

UNIVERSITY OF OKLAHOMA

GRADUATE COLLEGE

PERFORMANCE-DECLINE CURVE ANALYSIS OF VERTICAL AND  
HORIZONTAL WELLS  
IN ANISOTROPIC AND NATURALLY FRACTURED RESERVOIRS

A Dissertation

SUBMITTED TO THE GRADUATE FACULTY

in partial fulfillment of the requirements for the

degree of

Doctor of Philosophy

By

SCOTT BRADLEY CLINE  
Norman, Oklahoma  
1999

© Copyright by SCOTT BRADLEY CLINE 1999  
All Rights Reserved

PERFORMANCE-DECLINE CURVE ANALYSIS OF VERTICAL AND  
HORIZONTAL WELLS  
IN ANISOTROPIC AND NATURALLY FRACTURED RESERVOIRS

A Dissertation APPROVED FOR THE  
SCHOOL OF PETROLEUM AND GEOLOGICAL ENGINEERING

BY

The image shows five handwritten signatures stacked vertically, each preceded by a horizontal line. The signatures are: "Stephen Tyrell", "Ray Milner", "Dennis Myers", "John O'Reilly", and "Michael L. Wygant".

## Acknowledgements

I thank all faculty committee members for their various individual contributions during my tenure in the Petroleum Engineering Department and for putting up with a part time student for all these years. Foremost I thank Dr. Tiab for not only his challenging classes but for encouraging me to continue this project when, after unexpectedly leaving the petroleum industry, I could have easily given up. His persistent reminder to register each semester is the only reason I kept working. Thanks to Dr. Roy Knapp, who introduced me to simulation, who always stressed attention to detail and who may have finally succeeded in teaching me when to use the plural of “data”. Thanks to Dr. John Pigott for hopefully transferring some of his keen ability to see the “big picture” when presented with seeming chaos. I have never met anyone else that could so clearly see the important concepts in the midst of overwhelming data. Thanks to Dr. Wiggins for his great production class which introduced me to Muskat, Fetkovich and VanEverdingen and Hurst. Those class notes have been invaluable to me. Thanks to Dr. Osisanya whose teaching style made learning so fun and who set a great example by his hard work ethic. Each of you influenced my life in a positive way and for that I am eternally grateful. Thank you.

I also thank my daughter Charlotte Anne Cline, now a freshman at the University of Rochester, and my son Thomas Ansley Cline, a 10<sup>th</sup> grade student in Rushville, New York. Thank you both for sacrificing many of our precious moments together over these past few years and occasionally, but not often enough, convincing me to take a break

from this project to see what was happening in your own lives. Thank you Cindy Stewart for encouraging me to continue the project, for helping with the daily routines so that I could keep going, and for your general love and support. And thanks to all the rest of my family and friends who put up with my bad moods, understood or at least tolerated it when I gave up family functions to work on this project and gave me moral support.

I tried my best to keep a balance between family, friends and work despite the difficult circumstances of the past few years but I took too much from all of you. I did not however take your help for granted and therefore I hope now that through the grace of God and his Son Jesus Christ that I can pass on to others some of what you have all given me. Thank you and God bless you all.

## Table of Contents

|   |           |
|---|-----------|
| Acknowledgements.....   | iv        |
| Table of Contents.....  | vi        |
| List of Tables.....   | x         |
| List of Figures.....  | xiii      |
| Abstract.....   | xxi       |
|   |           |
| <b>CHAPTER ONE - Introduction .....</b>   | <b>1</b>  |
| 1.1 Introduction and Objectives.....  | 1         |
|   |           |
| <b>CHAPTER TWO - Decline Curve Background.....</b>  | <b>3</b>  |
| 2.1 History of Decline Curve Theory.....  | 3         |
| 2.2 Review of Decline Curve Methods.....  | 3         |
| 2.3 Characteristics of Decline Analysis.....  | 6         |
| 2.4 Special Case of Solution Gas Drive Reservoirs.....  | 8         |
|   |           |
| <b>CHAPTER THREE - Extending Analytical Solutions to Two Phase For Comparison With Reservoir Simulation Output.....</b> | <b>10</b> |
| 3.1 Introduction.....   | 10        |
| 3.2 Two Phase Background and Theory.....  | 12        |
| 3.3 Comparing Analytical Solutions to Two Phase Simulations.....  | 16        |
| 3.4 Evaluation of Effective Horizontal Permeability Assumptions – Vertical Well Case.....                               | 21        |
| 3.5 Evaluation of Effective Horizontal Permeability Assumptions - Horizontal Well Case.....                             | 21        |
|   |           |
| <b>CHAPTER FOUR - Decline Curve Theory.....</b>   | <b>26</b> |
| 4.1 Depletion Rate Decline (Pseudosteady State - PSS).....  | 26        |
| 4.2 Solution Gas Drive Meaning.....   | 33        |
| 4.3 Physical Meaning to Decline Analysis.....   | 34        |
| 4.3.1 Derivation of Fetkovich Type Decline Curves.....  | 36        |
| 4.3.2 Reservoir Parameters From Type Curves.....  | 38        |
|   |           |
| <b>CHAPTER FIVE - Decline Curve Construction Analysis and Use</b>   | <b></b>   |
| 5.1 – Introduction.....   | 43        |
| 5.2 - Theoretical Background for Dimensionless Solutions.....   | 43        |
| 5.2.1 Infinite Case.....  | 45        |
| 5.2.2 Solutions in Limited Reservoirs.....  | 47        |
| 5.2.2.1 Conditions.....   | 48        |
| 5.3 Generation of the Fetkovich Type Curves.....  | 50        |
| 5.4 Use of Decline Curves in Calculation of Reservoir Parameters and Future Production Calculations.....                | 56        |

|  |     |
|--|-----|
| 5.4.1 Calculation of transmissibility and apparent well bore radius.   | 56  |
| 5.4.2 Matching the PSS Portion - Calculation of N and Flow Rates..   | 57  |
| 5.4.3 Pseudosteady State Type Curve Matching for Reserve Estimates.....  | 58  |
| 5.4.4 Field - Wide Applications.....   | 61  |
| 5.5 Extensions of Fetkovich Radial Type Curves to Other Reservoir Shapes and Well Positions.....   | 61  |
| 5.5.1 Introduction.....  | 61  |
| 5.5.2 Overview of Derivation.....  | 62  |
| 5.5.2.1 Use in Calculating Reserves and Reservoir Parameters...  | 75  |
| 5.5.2.2 Use in Determining Contributions of Solution Gas Energy and Mobility Function.....   | 77  |
| 5.5.3 Extension to Fractured Reservoirs.....   | 79  |
| 5.6 Normalization Techniques.....  | 82  |
| 5.7 Derivative Methods.....  | 83  |
| 5.7.1 Closed Boundary Case-Radial Solutions.....   | 84  |
| 5.7.2 Construction of the Derivative Dimensionless Decline Curves.....   | 86  |
| 5.7.3 Extension to Other Reservoir Shapes.....   | 91  |
| 5.7.4 Use of the Derivative Curves in Reservoir Analysis.....  | 91  |
| 5.7.5 Data Smoothing Techniques.....   | 92  |
| 5.7.6 Example of Derivative Use.....   | 93  |
| 5.8 Chapter Summary.....   | 95  |
| <br>CHAPTER SIX - Horizontal Wells.....  | 96  |
| 6.1 Various Horizontal Well Analytical Equations.....  | 96  |
| 6.1.1 Mutalik-Joshi.....   | 96  |
| 6.1.2 Kuchuk et al.....  | 98  |
| 6.1.3 Babu and Odeh.....   | 99  |
| 6.2 Alternative Method Using Effective Wellbore Radius Concept...  | 103 |
| 6.3 Demonstration of Validity of 2-phase Horizontal Well Approximations.....   | 105 |
| 6.3.1 Validation Model Results and Discussion.....   | 106 |
| 6.4 Analysis of Analytical and Simulated Pseudosteady State Flow Equations for Horizontal Wells in Anisotropic Media.....                | 109 |
| 6.4.1 Anisotropic Experimental Results and Observations.....   | 110 |
| 6.4.2 Anisotropic Behavior Possibilities.....  | 112 |
| 6.4.3 Background Theory into Effective Permeability.....   | 113 |
| 6.5 Need to Re-Consider Effective Horizontal Permeability in Limited Reservoirs.....   | 115 |
| 6.6 Experimental Results and Observations of Variations in Simulated Output in Cases of Variable Horizontal Permeability Components..... | 118 |
| 6.6.1 Experiments.....   | 118 |
| 6.6.2 Effect of Grid Number.....   | 119 |

|   |     |
|---|-----|
| 6.6.3 Effect of Model Size and Penetration Ratios.....  | 123 |
| 6.6.4 Discussion of Experiment Results.....   | 131 |
| <br>  |     |
| CHAPTER SEVEN - Horizontal Well Decline Curve Analysis.....   | 132 |
| 7.1 Extension of Decline Analysis to Horizontal Wells.....  | 132 |
| 7.2 Dimensionless Decline Analysis Using the Horizontal Effective<br>Wellbore Radius Concept and Application.....                     | 133 |
| 7.3 Re-labeling of Decline Curves for Use in Decline Analysis.....  | 135 |
| 7.4 Calculation of Reserves from Horizontal Well Decline Curves.....  | 136 |
| 7.5 Comparison of Vertical and Horizontal Decline Curves.....   | 137 |
| 7.6 Decomposition of $k_x$ and $k_y$ .....  | 139 |
| 7.6.1 General Directional Permeability Background Discussion  | 140 |
| 7.6.2 Decomposing $k_x$ and $k_y$ .....   | 143 |
| 7.6.3 Studies in Anisotropic Media— $k_x$ , $k_y$ Experimental Results.   | 145 |
| 7.6.3.1 Visualization and Identification of Important Points on<br>the Rate Decline Curves .....                                      | 146 |
| 7.6.3.2 Experiments with Two Well System .....  | 156 |
| 7.6.4 Determination of the Principle $x$<br>and $y$ Permeability Components .....   | 160 |
| 7.7 Application to Decline Analysis Methods for<br>Horizontal Wells in Fractured Media.....   | 161 |
| 7.8 Extension to Determine Drainage Area.....   | 165 |
| 7.9 Chapter Summary.....  | 167 |
| <br>  |     |
| CHAPTER EIGHT - Extensions of Decline Curve Analysis to More<br>Complicated Reservoirs – Permeability Heterogeneity and Fractures.... | 168 |
| 8.1 Introduction.....   | 168 |
| 8.1.1 Heterogeneous Formation Considerations.....   | 168 |
| 8.2 Geological Model of a Fractured System.....   | 170 |
| 8.3 Mathematical Introduction and Overview of the Fracture Model .....  | 174 |
| 8.4 Construction and Development of the Type Curves.....  | 177 |
| 8.4.1 Model Assumptions.....  | 177 |
| 8.4.2 Limiting Equations Used in Construction.....  | 178 |
| 8.4.3 New Dual Porosity Dimensionless Parameters.....   | 186 |
| 8.5 Applications.....   | 190 |
| 8.6 Experiments with Fractured Media.....   | 191 |
| 8.7 Model Descriptions.....   | 192 |
| 8.8 Simulation Output.....  | 195 |
| 8.9 Analysis of Experimental Results.....   | 200 |
| 8.9.1 Matching of Experimental Rate-Time Data to<br>Posten-Chen Type Curves.....  | 205 |
| 8.9.2 Comparison of Rate-Time and Cumulative-Time<br>Data between Fracture Types.....   | 209 |

|   |     |
|---|-----|
| 8.9.3 Comparison of the $\Delta q/q$ vs. $q_{cum}/q$ Data between Fracture Types.....   | 216 |
| 8.9.4 Comparison of Derivative Data between Fracture Types.....   | 228 |
| 8.9.5 Comparison of $(t_p + \Delta t)/\Delta t$ vs. Time Data between Fracture Types.....   | 239 |
| 8.10 Summary of Surface Diagram Interpretation.....   | 242 |
| 8.11 Summary of Primary Diagnostic Indicators.....  | 243 |
| <br>CHAPTER NINE - Summary and Conclusions.....   | 245 |
| 9.1 Summary .....   | 245 |
| 9.2 Conclusions.....  | 251 |
| 9.3 Recommendations for Future Research.....  | 251 |
| <br>NOMENCLATURE.....   | 253 |
| <br>REFERENCES.....   | 255 |
| <br>Appendix A: Derivation of Use of Inflow Performance in Two Phase Approximations.....  | 259 |
| Appendix B: Algorithm for Estimating PVT Properties for use in Simulation ..  | 267 |
| Appendix C: Guide To Estimating And Deriving The Reservoir Properties Needed In Reservoir Simulation and Two Phase Analytical Calculations From Field Production Data ..... | 285 |
| Appendix D: Tabular Generalized Type Curve Solutions.....   | 311 |
| Appendix E: Derivation of Generalized Dimensionless Decline for General Reservoir Shapes and Well Positions.....  | 334 |
| Appendix F: Effective Wellbore Radius of a Horizontal Well.....   | 343 |
| Appendix G: Tabular Data-Fractured Reservoir Simulation Experiments.....  | 352 |

## List of Tables

|           |  |     |
|-----------|--|-----|
| Table 3.1 | Tabular Simulation Pressure Output.....  | 20  |
| Table 3.2 | Tabular Simulation Saturation Output.....  | 20  |
| Table 3.3 | Vertical Comparison Output .....   | 20  |
| Table 5.1 | Shape Factors for Use in Generalized Decline Curves .....                          | 69  |
| Table 5.2 | Correction Factors for Reservoir Shapes.....                                       | 82  |
| Table 5.3 | Derivative of Production Data from Golan Reference.....                            | 93  |
| Table 7.1 | Vertical and Horizontal Well Data.....   | 137 |
| Table 7.2 | Slopes of Various Portions of the Decline Curve.....                               | 150 |
| Table 7.3 | Relation of Permeability Ratio to Cumulative Departure Times..                     | 159 |
| Table 8.1 | Simulation Model Parameters.....   | 193 |
| Table 8.2 | Graph Output Generated.....  | 197 |
| Table 8.3 | Type Curve Match Summary Information.....  | 207 |
| Table 8.4 | Predominant Characteristics of Rate-Time and Rate<br>Cumulative Data Behavior..... | 215 |
| Table 8.5 | Predominant Characteristics from $\Delta q/q$ versus $q_{cum}/q$ .....             | 227 |
| Table 8.6 | Predominant Characteristics of the Derivative Plots.....                           | 238 |
| Table 8.7 | Comparisons of $(t_p + \Delta t)/\Delta t$ Plots.....                              | 241 |
| Table 8.8 | Summary of Other Fracture Type Characteristics.....                                | 244 |
| Table B-1 | Sample PVT Program Output.....   | 276 |
| Table C-1 | GOR Analysis for PVT Estimation .....  | 289 |
| Table C-2 | Program OILPROP Output .....   | 290 |

|           |  |     |
|-----------|--|-----|
| Table C-3 | Example Core Analysis .....  | 293 |
| Table C-4 | Relative Permeability Estimates From Willhite General Form ....                            | 293 |
| Table C-5 | Ratio Of Produced Fluid Flows .....  | 295 |
| Table C-6 | Gas-Oil Relative Permeability Data and Construction .....                                  | 300 |
| Table C-7 | Capillary Pressure Calculation Data.....   | 309 |
| Table D-1 | Tabular Data for Fetkovich Decline Type Curves<br>Figures 5.1 – 5.4.....                   | 312 |
| Table D-2 | Tabular Data for Fetkovich Decline Type Curves<br>Figures 5.1 – 5.4 Transient Portion..... | 314 |
| Table D-3 | Arps Depletion Solutions for Fetkovich Type Curves<br>Figures 5.1 – 5.4.....               | 315 |
| Table D-4 | Equivalent Radial Transient Generalized Solutions<br>Shape Factor 31.62.....               | 316 |
| Table D-5 | Depletion Solutions Generalized for Figure 5.9.....  | 318 |
| Table D-6 | Depletion Solutions Generalized for Figure 5.7 .....                                       | 322 |
| Table D-7 | Depletion Solutions Generalized for Figure 5.8 .....                                       | 326 |
| Table D-8 | Derivative Solutions For Type Curve.....   | 330 |
| Table D-9 | Arps Derivative Solutions For Type Curve.....  | 333 |
| Table G-1 | Model 1 Type 1 Fracture Simulation Output and Calculations.....                            | 353 |
| Table G-2 | Model 1h Type 1h Fracture Simulation Output and Calculations...                            | 356 |
| Table G-3 | Model 1n Type 1n Fracture Simulation Output and Calculations...                            | 360 |
| Table G-4 | Model 1nh Type 1nh Fracture Simulation Output and Calculation..                            | 364 |
| Table G-5 | Model 2 Type 2 Fracture Simulation Output and Calculations.....                            | 368 |
| Table G-6 | Model 2h Type 2h Fracture Simulation Output and Calculations...                            | 372 |
| Table G-7 | Model 3 Type 3 Fracture Simulation Output and Calculations....                             | 376 |

|           |  |     |
|-----------|--|-----|
| Table G-8 | Model 3h Type 3h Fracture Simulation Output and Calculations.... | 380 |
| Table G-9 | Model 4 Type 4h Fracture Simulation Output and Calculations..... | 384 |

## List of Figures

|  |    |
|--|----|
| Figure 2.1 Cartesian Rate versus Cumulative.....   | 6  |
| Figure 2.2 Log-Log Rate versus Cumulative .....  | 6  |
| Figure 2.3 Cartesian Rate versus Time.....   | 6  |
| Figure 2.4 Log-Log Rate versus Time.....   | 6  |
| Figure 3.1 Viscosity and Formation Volume Factor as a Function of Pressure....   | 13 |
| Figure 3.2 Mobility Factor as a Function of Pressure.....  | 15 |
| Figure 3.3 Relative Permeability versus Phase Saturation.....  | 17 |
| Figure 3.4 PVT Data as a Function of Pressure.....   | 17 |
| Figure 3.5 Relative Permeability-Viscosity-Formation Volume Factor Function<br>versus Pressure.....  | 18 |
| Figure 3.6 Oil Saturation versus Pressure.....   | 18 |
| Figure 3.7 Rate versus Pressure for Vertical Well Case of Permeability<br>Anisotropy but Constant Geometric Average Permeability.....                    | 19 |
| Figure 3.8 Comparison of Simulated Rate versus Pressure for Cases of Anisotropic<br>Horizontal Permeability but Constant Geometric Mean Permeability ... | 23 |
| Figure 3.9 Comparison of Simulated with Analytical for Isotropic Permeability...   | 24 |
| Figure 3.10 Comparison of Simulated and Analytical with Anisotropic<br>Permeability.....   | 24 |
| Figure 3.11 Comparison of Simulated and Analytical with Anisotropic<br>Permeability.....   | 25 |
| Figure 4.1 Dimensionless Rate versus Time.....   | 28 |
| Figure 4.2 Generalized Arps-Fetkovich Dimensionless Decline Curve.....   | 38 |
| Figure 5.1 Dimensionless Rate versus Dimensionless Time.....   | 47 |

|   |     |
|---|-----|
| Figure 5.2 Arps Depletion Decline for Values of b from 0 to 1.....  | 53  |
| Figure 5.3 Fetkovich Type Curve – Transient and Depletion.....  | 55  |
| Figure 5.4 Final Composite Fetkovich Type Curve – Transient and Depletion...  | 55  |
| Figure 5.5 Type Curve Matching.....   | 59  |
| Figure 5.6 Generalized Type Curve Transient and Exponential Depletion<br>for Circular Shape Factor.....               | 68  |
| Figure 5.7 Generalized Type Curve Rectangular Shape Factor x:y:2:1.....   | 72  |
| Figure 5.8 Generalized Type Curve Rectangular Shape Factor x:y:4:1.....   | 73  |
| Figure 5.9 Generalized Type Curve Rectangular Shape Factor x:y:2:1<br>Off-Center Close to Boundary.....               | 74  |
| Figure 5.10 Composite Fetkovich Type Curve.....   | 78  |
| Figure 5.11 Dimensionless Rate Derivative Radial Transient Portion.....   | 87  |
| Figure 5.12 Derivative Type Curve Radial Case.....  | 87  |
| Figure 5.13 Decline Dimensionless Rate Derivative Transient.....  | 88  |
| Figure 5.14 Arps Derivative Decline Dimensionless Rate Decline.....   | 89  |
| Figure 5.15 Composite Derivative Type Curve.....  | 90  |
| Figure 5.16 Example Production Data-Derivative Method.....  | 94  |
| Figure 5.17 Derivative Type Curve.....  | 94  |
| Figure 6.1 Schematic Diagram of Fully Penetrating Vertical Well versus<br>Equivalent Horizontal Well.....             | 102 |
| Figure 6.2 Comparison of Simulated Vertical and Equivalent Horizontal<br>Flow Rates.....                              | 102 |
| Figure 6.3 Simulated versus 2-Phase Analytical Equations $k_x=k_y=3.1$ md,<br>Geometric Mean Perm. Constant.....      | 108 |
| Figure 6.4 Simulated versus 2-Phase Analytical Equations $k_x=9.61$ , $k_y=1$ ,<br>Geometric Mean Perm. Constant..... | 108 |

|   |     |
|---|-----|
| Figure 6.5 Simulated versus 2-Phase Analytical Equations $k_x=19.22$ , $k_y=0.5$ , Geometric Mean Perm. Constant.....     | 109 |
| Figure 6.6 Simulated Rates For Various x and y Permeability Contrasts but Constant Geometric Means.....                   | 111 |
| Figure 6.7 Deviation from Isotropic as # Grid Blocks Increases L = 400 h=25, 2Xe/L=10 Case.....                           | 119 |
| Figure 6.8 Deviation from Isotropic as # Grid Blocks Increases L=600 h= 25, 2Xe/L=6.7 Case.....                           | 120 |
| Figure 6.9 Deviation from Isotropic as # Grid Blocks Increases L=1000 h= 25, 2Xe/L=4 Case.....                            | 120 |
| Figure 6.10 Variation in Rate-Pressure With Change in $k_x/k_y$ Ratio, L-1000, 2Xe/L=4.....                               | 121 |
| Figure 6.11 Variation in Rate-Pressure With Change in $k_x/k_y$ , L=1000, h=100, 2Xe/L=19.....                            | 121 |
| Figure 6.12 Deviation from Isotropic as L Changes $k_x/k_y=3.1$ case above 1500 psi, h=25.....                            | 122 |
| Figure 6.13 Deviation from Isotropic as L Changes, $k_x/k_y=6.2$ case above 1500 psi, h=25.....                           | 122 |
| Figure 6.14 Deviation from Isotropic with Change in L above 1500 psia, h=25 ft, 784 grids, 2Xe/L=4 to 10 Small Model..... | 124 |
| Figure 6.15 Deviation from Isotropic with Change in L above 1300 psia, h=25 ft, 784 grids, 2Xe/L=4 to 10 Small Model..... | 124 |
| Figure 6.16 Deviation from Isotropic with Change in L above 1500 psia, h=100 ft, 784 grids,2Xe/L= 4 to10 Small Model..... | 125 |
| Figure 6.17 Deviation from Isotropic with Change in L above 1300 psia, h=100 f, 784 grids,2Xe/L= 4 to10 Small Model.....  | 125 |
| Figure 6.18 Deviation from Isotropic with Change in L above 1500 psia, h=25 ft, 784 grids, 2Xe/L=19 to 48.....            | 126 |
| Figure 6.19 Deviation from Isotropic with Change in L above 1500 psia, h=25 ft, 784 grids, 2Xe/L=19 to 48.....            | 126 |

|  |     |
|--|-----|
| Figure 6.20 Deviation from Isotropic with Change in L above 1500<br>psia, h=100 ft, 784 grids, 2Xe/L=19 to 48.....               | 127 |
| Figure 6.21 Deviation from Isotropic with Change in L above 1500<br>psia, h=100 ft, 784 grids, 2Xe/L=19 to 48.....               | 127 |
| Figure 6.22 Deviation Trend as Ld Varies With Chang in h, Small Model-<br>$k_x/k_y=3.1$ .....                                    | 128 |
| Figure 6.23 Deviation Trend as Ld and L/2Xe Varies - Small Model-<br>$k_x/k_y=3.1$ .....   | 129 |
| Figure 6.24 Deviation Trend as Ld and L/2Xe Varies - Small Model-<br>$k_x/k_y=6.2$ .....   | 129 |
| Figure 6.25 Deviation Trend as Ld and L/2Xe Varies - Large Model-<br>$k_x/k_y=3.1$ .....   | 130 |
| Figure 6.26 Deviation Trend as L <sub>d</sub> and L/2Xe Varies - Large Model-<br>$k_x/k_y=6.2$ .....                             | 130 |
| Figure 7.1 Simulated Horizontal vs. Vertical Flow Rates-Same Reservoir<br>Parameters.....  | 138 |
| Figure 7.2 Generalized Type Curve Square Depletion.....  | 138 |
| Figure 7.3 Equivalent Horizontal Wellbore Radius.....  | 143 |
| Figure 7.4 Model Geometry.....   | 146 |
| Figure 7.5 3 Well System $k_x=19.22$ , $k_y=0.5$ md, with Isotropic<br>Case Displayed Geometric Mean Permeability is 3.1 md..... | 147 |
| Figure 7.6 3 Well System $k_x=19.22$ , $k_y=0.5$ md, Geometric Mean<br>Permeability is 3.1 md.....                               | 148 |
| Figure 7.7 3 Well System $k_x=3.1$ , $k_y=3.1$ md, Isotropic Case<br>Displayed Geometric Mean Permeability is 3.1 md.....        | 148 |
| Figure 7.8 3 Well System $k_x=3.1$ , $k_y=3.1$ md, Geometric Mean<br>Permeability is 3.1 md.....                                 | 149 |
| Figure 7.9 Depiction of Slope Areas for Table 7.....   | 149 |
| Figures 7.10 to 7.13 - Anisotropic Pressure Distribution Profiles for Figure 7.5   | 151 |

|   |     |
|---|-----|
| Figures 7.14 to 7.17 - Anisotropic Pressure Distribution Profiles for Figure 7.5  | 152 |
| Figures 7.18 to 7.21 Isotropic Case Pressure Distribution Profiles.....   | 153 |
| Figures 7.22 to 7.25 Isotropic Case Pressure Distribution Profiles.....   | 154 |
| Figure 7.26 3 Well System with Different Permeability Path Comparisons.....   | 155 |
| Figure 7.27 Productivity Index versus Time $k_x=19.22$ , $k_x = 0.5$ Case.....  | 155 |
| Figure 7.28 2 Competing Wells along Different Permeability Paths<br>Contrasted with Homogeneous Case Geometric Mean<br>Permeability is Identical.....                           | 157 |
| Figure 7.29 2 Competing Wells Along Different Permeability Directions.....  | 157 |
| Figure 7.30 Cumulative Production Versus Time Different Permeability Path..   | 157 |
| Figure 7.31 2 Competing Wells along Different Permeability Paths<br>Contrasted with Homogeneous Case Geometric Mean<br>Permeability is Identical.....                           | 158 |
| Figure 7.32 2 Competing Wells Along Different Permeability Directions.....  | 158 |
| Figure 7.33 Cumulative Production Versus Time Different Permeability Path..   | 158 |
| Figure 7.34 2 Well Case of Wells Oriented along Permeability Paths,<br>Equal Geometric Means.....   | 159 |
| Figure 7.35 Dimensionless Pressure versus Time for Horizontal Wells.....  | 164 |
| Figure 7.36 Drainage Area Over Time.....  | 165 |
| Figure 8.1 Posten-Chen Type Curve for Fractured Reservoir.....  | 172 |
| Figure 8.2 Posten-Chen Decline Type Curve Reconstruction - Fractured<br>Reservoir Model- $\omega$ (storage capacity) = 0.1.....   | 173 |
| Figure 8.3 Comparison Fetkovich(dashed lines) with Posten-Chen<br>Decline Type Curve Reconstruction - Fractured Reservoir<br>Model-Storage Compressibility $\omega = 0.1$ ..... | 183 |
| Figure 8.4 Fracture Dimensionless Rate versus Dimensionless Time<br>Horizontal Well.....  | 186 |

|  |            |
|--|------------|
| <b>Figure 8.6 Dimensionless Type Curve for Variations in Storage Compressibility.....</b>  | <b>189</b> |
| <b>Figure 8.7 Dimensionless Type Curves for Variations in Fracture Intensity.....</b>  | <b>189</b> |
| <b>Figures 8.8-16 Rate Time Plots For Various Fracture Types.....</b>  | <b>201</b> |
| <b>Figure 8.17 Composite Rate-Time Relationship Semi-Log Scale.....</b>  | <b>204</b> |
| <b>Figure 8.18 Composite Rate-Time Relationship Log-Log Scale.....</b>   | <b>204</b> |
| <b>Figure 8.19 Type Curve Matching Example.....</b>  | <b>206</b> |
| <b>Figure 8.20 Comparison of the Effect of Matrix Permeability in Cases of Large Matrix Storage Capacity – Types 2 and 3.....</b>                        | <b>209</b> |
| <b>Figure 8.21 Early Time Comparison of the Effect of Matrix Permeability in Cases of Large Matrix Storage Capacity – Types 2 and 3.....</b>             | <b>210</b> |
| <b>Figure 8.22 Late Time Comparison of the Effect of Matrix Permeability in Cases of Large Matrix Storage Capacity – Types 2 and 3.....</b>              | <b>211</b> |
| <b>Figure 8.23 Comparison of the Cumulative Production Effects of Matrix Permeability in Cases of Large Matrix Storage Capacity – Types 2 and 3.....</b> | <b>212</b> |
| <b>Figure 8.24 Effect of Increasing Fracture Storage Capacity on Systems with Low Matrix Permeability.....</b>   | <b>213</b> |
| <b>Figure 8.25 Effect of Increasing Fracture Storage Capacity from 1% to 18% of System Total.....</b>  | <b>214</b> |
| <b>Figure 8.26 Model Types 2 (log-log) <math>\Delta p/q</math> Compared to <math>\Delta q/q</math> versus <math>q_{cum}/q</math> .....</b>               | <b>218</b> |
| <b>Figure 8.27 Model Type 3 (semi-log) <math>\Delta p/q</math> Compared to <math>\Delta q/q</math> versus <math>q_{cum}/q</math> .....</b>               | <b>218</b> |
| <b>Figure 8.28 Model Type 3 (log-log) <math>\Delta p/q</math> Compared to <math>\Delta q/q</math> versus <math>q_{cum}/q</math> .....</b>                | <b>218</b> |
| <b>Figure 8.29 Type 1 Fracture Increasing Matrix Pore Volume Relative to Fracture Volume <math>\lambda'</math> .....</b>                                 | <b>220</b> |

|   |     |
|---|-----|
| Figure 8.30 Type 1 Fracture Increasing Matrix Pore Volume Relative to Fracture Volume $\lambda'$ .....  | 220 |
| Figure 8.31 Expanded Type 1,1n,1nh Fracture Model-Effect of Increasing Matrix Pore Volume Relative to Fracture and Change in $k_f/k_m$ Log-Log. ....                    | 221 |
| Figure 8.32 Expanded Type 1,1n,1nh Fracture Model-Effect of Increasing Matrix Pore Volume Relative to Fracture and Change in $k_f/k_m$ Semi-Log.....                    | 221 |
| Figure 8.33 Effect of Increasing Fracture Storage Capacity in Case of Poor Matrix Permeability Log-Log.....   | 222 |
| Figure 8.34 Effect of Increasing Fracture Storage Capacity in Case of Poor Matrix Permeability Expanded Semi-Log.....   | 223 |
| Figure 8.35 Effect of Increasing Matrix Permeability Relative to Fracture Permeability in Case of Large Matrix Storage Capacity.....                                    | 224 |
| Figure 8.36 Cartesian Plot of $\Delta q/q$ versus $q_{cum}/q$ Showing Effect of Matrix Pore Volume on Slope.....  | 225 |
| Figure 8.37 Expanded Cartesian Plot of $\Delta q/q$ versus $q_{cum}/q$ , type 2 – Effect of Fracture-Matrix Permeability in Large Relative Matrix Pore Volume Case..... | 226 |
| Figure 8.38 First Derivative of Rate with respect to Time.....  | 229 |
| Figure 8.39 Second Derivative of Cumulative with respect to Time.....   | 229 |
| Figure 8.40 $Q''$ versus Time-Effect of Change in $k_f/k_m$ , Large Constant Matrix Storage.....  | 230 |
| Figure 8.41 $Q''^*t$ versus Time-Effect of Change in $k_f/k_m$ , Large Constant Matrix Storage.....   | 231 |
| Figure 8.42 $(\Delta q/q)'$ versus Time-Effect of Change in $k_f/k_m$ , Large Constant Matrix Storage.....  | 231 |
| Figure 8.43 $Q''$ versus time- Effect of Changing the Relative Matrix to Fracture Storage.....  | 232 |
| Figure 8.44 $Q''^*t$ versus time- Effect of Changing the Relative Matrix to Fracture Storage.....   | 233 |
| Figure 8.45 $(\Delta q/q)'$ versus time- Effect of Changing the Relative Matrix to Fracture Storage.....  | 233 |

|  |     |
|--|-----|
| Figure 8.46 Effect of Permeability Compartments Inside Fracture.....   | 234 |
| Figure 8.47 Summary of Various Model Rate Derivatives.....   | 235 |
| Figure 8.48 Plot of $\Delta q$ and $q^*t$ versus time for the models exhibiting<br>10,000 md fracture permeability.....                              | 236 |
| Figure 8.49 Plot of $\Delta q/q$ and $q^*t$ versus time for the models exhibiting<br>10,000 md fracture permeability.....                            | 237 |
| Figure 8.50 Effect of Increase in Relative Matrix Storage Volume-Poor<br>Matrix Permeability- $\Delta q$ versus $(t_p + \Delta t)/\Delta t$ .....    | 239 |
| Figure 8.51 Effect of Change in Matrix Permeability in Case of Large<br>Matrix Storage Capacity- $\Delta q$ versus $(t_p + \Delta t)/\Delta t$ ..... | 240 |
| Figure 8.52 $\Delta q$ versus $(t_p + \Delta t)/\Delta t$ .....  | 241 |
| Figure 8.53 Surface Diagram of Average Pressure across Model Day 18 .....  | 242 |
| Figure 8.54 Surface Diagram of Oil Saturation across Model Day 18.....   | 242 |
| Figure A-1 Mobility Function versus Pressure.....  | 261 |
| Figure C-1 Graph of PVT Data From Oilprop Program.....   | 291 |
| Figure C-2 Derived Relative Permeability Curves.....   | 294 |
| Figure C-3 Final Relative Permeability Curve.....  | 296 |
| Figure C-4 Gas Oil Relative Permeability.....  | 300 |
| Figure C-5 Change in IPR with Depletion.....   | 305 |
| Figure C-6 Saturation v. Depth Profile.....  | 310 |
| Figure C-7 Capillary Pressure Profile.....   | 310 |
| Figure F1 Potential Flow to a Horizontal Well-Horizontal Plane.....  | 345 |
| Figure F-2 Division of 3D Horizontal Well Into Two 2-D Problems.....   | 346 |

## **Abstract**

This research extends previously developed dimensionless decline type curve concepts and techniques to more general cases of varying reservoir shapes, well locations and anisotropic permeability conditions. The research also introduces some novel approaches to estimating, from field production data, the simulation reservoir properties such as oil-water and gas-oil relative permeability relationships, PVT properties, and capillary pressure in the absence of laboratory measurements. Semi-analytical two-phase analytic equations are then developed that approximate the two phase flow in solution gas reservoirs for use as a “quick-look” tool to validate simulation model design by comparing expected and actual simulation output. Techniques and correlation curves based on simulation experiments are then generated to aid in proper simulation model design in cases where directional permeability is highly anisotropic. The last part of the research explores anisotropic and fracture permeability conditions for both vertical and horizontal wells where anisotropic and fractured reservoirs are modeled and studied in an effort to characterize fracture-matrix characteristics based on rate-time decline curve character.

It is not generally known that the “Fetkovich” decline type curves were developed for only single-phase radial systems with centrally located wells. This research derives the dimensionless decline rate and time relationships for the cases of more general reservoir geometry and well location. These relationships are then used to construct new type curves for various reservoir shapes and well locations. The data are then tabulated and

combined with "Arp's" depletion stems to form more general dimensionless decline curves and tabular data. A set of derivative curves is also generated, tabulated and plotted. These generalized decline curves are then modified for use with horizontal wells by incorporation of the equivalent well bore radius concept into the decline curve construction and display.

Extensive simulation experiments then demonstrate the effects of horizontal permeability anisotropy on well performance. The experiments confirmed the hypothesis that there are problems in properly simulating horizontal wells in horizontally anisotropic reservoirs. It is shown that unless the reservoir is extremely large in comparison to the length of the horizontal well, deviation from permeability isotropy in the principal x and y directions will yield results that deviate from that predicted by commonly accepted traditional geometric mean averaging. All analytical flow equations use the geometric mean permeability. Extensive experiments show however that as the contrast in x and y permeability increases, while maintaining a constant geometric mean horizontal permeability, the simulated horizontal flow rates deviate increasingly from one another. This deviation does not occur when simulating vertical wells. Graphical relationships showing the effect of permeability anisotropy as a function of dimensionless well length, grid block spacing etc. are presented based on the results of extensive simulation experiments.

Finally, the production rate decline characteristics of fractured reservoirs intersected by horizontal wells are studied through simulation experiments. Tables and charts are

produced that help classify each of four different fracture types through characteristic rate-time decline patterns. Pressure data is purposely ignored in an effort to utilize only data that would be typically available to the practicing engineer.

# **CHAPTER ONE**

## **Introduction and Objectives**

The two quantities one usually wishes to determine from decline curve analysis are remaining oil reserves and remaining productive life of the well or reservoir. The forecasts of reserves and future production are the most important items in a reservoir evaluation. Other desirable but normally difficult to determine reservoir parameters include permeability, drainage area, drainage shape and fracture characteristics. Reserve estimating methods are usually categorized into three families: analogy, volumetric, and performance techniques. Performance technique methods are usually further subdivided into simulation studies, material balance and decline-trend analysis.

Special problems occur with well prediction in anisotropic reservoirs particularly with well performance prediction in fractured reservoirs. The end of the infinite acting period is often abrupt and unpredictable. Post infinite acting flow is also quite variable depending on matrix supply support and micro fractures. Therefore decline curve analysis may give insight into fracture nature and type.

This research is primarily concerned with developing methods for better reservoir modeling and interpretation of decline curves using both analytical and empirical decline curve concepts for both vertical and horizontal wells in irregular shaped, anisotropic and fractured reservoirs. Specific attention is focused on reservoirs that in general exhibit

anisotropy in directional permeability. Recognition of fracture type from decline curves is also addressed. Inflow performance relations (IPR) and material balance concepts will also be addressed. Type curves, which combine 1) the rate and 2) rate derivative functions, or a group of terms involving these functions, with respect to time, or a group of terms involving time, will also be constructed for various reservoir systems. Adaptation to both vertical and horizontal wells will be addressed. Emphasis will be placed on developing equations and methods to forecast future performance, to calculate reserve estimates and ultimate recovery, classify fracture types and to identify permeability anisotropy. Both naturally fractured and heterogeneous media with vertical and horizontal wells will be examined.

## **CHAPTER TWO**

### **Decline Curve Background**

#### **2.1 History of Decline Curve Theory**

Decline curves are the most common means of forecasting production and estimating the value of oil and gas wells. The earliest literature reference to a mathematical decline analysis approach was by Arnold and Anderson in 1908.<sup>1</sup> The various methods used to interpret decline curves have generally been regarded as empirical and not reliable. However, in 1980 Fetkovich demonstrated that decline curve analysis not only has a solid fundamental base but also provides a tool with more diagnostic power than had been previously suspected. Fetkovich constructed log-log type curves, which combine all the standard exponential, hyperbolic and harmonic decline equations developed by Arps with the analytical constant-pressure infinite and finite reservoir solutions.<sup>2,3</sup> He showed that log-log type curves could be analyzed by the type curve matching technique. His type curves were developed for radial reservoirs only. This research will extend these curves to all reservoir shapes and well positions.

#### **2.2 Review of Decline Curve Methods**

Decline curve analysis adds the time dimension to the analysis of well performance. Traditional decline curve analysis considers particular cases of production decline in wells producing with constant wellhead pressure that can be treated without explicit material balance calculations. Constant pressure production implies a continuous drop of

production rate with time. Production with constant wellhead pressure of a separator or a pipeline without the restriction of a choke is typical of low productivity wells and old high rate wells when wellhead pressure has already reached the minimum delivery pressure required to maintain flow. The constant flowing wellhead pressure that exists in practical problems does not correspond rigorously to a constant flowing bottomhole pressure, which is assumed in developing traditional decline curve analysis. In fact, bottomhole pressure does change if the flow rate declines gradually and wellhead pressure is maintained constant. In many cases this is not a serious restriction as the changes are small and result in only minor losses of accuracy. However in many cases there is loss of accuracy and other methods must be developed to predict decline, ultimate recoveries and reserves in place.

From a practical standpoint, transient decline is only observed in wells with low permeability or during the early life of well production. Depletion decline, also known as pseudo steady state (PSS) decline, is observed for all wells producing by expansion, solution gas, gravity drainage or partial water drive. PSS decline occurs after the radius of drainage has reached the outer boundaries and the well is draining a constant reservoir volume.

Decline curve analysis assumes a tank type model. Important to the use of tank type models is the interpretation of a reservoir pressure or rate and production history to determine the oil in place and whether or not the reservoir has water influx. Tank type

models assume the 1) reservoir pore volume is constant, 2) the reservoir temperature is constant, 3) the reservoir has uniform porosity and relative permeability, 4) equilibrium conditions exist at all times in the reservoir. Pressure is assumed to be uniform throughout the reservoir. Deviations of decline or production performance curves from the homogeneous models may yield reservoir information.

It was first assumed that where water drive was absent, the pressure is proportional to the amount of remaining oil and that the productivity indices were constant throughout the well life. In such a hypothetical case, the relationship between cumulative oil produced and pressure would have to be linear and consequently, also the relationship between production rate and cumulative production. This linear relationship between rate and cumulative is typical of exponential or semi-log decline as will be shown later.

In most reservoirs, however, the aforementioned idealized conditions do not occur. Pressures usually are not proportional to the remaining oil, but seem to decline at gradually slower rates as the amount of remaining oil diminishes. At the same time the productivity indices are generally not constant, but show a tendency to decline as the reservoir is being depleted and the gas-oil ratios increase. The combined result of these two tendencies is a rate-cumulative relationship, which, instead of being a straight line on coordinate paper, shows up as a gentle curve, convex toward the origin.

## 2.3 Characteristics of Decline Analysis

Cumulative production and/or time are normally the independent variable (x) and production rate is the dependent variable (y). Figures 2.1-2.4 show the typical Cartesian and log-log plots of rate-cumulative and rate-time plots. The two most commonly used curves are rate-time and rate-cumulative production curves.

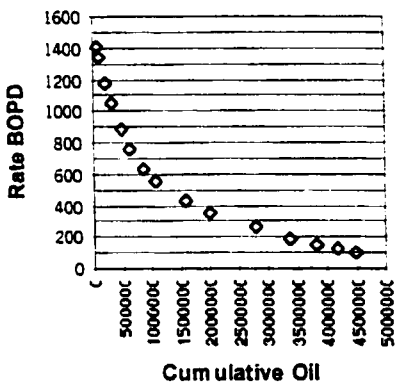


Figure 2.1 Cartesian Rate versus Cumulative

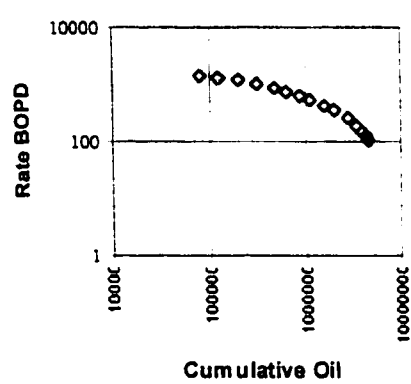


Figure 2.2 Log-Log Rate versus Cumulative

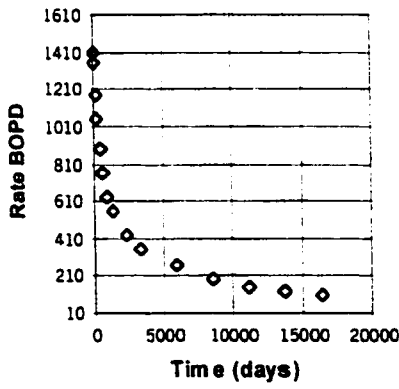


Figure 2.3 Cartesian Rate versus Time

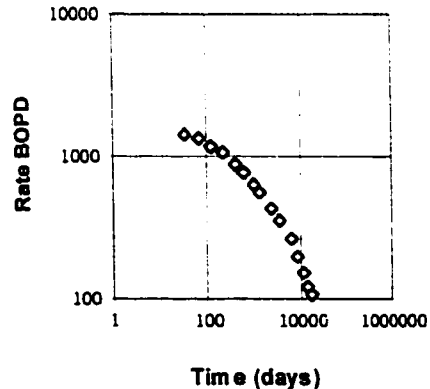


Figure 2.4 Log-Log Rate versus Time

Decline curve analysis is normally done by extrapolation of a performance trend that follows a certain pattern. For extrapolation purposes, this variable has to be 1) more or less a continuous function of the independent variable and 2) it must have a known endpoint. By plotting the continuously changing dependent variable (i.e. rate) vs. the independent variable (cumulative production or time) and extrapolating the trend until the known endpoint, an estimate of the remaining reserves, remaining life and future performance in time can be estimated. The method assumes that whatever caused the controlled trend of the curve in the past will continue in the future. This by nature then is empirical and mathematical expressions of the trend curve based on physical considerations are difficult and applicable in only a few simple cases.

Gradual changes in the production rate of a well may be caused by the 1) decreasing efficiency or effectiveness of the lifting equipment, 2) reduction of the productive index or increase in skin as a result of physical changes in the near well bore environment, 3) changes in bottomhole pressure, GOR, water percentage, or other reservoir conditions 4) Discontinuities in the outlying reservoir.

Production decline, caused by reservoir conditions, must be distinguished from that caused by wellbore conditions or failure of lifting equipment to be used for reserve estimation. When lifting equipment is operating properly and wellbore conditions are satisfactory, a declining production trend must reflect changing reservoir conditions and

the extrapolation of such a trend can then be a reliable guide to prediction of remaining reserves.

## **2.4 Special Case of Solution Gas Drive Reservoirs**

A solution gas drive reservoir is an oil reservoir that undergoes primary depletion with the main reservoir energy supplied by 1) the release of gas from the oil and 2) the expansion of the in-place fluids as the reservoir pressure drops. This excludes reservoirs that have significant water influx, oil and gas segregation and gravity assistance. Solution gas drive is also called dispersed gas drive or internal gas drive because the gas come out of solution throughout the portion of the oil zone that has a pressure below the bubblepoint. Initially, pore space contains interstitial water plus oil that contains gas in solution because of pressure. No free gas is assumed to be present in the oil zone. As production continues, the reservoir pressure drops below the bubblepoint, the oil shrinks, the gas that comes out of solution fills part of the pore space and there is minor water expansion. The drive mechanism (gas evolution and expansion) is dispersed or scattered throughout the oil zone.

The evolved gas, less any produced gas, fills the pore space vacated by the produced oil and by shrinkage of the remaining oil. The amount of oil recovered depends on the amount of pore space occupied by gas ( $S_g$ ) and the oil shrinkage ( $B_o$  vs. pressure). Gas-oil relative permeability characteristics and viscosity of oil and gas are important because

they determine the flowing GOR at a given  $S_g$  and thus the amount of free gas produced along with the oil.

Solution gas drive reservoir performance is characterized by 1) relatively rapid pressure decline, 2) low initial producing GOR rising to a much higher GOR, 3) oil production rates declining because of both 1 and 2, 4) little or no water production, 5) relatively low oil recovery. These reservoirs are ideal secondary waterflood candidates and thus merit considerable research.

## CHAPTER THREE

### Extending Analytical Solutions to Two Phase for Comparison with Reservoir Simulation Output

#### 3.1 Introduction

As mentioned previously, pseudosteady state, where pressure and thus well performance decreases with time, is the most common reservoir condition. Reservoir simulation is an important tool in reservoir modeling. However blindly jumping into simulation without accurately establishing reservoir and model parameters can lead to erroneous results. It is therefore desirable to develop and use simplified multi-phase analytical methods to estimate reasonable ranges of simulation results. In other words if the simulation yields performance data that deviate significantly from the basic multi-phase analytical methods presented in this paper then the model should be scrutinized for possible errors or simulation instabilities.

This chapter will demonstrate that pseudosteady state, multi-phase analytical approximations to vertical well fluid flow in both isotropic and anisotropic media closely match simulated results without the use of Muskat's pressure integral analysis.<sup>4</sup> The modification of single phase analytical fluid flow equations to include pressure dependant relative permeability, viscosity and formation volume factor at arithmetically averaged reservoir pressure and phase saturation (presented in this research) give results close to those when using more complicated methods. Thus a "quick-check" method is provided for use in verifying simulation parameters such as proper grid spacing, grid size and reservoir parameters.

It will also be demonstrated that, for vertical wells, the use of this effective horizontal permeability,  $k_h$ , as the geometric average, results in simulated rate versus pressure data that match analytical results quite well in both isotropic and highly anisotropic conditions. Simulation experiments with Boast-VHS simulation software indicate that vertical well inflow performance predictions match those predicted with analytical equations quite well no matter what the contrast in  $k_x$  and  $k_y$  as long as the geometric average is the same in each case compared. The match is also excellent between various simulation experiments in which the geometric average is the same but the components  $k_x$  and  $k_y$  vary widely. This match is good both above and below the bubble point.

Experiments with horizontal wells indicate that the match is often not good with horizontal wells unless the simulation model is closely monitored. This may be a result of either a lack of sufficient grid blocks near the well bore or other misconceptions as to what constitutes effective permeability to a lateral well. The horizontal well aspects will be explored in more detail in chapters six and seven.

### 3.2 Two Phase Background and Theory

This simplified analysis incorporates the effects of pressure-saturation dependant variables such as relative permeability, formation volume factor and viscosity. Relative permeability is indirectly related to pressure through the saturation-pressure function. The equation for single-phase pseudosteady state flow of a vertical well in a rectangular drainage area is given by the following equation.:

$$q = \frac{0.007078 k_h h (\bar{P}_R - P_{wf})}{\mu_o B_o \left( \ln \frac{r_e}{r_w} - 0.738 \right)} \quad 3.1$$

$P_R$  is the average reservoir pressure. Craft and Hawkins showed that for pseudosteady state conditions, the volumetric average reservoir pressure occurs at about one half the distance to the external radius ( $0.42R$ ).<sup>6</sup> It is very desirable to easily compute oil flow analytically, above and below the bubble point, for use in a “quick-check” comparison with simulated results since much of pseudosteady state flow occurs below the bubble point. In order to represent saturated oil flow in analytic equations it is necessary to begin with the pressure integral concept. Figure 3.1 shows that for solution gas drive reservoirs, viscosity and formation volume factors are pressure dependent properties.<sup>4</sup>

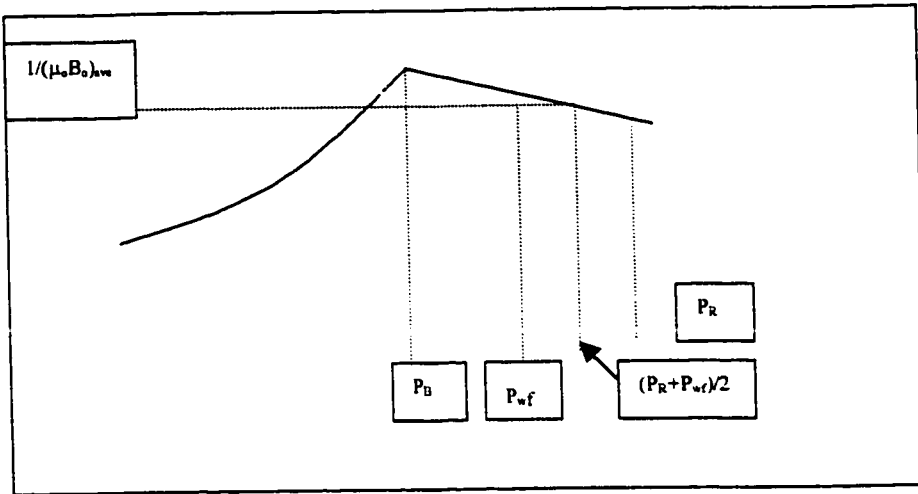


**Figure 3.1 Viscosity and Formation Volume Factor as a Function of Pressure**

For undersaturated conditions, the combined variation of viscosity and formation volume factor decreases approximately linearly with pressure. The above equation would then be modified above the bubble point as:

$$q = \frac{0.007078 k_h h}{\left( \ln \frac{r_e}{r_w} - 0.738 \right)} \int \frac{dp}{\mu_o B_o} \quad 3.2$$

The integral is evaluated from  $P_{wf}$  to  $P_e$  (the pressure at the external boundary). Since  $1/\mu_o B_o$  is a straight line, the area is a trapezoid (fig 3.1), so the integral can be represented by:

$$\int \frac{dp}{\mu_o B_o} = \frac{P_e - P_{wf}}{\left( \mu_o B_o \right)_{\bar{P}_R}} \quad 3.3$$

Where,  $\frac{1}{(\mu_o B_o)_{\bar{P}_R}}$  is the value at an average pressure  $P_R = (P_e + P_{wf})/2$ . The resulting inflow

equation, at average reservoir pressure for pseudosteady state conditions becomes:

$$q = \frac{0.007078 k_h h (\bar{P}_R - P_{wf})}{(\mu_o B_o)_{\bar{P}_R} \left( \ln \frac{r_e}{r_w} - 0.738 \right)} \quad 3.4$$

Golan<sup>4</sup> (166) and Muskat et al<sup>7</sup> note that below the bubble point, (i.e. saturated reservoir conditions) equation 3 would become (neglecting skin and turbulence effects):

$$q = \frac{0.007078 h k_h}{\left( \ln \frac{r_e}{r_w} - 0.738 \right)} \int \frac{k_{ro}}{\mu_o B_o} dp \quad 3.5$$

The integral is evaluated from  $P_{wf}$  to  $P_{Rave}$ .

As noted in the literature, solving the pressure integral is not a trivial procedure.<sup>4</sup> Evinger and Muskat<sup>7</sup> (1942) and later Vogel<sup>8</sup> et al noted however that the pressure function could be accurately represented versus pressure by a straight line ranging from  $k_{ro}/\mu_o B_o$  at reservoir pressure (up to the bubble point) to the origin. (Fig 3.2) However, if this is the case, there is no need to evaluate the integral this way. If the straight-line assumption is valid, the problem reduces to expressing the area under the trapezoid situation again, as in the above bubble point region. Appendix A shows the derivation and proof of the use of this approximation. It is shown in Appendix A that this method is equivalent to using the straight-line IPR relationship. Extensions to more complex curvature can be made.

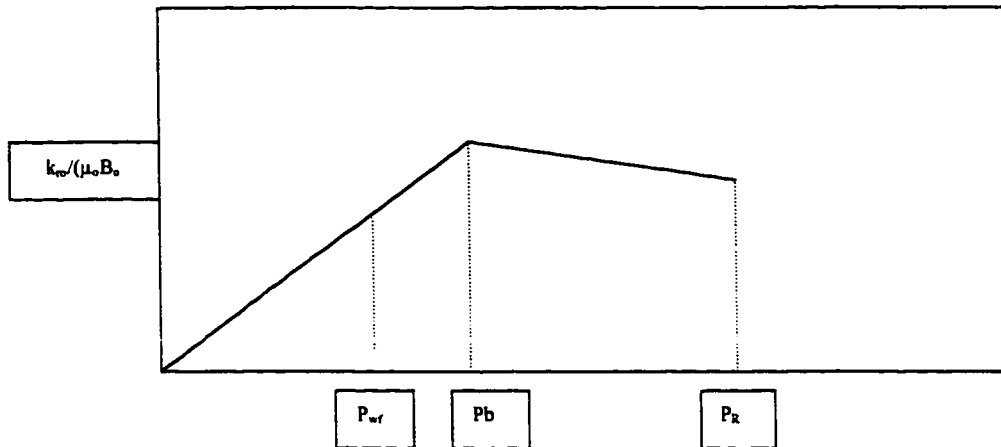


Figure 3.2 Mobility Factor as a Function of Pressure

It is then only necessary to evaluate the  $k_{ro}/\mu_o B_o$  at the average reservoir pressure at any given time. It will be shown that this method will give a good approximation. Two phase flow can then be described above and below the bubble point by equation 3.6 if one substitutes  $(k_{ro}/\mu_o B_o)_{ave}$  evaluated at average reservoir pressure.

$$q = \frac{0.007078 h k_h (\bar{P}_R - P_{wf})}{\left( \ln \frac{r_e}{r_w} - 0.738 \right)} \left[ \frac{k_{ro}}{(\mu_o B_o)} \right]_{S_o, \bar{P}_R} \quad 3.6$$

Therefore since one knows or assumes the mobility as a function of pressure and saturation that is input to simulators one can use the same function to analytically check against simulation output. Actually it seems to that  $k_{ro}$  should be computed at the average oil saturation at any given average pressure situation rather than at the average pressure as proposed in Muskat. Muskat never mentions this in his paper but the integral of  $k_{ro}$  should

not be from  $P_{wf}$  to  $P_e$  but from  $S_{oi}$  to  $S_{oe}$  since  $k_{ro}$  is only indirectly related to pressure through the saturation function.

In other words, the pressure integral in equation 3.5 can be approximated by  $(k_{ro}/B_o\mu_o)_{ave}$  where  $k_{ro}$  is taken as the relative permeability at the arithmetically averaged oil saturation across the simulation grid and  $B_o\mu_o$  is the value at average reservoir pressure over the entire simulation grid at any given time step as long as the straight line assumption is valid. Since a relative permeability function that is a function of fluid saturation is input to the simulator, knowing the average grid-block saturation yields the average relative permeability across the model to use in the equation for calculation purposes.

The averaging process is desirable because it is so easy to evaluate tabular simulation output in a spreadsheet. Typical simulators like Boastvhs provide tabular output that can be imported to spreadsheets and averaged over gridblocks in a single operation.<sup>5</sup> Then the data can be input into the analytical equations and compared to simulator calculations. The main question then is whether or not the straight-line assumption is really valid. As a test, equation 3.6 was tested against the simulation output of some real field examples of relative permeability, viscosity and formation volume factor values.

### 3.3 Comparing Analytical Solutions with Two Phase Simulations

An 11 by 13 block model (Table 1) was tested using real field data as shown in figures 3.3-3.6. Figure 3.5 shows  $(k_{ro}/\mu_o B_o)$  as a function of average reservoir pressure where  $k_{ro}$  is

derived from the simulation relative permeability function (defined in terms of fluid saturation) at the grid averaged oil saturation indicated in figure 3.6. Appendix B provides the reader with the algorithm to compute PVT properties.

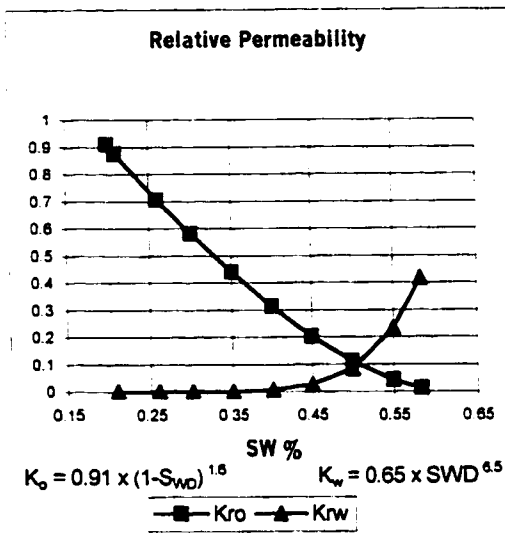


Figure 3.3 Relative Permeability versus Phase Saturation

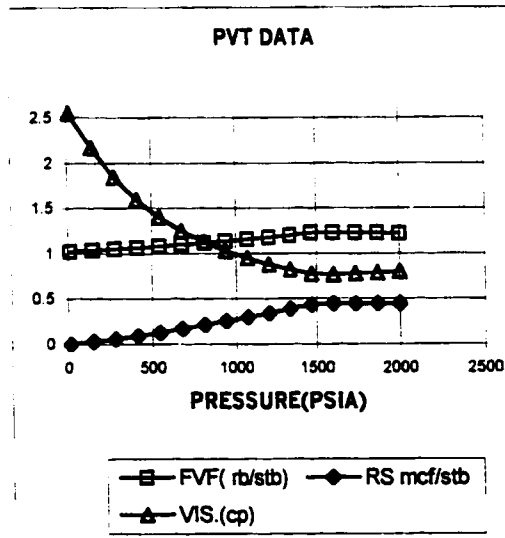


Figure 3.4 PVT Data as a Function of Pressure

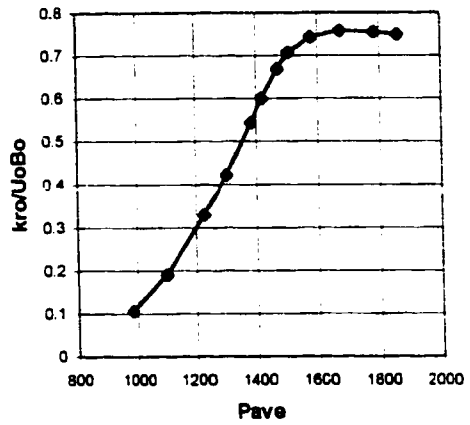


Figure 3.5 Relative Permeability-Viscosity-Formation Volume Factor Function versus Pressure

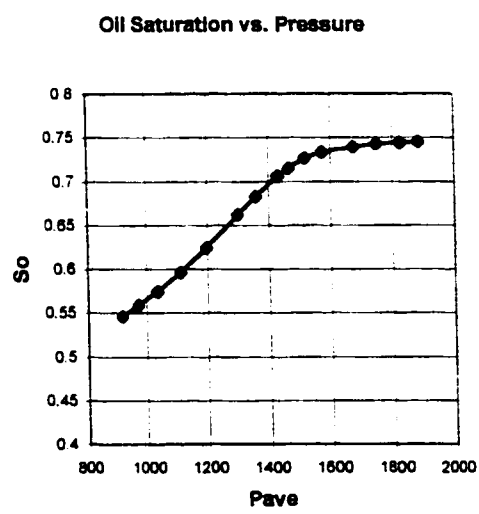


Figure 3.6 Oil Saturation versus Pressure

and Appendix C provides a good guide that has been developed for estimating, from oil-field data, all the necessary simulation inputs such as relative permeability, capillary pressure, etc. Tables 3.2 and 3.3 detail the typical simulation output from Boastvhs utilized to evaluate average saturation and pressures at any given time. Table 3.4 tabulates the actual simulation output values and the calculated analytical values. Figure 3.7 illustrates graphically the comparison of simulated oil rate vs. average reservoir pressure with analytical oil rates versus average pressure for the various models using the case of a vertical well. Average horizontal absolute permeability,  $k_h$  is 3.1 md in all cases although contrasts in directional permeability are varied in the simulation. Therefore using the values of  $(k_{vo}/\mu_o B_o)_{ave}$  at the grid-wide average reservoir pressure and saturation conditions seems to match actual simulated results very well thus confirming that the straight line assumption is reasonably a good approximation.

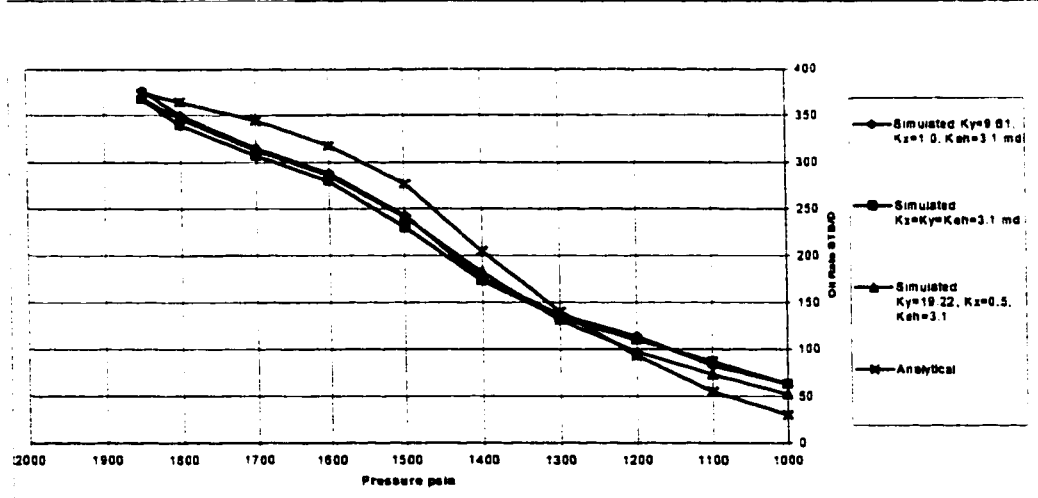
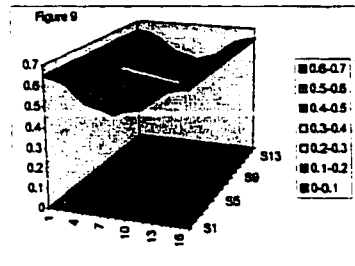


Figure 3.7 Rate versus Pressure for Vertical Well Case of Permeability Anisotropy but Constant Geometric Average Permeability

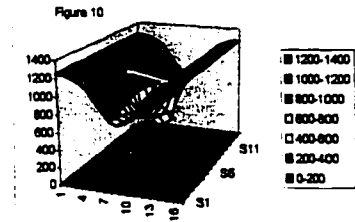
**Table 3.2 and 3.3 Saturation and Pressure Profiles –Tabular Output with Graphics from import to Excel Spreadsheet**

day 11188

|       |       | average S <sub>oi</sub> |       | 0.574722 |
|-------|-------|-------------------------|-------|----------|
| 0.545 | 0.545 | 0.545                   | 0.545 | 0.545    |
| 0.54  | 0.54  | 0.54                    | 0.54  | 0.54     |
| 0.527 | 0.527 | 0.527                   | 0.527 | 0.527    |
| 0.805 | 0.805 | 0.805                   | 0.804 | 0.805    |
| 0.585 | 0.585 | 0.585                   | 0.585 | 0.585    |
| 0.535 | 0.535 | 0.535                   | 0.535 | 0.535    |
| 0.523 | 0.523 | 0.523                   | 0.523 | 0.523    |
| 0.513 | 0.513 | 0.512                   | 0.511 | 0.513    |
| 0.495 | 0.494 | 0.493                   | 0.492 | 0.495    |
| 0.513 | 0.512 | 0.512                   | 0.511 | 0.513    |
| 0.523 | 0.523 | 0.524                   | 0.523 | 0.523    |
| 0.526 | 0.526 | 0.526                   | 0.526 | 0.526    |
| 0.567 | 0.566 | 0.565                   | 0.565 | 0.567    |
| 0.607 | 0.605 | 0.605                   | 0.604 | 0.607    |
| 0.527 | 0.527 | 0.527                   | 0.527 | 0.527    |
| 0.64  | 0.64  | 0.64                    | 0.64  | 0.64     |
| 0.645 | 0.645 | 0.645                   | 0.645 | 0.645    |



|      |      | Pressure |      | 1033.408 |
|------|------|----------|------|----------|
| 1255 | 1255 | 1255     | 1255 | 1255     |
| 1244 | 1244 | 1244     | 1244 | 1244     |
| 1233 | 1233 | 1233     | 1233 | 1233     |
| 1181 | 1181 | 1180     | 1179 | 1178     |
| 1118 | 1117 | 1115     | 1113 | 1110     |
| 998  | 994  | 987      | 977  | 964      |
| 678  | 672  | 654      | 623  | 594      |
| 791  | 782  | 763      | 734  | 694      |
| 758  | 750  | 731      | 702  | 682      |
| 761  | 762  | 763      | 734  | 694      |
| 978  | 970  | 954      | 930  | 904      |
| 994  | 984  | 987      | 977  | 964      |
| 1118 | 1117 | 1115     | 1113 | 1111     |
| 1181 | 1181 | 1180     | 1179 | 1178     |
| 1223 | 1223 | 1223     | 1223 | 1223     |
| 1244 | 1244 | 1244     | 1244 | 1244     |
| 1255 | 1255 | 1255     | 1255 | 1255     |



| rw = 0.5                               |      |          |         |      |          |         |      |          |         |           |                  |      |        |        |      |      |
|--|------|----------|---------|------|----------|---------|------|----------|---------|-----------|------------------|------|--------|--------|------|------|
| Same Ke but different distribution     |      |          |         |      |          |         |      |          |         |           |                  |      |        |        |      |      |
| vertcon=Ky=9.61, Kx=1, satby Ky=Ky=3.1 |      |          |         |      |          |         |      |          |         |           |                  |      |        |        |      |      |
| Day                                    | Rate | Pressure | cum oil | Rate | Pressure | cum oil | Rate | Pressure | vertcon | Ky=Ky=3.1 | analytical Rates | Muo  | Bo     | Kro    | So   |      |
| 31                                     | 383  | 1882     | 22.1    | 376  | 1857     | 21.6    | 380  | 1880     | 22.9    | 377.18    | 378              | 377  | 0.7862 | 1.2231 | 0.72 | 0.75 |
| 62                                     | 333  | 1788     | 32.2    | 322  | 1768     | 31.2    | 338  | 1784     | 33.4    | 358.3     | 359              | 362  | 0.7803 | 1.2239 | 0.72 | 0.75 |
| 123                                    | 298  | 1634     | 51.3    | 288  | 1625     | 49.7    | 307  | 1676     | 52.9    | 328.88    | 327              | 336  | 0.7689 | 1.2258 | 0.71 | 0.75 |
| 214                                    | 273  | 1551     | 77.1    | 261  | 1550     | 74.5    | 282  | 1580     | 79.6    | 304.26    | 304              | 311  | 0.7635 | 1.2268 | 0.7  | 0.74 |
| 395                                    | 243  | 1499     | 123.5   | 229  | 1500     | 118.8   | 248  | 1508     | 127.1   | 277.98    | 278              | 280  | 0.78   | 1.2273 | 0.68 | 0.73 |
| 576                                    | 219  | 1468     | 185     | 208  | 1467     | 157.6   | 221  | 1473     | 169.4   | 256.44    | 257              | 258  | 0.77   | 1.2216 | 0.63 | 0.72 |
| 942                                    | 179  | 1418     | 238.7   | 185  | 1420     | 228.7   | 198  | 1420     | 241.8   | 221.48    | 222              | 222  | 0.7877 | 1.2138 | 0.57 | 0.7  |
| 1308                                   | 166  | 1379     | 300.7   | 163  | 1384     | 291.8   | 170  | 1382     | 305.3   | 194.15    | 195              | 195  | 0.8031 | 1.2068 | 0.53 | 0.69 |
| 2304                                   | 137  | 1293     | 453.9   | 136  | 1303     | 438.7   | 131  | 1300     | 449.9   | 138.98    | 141              | 140  | 0.8361 | 1.1919 | 0.42 | 0.65 |
| 3400                                   | 121  | 1225     | 595.5   | 119  | 1232     | 578     | 104  | 1228     | 578.4   | 102.13    | 103              | 102  | 0.8722 | 1.1792 | 0.34 | 0.62 |
| 5688                                   | 86   | 1097     | 656.5   | 90   | 1108     | 843.7   | 76   | 1102     | 811.7   | 51.587    | 52.3             | 51.9 | 0.9088 | 1.1578 | 0.21 | 0.57 |
| 8892                                   | 59   | 986      | 1043    | 67   | 1013     | 1046    | 47   | 985      | 983.9   | 25.3      | 26.2             | 25.3 | 1.15   | 1.1112 | 0.14 | 0.53 |

**Table 3.3 Vertical Comparison Output**

### **3.4 Evaluation of Effective Horizontal Permeability Assumptions - Vertical Well Case**

Notice also that three cases of directional permeability distributions were simulated and compared in simulation illustrated in Figure 3.7. Figure 3.7 shows that they each match each other very well no matter what the contrast in  $k_x$  and  $k_y$  as long as the geometric average of  $k_x$  and  $k_y$  is constant. Overall the vertical simulations match both one another and the analytical results in both isotropic and anisotropic media. It is significant that the match is good for both isotropic and anisotropic media. This also indicates that the common assumption that the geometric mean of permeability ( $k_b = \sqrt{k_x k_y}$ ) is a valid assumption for a vertical well and that the simulator accurately describes this relationship.

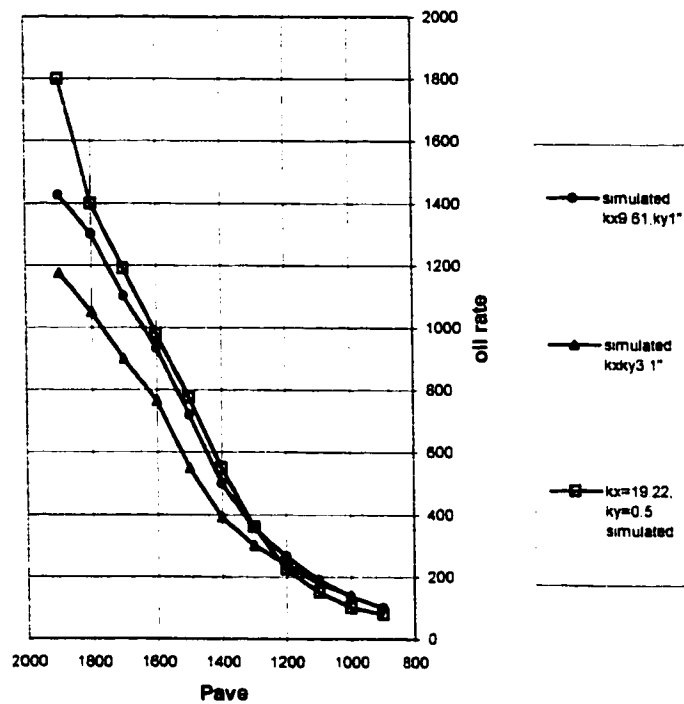
### **3.5 Evaluation of Effective Horizontal Permeability Assumptions - Horizontal Well Case**

Figure 3.8 however shows that the simulated results of horizontal wells do not match each other for anisotropic media even when the geometric mean is the same. It will be shown through simulation experiments, that published analytical solutions to horizontal well inflow at least track simulated results in cases of isotropic permeability (again above and below the bubble point) but they do not match simulated horizontal results as well in cases of horizontally anisotropic permeability (figures 3.9,3.10,3.11). This phenomenon may result from 1) the difficulty in properly modeling a horizontal well in a simple simulator like Boast and 2) the fact that if the well length is not small in comparison to the size of the reservoir, the geometric mean will not approximate the actual effective horizontal permeability. For

instance if the reservoir is semi-infinite, no other wells compete for drainage area, the reservoir is thick, and the well length is short compared to the reservoir dimensions then the geometric average of permeability may work well. The horizontal well would then appear small compared to the reservoir as a whole and the geometric average would give proper results. This is almost never the case in reality. The discrepancy in flow predictions seems to be related to well length, degree of penetration, permeability contrast and distance to the reservoir boundaries. If the simulator allows a large number of grid blocks then grouping smaller blocks near the horizontal wellbore may minimize problem. However in a simulator with grid block limitations such as Boastvhs, it does not appear that the horizontal well can be accurately modeled in cases of direction permeability anisotropy when the wellbore is long compared to the reservoir dimensions. This will be dealt with in more detail in chapters seven and eight.

Nevertheless equation 3.6 provides a framework to calibrate simulator parameters and resulting output for a test of “reasonableness”. This equation can be extended to use in horizontal wells, as will be demonstrated in chapter 6 and 7.

**Simulated Rates For Various Permeability Contrasts but Constant Geometric Means**



**Figure 3.8 Comparison of Simulated Rate versus Pressure for Cases of Anisotropic Horizontal Permeability but Constant Geometric Mean Permeability**

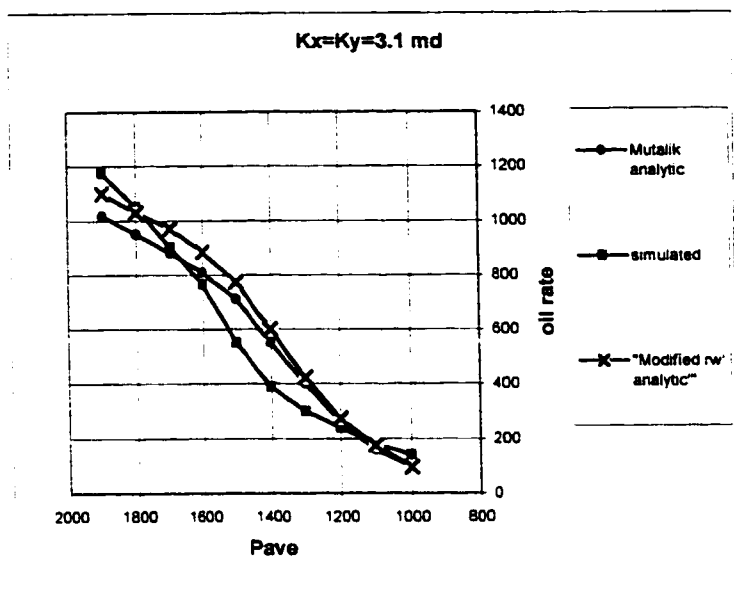


Figure 3.9 Comparison of Simulated with Analytical for Isotopic Permeability

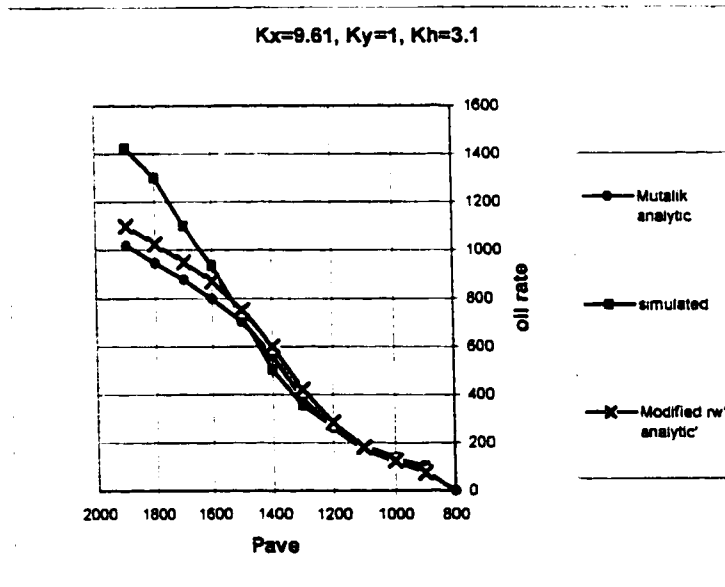
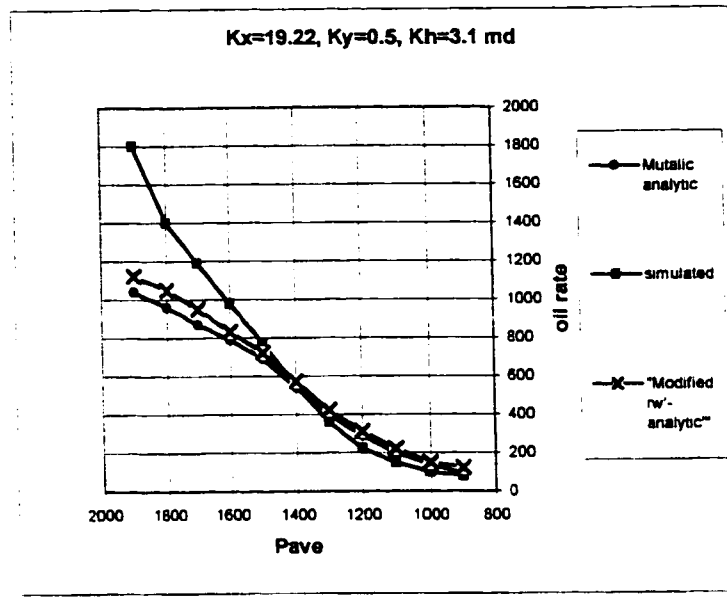


Figure 3.10 Comparison of Simulated and Analytical with Anisotropic Permeability



**Figure 3.1 Comparison of Simulated and Analytical with Anisotropic Permeability**

## CHAPTER FOUR

### Decline Curve Theory

#### 4.1 Depletion Rate Decline (Pseudosteady State-PSS)

Pressure decreases according to the following relation in the case of constant rate depletion for undersaturated reservoirs with no flow boundaries:

$$P_R = P_i - \frac{q_p B_o}{A h \phi c_t} t \quad 4.1$$

In cases of constant pressure depletion, the expression for undersaturated reservoir rate decline is expressed as:

$$q_o(t) = \frac{k h [p_e(t) - p_{wf}]}{141.2 \mu_o B_o [\ln(r_e / r_{wa})]} \quad 4.2$$

The material balance equation relates the cumulative production  $N_p$  to the pressure  $P_e(t)$  at the external boundary of the reservoir. It expresses the cumulative production as a function of the apparent total compressibility of the system  $c_{ta}$ , the hydrocarbon pore volume  $V_p(1-S_w)$ , and the pressure drop in the reservoir  $p_i - p_e(t)$ . Where  $c_{ta}$  is the apparent total compressibility of the system which varies with  $p_e(t)$

$$N_p = V_p (1 - S_w) c_{ta} [p_i - p_e(t)] \quad 4.3$$

More complicated expressions can be constructed for saturated oil reservoirs. Tracy<sup>9</sup>(1955) and Turner<sup>10</sup>(1944).

Rate time behavior during depletion has been treated rigorously by mathematicians who solve the flow equations analytically for particular boundary conditions of no flow at the outer boundary and constant pressure at the inner boundary (wellbore). Fetkovich<sup>3</sup> (1980) presented a useful form of the solution of Tsarevich and Kuranov<sup>11</sup> (1966) to prepare type curves of dimensionless rate versus dimensionless time (Figure 4.1). Observation of the type curves shows that transition from the infinite acting transient to the PSS is instantaneous at  $t_{ps}$  at least for the radial case. Irregular outer geometry will affect the infinite acting period and may accelerate true pseudo-steady state production. In contrast to Fetkovich's purely radial form, this research will show how to construct type curves to illustrate this irregular boundary phenomenon for various reservoir shape factors and well positions within the reservoir.

Fetkovich<sup>3</sup> prepared a type curve of dimensionless rate versus dimensionless time using the following relationship (figure 4.1):

$$q_D = \frac{141.5 q \mu B}{kh(P_i - P_{wf})} \quad 4.4$$

$$t_D = \frac{0.00634 k t}{\phi \mu c_r r_{wa}^2} \quad 4.5$$

$$r_{wa} = r_w e^{-s}$$

4.6

$$r_{wa} = \frac{x_f}{2}$$

4.7

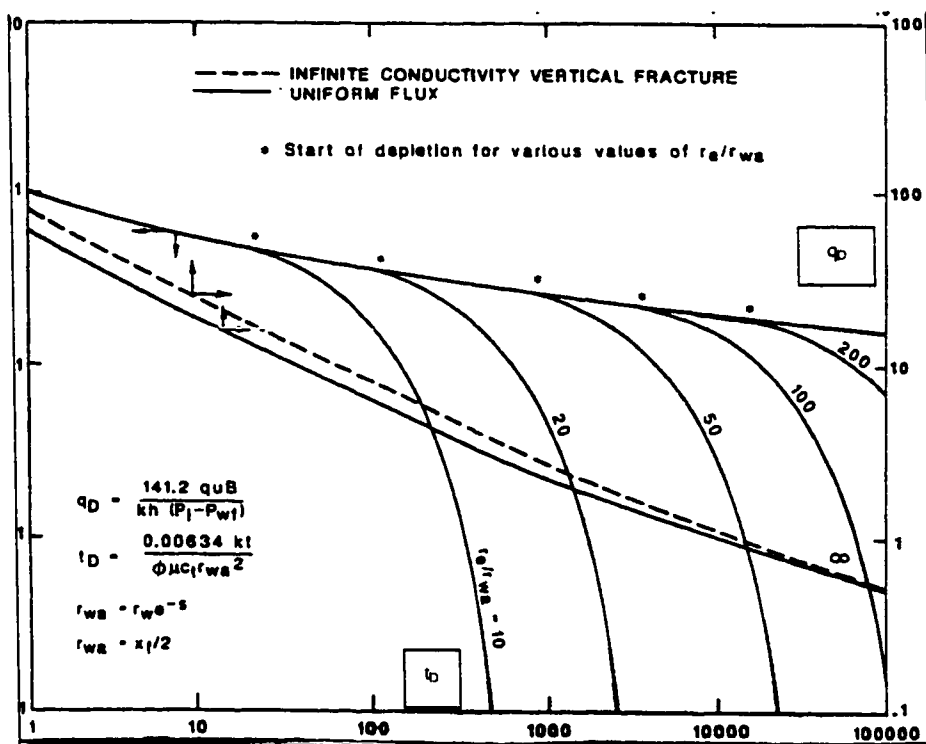


Figure 4.1 Dimensionless Rate versus Time<sup>3</sup>

An irregular outer geometry or off center well location can create a period of transition between transient and PSS production. This transition zone has not been the focus of much research but it may provide valuable information about the reservoir shape. Deviations from Fetkovich curves in the transition zone may indicate non-radial system geometry. The non-

radial relationships will be derived in chapter 5 and incorporated into a generalized decline curve system.

A general expression for PSS decline for constant pressure according to the analytical solution is:

$$q_D = A e^{-Bt_D} \quad 4.8$$

Where A and B are constants defined by the ratio  $r_e/r_{wa}$ . Fetkovich developed expressions for A and B which reflect different ratios of  $r_e/r_{wa}$ . The higher the ratio the larger is the time to pseudosteady state  $t_{Dps}$ .

$$A = \frac{I}{\ln(r_e / r_{wa}) - 0.5} \quad 4.9$$

$$B = \frac{2A}{(r_e / r_{wa})^2 - I} \quad 4.10$$

The expressions for A and B reflect the observation that different ratios of  $r_e/r_{wa}$  give different depletion stems. The higher the ratio of  $r_e/r_{wa}$ , the larger the time to pseudosteady state  $t_{Dps}$  and the lower is  $q_D$  at the start of depletion.

Exponential decline, according to the analytical solution, is substantiated by many field observations. The primary observation in Arp's<sup>2</sup> work (1945) suggested that three types of decline could express all conventional depletion declines: hyperbolic, exponential and

harmonic. The effective decline rate  $D_e$ , or  $D_{ei}$  at initial conditions, for the three types of production-decline curves is related to the nominal decline rate  $D$  or  $D_i$  for initial conditions as follows.

$$D_e = 1 - e^{-D} \quad 4.11$$

The nominal decline rate is the negative slope of the natural log of  $q$  vs. time plot. The effective decline  $D_e$  is a stepwise function whereas  $D$  is a continuous function.

For hyperbolic decline

$$D_{ei} = 1 - (1 + bD_i)^{-1/b} \quad 4.12$$

and for harmonic:

$$D_{ei} = \frac{D_i}{1 - D_i} \quad 4.13$$

Arps<sup>2</sup> classifies three types of decline:

A.

Hyperbolic decline where the decline  $D$  is proportional to a fractional power  $b$  of the production rate.

$$D = \frac{\frac{dq}{dt}}{q} = \left( \frac{D_i}{q_i^b} \right) q^b \quad 4.14$$

which upon integration becomes:

$$q_o = \frac{q_{oi}}{(1 + bDt)^{\frac{1}{b}}} \quad 4.15$$

Where  $q_{oi}$  = initial oil rate neglecting transient decline  
 $q_o$  = rate at time  $t$   
 $D$  = decline constant (Nominal decline rate = negative slope of  $\ln q$  vs. time)  
 $b$  = decline exponent  
Subscript i denotes initial conditions.

On second integration the rate cumulative expression becomes:

$$N_p = \frac{q_i^b}{(1-b)D_i} \left( q_i^{(1-b)} - q^{(1-b)} \right) \quad 4.16$$

and the time to abandonment becomes:

$$t_a = \frac{\left( \frac{q_i}{q_a} \right)^b - 1}{b D_i} \quad 4.17$$

and eliminating  $D_i$ :

$$t_a = \frac{\left[ \left( \frac{q_i}{q_a} \right)^b - 1 \right]}{b \left[ \frac{q_i^b}{(1-b) N_{pa}} \left( q_i^{1-b} - q^{1-b} \right) \right]} \quad 4.18$$

## B. Exponential $b=0$

Exponential decline exhibits a straight line on semi log plot of rate versus time. It is also called

constant percentage decline since it is characterized by the fact that the drop in production rate per unit of time is proportional to the production rate.

Constant percentage decline (exponential) the nominal decline rate D is constant of

$$D = -\frac{dq / dt}{q} \quad 4.19$$

which after integration yields:

$$q_o = q_{oi} e^{-Dt} \quad 4.20$$

After a second integration the rate-cumulative expression for cumulative production at any time t is:

$$N_p = \frac{q_i - q}{D} \quad 4.21$$

And the remaining life to abandonment time may be obtained by:

$$t_a = \frac{\ln(\frac{q_i}{q_a})}{D} \quad 4.22$$

or after eliminating D:

$$t_a = \frac{N_{pa}}{q_i} \left( \frac{\frac{q_i}{q_a} \ln \frac{q_i}{q_a}}{\frac{q_i}{q_a} - 1} \right) \quad 4.23$$

### C. Harmonic b=1

For harmonic decline where  $b= 1$  the nominal decline rate D is proportional to the production rate or:

$$D = \frac{dq}{dt} = \frac{D_i}{q_i} q \quad 4.24$$

or after integration:

$$q_o = q_{oi} \frac{1}{(1 + Dt)} \quad 4.25$$

After a second integration the rate cumulative relationship becomes:

$$N_p = \frac{q_i}{D_i} \ln \frac{q_i}{q} \quad 4.26$$

And time to abandonment  $t_a$  is:

$$t_a = \frac{N_{pa}}{q_i} \left( \frac{\frac{q_i}{q_a} - 1}{\ln \frac{q_i}{q_a}} \right) \quad 4.27$$

## 4.2 Solution Gas Drive Meaning

Arps<sup>2</sup> did not give physical reasons for the three observed declines but he indicated that exponential  $b=0$  was common and that  $b$  usually ranges from 0 to 0.5 in solution gas reservoirs. It has been observed that the  $b$  value in typical solution gas drive reservoirs

averages about 0.3 while a 0.5 value indicates water drive or gravity drainage. Exponential is the most rapid decline observed and thus exponential is used for the most conservative estimates for reserves. Recall that exponential decline implies that the total compressibility of the rock and fluid is the only mechanism providing pressure support for the system. Departure from exponential decline in solution gas reservoirs should then be useful in estimating the mobility function shown if figure 3.1. This will be explored further in chapters 5 and 6.

### 4.3 Physical Meaning to Decline Analysis

Fetkovich<sup>3</sup> expressed Arp's<sup>2</sup> exponential decline equation in terms of reservoir variables and thus gave physical meaning to Arp's observations. He obtained the following expressions for the Arps empirical constants  $q_{oi}$  and D.

$$q_{oi} = \frac{kh(p_i - p_{wf})}{141.2 \mu_o B_o [\ln(r_e / r_{wa}) - 0.5]} \quad 4.28$$

$$D = \frac{2(0.000264)k}{\phi \mu_o c_n (r_e^2 - r_{wa}^2) [\ln(r_e / r_{wa}) - 0.5]} \quad 4.29$$

These expressions can be used to forecast rate decline if production data are not available to identify the actual decline trend.

Since the transition from infinite to PSS is practically instantaneous in the radial system, a natural extension of the decline type curve is to combine transient and depletion relations onto a single graph. Fetkovich did this and used the unit variable  $t_{Dd}$  and  $q_{Dd}$  to define the type curves. (Figure 4.2 Combined Fetkovich-Arps analysis)

Hyperbolic decline ( $1 < b > 0$ ) results from natural and artificial driving energies that slow down the pressure depletion compared with the depletion caused by pure expansion of a slightly compressible oil. Hyperbolic decline is exhibited if the reservoir drive mechanism is solution gas drive, gas cap expansion, or water drive. It is also exhibited when the natural drive mechanism is supplemented by water or gas injection. The presence of these driving energies implies that total compressibility increases and recovery is improved compared with the pure oil expansion drive mechanism.

When plotted on semi-log paper (rate vs. time) data showing hyperbolic declines tend to curve upward while exponential decline is a straight line of unit slope. The hyperbolic upward curvature is illustrated on figures 2.1 and 2.3.

$$D = -\frac{\ln[q_o(t^*)/q_{oi}]}{t^*} = -2.302 \frac{\log[q_o(t^*)/q_{oi}]}{t^*} \quad 4.30$$

Where  $t^*$ ,  $q_o(t^*)$  is any rate-time point on the semi-log straight line and an intercept of:

$$q_{oi} = q_o(t=0).$$

### 4.3.1 Derivation of Fetkovich Type Decline Curves

Arps equation for hyperbolic decline can also be expressed in terms of dimensionless variables and the coefficients of the analytical decline equation (4.4) to yield:

$$q_{Dd} = \frac{A}{(1 + bBt_D)^{\frac{1}{b}}} \quad 4.31$$

To plot as a single type curve that exhibits exponential harmonic and hyperbolic declines, Fetkovich defined new dimensionless unit variable  $q_{Dd}$  and  $t_{Dd}$  where:

$$q_{Dd} = \frac{q_o}{q_{oi}} = \frac{q_D}{A} \quad 4.32$$

and

$$t_{Dd} = Dt = B t_D \quad 4.33$$

Where A and B have been previously defined.

In terms of the unit variable for exponential decline:

$$q_{Dd} = e^{-r_{Dd}} \quad 4.34$$

and for hyperbolic decline:

$$q_{Dd} = \frac{1}{(1 + bt_{Dd})^{1/b}} \quad 4.35$$

Fetkovich plotted these equations as type curves with unit dimensionless variable for  $b=0$  up to  $b=1$ . (See Figure 4.2) Since the transition from infinite acting to PSS is practically instantaneous in a radial system, a natural extension is to combine transient with PSS onto a single graph.

When the unit variable  $q_{Dd}=q_D/A$  and  $t_{Dd}=Bt_D$  are expressed with previously defined A and B definitions then the units are related to the ratio  $r_e/r_{wa}$  by:

$$q_{Dd} = [\ln(r_e/r_{wa}) - 0.5] q_D = \left[ \ln\left(\frac{r_e}{r_{wa}}\right) - 0.5 \right] \frac{141.2 \mu B q(t)}{kh(p_i - p_{wf})} \quad 4.36$$

and

$$t_{Dd} = \frac{2}{[(r_e/r_{wa})^2 - 1][\ln(r_e/r_{wa}) - 0.5]} t_D = \frac{\frac{0.00634 k t}{\phi \mu c_i r_{wa}^2}}{0.5 \left[ \left( \frac{r_e}{r_{wa}} \right)^2 - 1 \right] \left[ \ln\left(\frac{r_e}{r_{wa}}\right) - 0.5 \right]} \quad 4.37$$

Combining these expressions with those of Arps for the depletion period resulted in a general type curve for transient and depletion periods as in Fig 4.2.

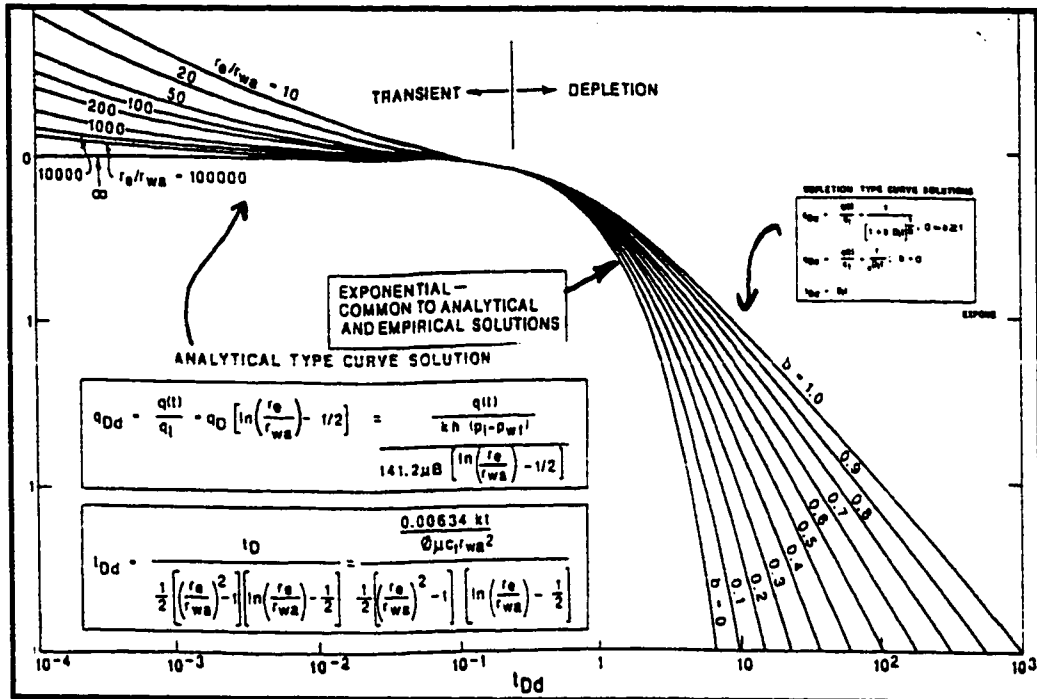


Figure 4.2 Generalized Arps-Fetkovich Dimensionless Decline Curve<sup>3</sup>

#### 4.3.2 Reservoir Parameters From Type Curves

Type curve match points can then be used to calculate permeability, skin and drainage radius which yields initial oil in place. Using  $r_e / r_{w\alpha}$  from the match, the transmissibility is determined from the match point by:

$$q_D = \frac{141.2 \mu B q(t)}{k h (P_i - P_{wf})} \quad 4.38$$

$$q_{Dd} = q_D \left[ \ln \frac{r_e}{r_w} - \frac{1}{2} \right] \quad 4.39$$

and combining yields:

$$kh = \frac{1412 \mu B}{(P_i - P_{wf})} \left( \ln \frac{r_e}{r_w} - \frac{1}{2} \right) \frac{q_r}{q_{dD}}_{match} \quad 4.40$$

While the apparent wellbore radius is calculated from the following expressions:

$$t_D = \frac{0.00634 k t}{\phi \mu c, r_w^2} \quad 4.41$$

$$t_{Dd} = \frac{t_D}{\frac{1}{2} \left[ \left( \frac{r_e}{r_w} \right)^2 - 1 \right] \ln \left( \frac{r_e}{r_w} \right) - \frac{1}{2}} \quad 4.42$$

and combining to yield:

$$r_{wa}^2 = \frac{0.00634 k}{\phi \mu c, \frac{1}{2} \left[ \left( \frac{r_e}{r_{wa}} \right)^2 - 1 \right] \ln \left( \frac{r_e}{r_{wa}} \right) - \frac{1}{2}} \left( \frac{t \text{ (days)}}{t_{dD}} \right)_{match} \quad 4.43$$

from which  $s = -\ln(r_{wa}/r_w)$  and drainage radius is calculated as :

$$r_e = r_{wa} \left( \frac{r_e}{r_{wa}} \right)_{match} \quad 4.44$$

By knowing the drainage radius then N reserves in place can be calculated from:

$$N(\text{well}) = \frac{\pi r_e^2 h \phi (1 - S_w)}{5.615 B_o} \quad 4.45$$

An example of this calculation is shown in Section 5.4.1.

Thus Fetkovich<sup>3</sup> gave physical meaning to decline curves in radial systems and showed that they could be combined with Arps empirical relationships in the pseudosteady state region. Methods to use the deviation from exponential decline to gain information about the fluid properties, relative permeability and pore volume are explored as part of Appendix C. These concepts will be extended to non-radial geometry and horizontal well analysis in chapters 5 and 6. This should further enhance the decline curve matching process in non-radial reservoirs.

According to Mathews<sup>21</sup>, during pseudo steady state, the drainage volumes in a bounded reservoir are proportional to the rates of withdrawal from each drainage volume. Therefore the ratio  $q_i/N_{pi}$  will be identical for each well and, thus, the sum of the results from each well should give the same results as from analyzing the total lease or field production rate. Field experience often demonstrates how rapidly readjustments in drainage volumes can take place by changes in the production rate or depletion by offset wells. This of course assumes that the field is not stratified or separated by a fault or drastic anisotropy. The effect compartmentalization by permeability or stratification would be interesting to experiment with in the future.

It is not well known that the Fetkovich Type Curves are based on a strictly radial system operating above the bubble point with the well centrally located. It is obviously desirable to derive a more general case that would apply to any particular reservoir drainage shape such as rectangular, triangular, and reservoirs in which the well is displaced from the reservoir center. It would also be desirable to modify the curves for cases below the bubble point and extract information from that deviation from the strictly exponential case. In the radial case, the transition from infinite acting to pseudosteady state is almost instantaneous.

However in a non-radial reservoir the transition from infinite to pseudosteady state is prolonged. Significant error in type curve matching may result from using the radial form. In low permeability formations rapidly declining transient production can be confused with depletion and an attempt to fit the transient data to the depletion portion of the type curve will result in Arps "b" values that are unrealistically high. It is therefore desirable to properly define the full shape of the type curve over the transient and depletion period properly apply the techniques and analysis.

This method, shown in this section and fully derived in Appendix E utilizes shape factors derived for these various conditions such as shown in Earlouger's Table C-1 *in Advances in Well Testing*<sup>22</sup>. Application of these factors to the Fetkovich system is neither direct nor straightforward. A system was derived that will incorporate all reservoir shapes, positions and later will be applied to vertically fractured and horizontal wells using an equivalent well

bore radius concept. The complete derivation is shown in Appendix E and applications to actual field production data is detailed in Chapter 5.

## CHAPTER FIVE

### Decline Curve Construction, Analysis and Use

#### 5.1 – Introduction

In chapters one and four it was shown that Fetkovich<sup>3</sup> combined the transient analytical solution with the pseudo-steady state (boundary-dominated flow) to develop a single type curve system. In that work, Fetkovich developed the dimensionless terms,  $q_{\text{AD}}$ , the dimensionless flow rate and  $t_{\text{AD}}$  the dimensionless time based on the initial flow rate and initial decline. Fetkovich developed his decline curves for radial geometry only. That derivation will be extended to a more general geometry and well position application. Reservoir parameters such as permeability, pore volume, skin etc were then extracted from the transient portion. Fetkovich indicated that reservoir parameters such as pore volume should not be computed until the onset of depletion when an approximation of the Arps<sup>1</sup> decline exponent  $b$  could be made. Reservoir and fluid properties can affect the value of the decline exponent  $b$ . Solution gas increases the value of  $b$  so that the production tail is extended in time. Fractured reservoirs with matrix support also show extended tails.

#### 5.2 Theoretical Background for Dimensionless Solutions

In 1949, Van Everdingen and Hurst<sup>17</sup>, first developed the equations used to generate the dimensionless pressure and time values that were later used in decline curves as shown in

subsequent section 5.3. These were later extended by Fetkovich<sup>3</sup> to define dimensionless decline parameters. The theory began with the diffusivity equation, the application of certain boundary equations and the application of the Laplace transformation solution. The basic diffusivity equation is:

$$\frac{1}{r} \frac{\partial}{\partial r} \left( r \frac{\partial P}{\partial r} \right) = \frac{\phi \mu c}{k} \frac{\partial P}{\partial t} \quad 5.1$$

The treatment of the diffusivity equation had been essentially the application of the Fourier-Bessel series. VanEverdingen and Hurst<sup>17,18</sup> presented a new approach to the solution in the form of the Laplace transformation since it was recognized that Laplace transformations offered an easier approach. The primary case of interest in decline analysis was the solution to the constant terminal pressure case solved for both the infinite and limited reservoirs. The constant terminal pressure and the constant terminal rate cases are not independent of one another, as knowing the operational form of one, the other can be determined. The initial condition is that at time zero the pressure at all points in the formation is constant and equal to unity. The inner boundary condition is that when the well or reservoir is opened, the pressure at the well or reservoir boundary,  $r_D=1$ , immediately drops to zero and remains zero for the duration of the production history.

### 5.2.1 Infinite Case

The outer boundary case for the infinite reservoir is as the reservoir reaches infinity, the pressure drop is zero. This is expressed as:

$$\lim(r_{eD} \rightarrow \infty) P_D = 0 \quad 5.2$$

VanEverdingen and Hurst<sup>17</sup> gave the solution in Laplace space:

$$\bar{Q}_D = \frac{K_1(\sqrt{p})}{z^{3/2} K_0(\sqrt{p})} \quad 5.3$$

where  $Q_D$  is the cumulative production,  $p$  is the Laplace transform variable and  $K_0$  and  $K_1$  are modified Bessel functions of the order zero and one. The application of Mellin's inversion formula to the equation yields the analytical expressions for  $Q_D$ :

$$Q_D = \frac{4}{\pi^2} \int_0^\infty \frac{1 - e^{-u^2}}{u^3 [J_0^2(u) + Y_0^2(u)]} du \quad 5.4$$

where  $J_0$  and  $Y_0$  are Besel functions of the first and second kind, respectively of order zero.

Since cumulative production  $Q_D$  is defined as :

$$Q_D = \int_0^t q_D(t) dt \quad 5.5$$

the Laplace equivalent of  $q_D$  is:

$$\bar{q}_D = \frac{K_1(\sqrt{p})}{z^{1/2} K_0(\sqrt{p})} \quad 5.6$$

This equation is inverted numerically by the Stehfest<sup>19</sup> method to obtain the variation of  $q_D$  with  $t_D$ . The corresponding analytical expression is:

$$q_D = \frac{4}{\pi^2} \int_0^\infty \frac{e^{-u^2 t_D}}{u[J_0^2(u) + Y_0^2(u)]} du \quad 5.7$$

The dimensionless flow rate  $q_D$  in field units is of course:

$$q_D = \frac{141.2 \mu B q(t)}{kh(P_i - P_{wf})} \quad 5.8$$

and the dimensionless time in field units is:

$$t_D = \frac{0.00634kr}{\phi \mu c_i r_w} \quad 5.9$$

After considerable work a program was used to invert these equations numerically using the Stehfest numerical Laplace algorithm. The results of this inversion yield values for infinite  $q_D$  versus  $t_D$  that are tabulated in the Appendix D and plotted on figure 5.1 as the infinite solutions. Notice the divergence of the solutions from the bounded solutions at increasing reservoir sizes (see limited reservoir theory next section.)

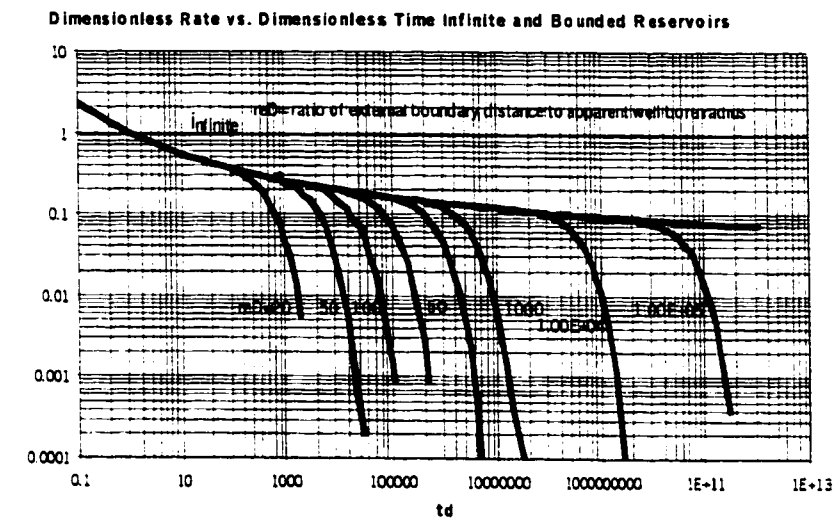


Figure 5.1 Dimensionless Rate versus Dimensionless Time

### 5.2.2 Solutions in Limited Reservoirs

The Fourier-Bessel type of expansions first developed the solutions for limited reservoirs of radial symmetry. VanEverdingen and Hurst<sup>17</sup> showed how the solutions could be obtained more easily using the Laplace transformation.

### 5.2.2.1 Conditions

The limited reservoir case is essentially the case of no fluid flow across the exterior boundary where:

$$\left(\frac{\partial P}{\partial r}\right)_{r=r_e} = 0 \quad 5.10$$

The VanEverdingen and Hursts solution to the cumulative production in Laplace space was given by:

$$Q_D = \frac{I_1(r_{eD}\sqrt{p})K_1(r_{eD}\sqrt{p}) - K_1(r_{eD}\sqrt{p})I_1\sqrt{p}}{p^{3/2}[K_1(r_{eD}\sqrt{p})I_o(\sqrt{p}) + I_1(r_{eD}\sqrt{p})K_o(\sqrt{p})]} \quad 5.11$$

In order to apply Mellin's inversion formula, the first consideration is the roots of the denominator of this equation, which indicates the poles. Since the modified Bessel functions for positive real arguments are either increasing or decreasing, the bracketed term in the denominator does not indicate any poles for positive real values for p. An investigation of the integration along the negative real axis both for the upper and lower portions reveals that the above equation is an even function for which the integration along the paths is zero. However poles are indicated along the negative real axis and these residuals help make up the solution for the constant terminal pressure case for the limited radial system. The analytical solution reduces to:

$$Q_D = \frac{r^2 - 1}{2} - 2 \sum_{a_1, a_2, \text{etc}}^{\infty} \left\{ \frac{e^{-a_n^2 p} J_1^2(a_n, r_{eD})}{a_n^2 [J_0^2(a_n) - J_1^2(a_n, r_{eD})]} \right\} \quad 5.12$$

As with the infinite solution, differentiation of cumulative production yields the Laplace and analytical solutions for dimensionless flow rate:

$$q_D = \frac{I_1(r_{eD}\sqrt{p})K_1(r_{eD}\sqrt{p}) - K_1(r_{eD}\sqrt{p})I_1(\sqrt{p})}{\sqrt{p}[K_1(r_{eD}\sqrt{p})I_o(\sqrt{p}) + I_1(r_{eD}\sqrt{p})K_o(\sqrt{p})]} \quad 5.13$$

$$q_D = 2 \sum_{a_1, a_2, \text{etc}}^{\infty} \left\{ \frac{e^{-a_n^2 r_{eD}} J_1^2(a_n, r_{eD})}{[J_0^2(a_n) - J_1^2(a_n, r_{eD})]} \right\} \quad 5.14$$

Where the values of  $a_1, a_2$  etc are determined as multiple roots of the equation :

$$[J_1(a_n r_{eD})Y_0(a_n) - Y_1(a_n r_{eD})J_0(a_n)] = 0 \quad 5.15$$

Once the roots are found the summation is done for the various roots until convergence is obtained. The above two expressions are used to generate the solution for the closed boundary case for various distances to the external boundary. These are also shown in Figure 5.1.

### **5.3 Generation of Fetkovich Type Curves.**

The method of generating the Fetkovich type curves is not a trivial process and is not widely known. The method must be understood and duplicated in order to extend the method to other shapes and well positions. The methodology of duplicating the Fetkovich curves is summarized as follows:

1. Generate the transient solutions for both infinite and closed reservoir systems by the methods of VanEverdingen and Hurst. Lee<sup>20</sup> in his Appendix C Table C-5 published the tabular solutions to the finite radial system with closed exterior boundary. Those values are also tabulated in this Appendix D along with all the solutions needed for finite and infinite cases generated with the Stehfest algorithm and extensions to the general cases. Figure 5.1 showed a graph of the dimensionless rate vs. dimensionless time for the infinite and bounded reservoirs using the tabular results of Lee and those generated from the program. Notice that the finite reservoir solutions for increasingly large reservoirs (i.e.  $r_{eD}$  increasing) converge into the infinite solution at increasing dimensionless time values and decreasing dimensionless rate values. The solutions for the infinite case are common to the bounded case where the outer boundary has not been sensed by the well. As the distance to the outer boundary increases, the time taken to reach the pseudo-steady state flow increases. This construction is specifically for radial cases. This research will extend those solutions to other reservoir shapes.

2. The next step is to convert those dimensionless rates and times from the table into the new Fetkovich type dimensionless decline parameters  $q_{Dd}$  and  $t_{Dd}$  by multiplying or dividing the dimensionless rate and time values in the table by the appropriate Fetkovich A and B values previously discussed in Chapter 4.

$$q_{Dd} = \frac{q_o}{q_{oi}} = \frac{q_D}{A} \quad 5.16$$

where A is given by:

$$A = \frac{1}{\left[ \ln \frac{r_e}{r_{wa}} - \frac{1}{2} \right]} = \frac{1}{c_1} \quad 5.17$$

and the dimensionless time scale

$$t_{Dd} = Dt = Bt_D \quad 5.18$$

where:

$$B = \frac{2A}{\left( \frac{r_e}{r_{wa}} \right)^2 - 1} = \frac{1}{0.5 \left[ \left( \frac{r_e}{r_{wa}} \right)^2 - 1 \right] \left[ \ln \frac{r_e}{r_{wa}} - 0.5 \right]} = \frac{2}{c_2 c_1} \quad 5.19$$

This was shown in chapter four. The dimensionless rate and time is thus expressed as:

$$q_{Dd} = [\ln(r_e/r_{wa}) - 0.5] q_D = \frac{\frac{q(t)}{kh(p_i - p_{wf})}}{141.2 \mu B \left[ \ln\left(\frac{r_e}{r_{wa}}\right) - 0.5 \right]} \quad 5.20$$

and

$$t_{Dd} = \frac{2}{[(r_e/r_{wa})^2 - 1][\ln(r_e/r_{wa}) - 0.5]} t_D = \frac{\frac{0.00634kt}{\phi \mu c_1 r_{wa}^2}}{0.5 \left[ \left( \frac{r_e}{r_{wa}} \right)^2 - 1 \left[ \ln\left(\frac{r_e}{r_{wa}}\right) - 0.5 \right] \right]} \quad 5.21$$

The tabular values used in these plots are shown in Appendix D.

3. Calculate the Arps empirical dimensionless time and rate from the expression:

$$q_o = \frac{q_{oi}}{(1 + bDt)^{\frac{1}{b}}} \quad 5.22$$

or defined in dimensionless decline terms:

$$q_{Dd} = \frac{q'}{q_i} = [1 + bDt]^{-1/b} \quad 5.23$$

The decline D is assumed as unity in the calculation of the terms. These values are also computed in a spreadsheet and tabulated in the appendix D for all b values greater than zero and up to one. The exponential decline with  $b=0$  is calculated as:

$$q_{dD} = e^{-tdD} \quad 5.24$$

The results are tabulated in the appendix D and plotted on figure 5.2.

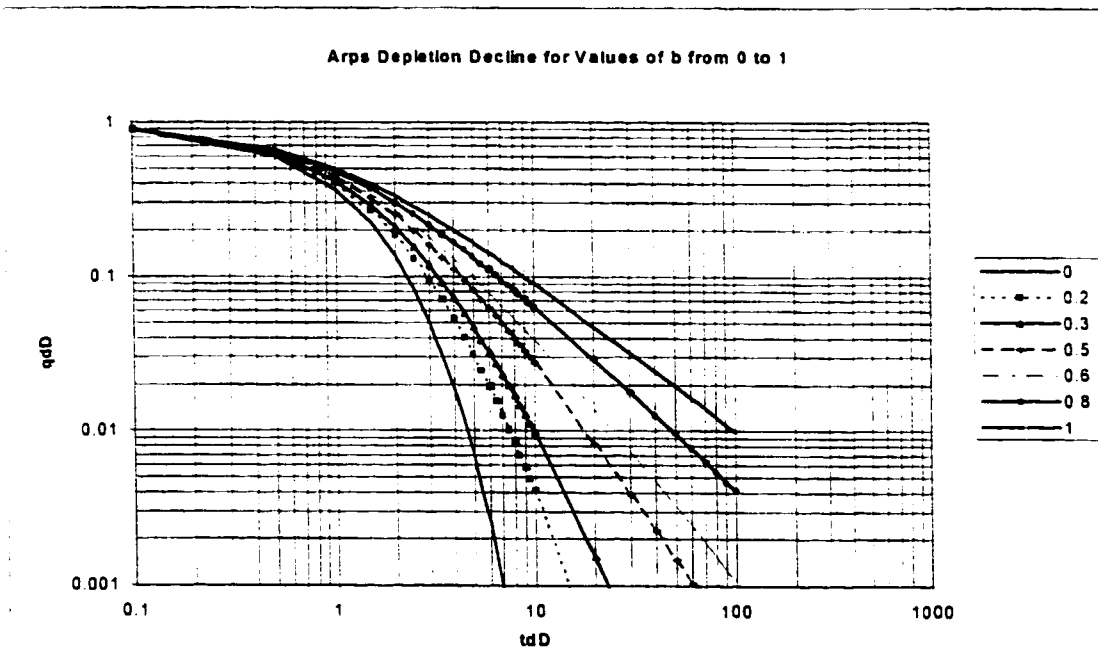


**Figure 5.2 Arps Depletion Decline for Values of b from 0 to 1**

As discussed before, Fetkovich discovered that the analytical dimensionless rate solution converges with the empirical dimensionless exponential rate solution for pseudo-steady state by defining the dimensionless rate scale.

Combining these expressions from steps one and two with those of Arps for the depletion period resulted in a general type curve for transient and depletion periods (exponential decline only  $b=0$ ) as reconstructed in Fig 5.3. The transient portion was generated for different sizes of drainage area by  $r_{eD}$ . Again the numerical results are shown tabular form in the appendix D. The complete set of tabular results is not available from any other source in the literature. Figure 5.4 shows the final composite curve for the transient and depletion stages.

**Fetkovich Type Curve Transient and Exponential Depletion Type Curves**

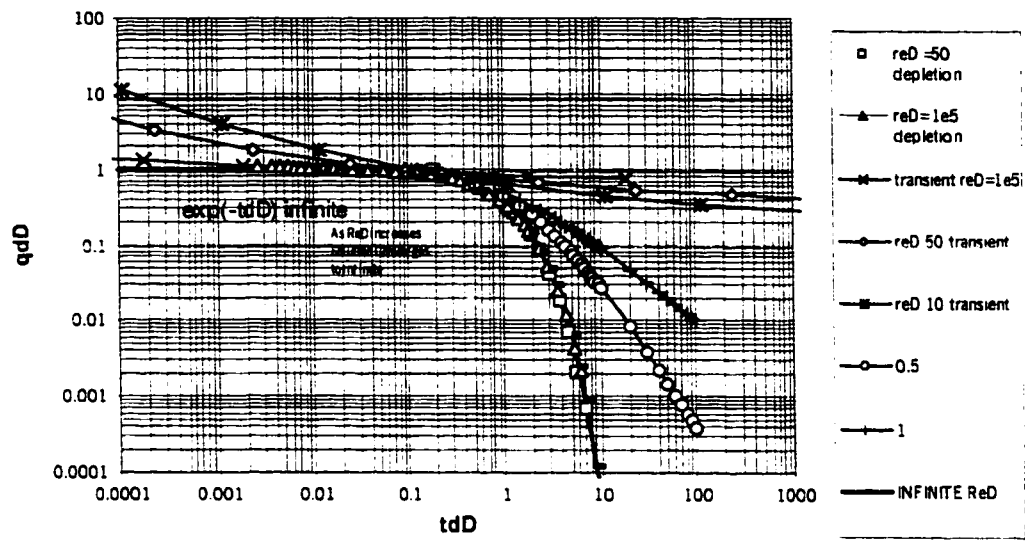


**Figure 5.3 Fetkovich Type Curve – Transient and Depletion**

**Composite Fetkovich Type Curve Transient and Exponential Depletion**

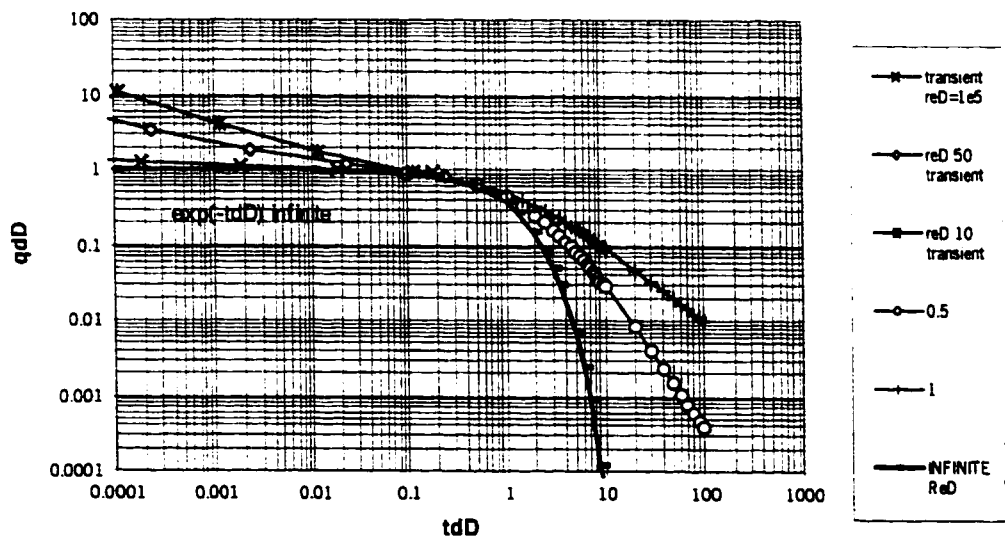


**Figure 5.4 Final Composite Fetkovich Type Curve – Transient and Depletion**

## 5.4 Use of Decline Curves in the Calculation of Reservoir Parameters and Future Production Calculations

The type curves can be used to calculate reservoir parameters such as permeability and apparent well bore radius. Data from the infinite acting portion of the type curve is used for these calculations. However points from both the infinite and pseudosteady state portion are needed for the best curve fitting.

### 5.4.1 Calculation of Transmissibility and Apparent Well Bore Radius

As previously derived:

$$kh = \frac{141.2 \mu B}{(P_i - P_{wf})} \left( \ln \frac{r_e}{r_w} - \frac{1}{2} \right) \frac{q_t}{q_{dD}} \quad 5.25$$

and apparent well bore radius is expressed as:

$$r_{wa}^2 = \frac{0.00634 k}{\phi \mu c_s} \frac{1}{2} \left[ \left( \frac{r_e}{r_{wa}} \right)^2 - 1 \right] \left[ \ln \left( \frac{r_e}{r_{wa}} \right) - \frac{1}{2} \right] \left( \frac{t \text{ (days)}}{t_{dD}} \right) \quad 5.26$$

In each case  $r_{eD} = r_e/r_{wa}$  is read from the type curve match.

For example:

If from the type curve match,  $r_e/r_{wa}$  is best represented by 50,  $q_{Dd}$  is 0.54,  $q_t$  is 10,000 BOPM

(333 BOPD) and  $\frac{(P_i - P_{wf})}{\mu B} = 7259$  from reservoir production data, then from equation

above  $kh$  is 40.5 md-ft. Then knowing the thickness  $h$ , yields  $k$ .

Likewise if the corresponding time match points are  $t=10$  months (300 days) and  $t_{Dd}=1.22$  with  $r_e/r_{wa} = 50$ , and reservoir characteristics are porosity of 10.1%, viscosity of 1 cp and total compressibility of  $20 \times 10^{-6}$ , and permeability is 0.33 md then the apparent well bore radius is: 1.042 feet.

#### 5.4.2 Matching the PSS Portion for Calculation of N and Future Flow Rates

The drainage radius can then be calculated from the following expression:

$$r_e = r_{wa} \left( \frac{r_e}{r_{wa}} \right)_{match} \quad 5.27$$

In the above example, with  $r_e/r_{wa} = 50$  from the match of the transient portion of the curve,  $r_{wa}$  from the previous step = 1.042 then the drainage area is  $r_e = 52$  feet.

The reserves in place can then be determined by the expression<sup>4</sup> (399)

$$N(\text{well}) = \frac{\pi r_e^2 h \phi (1 - Sw)}{5.615 B_{oi}} \quad 5.28$$

or by:

$$N = \frac{A \phi c_i h P_i}{5.615 B} \quad 5.29$$

#### 5.4.3 Pseudosteady State Type Curve Matching for Reserve Estimates

Fetkovich type expressions can be adapted to determine initial reserves in place and forecast future flow rates. Then if we know the cumulative production, the remaining reserves in place can be calculated. Using a data set from the Fetkovich paper<sup>3</sup>, the match (fig 5.5) followed the b=0.5 type curve.

Future producing rates can than be read directly from the real time scale on which the data are plotted.  $q_i$  and  $D_i$  can be determined from the match points and that data can be used to determine the reserves. The following match points were obtained:

$$q_t = 1000 \text{ BOPM}, q_{Dd} = 0.033$$

Therefore:

$$q_{Dd} = 0.033 = \frac{q(t)}{q_i} = \frac{1000 \text{ BOPM}}{q_i}$$

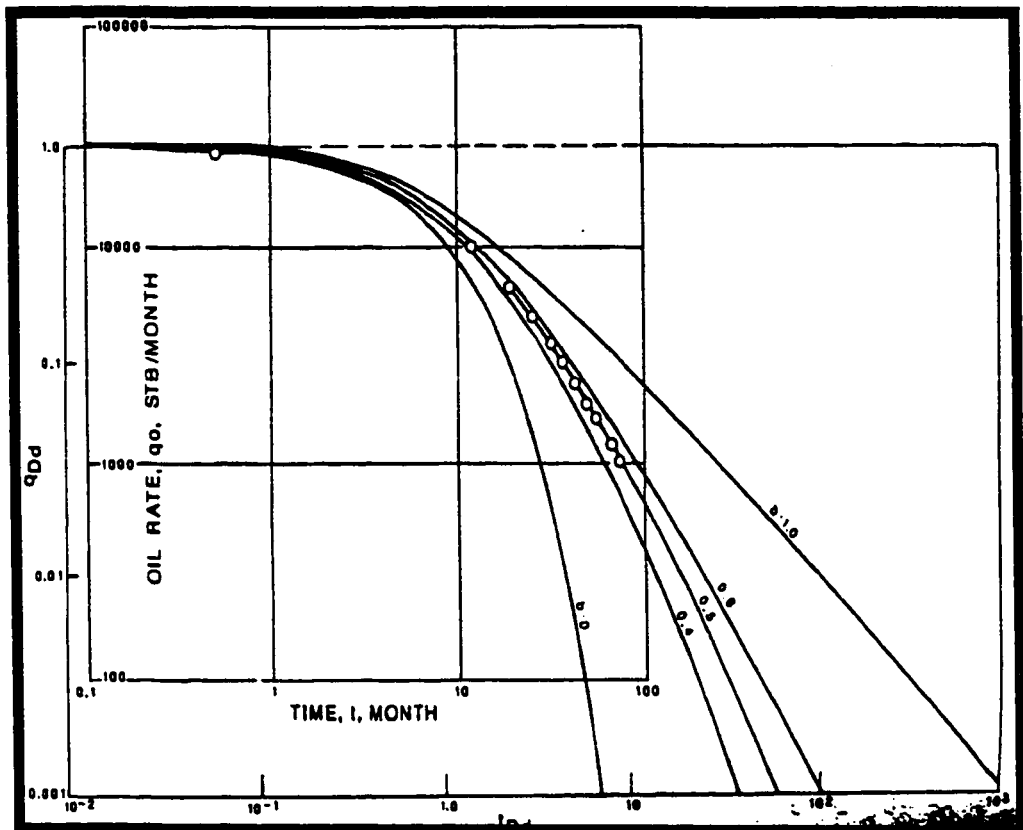


Figure 5.5 Type Curve Matching

therefore the initial production rate is:

$$q_i = 30,303 \text{ BOPM}$$

and the time match points were:

$$t_{Dd} = 12, t = 100 \text{ months}$$

therefore the initial decline rate is:

$$D_i = \frac{t_{Dd}}{t} = \frac{12}{100 \text{ months}} = 0.12$$

Once the initial decline rate and initial production rate are known, the initial reserves in place can be calculated since the cumulative oil in place would be the integration of the initial flow rate expression:

$$N_p = \int_0^t q_i = q_i [1 + bD_i t]^{-\frac{1}{b}} \quad 5.30$$

which yields the expression for the hyperbolic ( $0 < b < 1$ ) expression for cumulative oil produced.

$$N_p = \frac{q_i^b}{(1-b)D_i} (q_i^{1-b} - q^{1-b}) \quad 5.31$$

If the initial oil in place is defined as the cumulative oil produced to a reservoir pressure of zero, then the expression reduces to:

$$N_{pi} = \frac{q_i}{(1-b)D_i} \quad 5.32$$

Therefore using the above match points along the  $b=0.5$  curve we have:

$$N_{pi} = \frac{30,303}{(1-0.5) * 0.12} = 505,050$$

If the decline is exponential then the expression reduces even further. Alternate methods for calculating pore volume and thus reserves with a known initial oil saturation above and below the bubble point are presented in Appendix C. Methods of using the type curve matches for computing oil relative permeability are also presented in Appendix C.

#### **5.4.4 Field Wide Application**

According to Mathews<sup>21</sup>, during pseudo steady state, the drainage volumes in a bounded reservoir are proportional to the rates of withdrawal from each drainage volume. Therefore the ratio  $q_i/N_{pi}$  will be identical for each well and, thus, the sum of the results from each well should give the same results as from analyzing the total lease or field production rate. Field experience often demonstrates how rapidly readjustments in drainage volumes can take place by changes in the production rate or depletion by offset wells. This of course assumes that the field is not stratified or separated by a fault or drastic anisotropy. The effect compartmentalization by permeability or stratification would be interesting to experiment with in the future.

### **5.5 Extensions of Fetkovich Radial Type Curves to Other Reservoirs Shapes and**

#### **Well Positions**

##### **5.5.1 Introduction**

It is not well known that the Fetkovich Type Curves are based on a strictly radial system operating above the bubble point with the well centrally located. It is obviously desirable to derive a more general case that would apply to any particular reservoir drainage shape such as rectangular, triangular, and reservoirs in which the well is displaced from the reservoir center. It would also be desirable to modify the curves for cases below the bubble point and

extract information from that deviation from the strictly exponential case. In the radial case, the transition from infinite acting to pseudosteady state is almost instantaneous. However in a non-radial reservoir the transition from infinite to pseudosteady state is prolonged. Significant error in type curve matching may result from using the radial form. In low permeability formations rapidly declining transient production can be confused with depletion and an attempt to fit the transient data to the depletion portion of the type curve will result in Arps "b" values that are unrealistically high. It is therefore desirable to properly define the full shape of the type curve over the transient and depletion period properly apply the techniques and analysis.

This method, shown in this section and fully derived in Appendix E utilizes shape factors derived for these various conditions such as shown in Earlouger's Table C-1 in *Advances in Well Testing*<sup>22</sup>. Application of these factors to the Fetkovich system is neither direct nor straightforward. A system was derived that will incorporate all reservoir shapes, positions and later will be applied to vertically fractured and horizontal wells using an equivalent well bore radius concept. The complete derivation is shown in Appendix E.

### 5.5.2 Overview of Derivation

Recall that the productivity and decline theory of the previous section Fetkovich defined  $q_{Dd}$  as:

$$q_{Dd} = \frac{q(t)}{q_{\max}} = \frac{141.3 \mu B q(t)}{kh(P_i - P_w)} \left[ \ln \frac{r_e}{r_w} - \frac{1}{2} \right] = q_D \left[ \ln \frac{r_e}{r_w} - \frac{1}{2} \right] = q_D c_1 \quad 5.33$$

In a similar manner the dimensionless time  $t_{Dd}$  was defined as:

$$t_{Dd} = \left[ \frac{q_{\max}}{N_p} \right] t = D_t t = \frac{0.00634 k t}{\phi \mu C_t r_w^2} \left[ \frac{1}{\frac{1}{2} \left[ \left( \frac{r_e}{r_w} \right)^2 - 1 \right] \ln \left( \frac{r_e}{r_w} \right) - \frac{1}{2}} \right] = t_D \left[ \frac{1}{\frac{1}{2} \left[ \left( \frac{r_e}{r_w} \right)^2 - 1 \right] \ln \left( \frac{r_e}{r_w} \right) - \frac{1}{2}} \right] \quad 5.34$$

or:

$$t_{Dd} = t_D \frac{2}{c_1 c_2} \quad 5.35$$

Now instead of using the radial form one begins with a more general equation in terms of the shape factors and drainage area A such as that found on page 243 in Craft and Hawkins<sup>6</sup> so that:

$$q(t) = \frac{k h (\bar{P}_R - P_w)}{162.6 \mu B} \left[ \log \frac{4A}{1.781 C_A r_w^2} \right] \quad 5.36$$

Then applying the Fetkovich definition above and converting constants to Fetkovich's definitions of  $q_D$ :

$$q_{Dd} = \frac{q(t)}{q_{\max}} = q_D \left[ 1.151 \left[ \log \frac{4A}{1.781 C_A r_w^2} \right] \right] = \frac{141.3 \mu B q(t)}{kh(P_i - P_w)} \left[ 1.151 \log \frac{4A}{1.781 C_A r_w^2} \right] \quad 5.37$$

Or condensing notation:

$$q_{Dd} = q_D \left[ 1.151 \left[ \log \frac{4A}{1.781 C_A r_w^2} \right] \right] = q_D (1.151 c_1) \quad 5.38$$

where  $c_1$  is:

$$c_1 = \log \frac{4A}{1.781 C_A r_w^2} \quad 5.39$$

The equivalent Fetkovich form was:

$$q_{Dd} = q_D \left[ \ln \frac{r_e}{r_w} - \frac{1}{2} \right] = q_d c_1 \quad 5.40$$

Where  $c_1$  was:

$$c_1 = \left[ \ln \frac{r_e}{r_w} - \frac{1}{2} \right] \quad 5.41$$

Likewise the dimensionless time decline can be derived in a manner similar to that of Fetkovich but in terms of the reservoir shape and drainage size factors:

$$t_{Dd} = \left[ \frac{q_{i,\max}}{N_{pi}} \right] t = D_i t \quad 5.42$$

where :

$$q_{\text{max}} = \frac{k h P_t}{162.6 \mu B} \left[ \frac{1}{\log \frac{4A}{1.781C_A r_w^2}} \right] \quad 5.43$$

and :

$$N_t = \frac{A \phi c_t h P_t}{5.615 B} \quad 5.44$$

and applying the definition of  $t_{Dd}$  and converting constants:

$$t_{Dd} = \frac{q_{\text{max}}}{N_t} t = \frac{0.00634 k t}{\phi \mu c_t A} \left[ \frac{5.44678}{\log \frac{4A}{1.781C_A r_w^2}} \right] \quad 5.45$$

$$t_{Dd} = \frac{0.00634 k t}{\phi \mu c_t r_w^2} \frac{r_w^2}{A} \left[ \frac{5.44678}{\log \frac{4A}{1.781C_A r_w^2}} \right] = t_D \frac{r_w^2}{A} \left[ \frac{5.44678}{\log \frac{4A}{1.781C_A r_w^2}} \right] \quad 5.46$$

or putting in a similar arrangement to that of the Fetkovich radial form:

$$t_{Dd} = \frac{\frac{t_D}{4A}}{\frac{A \log \frac{4A}{1.781C_A r_w^2}}{r_w^2 - 5.44678}} = \frac{t_D}{\frac{0.183594A}{r_w^2} \log \frac{4A}{1.781C_A r_w^2}} = \frac{t_D}{0.183594(c_1 c_2)} \quad 5.47$$

Where  $c_2$  is:

$$c_2 = \frac{A}{r_w^2} \quad 5.48$$

As compared to  $c_2$  in the Fetkovich radial case:

$$c_2 = \frac{r_e}{r_w^2} - 1 \quad 5.49$$

And:

$$c_1 = \log \frac{4A}{1.781C_A r_w^2} \quad 5.50$$

Again comparing this to the Fetkovich equivalent forms one notes the similarities:

$$c_1 = \ln \frac{r_e}{r_w} - \frac{1}{2} \quad 5.51$$

The complete derivation of the more general shape and well location case is shown in the Appendix E.

Now if the drainage area can then be expressed in terms of the equivalent radial system  $r_{eD}=r_e/r_w$  then the published values of  $q_D$  and  $t_D$  can be converted directly to decline dimensionless terms for any drainage shape and can also be extended to fractured vertical wells and horizontal wells as will be demonstrated. Therefore define the equivalent drainage area for the radial system as:

$$A = \pi(r_e^2 - r_w^2) = \pi r_e^2 - \pi r_w^2 \quad 5.52$$

and rearranging:

$$\frac{A}{r_w^2} = \pi \left( \frac{r_e}{r_w} \right)^2 - \pi = \pi \left( \left( \frac{r_e}{r_w} \right)^2 - 1 \right) \quad 5.53$$

Therefore using the radial solutions to  $q_D$  and  $t_D$  at the various  $r_{eD} = r_e/r_w$  values and the new constants  $c_1$  and  $c_2$  we can find equivalent expressions in terms of  $A/r_w^2$  and the various shape factors.

Decline curve construction using the shape factor approach has confirmed that when the circular shape factor is used, the above derivation is identical to the Fetkovich radial form. Figure 5.6 is the equivalent radial form using the above derivation with the centrally located circular shape factor  $A = 31.62$ . It is identical to the Fetkovich radial solution in figure 5.2. Tabular data for all rectangular comparisons from equations above are provided in the appendix D. Shape Factors are shown in Table 5.1. These shape factors are used for the transition and depletion portions of the type curve. The infinite portion retains the radial form without shape factor adjustment. The change to shape

factors is valid for  $t_{DA} = \frac{r_w^2}{A}$  greater than 0.025 for a rectangular shape factor of x:y = 2:1 and 0.01 for a rectangular shape factor of x:y = 4:1. This corresponds to a  $t_{Dd}$  range from 0.4 to 0.2 on the generalized type curves in the transition and depletion area.

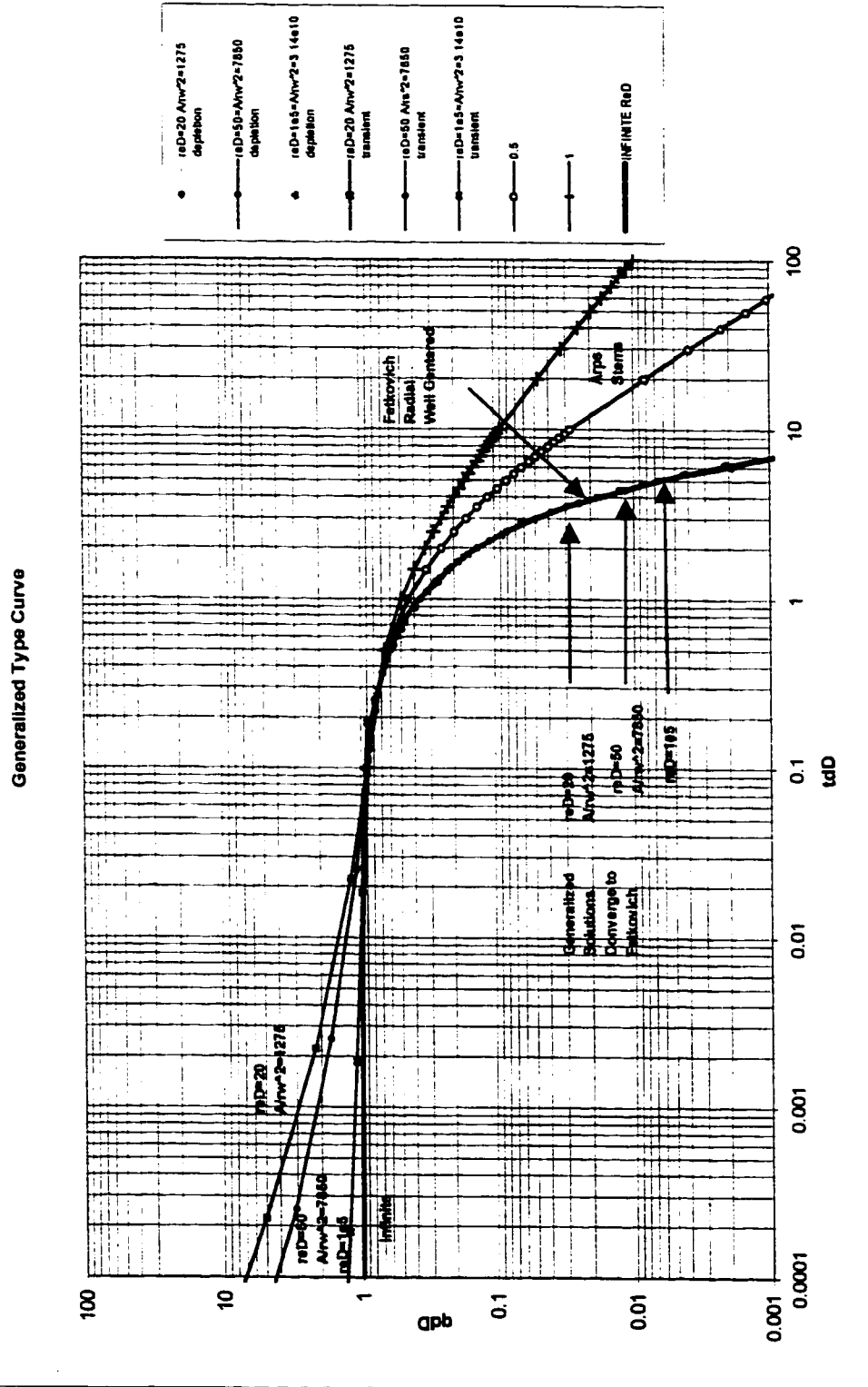


**Figure 5.6 Generalized Type Curve -Circular Shape Factor, Well Centered, CA=31.62**

Table 5.1

Shape Factors for  
Use in Generalized  
Decline Curves<sup>22</sup>

| <i>N BOUNDED RESERVOIRS</i> | <i>C<sub>A</sub></i> | < 1%<br>error<br><i>t<sub>OA</sub></i> > |       |
|-----------------------------|----------------------|--|-------|
| •                           | 31.62                | 0.06                                     | 0.10  |
| •                           | 31.6                 | 0.06                                     | 0.10  |
| •                           | 27.6                 | 0.07                                     | 0.09  |
| •                           | 27.1                 | 0.07                                     | 0.09  |
| •                           | 21.9                 | 0.12                                     | 0.08  |
| 3 {<br>4 }<br>△             | 0.098                | 0.60                                     | 0.015 |
| •                           | 30.8828              | 0.05                                     | 0.09  |
| •                           | 12.9851              | 0.25                                     | 0.03  |
| •                           | 4.5132               | 0.30                                     | 0.025 |
| •                           | 3.3351               | 0.25                                     | 0.01  |
| •<br>1<br>2                 | 21.8369              | 0.15                                     | 0.025 |
| •<br>1<br>2                 | 10.8374              | 0.15                                     | 0.025 |
| •<br>1<br>2                 | 4.5141               | 0.50                                     | 0.06  |
| •<br>1<br>2                 | 2.0769               | 0.50                                     | 0.02  |

Thus the dimensionless decline type curves can now be generated for any drainage shape and well bore position if a shape factor is available. Shape factors are available for a wide range of reservoir situations. For instance the shape factor  $C_A$  is 31.62 for a circle, 30.8828 for a square, 21.8369 for a rectangle of dimensions  $x_e/y_e=1/2$ , and 5.379 for a rectangle of dimensions  $x_e/y_e =1/4$ . These various shape and well location factors  $C_A$  are reproduced in Table 5.1<sup>22</sup>.

The decline curves have been presented in terms of  $A/r_w^2$  or alternatively  $\sqrt{A/r_w}$  and the equivalent  $r_e/r_w = r_{eD}$ .  $A/r_w^2$  seems more appropriate for rectangular reservoir shapes. During the transient period the radial solution would still be used as the reservoir boundaries have not yet affected the drainage. However the transient period can be very short with some reservoir shapes with wells near the boundary as will be shown. As the reservoir boundaries are felt a transition period will occur before pseudosteady state is observed. It is this early transition zone that will indicate deviation from radial system and the portion that is most pertinent to this generalized shape method. Theoretically it should be possible to extract reservoir shape information from deviation from radial dimensionless decline curves.

If the well bore radius is small compared to the reservoir size then the area can be approximated by:

$$A \approx \pi r_e^2 \therefore \frac{A}{r_w^2} = \pi \frac{r_e^2}{r_w^2} \quad 5.54$$

or upon rearranging:

$$r_{eD} = \frac{r_e}{r_w} = \frac{\sqrt{A}}{\sqrt{\pi r_w}} \quad 5.55$$

This provides the solution in terms more similar to the Fetkovich type curves. However the more exact solution is necessary when considering horizontal wells since one can define the horizontal well in terms of an apparent well bore radius.

Figures 5.7 and 5.8 show the dimensionless decline curve results of applying the above relationships for a rectangle of dimensions  $x_e/y_e = 0.5$  and  $x_e/y_e = 0.25$  respectively. Figure 5.9 shows the case where the  $C_A$  value is very small in a rectangular reservoir with the well close to the boundary ( $C_A=10.8374$ ). Notice how the transition zone from infinite to finite acting has shifted to the left as the time to PSS has decreased. Also notice that for small values of  $r_{eD}$  such as 50, the infinite and finite solutions do not converge as well. The difference between a rectangle of dimension ration 2 to 1 is not easily distinguished from the radial solution. The method is most useful when the geometry departs significantly from radial or the well is close to a boundary. Reservoir parameters can then be calculated from the type curve match points in the usual way.

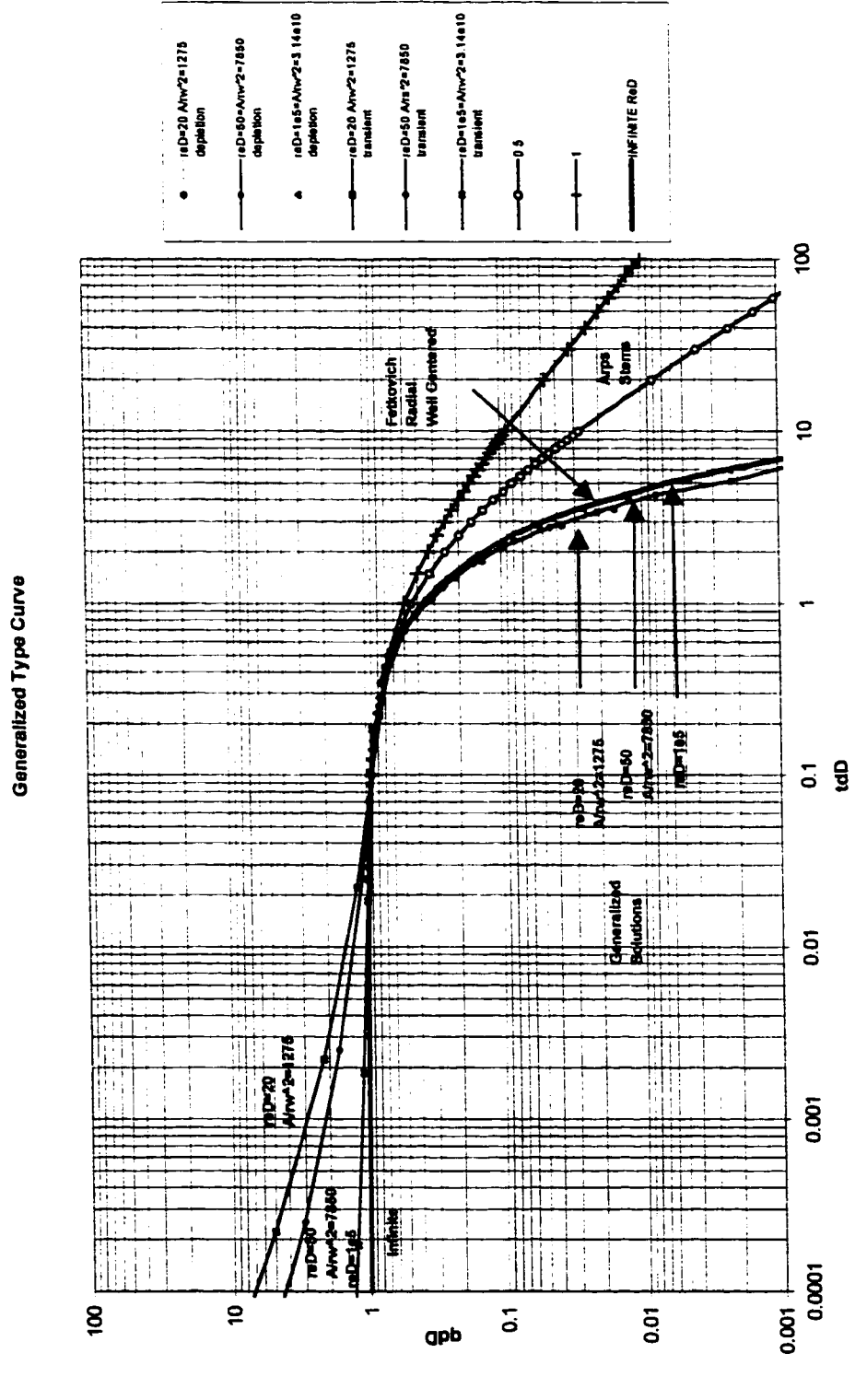


**Figure 5.7 Generalized Type Curve -Rectangular Shape Factor x:y 2:1 Offcenter close to boundary, CA=10.374**

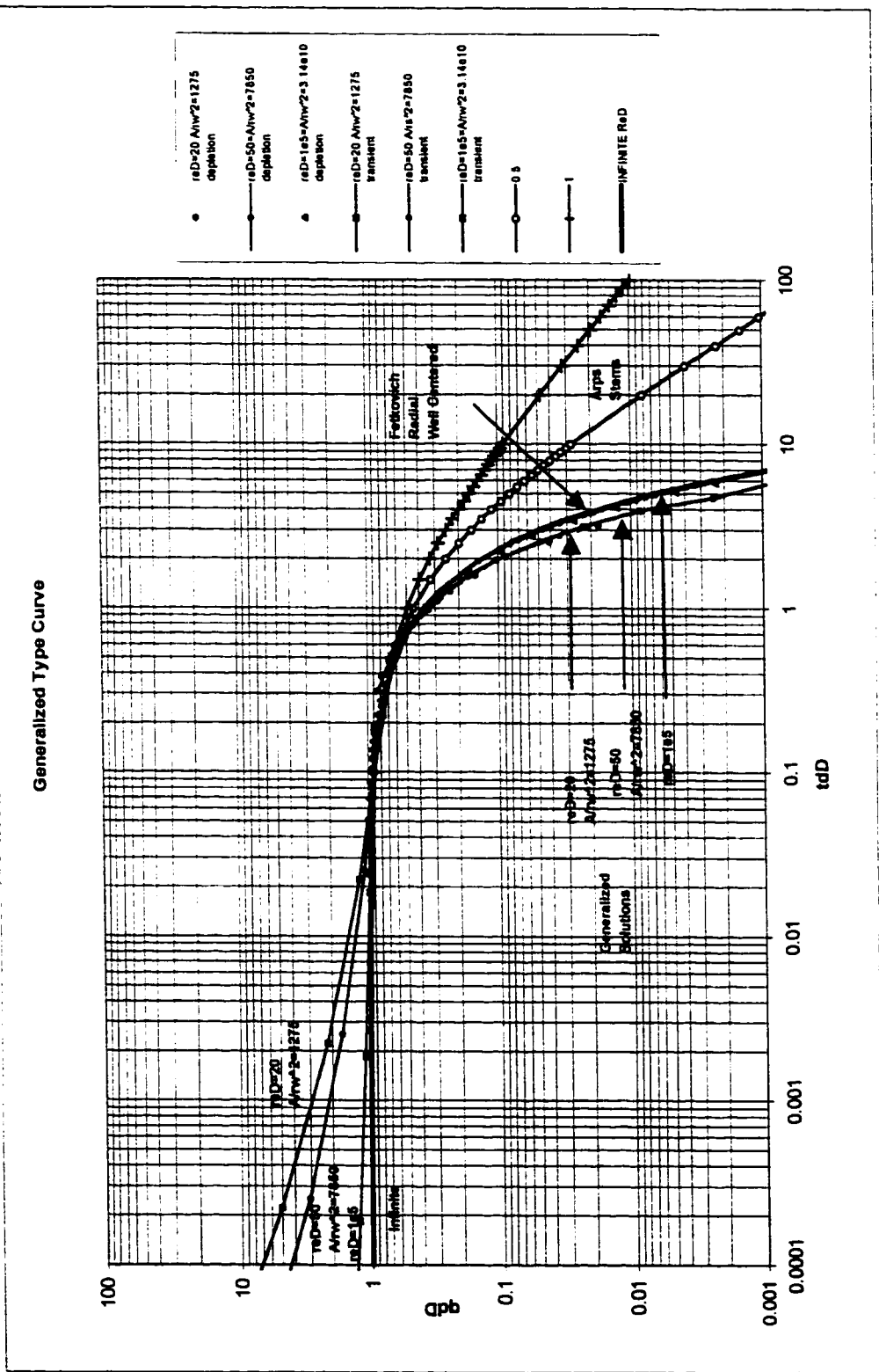


Figure 5.8 Generalized Type Curve -Rectangular Shape Factor x:y 4:1 Well Centered, CA=5.3790

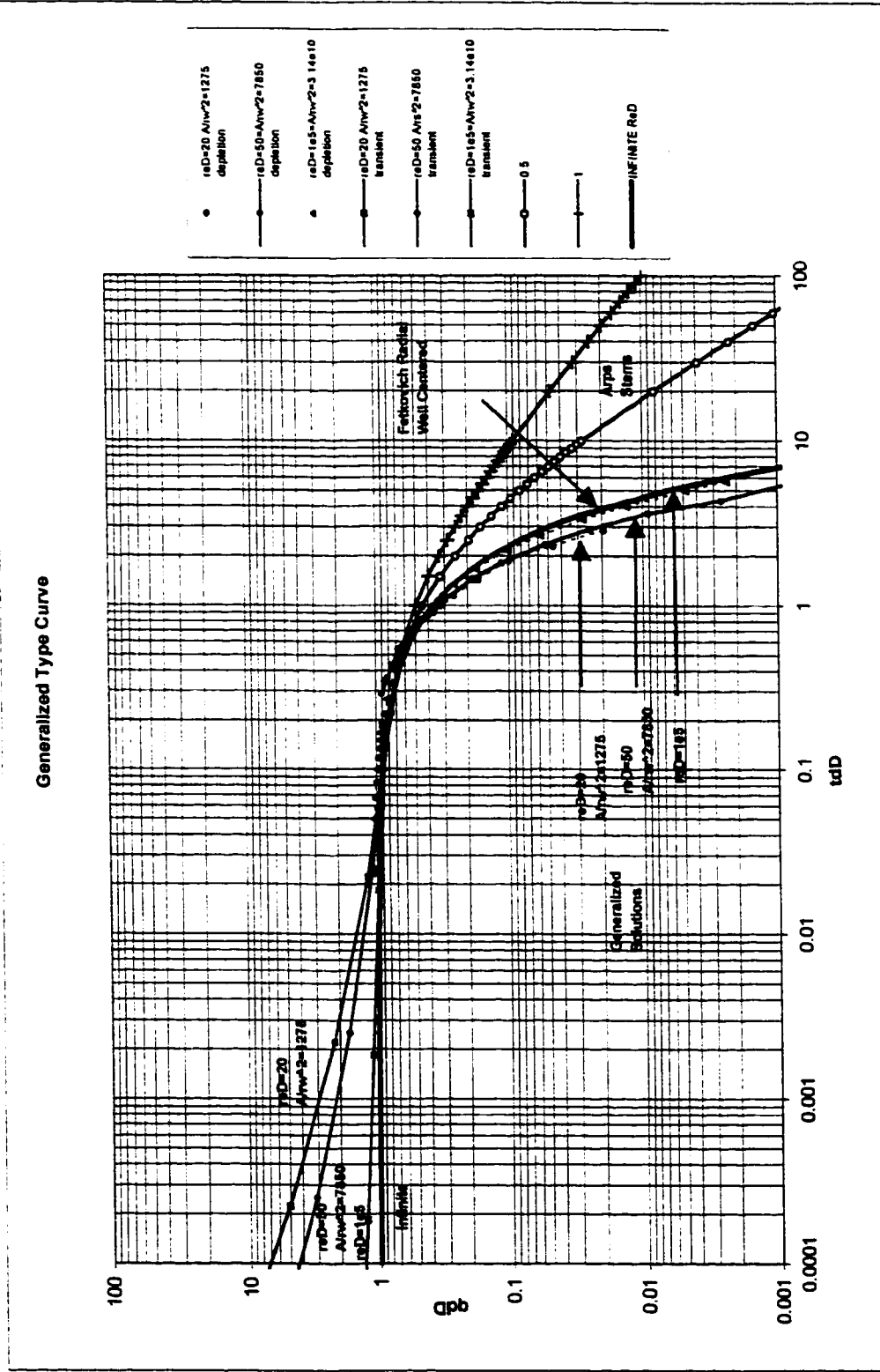


Figure 5.9 Generalized Type Curve -Rectangular Shape Factor x:y 4:1 Offcenter close to boundary, CA=2.6896

### 5.5.2.1 Use in Calculating Reserves and Reservoir Parameters

The transmissibility ( $kh$ ) and permeability (if reservoir thickness is known) can be computed by solving the my dimensionless decline equation for  $kh$  and using the match point:

$$q_{Dd} = q_D \left[ 1.151 \log \frac{4A}{1.781C_A r_w^2} \right] = \frac{1413 \mu B q(t)}{kh(P_i - P_{wf})} 1.151 \log \frac{4A}{1.781C_A r_w^2} \quad 5.56$$

and solving for  $kh$ :

$$kh = \frac{1413 \mu B}{P_i - P_{wf}} 1.151 \log \frac{4A}{1.181C_A r_w^2} \left( \frac{q(t)}{q_{Dd}} \right)_{match} \quad 5.57$$

Since we know  $A/r_w^2$ , the match point, and the shape factor we can compute  $kh$  for the particular reservoir conditions.

The apparent well bore radius, drainage area and initial reserves can then be computed from the dimensionless decline parameter  $t_{Dd}$  and the match points. Ultimate reserves are then computed from the difference between initial reserves and cumulative reserves.  $r_{wa}$  is computed from the following relationship derived for the more general shape factor form:

Since  $t_D$  is defined before as:

$$t_{Dd} = \frac{t_D}{\frac{0.183594A}{r_w^2} \log \frac{4A}{1.781C_A r_w^2}} \quad 5.58$$

Now inserting the definition of  $t_D$ :

$$t_D = \frac{0.0063kt}{\phi\mu c_i r_{wa}^2} \quad 5.59$$

Solving the dimensionless time equation for  $r_{wa}^2$ :

$$r_{wa}^2 = \frac{0.00634k}{\phi\mu c_i \frac{A}{r_w^2} \left( \frac{\log \frac{4A}{1.781C_A r_w^2}}{5.44678} \right)} \left( \frac{t}{t_{Dd}} \right)_{match} \quad 5.60$$

We know the ratio  $A/r_w^2$  and  $t/t_{Dd}$  from the type curve match points therefore we can compute the apparent well bore radius,  $r_{wa}$ . This apparent well bore radius will be used later.

Now since we know  $r_{wa}$  we can calculate the drainage area  $A$  since from knowing  $A/r_w^2$  from the type curve match and computing  $r_w^2$  we can solve for the drainage area  $A$  by:

$$A = r_{wa}^2 \left( \frac{A}{r_{wa}^2} \right)_{match} \quad 5.61$$

This allows for the computation of the original reserves in place from the relationship:

$$N = \frac{A \phi c_i h P_i}{5.615 B} \quad 5.62$$

### **5.5.2.2 Use in Determining Contributions of Solution Gas Energy and Mobility Function**

The decline path will be exponential where  $b=0$  and the Fetkovich solutions converge when the only reservoir energy is the compressibility of the rock and fluid. In a solution gas reservoir where water drive is absent the decline path will be more hyperbolic where  $b$  values of 0 to 0.5 exist. This deviation from  $b=0$  can give information that can be used in determining the mobility-pressure function that was described in chapter 3 and the appendix C. This concept can be shown in the following figure 5.10.

### Composite Fetkovich Type Curve Transient and Exponential Depletion

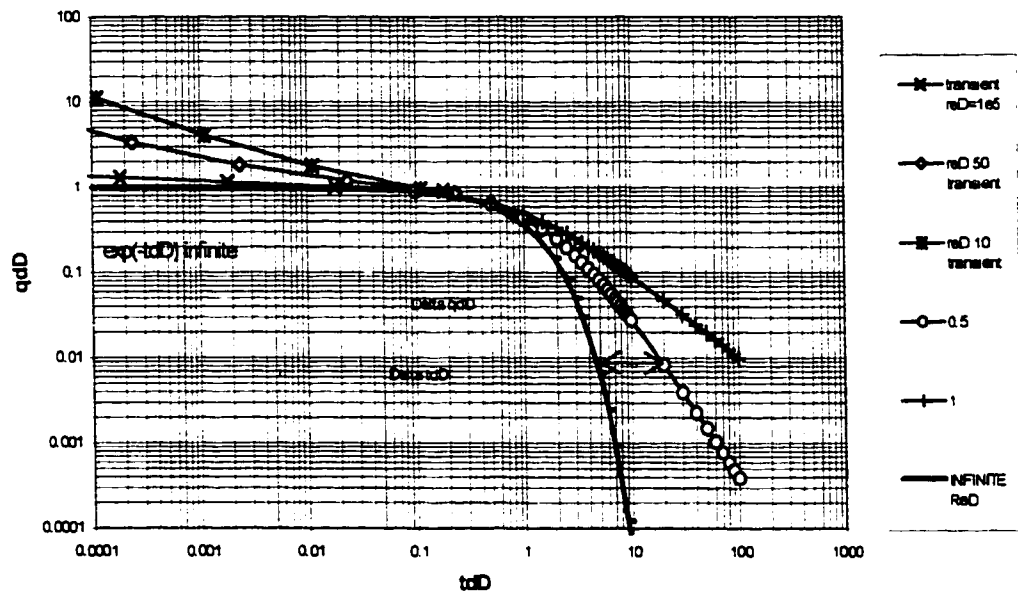


Figure 5.10 Composite Fetkovich Type Curve

Where  $\Delta q_{Dd}$  represents the difference from the actual path and that predicted with no energy in the system other than the fluid and rock compressibility. The solution gas provides additional pressure support that more than offsets the increased resistance from the reduction in  $k_{ro}/(\mu_o B_o)$  with a reduction in pressure and oil saturation. Also with a purely exponential decline with no additional drive energy, the IPR will be constant with declining pressure. Field experience indicates that the IPR does change with depletion since exponential depletion is rare. Once the decline path is known from the above chart, the difference between the decline path and the predicted exponential path should give information about the pressure mobility function and adjustments to IPR over time without the need for well testing techniques.

$$\int \frac{k_{ro}}{\mu_o B_o} dp \equiv \frac{(P_R - P_{wf})k_{ro}}{(\mu_o B_o)_{P_{sw}}} \quad 5.63$$

Some of these ideas as well as some methods for estimating the relative permeability to oil are discussed in more detail in the guide to reservoir parameters in appendix C.

### 5.5.3 Extension to Fractured Wells

Fetkovich showed an example, which indicated that the “Arps b” value in pseudosteady state condition did not change with a fractured well but the  $r_{eD}=r_e/r_{ws}$  did shift to a smaller match ratio. He used type curves to indicate that the reserves increased as a

result of the increase in the effective well bore radius and the resulting shift of the curve to lower values of  $r_{eD} = r_e/r_{wa}$ . But reserves do not seem to increase in direct proportion to the increase in producing rate as a result of the treatment. He did not derive a relationship to account for these conditions. However if the effective or apparent well bore radius can be calculated after fracture stimulation then the same curves can be used.

As with the dimensionless pressure evaluation of reservoirs that have been fracture stimulated, the  $A/r_w^2$  term can be replaced by  $x_e^2/x_f^2$  or by  $A/x_f^2$  in the equations in the previous section and the same type of analysis could be applied as for the vertical well. Alternatively the fractured well approximations could be used to generate the  $q_D$  and  $t_D$  terms as follows:

$$q_D = \frac{1}{P_D} = \frac{1}{2\pi t_{DA} + \frac{1}{2 \left[ \ln \left( \frac{x_e}{x_f} \right)^2 \right] + \frac{1}{2} \frac{2.2458}{C_A}}} \quad 5.64$$

for the pseudosteady state portion and :

$$q_D = \frac{1}{P_D} = \frac{1}{2\pi t_{DA} + \left[ \frac{1}{2 \left[ \ln \left( \frac{x_e}{x_f} \right)^2 \right] + 0.80907} \right]} \quad 5.65$$

for the transient portion. The Fetkovich type curves can then be plotted using the standard relationship adjusted for the differences in  $t_{DA}$  and  $t_D$ :

$$q_{Dd} = q_D \left[ 1.15 \log \left( \frac{4A}{1.781C_A x_f^2} \right) \right] \quad 5.66$$

and

$$t_{Dd} = \frac{t_D}{\left( \frac{A}{x_f^2} \right) \frac{\log \frac{4A}{1.781C_A x_f^2}}{5.44678}} \quad 5.67$$

where  $t_D$  is related to  $t_{DA}$  by:

$$t_{DA} = t_D \frac{x_f^2}{A} \text{ or } \frac{x_f^2}{x_e^2} \quad 5.68$$

Appropriate decline dimensionless graphs can then be easily generated. The following table 5.4 for vertical fractured wells gives the shape factors for variations in reservoir shape and size. These tabular values are a compilation of various experiments, Table C.1 values of Earlougher<sup>22</sup> (modified) and Joshi<sup>23</sup> Table 7-3.

| $C_f$     | $x_e/y_e$ |        |       |        |        |          |
|-----------|-----------|--------|-------|--------|--------|----------|
|           | 1         | 2      | 3     | 5      | 10     | 20       |
| $x_w/x_e$ | 2.020     | 1.4100 | 0.751 | 0.2110 | 0.0026 | 0.000005 |
| 0.3       | 1.820     | 1.3611 | 0.836 | 0.2860 | 0.0205 | 0.000140 |
| 0.5       | 1.600     | 1.2890 | 0.924 | 0.6050 | 0.1179 | 0.010550 |
| 0.7       | 1.320     | 1.1100 | 0.880 | 0.5960 | 0.3000 | 0.122600 |
| 1.0       | 0.791     | 0.6662 | 0.528 | 0.3640 | 0.2010 | 0.106300 |

**Table 5.2 Correction Factors for Reservoir Shapes**

Therefore the type curves can be generated for any rectangular reservoir shape and fracture penetration ratio using the methods developed in the previous sections..

## 5.6 Normalization Techniques

Flowing bottomhole pressure may vary simultaneously with production rate. If the pressure varies in a smooth manner, rate decline can be treated with a constant pressure type curve if the rate used in the curve is normalized by pressure drop according to the relationship:

$$q_n = \frac{q_o(t)}{[P_i - P_{wf}]} \quad 5.69$$

Strictly speaking normalization should only be used during the infinite acting period. Golan and experience show that this use after the onset of PSS does not cause a problem since simultaneous pressure and rate decline usually stabilizes to a constant pressure condition before PSS state condition is reached. Normalization can not be used when flowing pressure changes stepwise. Superposition is used then. This normalization process will be extended in the horizontal well technique sections.

## 5.7 Derivative Methods

In the previous chapter the Fetkovich type curves were generated using the solutions of VanEverdingen and Hurst. This section attempts to derive and use the derivative type curves for both the vertical and horizontal well cases. The use of derivative curves for pressure transient analysis is not new. Tiab<sup>24,25,26</sup>, Bourdet etc presented derivative type curves and direct synthesis techniques for pressure analysis. These methods typically involve the log-log plot of the derivative of a dimensionless pressure or group of terms vs. dimensionless time or a group of terms involving time. The derivative techniques often have more curvature and definition and thus it is easier to obtain unique characteristic type curve matches. However because of the noisy nature of production

data derivative curves have had limited usefulness. Nevertheless for the sake of completeness the derivative type curves should be presented.

Decline analysis utilizes flow rate or cumulative production vs. time rather than pressure. Of course the dimensionless pressure  $P_D$  is simply the reciprocal of dimensionless rate  $q_D$  with a constant applied. Production rate data are much more difficult to uniquely match since conditions are not always ideal. Common data problems are related to such things as well shut-in periods, variations in well bore flowing pressures, mechanical problems, workovers, and erratic daily production recording. It is possible that rate derivative techniques may help in decline analysis using the methods of Fetkovich. Therefore the following methods are presented.

### 5.7.1 Closed boundary Case

The derivative of VanEverdingen and Hurst's relationships of sections 5.3.1 and 5.3.2 are given as:

$$\frac{\partial q_D}{\partial t} = -2 \sum_{a_1, a_2, \dots}^{\infty} \left[ \frac{a_n^2 e^{-a_n^2 t_D} J_1^2(a_n, r_{eD})}{J_0^2(a_n) - J_1^2(a_n, r_{eD})} \right] \quad 5.70$$

Recalling from the previous section that Fetkovich defined the parameters from conversion from dimensionless to type curve dimensionless using the following:

$$A = \frac{1}{\left[ \ln \frac{r_e}{r_{wa}} - \frac{1}{2} \right]} \quad 5.71$$

and :

$$B = \frac{2A}{\left( \frac{r_e}{r_{wa}} \right)^2 - 1} = \frac{1}{0.5 \left[ \left( \frac{r_e}{r_{wa}} \right)^2 - 1 \right] \left[ \ln \frac{r_e}{r_{wa}} - 0.5 \right]} \quad 5.72$$

It should be possible to easily convert the derivative of the closed boundary case to type curve dimensionless form since:

$$q_{Dd} = \frac{q_o}{q_{oi}} = \frac{q_D}{A} \quad 5.73$$

so that :

$$\frac{\partial q_{Dd}}{\partial t_{Dd}} = q'_{Dd} = \frac{\partial q_D}{\partial t_D} \left[ \frac{1}{A} \right] = \frac{\partial q_D}{\partial t_D} \left[ \ln \frac{r_e}{r_{wa}} - \frac{1}{2} \right] \quad 5.74$$

Likewise from the previous relationship:

$$t_{Dd} = Dt = Bt_D \quad 5.75$$

$$t_{Dd} = \frac{t_D}{\frac{1}{2} \left[ \left( \frac{r_e}{r_{wa}} \right)^2 - 1 \right] \left[ \ln \frac{r_e}{r_{wa}} - \frac{1}{2} \right]} \quad 5.76$$

It is customary to multiply the derivative by  $t_{Dd}$  for plotting at the same time scale as the traditional  $q_{dD}$  vs.  $t_{dD}$  plots for comparison. Therefore the form used in the analysis is:

$$q'_{Dd} * t_{Dd} = -q'_D * t_D * \left[ \ln \frac{r_e}{r_{wa}} - \frac{1}{2} \right] \quad 5.77$$

### 5.7.2 Construction of the Derivative Dimensionless Decline Curves

A computer program was written to compute the derivative as well as the  $q_D$  values from the VanEverdingen and Hurst relationships. This is done for the radial and then converted to the more general formulation for all reservoir shapes by the application of the appropriate shape and position terms.

Figure 5.11 shows the construction of the transient portion of the curve from the derivative of the radial solutions for various  $r_{eD}$  values. Figure 5.12 shows the dimensionless decline rate derivative  $q'_{Dd}$  plot. And figure 5.13 shows the dimensionless decline rate derivative  $q'_{Dd}$  in the transient region multiplied by  $t_{Dd}$  for plotting purposes. Tabular data from the program generated values that are included again in Appendix D.

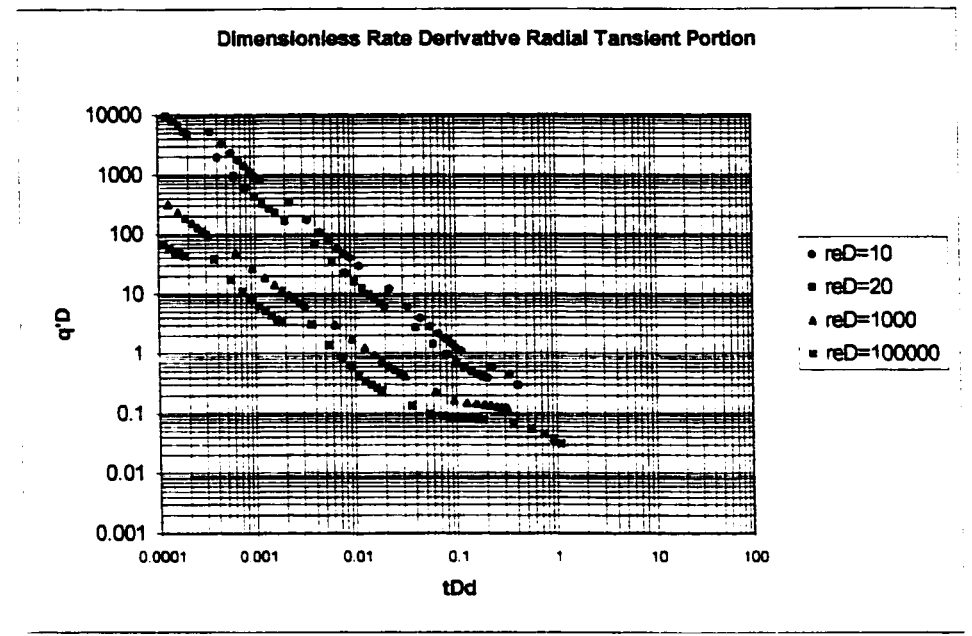


**Figure 5.11 Dimensionless Rate Derivative Radial Transient Portion**

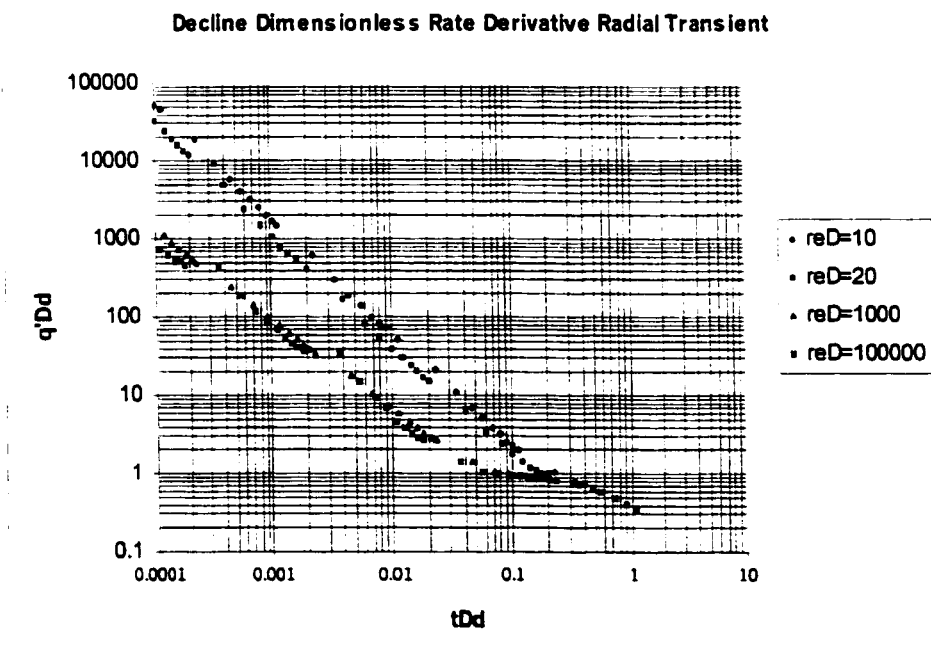


**Figure 5.12 Derivative Decline Type Curve Radial Case**

**Derivative Type Curve Radial Case Transient Solution**

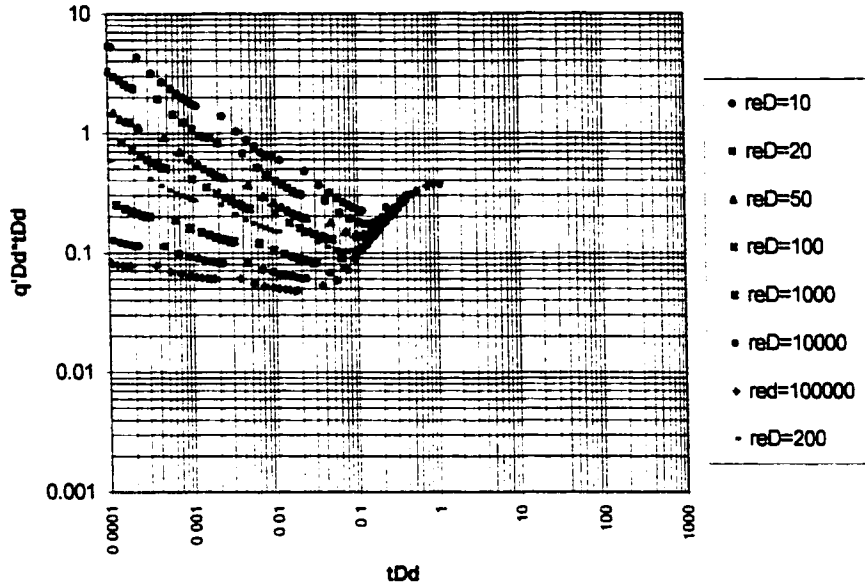


**Figure 5.13 Decline Dimensionless Rate Derivative Transient**

The depletion portion of the derivative dimensionless decline curve can be constructed by simply differentiating the Arps equations for exponential, hyperbolic and harmonic declines. Therefore the following expressions give the derivatives of the Arps expressions: Exponential:

$$\frac{\partial q_{Dd}}{\partial \alpha_{Dd}} = -\frac{1}{e^{t_D}} \quad 5.78$$

Hyperbolic:

$$\frac{\partial q_{Dd}}{\partial \alpha_{Dd}} = -\frac{1}{(1+bt_{Dd})^{\frac{1}{b}+1}} \quad 5.79$$

Harmonic:

$$\frac{\partial q_{dD}}{\partial t_{Dd}} = -\frac{1}{(1+t_{Dd})^2} \quad 5.80$$

These expressions are easily computed in a spreadsheet and displayed in figure 5.13 for the depletion portion of the dimensionless derivative decline type curve. The transient and depletion curves are then combined into one graph as shown in figure 5.14. Again notice that the expressions are multiplied by the dimensionless decline time for plotting purposes. Although the data are rather noisy, the depletion and transient portions converge at about time 0.1.

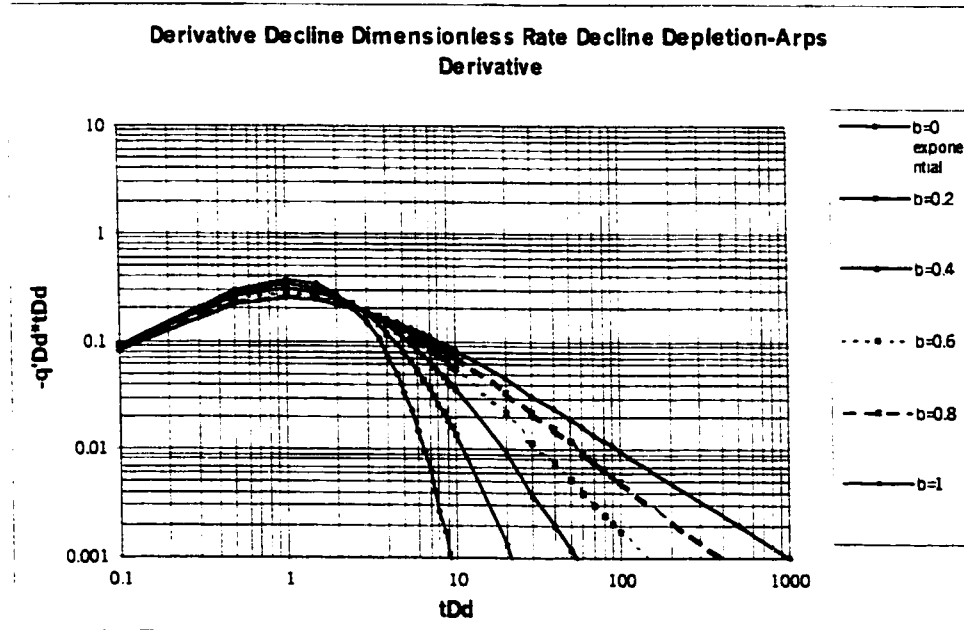
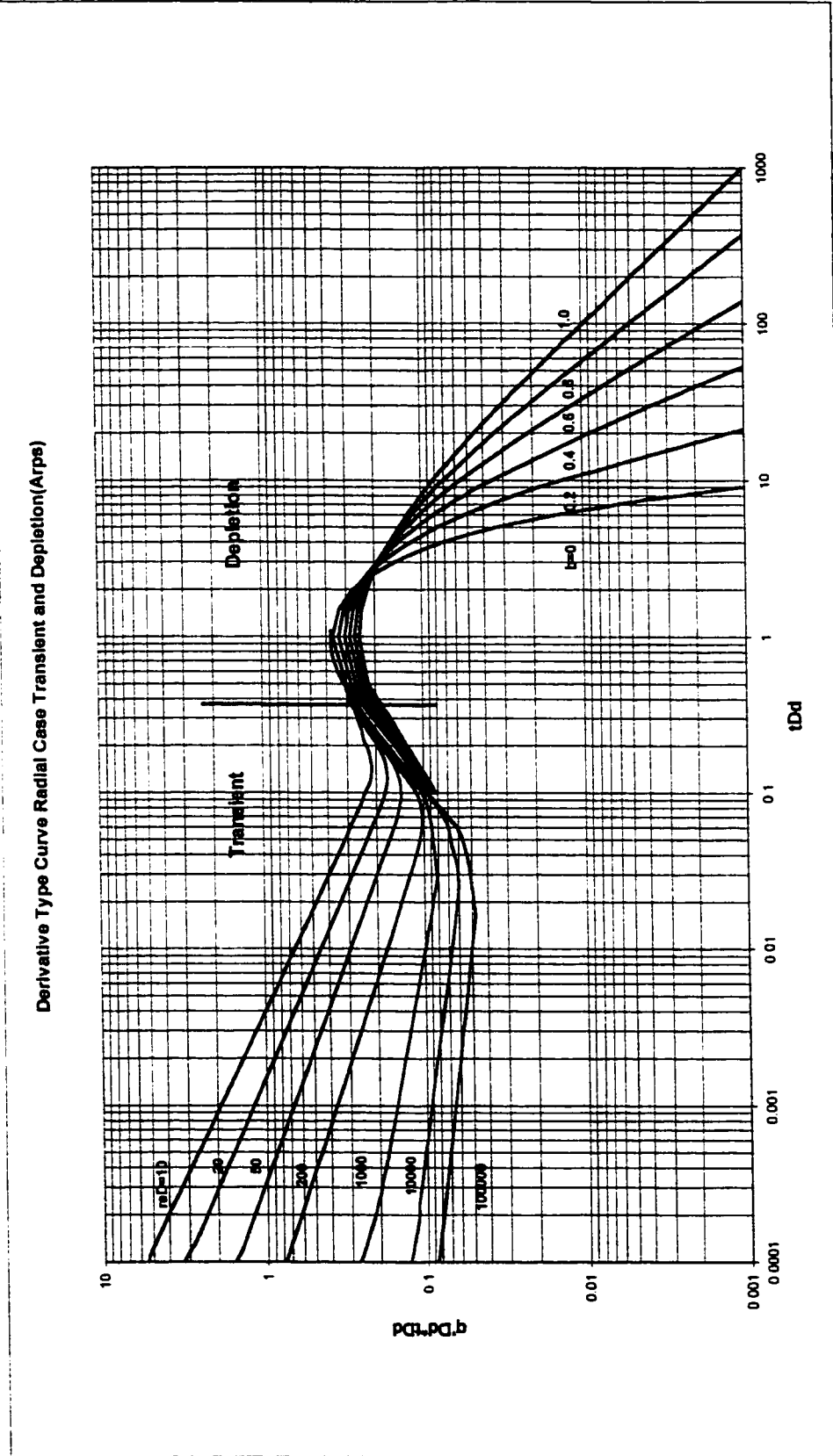


Figure 5.14 Arps Derivative Decline Dimensionless Rate Decline



**Figure 5.15 Composite Dimensionless Decline Derivative Type Curve - Transient and Depletion**

### 5.7.3 Extension to Other Reservoir Shapes

The above construction can be extended to the other reservoir shapes by application of my methods from section 5.6. As the data are so noisy for even the radial case this has not been done in this research. However the extension is straightforward.

### 5.7.4 Use of the Derivative Curves in Reservoir Analysis

The use of the type curve in reservoir analysis was done in the previous sections. This section will explain the use of the derivative in the analysis. Limited success has been found in using derivatives for decline curve analysis. The derivative type curves primary use as an aid in picking the proper  $r_{eD}$  and  $b$  curves for decline curve matching. This is done by first converting the field production data to a derivative and then matching to the derivative type curve.

The first step is to compute the numerical derivative of the production data using a derivative approach such as the three-point derivative as follows:

$$t_i \left[ \frac{\partial p}{\partial t} \right]_i = t_i \left[ \frac{(t_i - t_{i-1}) \Delta P_{i+1}}{(t_{i+1} - t_i)(t_{i+1} - t_{i-1})} \right] + \left[ \frac{(t_{i+1} + t_{i-1} - 2t_i) \Delta P_i}{(t_{i+1} - t_i)(t_i - t_{i-1})} \right] - \left[ \frac{(t_{i+1} - t_i) \Delta P_{i-1}}{(t_i - t_{i-1})(t_{i+1} - t_{i-1})} \right] \quad 5.81$$

This derivative will often give adequate results. If the derivative results in noisy data then certain smoothing techniques can be used.

### 5.7.5 Data Smoothing Techniques

Data smoothing techniques are varied. For instance one method to reduce noise might include using data points that are separated by at least 0.2 of a log cycle., rather than points that are immediately adjacent and using the natural logarithm of time.

$$t \left[ \frac{\partial p}{\partial} \right]_i = \left[ \frac{\partial p}{\partial \ln t} \right]_i \quad 5.82$$

So that the expression for the numerical differentiation would then be:

$$t \left[ \frac{\partial p}{\partial} \right]_i = \left[ \frac{\partial p}{\partial \ln t} \right]_i = \frac{\ln(t_i/t_{i-k})\Delta P_{i+1}}{\ln(t_{i+j}/t_i)\ln(t_{i+j}/t_{i-k})} + \frac{\ln(t_{i+j}t_{i-k}/t_i^2)\Delta P}{\ln(t_{i+j}/t_i)\ln(t_i/t_{i-k})} - \frac{\ln(t_{i+j}/t_i)\Delta P_{i-1}}{\ln(t_i/t_{i-k})\ln(t_{i+j}/t_{i-k})}$$

$$\ln t_{i+j} - \ln t_i \geq 0.2$$

$$\ln t_{i+j} - \ln t_{i-k} \geq 0.2$$

The value of 0.2 is known as the differentiation interval and could be replaced by smaller or larger values (usually between 0.1 and 0.5) with consequent differences in the smoothing of the noise. The differentiation interval may cause problems in determining the derivative for the last part of the derivative curve, since the data runs out within the

last differentiation interval. Therefore some noise is expected at the end of the data string.

The primary benefit of the derivative curve is for an aid in picking the proper  $r_{eD}$  and  $b$  values with which to match and diagnosing characteristic reservoir types. The calculation of reservoir parameters is identical to the method discussed before. It is difficult to use the derivative type curve unless sufficient data is available in both the transient and depletion portions of the curve.

### 5.7.6 Example of Derivative Use

The table below is a data set from Golan's book<sup>4</sup> as noted in the table 5.3 below. Applying the above concepts and plotting results in the following graphs in figure 5.16. Figure 5.17 is the derivative type curve developed in the prior sections.

| Production Data from Golan page 393 Table E.4.5<br>b=0.5 considered best match by author |       |         |           |          |          |          |
|--|-------|---------|-----------|----------|----------|----------|
| Delta T  | Q/mo  | Delta q | Q'        | Q'alt    | t"Q'     | t"Q'alt  |
| 0  | 0     |         |           |          |          |          |
| 0.5  | 30000 | 30000   | 218.0000  |          |          |          |
| 14   | 9000  | 39000   | 826.1702  | 1072.949 | 11566.38 | 15021.29 |
| 19.3   | 6532  | 45532   | 1004.7748 | 1024.402 | 19392.15 | 19770.96 |
| 25.1   | 4621  | 50153   | 691.6949  | 695.1959 | 17361.54 | 17449.42 |
| 31.1   | 3541  | 53694   | 477.8358  | 499.0876 | 14860.69 | 15521.62 |
| 38.5   | 2862  | 56556   | 370.5797  | 368.052  | 14267.32 | 14170    |
| 44.9   | 2252  | 58808   | 355.2586  | 356.0395 | 15951.11 | 15986.17 |
| 50.1   | 1869  | 60677   | 320.5556  | 323.3318 | 16059.83 | 16198.92 |
| 55.7   | 1593  | 62270   | 161.8235  | 224.2197 | 9013.571 | 12489.04 |
| 67.1   | 1158  | 63428   | 115.7368  | 122.8158 | 7765.942 | 8240.939 |
| 74.7   | 1041  | 64469   | 945.2757  | 54.7368  |          |          |

Table 5.3 Derivative of Production Data from Golan Reference

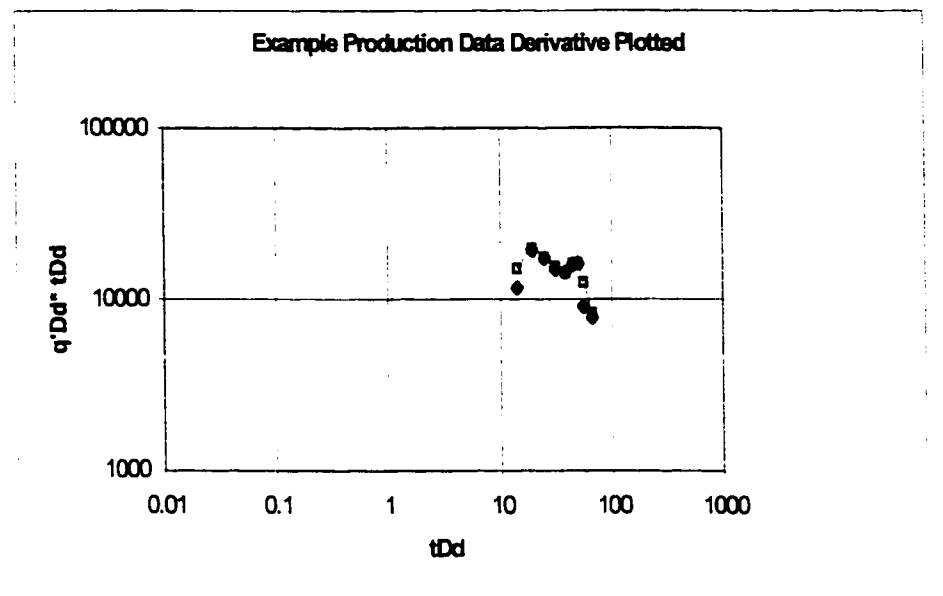


**Figure 5.16 Example Production Data-Derivative Method**

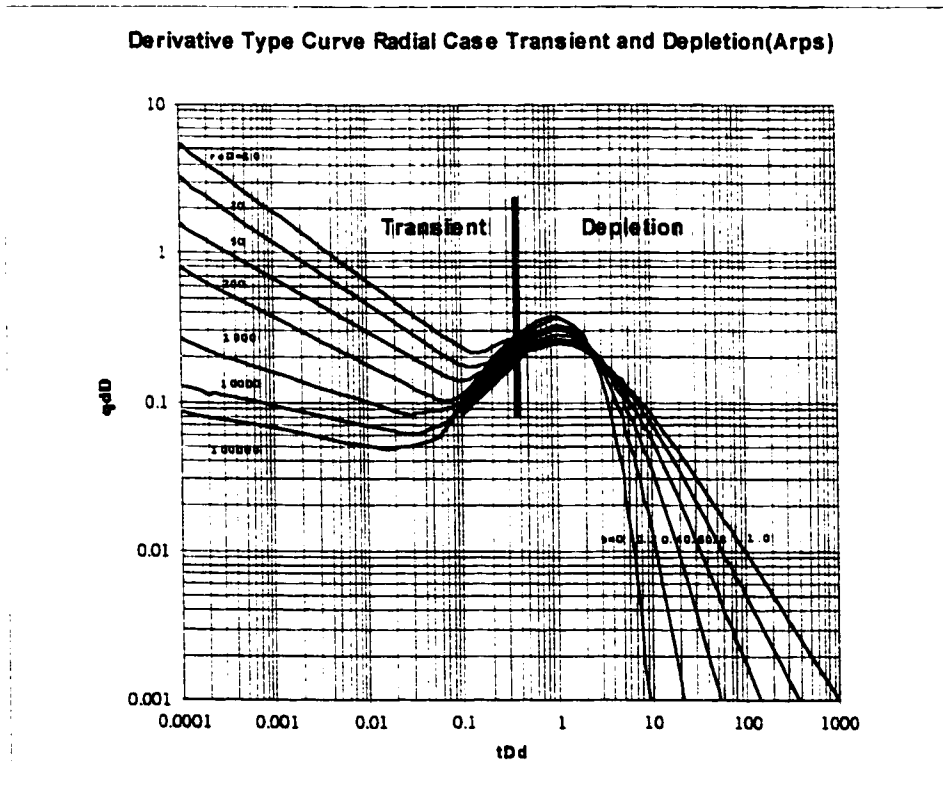


**Figure 5.17 Dimensionless Decline Derivative Type Curve**

The hope is that the derivative of the production data will help the user pick the appropriate “Arps b” value and the appropriate  $r_{eD}$  or  $A/r_w^2$  term to be used in the analysis of reservoir parameters and production forecasting. An examination of the plot of the production derivative shows the same general curvature of the type curve but there is not sufficient data to really help in the transient portion of the curve. Therefore the usefulness in picking the reservoir radius is limited. If early production data can be obtained then this method should help.

## **5.8 Chapter Summary**

This chapter and associated appendices provide one of the most comprehensive treatments of decline curve construction and use available. Compete theory, methodology and tabular data are provided for both Fetkovich type curves construction, extensions of type curve to all reservoir shapes and well positions as well as derivative type curves. These concepts will be extended to the analysis of horizontal wells in the next few chapters.

## CHAPTER SIX

### Horizontal Wells

#### 6.1 Various Horizontal Well Analytical Equations

There are three popular PSS equations for horizontal well flow. These methods are summarized in the following sub-sections.

##### 6.1.1 Method One: Infinite Conductivity Fracture Method

The method, introduced by Mutalik, Joshi et al<sup>27</sup> assumes that a horizontal well is equivalent to an infinite conductivity fracture. The proposed equation is an extension of fractured vertical well theory. Mutalik et al's equation for flow during pseudosteady state conditions is expressed as:

$$q = \frac{0.007078 k_h h (\bar{P}_R - P_{wf})}{\mu_o B_o \left( \ln \frac{r_e}{r_w} - A' + s_f + s_m + s_{CA,h} - c' + Dq \right)} \quad 6.1$$

Where:

$$r_e = \sqrt{\frac{A * 43560}{\pi}} \quad 6.2$$

and

|            |   |  |
|------------|---|--|
| $S_m$      | = | mechanical skin factor, dimensionless  |
| $S_f$      | = | - $\ln[L/(4r_w)]$ = negative skin factor of an infinite conductivity fully penetrating fracture of length L. |
| $S_{CA,h}$ | = | shape related skin factor  |
| $c'$       | = | shape factor conversion constant = 1.386   |
| $A'$       | = | 0.75 for circular drainage areas   |
|            | = | 0.738 for rectangular areas  |
| $D_q$      | = | Near well turbulence factor  |

The skin factor  $S_{CA,h}$  is determined from published charts such as shown in Joshi's Horizontal Well Technology book<sup>23</sup> (figures 7-5 to 7-7) for centrally located wells within drainage areas based on the ratios of  $2x_e/2y_e$  for each particular case. The Mutualik method gives the highest flow rates of the three published methods.

Again  $k_h$  is always in the formula and is assumed to be represented by the geometric mean of permeability in the principle x and y directions. The analytic equation would thus predict that no matter what the contrast between  $k_x$  and  $k_y$ , the solution should remain constant as long as the square root of  $k_x k_y$  is the same and all other parameters remain constant as shown before. This is probably only the case when the horizontal well is small compared to the reservoir dimensions. The skin factor for shape considerations,  $S_{CA,h}$ , only accounts for variations in vertical versus horizontal permeability. It does not account for average directional horizontal permeability,  $k_h$ , variations.

### 6.1.2 Method Two – Kuchuk Method

Another method, proposed by Kuchuk et al<sup>28</sup> used the approximate infinite conductivity solution where constant wellbore pressure is obtained by averaging pressure values of the uniform flux solution along the well length. This equation gives the lowest flow rates of the various methods. The term  $B_o$  was left off the equation in the literature but it has been added to the equation below to convert the flow to surface conditions for proper comparison. These authors present the following equation to describe single-phase flow in a horizontal

$$q_h = \frac{(P_R - P_{wf})k_h h}{70.6 B_o \mu_o \left( F + \frac{h}{0.5L} \sqrt{\frac{k_h}{k_v}} s_x \right)} \quad 6.3$$

well.

Charts such as Table 7-6 in Joshi's book give the  $F$  term.  $F$  is dependent on  $y_w/2y_c$ ,  $x_w/2x_c$ ,  $L/4x_c$ , and  $(y_c/x_c)^*$   $\text{sqrt}(k_x/k_y)$ .  $z_w$ ,  $y_w$  and  $x_w$  are the distances from the center of the horizontal well to the boundaries of the reservoir in the  $z$ ,  $y$ , and  $x$  directions respectively. The  $s_x$  term is calculated with the following equation.

$$s_x = \ln \left[ \left( \frac{\pi r_w}{h} \right) \left( 1 + \sqrt{\frac{k_v}{k_h}} \right) \sin \left( \frac{\pi z_w}{h} \right) \right] - \sqrt{\frac{k_h}{k_v}} \left( \frac{2h}{L} \right) \left[ \frac{1}{3} - \frac{z_w}{h} + \left( \frac{z_w}{h} \right)^2 \right] \quad 6.4$$

Again  $k_h$  and  $k_v$  are considered but not variations in  $k_x$  and  $k_y$  other than geometrical averaging of  $k_x$  and  $k_y$  for  $k_h$ . This method seems especially poor at predicting rates above the bubble point for some reason.

### 6.1.3 Method Three

Another method was presented by Babu and Odeh<sup>29</sup> which is based on a partially penetrating vertical well-turned sideways. This method yields flow rate results in between the Mutualik-Joshi and Kuchuk methods.

Babu and Odeh's<sup>29</sup> equation is expressed as:

$$q = \frac{.007078(2X_e)\sqrt{k_y k_v(P_R - P_{wf})}}{B_o \mu_o \ln(\sqrt{A} / r_w) + \ln C_H - 0.75 + s_R} \quad 6.5$$

$C_H$  is the geometric shape factor given as:

$$\ln C_H = 6.28 \left( \frac{2y_e}{h} \right) \sqrt{\frac{k_v}{k_y}} \left[ \frac{1}{3} - \left( \frac{y_w}{2y_e} \right) + \left( \frac{y_w}{2y_e} \right)^2 \right] \cdot \ln \left[ \sin \left( 180 \frac{z_w}{h} \right) \right] - 0.5 \ln \left[ \left( 2 \frac{y_e}{h} \right) \sqrt{\frac{k_v}{k_y}} \right] - 1.088 \quad 6.6$$

$S_R$  is the skin factor attributable to partial penetration.  $S_R$  will be zero when  $L = 2x_e$  i.e. fully penetrating horizontal well. If  $L < 2x_e$  then the value depends on the two conditions:

Case 1:

$$2 \frac{y_e}{\sqrt{k_y}} \geq 1.5 \frac{x_e}{\sqrt{k_x}} \ll 0.75 \frac{h}{\sqrt{k_v}} \quad 6.7$$

Case 2:

$$2 \frac{x_e}{\sqrt{k_x}} \geq 2.66 \frac{y_e}{\sqrt{k_y}} \ll 1.33 \frac{h}{\sqrt{k_v}} \quad 6.8$$

Case 1

$$S_R = PXYZ + PXY'$$

PXYZ is given by:

$$PXYZ = \left[ 2 \frac{x_e}{L} - 1 \left[ \ln\left(\frac{h}{r_w}\right) + 0.25 \ln\left(\frac{k_y}{k_v}\right) - \ln\left(\sin \frac{180^\circ z_w}{h}\right) - 1.84 \right] \right] \quad 6.9$$

The PXY' component is given by:

$$PXY' = \left( \frac{2(2x_e)^2}{Lh} \sqrt{\frac{k_v}{k_x}} \right) [f(x) + 0.5[f(y_1) - f(y_2)]] \quad 6.10$$

$x_w$  is the distance from the horizontal well mid point to the closest boundary in the x direction.

Pressure computations are made at the mid point along the well length.

$$x = \frac{L}{4x_e} \quad y_1 = \frac{4x_w + L}{4x_e} \quad y_2 = \frac{4x_w - L}{4x_e}$$

$$f(x) = -x[0.145 + \ln(x) - 0.137(x)^2] \quad 6.11$$

$$f(y) = (2-y)[0.145 + \ln(2-y) - 0.137(2-y)^2] \quad 6.12$$

where  $y = y_1$  or  $y_2$

Case 2:

$$SR = PXYZ + PY + PXY \quad 6.13$$

PXYZ is calculated as above while PY comes from the relation:

$$PY = 6.28 \frac{(2x_e)^2 \sqrt{k_y k_v}}{2y_e h} \left[ \left( \frac{1}{3} - \left( \frac{x_w}{2x_e} \right) + \left( \frac{x_w}{2x_e} \right)^2 \right) + \frac{L}{48x_e} \left( \frac{L}{2x_e} - 3 \right) \right] \quad 6.14$$

$x_w$  is the mid-point coordinate of the well. PXY is:

$$PXY = \left( \frac{2x_e}{L} - 1 \right) \frac{6.28(2y_e)}{h} \sqrt{\frac{k_v}{k_y}} \left[ \frac{1}{3} - \left( \frac{y_w}{2y_e} \right) + \left( \frac{y_w}{2y_e} \right)^2 \right] \quad 6.15$$

$$\text{For } [\text{Min}\{y_w, (2y_e - y_w)\}] = 0.5y_e$$

This method is predicated on the assumption that a “fully penetrating horizontal well should be identical in behavior to a fully penetrating vertical well, provided that the drainage volumes are similar and it is recognized that the horizontal well is parallel in the y direction while the vertical well is parallel to the z direction”<sup>29</sup>. This basic assumption has been bothersome for several reasons as indicated in the following paragraph.

To test the assumption of this method, a comparison was made of the simulated results of a vertical well model to the equivalent horizontal model of the vertical well turned sideways. As suspected the results were not identical. Figure 6.1 illustrates the models used in the validation and comparison experiment. Figure 6.2 shows the comparison of the two cases. In general the equivalent horizontal well gave higher simulated flow results. Variations of pressure with depth were purposely omitted in the experiment, as this would make the

difference even larger than observed in thick formations. According to the Babu and Odeh's<sup>29</sup> publication, they only tested the validity of the equivalency of a vertical well turned sideways in the transient regime.

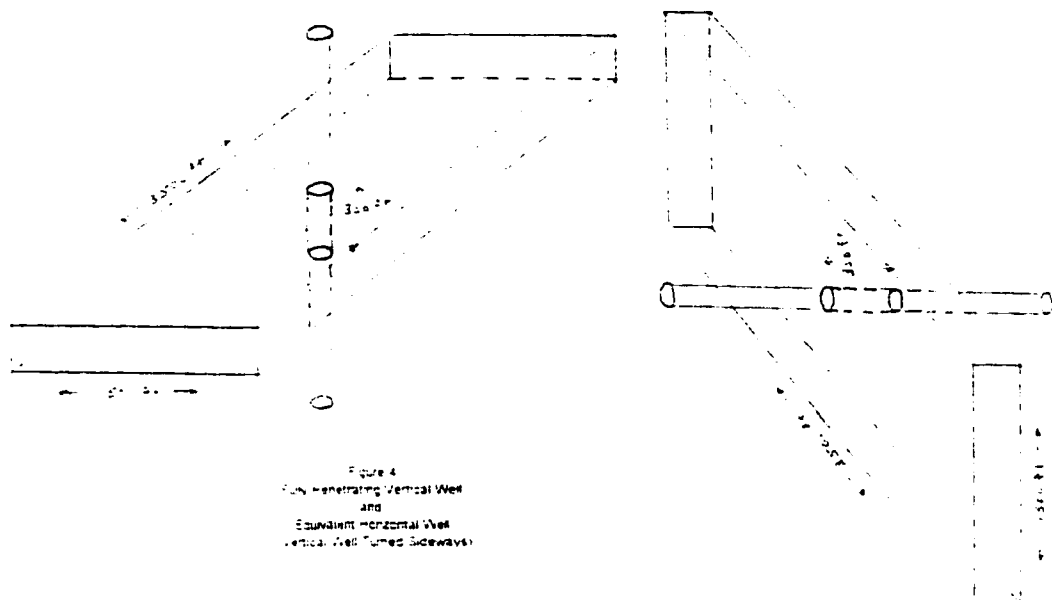


**Figure 6.1 Schematic Diagram of Fully Penetrating Vertical Well versus Equivalent Horizontal Well**

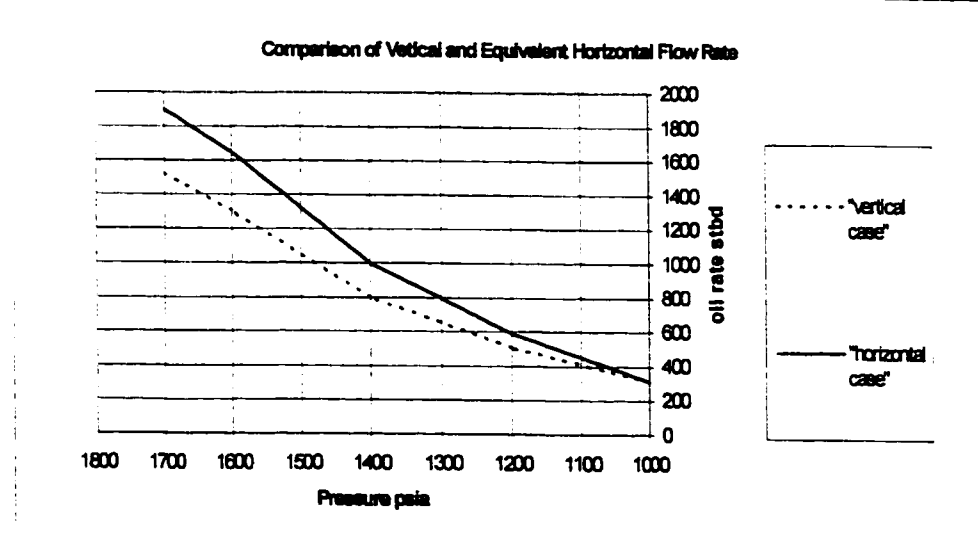


**Figure 6.2 Comparison of Simulated Vertical and Equivalent Horizontal Flow Rates**

This basic assumption of the Babu and Odeh<sup>29</sup> method may not be valid for several reasons. First, the condition of equal drainage volumes does not seem sufficient. The drainage shape and dimensions would also have to be the same. When a vertical well is turned sideways the reservoir is then very thin horizontally compared to the vertical dimension and severe boundary effects may result. Generally a reservoir is thin compared to its horizontal areal size. If a vertical well is turned sideways then the dimensions in the y and z directions are then distorted compared to the x direction (parallel to the well). Second there are basic pressure differences to take into account. The pressure differences of a vertical versus horizontal slice can be different depending on the formation thickness. Third, there are gravity considerations.

The Babu and Odeh method is also very cumbersome to use. If analytical methods of accounting for horizontal permeability contrasts and situations below the bubble point could be adapted to vertical style methods then a easy and more accurate predictive model might result that could be used to verify, calibrate and validate simulation output.

## **6.2 Alternative Method Using Effective Wellbore Radius Concept**

A horizontal well should be capable of being modeled in terms of familiar vertical equations by the introduction of an equivalent wellbore radius concept. The derivation of the effective radius of a horizontal well as adapted from Joshi<sup>30,32</sup> is shown in appendix F. It will then be shown that the use of the equivalent well bore radius  $r_w$  in vertical style equations, modified

for incorporation of solution gas cases below the bubble point, is not only easier to use but is also accurate and thus useful in validating simulation models and simulation output.

The equivalent well bore radius of a horizontal well in comparison to a vertical well is expressed as:

$$r_w = \frac{0.5r_{eh}L}{a \left[ 1 + \sqrt{1 - \left[ \frac{L}{2a} \right]^2} \right] \left[ \frac{\beta h}{2r_w} \right]^{\frac{h}{L}}} \quad 6.16$$

where a is defined as:

$$a = 0.5L \left[ 0.5 + \sqrt{0.25 + \left( \frac{2r_{eh}}{L} \right)^4} \right]^{\frac{1}{2}} \quad 6.17$$

And

$$\beta = \left( \frac{k_h}{k_v} \right)^{\frac{1}{2}}, \quad r_{eh} = \sqrt{\frac{A}{\pi}} \quad 6.18$$

Where A is in square feet. In a homogeneous reservoir the  $\beta$  term is unity and the apparent well bore radius expression reduces to:

$$r_w = \frac{0.5r_{eh}L}{a \left[ 1 + \sqrt{1 - \left[ \frac{L}{2a} \right]^2} \right] \left[ \frac{h}{2r_w} \right]^{\frac{h}{L}}} \quad 6.19$$

Therefore the equation for the horizontal well would then reduce to:

$$q = \frac{0.007078 k_h h (\overline{P_R} - P_{wf})}{\mu_o B_o \left( \ln \frac{r_e}{r_w} - 0.75 \right)} \quad 6.20$$

Where  $r_w$  is defined above and  $k_{eh}$  is as usual the geometric mean of the permeability in the principle x and y directions. As shown in chapter 3 this equation can be converted to a 2-phase flow estimate by estimating and incorporating the mobility as a function of pressure and average saturation. Thus the generalized multi-phase equation approximation for a horizontal flow in terms of equivalent vertical well parameters should be:

$$q = \frac{0.007078 k_h h (\overline{P_R} - P_{wf})}{\left( \ln \frac{r_e}{r_w} - 0.75 \right)} \left( \frac{k_{ro}}{\mu_o B_o} \right)_{P_{ave}} \quad 6.21$$

The other three published methods can also be modified to incorporate the 2 phase flow characteristics. As a validation check of this modification experimental comparisons will be shown as done previously for the vertical well case. The next section will detail validation comparisons for the isotropic results followed by an application to anisotropic cases.

### 6.3 Demonstration of Validity of 2-phase Horizontal Well Approximations

As a test of the validity and accuracy of these published equations and as a test of the more usable equivalent wellbore radius concept, simulation tests were conducted using horizontal wells in isotropic media compared to the analytical equations. Later anisotropic cases will be presented. Simulated results of each anisotropic model were compared with one another and

the 2-phase analytical results were then compared to simulated results. It is important to note that the  $k_h$  in the above equations is the absolute horizontal permeability, which must be multiplied by the relative permeability to the desired phase such as oil in this case. Therefore in equations 6.20 and 6.21, for instance,  $k_h$  would be multiplied by  $k_{ro}$  at each oil saturation point if the flow rate for oil is desired and by  $1/(\mu_o B_o)$  and average reservoir pressures as demonstrated previously for the vertical comparisons. This has been done in the analysis but is never presented or addressed in the various papers.

For this project, a test was conducted to see if these saturation and pressure averaged mobility functions would work as well with both vertical and horizontal wells. If the averaging process works as well for horizontal well conditions as it did for vertical wells then it will be easier to perform some other tests on absolute permeability anisotropy and extensions to decline analysis.

### 6.3.1 Validation Model Results and Discussion

The basic model parameters for horizontal test cases are given in Appendix E. Vertical permeability is 0.1 md in all cases. The average effective horizontal permeability in all cases is 3.1 md. A 15 by 17 by 3-grid block model was used for the horizontal cases. Three models were tested. The first model depicts the isotropic model of constant permeability in both x and y direction ( $k_x=k_y=3.1$  md). Models 2 and 3 are the cases in which  $k_y=9.61$ ,  $k_x=1.0$  md and  $k_y=19.22$ ,  $k_x=0.5$  md but the average horizontal permeability was still 3.1 md ( $\sqrt{(k_x k_y)}$ ) in all cases. The averaging process is desirable because it is so easy to evaluate in a spreadsheet.

Typical simulators give tabular output that can be imported to spreadsheets and averaged over gridblocks in a single operation. Typical simulation output was previously shown in Tables 3.2, 3.3.

Figures 6.3 through 6.5 show the oil rate vs. average pressure plot with the above model. Figure 6.3 is a comparison of the isotropic permeability case ( $k_x=k_y=3.1 \text{ md}$ ) compared to the various 2-phase analytical equations presented in section 6.2 of this chapter. There are several things to note. First of all the match between the simulated output for the isotropic case of constant x and y permeability and the analytical results is not quite as good as with a vertical well for several of the methods. Note however that the equivalent wellbore radius incorporation using the 2-phase adaptation is one of the best matches to the simulated results. This is very important because it validates the idea that the equivalent wellbore 2-phase analytical equations are reasonable approximations to actual reservoir performance. And because the equivalent wellbore concept is in terms of vertical well terminology and conventions it is immediately applicable to decline analysis as will be shown in chapter 7. In fact the equivalent wellbore radius concept will be shown to also give superior results to the other methods in the case of anisotropic media.

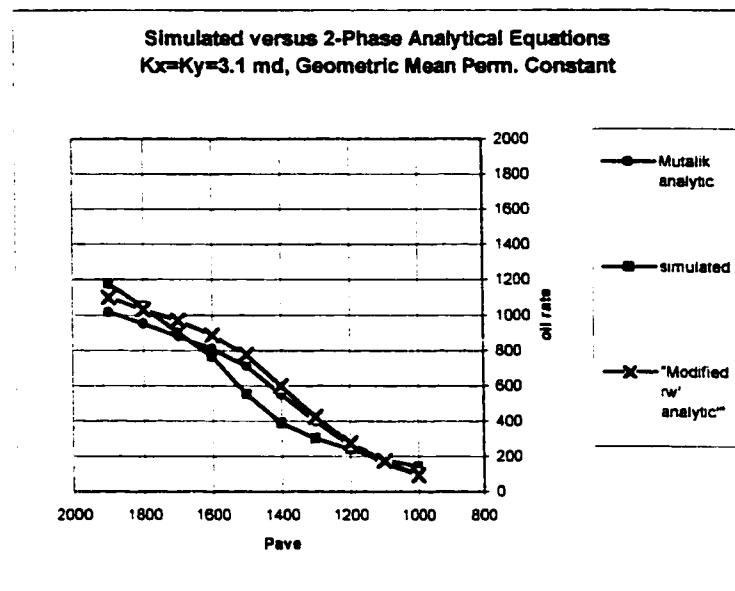


**Figure 6.3 Simulated versus 2-Phase Analytical Equations  $k_x=k_y=3.1$  md, Geometric Mean Permeability Constant**

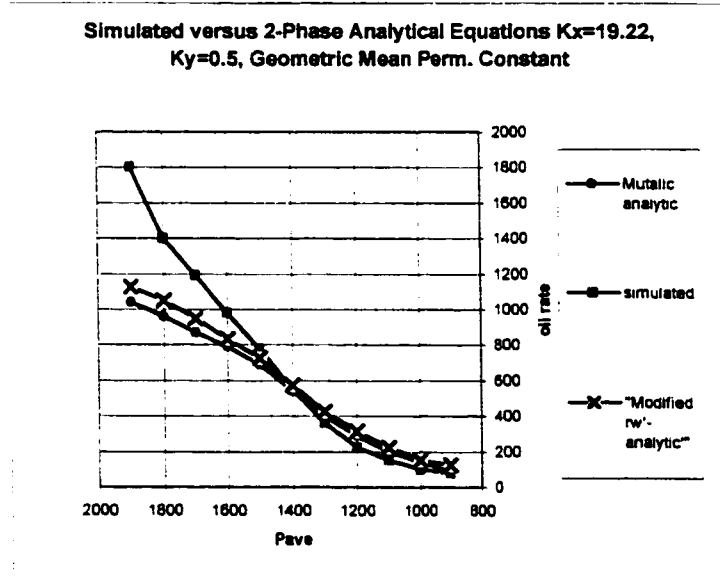


**Figure 6.4 Simulated versus 2-Phase Analytical Equations  $k_x=19.22$ ,  $k_y=1$ , Geometric Mean Permeability Constant**

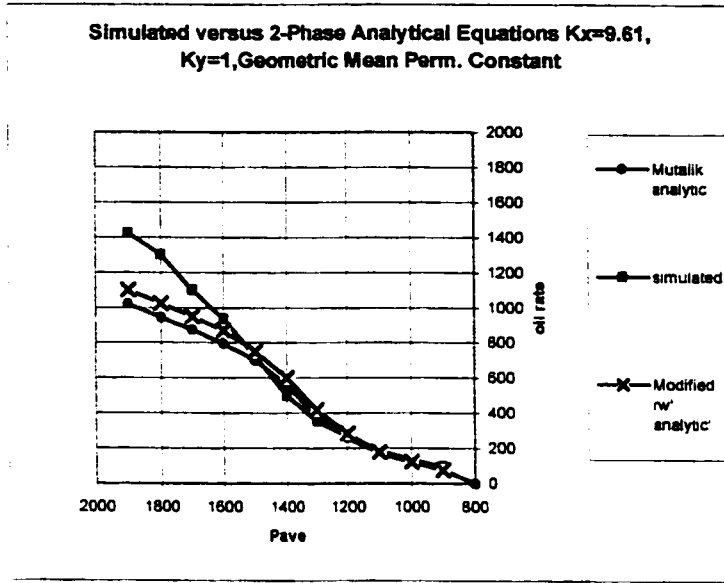


**Figure 6.5 Simulated versus 2-Phase Analytical Equations  $k_x=9.61$ ,  $k_y=1.0$ , Geometric Mean Permeability Constant**

#### 6.4 Analysis of Analytical and Simulated Pseudosteady State Flow Equations for Horizontal Wells in Anisotropic media.

As mentioned in chapter 3, vertical well-modified 2-phase analytical solutions match simulated results quite well for fluid flow in both isotropic and highly anisotropic media above and below the bubble point. This showed that no matter what the contrast in  $k_x$  and  $k_y$ , the simulated rate vs. pressure results were essentially identical. Also the analytical computations were shown to be good estimates of simulated results. In contrast, analytical solutions to horizontal well flow generally follow simulated solutions in isotropic media but do not match simulated horizontal results very well in horizontally anisotropic media. The mismatch is especially pronounced above the bubble point. What

is the cause of this phenomenon and what can be done to improve the match? Let's first look at the results and see what we can observe.

#### 6.4.1 Anisotropic Experimental Results and Observations

Simulation experiments indicate that published analytical solutions to horizontal well inflow at least track simulated results in cases of isotropic permeability (again above and below the bubble point) (figure 6.3) but they do not match simulated horizontal results as well in cases of horizontally anisotropic permeability. Figures 6.3-6.5 illustrate the comparison of three horizontal permeability cases (single layer model) each with a geometric average of 3.1 m.d. but with varying degrees of anisotropy. Figure 6.4 shows the comparison with simulated  $k_x=9.61$  md,  $k_y=1$  while figure 6.5 shows output for the case of  $k_x=19.22$ ,  $k_y=0.5$ . Each case has the same geometric mean permeability. If  $k_y$  is set to a constant 9.61 md and  $k_x$  to 1.0 md, the match is very poor even though the horizontal average permeability remains at 3.1 md. The deviation between the simulation case and analytical results is even greater if  $k_y$  is magnified to 19.22 md vs.  $k_x=0.5$  while keeping  $k_{eh}$  equal to 3.1. Therefore the traditional use of a geometric average of  $k_x$  and  $k_y$  for the effective horizontal permeability is not a good approximation for the horizontal well at least when the wellbore is long in comparison the reservoir dimensions and the maximum grid block number is limited. Since no other parameters have been changed between models, the difference must be in the way  $k_{eh}$  is calculated for horizontal wells in the simulation or in some type of numerical or boundary effects due to model design. These are compared with two popular analytic prediction

methods discussed earlier in this chapter as well as the modified equivalent wellbore radius method presented in this chapter. Notice also in figure 6.6 that in each case, the simulated horizontal flow rates increase with increasing permeability perpendicular to the well bore despite constant horizontal geometric mean permeability. Theory would predict that anisotropy would not affect results as long and the geometric mean permeability remained constant. There are then two questions to answer. 1) Why do the analytical and simulated results vary and 2) why do the simulated results themselves vary when theory would predict that the permeability contrast would not affect results?

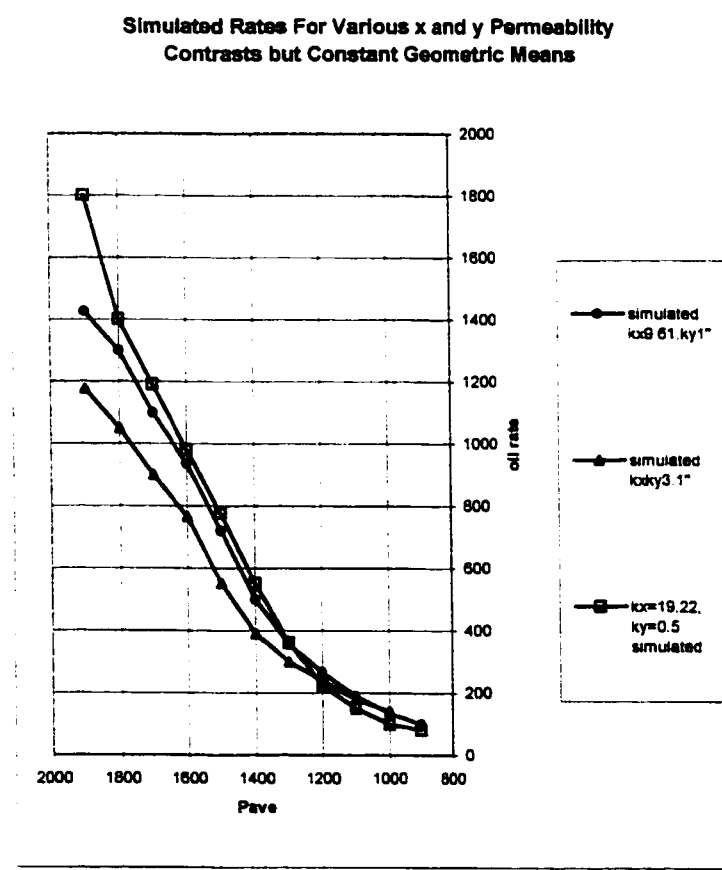


**Figure 6.6 Simulated Rates For Various x and y Permeability Contrasts but Constant Geometric Means**

#### **6.4.2 Anisotropic Behavior Possibilities**

As in the vertical well situation, each horizontal well analytical method requires the use of effective horizontal permeability,  $k_h$ , in the calculation. Perhaps one of the problems is a misconception as to what effective horizontal permeability is to a horizontal well. Other possible explanations include the need to include more reservoir blocks in the vicinity of the wellbore and boundary effects when the well is close to the reservoir edge.

If the reservoir is semi-infinite, no other wells compete for drainage area, and the reservoir is thick, then the geometric average of permeability may work satisfactorily. The horizontal well would then appear small compared to the reservoir as a whole and the geometric average would give proper results. This is almost never the case in reality. In practice, reservoirs are limited, compete for drainage area, and are anisotropic. The discrepancy in flow predictions may be a function of well length, degree of penetration, permeability contrast, distance to the reservoir boundaries and number of simulation blocks. This also demonstrates the usefulness of the 2-phase analytical approximations presented in this work as they help to validate simulation model parameters.

All published horizontal well inflow solutions use the geometric average for effective horizontal permeability. If the reservoir is very large compared to the horizontal well length, and the reservoir is isotropic, then the geometric average can be used. In simulation experiments, as the permeability perpendicular to the horizontal well increases over the

permeability parallel to the well bore, keeping the square root of  $k_x k_y$  constant, the simulated flow rates increase dramatically while the analytical flow rate predictions remain fairly constant depending on the analytical method used. Simulation experiments were conducted to see if this discrepancy appears to be a function of primarily the x, y and z directional permeability contrast, the length of the horizontal well, the distance from the well to the reservoir boundaries and possibly other parameters such as grid size and number of grids in the model.

#### **6.4.3 Background Theory into Effective Horizontal Permeability**

In naturally fractured wells, the permeability along the fracture trend is larger than the direction perpendicular to the fractures. As such, a vertical well would drain more length along the fracture trend. Assuming a single phase, steady state flow, one can write the following equation.

$$\frac{\partial}{\partial x} \left( k_x \frac{\partial p}{\partial x} \right) + \frac{\partial}{\partial y} \left( k_y \frac{\partial p}{\partial y} \right) = 0 \quad 6.22$$

Assuming non-variant values of  $k_x$  and  $k_y$  in the principal x and y directions one can rewrite the equation as:

$$k_x \frac{\partial^2 p}{\partial x^2} + k_y \frac{\partial^2 p}{\partial y^2} = 0 \quad 6.23$$

and multiplying and dividing throughout by  $\sqrt{(k_x k_y)}$  the equation can be rewritten as:

$$\sqrt{k_x k_y} \left[ \sqrt{\frac{k_x}{k_y}} \frac{\partial^2 p}{\partial x^2} + \sqrt{\frac{k_y}{k_x}} \frac{\partial^2 p}{\partial y^2} \right] = 0 \quad 6.24$$

Which can be rearranged and transformed as follows:

$$\sqrt{k_x k_y} \left[ \frac{\partial^2 p}{\partial x^2} + \frac{\partial^2 p}{\partial y^2} \right] = 0 \quad 6.25$$

where:

$$y' = y \sqrt{\frac{k_x}{k_y}} \quad 6.26$$

Therefore in an anisotropic reservoir the effective horizontal permeability would be  $\sqrt{(k_x k_y)}$  and the drainage length along the high permeability side is  $\sqrt{(k_x/k_y)}$  times the length along the low permeability side. Thus if the permeability along the fracture trend is 16 times greater than that perpendicular to the trend then the drainage length along the fracture trend is four times larger than the length perpendicular to the fracture trend.

A horizontal well drilled along the low permeability direction has the potential to drain a significantly larger area than a vertical well, resulting in a larger reserve for horizontal wells versus vertical wells. Now so far the above discussion concerns only a vertical well in anisotropic media. There is limited data for fractured vertical wells with which to calculate the time to reach pseudo-steady state. Horizontal well data are also not extensive.

## 6.5 Need to Re-Consider Effective Horizontal Permeability in Limited Reservoirs

Due to the longer well length, a horizontal well would drain a larger reservoir area than a vertical well within a given specific time interval. If a vertical well drains a certain reservoir volume in a given time then that information can be used to calculate a horizontal well drainage area. A horizontal well can be looked at as a number of vertical wells drilled in succession. However unless the reservoir is very large compared to the horizontal well length a distortion may be introduced into the effective horizontal permeability that is not captured in the shape factor alone. As noted in the preceding sections, all horizontal well flow equations assume the square root effective horizontal permeability concept. Various shape and pseudo-skin factors have been developed to account for variations in reservoir shape, well penetration ratios and dimensionless well length but no studies have been performed to investigate the effect of contrasts in  $k_x$  and  $k_y$  on flow rates versus pressure. This is because it has been assumed that the effective horizontal permeability can be adequately described by the square root of permeability in the principle x and y directions.

This simple geometric average of permeability alone does not appear to work well for horizontal wells in simulation experiments involving Boast reservoir simulator. This is not just related to a shape factor to account for the degree of penetration of the horizontal well relative to the reservoir dimension. For instance Earlougher<sup>22</sup> published shape factors for vertically fractured wells with different ratios of the fracture length  $x_f$  relative to the length of the reservoir in the direction parallel to the fracture. If the ratio of  $x_f$  to  $x_e$  was 0.5 (i.e. the

fracture was half as long as the reservoir length parallel to the fracture) then the  $C_A$  factor in the equation was 1.662 compared to 2.654 when the fracture was very short and  $x_f/x_e$  was 0.1. This would also be the case with the horizontal well where the length varied in comparison to the reservoir  $x$  dimension. However given a certain well or fracture length which would still yield a certain shape factor, the equations would all predict a certain constant behavior irrespective of the contrast in  $k_x$  and  $k_y$  as long as the square root of the product was constant. Likewise Joshi<sup>23</sup> published various shape and skin factors (page 217-219) for use in the traditional horizontal well flow rate equations. However all methods assume horizontal permeability is the square root of  $x$  and  $y$  permeability.

As previously shown, a reasonable match was obtained between analytical published equations modified by using the modified 2-phase equivalent wellbore radius approximation and simulated results for isotropic permeability. Theoretically equation 6.16 can be used for horizontal wells in both anisotropic and isotropic media. The only difference would be the deletion of the beta term in equation 6.16 for the isotropic case. However inspection of the beta term shows that this term is only introducing variations in the ratio of vertical to horizontal permeability. It does not account for variations in  $k_x$  and  $k_y$  distributions. As long as the effective horizontal permeability given by the square root of  $k_x k_y$  is the same, the analytical results predict no change in flow rate with anisotropy. Clearly this is not always the case in reality. The beta term in the equation and the skin factors in the other methods only address the ratio of vertical and horizontal anisotropy, not the issue of horizontal anisotropy itself. The use of skin factors and Kuchuk's equation yield even worse results.

Simulation results indicate that a simple geometric averaging of x and y permeability does not suffice in the case of a horizontal well.

Notice in the various experiments that as the contrast in x and y permeability was increased (geometric mean constant), the flow rates diverged significantly, especially at higher pressures above the bubble point. This was perplexing and deserved further investigation. Intuition would also indicate that high permeability perpendicular to the horizontal wellbore would yield higher flow rates than equal but lower permeability in both directions. In other words if  $k_x=9.61$  md perpendicular to the wellbore and  $k_y=1$  md parallel to the wellbore one might intuitively expect higher flow rates than if  $k_x=k_y=3.1$  md even though both cases give the same geometric mean  $k_h$  of 3.1 md. But analytical equations predict the same productivity no matter what the values of  $k_x$  and  $k_y$  as long as the square root of the product of  $k_xk_y$  is the same.

There were several hypotheses to explain this divergence in flow rate versus average reservoir pressure. First it was thought that perhaps not enough grid blocks were used to define the model. Secondly perhaps distortion was introduced when the well penetration was long compared to the reservoir dimensions. In other words if the well length was insignificant compared to the horizontal dimensions then perhaps the deviation would disappear. Thirdly perhaps the simulator itself is not designed properly to account for such variations. It was not possible to test the third possibility since no access to other simulators was possible but such a comparison should be made to determine if this is a simulator artifact.

## **6.5 Experimental Results and Observations of Variations in Simulated Output in Cases of Variable Horizontal Permeability Components**

This phenomenon was first observed while preparing a class project in 1995. Though a class project paper was written on the subject the paper generated no real interest and it was uncertain what the results really meant. For the past four years the subject has periodically resurfaced in this research and since no flaws are apparent in the observation, the experimental analysis continued. As a test of the above theory that additional skin factors are needed to account for horizontal anisotropy, scores of simulation experiments were conducted in which the grid blocks, well length and, reservoir size was varied versus contrasts in x and y directional permeability. If the simulated results match analytical results in isotropic media as grids become more numerous then it will be apparent that the explanation lies only in the simulation model itself. The geometric mean would then be validated and discrepancies will be explained by simulation limitations. If this is not the case other explanations must be considered. The "quick-look" 2-phase approximations are used to check results.

### **6.6.1 Experiments**

The first hypothesis tested was the effect of the number and size of the grid blocks used. Boast is limited to 810 grid blocks but this should be sufficient to test the hypothesis. Reservoirs ranging from as small as 0.8 square miles up to 3.6 square miles were tested using various permeability contrasts and well lengths ranging from 400 to 1000 feet ( $L/X_e$  ratios from 10 up to 50,  $L/X_e = 0.02$  to 0.1). Details of the experimental parameters are available

from the author. The complete experimental output files are available for inspection and use by the reader however they are too voluminous to include in this document. The following sections summarize some of the findings from those studies.

### 6.6.2 Effect of Grid Number

The first thing to note is that as the contrast in  $k_x$  and  $k_y$  becomes more pronounced, the deviation from the isotropic case becomes more pronounced. However the effect of the number of grid blocks is relatively minor. Figures 6.7 through 6.9 show the effect of variations in the # of grid block with increasing contrast in  $k_x$  and  $k_y$  (geometric mean constant).

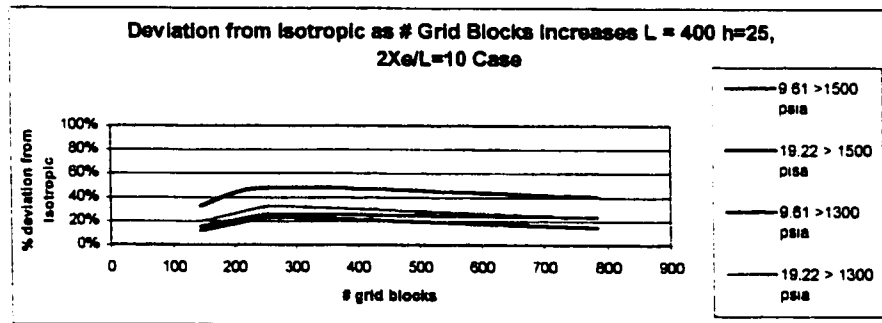
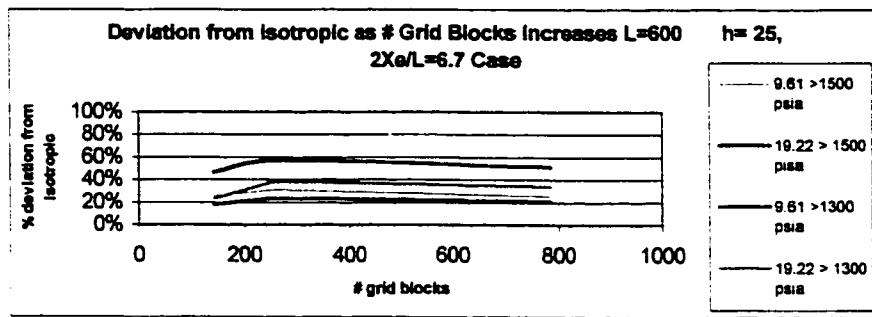
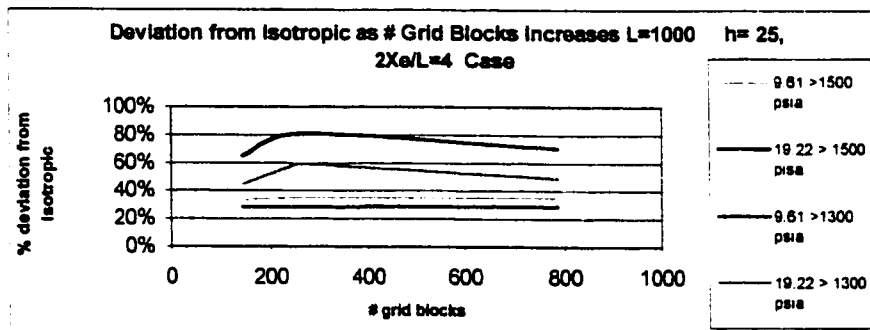


Figure 6.7 Deviation from Isotropic as # Grid Blocks Increases L = 400 h=25, 2Xe/L=10 Case, Geometric Mean  $k_x k_y$  Constant.



**Figure 6.8 Deviation from Isotropic as # Grid Blocks Increases L=600 h= 25, 2Xe/L=6.7 Case Geometric Mean  $k_x, k_y$  Constant.**



**Figure 6.9 Deviation from Isotropic as # Grid Blocks Increases L=1000 h= 25, 2Xe/L=4 Case Geometric Mean  $k_x, k_y$  Constant.**

Note that as the grid blocks increase, keeping the total model size constant, there is relatively little change in the average deviation from the isotropic case. Note also that the average deviation increases with increasing pressure but becomes less noticeable as the reservoir size increases relative to the well length. This can also be shown in the following figures 6.10 and 6.11 from one of the experiments.

**Figure 6.10 Variation in Rate-Pressure With Change in  $k_x/k_y$  Ratio, L=1000,  
 $2Xe/L=4$**

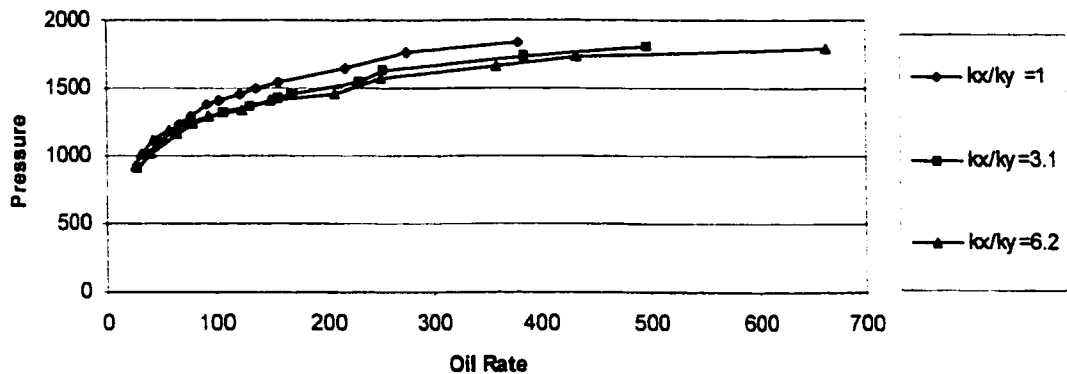


**Figure 6.10 Variation in Rate-Pressure With Change in  $k_x/k_y$  Ratio, L=1000,  $2Xe/L=4$**

**Figure 6.11 Variation in Rate-Pressure With Change in  $k_x/k_y$ , L=1000, h=100,  
 $2XeL=19$**

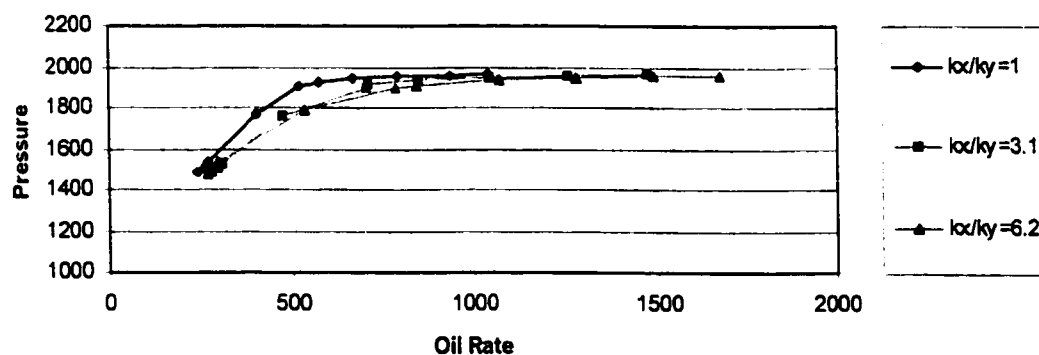


**Figure 6.11 Variation in Rate-Pressure With Change in  $k_x/k_y$ , L=1000, h=100,  $2Xe/L=19$**

The following plots also show that although the deviation from isotropic increases with increasing well length relative to the reservoir dimensions, the effect of grid size and number is relatively insignificant for any given well length or dimensionless well length.

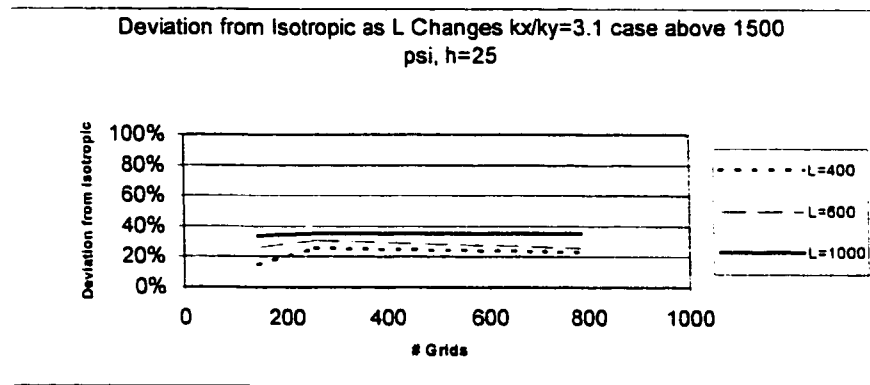


Figure 6.12 Deviation from Isotropic as L Changes  $k_x/k_y=3.1$  case above 1500 psi,  $h=25$

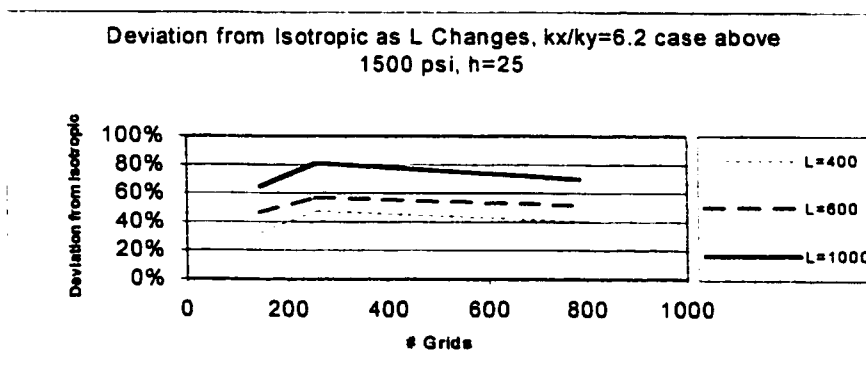


Figure 6.13 Deviation from Isotropic as L Changes,  $k_x/k_y=6.2$  case above 1500 psi,  $h=25$

Similar results can be shown for other cases of larger reservoir to well-length ratios. More complete results are available from the author. Since the effect of grid spacing and

number is inconsequential hypothesis one is rejected and the experiments focused on variations in well length and reservoir size.

### 6.6.3 Effect of Model Size and Penetration Ratios

Dimensionless well length  $L_D$  is defined as:

$$L_D = \frac{L}{2h} \sqrt{\frac{k_v}{k_h}} \quad 6.27$$

Where L is the horizontal well length and h is the reservoir thickness in feet.

Figures 6.7 through 6.13 demonstrated that although grid number is not that important, there is a general increase in divergence from the isotropic case as the permeability contrast increases and as the well length increases relative to the reservoir dimensions. This can be further demonstrated graphically by figures 6.14 through 6.15 which collectively show the deviation from isotropic for the smaller model where reservoir thickness is constant but the ratio of horizontal dimension to well length varies. These graphs show that for a given reservoir size, as the well length increases relative to the reservoir dimensions, the deviation in flow rates for a given pressure increasingly deviate from the isotropic case. It also shows the deviation is more pronounced as the anisotropy in  $k_x$  and  $k_y$  increases.

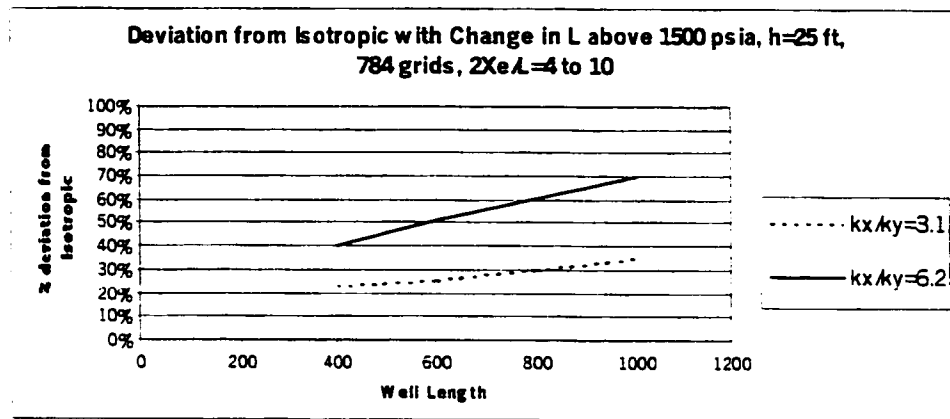


**Figure 6.14 Deviation from Isotropic with Change in L above 1500 psia,  
h=25 ft, 784 grids, 2Xe/L=4 to 10, Small Model**

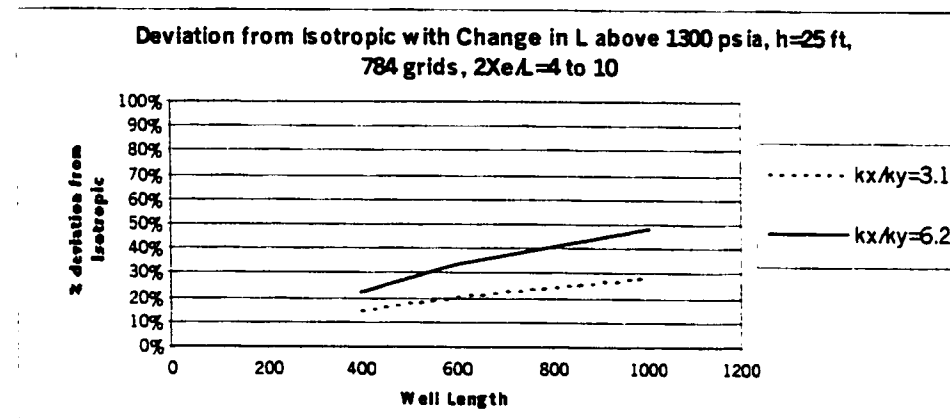


**Figure 6.15 Deviation from Isotropic with Change in L above 1300 psia,  
h=25 ft, 784 grids, 2Xe/L=4 to 10, Small Model**

Similarly, figures 6.16 and 6.17 show that as the reservoir thickness increases from 25 ft in the previous figures, keeping other parameters constant, the trend to increasing deviation from the isotropic is the same although the deviation magnitude decreases.

**Deviation from Isotropic with Change in L above 1500 psia,  $h=100$  ft, 784 grids,**

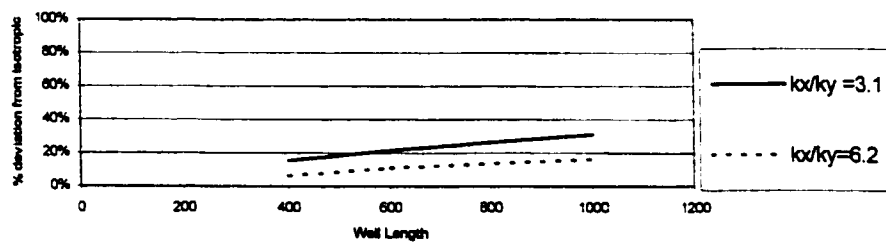


**Figure 6.16 Deviation from Isotropic with Change in L above 1500 psia,  $h=100$  ft, 784 grids,  $2X_e/L = 4$  to 10, Small Model**

**Deviation from Isotropic with Change in L above 1300 psia,  $h=100$  ft, 784 grids**

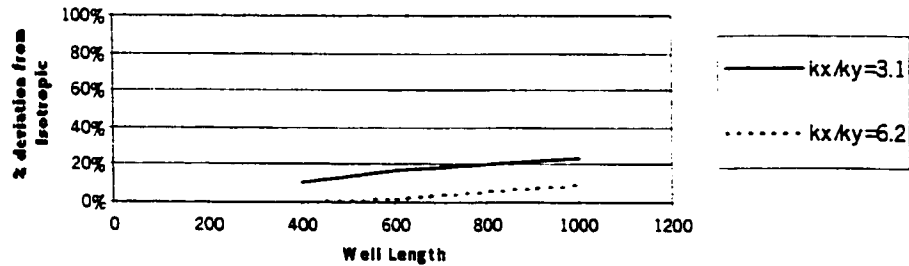


**Figure 6.17 Deviation from Isotropic with Change in L above 1300 psia,  $h=100$  f, 784 grids,  $2X_e/L = 4$  to 10, Small Model**

As the reservoir becomes larger and the ratio of  $2X_e/L$  increases, the trend towards increasing deviation from isotropic with increasing well length and reservoir to well length ratio remains the same. However note that the magnitude of the relative deviation from isotropic diminishes. This is shown in figures 6.18 – 6.21.

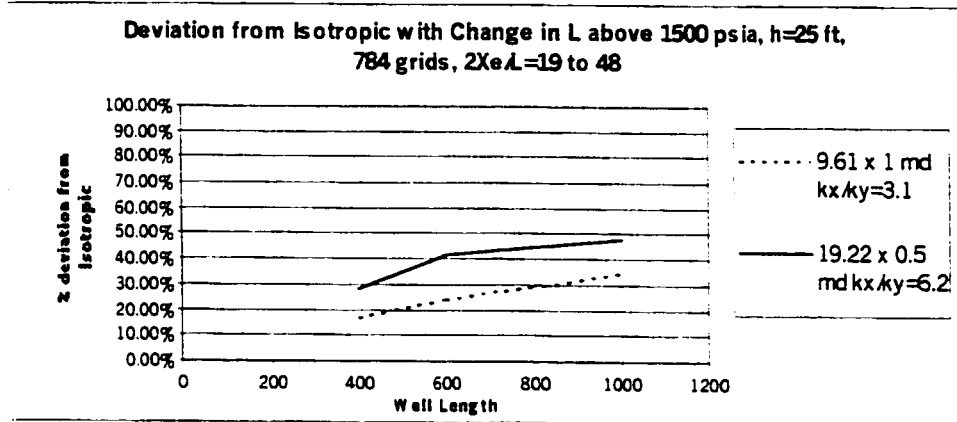


Figure 6.18 Deviation from Isotropic with Change in L above 1500 psia,  
h=25 ft, 784 grids,  $2X_e/L=19$  to 48, Large Model

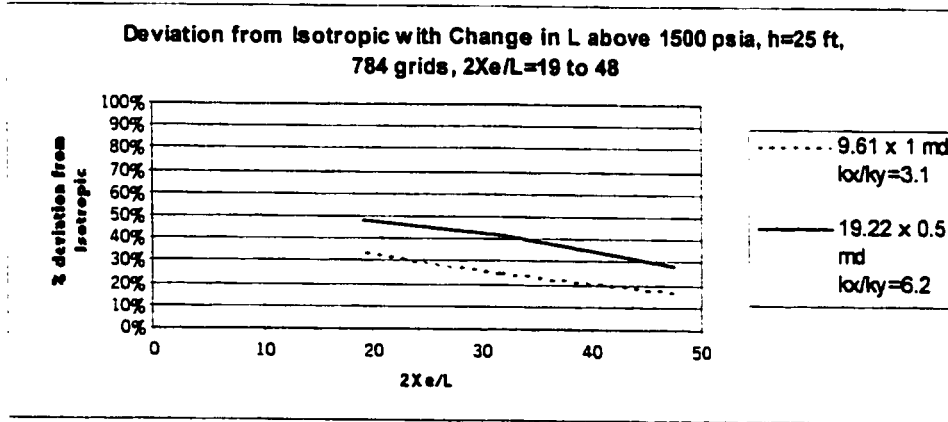
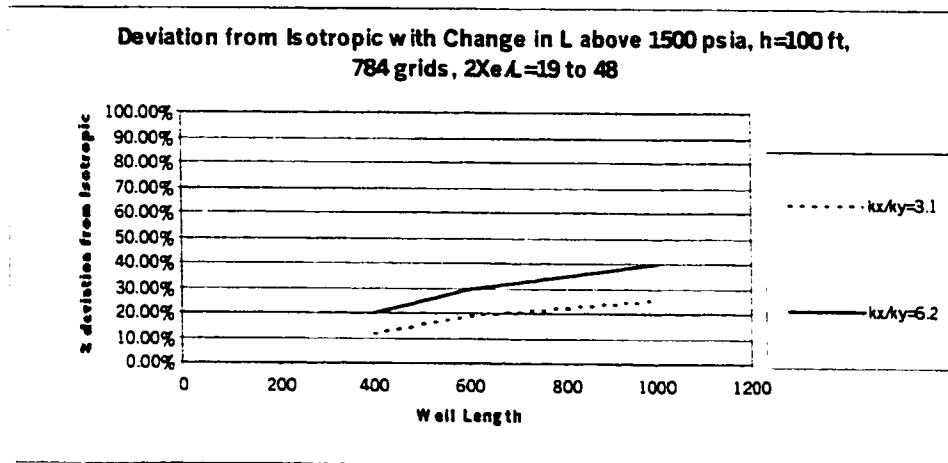
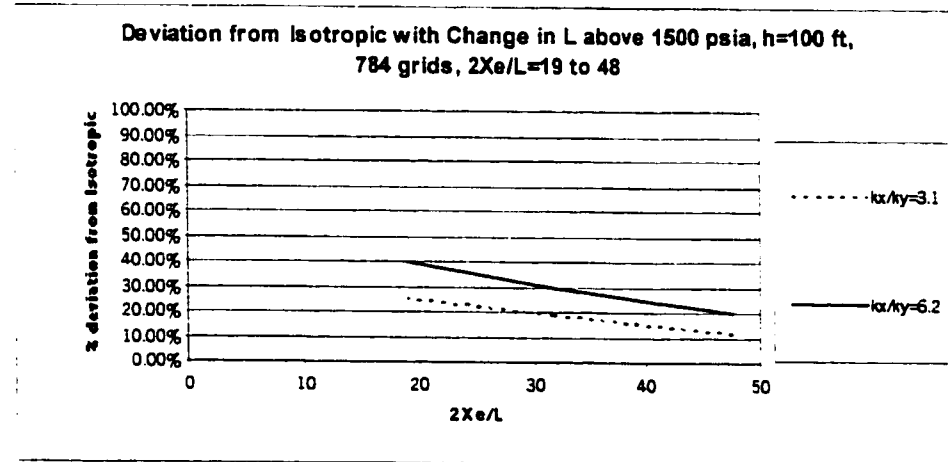


Figure 6.19 Deviation from Isotropic with Change in L above 1500 psia,  
h=25 ft, 784 grids,  $2X_e/L=19$  to 48, Large Model

Again an increase in the reservoir thickness also diminishes the deviation from isotropic horizontal permeability as shown by contrasting figures 6.18 and 6.19 with 6.20-1.



**Figure 6.20 Deviation from Isotropic with Change in L above 1500 psia,  
h=100 ft, 784 grids, 2Xe/L=19 to 48, Large Model**



**Figure 6.21 Deviation from Isotropic with Change in L above 1500 psia,  
h=100 ft, 784 grids, 2Xe/L=19 to 48, Large Model**

These trends can also be portrayed in more familiar horizontal well terminology as shown in figures 6.22 through 6.25. Though not plotted here, this same general trend toward increasing deviation from isotropic is seen as  $k_x/k_y$  increases and  $L_d$  increases for any given thickness. Note however the decrease in deviation from isotropic as the thickness increases. The trends are not as clear at lower reservoir pressures however.

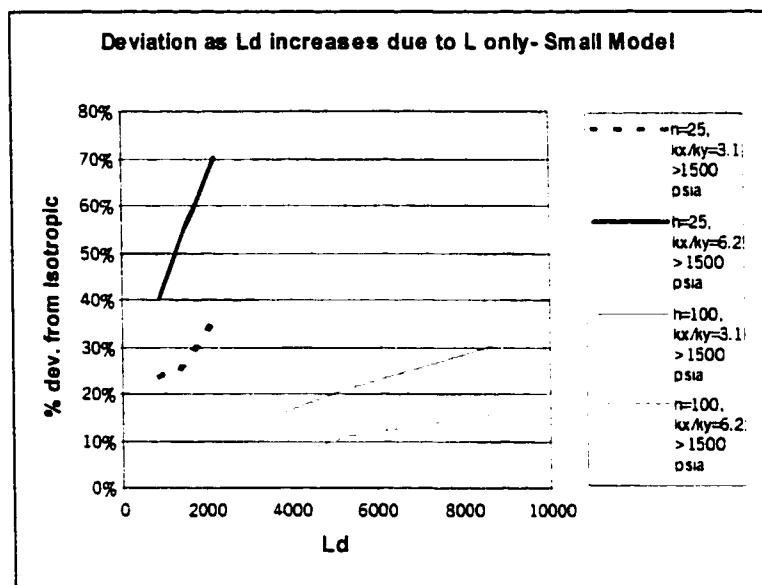


**Figure 6.22 Deviation Trend as  $L_d$  Varies with Different Thickness (h) - Small Model-**

If one tries to make a comparison of changes in deviation as a result of changes in  $L_d$  (essentially showing change in  $L/2h$ ) for any constant ratio of  $L/2X_e$  within model types, some confusing results are seen. For instance if one plots the deviation from isotropic of identical well length to horizontal reservoir width ratios, against  $L_d$  (essentially  $L/2h$ -i.e.combinations of  $L$  from 400-1000 and  $h$  from 25 to 100) it is apparent that certain trends are evident that are confusing. Figures 6.23 through 6.26 show the comparisons.

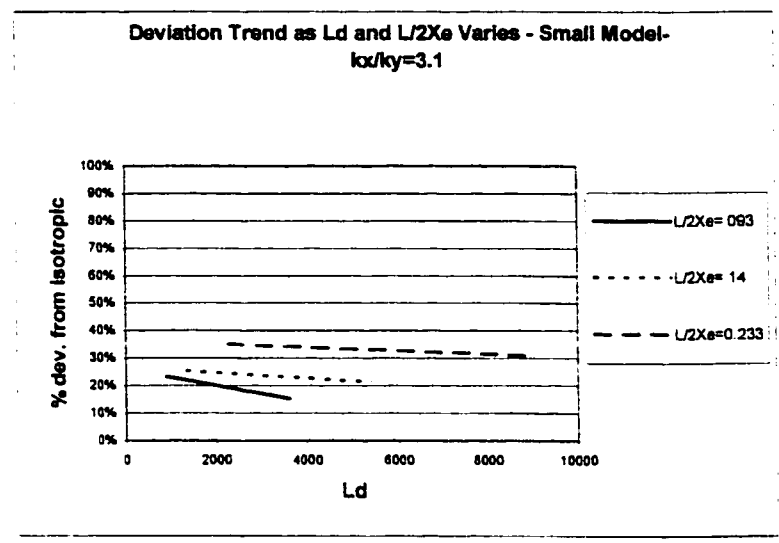


Figure 6.23 Deviation Trend as  $L_d$  and  $L/2Xe$  Varies - Small Model- $k_x/k_y=3.1$

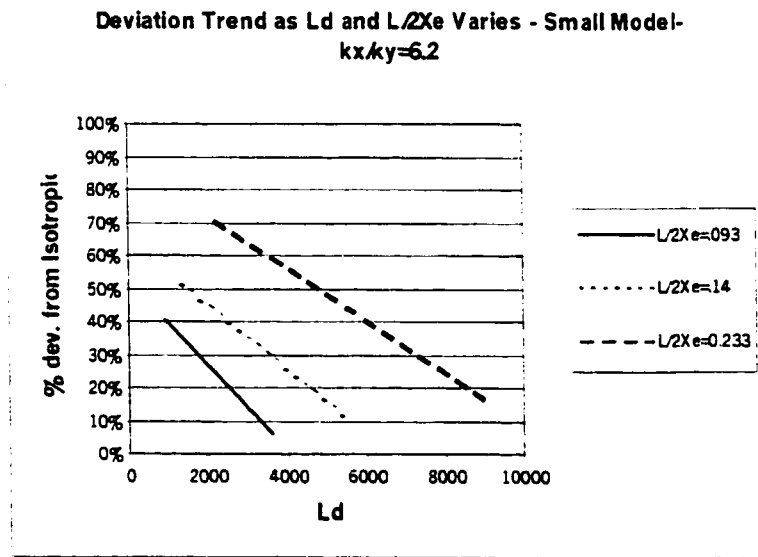
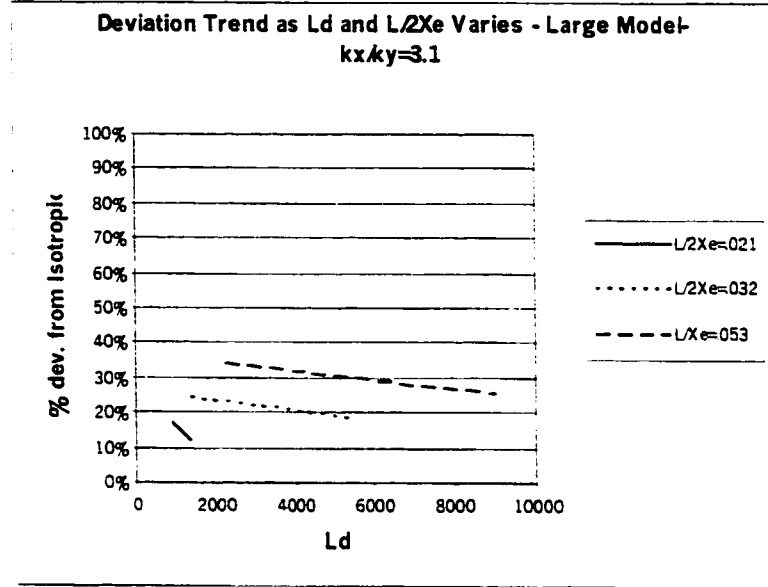
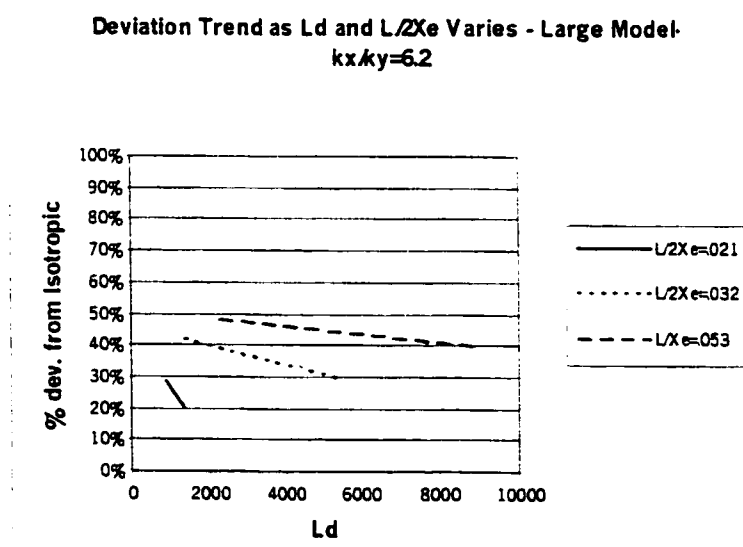


Figure 6.24 Deviation Trend as  $L_d$  and  $L/2Xe$  Varies - Small Model- $k_x/k_y=6.2$



**Figure 6.25 Deviation Trend as  $L_d$  and  $L/2Xe$  Varies - Large Model- $k_x/k_y=3.1$**



**Figure 6.26 Deviation Trend as  $L_d$  and  $L/2Xe$  Varies - Large Model- $k_x/k_y=6.2$**

#### 6.6.4 Discussion of Experiment Results

Though the expected trend of generally increasing deviation from isotropic, as the ratio of  $L/2X_e$  increases (ie the well length increases with respect to the horizontal dimensions) , the unexpected trend is that within each  $L/2X_e$  group the deviation decreases with increasing  $L_d$  ( $L/2h$ ). This is confusing but must be a function of the change in  $h$ .

The more important things to note in these experiments are:

1. The deviation from the isotropic case increases as the well length increases for any given reservoir thickness and dimension.
2. The deviation becomes more severe with increasing contrast in  $k_x$  and  $k_y$ .
3. The deviation becomes more severe with decreasing reservoir thickness given a constant well length and horizontal dimension reservoir dimension.
4. The deviation becomes more severe with increasing reservoir pressure.
5. The grid number and size has a relatively minor effect.
6. The flow rate versus pressure deviation from the isotropic horizontal permeability case increases as the ratio of well length to reservoir dimension increases (i.e. the well more fully penetrates the horizontal dimension).
7. The deviation becomes more severe as the contrast in  $k_x$  and  $k_y$  increases.
8. The deviation becomes more apparent as reservoir pressure increases above the bubble point.

More extensive experiments could be conducted. However until such time as it is determined whether or not these deviations are due to an artifact of the simulator or to a fundamental misconception about effective horizontal permeability, it is sufficient to note that care must be used in interpreting horizontal well simulations in horizontally anisotropic media. Anisotropic permeability is the most common reservoir condition. Traditional theory and analytical equations do not predict that flow rates should vary with changes in horizontal permeability as long as the geometric average of  $k_x$  and  $k_y$  is constant. Experiments show that as the reservoir becomes large compared to the well length that the deviation becomes less. However the reservoir must become far greater in size relative to the well length than is normally found in practice. With a horizontal well 1000 feet long and a reservoir 19 times that length, the deviation from isotropic case was still significant and the deviation increased as the contrast in  $k_x$  and  $k_y$  became more pronounced. A comparison of these experiments with other horizontal well simulators would be needed to further study this phenomenon. If the results are the same then more time could be justified in finding empirical correction factors to use with analytical equations.

## CHAPTER SEVEN

### Horizontal Well Decline Curve Analysis And Studies in Permeability Anisotropy

#### 7.1 Extension of Decline Analysis to Horizontal Wells

If a fractured vertical well increases production rates and increases cumulative production over a certain time period then a horizontal well should have a similar result. In fact if a horizontal well is sufficiently long, (i.e.  $L_D > 10$ ) then the performance of a horizontal well approaches that of a fully penetrating infinite-conductivity fracture and the shape factors will approach those given for fractured wells.

Dimensionless well length  $L_D$  is defined as:

$$L_D = \frac{L}{2h} \sqrt{\frac{k_v}{k_h}} \quad 7.1$$

Where L is the horizontal well length and h is the reservoir thickness in feet. And the previously derived general dimensionless decline analysis should be immediately applicable to a horizontal well by defining the horizontal well in terms of an apparent well bore radius as long as the dimensionless well length is relatively small in comparison to the reservoir dimensions.

## 7.2 Dimensionless Decline Analysis Using the Horizontal Effective Wellbore

### Radius Concept and Application

Since it was shown in section 6.2 that an equivalent wellbore radius well could represent the horizontal well it should be possible to extend the generalized decline curve analysis to horizontal wells. Recall that the equivalent well bore radius was expressed as:

$$r_w = \frac{0.5 r_{eh} L}{a \left[ 1 + \sqrt{1 - \left[ \frac{L}{2a} \right]^2} \right] \left[ \frac{\beta h}{2r_w} \right]^{\frac{\beta h}{L}}} \quad 7.2$$

And the single-phase flow rate was defined in terms of this wellbore radius as:

$$q = \frac{0.007078 k_h h (\overline{P}_R - P_{wf})}{\mu_o B_o \left( \ln \frac{r_e}{r_w} - 0.75 \right)} \quad 7.3$$

Therefore it is only necessary to follow the derivations of the dimensionless decline curve for vertical wells and the extension to horizontal wells is immediate with incorporation of the equivalent wellbore radius. Then as with the radial case, the dimensionless decline rate and time are given by the following expressions (derived in chapters 4 and 5) by just replacing the well bore radius by the effective well bore radius to a horizontal well:

$$q_{Dd} = q_D \left[ \ln \frac{r_e}{r_w} - \frac{1}{2} \right] \quad 7.4$$

or the more general version for other drainage shapes derived in this research:

$$q_{Dd} = \frac{q(t)}{q_{\max}} = q_D \left[ 1.151 \left[ \log \frac{4A}{1.781C_A r_w^2} \right] \right] \quad 7.5$$

And the decline dimensionless time is:

$$t_{Dd} = \frac{t_D}{\frac{1}{2} \left[ \left( \frac{r_e}{r_w} \right)^2 - 1 \right] \ln \left( \frac{r_e}{r_w} \right) - \frac{1}{2}} \quad 7.6$$

or again for more general drainage shapes derived in my previous work:

$$t_{Dd} = \frac{0.00634kt}{\phi\mu c_i r_w^2} \frac{r_w^2}{A} \left[ \frac{5.44678}{\log \frac{4A}{1.781C_A r_w^2}} \right] = t_D \frac{r_w^2}{A} \left[ \frac{5.44678}{\log \frac{4A}{1.781C_A r_w^2}} \right] \quad 7.7$$

Where the  $r_w$  has been replaced by the equivalent well bore radius  $r_w'$ . This method will give results that compare well with more laborious equations involving charts and shape factors described in the literature and Joshi's book<sup>23</sup>. However as previously

demonstrated (figures 6.3-6.5) the use of the modified  $r_w$  method will yield results as good as the more tedious horizontal shape factors in conjunction with skin factors.

### 7.3 Re-labeling of Decline Curves for Use in Decline Analysis

The horizontal decline curves then are identical to the previously generated vertical case but relabeled in terms of  $A/r_w$  or  $r_e/r_w$  instead of  $r_e/r_w$ . The curves in terms of  $A$  are more appropriate to the linear reservoir convention used with horizontal wells as well as more adaptable to the general shape factors that were previously introduced. The only difference with a horizontal well then is that the apparent well bore radius will be greater than that of the equivalent vertical well. That means the ratio  $r_e/r_{wa}$  ( $r_{eD}$ ) will decrease on the dimensionless decline type curves.  $k_h$  and  $r_{wa}$  should be calculated exactly as they are for the vertical well except the  $r_{wa}$  calculated is a pseudo radius equivalent given by the above expression. Then using the following techniques as with the vertical well we can determine the effect of the horizontal over the vertical well. Therefore the transmissibility can be expressed as:

$$kh = \frac{141.3 \mu B}{P_i - P_{wf}} 1.151 \log \frac{4A}{1.181 C_A r_w^2} \left( \frac{q(t)}{q_{Dd}} \right)_{\text{match}} \quad 7.8$$

Since we know  $A/r_w^2$  from the type curve match, the match point of  $q(t)/q_{Dd}$ , and the shape factor from the proper curve match we can compute  $kh$  for the particular reservoir conditions as we did previously for the vertical well case.

The apparent well bore radius, drainage area and initial reserves can then be computed from the dimensionless decline parameter  $t_{Dd}$  and the match points. We know  $A/r_w^2$  and  $t/t_{Dd}$  from the type curve match point therefore we can compute the apparent well bore radius  $r_{wa}$ :

$$r_{wa}^2 = \frac{0.00634k}{\phi \mu c, \frac{A}{r_w^2}} \left( \frac{\log \frac{4A}{1.781C_A r_w^2}}{5.44678} \right)_{match} \quad 7.9$$

Now since we have computed  $r_{wa}$  we can calculate the drainage area since from knowing  $A/r_w^2$  and computing  $r_{wa}^2$  we can solve for the drainage area A by:

$$A = r_{wa}^2 \left( \frac{A}{r_{wa}^2} \right)_{match} \quad 7.10$$

#### 7.4 Calculation of Reserves from Horizontal Well Decline Curves

Remaining reserves are then computed from the difference between initial reserves and cumulative reserves. This allows for the computation of the original reserves in place from the relationship:

$$N = \frac{A \phi c_i h P_i}{5.615 B} \quad 7.11$$

## 7.5 Comparison of Vertical and Horizontal Decline Curves

Theoretically then the horizontal and vertical well log-log plots should overlie one another in the pseudosteady state region just as Fetkovich theorized for vertically fractured wells. In other words they would have the same Arps "b" value but exhibit different  $r_e/r_w$  ( $r_{eD}$ , or the equivalent  $A/r^2 w$ ) values and thus different  $q_{Dd}$  values.

Several horizontal simulation models were conducted to investigate this theory of method equivalency. The simulated vertical vs. horizontal well data of Table 7.1 is graphed in Figure 7.1 and shows this phenomenon.

| Horizontal vs. Vertical Comparison of Decline Curves-Simulated Experimental Results. |       |       |       |       |              |    |     |  |
|--|-------|-------|-------|-------|--------------|----|-----|--|
| re   | 1785  | L     | 1275  | coip  | 5.48 million | h  | 100 |  |
| $r_w'$   | 39    | $r_w$ | 0.5   | $S_w$ | 0.25         |    |     |  |
| a  | 1842  | khor  | 3.1   | x     | 3315         | kv | 0.1 |  |
| beta   | 5.568 | phi   | 0.05  | y     | 3014         |    |     |  |
| time   | hours | ratev | rateh |       |              |    |     |  |
| 31   |       | 372   | 1765  |       |              |    |     |  |
| 62   |       | 320   | 850   |       |              |    |     |  |
| 123  |       | 294   | 854   |       |              |    |     |  |
| 214  |       | 266   | 707   |       |              |    |     |  |
| 395  |       | 239   | 569   |       |              |    |     |  |
| 576  |       | 219   | 456   |       |              |    |     |  |
| 942  |       | 187   | 372   |       |              |    |     |  |
| 1308   |       | 157   | 332   |       |              |    |     |  |
| 2304   |       | 142   | 232   |       |              |    |     |  |
| 3400   |       | 128   | 180   |       |              |    |     |  |
| 5996   |       | 99    | 93    |       |              |    |     |  |
| 8592   |       | 83    | 51    |       |              |    |     |  |

Table 7.1 Simulated Vertical and Horizontal Well Data

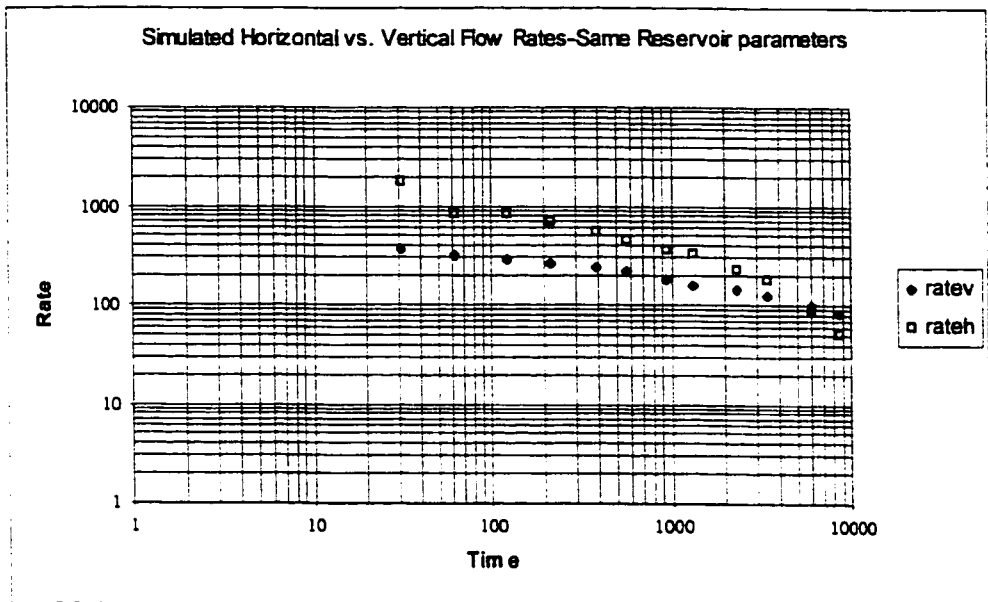


**Figure 7.1 Simulated Horizontal vs. Vertical Flow Rates-Same Reservoir Parameters**

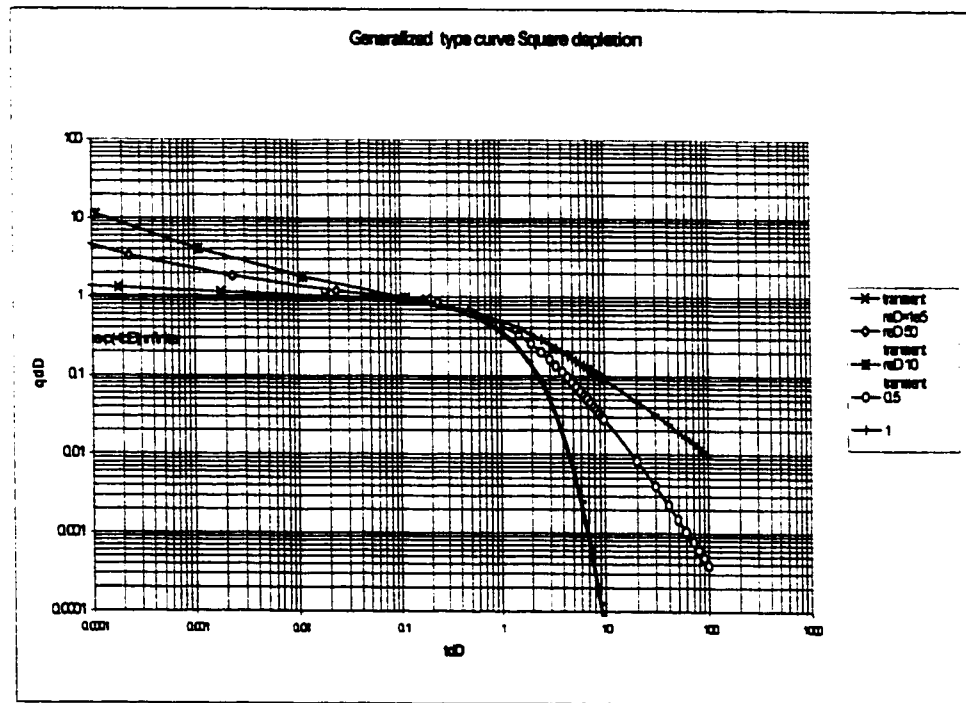


**Figure 7.2 Generalized Type Curve Square Depletion**

Though the simulation could have been run longer, it still shows the essential effect of a vertical vs. horizontal well on the identical reservoir parameters and size. When Figure 7.2, the dimensionless decline curve, is plotted at the same scale as figure 7.1 a type curve match is made. Using the match points for the vertical well vs. the horizontal well and applying the relationships presented in sections 7.2 through 7.4 yields a match of  $r_{eD}$  of 10 for the horizontal well and  $r_{eD}$  of 50 for the vertical well. This verifies the prediction of the previous statement that  $r_{eD}$  would decrease for the horizontal well because of a larger apparent wellbore radius. Therefore the value of the  $r_{eD}$  match can then be used to determine the apparent effective wellbore radius  $r_{wa}$  from the time match points and  $kh$  from the rate matches. Once the apparent well bore radius of the horizontal well is determined it can be multiplied by the  $r_{eD}$  match point to determine the drainage radius and then used to calculate the reserves as shown in previous chapters.

## 7.6 Decomposition of $k_x$ and $k_y$

If the horizontal well is long in comparison to the reservoir dimensions then the drainage shape and well penetration factors become important as was shown in the previous chapter. The horizontal shape expressions can then be incorporated as functions of the following factors:

1. Drainage area shape:  $2X_0/2Y_0$ , where  $x$  and  $y$  are the half-length of the reservoir in the  $x$  and  $y$  directions respectively.

2. Well Penetration ratio:  $L/2x_e$

3. Dimensionless well length defined before as:  $L_D = \frac{L}{2h} \sqrt{\frac{k_v}{k_h}}$

Methods to predict the performance of horizontal wells in anisotropic, naturally fractured reservoirs require knowledge of or assumptions regarding  $k_x$  and  $k_y$  since rectangular drainage shapes are usually assumed. And  $k_x$  and  $k_y$  will determine, to a large extent, the dimensions of the drainage shape. The basic drainage shape is defined as  $2X_e/2Y_e$ . Unfortunately the horizontal permeability components  $k_x$  and  $k_y$  ( $k_h = \sqrt{k_x k_y}$ ) are rarely known. Interference test data, which can provide  $k_x$  and  $k_y$  information, is also rarely available. However it may be possible to estimate these directional permeabilities if drainage shapes can be inferred from an analysis of actual production decline curve characteristics among offset wells.

#### **7.6.1 General Directional Permeability Background Discussion**

Several methods have been introduced to determine productivity and predict future horizontal well performance in anisotropic naturally fractured reservoirs. These methods require assumptions as to directional permeability,  $k_x$ ,  $k_y$ ,  $k_z$  which are almost never known. It seems that we should be able to perform the inverse and determine reservoir drainage area and shape, and thus infer directional permeabilities, if sufficient production history is known. Predicting the total drainage area around the producing well should be obtainable. However a prediction of how this drainage area is distributed

may be difficult to determine. Distribution depends on the value of  $k_x$  and  $k_y$ . The larger the value of  $k_y/k_x$  the longer the drainage distance along the high permeability  $y$  direction. A literature review indicates no other attempts to obtain this information with horizontal wells in anisotropic media.

Indeed a determination of reservoir shape and  $k_x$ ,  $k_y$ ,  $k_z$  could then be used to input to established predictive equations to predict future production more accurately. Also most models seem to ignore relative permeability. The permeability in these equations in fact should be replaced with relative permeability but this is often not done.

Recall that Arps<sup>1,2</sup> and Fetkovich<sup>3</sup> developed decline curve equations, based on pseudosteady state theory as early as 1945, which are still used today. As previously discussed, these relations take the form of:

$$q = \frac{q_i}{(1 + b D_i t)^{1/b}} \quad 7.12$$

where:

$$D_i = \frac{0.00634 k}{0.5 \phi \mu c_i r_w^2 \left( \frac{r_e}{r_w^2} - 1 \right) \ln \frac{r_e}{r_w} - 0.5} \quad 7.13$$

For a horizontal well, the effective well bore radius  $r_w'$  can be expressed as:

$$r_w = \frac{0.5 r_{eh} \frac{L}{a}}{\left(1 + \sqrt{1 - \left(\frac{0.5L}{a}\right)^2} \right) \left(0.5 \beta \frac{h}{r_w}\right)^{\frac{\beta h}{L}}} \quad 7.14$$

and

$$a = 0.5L \left(0.5 + \sqrt{0.25 + \left(\frac{2r_{eh}}{L}\right)^4}\right)^{0.5} \quad 7.15$$

$$\beta = \left(\frac{k_h}{k_v}\right)^{0.5} \quad 7.16$$

$$k_h = \sqrt{k_x k_y} \quad 7.17$$

where  $r_{eh}$  is the equivalent drainage area of the horizontal well. If vertical wells are available in the area, traditional test methods and production data can give an estimate of the total drainage area. For instance if the drainage area of a vertical well is 40 acres then the equivalent vertical radius,  $r_{ev}$  is 745 feet by using the relationship<sup>6</sup>:

$$\text{Area of Circle} = \pi r_{ev} = \text{acres} * 43560 \quad 7.18$$

$$r_{ev} = \sqrt{\frac{A * 43560}{\pi}} \quad 7.19$$

Joshi presents a method for finding the equivalent horizontal well drainage area based on a rectangle bounded on the long sides by semi-circles<sup>23</sup>. Now applying that  $r_{ev}$  to the diagram below, the following relationships can be derived:

$$A = \frac{\pi r_{ev}^2 + 2Lr_{ev}}{43560} \quad 7.20$$

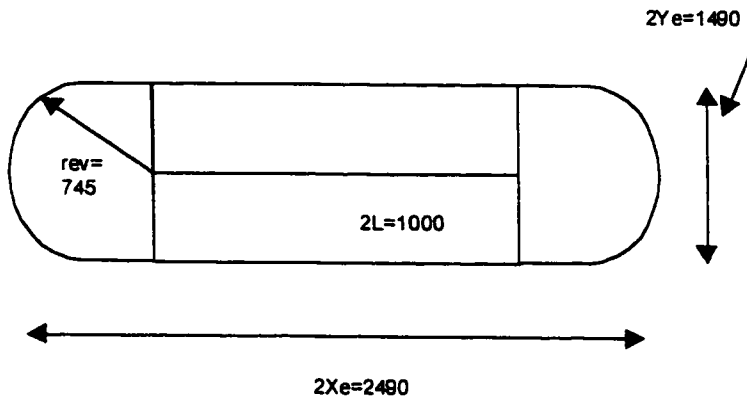


**Figure 7.3 Equivalent Horizontal Wellbore Radius**

In the above example the equivalent horizontal wellbore radius,  $r_{eh}$ , would be 1014 feet for a lateral well of 1000 feet and  $r_{ev}$  of 745 feet.

### 7.6.2 Decomposing $k_x$ and $k_y$

With this equivalent radius information,  $r_{eh}$ , it is possible to insert into equation 7.14 to solve for  $r_w$ . If the reservoir thickness is 100 feet this would yield  $r_w = 406/(100\beta)^{0.28}$ .

Now  $r_w$  can be obtained by the decline curve methods introduced in Section 7.3 to solve for  $\beta = (k_y/k_x)^{0.5}$ . Once  $k_h$  is found in this manner one can concentrate on decomposing  $k_h$  into  $k_x$  and  $k_y$  if rectangular or elliptical drainage shape is assumed which is reasonable in horizontal wells in naturally fractured reservoirs as well as many drainage shapes in vertical well situations.

It can be shown that the drainage shape is dictated by the contrast in  $k_x$  and  $k_y$  so that:<sup>23</sup>

$$\frac{2Y_e}{2X_e} = \sqrt{\frac{k_y}{k_x}} \quad 7.21$$

Therefore it seems that it should be possible to decompose  $k_x$  and  $k_y$  if there are competing wells with sufficient drainage history to identify the time to competition for drainage area. The hypothesis is that there should be an observable break in the production decline or cumulative versus time plots when wells begin competing for drainage. In other words there should be some type of interference imprint or deviation from the drainage area predicted from early time rate and cumulative data (see figure 7.36 for example). Or alternatively if several wells experience interference at roughly the same time, the distance between the two wells should give the ratio of  $2Y_e/2X_e$  by approximately:

$$\frac{t_{y_{\text{int}}}}{t_{x_{\text{int}}}} \frac{2Y_e}{2X_e} = \sqrt{\frac{k_y}{k_x}} \quad 7.22$$

$$2 X_e * 2 Y_e = A * 43560$$

7.23

where  $t$  is the interference time in the various directions. Vector analysis could be applied to resolve the potential angular problems.

If the time or distance ratio is known then the relative relationship between  $k_x$  and  $k_y$  should be obtainable. For instance if the time/distance ratios are 3 then  $k_y=9k_x$ . Extensive simulation experiments and pressure versus time visualization analysis were conducted to study this hypothesis. The complete graphical output and tabular experimental output is very voluminous but is available from the author.

### 7.6.3 Studies in Anisotropic Media – $k_x$ , $k_y$ Experimental Results

Numerous experiments were conducted to study the effects of horizontal anisotropy on well performance with the objective of finding ways to decompose  $k_x$  and  $k_y$  using production data that would normally be available to the practicing engineer. Normal data available would be limited to fluid rates, cumulative production volumes and time. Monthly production data are all that can be expected after the first few months of production. Although not published, daily rates are often kept by the operator for early time periods and can be obtained by contacting operators. Thus this analysis will be restricted to that data that can be normally obtained. Unfortunately pressure data are

rarely available. Pressure will be used in this analysis but only as a visualization technique to illustrate the various rate decline points of the rate decline curves.

#### 7.6.3.1 Visualization and Identification of Important Points - Rate Decline Curves

A 14,000 ft. by 14,000 ft. 3-well system was tested with orientation as in figure 7.4. The wells are equal distance from each other (3000 feet) and oriented along separate permeability paths, which would be realistic in some field spacing units initially.

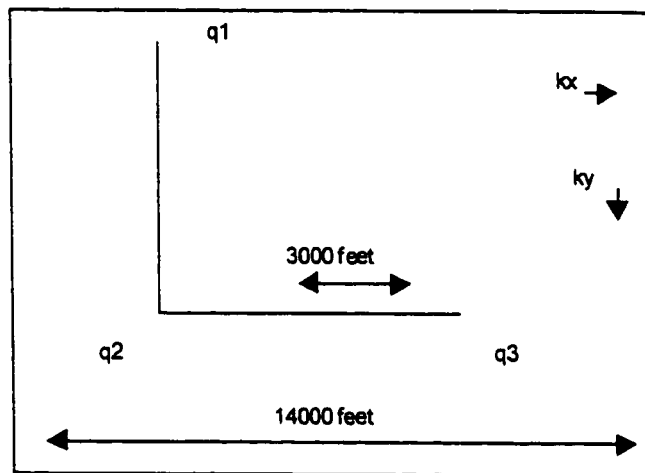


Figure 7.4 Model Geometry

The following graphs depict the rate-time, cumulative-time and pressure distribution versus time. The case of  $k_x=19.22$ ,  $k_y=0.5$  (geometric mean 3.1 md) is contrasted with the isotropic case of 3.1 md. Figures 7.5 and 7.7 show the rate-time plot for the anisotropic and isotropic cases respectively. Figures 7.6 and 7.8 are the cumulative

versus time plot for the anisotropic and isotropic cases respectively. The times to the various slope changes are noted on Figure 7.5 and 7.7 and visual pressure distribution diagrams are plotted for each of these times in figures 7.10 to 7.17 for the anisotropic case and 7.18 through 7.26 for the isotropic case. Figure 7.9 shows the various portions of the rate time curve for which slopes are calculated for each well in the model.

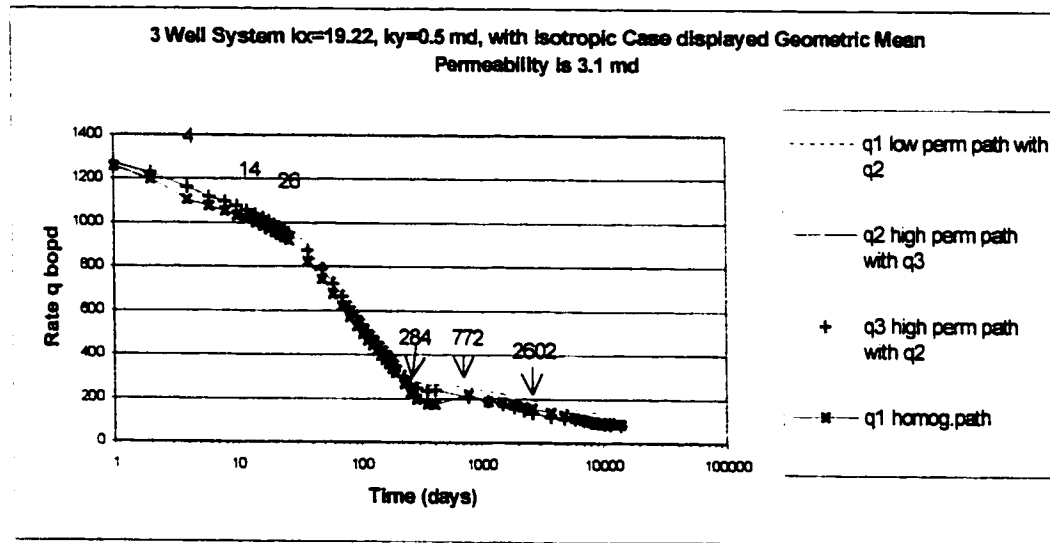


Figure 7.5 3 Well System  $k_x=19.22$ ,  $k_y=0.5$  md, with Isotropic Case Displayed Geometric Mean Permeability is 3.1 md

Figure 7.6 shows the effect of the rates illustrated in figure 7.5. Notice the dramatic departure in cumulative production where the well (q1) that is oriented along the low permeability path with respect to q2 retains its higher rates and therefore its higher cumulative production compared to well q3 along the high permeability path. This shows the clear mark of drainage competition more quickly along the high permeability

path. Compare this to figure 7.8 which shows the cumulative departure between wells at a much later time with the isotropic case.

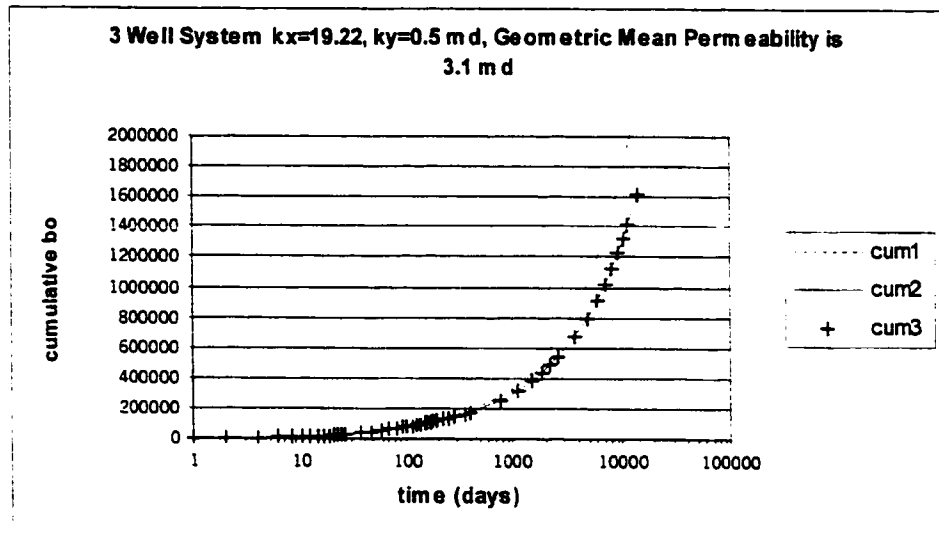


Figure 7.6 3 Well System  $k_x=19.22$ ,  $k_y=0.5$  md, Geometric Mean Permeability is 3.1 md

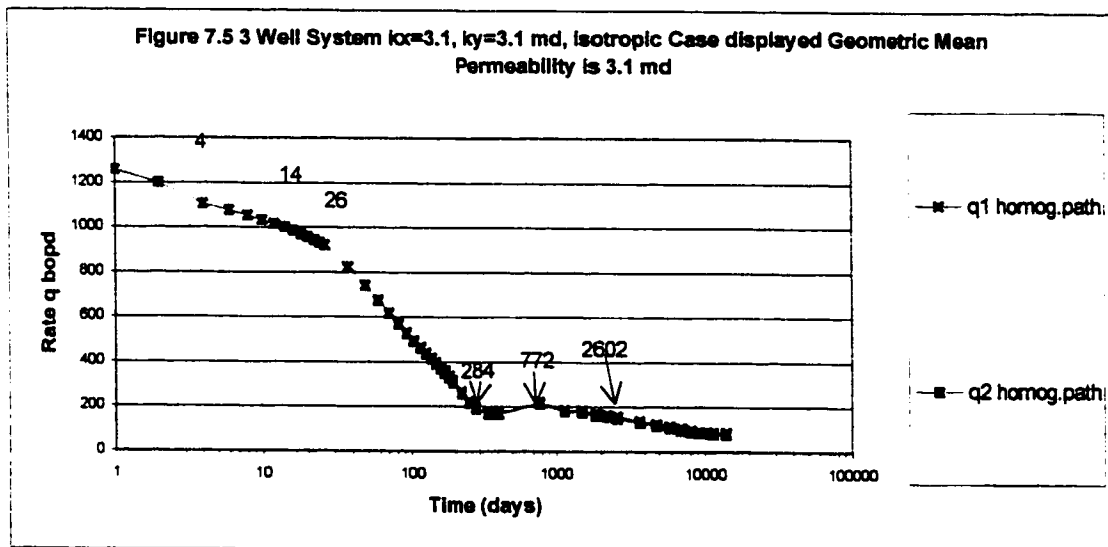
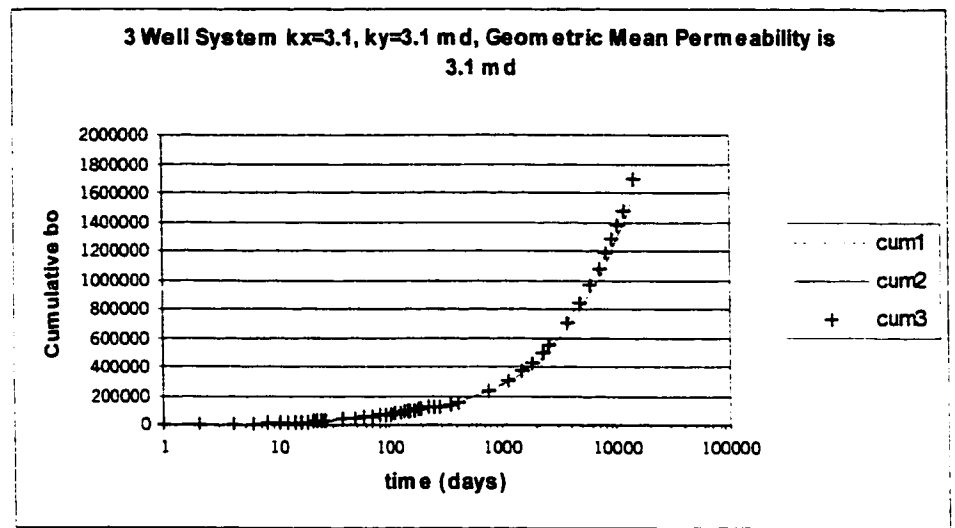
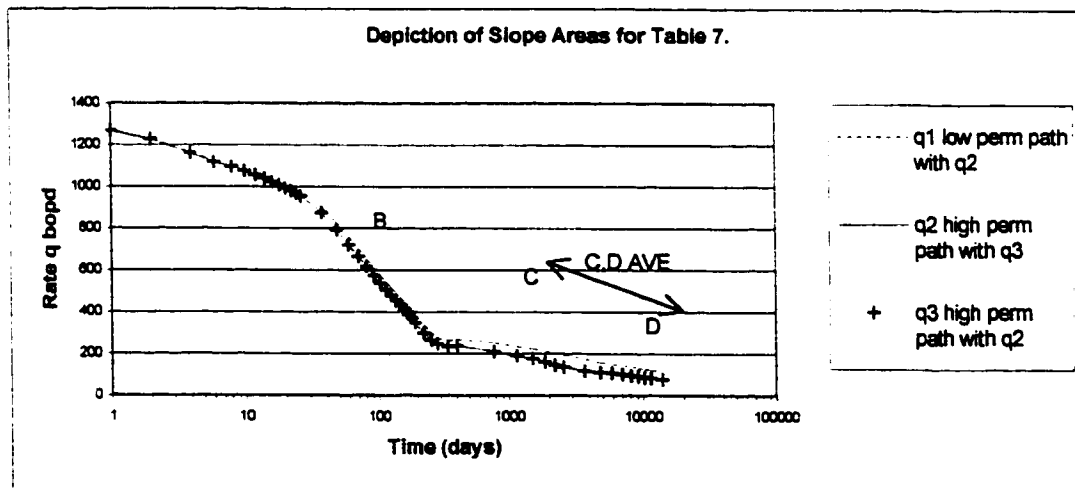


Figure 7.7 3 Well System  $k_x=3.1$ ,  $k_y=3.1$  md, Isotropic Case Displayed Geometric Mean Permeability is 3.1 md



**Figure 7.8 3 Well System  $k_x=3.1$ ,  $k_y=3.1$  md, Geometric Mean Permeability is 3.1 md**



**Figure 7.9 Depiction of Slope Areas for Table 7.**

Table 7.2 shows the various slopes and departure times of cumulative production between the various competing paths of the two cases as well as the slopes for an intermediate case of  $k_x = 9.61$  and  $k_y = 1.0$  md. Figures 7.10 through 7.25 show the pressure distribution profiles that help in understanding what is happening in the model at the various time steps. Figures 7.36 and 7.27 illustrate the effect on the productivity index.

| Slopes of Semilog rate versus time plots |           |     |       |     |       |    |       |        |
|--|-----------|-----|-------|-----|-------|----|-------|--------|
| SQRT(KX/KY)                              |           | q1  | q2,q3 | q1  | q2,q3 | q1 | q2,q3 | q1     |
| CONTRAST                                 | Region    | B1  | B2    | C1  | C2    | D1 | D2    | CD1AVE |
| 6.2                                      | 19.22,0.5 | 710 | 706   | 138 | 106   | 80 | 96    | 103    |
| 3.1                                      | 9.61,1    | 697 | 693   | 100 | 89    | 72 | 69    | 95     |
| 1  | 3.1,3.1   | 714 | 707   | 118 | 118   | 22 | 22    | 93     |
|  |           |     |       |     |       |    |       | 103    |

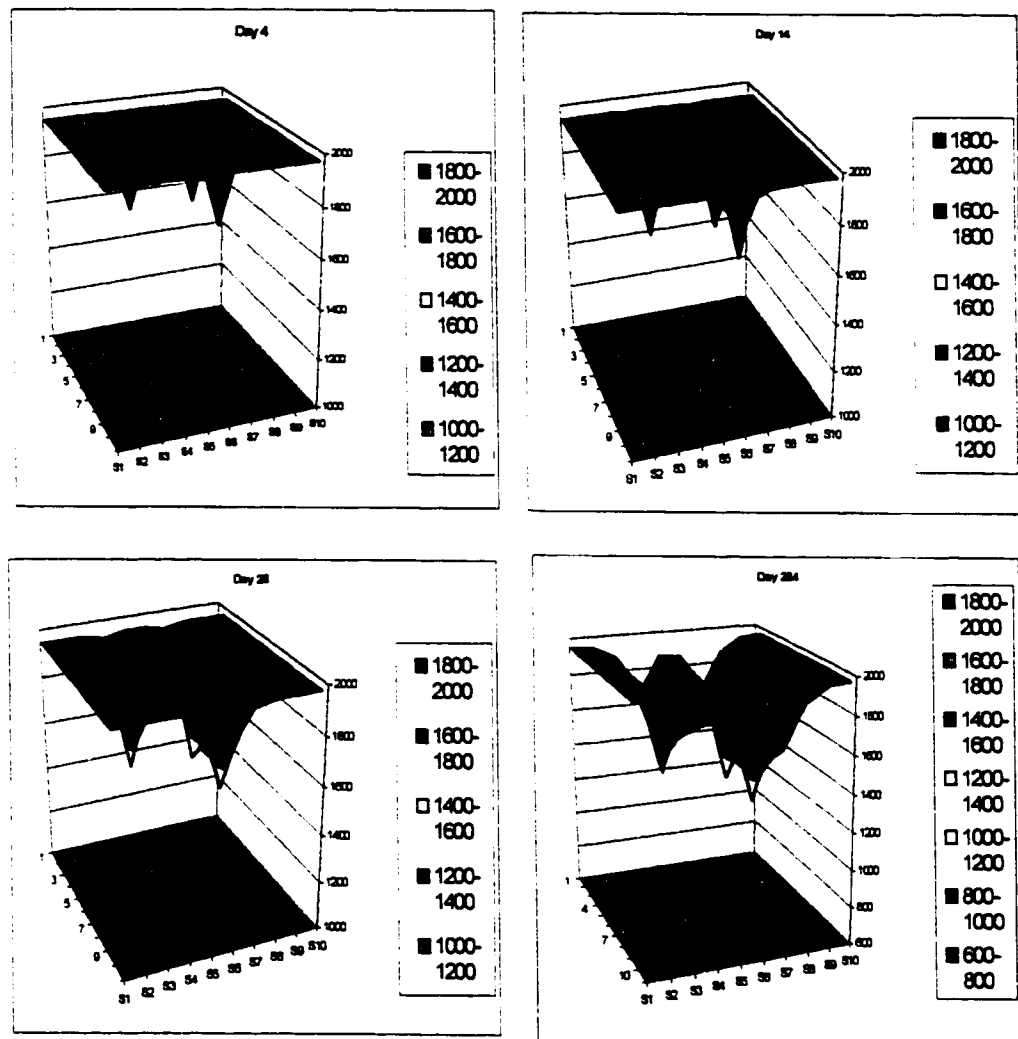
  

| Times at which q1 deviates from q2,q3 rates for different permeability ratios (geometric mean equal 3.1 md) |           |                     |       |                    |       |  |  |  |
|---|-----------|---------------------|-------|--------------------|-------|--|--|--|
| SQRT(KX/KY)   |           | Noticable on        |       | Noticable on q1/q3 |       |  |  |  |
| CONTRAST  | Region    | Cumulative vs. Time |       | Ratio              |       |  |  |  |
|   |           | time                | ratio | time               | ratio |  |  |  |
| 6.2   | 19.22,0.5 | 284                 | 5.30  | 8                  | 4.6   |  |  |  |
| 3.1   | 9.61,1    | 406                 | 3.70  | 14                 | 2.6   |  |  |  |
| 1   | 3.1,3.1   | 1504                |       | 37                 |       |  |  |  |

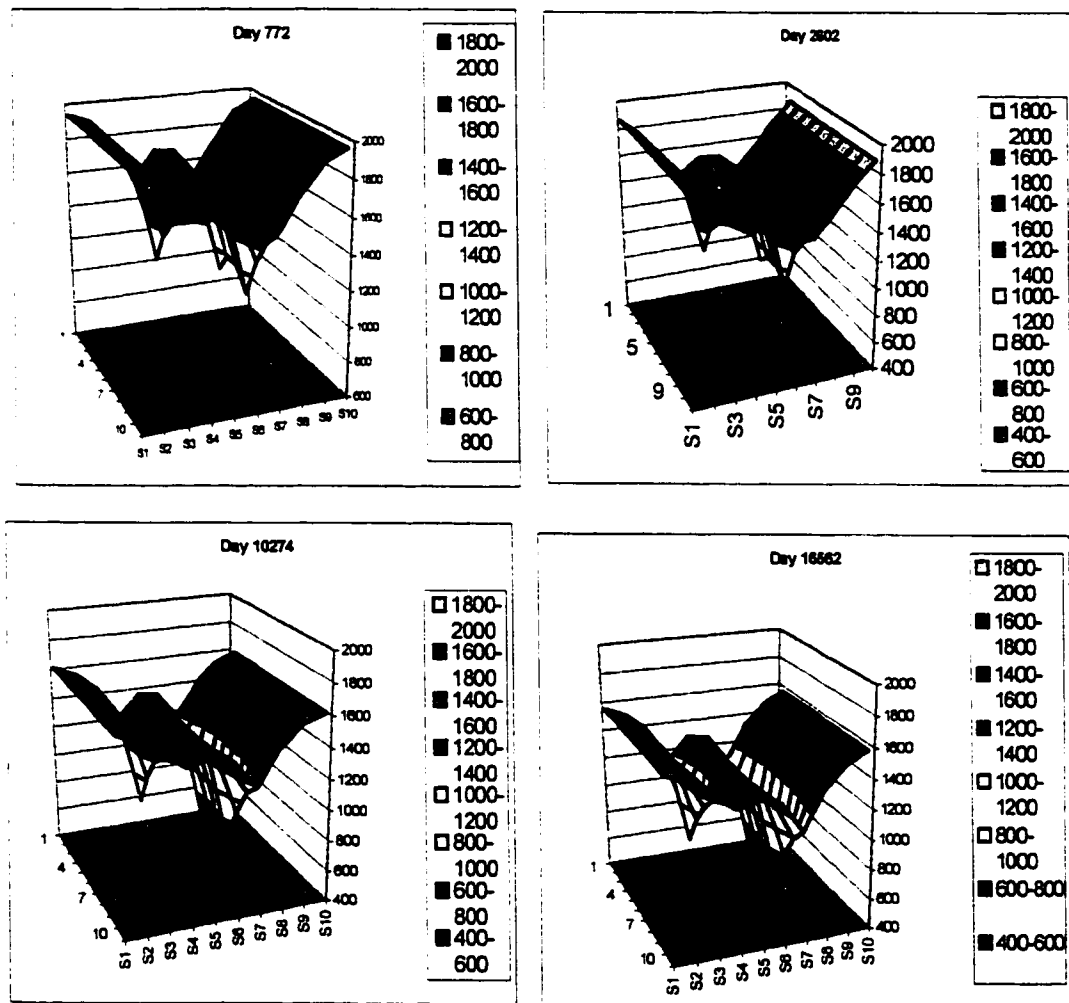
**Table 7.2 Slopes of Various Portions of the Decline Curve**

The data suggest that the cumulative time versus departure time comparison can give a rough approximation of the ratio of permeability in the x and y directions.

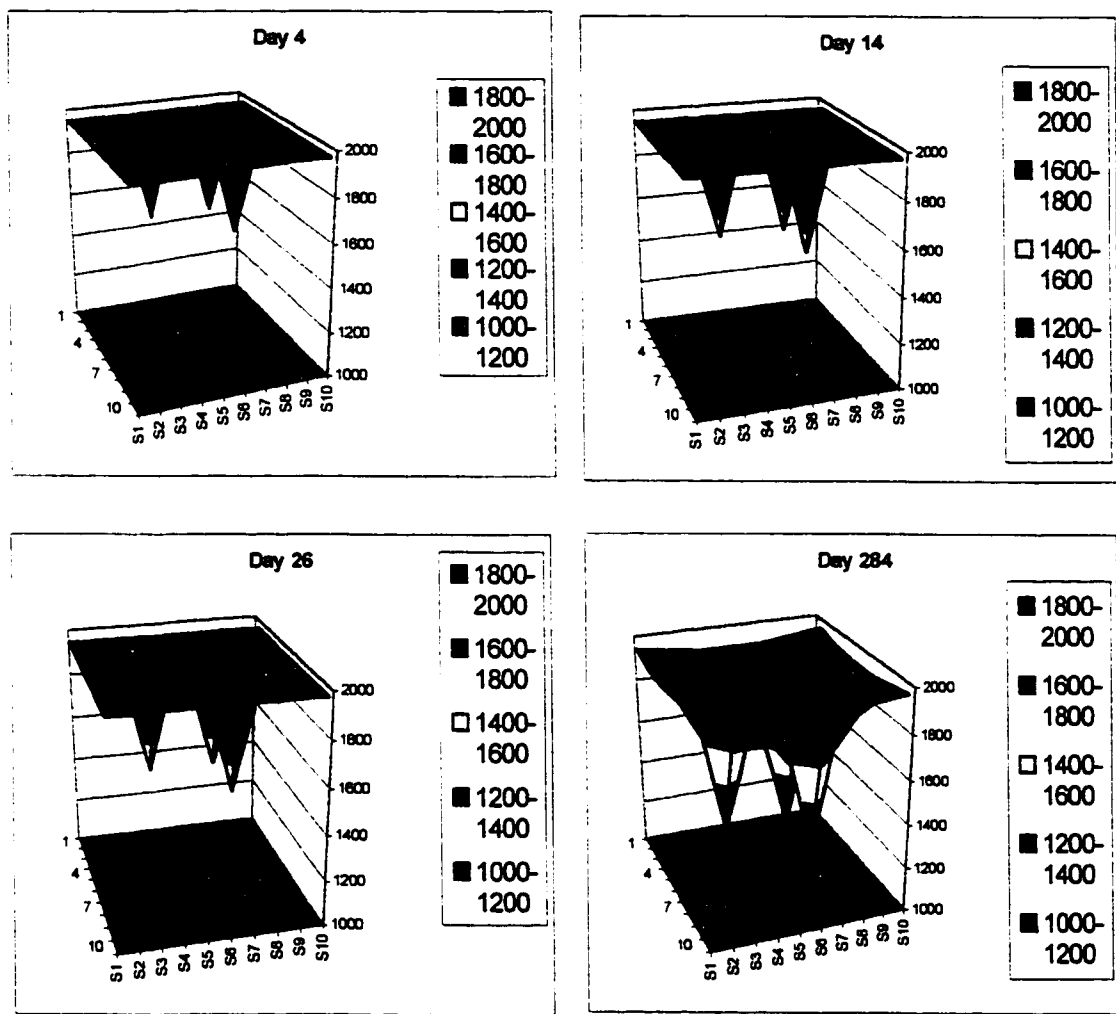
**Figures 7.10 to 7.13 - Anisotropic Pressure Distribution Profiles for Figure 7.5**



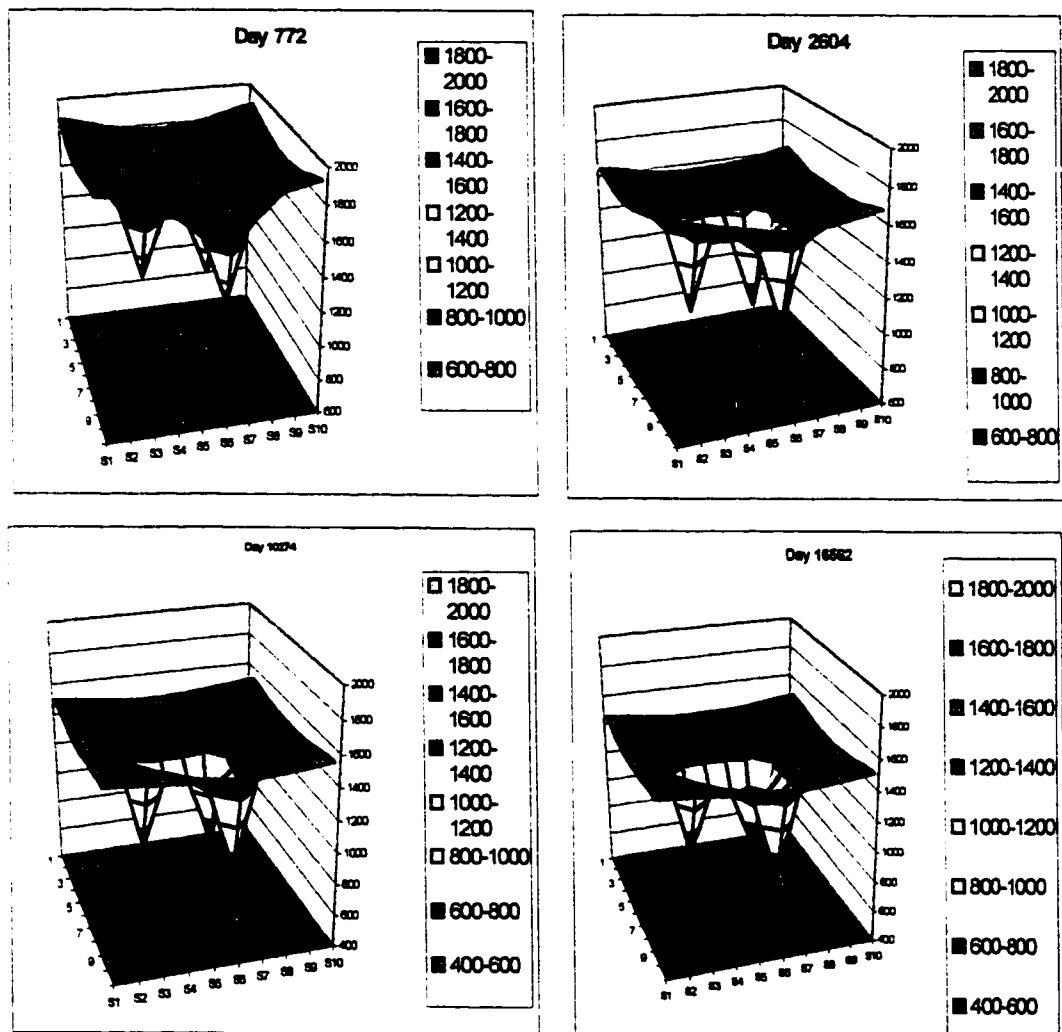
**Figures 7.14 to 7.17 - Anisotropic Pressure Distribution Profiles for Figure 7.5**

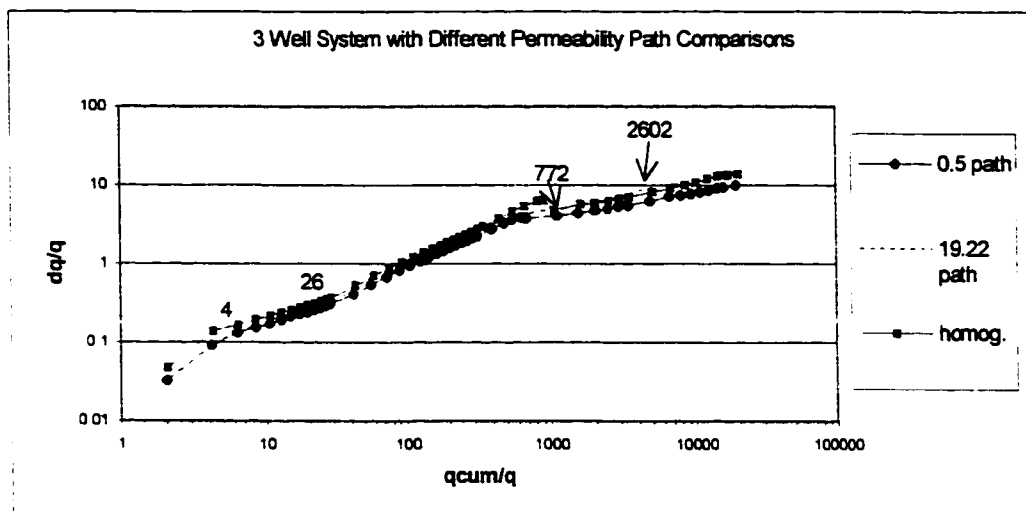


**Figures 7.18 to 7.21 Isotropic Case Pressure Distribution Profiles**

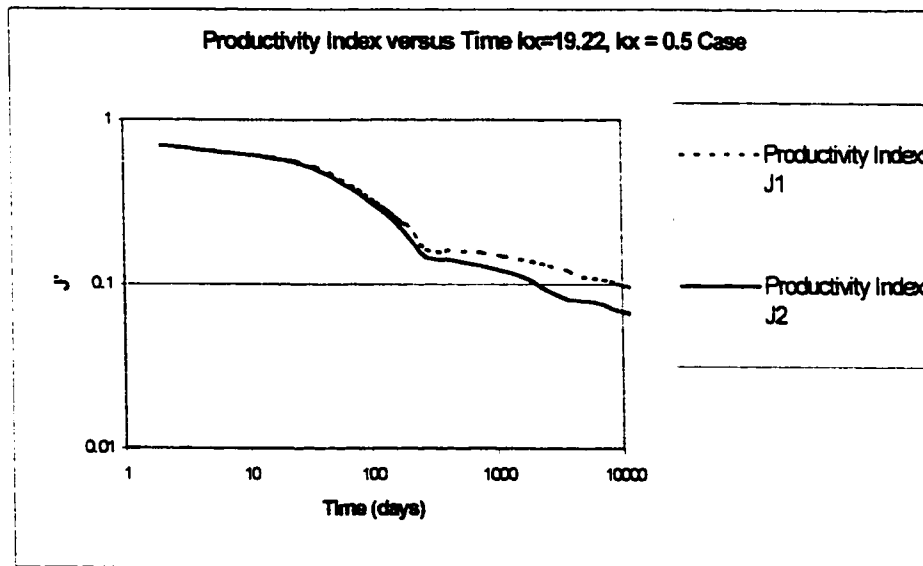


**Figures 7.22 to 7.25 Isotropic Case Pressure Distribution Profiles**





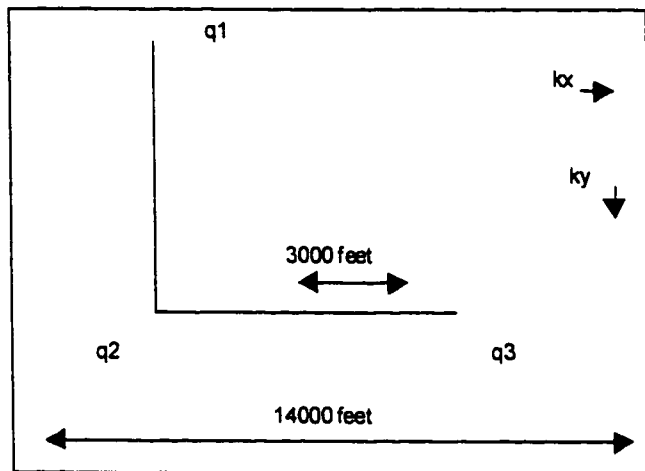
**Figure 7.26 3 Well System with Different Permeability Path Comparisons**



**Figure 7.27 Productivity Index  $J = q / (p_{ave} - p_w)$  versus Time  $k_x=19.22$ ,  $k_x = 0.5$  Case**

### 7.6.3.2 Anisotropic Experiments in Two Well System

The same type of analysis can be conducted for the case of a two well system in which the two wells are parallel to the x and y directional permeability. In other words the experiment involves wells q<sub>1</sub> and q<sub>2</sub> alone and then q<sub>2</sub> and q<sub>3</sub> alone from the previous model. Then the same type of analysis is shown below for the various anisotropic cases.



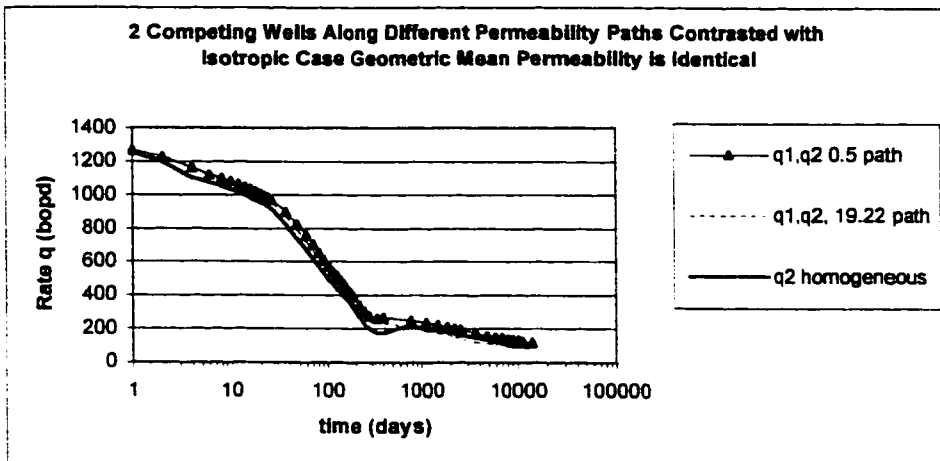


Figure 7.28 2 Competing Wells Along Different Permeability Paths Contrasted with Isotropic Case Geometric Mean Permeability is Identical

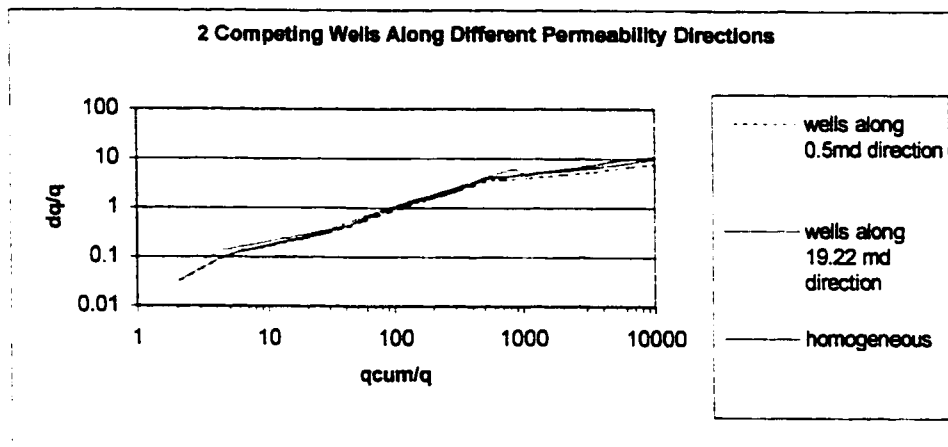


Figure 7.29 2 Competing Wells Along Different Permeability Directions

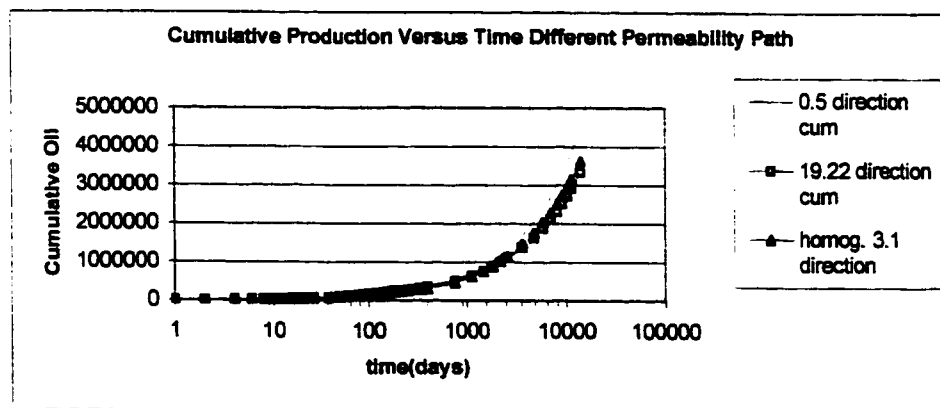
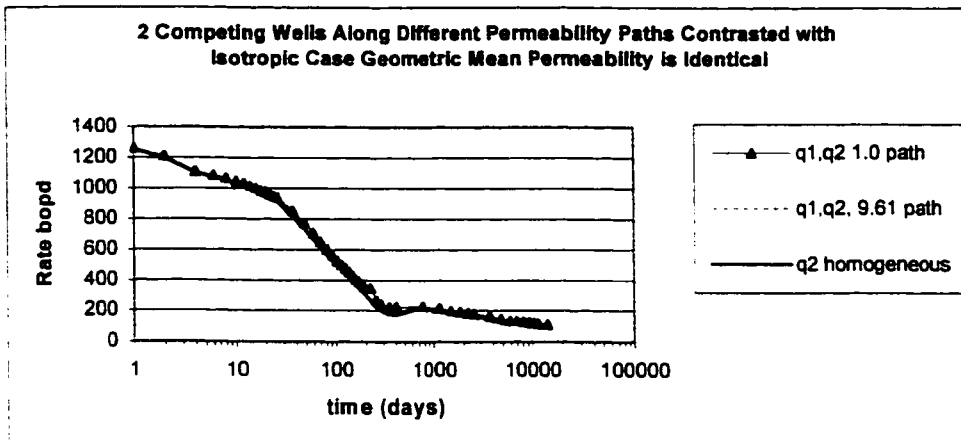
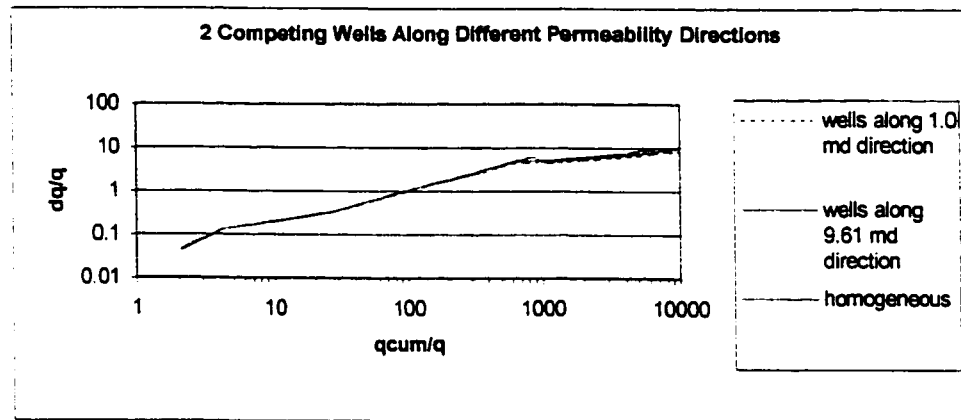


Figure 7.30 Cumulative Production Versus Time Different Permeability Path



**Figure 7.31 2 Competing Wells Along Different Permeability Paths Contrasted with Isotropic Case Geometric Mean Permeability is Identical**



**Figure 7.32 2 Competing Wells Along Different Permeability Directions**

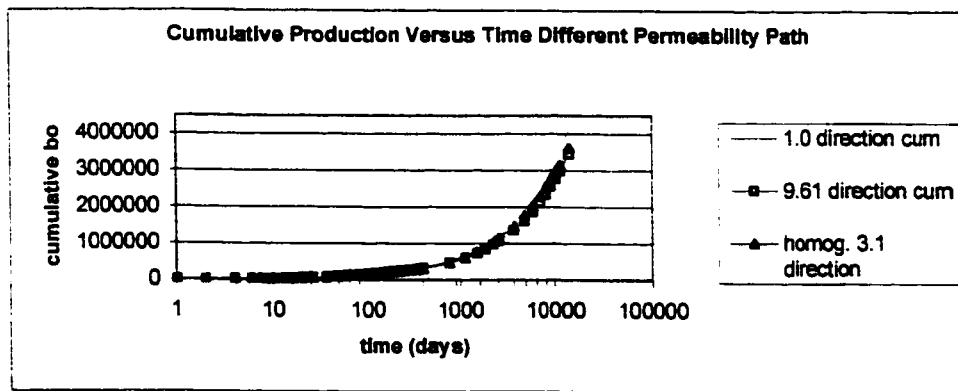


**Figure 7.33 Cumulative Production Versus Time Different Permeability Path**

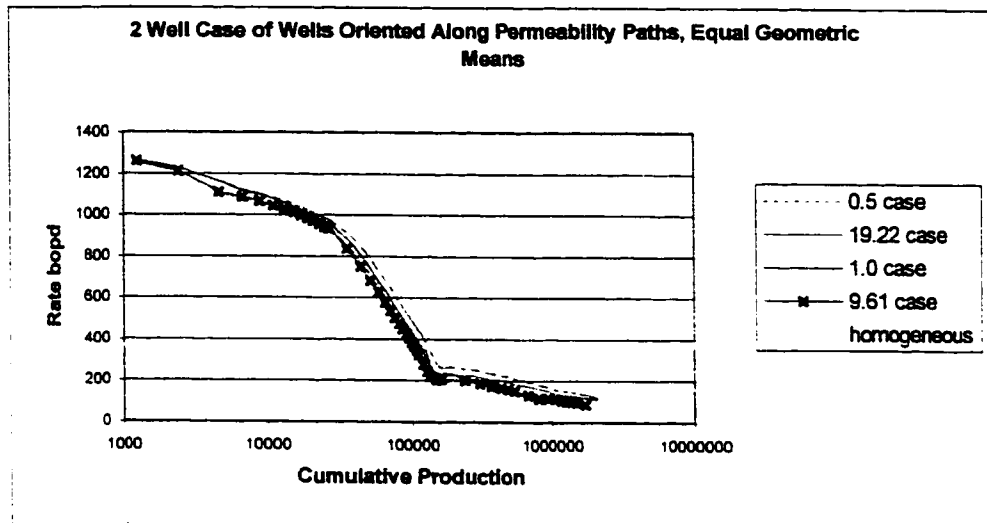


**Figure 7.34 2 Well Case of Wells Oriented Along Permeability Paths, Equal Geometric Means**

Table 7.3 shows the times at which the various wells along certain permeability paths depart from the isotropic case. Note that the ratio of the times (distance between wells is identical) seems to follow the ratio of the square root of the permeability ratios in the x and y directions.

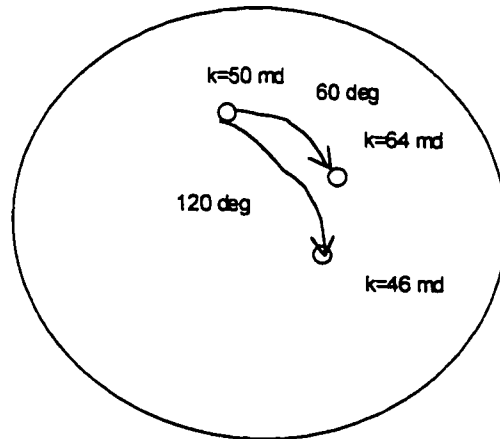
|  |            |        |
|--|------------|--------|
| Permeability Contrast (geometric mean both 3.1 md) | 0.5, 19.22 | 1.9.61 |
| Sqr (kx/ky)  | 6.2        | 3.1    |
| Departure Times from Isotropic                     | 406        | 345    |
| Departure Times from Each Other                    | 2602       | 1138   |
| Time Ratio   | 6.4        | 3.3    |

**Table 7.3 Relation of Permeability Ratio to Cumulative Departure Times**

The method thus seems to give a rough approximation to directional permeability.

#### 7.6.4 Determination of the Principle X and Y Permeability Components

If three values of permeability can be determined and the angle between those three values is known then the permeability in the principle x and y directions can be determined by application of rock mechanics techniques. (homework in Rock Mechanics, 1995) For instance in the following diagram:



If three points (strain or permeability) and the angles between the observation points are known a Mohr circle approach can be used to calculate the principle values. Alternatively rock mechanics homework indicated that a matrix solution could be used

also. These methods used strain values but extension to permeability values should work also.

$$k_x = \begin{pmatrix} \cos^2 \alpha_A & \sin^2 \alpha_A & \frac{\sin 2\alpha_A}{2} \\ \cos^2 \alpha_B & \sin^2 \alpha_B & \frac{\sin 2\alpha_B}{2} \\ \cos^2 \alpha_C & \sin^2 \alpha_C & \frac{\sin 2\alpha_C}{2} \end{pmatrix} \begin{pmatrix} k_A \\ k_B \\ k_C \end{pmatrix} \quad 7.24$$

$$k_y = \begin{pmatrix} \cos^2 \alpha_A & \sin^2 \alpha_A & \frac{\sin 2\alpha_A}{2} \\ \cos^2 \alpha_B & \sin^2 \alpha_B & \frac{\sin 2\alpha_B}{2} \\ \cos^2 \alpha_C & \sin^2 \alpha_C & \frac{\sin 2\alpha_C}{2} \end{pmatrix}^{-1} \begin{pmatrix} k_A \\ k_B \\ k_C \end{pmatrix} \quad 7.25$$

This yields  $k_x=46$  and  $k_y=61$  and  $k_{xy}=16$ . This in turn can be used to compute  $k_1$  and  $k_2$  as 64 and 42 md. Alternatively the Mohr circle can be used to arrive at the same results.

## 7.7 Application to Decline Analysis Methods for Horizontal Wells in Fractured Reservoirs

When a well is first put on production, the pressure transient travels away from the well towards the well drainage boundaries. Once the pressure transient has reached all the drainage boundaries then the average reservoir pressure starts dropping with time. This flow period before the well sees the drainage boundary is known as the transient state.

Depletion state is the post-transient flow period and is also known as the pseudosteady state flow period.

For mathematical treatment, either constant flowing well bore pressure or constant production rates are normally assumed. A constant production rate implies that flowing bottom hole and wellhead pressures are declining with time. This is typical of fields where the production level is limited by such things as production allowable or critical rates due to gas/water coning problems. A constant bottomhole flowing pressure is the more typical situation. Actually this is in reality a constant flowing wellhead pressure which is maintained constant against the backpressure of a production facilities. This constant wellhead pressure implies a decline in production rates.

Type curves for horizontal well flow in a closed rectangle have been constructed in the past. As discussed before these do not model the fractured reservoir well but serve as a starting point for analysis. The methods essentially involve solving the dimensionless pressure solution  $P_d$  using the exact mathematical solution of the Laplace transform of the constant production rate equation<sup>33,39,40</sup>. The objective is to calculate dimensionless pressure,  $P_D$  and dimensionless rate  $q_D$  for different values of dimensionless time  $t_D$ . This is done by taking any dimensionless time  $t_D$ , calculating the dimensionless pressure, converting to dimensionless rate ( $q_D = 1/P_D$ ) then converting to real rates.

If  $k_h$  can be determined, then the following procedure can be used to generate well performance predictions for horizontal wells with the aid of published type curves.

1. Calculate  $t_D$  from the various user specified time steps using the following equation:

$$t_D = \frac{0.001055kt}{\phi\mu c_i L^2} \quad 7.26$$

2. Determine  $L_D$ :

$$L_D = \frac{L}{2h} \left( \frac{K_v}{K_h} \right)^{0.5} \quad 7.27$$

3. Calculate the term  $L/2X_e = L/r_{eh}$ , approximated by  $= L/A^{0.5}$
4. Calculate  $r_{wD} = r_w/h$
5. Use the proper type curve (Figure 7.35) corresponding to the well specifications  $L_D$  and  $L/2X_e$  (from step 2 and 3) (similar to the one shown in Figure 7.33 from ref 32 and 34) to determine  $q_D$  corresponding to the  $t_D$  calculated in step one.

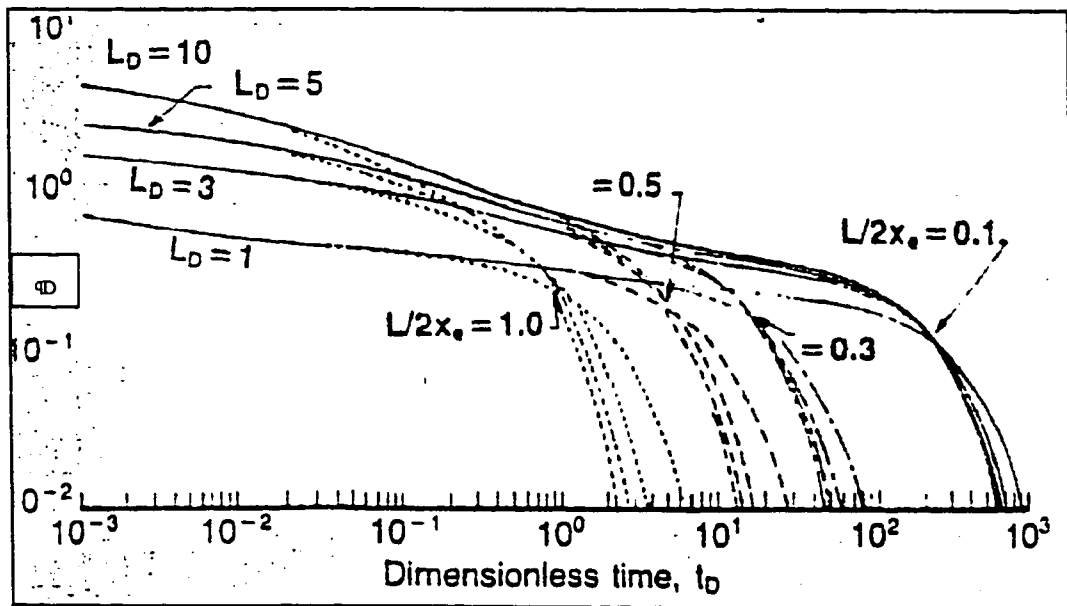


**Figure 7.35 Dimensionless Pressure versus Time for Horizontal Wells  
From Refs 32,34**

6. Calculate  $q$  from the  $q_D$  value determined in step 5 from the following equation:

$$q_D = \frac{141.3 \mu B q}{k h (p_i - p_{wf})} \quad 7.28$$

7. Repeat the calculation for various times (days) and plot as cumulative oil production versus time. This procedure can be repeated for any desired drainage area A and well parameters. For a particular well that is 1500 feet long, 35 feet thick, permeability of 0.7, figure 7.4 shows the predicted production at any particular time for various drainage size assumptions.

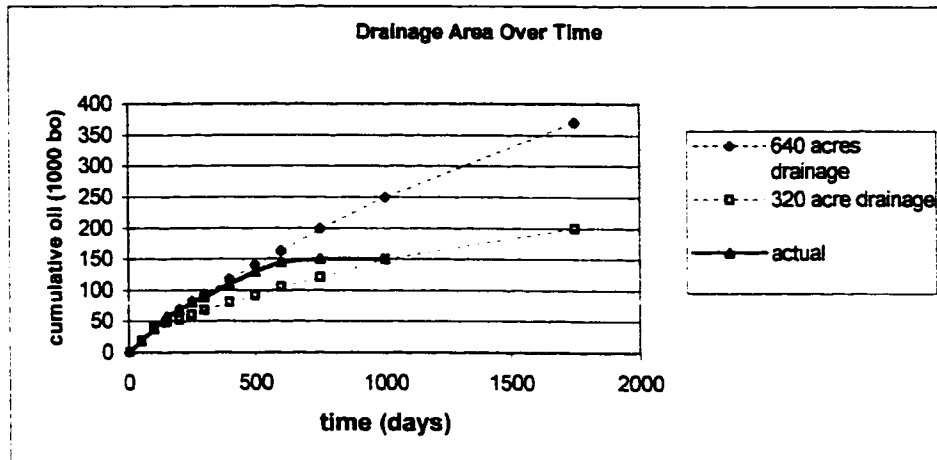


**Figure 7.36 Predicted Performance Based on Actual Drainage Area Over Time versus Actual**

Thus for a particular set of horizontal well lengths and reservoir parameters the performance can be predicted at any particular drainage size. Notice the deviation of the actual well production from the early time data. This is a result of the well beginning to sense the drainage area from competing wells. These times to drainage competition can be plotted to outline a drainage shape and the permeability contrast can be inferred.

## 7.8 Extension to Determine Drainage Area – Homogeneous and Fractured Reservoirs

The above method can be modified to predict the drainage area of a well and reservoir parameters in naturally fractured reservoirs by using the fractured type curve since the behavior of horizontal wells approaches that of the infinite conductivity fractured

vertical well with long well lengths in thin reservoirs. Thus a set of performance type curves for various reservoir sizes can be constructed just as above in figure 7.36.

Then actual production data from the well can then be compared to the predicted curves for various reservoir sizes to determine the best fit. These can also be used to help identify interference in drainage areas that were referred to in a previous section. The method of construction for fractured wells is as follows:

Repeat steps one through four as above. Instead of step 5, use the fully penetrating vertical fracture type curve. Repeat step six above then repeat for various times and plot as cumulative oil versus time for various drainage areas A again. Then plot the actual production profile on the same graph (Figure 7.36 dashed line) and see which drainage area fits best and note at which time if any the curve deviates from the best fit drainage area. Any flattening as shown in the diagram indicates a reduction in original drainage area. This can be attributable to the time at which drainage areas begin overlapping because of well competition. That information can be used as described in Section 7.6 and 7.7 to decompose  $k_x$  and  $k_y$ . It is especially useful if several wells are available to gauge changes versus direction and distance.

## **7.9 Chapter Summary**

The determination of directional permeability in an anisotropic reservoir is a difficult but important problem. Knowledge of this directional permeability can lead to better production prediction and design of proper well spacing. Without interference testing there is currently no direct way to estimate the directional permeability  $k_x$  and  $k_y$ . Decline curve analysis of wells that compete for drainage area provides a method of roughly estimating drainage shape and therefore directional permeability.

## **CHAPTER EIGHT**

### **Extensions of Decline Curve Analysis To More Complicated Reservoirs -Permeability Heterogeneity And Fractures**

#### **8.1 Introduction**

The decline curve analysis of this research has so far dealt with vertical and horizontal wells in homogeneous-isotropic and anisotropic reservoirs of constant directional permeability. More common situations involve highly heterogeneous formations where permeability variations are erratic and sometimes compartmentalized. Other common situations involve fractures of various types. This chapter will explore rate decline behavior in heterogeneous and fractured reservoirs through simulation experiments in controlled models. The analysis seeks to characterize various fracture types through characteristics exhibited in certain plotting techniques as well as type curve matching utilizing type curves developed by Poston and Chen for fractured reservoirs.<sup>43,44,45</sup>

##### **8.1.1 Heterogeneous Formation Considerations**

Heterogeneous formations can give rise to serious problems in the decline curve analysis and ultimate recovery projections. Heterogeneity can stem from either reservoir layering or rapid changes in spatial permeability within the reservoir<sup>38</sup>. Material balance is also predicated on the single tank model. Reservoir heterogeneity can also give rise to pressure gradients within the reservoir resulting in non-linearity of the pressure vs.

cumulative production plots. This leads to misinterpretation of future production and ultimate recoveries in low permeability and heterogeneous formations.

Scatter and curvature (which is also rate dependent) in the pressure decline vs. cumulative production plots can sometimes be attributed to pressure gradients in tight or heterogeneous reservoirs. It was already noted that late time deviations from early time decline curve predictions occur in reservoirs exhibiting drainage overlap. Scatter and curvature may contain valuable information that can be used to understand the heterogeneity, better predict reserves and forecast future development potential.

Experiments will be conducted with a number of models containing various types of heterogeneity in solution gas oil reservoirs. Experiments that model various fracture types and blocks of varying permeability are especially stressed in this chapter. The decline curves associated with production from those models will be analyzed in detail. Many plotting schemes are introduced in this chapter in an effort to help identify particular reservoir characteristics. For instance rather than plotting simply rate vs. time, the rate decline can be compared with actual rate as a function of rate-cumulative-time functions. Some of the normalization techniques of the previous chapter will also be applied in an effort to present the data in a form more suitable for well test analysis. However pressure is purposely ignored in the analysis since the purpose is to utilize only the rate decline data that is commonly available to the practicing engineer.

## **8.2 Geological Model of a Fractured System**

Decline curves used to predict future production from fractured flow regimes should model those geological-physical regimes. In other words the model should depict the geological system if possible. Poston and Chen<sup>43,44,45</sup> developed a naturally fractured reservoir model composed of a major and at least one additional minor fracture system and a matrix system of smaller blocks. Type curves were developed to represent a combination of flow through a major fracture system with infinite conductivity, linear flow through a set of lesser subsidiary micro-fractures and flow from the matrix block system. Flow from this system would also be predominately linear rather than radial. Flow from the macro fracture would not affect the shape of the curve since it is treated as infinite acting.

The authors noted that one would expect a horizontal well to intersect a greater number of fractures and thus have a different characteristic decline curve. However their analysis of Austin Chalk wells indicated that this was not the case. Rather, the family of curves that they developed matched for both horizontal and vertical wells except for the early data which is due (according to them) to the transient period being masked in the horizontal wells. This was confirmed by the simulation experiments.

Their model consists of the following attributes:

- 1) Major fracture with infinite conductivity
- 2) At least one minor fracture system with linear flow and

- 3) Rock matrix composed of small blocks
- 4) Linear rather than radial flow model

To summarize, the objective of their model is to:

- 1) Couple a single fracture type model to a dual porosity type model.
- 2) The model should consider the spatially dependent fracture orientation, connectivity, distribution and intensity of fractures.
- 3) Differentiate between the bounded PSS and transient flow and to predict future producing characteristics.
- 4) Distinguish macro from micro fractures.

The model would encompass the following assumptions:

- 1) The wellbore encountered macro fracture is a vertical plane of zero thickness with height equal to the formation thickness and of finite length in the lateral direction.
- 2) The fracture parallel to the drainage boundary. Uniform flux, infinite conductivity, or uniform flux can be used.
- 3) Micro fractures are more or less connected and continuous.
- 4) Production is from the wellbore fractures only. Micro-fractures feed the macro-fractures. Matrix acts as supporting sources to feed the fractures with fluid.
- 5) Constant pressure production condition.

Chen and Poston developed the following type curves representing the expected producing characteristics for a reservoir of this type<sup>41,42,43</sup>. (Figure 8.1)

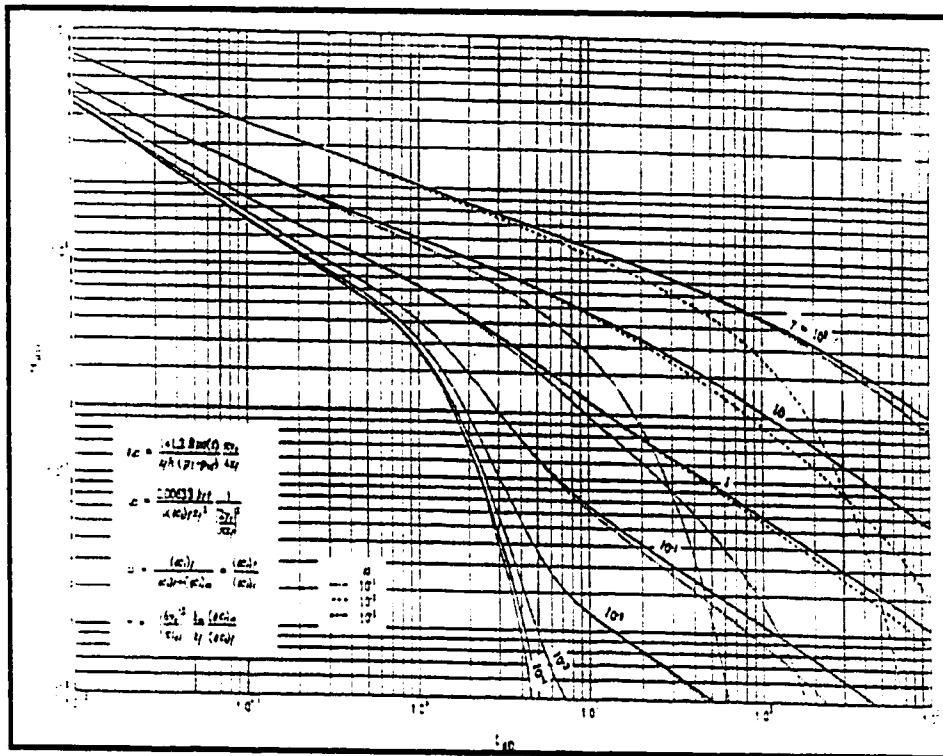


**Figure 8.1 Poston-Chen Type Curve for Fractured Reservoir<sup>41</sup>**

Three flow regimes would be recognized from these type curves but the flow from the macro-fracture would be treated as infinite acting and thus does not affect the curve shape:

**Regime One:** Unsteady state flow from the micro-fractures.

**Regime Two:** Transition of the flow system from mainly the micro-fractures to mainly the matrix.

**Regime Three:** Pseudo-steady state boundary dominated matrix flow.

Type curves should not only permit differentiation of the pseudosteady state and transient region but also aid in the estimation of future producing characteristics.

Figure 8.2 (reconstruction method explained later) shows the various theorized parts of the curve for the case of storage capacity of 0.1 and various degrees of fracture intensity as defined by Poston and Chen.

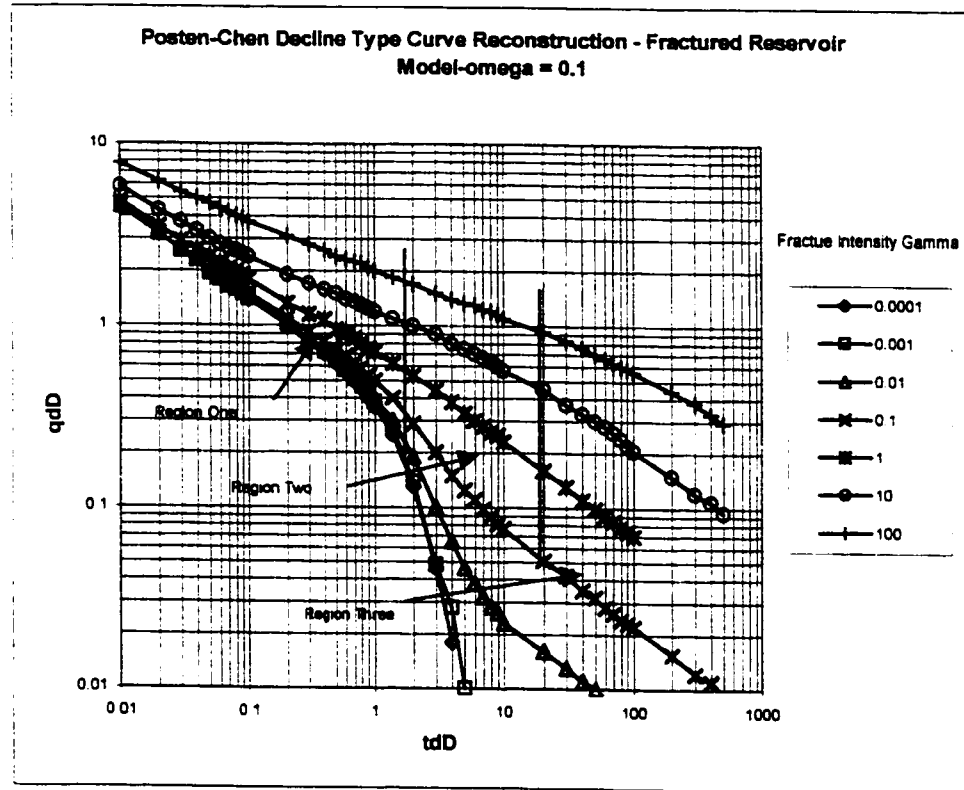


**Figure 8.2 Poston-Chen Decline Type Curve Reconstruction - Fractured Reservoir Model- $\omega$  (storage capacity) = 0.1**

Four fracture system types have been proposed and will be investigated.<sup>49</sup>

**Type One:** Fractures provide the significant reservoir storage capacity and permeability, which is thought to be characterized by high flow rate and short reservoir life.  $k_f \gg k_m$  and  $\phi_f \gg \phi_m$

**Type Two:** The matrix has good permeability and provides a good feed to the fracture system. High flow rates and longer reservoir life should result.

Type Three: The matrix permeability is low but contains most of the oil. The fractures contain high permeability.

Type Four: The fractures are filled with minerals and partition the formation into blocks.

These various types of fractures will be studied in this chapter.

### 8.3 Mathematical Introduction and Overview of the Poston-Chen Fracture

#### Model<sup>41,42,43</sup>

A Laplace and Green's function approach is used to provide analytical solutions for the model problem. The details as well as the formulation and construction of the type curves are summarized in the next section. The decline curve dimensionless rate and dimensionless time corresponding to the rectangular coordinates are defined respectively as:

$$q_{dD} = \beta_2 q_D \quad 8.1$$

and

$$t_{dD} = t_D / (\beta_1 \beta_2) \quad 8.2$$

where the normalizing factors are:

$$\beta_1 = (16 / \pi^3) / (y_e / x_f) \quad 8.3$$

$$\beta_2 = (\pi / 4) / (y_e / x_f) \quad 8.4$$

The dimensionless rate for the model is given as:

$$q_D(t_D) = \frac{141.2B\mu q(t)}{k_f h(p_i - p_{wf})} \quad 8.5$$

or rearranging and substituting for the normalizing factors and rectangular coordinates:

$$q_{dD} = \left( \frac{\pi}{4} \frac{y_e}{x_f} \right) \frac{141.2B\mu q(t)}{k_f h(p_i - p_{wf})} \quad 8.6$$

Note the similarity with the Fetkovich decline dimensionless decline:

$$q_{Dd} = \left[ \ln \left( \frac{r_e}{r_{wa}} \right) - 0.5 \right] \frac{141.2\mu B q(t)}{kh(p_i - p_{wf})} \quad 8.7$$

or using my more general form:

$$q_{Dd} = \frac{141.3\mu B q(t)}{kh(P_i - P_{wf})} \left[ 1.151 \log \frac{4A}{1.781C_A r_w^2} \right] \quad 8.8$$

Where  $p_{wf}$  is the constant bottom hole pressure and  $q(t)$  is the time dependent production rate at the wellbore. The dimensionless time is given as:

$$t_D = \frac{0.00633 k_f t}{\mu (\phi c_t)_f x_f^2} \quad 8.9$$

or rearranging and substituting for the normalizing factors and rectangular coordinates

$$t_{dD} = \frac{0.00633 k_f t}{\mu (\phi c_i)_f x_f^2 \left( \frac{2 y_e}{\pi x_f} \right)^2} \quad 8.10$$

These relationships, similar to the form of Fetkovich's radial systems and my general system equations, appear to be rectangular and linear. Note the similarities to the dimensionless decline time Fetkovich type equivalents reproduced below.

$$t_{Dd} = \frac{0.00634 k t}{\phi \mu c_i r_w^2} \left[ \frac{1}{\frac{1}{2} \left[ \left( \frac{r_e}{r_w} \right)^2 - 1 \right] \left[ \ln \left( \frac{r_e}{r_w} \right) - \frac{1}{2} \right]} \right] \quad 8.11$$

or using my more general form:

$$t_{Dd} = \frac{0.00634 k t}{\phi \mu c_i r_w^2} \frac{r_w^2}{A} \left[ \frac{5.44678}{\log \frac{4A}{1.781C_A r_w^2}} \right] = t_D \frac{r_w^2}{A} \left[ \frac{5.44678}{\log \frac{4A}{1.781C_A r_w^2}} \right] \quad 8.12$$

and putting in a similar arrangement to that of the Fetkovich radial form:

$$t_{Dd} = \frac{\frac{t_D}{\log \frac{4A}{1.781C_A r_w^2}}}{\frac{A}{r_w^2} \frac{5.44678}{1.781C_A r_w^2}} = \frac{t_D}{\frac{0.183594 A}{r_w^2} \log \frac{4A}{1.781C_A r_w^2}} = \frac{t_D}{0.183594 (c_1 c_2)} \quad 8.13$$

## **8.4 Construction and Development of the Decline Curves**

Poston and Chen developed type curves based on the fractured reservoir model<sup>41</sup>. The solution to the dimensionless rate and time are based on an iterative calculation of the Laplace transform of the constant production rate equations. Conversion to dimensionless decline parameters follows in a manner similar to that of Fetkovich. An extension to horizontal wells in the transient regime is investigated utilizing the equivalent wellbore radius concept.

### **8.4.1 Model Assumptions**

There are two basic groups of assumptions regarding the geometry and rock properties of the model as follows:

1. A horizontal, uniform thickness, naturally fractured reservoir completely filled with a fluid of small and constant compressibility and constant viscosity, bounded by an upper and lower impermeable strata is considered. The drainage area is assumed rectangular with closed outer boundaries. The wellbore fracture is represented by a vertical plane of zero thickness in the y direction with a height equal to the formation thickness and of finite length in the lateral x directions and symmetrical with respect to the wellbore and parallel to the drainage boundary.

2. The micro-fractures are more or less connected and are considered as a continuous network. Uniform spheres are used to approximate the geometry of the matrix blocks. The permeability of the fractures is much larger than that of the matrix blocks. In other words the micro fracture network is visualized as a large-scale version of a conventional intergranular porous medium. Such a continuum model implies that both the size and permeability of the intervening matrix blocks are small enough to avoid disturbance of the macroscopic flow. Fluid flow toward the well and wellbore fracture in the reservoir is considered entirely through the natural fracture network. The fluid in the matrix blocks acts a source to the natural fracture network. Communication between the matrix blocks is not allowed. The mathematical formulation is developed in SPE paper 23527<sup>42</sup>. The wellbore-intercepted fracture is assumed to extend over the entire vertical extent of the formation but is bed contained. Both infinite conductivity and uniform-flux conditions are considered.

#### **8.4.2 Limiting Equations Used in Construction**

By solving the governing equation by the Laplace domain instantaneous source and Green's function with product solution approach and defining dimensionless parameters as defined in the previous section, the authors develop the dimensionless rate equation of a fully penetrating fracture intersecting the wellbore as:

$$\bar{q}_D(s) = \frac{2}{\pi y_{eD}} \frac{1}{s} \left[ y_{eD} \sqrt{sf(s)} \operatorname{th}(y_{eD} \sqrt{sf(s)}) \right] \quad 8.14$$

where the decline curve dimensionless rate and time are given as before as:

$$q_{dD} = \beta_2 q_D = q_D \frac{\pi v_e}{4x_f} \quad 8.15$$

and the dimensionless time is:

$$t_{dD} = \frac{t_{fD}}{\beta_1 \beta_2} = \frac{4x_f^2 t_{fD}}{y_e^2} \quad 8.16$$

Seven limiting forms can be derived from which the decline curves are constructed in a similar way to that of Fetkovich type curves. These limiting forms can be shown to be dependent on two parameters  $\omega$  and  $\gamma$  as previously defined. These parameters are the storage expansion ratio and the inter-porosity flow or fracture intensity parameters. These two parameters characterize the behavior of the dual porosity system. The seven limiting forms with the constraints are expressed below:

#### Infinite Region:

$$q_D(t_{fD}) = \frac{2}{\pi^{2/3}} \frac{1}{\sqrt{t_{fD}}} \left[ t_{fD} < \frac{1}{(3\lambda\omega)} \right] \quad 8.17$$

This limiting form corresponds to the approximations of  $(3\lambda\omega/s) \ll 1$  and hence  $f(s)=1$ .

$$q_D(t_{JD}) = \frac{2}{\pi^{2/3}} \frac{1}{\sqrt{t_{JD}}} + \frac{\sqrt{3\lambda\omega}}{\pi} ; \left[ \frac{1}{3\lambda\omega} < t_{JD} < \frac{0.3\omega}{\lambda} \right] \quad 8.18$$

$$q_D(t_{JD}) = \frac{2(\lambda\omega)^{1/4}}{\pi\Gamma(3/4)} \frac{1}{t_{JD}^{1/4}} ; \left[ t_{JD} > \frac{0.3\omega}{\lambda} \right] \quad 8.19$$

where  $\Gamma$  is the Gamma function and  $\Gamma(3/4)$  is 1.225420.

The finite acting limiting forms are:

$$q_D(t_{JD}) = \frac{1}{\beta_2} \sum_{n=1}^{\infty} \exp \left[ -(2n-1)^2 \frac{t_{JD}}{\beta_1 \beta_2} \right] \quad 8.20$$

$$q_D(t_{JD}) = \frac{1}{\beta_2} \sum_{n=1}^{\infty} \exp \left[ -(2n-1)^2 \frac{\omega t_{JD}}{\beta_1 \beta_2} \right] \quad 8.21$$

$$q_D(t_{JD}) = \frac{1}{\beta_2} \sum_{n=1}^{\infty} \frac{1}{a} \exp \left[ \frac{-(2n-1)^2}{a} \frac{\omega t_{JD}}{\beta_1 \beta_2} \right] \quad 8.22$$

and

$$q_D(t_{JD}) = \frac{1}{\beta_2} \sum_{n=1}^{\infty} \frac{\gamma}{\gamma - (2n-1)^2} \operatorname{erfc} \left[ b \sqrt{\frac{t_{JD}}{\beta_1 \beta_2}} \right] \exp \left[ b^2 \frac{t_{JD}}{\beta_1 \beta_2} \right] \quad 8.23$$

where:

$$\alpha = 1 + (2n-1)^2 \frac{3(1-\omega)^3}{5\omega} \frac{1}{\gamma} \quad 8.24$$

$$b = \frac{(2n-1)^2 \sqrt{\gamma}}{\gamma - (2n-1)^2} \quad 8.25$$

$$\gamma = 3\lambda\omega / \beta_1 \beta_2 = 3\lambda[(1-\omega)/\omega] \beta_1 \beta_2 \quad 8.26$$

$$\beta_1 = \frac{16y_{eD}}{\pi} \quad 8.27$$

$$\beta_2 = \frac{\pi y_{eD}}{4} \quad 8.28$$

If the erfc function is approximated as  $\operatorname{erfc}(z) \approx \exp(-z)^2 / \sqrt{\pi z}$  for large values of the argument then the last limiting equation can be approximated by:

$$q_D(t_{JD}) = \frac{1}{\beta_2} \sum_{n=1}^{\infty} \frac{\sqrt{\gamma/\pi}}{(2n-1)^2} \frac{1}{\sqrt{t_{JD}/(\beta_1 \beta_2)}} \quad 8.29$$

The limiting equations can then be plotted for various ranges of reservoir size and limiting parameters just as with the Fetkovich construction where the  $q_{Dd}$  was constructed for increasing reservoir size  $r_{eD}$ . The fracture dimensionless curves are constructed for increasing  $y_e/x_f$ .

$$q_{Dd} = \beta_2 q_D = q_D \frac{\pi y_e}{4x_f} \quad 8.30$$

and the dimensionless time is:

$$t_{Dd} = \frac{t_D}{\beta_1 \beta_2} = \frac{4x_f^2 t_D}{y_e^2} \quad 8.31$$

The lines will converge and overlap. The values of the limiting areas can then be extracted and re-plotted to form the Type curve shown in figure 8.3 which closely replicates the Poston and Chen curves in Figure 8.1.

The Poston-Chen curve for a storage compressibility of 0.1 with superimposed Fetkovich type curve is shown in figure 8.3. Note the convergence of the two type curves in the depletion period for low values of fracture intensity. The transient period is also markedly different in the fractured regime.

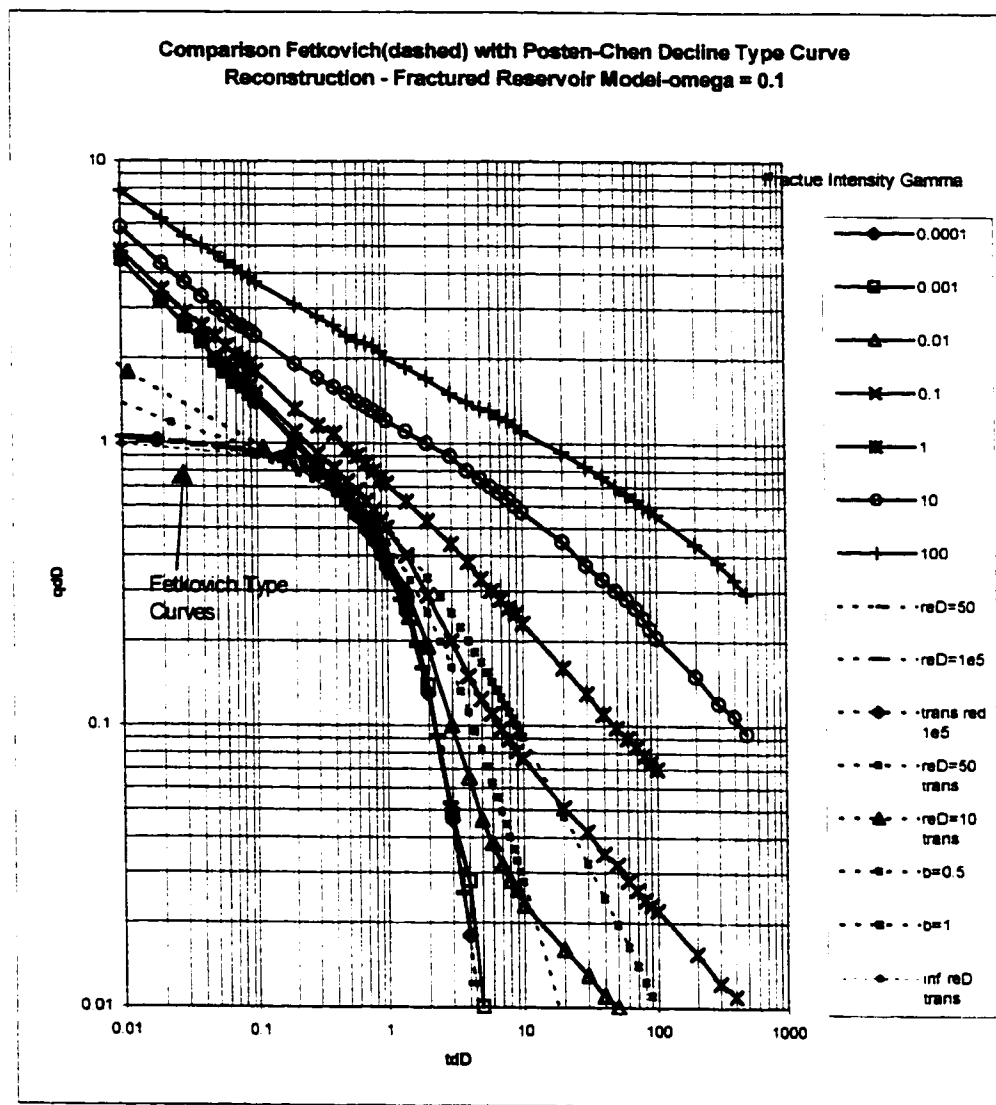


**Figure 8.3 Comparison Fetkovich (dashed lines) with Poston-Chen Decline Type Curve Reconstruction - Fractured Reservoir Model-Storage Compressibility  $\omega = 0.1$**

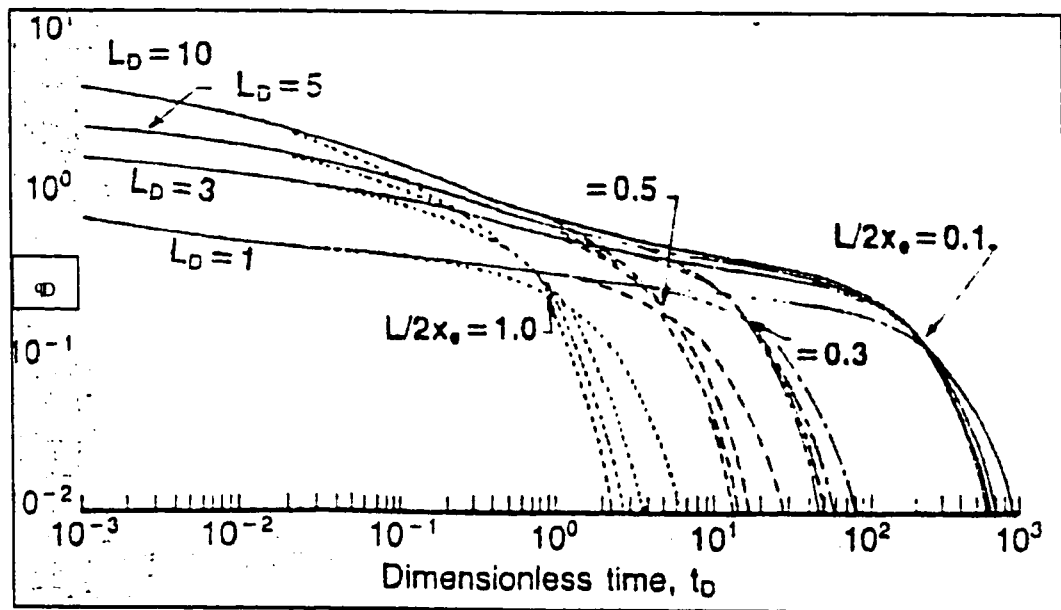
An examination of the curves indicates that the Poston and Chen curves treat the initial period, as infinite acting which is not always typical of a horizontal well in fractured media. As the simulation experiments indicate even with fracture permeability of as much as 4000 md the initial flow does not always follow the early time Poston-Chen curves but does match the late time portions very well. The examples in their published papers from Austin Chalk reservoirs also did not match the early time behavior but similar to the simulation experiments showed a much "flatter" early time slopes. However the combined Fetkovich type superimposed on the Poston Chen curves in Figure 8.3 do provide the extremes to compare. The actual early time path of a fractured well will be somewhere in between the two cases. Since the curves are primarily being used to classify fracture types this is not a serious limitation but does present some difficulties in curve matching.

If the dimensionless well length is known then an alternative early time behavior can be approximated using the Poston Chen's Fetkovich equivalent dimensionless constants and applying the horizontal dimensionless rate and time values

$$q_{dD} = \left( \frac{\pi}{4} \frac{y_e}{x_f} \right) \frac{141.2 B \mu q(t)}{k_f h (p_i - p_{wf})} = \left( \frac{\pi}{4} \frac{y_e}{x_f} \right) q_D \quad 8.32$$

$$t_{dD} = \frac{0.00633 k_f t}{\mu (\phi c_r)_f x_f^2 \left( \frac{2 y_e}{\pi x_f} \right)^2} = \frac{t_D}{\left( \frac{2 y_e}{\pi x_f} \right)^2} \quad 8.33$$

similar to values from figure 7.33 of the previous chapter.



Reproduced Figure 7.33<sup>32,34</sup>

The Poston-Chen early time infinite conductivity assumptions are more similar to using the fully penetrating infinite conductivity fracture such as shown in figure 8.4.<sup>33</sup>

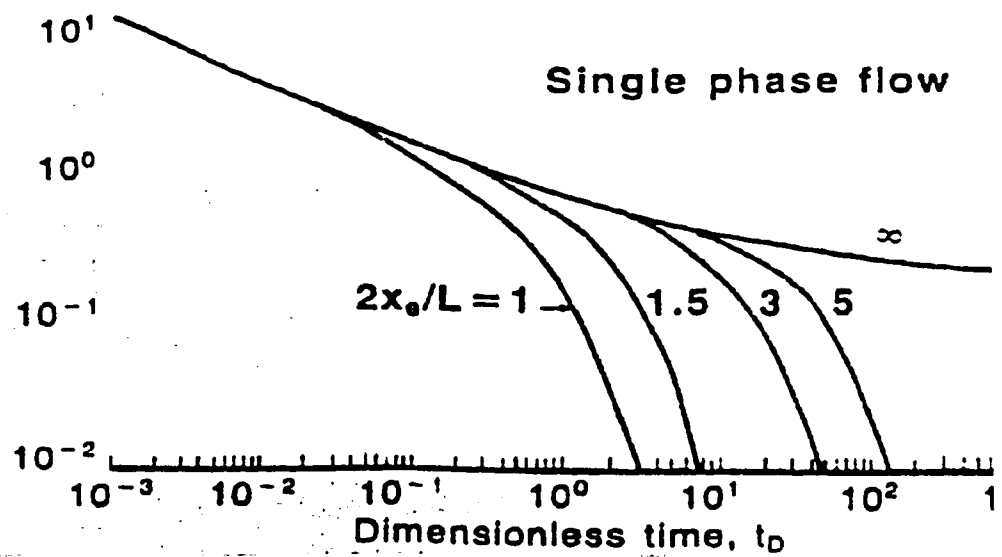


Figure 8.4 Fracture Dimensionless Rate versus Dimensionless Time Horizontal Wells<sup>13</sup>

Thus a more reasonable early time curve falls in between the Fetkovich type curve and the Poston-Chen early time. This preserves the Poston Chen late time behavior but changes the early time behavior to that actually seen in some of the field and in the simulation experiments.

#### 8.4.3 New Dual Porosity Dimensionless Parameters

For the standard homogeneous type curve models of Arps and Fetkovich there is just one correlation parameter  $r_c/r_w$  or  $\sqrt{A}/r_w$  for the more general case in the transient portion and one parameter "b" for the pseudosteady state decline solution. Dimensionless parameters characterizing a dual porosity behavior are traditionally defined as the 1) storage expansion ratio  $\omega$  and 2) the inter-porosity flow parameter  $\lambda$ . The storage capacity expansion factor is defined as:

$$\omega = \frac{(\phi c_t)_f}{(\phi c_t)_f + (\phi c_t)_m} = \frac{(\phi c_t)_f}{(\phi c_t)_t} \quad 8.34$$

which is known as the ratio of storage expansion of the fracture system to the total system. For many fractured systems (Type 3 fractures) the fracture porosity is low and the storage expansion ratio is just the ratio of  $\phi_f/\phi_m$ . The presence of fluid influx from the matrix blocks will thus override the compressibility effect and produce a production "tail".

A useful variation of this storage expansion factor is:

$$\omega' = (1-\omega)/\omega = (\phi_{ct})_m / (\phi_{ct})_f \quad 8.35$$

Thus  $\omega$  is based on expressions for inter-porosity flow and storage compressibility. The term defines the difference between the fracture and matrix flow, which can theoretically be used to characterize the type of fracture system.

For a formation such as the Austin Chalk which has low fracture porosity  $\phi_f$  but good fracture permeability  $k_f$  (type 3) and often also has good matrix support, values of  $\omega$  averages about  $10^{-3}$ . The Austin Chalk has fracture porosity of about 0.005. So  $\omega$  is approximately  $(\phi_f)/(\phi_m)$  or  $0.005/0.16$ . The presence of fluid influx from the matrix blocks will override the compressibility effect and produce a production tail in such cases.

The second limiting parameter  $\lambda$  can be re-characterized and defined as  $\gamma$ . The  $\gamma$  term is proportional to the fracture intensity, FI, and is thus a direct indicator of fracture intensity if the matrix and fracture compressibility are the same and  $\omega$  is of the order  $10^{-3}$ . The smaller the value of  $\gamma$  the smaller the production rate, life of the well and thus less tail on the decline curve. A large value of  $\gamma$  can imply a high fracture intensity and good fracture connectivity and tends to be characteristic of small values of storage expansion ratio. Thus according to Poston and Chen, the extended production tailing is a result of primarily matrix fluid contribution and not compressibility effects.

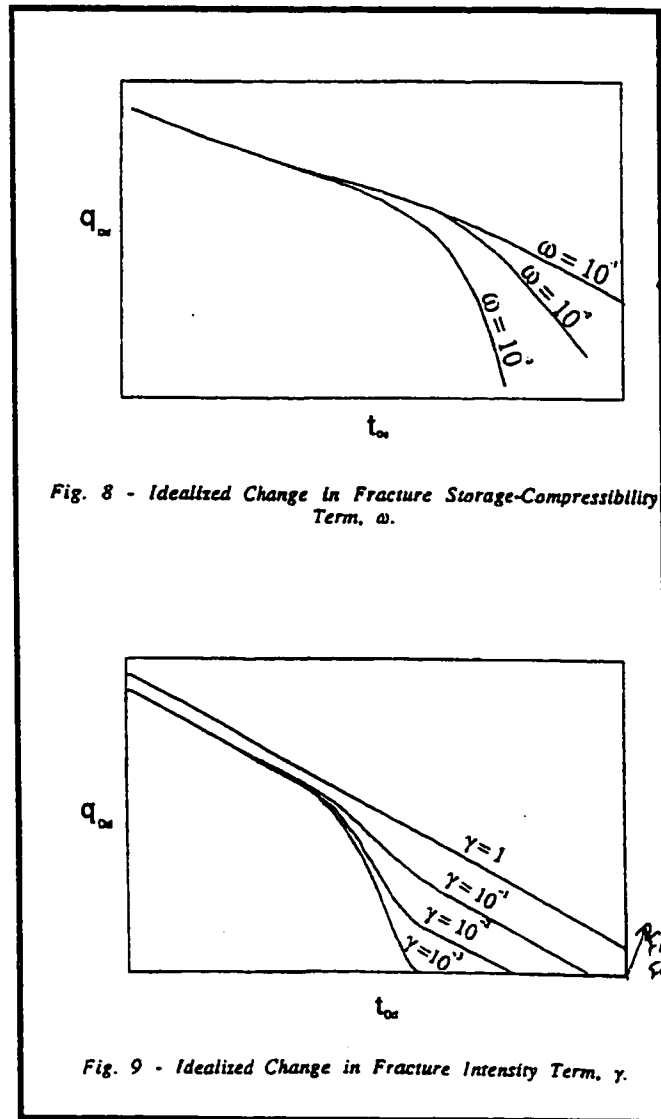
$\gamma$  is related to the inter-porosity parameter  $\lambda$  and  $\omega$  by:

$$\gamma = 3\lambda\omega\beta_1\beta_2 = 3\lambda\beta_1\beta_2(1-\omega)/\omega \quad 8.36$$

$$\gamma = (FI)^2 x_f^2 \frac{k_m(\phi c_t)_m}{k_f(\phi c_t)_f} \beta_1 \beta_2 = \left( \frac{6}{\pi} \frac{y_e}{l_c} \right)^2 \frac{k_m(\phi c_t)_m}{k_f(\phi c_t)_f} \quad 8.37$$

Poston and Chen state that in the Austin Chalk,  $\gamma$  can often be a direct indicator of fracture intensity if the ratio of  $k_m\phi_m c_m / k_f\phi_f c_f$  is approximately one. Whether this is a common occurrence is unknown however it will be tested in the simulation experiments.

Figures 8.4 and 8.5 show Poston and Chen's general storage compressibility  $\omega$  and fracture intensity relationships.



Figures 8.6 and 8.7 Dimensionless Type Curves for Variations in Storage Compressibility and Fracture Intensity<sup>41,42,43</sup>

## 8.5 Application

The Austin Chalk of south Texas and the Viola of Oklahoma provide two good contrasting fractured carbonate examples. The Austin Chalk exhibits high initial production from the fracture system followed by a steep drop off in production as the fracture systems are depleted. The Austin Chalk does, in many cases, continue to provide some support to production from the matrix after the steep initial drop. However, the Viola rate drop-off is very abrupt and provides little post drop off production support from the outlying matrix system. Once the fracture system is depleted the wells are usually abruptly uneconomic. Presumably the matrix permeability is too limited to provide pressure support.

The unique feature of the dual fracture - matrix type curves lies in the abrupt decline followed by the extended production tail of the decline curve for certain storage compressibility conditions. The author's indicate that the tail is a consequence of the matrix contribution in this formulation. The simulation experiments indicate that the tail may also be a result of the solution gas effect. Naturally fractured reservoirs with small matrix permeability would display a pronounced fall off later in the life of the well.

Recall that the Poston Chen models use the following relationships:

$$q_{dD} = \left( \frac{\pi}{4} \frac{y_e}{x_f} \right) \frac{141.2 B \mu q(t)}{k_f h (p_i - p_{wf})} \quad 8.38$$

$$t_D = \frac{0.00633 k_f t}{\mu (\phi c_i)_f x_f} \quad 8.39$$

with correlation parameters:

$$\omega = \frac{(\phi c_i)_f}{(\phi c_i)_f + (\phi c_i)_m} = \frac{(\phi c_i)_f}{(\phi c_i)_t} \quad 8.40$$

$$\gamma = (FI)^2 x_f^2 \frac{k_m (\phi c_i)_m}{k_f (\phi c_i)_f} \beta_1 \beta_2 = \left( \frac{6}{\pi} \frac{y_e}{l_c} \right)^2 \frac{k_m (\phi c_i)_m}{k_f (\phi c_i)_f} \quad 8.41$$

Poston and Chen used these type curves and drew certain conclusions based on matching of data for Austin Chalk production data. Since actual reservoirs are heterogeneous and anisotropic in unknown ways, simulation experimentation offers a method to test and properly validate the type curve model. Only then can they be used to help characterize fracture types. Comparisons of short and long term production decline curves are useful.

## 8.6 Experiments with Fractured Media

In an effort to both test the Poston Chen Type curves, to try to classify the various fracture types by decline curve characteristics and to possibly modify the Poston Chen curves to a more realistic early time behavior, simulation models were constructed for

each fracture type. The type curves were then applied to each experimental output and comparisons are made between various graphical output of the various fracture types. Recall that the fractures were classified by types into the following four categories.<sup>49</sup>

- Type One:** Fractures provide the majority of the movable reservoir storage capacity and permeability, which is characterized by high flow rate and short reservoir life.  $k_f \gg k_m$  and  $\phi_f \gg \phi_m$
- Type Two:** The matrix has good permeability and provides a good feed to the fracture system. High flow rates and longer reservoir life result.
- Type Three:** The matrix permeability is low but contains most of the oil. The fractures contain high permeability.
- Type Four:** The fractures are filled with minerals and partition the formation into blocks.

Unfortunately it was difficult to model an extreme case type 1 fracture where there was almost no storage capacity in the matrix while keeping other parameters fairly constant. However it was possible to model a system that contained a large part of the storage capacity in the fracture (18%) relative to the type two and three fractures cases where fracture storage was only 1%. A reasonable qualitative comparison could thus be obtained. This is not considered a serious limitation since even in very tight formations such as the Viola of Oklahoma there is significant though immovable oil in the matrix.

## 8.7 Model Descriptions

To properly compare and classify the various fracture types it was necessary to construct models that contained, as much as feasible, identical characteristics such as

reservoir dimensions, total pore volume, total fluid volumes, initial fluid saturation, grid spacing, grid number and PVT parameters. In other words the experiments were designed to test fracture type classifications in a scenario that compared only the relative changes in matrix and fracture storage capacity and permeability by keeping the sum total reservoir rock and fluid volumes and initial saturation identical. Therefore models were constructed as follows:

All models contained 784 grid blocks (near the capacity of the boastvhs simulator) in a nearly square reservoir. The total system oil in place was a constant 3.37 million stock tank barrels and initial gas in solution was 1.5 bscf in all cases. Relative matrix-fracture pore volume was adjusted to maintain a constant total system pore volume within each model but was distributed between the fracture and matrix to fit the model type as well as possible according to the following generalized summary table 8.1. The initial reservoir pressure is 2000 psia and bubble point is 1600 psia. The horizontal reservoir length to horizontal well length ratio  $X_e/L$  was a constant 8.5 for all cases.

#### Constant OOIP is 3.37 Million Stock Tank Barrels

| Model    | Order of<br>initial q<br>Highest<br>→1 | Matrix<br>k. md | Fracture<br>k. md            | coip/coip, | Storage<br>Factor<br>$\omega$ | $k_f/k_m$<br>$1/\lambda'$ | $k_w/k_f$<br>$\lambda'$ | $k_{pw}$ | Fracture<br>Intensity |
|----------|--|-----------------|------------------------------|------------|-------------------------------|---------------------------|-------------------------|----------|-----------------------|
| Type 1   | 6                                      | 0.1             | 1000                         | 4%         | .036                          | 10000                     | .0001                   | 44.6     | .00036                |
| Type 1h  | 5                                      | 0.1             | 4000                         | 4%         | .036                          | 40000                     | .000025                 | 178.1    | .00036                |
| Type 1n  | 4                                      | 0.1             | 1000                         | 18%        | .146                          | 10000                     | .0001                   | 177.6    | .0015                 |
| Type 1hn | 3                                      | 0.1             | 4000                         | 18%        | .146                          | 40000                     | .000025                 | 710.4    | .0015                 |
| Type 2   | 2                                      | 10.1            | 1000                         | 1%         | .007                          | 100                       | .01                     | 18.62    | .00038                |
| Type 2h  | 1                                      | 10.1            | 4000                         | 1%         | .007                          | 400                       | .0025                   | 44.43    | .00038                |
| Type 3   | 8                                      | 0.1             | 1000                         | 1%         | .007                          | 10000                     | .0001                   | 8.7      | .00038                |
| Type 3h  | 7                                      | 0.1             | 4000                         | 1%         | .007                          | 40000                     | .000025                 | 34.52    | .00038                |
| Type 4   |  | 10.1            | 4000<br>with<br>compartments | 1%         | .007                          | 400                       | .0025                   | 34.43    | .00038                |

**Table 8.1 Simulation Model Parameters**

It was shown in the master's thesis that as the fracture intensity increases, the performance derived oil relative permeability approaches a straight line between zero and irreducible liquid saturation.<sup>12</sup> Low fracture intensity wells have  $k_{ro}$  similar to laboratory determined matrix curves. Wells with higher fracture intensity generally exhibit more favorable  $k_{ro}$  at high gas saturation and approach straight lines. As the degree of fracturing increases,  $k_g/k_o$  becomes more unfavorable toward oil recovery. In this case however the relative permeability curves were kept constant in the experiments to avoid introducing an unknown parameter. The effect of the relative permeability in the matrix versus the fracture could be investigated later.

The author has used traditional fractured reservoir parameters in Table 8.1 as well as defined several variables that are variations of the traditional fracture parameters. Traditional parameters include storage coefficient,  $\omega$ , fracture transfer rate,  $\lambda$ , fracture intensity term  $\nu = \frac{\phi_f - \phi_m}{1 - \phi_m}$ , and Poston Chen correlation, parameter  $\gamma$ .<sup>44,47,48</sup> The fracture intensity term requires a calculation of the total system porosity using the pore volume weighted porosity of the fracture and matrix. Modified parameters are also used since it is difficult to estimate the compressibility. A simple storage factor  $\omega'' = \frac{V_f \phi_f}{V_f \phi_f + V_m \phi_m}$  is used for discussion purposes to show the relationship of fracture porosity to total system porosity. This is essentially the same as the traditional  $\omega$  without the compressibility terms (see equation 8.40). The oil filled fracture pore volume to total system pore volume (ooip/ooip<sub>t</sub>) can also approximate the storage coefficient. This term allows a more direct conceptual

comparison of the various experimental outputs. Likewise the traditional  $\lambda = c r_w^2 k_m / k_f$ , which is an indication of fluid transfer rate from matrix to fractures is simplified in the discussions to  $\lambda = k_m / k_f$  for conceptual clarity since only one well dimension is used. This term is then further modified to incorporate pore volume weighted permeability for the system. This should provide another possible useful parameter to classify the system in the presence of a horizontal well that intersects both matrix and fractures.

For instance  $k_{pv}$ , for comparison purposes, will be defined as the pore volume weighted bulk permeability:

$$k_{pvt} = \frac{\sum k_f V_{pvf} + \sum k_m V_{pvm}}{V_{pvt}} \quad 8.42$$

$V_{pvf}$  = Pore volume of fracture

$V_{pvm}$  = Pore volume of matrix

$V_{pt}$  = Total model pore volume

All of these various traditional and modified parameter values are shown in table 8.1 so that a comparison can be made as the individual model outputs are compared and contrasted. It will be useful to refer to Table 8.1 during the discussion of the graphical output.

## 8.8 Simulation Output

The reservoir simulation output is too voluminous to include in this report but the following sections summarize some of the main points of the various experiments. More

complete tabular simulation output and calculations are included in the appendix G.

More complete experimental and graphical output is available from the author.

The experimental output collected consisted of tabular pressure, oil, gas, water rate and cumulative data as well as phase saturation data for each time step. That output was input to spreadsheets and used in various calculations that were graphed. As mentioned before, pressure data was collected to help in the analysis of the rate data but is not used in the characterization since this type of data will not be available for most reservoir situations. Even valuable early time daily rate data are hard to obtain. One can only reasonably expect to have monthly rate and cumulative production data after the first year of production and occasionally some sporadic bottomhole shut-in pressure data. Since most domestic onshore wells produce at maximum rate limited only by separator backpressure, flowing wellhead pressures are of little value and can give misleading results. Poston and Chen used those values in their analysis but the general applicability and availability of such data is questionable. This analysis is restricted to data that can be obtained by the practicing from traditional public data sources. Graphical output for each fracture experiment as well as tabular results (included in Appendix G) consisted of the information listed in Table 8.3. Only selected output that was deemed most relevant is included in this report.

| Graph Type   | Cartesian | Semi-Log | Log-Log |
|--|-----------|----------|---------|
| Oil Rate versus Time: $q$ vs. $t$  | X         | X        | X       |
| Oil and Gas Rate versus Cumulative: $q$ vs. $q_{cum}$  | X         | X        | X       |
| Cumulative Oil and Gas vs. Time: $q_{cum}$ vs. $t$   | X         | X        | X       |
| Oil Rate $q$ vs. $(t_p + \Delta t)/\Delta t$ Note: not well testing definition (see report body)               |           |          | X       |
| Pressure Average vs. $(t_p + \Delta t)/\Delta t$ Note: not well testing definition                             |           | X        | X       |
| Oil Rate Change $\Delta q$ vs. $(t_p + \Delta t)/\Delta t$ Note: not well testing definition (see report body) |           |          | X       |
| Average Reservoir Pressure versus Cumulative Oil: $P$ vs. $q_{cum}$  | X         |          | X       |
| Oil Rate Change/Oil Rate versus Cumulative Oil/Rate: $(\Delta q/q)$ vs $q_{cum}/q$                             | X         | X        | X       |
| Pressure Change/Rate vs Cumulative Oil/Rate: $(\Delta p/q)$ vs $q_{cum}/q$                                     |           | X        | X       |
| Pressure Change vs time: $\Delta p$ vs. $t$  |           | X        | X       |
| Oil Rate Change vs time: $\Delta q$ vs. $t$  |           | X        | X       |
| Oil Rate Change vs Pressure Change: $\Delta q$ vs. $\Delta p$  |           | X        | X       |
| Pressure Change vs Cumulative: $\Delta p$ vs. $q_{cum}$  |           | X        | X       |
| Pressure Change vs square root of time: $\Delta p$ vs. $\sqrt{t}$  |           | X        | X       |
| Oil Rate Derivative versus Cumulative Oil: $q'$ vs. $q_{cum}$ (also smoothed)                                  |           | X        | X       |
| Oil Rate Derivative versus Time: $q'$ vs. $t$ (also smoothed )   |           | X        | X       |
| Pressure $P'$ , Oil Rate Derivative versus Time: $P'$ vs. $t$ (also smoothed )                                 |           | X        | X       |
| Oil Rate Derivative * Time vs Cumulative Oil: $q' * t$ vs. $q_{cum}$   |           | X        | X       |
| Oil Rate Change/Oil Rate Derivative versus Time: $(\Delta q/q)'$ vs $t$  |           | X        | X       |

Table 8.2 Graph Output Generated

Surface diagrams of the pressure and saturation conditions for each grid block at selected time steps were also utilized in the analysis. The primary graphs that proved diagnostic in classifying the fracture types were the rate-time, cumulative-time, rate derivative-time, rate- $(t_p + \Delta t)/\Delta t$ ,  $\Delta q$ -time and the  $(\Delta q/q)$  vs.  $(q_{cum}/q)$  plots. Note that  $t_p$

is not the traditional well test parameter but rather defined as  $t_p = [(q_{cum}/q) + \Delta t]/\Delta t$ . The physical significance, if any, of this parameter is unknown but it seemed to have some value in classifying the reservoirs.

The  $(\Delta q/q)$  vs.  $(q_{cum}/q)$  plots were generated to approach the problem from a normalization and material balance standpoint that seems to have some semi-quantitative usefulness. This type of plot presents the data in a manner similar to well test analysis. A plot of  $\log(\Delta p/q)$  or  $(\Delta q/q)$  vs.  $\log(q_{cum}/q)$  (or the inverse) should transfer the data to data suitable for well test analysis. If pressure was available then linear flow would be characterized by 1/2 slope and pseudosteady state exponential decline would exhibit unit slope. Plateaus in the plot could be characteristic of possible hierarchical fracture systems and dual porosity character should be visible. Qualitative extension to rate data may be possible.

Decline curves were developed under the assumption of constant flowing bottom hole pressure but most wells declining to production capability, exhibit decreasing tubing head pressure which reflects a declining flowing bottom hole pressure. Therefore a normalization technique should be useful. Normalizing the flow rates by dividing the production rates by the change in tubing head pressure ( $FTHP_{initial} - FTHP_{current}$ ) was used by Poston and Chen to approximate the constant flowing bottomhole pressure assumptions. Though this is an ideal situation, using that data to approximate actual bottomhole flowing pressures is dangerous since practically speaking most US wells

decline to pipeline or separator pressure very quickly and produce against a constant backpressure.

Since this type of data are not often available, this work modified the method to use rate divided by changes in rate ( $q/\Delta q$ ), (or the inverse) which seem to approximate the general shape of the  $q/\Delta p$  curves. Although this ( $q/\Delta q$ ) cannot be used in a strictly quantitative sense it does give relative characteristics of the various fracture types. The normalization should also magnify the changes in storage compressibility and fracture intensity terms.

If the material balance equation is arranged in the form of a straight line for PSS flow then a Cartesian plot of  $\Delta p/q$  vs.  $q_{cum}/q$  should yield a straight line of slope  $m$  that defines the matrix pore volume where the slope ( $m$ ) =  $5.615^* (B_o/V_p c_t)$  where  $V_p$  is the pore volume. The rate of change of  $\Delta q/q$  vs. cumulative  $q/q$  is plotted as an approximation to such pressure data. As such the actual pore volume can not be computed exactly but the relative slope can be used for qualitative interpretation.

As with the derivative of pressure ( $\Delta p/dt$ ), the derivative of rate with respect to time ( $\Delta q/dt$ ) should give an indication of the storage compressibility since pressure and rate are related quantities. The deeper the trough on the pressure derivative plots the lower the storage factor (i.e. lower fracture storage). This parameter can also be seen on the semi-log pressure-time plot as a double straight line offset. The larger the offset the

lower the storage factor and the more time delayed is the offset to the lower value of  $\lambda$ .

Although pressure is not used here it was hoped that the  $(\Delta q/q)$  vs.  $\log(q_{cum}/q)$  plot would transfer the rate data to a pseudo-pressure plot which will exhibit the same phenomenon. These topics will be discussed in more detail as each graph is discussed.

## 8.9 Analysis of Experimental Results

To summarize, the analysis consists of an examination of the following types of data:

1. Simulation experiments to approximate rate decline performance of four different fracture types.
2. Type curve matching of the rate-time experimental output to the Poston-Chen-Fetkovich curves.
3. Comparison to conclusions and results obtained by Poston and Chen from actual field data from Austin Chalk reservoirs.
4. Graphical analysis of various calculation data from simulation output.
5. Visualization of pressure and saturation profiles using surface diagrams from simulation tabular output.

Figures 8.9 through 8.16 show the basic rate versus time data for the various fracture experiments on log-log plots. This is the first data to examine for general comparison between the experiments.

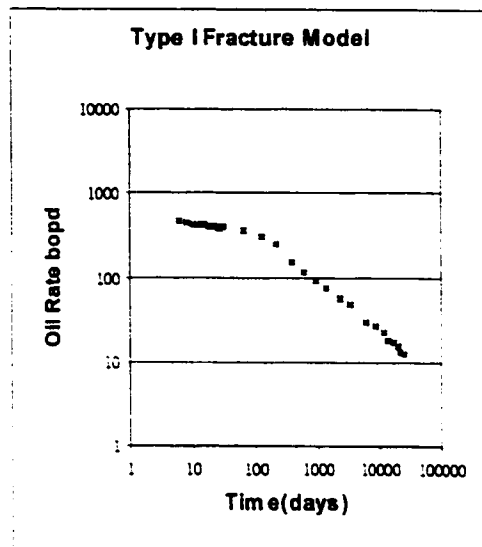


Figure 8.8 - Rate Time Plots Type 1

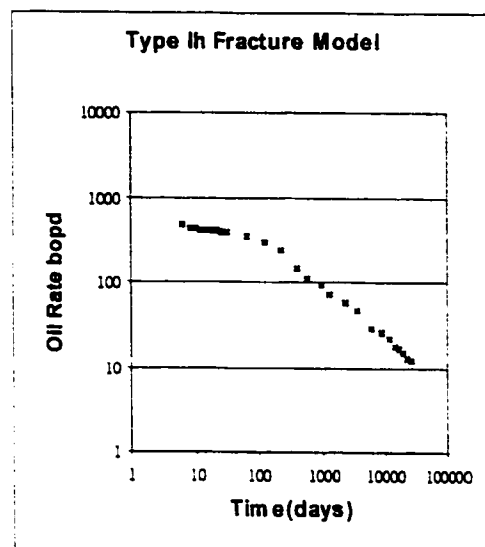


Figure 8.9 - Rate Time Plots Type 1h

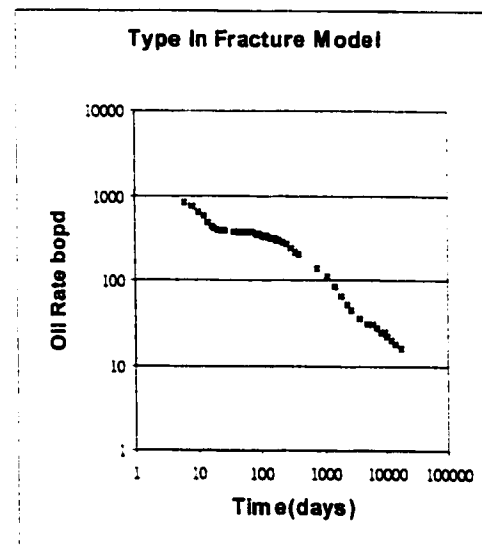


Figure 8.10 - Rate Time Plots Type 1n

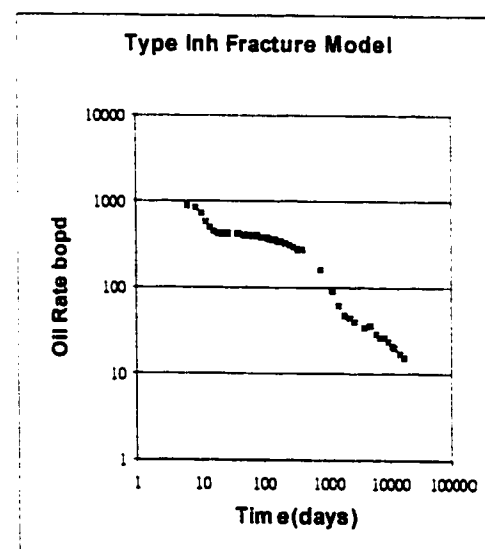


Figure 8.11 - Rate Time Plots Type 1nh

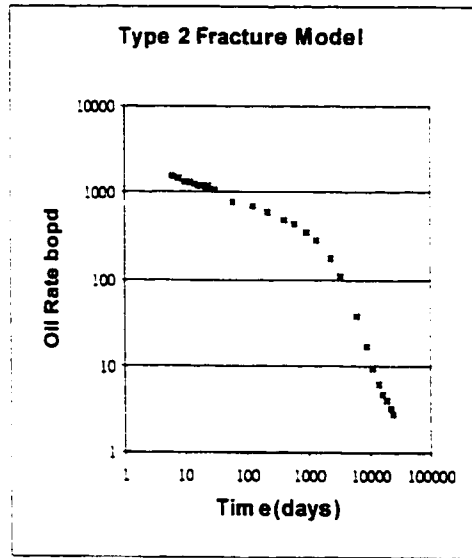


Figure 8.12 - Rate Time Plots Type 2

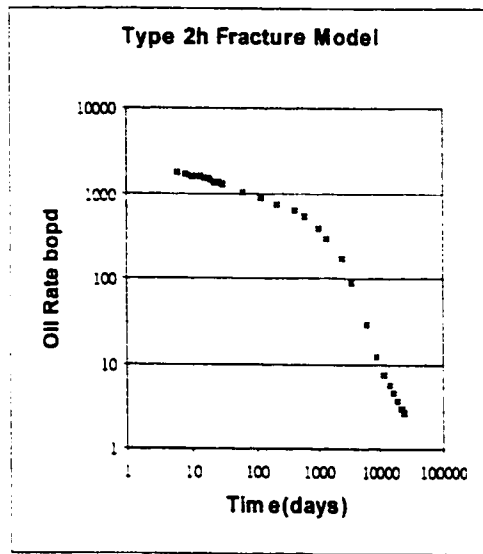


Figure 8.13 - Rate Time Plots Type 2h

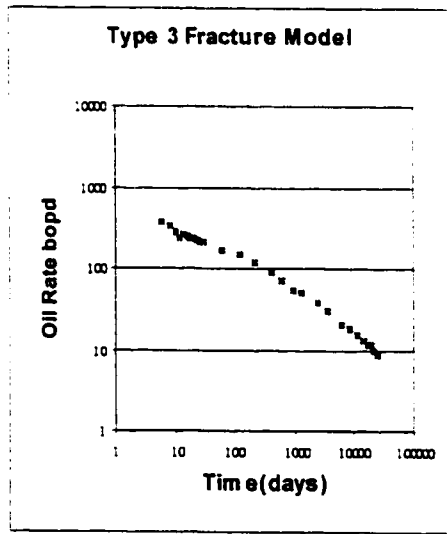


Figure 8.14 - Rate Time Plots Type 3

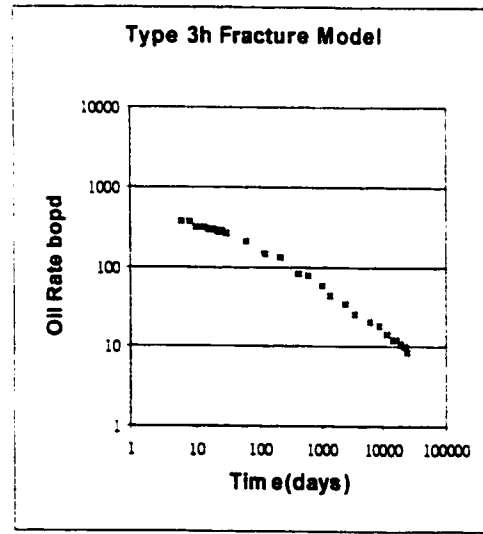
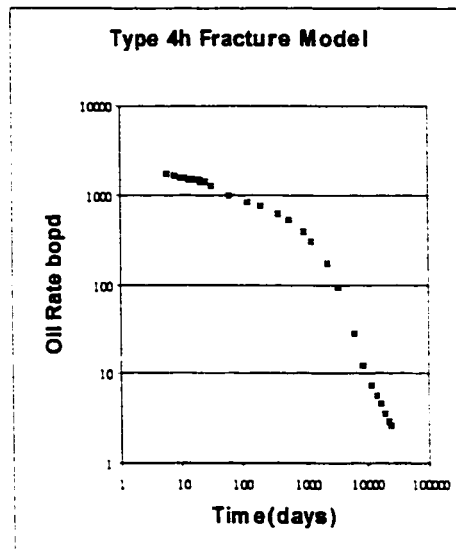
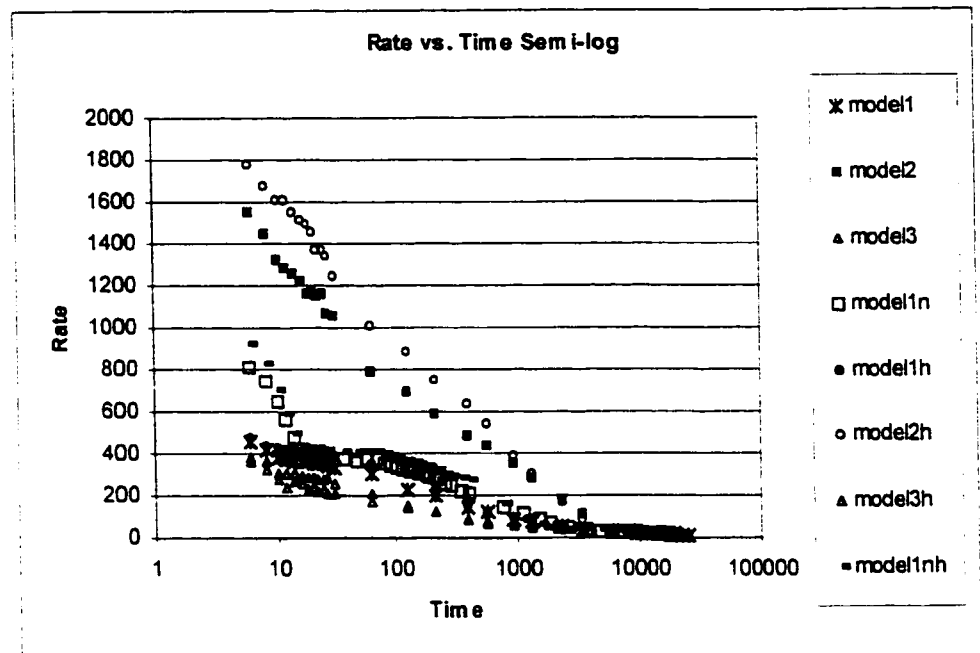


Figure 8.15 - Rate Time Plots Type 3h



**Figure 8.16 Rate Time Plots Type 4h**

This rate-time output indicates that though there are distinct differences between model types there is very little difference in curve shape within each type of model when only fracture permeability is increased from 1000 to 4000 md (i.e. type 1 versus type 1h). However there are significant differences between fracture types. Type 1 fractures predictably show modest initial production rates followed by steep decline. Figures 8.17 and 8.18 show the composite curve for all model types superimposed on both semi-log and log-log scales.



**Figure 8.17 Composite Rate-Time Relationship Semi-Log Scale**

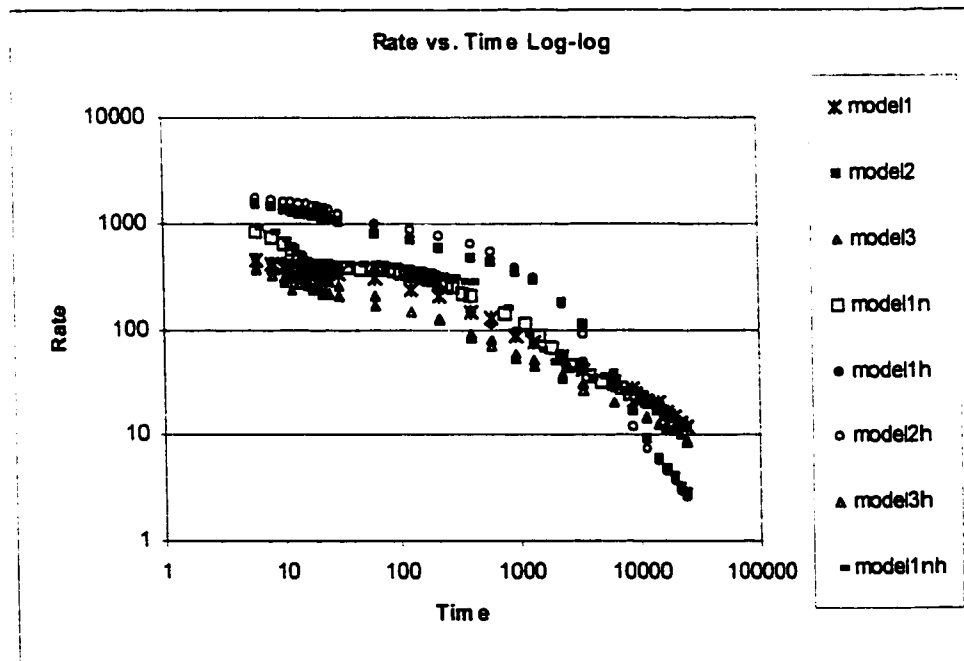
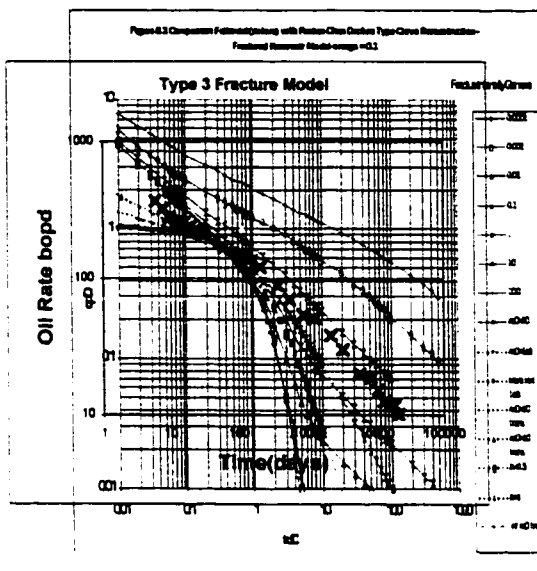


**Figure 8.18 Composite Rate-Time Relationship Log-Log Scale**

### 8.9.1 Matching of Experimental Rate-Time Data to Poston-Chen Type Curves

Figure 8.18 shows the expected trends based on the Poston-Chen type curves where the pseudo-fracture intensity term,  $\gamma$ , is increasing as the curves flatten out for any given storage compressibility coefficient,  $\omega$ . Likewise as the transfer rate  $\lambda' = k_m/k_f$  decreases ( $\omega$  held constant), the curves flatten at late times. Also for a given fracture intensity the flattening of the curves indicates larger fracture storage capacity. Other broad features to note include the high initial rate exhibited by the type 2-fracture case where both the matrix and the fractures exhibit good permeability and the fracture storage capacity is low relative to the matrix. Also note that when the fracture storage increases to almost 20% of total pore volume the flow rate approaches that of the type two case but decreases very rapidly while the type two continues on a less steep decline rate presumably due to the matrix contribution.

The Poston-Chen and superimposed Fetkovich type curves were overlaid on the rate time output at the appropriate scales for comparison. For instance the following diagrams show the type curves plotted at the same scale as the rate time output. When overlain the storage compressibility and fracture intensity terms can be matched and used for interpretation. Recall that Poston and Chen claimed that the parameter  $\gamma$  was a direct indicator of fracture intensity if  $\omega$  is on the order of  $10^{-3}$ . This claim will be checked in the analysis.



This type curve matching process can be applied to each simulation model output. The following table illustrates the best matches of the rate-time data using the combined Fetkovich-Poston Chen type curve matches of the various models that were depicted in Table 8.1. Though the overall expected trends were present, the type curves did not prove useful in quantitative analysis.

| Model Type              | 1         | 1h        | 1n  | 1nh   | 2   | 2h  | 3        | 3h       | 4   |
|-------------------------|-----------|-----------|---|---|---|---|----------|----------|---|
| $\alpha$                |           |           | $\alpha$ Values<br>Merge at<br>Low $\gamma$<br>Values | $\alpha$ | $\alpha$ | $\alpha$ Values<br>Merge at<br>Low $\gamma$<br>Values |
| <b>Very Early Time</b>  | Fetkovich | Fetkovich |   |   | ?   | ?   | ?        | ?        |   |
| <b>Early Time</b>       |           |           |   |   | 0.001   | 0.001   | ?        | ?        | 0.001   |
| <b>Middle-Late Time</b> | 0.01      | 0.01      | 0.01  | 0.01  | 0.001   | 0.001   | 0.01     | 0.01     | .001  |
| <b>Very Late Time</b>   | 0.01      | 0.01      | 0.01  | 0.01  | ?   | ?   | 0.01     | 0.01     | .001  |
| $\gamma$                |           |           |   |   |   |   |          |          |   |
| <b>Very Early Time</b>  | Fetkovich | Fetkovich | 0.001   | 0.001   | $R_{eD}=10$   | $R_{eD}=10$   | 10       | 10       | $R_{eD}=10$   |
| <b>Early Time</b>       | 10        | 10        | 0.001   | 0.001   | 10  | 10  | 10       | 10       | 10  |
| <b>Middle-Late Time</b> | 1         | 1         | 0.1   | 0.1   | 10  | 10  | 10       | 10       | 10  |
| <b>Very Late Time</b>   | 1         | 1         | 0.1   | 0.1   | 0.001   | 0.001   | 10       | 10       | 0.001   |

**Table 8.3 Type Curve Match Summary Information**

Recall in figure 8.1 that the storage compressibility term converged at short times and large values of  $\gamma$  so that these values are not distinguishable on the Poston-Chen curves. Also as the storage compressibility term approaches values of  $10^{-3}$ , the curves are only dependent on the  $\gamma$  term and can theoretically be used as a direct indicator of fracture intensity. At intermediate to late time the values of  $\gamma$  did seem to be an inverse indicator of fracture intensity. Poston and Chen also noted that storage compressibility remained fairly constant over time for any particular model but that fracture intensity seemed to increase after shut-in periods. They related this to the system “sensing” more fractures

further into the reservoir system with time. In general the type curve match to the experimental data of this study seemed to change over time to less fracture intensity at very late time values. Since only one type of fracture system was present in each model this change must indicate that over time the relative total compressibility of the matrix and fracture is changing over time in different ways with different fracture types. This could be the only explanation (assuming the type curves are valid) since the fracture intensity term was defined as  $\gamma = (FI)^2 x_f^2 \frac{k_m}{k_f} \frac{(\phi c_f)_m}{(\phi c_f)_f}$  and all other parameters are invariant in the experiments. The implication is that the total compressibility in the fractures is increasing relative to the matrix over time for the cases of low matrix permeability and low fracture storage capacity. This should be reflected also by changing values of  $\omega = \frac{(\phi c_f)_m}{(\phi c_f)_f + (\phi c_f)_m}$  however the observed values are in the range that merges into the main stem so that it is difficult to distinguish. These results are very confusing in light of the known experimental model parameters and cast some doubt on the use of the Poston-Chen curves for use as fracture storage compressibility and fracture intensity indicators.

In general it did not appear that the experimental results correlated precisely with these Poston and Chen curves except in a very general sense. However one could say that there was a general shift toward lower  $\gamma$  values as the fracture storage increased relative to the matrix and as the fracture intensity increased. There was also a decrease in the  $\omega$  term as the matrix permeability increased which must be related to the compressibility of the system since permeability is not directly related by the definition.

### 8.9.2 Comparison of Rate-Time and Cumulative-Time Data

Figure 8.20 depicts the log-log rate-time behavior comparison of fracture systems with relatively high matrix storage capacity relative to the fracture storage capacity but with varying matrix permeability so that principally  $\lambda$  is contrasted.

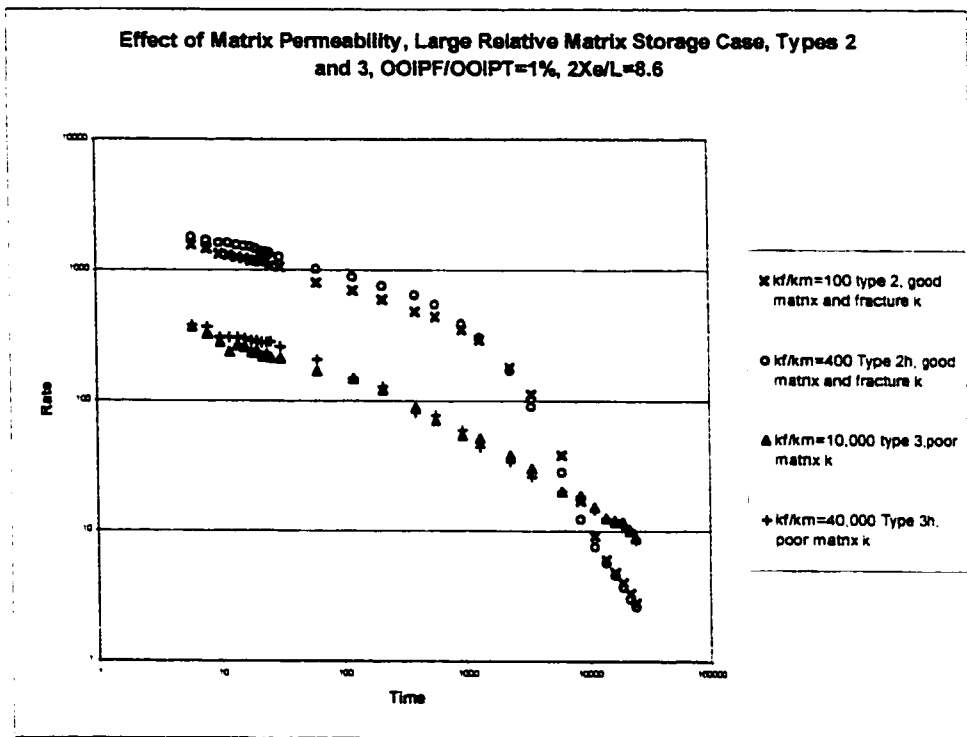


**Figure 8.20 Comparison of the Effect of Matrix Permeability in Cases of Large Matrix Storage Capacity – Types 2 and 3**

The comparison shows the marked contrast of high initial rates for the cases where the matrix and fractures have high permeability compared to cases where only the fracture has high permeability. The decline paths cross at late times. Note that the effect of increasing the fracture permeability from 1000 to 4000 md, (decreasing  $\lambda$ ) increases flow

rate within each group as expected by theory but notice that it is a relatively minor effect compared to increasing the matrix permeability.

Figures 8.21 and 8.22 show the magnified early and late time portions of the decline curves to better illustrate this phenomenon.

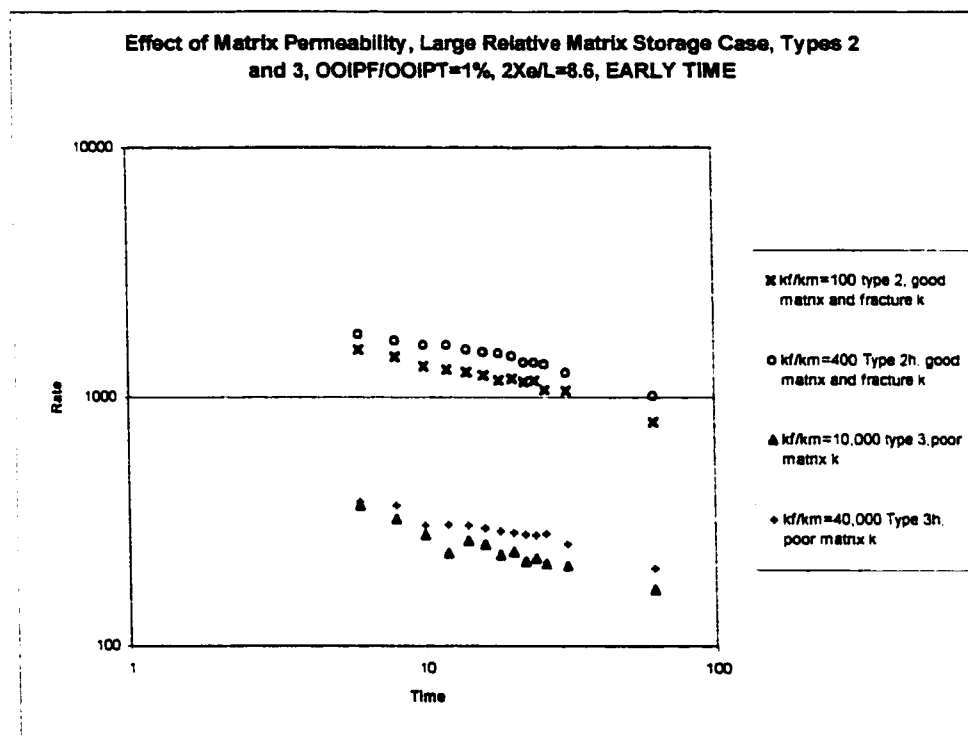


**Figure 8.21 Early Time Comparison of the Effect of Matrix Permeability in Cases of Large Matrix Storage Capacity – Types 2 and 3**

Notice in Figure 8.22 that the effect diminishes at late times and at very late times the curves even cross.

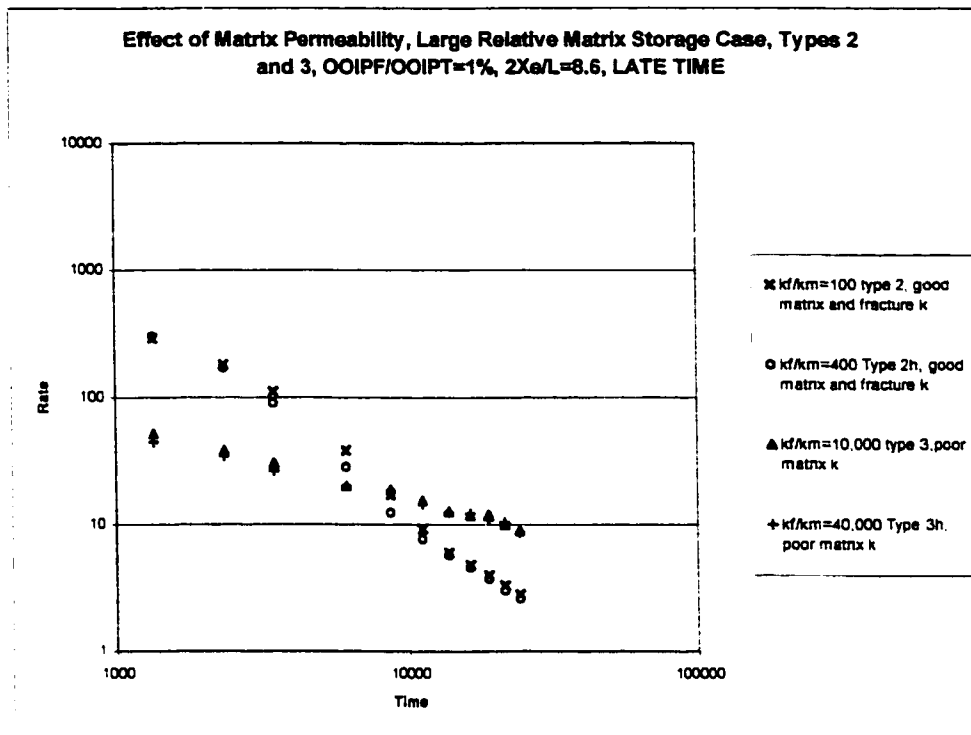


**Figure 8.22 Late Time Comparison of the Effect of Matrix Permeability in Cases of Large Matrix Storage Capacity – Types 2 and 3**

These effects can also be illustrated through the cumulative production versus time plots. Note in Figure 8.23 that the slope of the high matrix permeability case is very large compared to the low matrix permeability case. However they slowly converge at late times, presumably as the matrix and fractures have been depleted in the high permeability cases. Again the shift to higher cumulative production as a result of higher initial flow rates with increasing matrix permeability is shown.

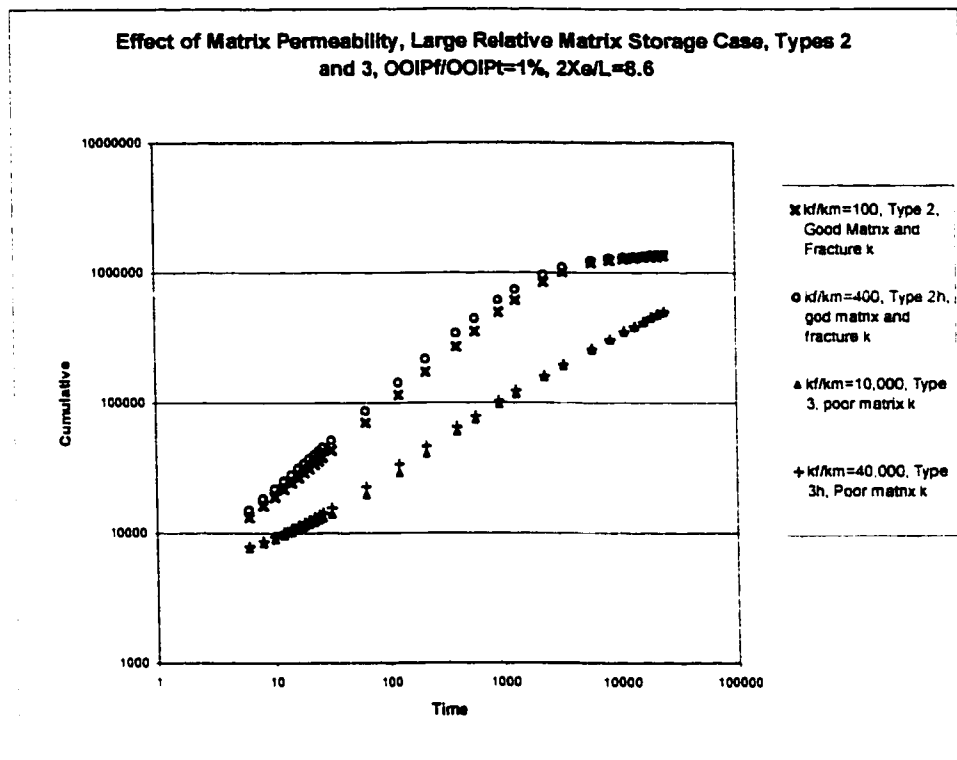


**Figure 8.23 Comparison of the Cumulative Production Effects of Matrix Permeability in Cases of Large Matrix Storage Capacity – Types 2 and 3**

Figure 8.24 illustrates the effect of increases in the relative storage capacity of the fracture relative to the matrix system in cases where the matrix permeability is poor. As the storage capacity of the fracture increases from 1% to 18% of the total system storage capacity (total system ooip remaining constant) the initial flow rates increase substantially and shift the curves upward to the right. The rate-time behavior converges at late times as the fracture is depleted. As before the effect of the fracture permeability is less important than as associated matrix support even at early times.

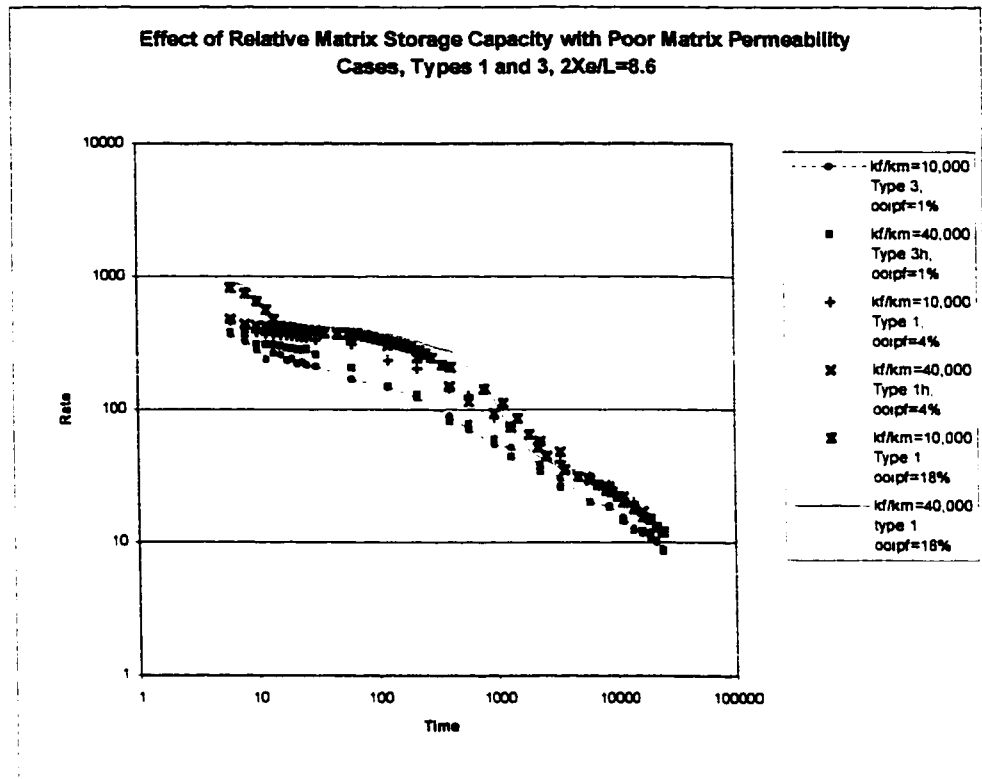


**Figure 8.24 Effect of Increasing Fracture Storage Capacity on Systems with Low Matrix Permeability**

Notice how the effect of additional fracture storage results in a plateau in the rate decline followed by a rapid decline to the rate exhibited by the model containing less fracture storage.

Again a similar effect can be seen on the cumulative versus time plot shown in Figure 8.25. The curves are shifted upward and to the left as a result of the more rapid cumulative production build-up resulting from the higher flow rates.

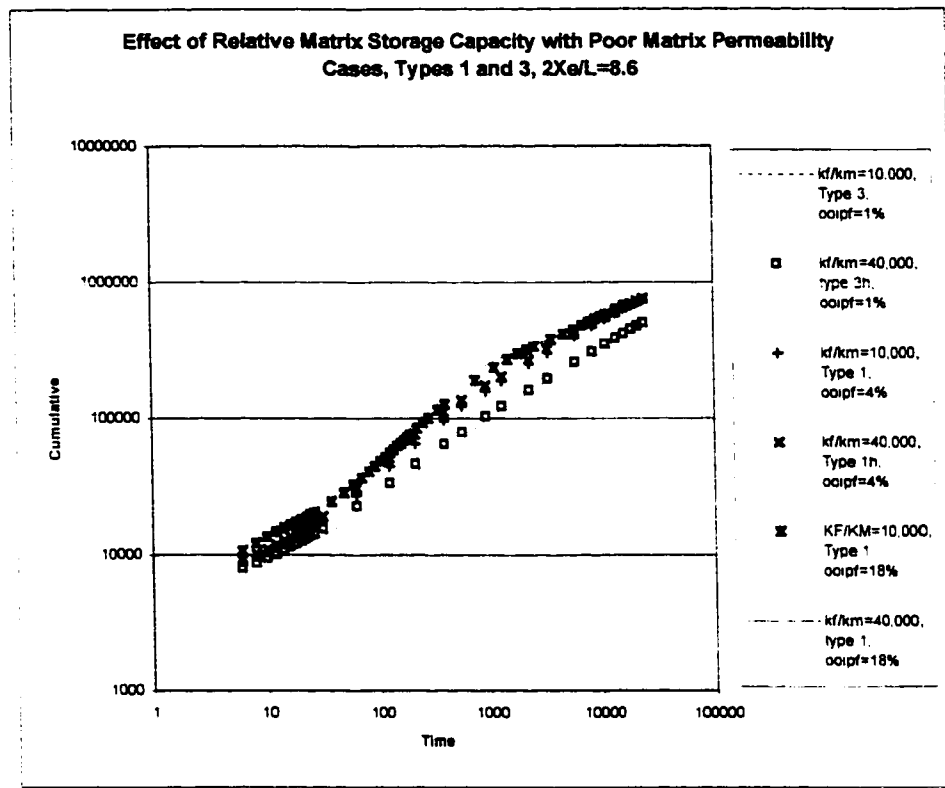


**Figure 8.25 Effect of Increasing Fracture Storage Capacity from 1% to 18% of System Total**

Table 8.4 illustrates the predominant characteristics of the rate-time and cumulative time data for the various fracture types.

| Type | Characteristics  |
|------|--|
| 1    | <ul style="list-style-type: none"> <li>Modest initial rate but initial rate increasing and approaching Type 2 as <math>\omega'</math> approaches 0.15.</li> <li>Rapid initial decline followed by relatively long transition period.</li> <li>Semi-log and log-log plots show four linear slope changes with steep early decline, a long zero slope transition, a long linear portion and a very late time low slope linear portion. The middle zero slope transition diminish as <math>\omega'</math> drops to 0.04.</li> <li>The cumulative-time plot exhibits an increasingly "S" shape with <math>\omega'</math> increasing and late time flattening but not as flat as type 2.</li> </ul> |
| 2    | <ul style="list-style-type: none"> <li>High initial flow rates.</li> <li>Very little early time character. Initial linear decline is short with very indistinct transition on log-log. Very modest early-middle slope change on semi-log plot only.</li> <li>Low and prolonged subsequent decline rate compared to type 1 with a rapid rate decline at late time beginning later than type 1 but slope is greater and eventually crosses type 1 decline.</li> <li>The cumulative-time plot is linear on log-log with very late time slope change to near zero slopes.</li> </ul>   |
| 3    | <ul style="list-style-type: none"> <li>Low initial rates.</li> <li>Similar early characteristics to type 2 but lower initial rates and longer period of middle linear behavior with slope similar to type 2 but at lower rates.</li> <li>Very late time slope increase after the curve crosses the type 2 plot.</li> <li>The cumulative-time plot shows an early time linear slope changing to a steeper prolonged linear shape on log-log until very late slope change. Curve converges to type 2 at late time</li> </ul>   |
| 4    | <ul style="list-style-type: none"> <li>No distinguishing characteristics from type 2.</li> </ul>   |

**Table 8.4 Predominant Characteristics of Rate-Time and Rate-Cumulative Data Behavior**

### 8.9.3 Comparison of the $\Delta p/q$ vs. $q_{cum}/q$ Data between Fracture Types

As mentioned before, the  $\Delta p/q$  vs.  $q_{cum}/q$  plot is very useful in reservoir analysis of fracture type, calculation of pore volume and estimation of storage compressibility. However as noted, pressure data are almost never available to a practicing engineer. Therefore  $\Delta q/q$  has been plotted as an approximation to  $\Delta p/q$ . A comparison of  $\Delta q/q$  vs.  $q_{cum}/q$  with  $\Delta p/q$  vs.  $q_{cum}/q$  plots below (figures 8.25-8.28) show that the plots are very similar in shape. The interesting thing to note is that if one uses rates instead of pressure, such as  $\Delta q/q$  vs.  $q_{cum}/q$ , then the same general patterns are seen in the plots. The later unit slope on the pressure plots corresponds to an exponential decline on the production curve. Although the unit pressure slopes are not exhibited on the rate declines, the semi-unit linear characteristics are the same and can be used to classify the matrix-fracture system.

With this type of plot using pressure, one would typically expect a  $\frac{1}{2}$  slope in the early time region characteristic of linear flow. Also the unit slope pseudosteady region is magnified. The late time would be characterized by exponential decline because the boundary effects are felt by the system. This would result in a unit slope on such plots. Figure 8.25 shows this early  $\frac{1}{2}$  slope followed by a transition period and subsequent unit slope. Figure 8.26 shows the same type of plot using  $\Delta q/q$ , as an approximation for  $\Delta p/q$  since the flowing pressure data are rarely available. Note that although the slopes are

not  $\frac{1}{2}$  and unity, the curves do show the same basic shape and can be used to indicate the time at which pseudosteady state is obtained.

Note in figure 8.27 that the early time  $\frac{1}{2}$  slope is not apparent on the graph. This is probably because of the small amount of oil in the fractures and the system senses the fracture depletion relatively quickly. There is also relatively little matrix permeability support. The unit slope is present but without an apparent transition zone. Conversely, the  $\Delta q/q$  plot shown in figure 8.28 does show an early break in slope at approximately 62 days. Surface diagrams of the pressure field indicate that this corresponds to the time that the system first senses the exterior boundaries of the model. This phenomenon is not exhibited as well on the  $\Delta p/q$  plot. But it does show the possible value of the  $\Delta q/q$  type of diagram, which will be used to compare and contrast the various models.

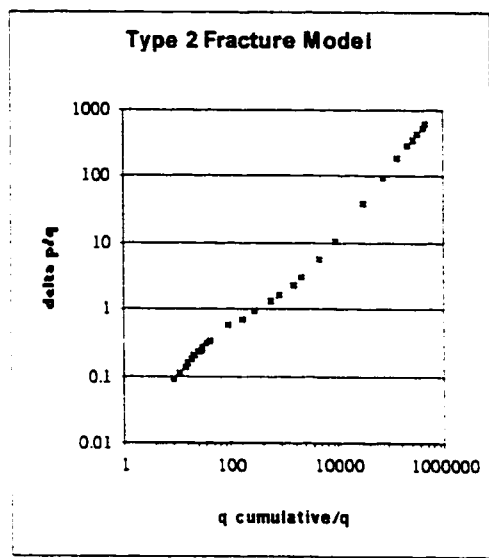


**Figure 8.25 Model Types 2 (semi-log)**  
 $\Delta p/q$  versus  $q_{\text{cum}}/q$

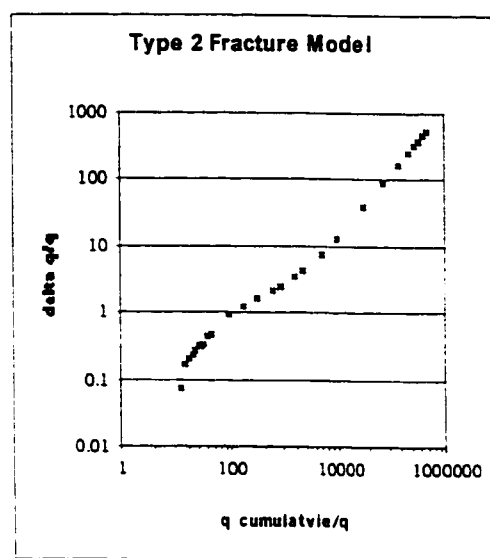


**Figure 8.26 Model Types 2 (log-log)**  
 $\Delta q/q$  versus  $q_{\text{cum}}/q$

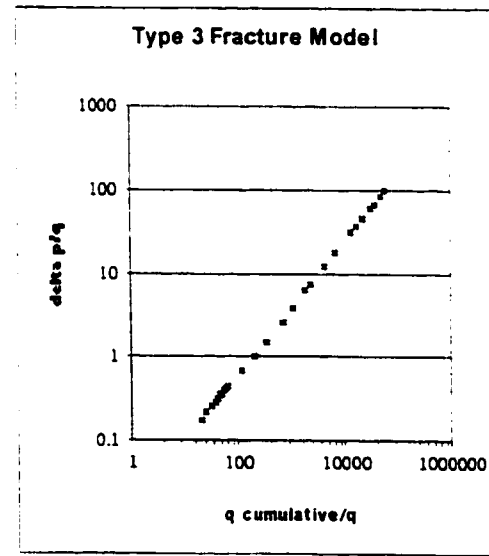


**Figure 8.27 Model Type 3 (semi-log)**  
 $\Delta p/q$  versus  $q_{\text{cum}}/q$

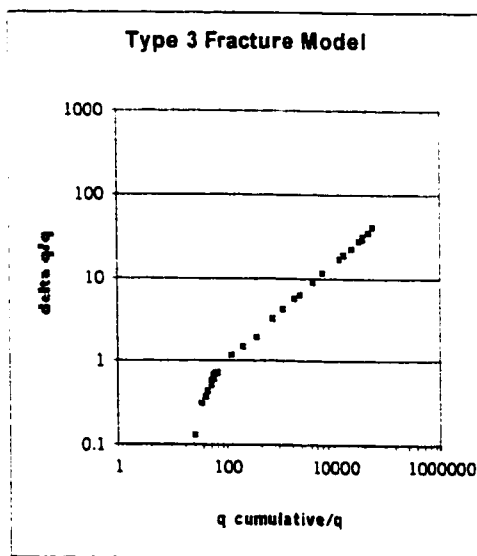


**Figure 8.28 Model Type 3 (log-log)**  
 $\Delta q/q$  versus  $q_{\text{cum}}/q$

The following section discusses an examination of the graphs of  $\Delta q/q$  vs.  $q_{cum}/q$  plots for the various models. Figures 8.29 and 8.30 show the effect of changing the relative fracture to matrix storage volume,  $\omega$ , but keeping the ratio of matrix to fracture permeability,  $\lambda$  constant. Note in both figures 8.29 and 8.30 that as the fracture storage capacity increases, there is a pronounced change in the shape and in fact a double offset character is exhibited even though the matrix permeability is very low. Also note that as the fracture storage is increased, that the time between the slope change is delayed. This shows that the time delay may indicate the relative contrast in fracture to matrix storage or an indicator of  $\omega'$ . Also of note is that as  $\lambda$  increases, given a constant relative fracture to matrix storage ratio, there are an increase in the "width" of the transition zone. In other words there is more of a time delay from the onset of the first slope change to the second. Figure 8.31 and 8.32 show the log-log and semi-log expanded views to better show these phenomenon. These diagrams illustrate an important discovery that the ratio of the  $\Delta q/q$  for the beginning or the transition zone yields an indicator of the relative storage capacity of the fracture system. In other words on figure 8.31, the ratio of  $\Delta q_A/q_A$  to  $\Delta q_B/q_B$  is 4.38 (1.1698/0.2672), which corresponds to the ratio of the relative fracture storage capacities of the two models. Thus if one has a reference well, all other field well decline curves can be used as an indicator of relative fracture storage capacity.

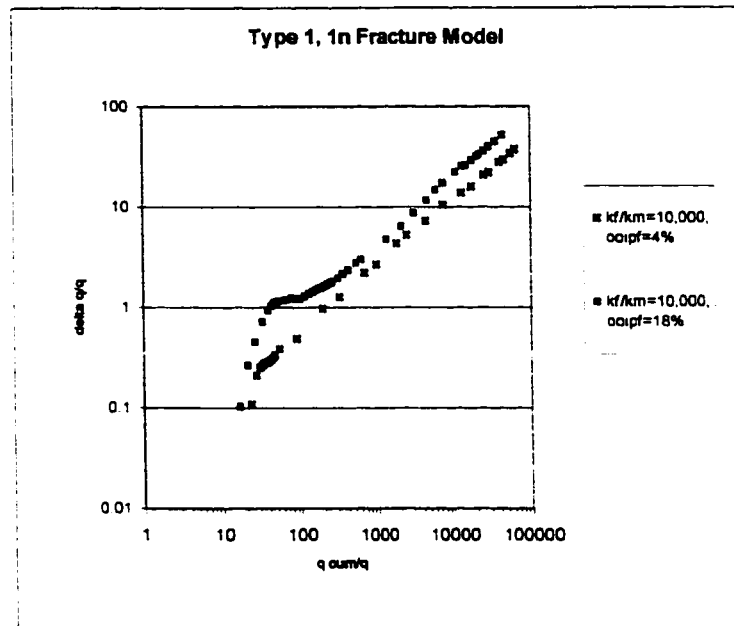


Figure 8.29 Type 1 Fracture Increasing Matrix Pore Volume Relative to Fracture  $\lambda'=1 \text{ ee}^{-4}$

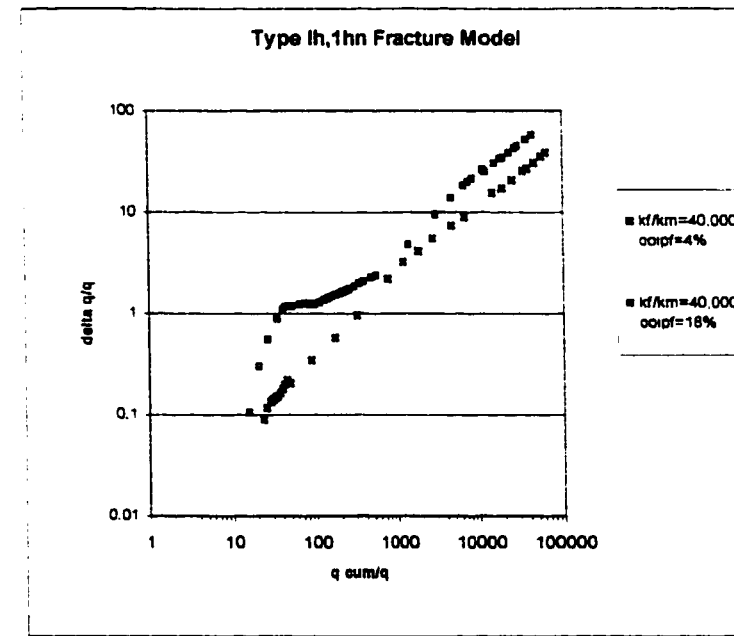
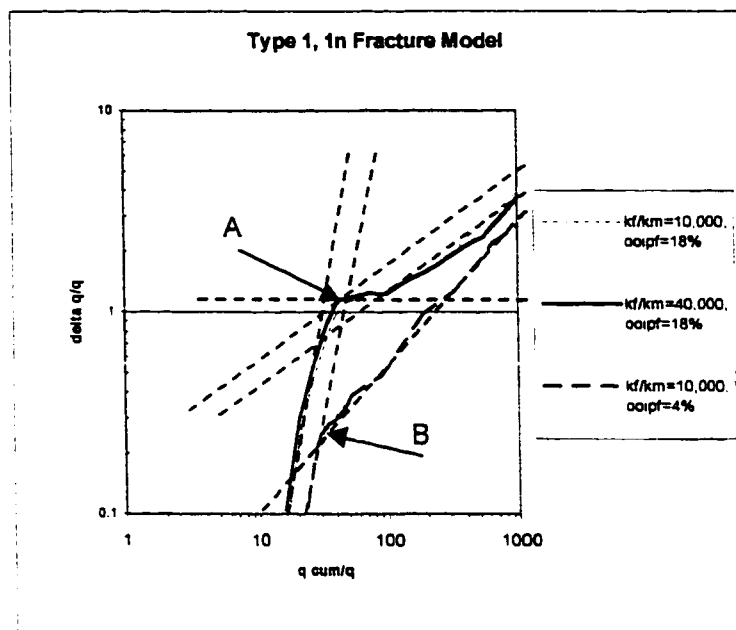
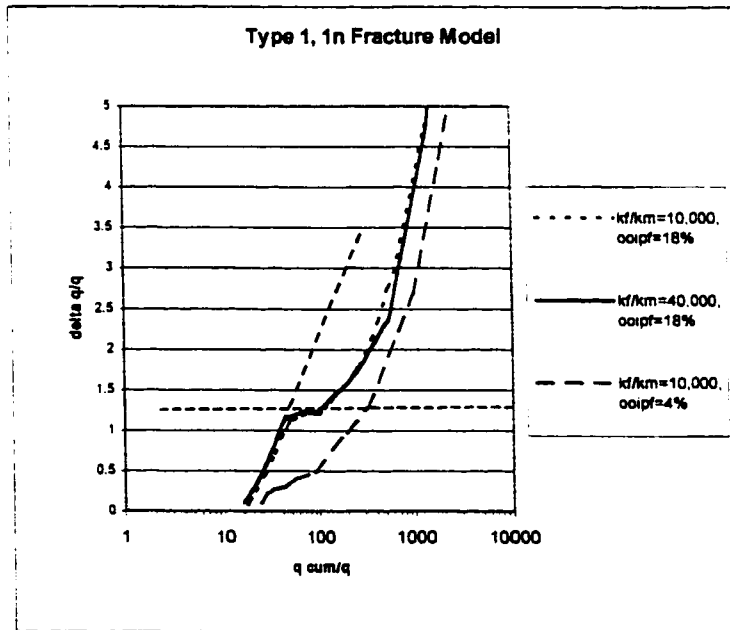


Figure 8.30 Type 1 Fracture Increasing Matrix Pore Volume Relative to Fracture  $\lambda'=2.5 \text{ ee}^{-6}$

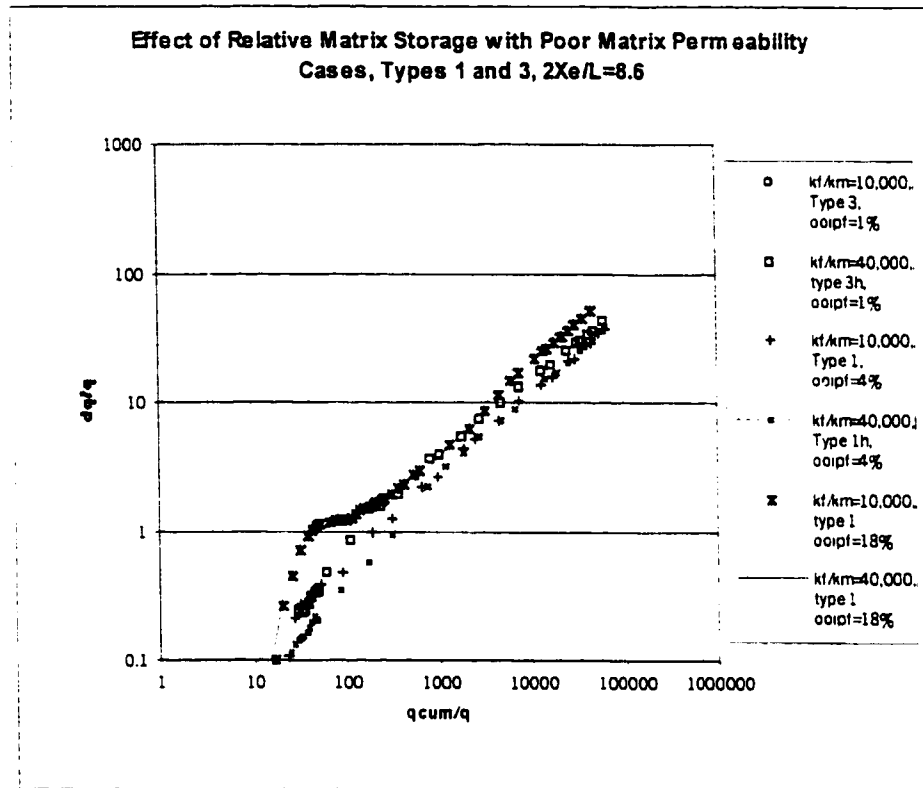


**Figure 8.31 Expanded Type 1,1n,1nh Fracture Model-Effect of Increasing Matrix Pore Volume Relative to Fracture and Change in  $k_f/k_m$  Log-Log**

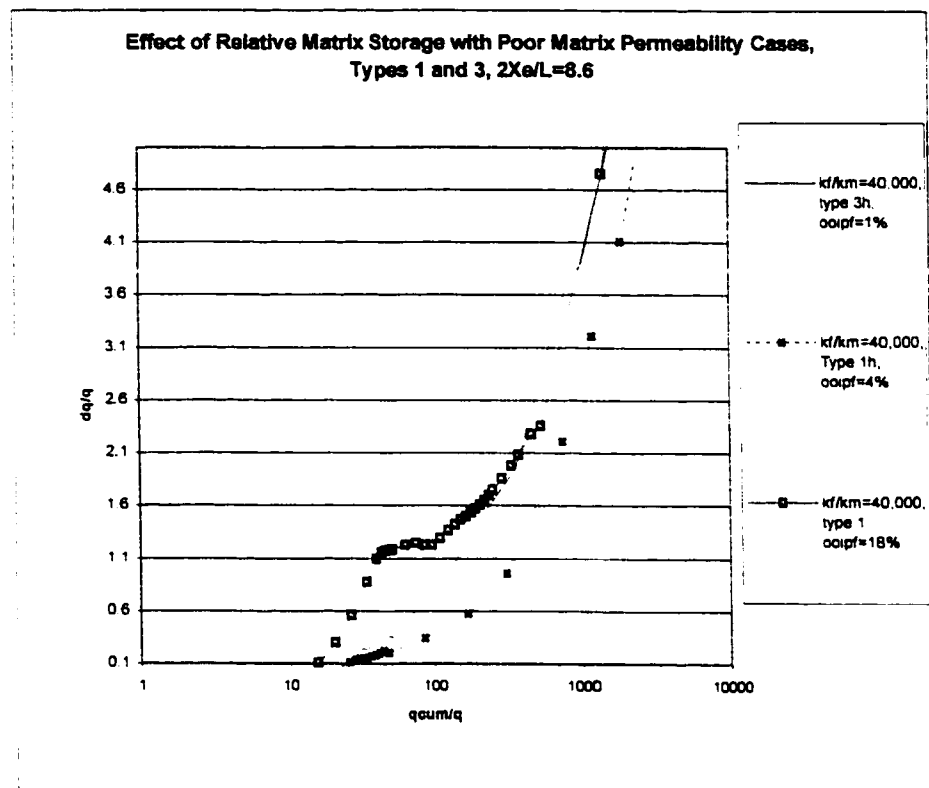


**Figure 8.32 Expanded Type 1,1n,1nh Fracture Model-Effect of Increasing Matrix Pore Volume Relative to Fracture and Change in  $k_f/k_m$  Semi-Log**

Figure 8.33 shows the effect of increasing the fracture storage volume in cases of poor matrix permeability. Except for early time data, which is often not recorded, the slopes again show near unit slopes.

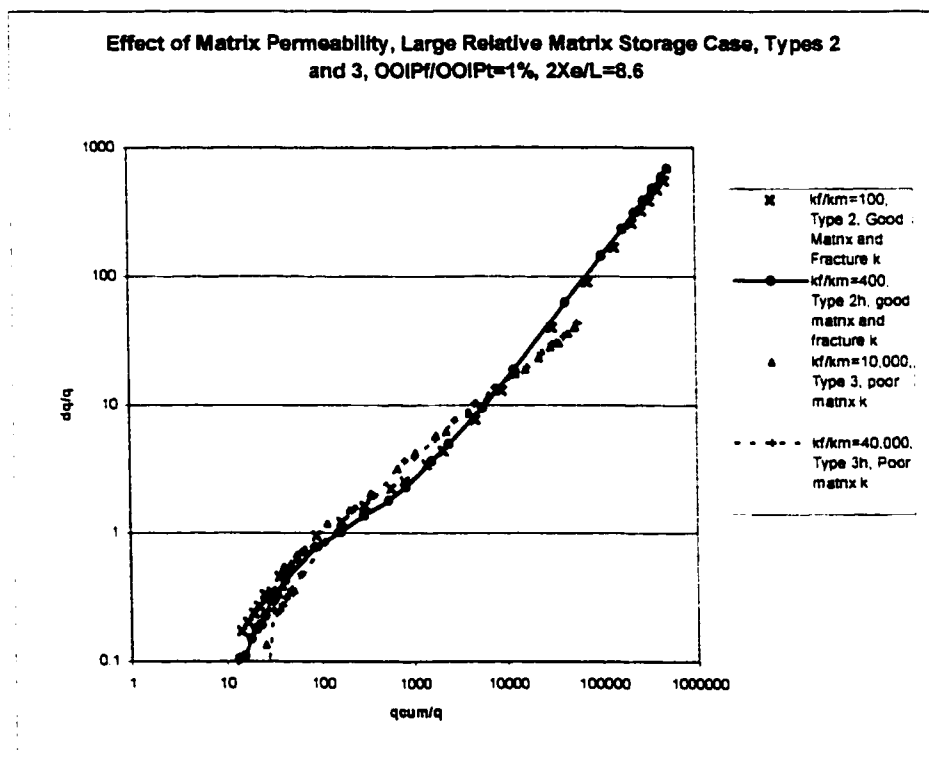


**Figure 8.33 Effect of Increasing Fracture Storage Capacity in Case of Poor Matrix Permeability Log-Log**



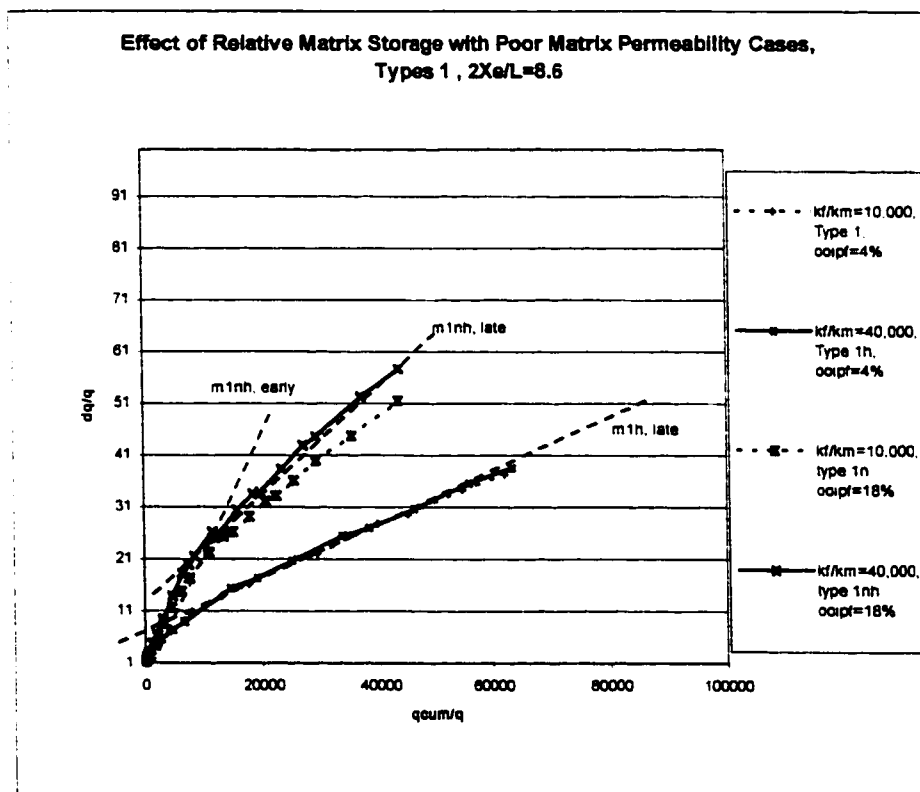
**Figure 8.34 Effect of Increasing Fracture Storage Capacity in Case of Poor Matrix Permeability  
Expanded Semi-Log**

Figure 8.35 shows the effect of changes in matrix permeability in cases of large matrix storage capacity relative to fracture storage capacity. Note the typical dual porosity offset in the slope for the Type 2 fracture.



**Figure 8.35 Effect of Increasing Matrix/Fracture Permeability-Large Matrix Storage Capacity**

The slope of the Cartesian plot can also give a qualitative indication of pore volume. Actual values of pore volume can be obtained if pressures instead of rate data are available. However using the same techniques on  $\Delta q/q$  versus  $q_{cum}/q$  data can give a relative value of pore volume between the fracture types from the relationship: slope ( $m$ )= $5.615^*$  ( $B/V_p c_t$ ). In other words the matrix pore volume will be inversely proportional to the slope of the Cartesian straight-line portions at late time. The steeper the slope the less the  $V_{pm}$ .



**Figure 8.36 Cartesian Plot of  $\Delta q/q$  versus  $q_{cum}/q$  Showing Effect of Matrix Pore Volume on Slope**

The graphs generally confirm that the late time slope increases with increasing fracture and decreasing matrix pore volume since the lower slope indicates more matrix pore

volume. However there is also an unexpected secondary effect related to  $\lambda$  since the slope steepens slightly with increasing fracture permeability ( $\lambda$  decreasing). This phenomenon is most apparent as the fracture volume increases to 18% of the total. Although the phenomenon is also seen on the Type 1 and 3 it is much less noticeable.

Figure 8.35 shows the Cartesian case of the Type 2 models. . Notice that the late time portion is again linear and the early time linear portion is not visible, as the duration is very short.

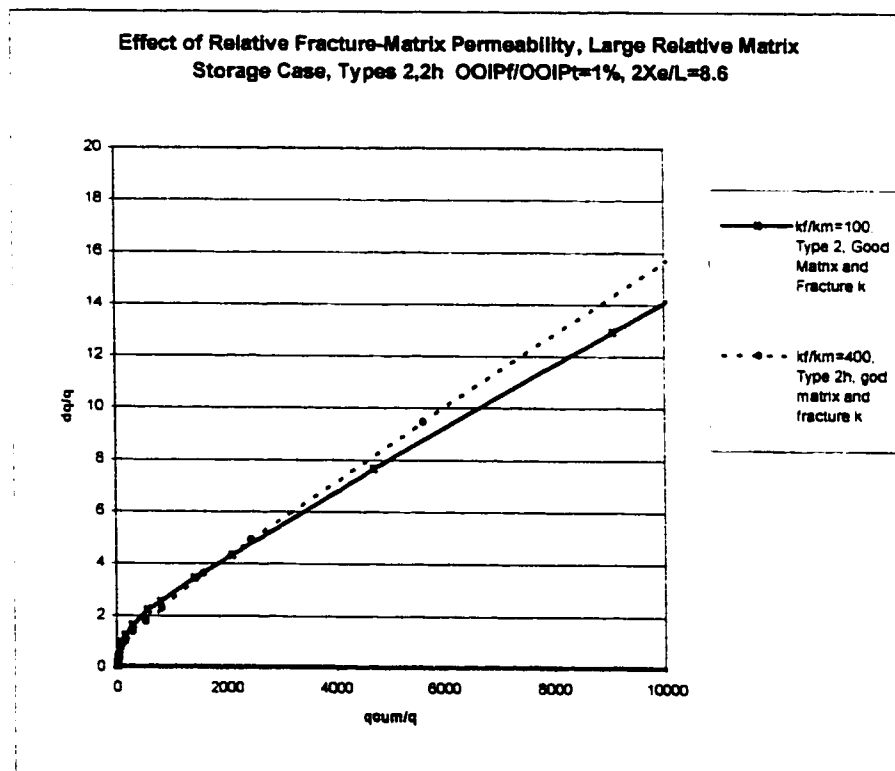


**Figure 8.37 Expanded Cartesian Plot of  $\Delta q/q$  versus  $q_{cum}/q$ , type 2 - Effect of Fracture-Matrix Permeability in Large Relative Matrix Pore Volume Case**

Table 8.5 summarizes the predominant characteristics from  $\Delta q/q$  versus  $q_{cum}/q$  graphs that have been discussed.

| Type | Cartesian  | Semi-Log  | Log-Log   |
|------|--|---|---|
| 1    | <ul style="list-style-type: none"> <li>2-linear slopes, intersecting at increasing <math>\Delta q/q</math> as <math>\omega'</math> increases.</li> <li>Intersection shifts to lower <math>q_{cum}/q</math> and slope increases as <math>\lambda'</math> decreases.</li> <li>Late time linear slope increases as matrix pore volume increases.</li> </ul> | <ul style="list-style-type: none"> <li>Early semi-linear slope with zero slope transition to later concave upward shape.</li> <li>Zero slope transition disappears at low <math>\omega'</math>.</li> <li>The early linear period remains as as <math>\omega'</math> shrinks until it disappears as the model approaches type 3.</li> <li>Duration of the zero slope transition decreases slightly with increasing <math>\lambda'</math> for a given <math>\omega'</math></li> </ul> | <ul style="list-style-type: none"> <li>Early semi-linear slope (approx. <math>1/2</math> slope) with zero slope transition to later semi-linear shape.</li> <li>Zero slope transition disappears at low <math>\omega'</math>.</li> <li>The early linear period remains as as <math>\omega'</math> shrinks until it disappears as the model approaches type 3.</li> <li>Duration of the zero slope transition decreases slightly with increasing <math>\lambda'</math> for a given <math>\omega'</math></li> </ul> |
| 2    | <ul style="list-style-type: none"> <li>Early very short duration linear followed by prolonged linear slope that shifts to higher slope with decreasing <math>\lambda'</math></li> </ul>  | <ul style="list-style-type: none"> <li>Concave upward in entirety with shift to higher <math>\Delta q/q</math> with decreasing <math>\lambda'</math></li> </ul>   | <ul style="list-style-type: none"> <li>Double offset "dual-porosity" unit slope shape is present with early and late time slopes almost parallel.</li> <li>Transition zone offsets the two linear portions but is not zero slope.</li> </ul>  |
| 3    | <ul style="list-style-type: none"> <li>2-linear slopes, intersecting at increasing <math>\Delta q/q</math> as <math>\omega'</math> increases.</li> <li>Intersection shifts to lower <math>q_{cum}/q</math> and slope increases as <math>\lambda'</math> decreases.</li> </ul>  | <ul style="list-style-type: none"> <li>Early, very short duration semi-linear slope but no zero slope transition.</li> <li>Concave upward shape begins immediately after early linear.</li> </ul>   | <ul style="list-style-type: none"> <li>Early, very short duration semi-linear slope with change to prolonged linear middle-late time and shift to higher <math>\Delta q/q</math> with decreasing <math>\lambda'</math></li> </ul>   |

Table 8.5 Predominant Characteristics from  $\Delta q/q$  versus  $q_{cum}/q$  Graphs

#### **8.9.4 Comparison of Derivative Data between Fracture Types**

The derivative of rate with respect to time is examined next. The rate derivative is often so noisy that it is useless in quantitative analysis. The derivatives of simulated rate data are no exception. However, qualitative comparisons between the various data can be made. Also an additional smoothing technique is introduced that seems to be useful. This technique involves not only using a smoothed derivative as introduced in Chapter 5 but utilizes the cumulative data instead of the rate data. Using cumulative data is itself a method of smoothing. And since cumulative production is the integral of rate data, taking the second derivative of the cumulative data appears to result in a better smoothed derivative of rate versus time. Figures 8.38 and 8.39 illustrate this concept. Notice the significant improvements in the derivative with the use of the second derivative of cumulative over the erratic nature of the simple smoothed rate derivative. This type of derivative will be used in the following analysis whenever it appears to offer a smoother pattern in the early time region. However the pure rate derivatives were always plotted for comparison in the analysis. The rate derivative analysis is followed by a comparison to the derivative of  $\Delta q/q$  with respect to time. The derivative of  $\Delta q/q$  with respect to time appears to offer some aid in better direct comparison with pressure derivative analysis.

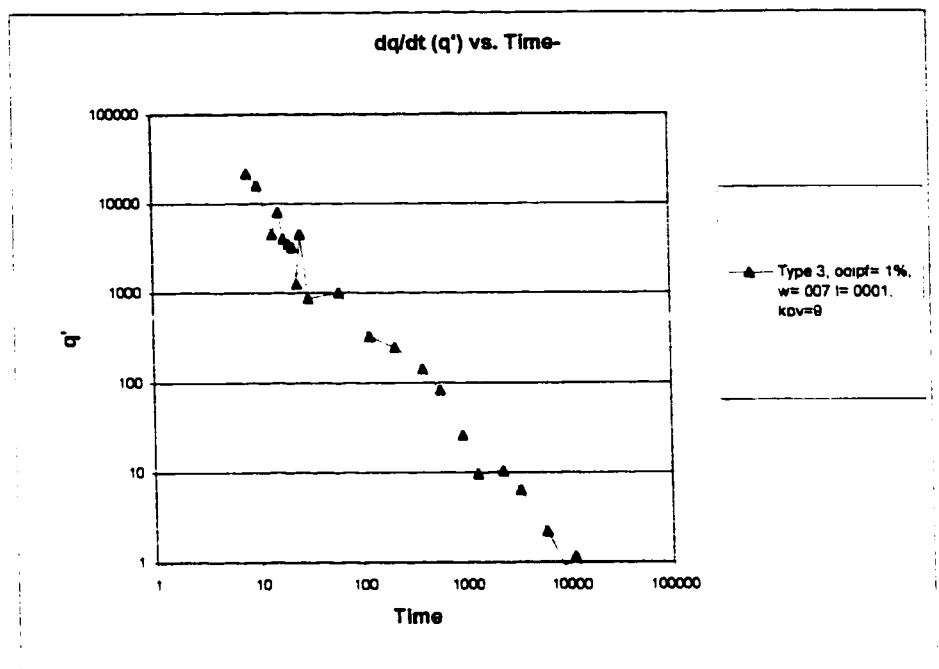


**Figure 8.38 First Derivative of Rate with respect to Time**

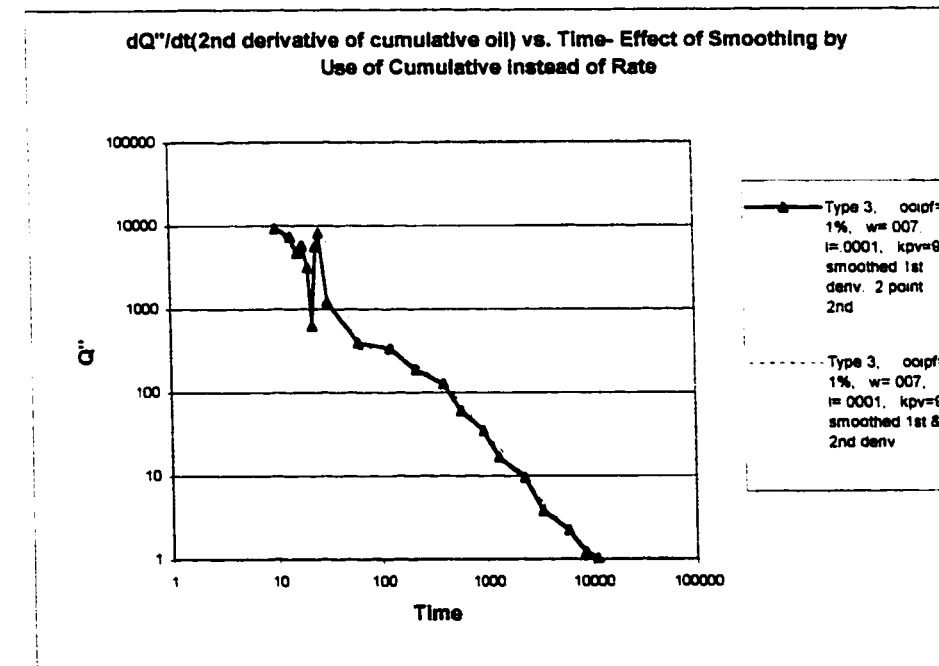


**Figure 8.39 Second Derivative of Cumulative with respect to Time**

Figure 8.40 shows the rate derivative comparison of the Type 2 and Type 3 fracture models illustrating the effect of changes in the matrix permeability but constant low fracture to storage capacity ratio. Figure 8.41 shows the derivative plotted on a scale modified by time ( $Q'' * t$ ) to level the plot for analysis purposes Note that the depth of the minimum is slightly greater with the type2. Typically one expects the depth of the minimum to be the same when storage coefficient is identical so that compressibility factors must also be present. Also note that as  $\lambda' = k_m/k_f$  decreases (from Type 2 to Type 3), the minimum shifts to the right toward more time delay. The minimum delay is opposite on the  $(\Delta q/q)'$  plot which is more consistent with pressure data. However the time delay is so small and happens at such an early time that it may not be useful in classifying the reservoir types.

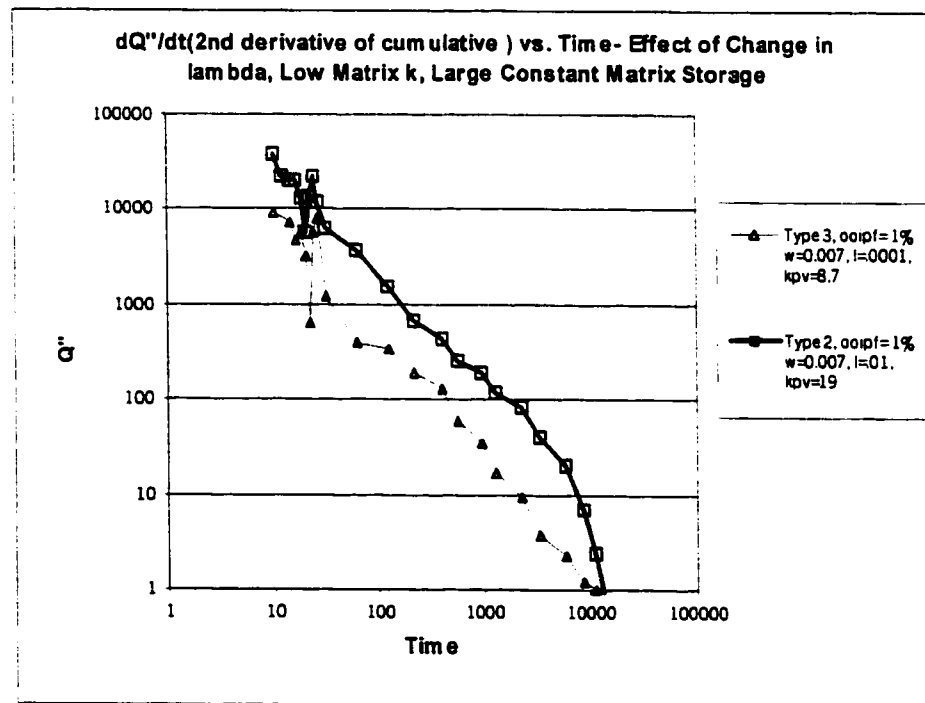


Figure 8.40  $Q''$  versus Time-Effect of Change in  $k_m/k_f$ , Large Constant Matrix Storage

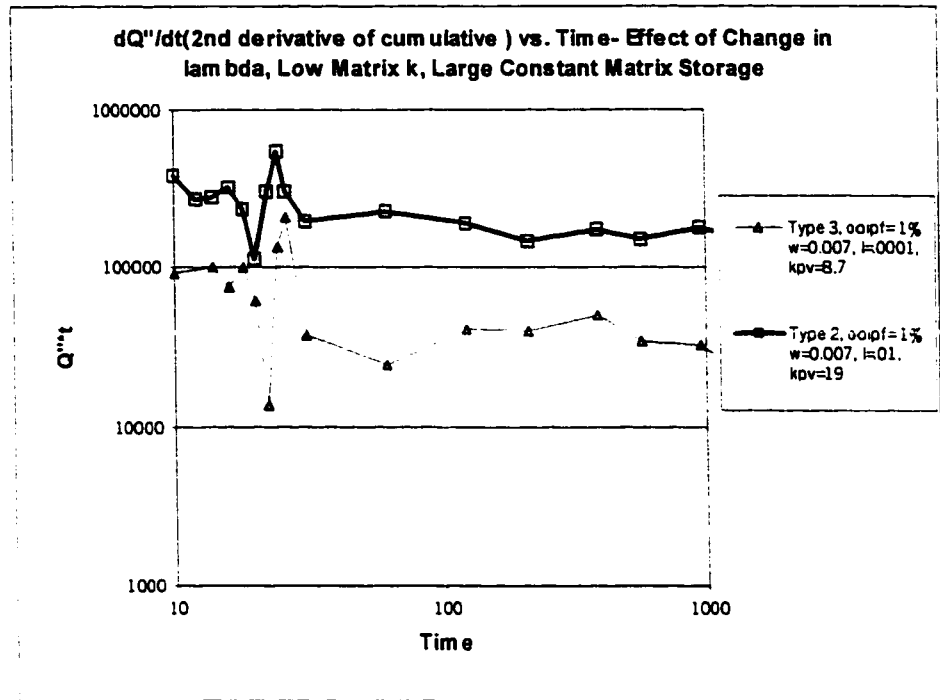


Figure 8.41  $Q''^*t$  versus Time-Effect of Change in  $k/k_m$ , Large Constant Matrix Storage

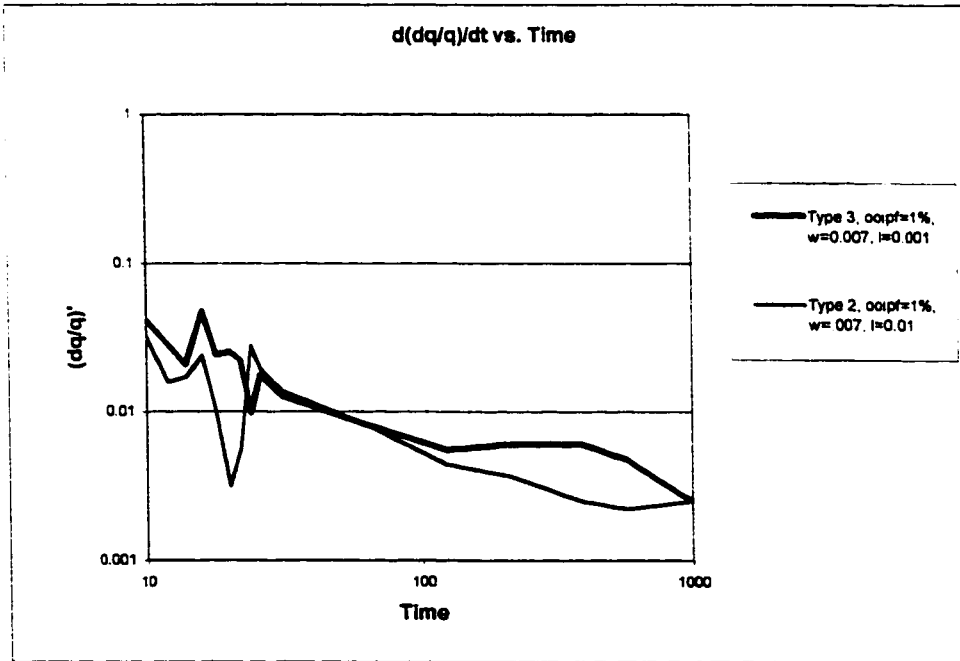


Figure 8.42  $(\Delta q/q)'$  versus Time-Effect of Change in  $k/k_m$ , Large Constant Matrix Storage

Figures 8.43, 8.44 and 8.45 show the effect of changing the relative storage capacity  $\omega$  while the relative matrix to fracture permeability ratio remains constant. As expected the increase in  $\omega$  (increasing fracture storage) shifts the minimum to a higher time delay, however the depth of the minimum also increases with increasing  $\omega$  which is the opposite of that seen in pressure derivative data. Also note that the derivative minimum is time delayed and deeper and wider than either the Type 2 or Type 3.

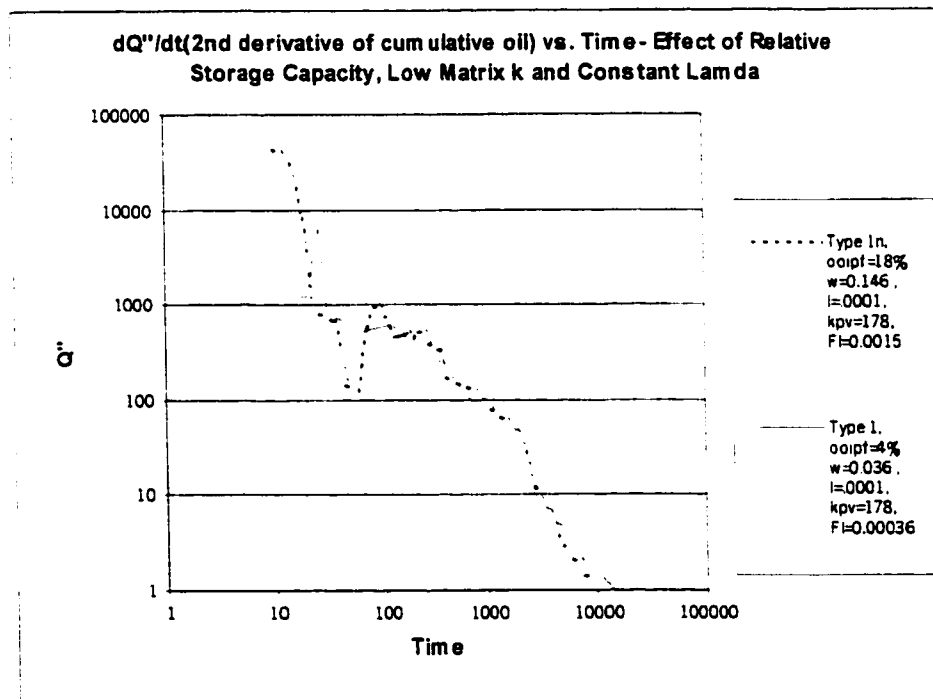
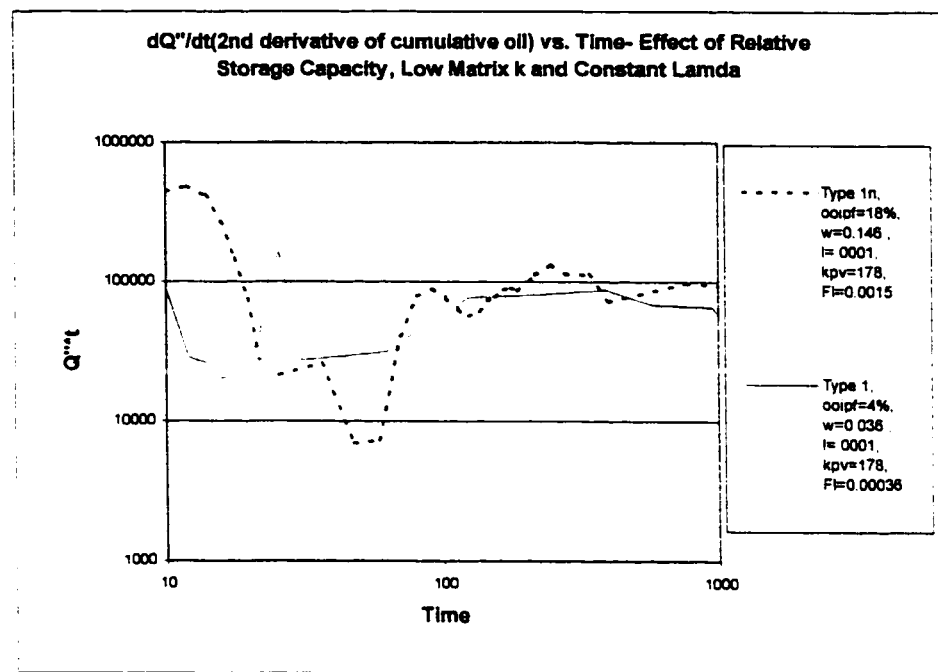
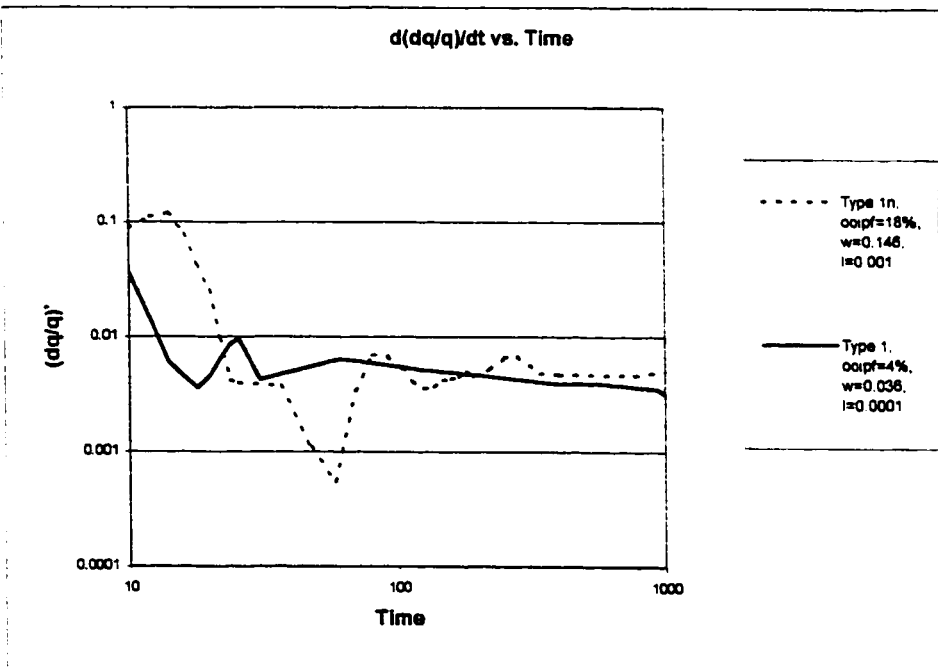


Figure 8.43  $Q''$  versus time- Effect of Changing the Relative Matrix to Fracture Storage



**Figure 8.44**  $Q''^*t$  versus time- Effect of Changing the Relative Matrix to Fracture Storage



**Figure 8.45**  $(\Delta q/q)'$  versus time- Effect of Changing the Relative Matrix to Fracture Storage

Figure 8.46 shows the effect of the Type 4 case where the fracture has developed compartments or permeability barriers within the fracture. No effect was detected on the rate time plots of the previous sections. However there does appear to be an effect on the derivative curve. Note that the derivative contains many early spikes rather than one single spike. This may be useful in distinguishing this fracture type. The only difference in the two curves is the effect of placing several low permeability barriers in the fracture.

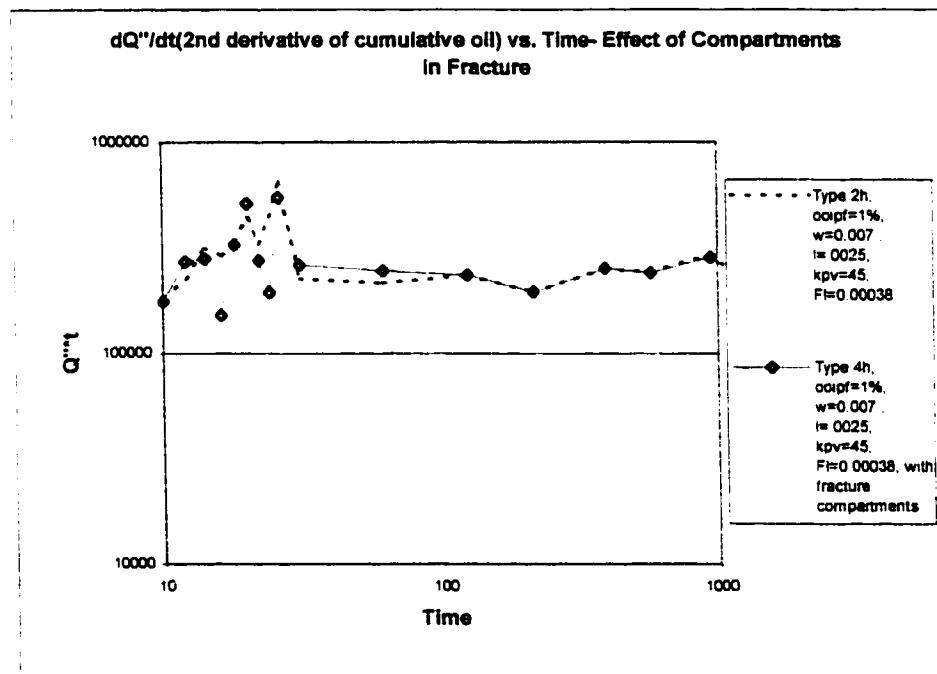
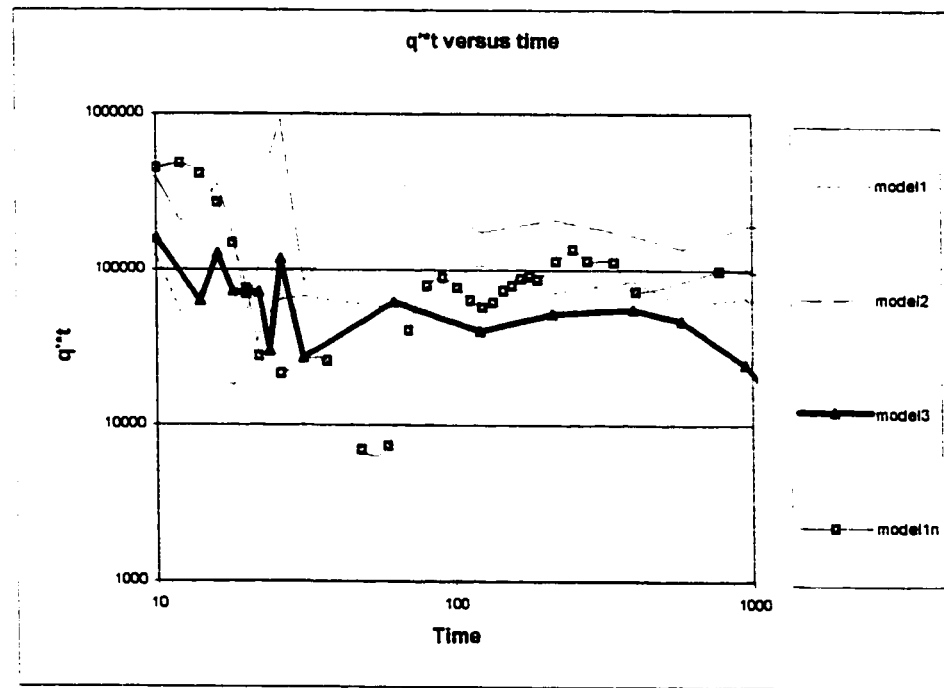


Figure 8.46 Effect of Permeability Compartments Inside Fracture-Q'''t Plot

In summary, the derivatives appear to have limited usefulness in quantitatively characterizing the fractures because of the early time data necessary to use the techniques and the erratic nature of the typical rate derivatives and even the cumulative production derivatives. As figure 8.47 indicates there are few distinguishing characteristics between the various fracture types except at very early times. However the depth and time delay to the minimums can be used in a qualitative sense to help characterize the fractures.



**Figure 8.47 Comparison of Various Model Rate Derivatives –  $q'^*t$**

If the engineer is fortunate enough to have flow pressures then those can be used to apply more typical pressure derivative analysis for quantitative analysis of the reservoir.

Well test analysis employs techniques where  $\Delta p$  and  $p^*t$  are plotted so that the  $\Delta p$  vs. time, derivative early time unit slope, width, depth, and characteristic line intersections can yield values of fracture length, fracture permeability, well bore storage, as well as  $\lambda$  and  $\omega$ .<sup>49</sup> Very early time data are also needed in that analysis. Since neither pressure nor early time data are normally available, a plot of similar nature encompassing  $\Delta q$  and the rate derivative might at least yield some qualitative characteristics of the respective fracture types. Figure 8.48 is the plot of  $\Delta q$  and  $q^*t$  versus time for the models exhibiting the  $1/\lambda = 10,000$  permeability ratio case. Figure 8.49 is the plot of the normalized  $\Delta q/q$  and  $q^*t$  versus time.

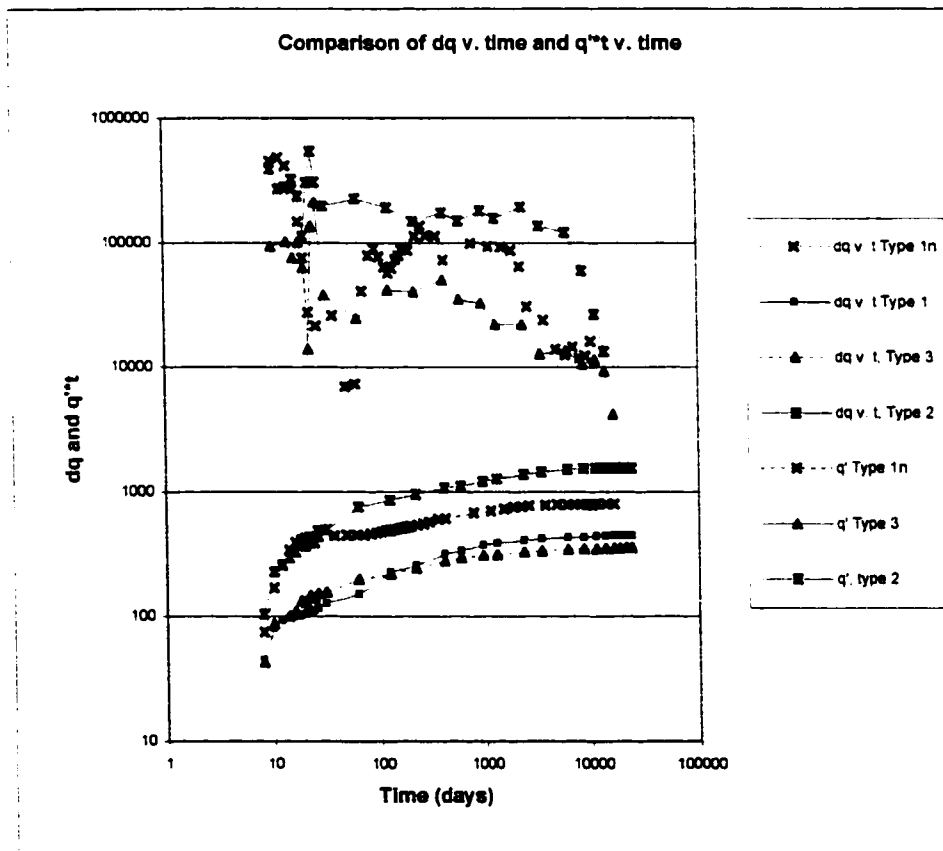
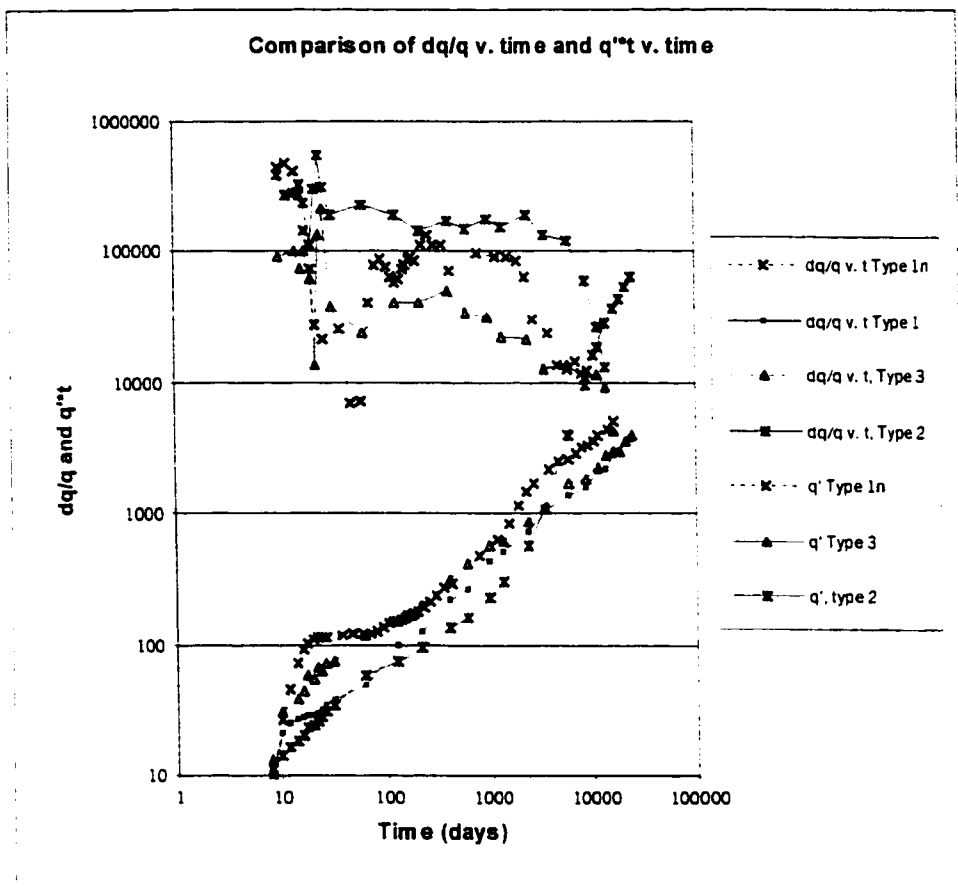


Figure 8.48 Plot of  $\Delta q$  and  $q^*t$  vs time-Models Exhibiting 10,000 md Fracture Permeability



**Figure 8.49 Plot of  $(\Delta q/q)^*1000$  and  $q''t$  vs time-Models Exhibiting 10,000 md Fracture Permeability**

An interesting feature of figure 8.49 is the way the Type 1n and Type 3 models converge at the end of the zero slope transition zone. The area between the two curves probably yields some measure of the fracture storage capacity since that is the only differing parameter. The derivative helps better locate the slope changes. Table 8.6 summarizes some of the distinguishing characteristics of the derivative plots.

| Type | Characteristics   |
|------|---|
| 1    | <ul style="list-style-type: none"> <li>• Minimum is time delayed, longer duration and deeper than Types 2 and 3.</li> </ul>   |
| 2    | <ul style="list-style-type: none"> <li>• Early short duration rate derivative minimum.</li> <li>• Shallow depth to minimum compared to Type 1.</li> <li>• Onset of minimum is very early</li> </ul>   |
| 3    | <ul style="list-style-type: none"> <li>• Early short duration rate derivative minimum.</li> <li>• Shallow depth to minimum compared to Type 1 but similar to Type 2.</li> <li>• Onset of minimum is earliest and slightly before Type 2.</li> </ul> |
| 4    | <ul style="list-style-type: none"> <li>• Numerous early derivative spikes. Otherwise the same as Type 2.</li> </ul>   |

**Table 8.6 Predominant Characteristics of the Derivative Plots**

### 8.9.5 Comparison of $q$ vs. $(t_p + \Delta t)/\Delta t$ Data between Fracture Types

Other distinguishing plots include the rate,  $q$ , and rate-change  $\Delta q$  versus  $(t_p + \Delta t)/\Delta t$  plots. This  $t_p$  is not the same as that used in constant rate well testing but is rather an averaging type of function where  $t_p$  is the cumulative oil produced up to a certain time step divided by the current instantaneous producing rate. This quantity is then added to the cumulative producing time and divided by cumulative time. The physical significance, if any, of this plot is not known but it does seem to distinguish the various fracture types. The following graphs (figures 8.50-8.51) show the comparison.

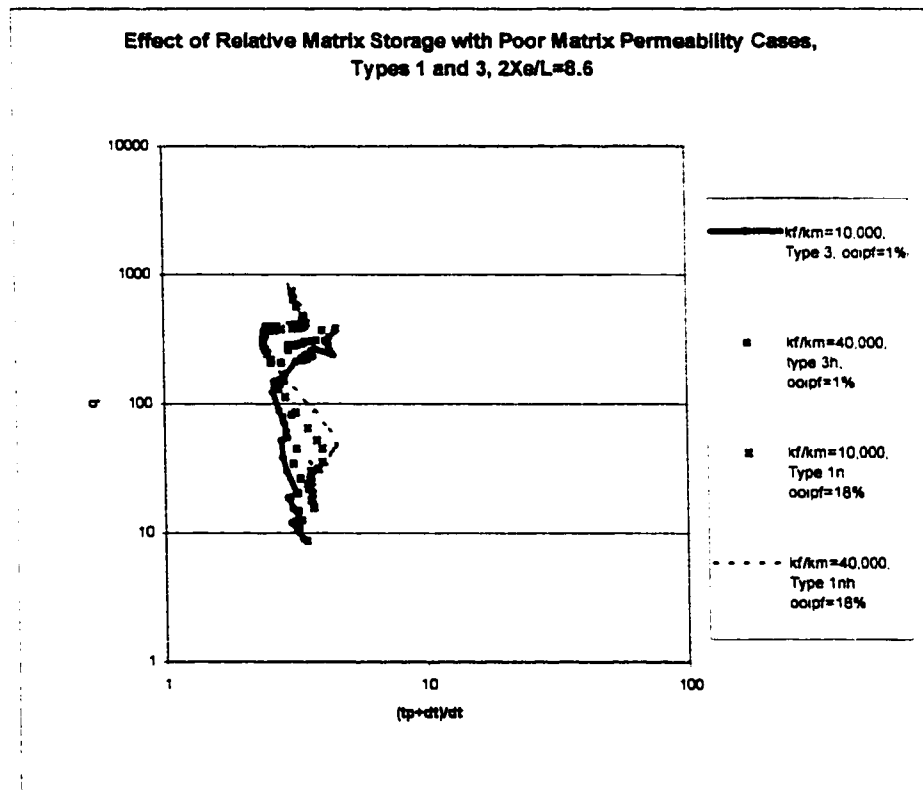
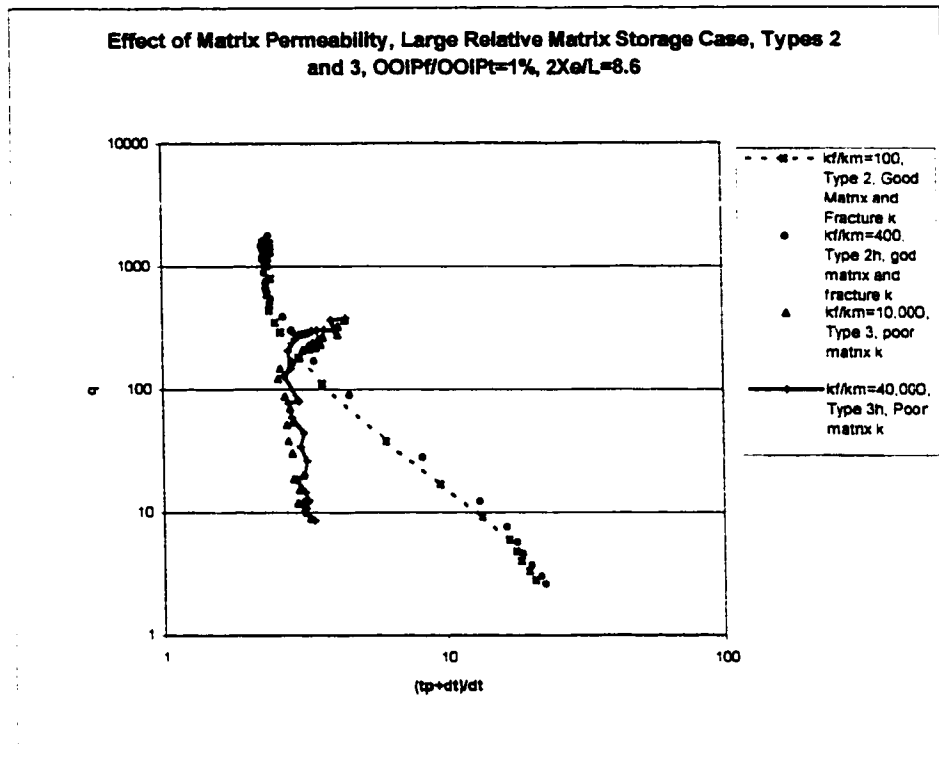


Figure 8.50 Effect of Increase in Relative Matrix Storage Volume-Poor Matrix Permeability

Again the complete tabular output is listed in appendix G. Table 8.7 describes the distinguishing characteristics for each type.



**Figure 8.51 Effect of Change in Matrix Permeability in Case of Large Matrix Storage Capacity-q vs.  $(t_p + \Delta t)/\Delta t$**

The pressure and saturation surface diagrams in combination with the graphical and tabular data help illustrate what is happening throughout the reservoir model as a function of time and space at the inflection points. For instance, the tabular data help to identify the actual producing times for the  $(t_p + \Delta t)/\Delta t$  minimums and reference to the pressure or saturation surface diagram helps interpret the physical significance of such points. This is also helpful in interpreting slope changes in the rate-time type plots. Complete surface diagrams of the pressure profiles are available from the author.

| Model Type | Time Corresponding to $(t_p + \Delta t)/\Delta t$<br>Minimum | Description  |
|------------|--|--|
| Type 1     | Sharp Day 147  | Tight (less than one q cycle) double minimum, double maximum curvature exhibiting a " <u>snake</u> " like appearance |
| Type 2     | Day 576  | Near linear elongated (3 q cycles) " <u>big-dipper</u> " pattern.  |
| Type 3     | Day 1308   | Tight (less than one q log cycle) single minimum curvature " <u>toboggan</u> " pattern.                              |
| Type 4     | Day 576  | Same as Type 2   |

Table 8.7 Comparisons of  $(tp + dt)/dt$  Plots

This type of plot shows one of the most distinguishing signatures of the various fracture types as can be seen on figures 8.50 and 8.51. Similarly the  $\Delta q$  versus  $(t_p + \Delta t)/\Delta t$  plots (figure 8.52) show some distinctive patterns that can be used in characterization.

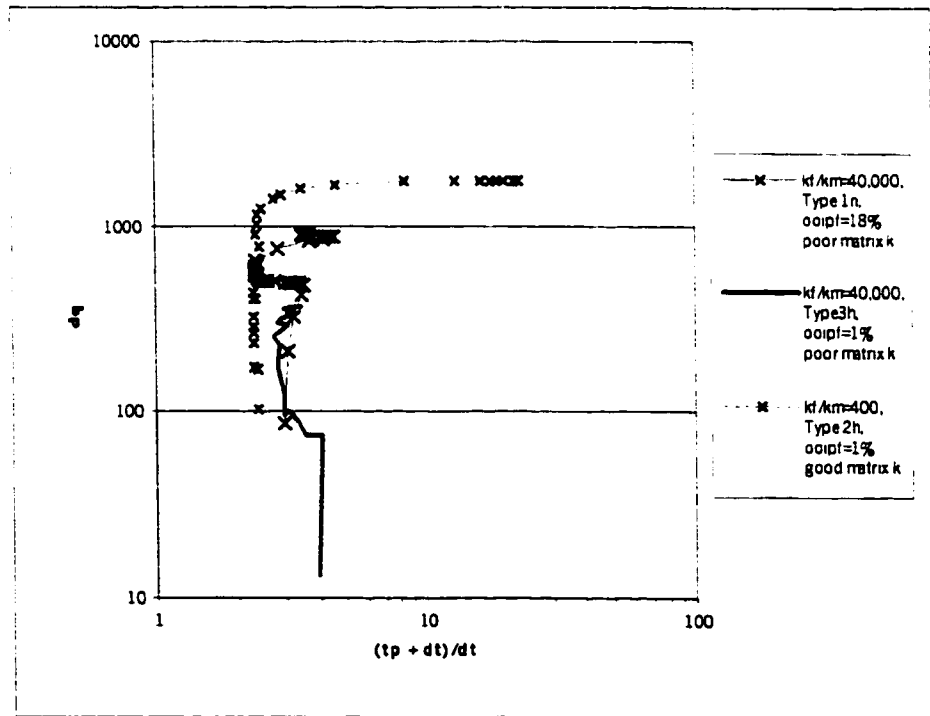


Figure 8.52  $\Delta q$  versus  $(t_p + \Delta t)/\Delta t$

## 8.10 Discussion of the Surface Diagram Interpretation

The average grid block and saturation surface diagrams are helpful in identifying to various changes in the graphs that have been discussed. A few things that are illustrated by the surface diagrams that might not be obvious from general graphing techniques presented (figures 8.53 and 8.54). First of all the reservoir is sensing the pressure drop and saturation change throughout the fracture by day 18. Also the average reservoir pressure and saturation by grid block shows a pattern that is more elongated with type 1 and 3 than for type 2 and 4 where the matrix permeability support is better. All external boundaries are beginning to sense the pressure drop by day 125 for types 1 and 3.

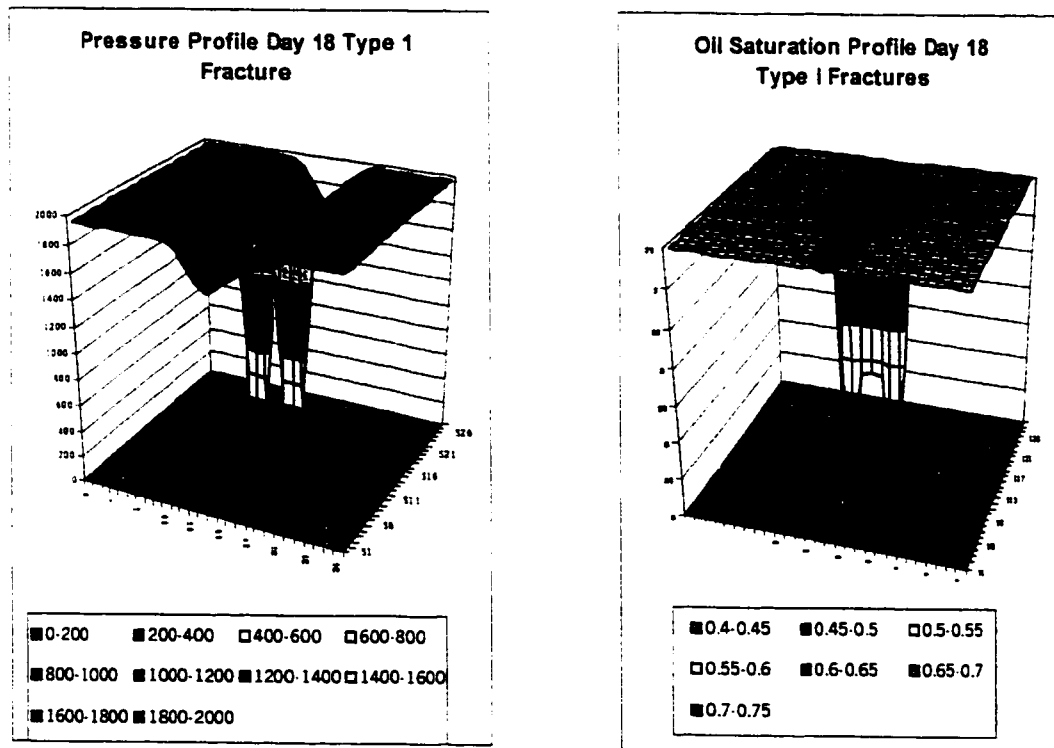


Figure 8.53 Surface Diagram of Average Pressure across Model Day 18

Figure 8.54 Surface Diagram of Oil Saturation across Model Day 18

## **8.11 Summary of Primary Diagnostic Indicators**

The characteristic patterns of the various fracture types have been discussed in detail and summaries were presented in Tables 8.3- 8.7. Although many more types of graphs were generated, as indicated in Table 8.2, the more diagnostic plots included rate-time, cumulative-time,  $\Delta q/q$  vs.  $q_{cum}/q$ ,  $q$  vs.  $(t_p + \Delta t)/\Delta t$  plots, and various derivatives such as rate-time, cumulative-time,  $\Delta q/q$ -time, and  $\Delta q$ -time plots. Table 8.8 summarizes some of the more distinctive points from the previous tables as well as some additional information from plots listed in Table 8.2 that were not discussed or presented. For a "quick-look" classification, the  $(t_p + \Delta t)/\Delta t$  plot gives a good indicator of general fracture type. More extensive experiments should be conducted to verify the general usefulness of this type of graph. Further experimentation with changes in well length down should also be pursued. Although initially it appeared that the Poston-Chen type curves could provide a framework for further rate decline analysis, after considerable work in duplicating and applying the curves it appeared that they were useful in only a limited qualitative sense. They do however allow better curve fitting of the late time "tail" section, which is characteristic of some dual porosity systems.

| Type | Characteristics   |
|------|---|
| 1    | <ul style="list-style-type: none"> <li>Modest initial rate but rate increasing and approaching type 2 as <math>\omega'</math> increases.</li> <li>Rapid initial decline followed by relatively long transition period.</li> <li>Semi-log and log-log plots show four linear slope changes with steep early decline, a long zero slope transition, a long linear portion and a very late time low slope linear portion. The middle zero slope transition diminish as <math>\omega'</math> drops.</li> <li>Cumulative versus time log-log plot shows "s" curvature with <math>\omega'</math> increasing and late time flattening but not as flat as type 2.</li> <li>Early semi-linear log-log slope with zero slope transition to later semi-linear shapes again.</li> <li>The early log-log linear period remains as as <math>\omega'</math> shrinks until it disappears as the model approaches type 3.</li> <li>Double porosity offset parallel unit slope behavior is <u>not present</u> on log-log <math>\Delta p/q</math> vs. <math>q_{cum}/q</math> plot but unit slope late time is observed. If tangent drawn from beginning of transition, a double parallel slope can be created.</li> <li>Cartesian 2-linear slopes, intersecting at increasing <math>\Delta q/q</math> as <math>\omega'</math> increases.</li> <li>Approximate early half slope is observed on log-log plot.</li> <li>Well-defined early time rate-time and rate-cumulative derivative minimum with "deep" minimum, time delayed and longer duration than type 2 and 3.</li> <li>Poston-Chen fracture intensity <math>\gamma</math> term is low during middle-late time compared to type 2,3.</li> <li>Poston-Chen storage compressibility term <math>\omega</math> is fairly constant and higher than type 2 over time.</li> <li><math>(t_p + \Delta t/\Delta t)</math> shows tight (less than one q log cycle) double minimum, double maximum curvature exhibiting a "snake" like appearance.</li> <li><math>\Delta q</math> versus time log-log plot shows increased late time flattening from type 1 to type 3.</li> <li><math>\Delta q/q</math> versus time, log-log plot early time deviation from linear seems to be an indicator of fracture storage volume.</li> </ul> |
| 2    | <ul style="list-style-type: none"> <li>High initial rate</li> <li>Very little early time character. Initial linear decline is short with very indistinct transition on log-log. Very modest early-middle slope change on semi-log plot only.</li> <li>Low and prolonged subsequent decline rate compared to type 1 with a rapid rate decline at late time beginning later than type 1 but slope is greater and eventually crosses type 1 decline.</li> <li>The cumulative-time plot is linear on log-log with very late time slope change to near zero slopes.</li> <li>Double porosity offset parallel unit slope behavior is <u>present</u> on log-log <math>\Delta q/q</math> vs. <math>q_{cum}/q</math> plot but transition is not zero slope.</li> <li>Cartesian early very short duration linear followed by prolonged linear slope.</li> <li>Less well defined early time rate-time and rate-cumulative derivative with shallower minimum than type 1.</li> <li>Near linear elongated (3 q cycles) "big-dipper" pattern on <math>(t_p + \Delta t/\Delta t)</math>.</li> <li>Poston-Chen fracture intensity term <math>\gamma</math> is high and appears to be more constant than type 1 except a very late time.</li> <li>Poston-Chen storage compressibility term <math>\omega</math> is generally lower than the type 1 or 3.</li> <li>The very early time type curve match is more "setkovich" type than Poston-Chen fracture type.</li> <li><math>\Delta q</math> versus time log-log plot shows increased late time flattening from type 1 to type 3.</li> </ul>  |
| 3    | <ul style="list-style-type: none"> <li>Low initial rates.</li> <li>Similar early characteristics to type 2 but lower initial rates and longer period of middle linear behavior with slope similar to type 2 but at lower rates.</li> <li>Very late time slope increase after the curve crosses the type 2 plot.</li> <li>The cumulative-time plot shows and early time linear slope changing to a steeper prolonged linear shape on log-log until very late slope change. Curve converges to type 2 at late time.</li> <li>Log-log early, very short duration semi-linear slope with change to prolonged linear middle-late time and shift to higher <math>\Delta q/q</math> with decreasing <math>\lambda'</math>.</li> <li>Double porosity offset parallel unit slope behavior is <u>not present</u> on log-log <math>\Delta p/q</math> vs. <math>q_{cum}/q</math> plot and unit slope late time is not observed but slope is close to unity.</li> <li>Cartesian 2-linear slopes, intersecting at increasing <math>\Delta q/q</math> as <math>\omega'</math> increases.</li> <li>Poorly defined early time rate-time and rate-cumulative derivative minimum with erratic late time slope</li> <li>Tight (less than one q log cycle) single minimum curvature "toboggan" pattern.</li> <li>Poston-Chen fracture intensity term is high compared to type 1 and more consistent than type 2.</li> <li><math>\Delta q</math> versus time log-log plot shows increased late time flattening from type 1 to type 3.</li> </ul>  |
| 4h   | Same as Type 2 except derivative exhibits very "spiky" early nature   |

Table 8.8 Summary of Fracture Type Characteristics

## **Chapter 9**

### **Summary and Conclusions**

#### **9.1 Summary**

This research has resulted in several new contributions to the area of performance and decline curve analysis of both vertical and horizontal wells in anisotropic and fractured porous media. The important discoveries and future research ideas have been summarized by topic in the following sections.

#### **Generalized Dimensionless Decline Curves**

This area of research extends the previously developed dimensionless decline type curve concepts and techniques to more general cases of varying reservoir shapes and well locations. Fetkovich<sup>3</sup> had previously derived dimensionless decline curves for single-phase radial systems with centrally located wells. He then combined these relationships with the empirical hyperbolic pseudo-steady state relationships of Arps, to formulate a combined dimensionless decline curve as previously shown in Chapter 5. This research derives the dimensionless decline rate and time relationships for the cases of more general reservoir geometry and well location. These relationships are then used to construct new type curves for various reservoir shapes and well locations for single-phase cases. The data are then tabulated and combined with the Arps depletion stems to form a more generalized dimensionless decline curve system. This is the only

publication that contains the complete set of tabulated dimensionless rate and time data for both infinite and bounded reservoir cases as well as the dimensionless decline rate and time data for the Fetkovich and new generalized type curves. The more generalized equations for calculation of transmissibility, permeability, reservoir area or radius and reserve estimation are also derived and presented for the first time in this research.

Chapter 5 figures show the effect of the more generalized dimensionless decline form as a shift in the single-phase pseudosteady state decline stem toward the origin for cases of increasing shape irregularity and wells closer to the boundaries. This effect manifests itself by an increasing deviation from the Fetkovich radial-well centered solution as the shape factor decreases. Without the use of such a system the user would choose the wrong depletion stem resulting in errors in the computation of reserves and permeability.

### Solution Gas Reservoir Parameter Estimation

This research also introduces some novel approaches for estimating, from field production data, the simulation reservoir properties such as oil-water and gas-oil relative permeability, PVT properties, and capillary pressure in the absence of laboratory measurements. Appendix B and C contain the techniques and references for estimating all the reservoir properties needed for input to reservoir simulations. Of particular note are the techniques introduced to estimate flow rates in cases of two phase flow where a  $k_r/\mu_o B_o$  correlation as a function of grid block averaged pressure

and saturation is used to modify the single phase flow equation in cases above and below the bubble point in solution gas reservoirs. Experimental results show that these methods yield good approximations to simulated results. Also of note are the techniques for estimating relative permeability in cases of solution gas reservoirs.

#### Flow Rate Correction Factors in Cases of Horizontal Permeability Anisotropy

Extensive simulation experimentation confirms that corrections must be applied to traditional horizontal well inflow performance relationships in cases of horizontal permeability anisotropy. This research demonstrates that unless the reservoir is extremely large in comparison to the length of the horizontal well, deviation from permeability isotropy in the principal x and y directions will yield results that deviate from those predicted by commonly accepted geometric mean averaging. All analytical flow equations incorporate the geometric mean horizontal permeability concept and thus predict that if the geometric mean is constant, the flow rate will remain constant. As demonstrated in Chapter 6, extensive experiments demonstrate however that as the contrast in x and y permeability increases, while maintaining a constant geometric mean horizontal permeability, the simulated horizontal flow rates deviate increasingly from one another. With vertical wells however, the simulated flow rate remains constant no matter what the contrast in x and y permeability as long as the geometric mean permeability is invariant.

Graphical relationships are presented showing the effect of permeability anisotropy on flow rate as a function of dimensionless well length, grid block size and well to boundary ratios. The experiments also indicate that the deviance from isotropic cases increases above the bubble point pressure. This is an important observation that should lead the engineer to exercise caution when interpreting rate data.

#### Decomposition of x and y Directional Permeability

Chapter 7 introduces new techniques to estimate directional permeability contrasts from the decline characteristics of both horizontal and vertical wells that compete for drainage area. The techniques are validated with simulation data and an example from actual field data is introduced. The research shows both experimentally and mathematically that departures of cumulative production data trends from the early time trends of competing wells will indicate relative contrasts in directional permeability that is approximately related to the ratio of the square root of  $k_y/k_x$ . Dual and multi-well experiments illustrate this phenomenon. The concept is also expanded to horizontal wells and vertically fractured reservoirs using a method that makes use of the horizontal well decline type curves applied to cumulative-time production data.

#### Horizontal Well Decline Curve Analysis and Effective Wellbore Radius

This research also showed that the traditional pseudosteady state horizontal well equations that utilize skin factors to account for well length, dimensionless well length

and reservoir to well length can instead be expressed in terms of an effective wellbore radius. This concept not only allows the flow rate to be expressed in terms of one term that incorporates a number of skin factors but it is easier to use since the user does not need to use charts and graphs to determine skin factors. Therefore the generalized decline curves introduced in chapter 5 or Fetkovich radial type curves can be used directly with horizontal wells since the skin factors have been incorporated into the effective well bore radius. Theoretically then the horizontal and vertical well log-log plots should overlie one another in the pseudosteady state region just as Fetkovich theorized for vertically fractured wells. In other words they would have the same Arps "b" value but exhibit different  $r_e/r_w$  ( $r_{eD}$ , or the equivalent  $A/r_w^2$ ) values and thus different  $q_{Dd} - t_{Dd}$  match values. An example was introduced for isotropic conditions where the effect of the horizontal well was to shift the match to a lower  $r_{eD}$  match value in the transient area thus resulting in the calculation of larger radius of drainage,  $r_e$ . It was found that this method did not work as well when the horizontal well length became very large in comparison to the reservoir size and the permeability field was anisotropic.

### Fractured Reservoir Classifications

The simulated production rate decline characteristics of fractured reservoirs that are intersected by horizontal wells were studied through the use of simulation experiments. Tables and charts were produced that help classify each of four different fracture types through characteristic rate-cumulative-time decline patterns. Pressure data is purposely

ignored in an effort to utilize only data that would typically be available to the practicing engineer. Although many types of graphs were generated, as indicated in Table 8.2, the more diagnostic plots included rate-time, cumulative-time,  $\Delta q/q$  vs.  $q_{cum}/q$ ,  $q$  vs.  $(t_p + \Delta t)/\Delta t$  plots, and various derivatives such as rate-time, cumulative-time,  $\Delta q/q$  – time, and  $\Delta q$ -time plots. These diagrams illustrate an important discovery that the ratio of the  $\Delta q/q$  for the beginning of the transition zone yields an indicator of the relative storage capacity of the fracture system. Thus if one has a reference well, all other field well decline curves can be used as an indicator of relative fracture storage capacity. For a “quick-look” classification, the  $(t_p + \Delta t)/\Delta t$  plot gives a good indicator of general fracture type. Poston and Chen’s fractured reservoir type curves were plotted on the same graph as the Fetkovich type curves in an effort to classify fracture types. Though the Posten and Chen type curves proved less useful than anticipated, the difference in the Fetkovich and Posten and Chen curves did provide some useful information.

## 9.2 Conclusions

1. The generalized decline curves confirm that the Fetkovich dimensionless decline type curves change significantly as the reservoir geometry and well location become more irregular.
2. The more generalized equations for calculation of transmissibility, permeability, reservoir area or radius and reserve estimation are also derived and presented for

the first time in this research which will result in more accurate parameter estimation in cases of non radial geometry.

3. All the required simulation PVT and relative permeability data can be calculated from production field data by the methods of Appendix B and C.
4. A two-phase flow approximation utilizing grid block averaged pressure and saturation has been developed to use with calibrating and validating simulation output in cases of solution gas reservoirs.
5. Graphical relationships showing the effect of permeability anisotropy on flow rate as a function of dimensionless well length, grid block size and well to boundary ratios are presented that will help better predict the horizontal flow rate in bounded and horizontally anisotropic reservoirs.
6. It is shown that the generalized dimensionless decline curves can be used with horizontal wells by introducing the equivalent horizontal well radius as long as the horizontal well length is not too long compared to the reservoir dimensions.
7. The research shows both experimentally and mathematically that departures of cumulative production data trends from the early time trends of competing wells will indicate relative contrasts in directional permeability that is approximately related to the ratio of the square root of  $k_y/k_x$ .
8. Fracture types can be classified and sometimes quantified by the use of certain plotting techniques and deviation from Fetkovich dimensionless type curve behavior.

### **9.3 Recommendations for Future Research**

Although many new concepts have been introduced, there are still several areas that merit further investigation. First, the generalized decline formulation has not been incorporated into the Arps empirical hyperbolic stems since there is no simple mathematical formulation for the cases in which additional reservoir energy, besides the rock and fluid compressibility, is present. Presumably however a downward shift to the origin similar to that of the mathematically derived single-phase solution would occur. This could be explored in future research by the use of simulation experimentation and examination of the depletion stems in the case of various solution gas and water drive conditions for non-radial and non well centered situations. The departure of the dimensionless decline curves from the exponential single-phase solution should give relative permeability information and should be explored further. Secondly, future research should be conducted with other simulators to test the observation that as the contrast in x and y permeability increases, while maintaining a constant geometric mean horizontal permeability, the simulated horizontal flow rates deviate increasingly from one another. This has been observed in an extensive set of experiments but should be further investigated with other simulators. Thirdly, further research is needed in using the departure in the Arps depletion stems from the single-phase solution as a tool of estimating relative permeability and drive energy. Fourthly more research is needed in applying the Posten Chen-Fetkovich type curves for characterization of reservoirs. There is also a need for more research in extracting more quantitative information from the  $\Delta q/q$  vs.  $q_{\text{cum}}/q$ ,  $q$  vs.  $(t_p + \Delta t)/\Delta t$  plots.

## NOMENCLATURE

|                   |   |
|-------------------|---|
| A                 | Well drainage area in acres   |
| A'                | 0.75 for circular drainage areas<br>0.738 for rectangular areas   |
| B <sub>o</sub>    | Oil formation volume factor   |
| b                 | Decline exponent(dimensionless) b=0 for exponential, 0<b<1 for hyperbolic   |
| B <sub>o</sub>    | Formation volume factor   |
| c'                | Shape factor conversion constant = 1.386  |
| c <sub>t</sub>    | Total compressibility   |
| c <sub>f</sub>    | Fracture compressibility  |
| c <sub>m</sub>    | Matrix compressibility  |
| D <sub>i</sub>    | Decline coefficient in days <sup>-1</sup>   |
| D <sub>q</sub>    | Near well turbulence factor   |
| GOR               | Gas to oil ratio  |
| h                 | Reservoir thickness   |
| IPR               | Inflow performance relationship   |
| k                 | Permeability, md  |
| k <sub>v</sub>    | Vertical permeability   |
| k <sub>h</sub>    | Horizontal permeability   |
| k <sub>ro</sub>   | Relative Permeability to Oil  |
| k <sub>x</sub>    | Permeability perpendicular to fractures(along well bore)  |
| k <sub>y</sub>    | Permeability along fractures(perpendicular to wellbore)   |
| L                 | Length of horizontal well   |
| L <sub>D</sub>    | Dimensionless well length   |
| p <sub>D</sub>    | Dimensionless pressure  |
| p <sub>i</sub>    | Initial reservoir pressure  |
| p <sub>wf</sub>   | Well flowing pressure   |
| PSS               | Pseudosteady state  |
| q                 | Oil production rate STB/day   |
| q <sub>D</sub>    | Dimensionless oil production rate   |
| q <sub>dD</sub>   | Decline Dimensionless oil rate  |
| q <sub>i</sub>    | Production rate at start of depletion STB/day   |
| r <sub>e</sub>    | Well drainage radius in feet  |
| r <sub>eh</sub>   | Horizontal well drainage radius   |
| r <sub>w</sub>    | Well radius in feet   |
| r <sub>w'</sub>   | Effective well radius   |
| S                 | Saturation  |
| s <sub>m</sub>    | Mechanical skin factor, dimensionless   |
| s <sub>f</sub>    | -ln[L/(4r <sub>w</sub> )]= negative skin factor of an infinite conductivity fully penetrating fracture of length L. |
| S <sub>CA,b</sub> | Shape related skin factor   |
| t                 | Time in hours   |
| t <sub>D</sub>    | Dimensionless time  |
| t <sub>da</sub>   | Dimensionless time based on drainage area   |

|                 |  |
|-----------------|--|
| $V_p$           | Pore Volume  |
| $x_e, y_e$      | Half the drainage distance in the x and y direction                      |
| $x_w, y_w, z_w$ | Distance of horizontal well center from drainage area boundaries in feet |
| $\mu$           | Viscosity  |
| $\Delta$        | Change   |
| $\lambda$       | Fluid transfer coefficient   |
| $\rho_w$        | Water density  |
| $\rho_o$        | Oil density  |
| $\phi$          | Porosity   |
| $\phi_m$        | Matrix Porosity  |
| $\phi_f$        | Fracture Porosity  |
| $\phi_e$        | Effective porosity   |
| $\gamma$        | Poston-Chen Fracture Intensity   |
| $\omega$        | Storage Compressibility  |
| $\omega'$       | Ratio of Matrix to Fracture Storage                                      |

## REFERENCES

1. Arps, J. J.: "Analysis of Decline Curves", *Petroleum Technology* (September 1944), May 1944 TP 1758.
2. Arps, J.J. : "Analysis of Decline Curves," *Petroleum Transactions*, AIME, Vol. 160, 1945, 228-47.
3. Fetkovich, M.J.: "Decline Curve Analysis Using Type Curves," *JPT*, (June 1980). 1065-77.
4. Golan, M., Whitson, C.: *Well Performance*, 2<sup>nd</sup> edition, Prentice Hall, Englewood Cliffs, NJ, (1991). (121)
5. Chang, M.M. et al, "User's Guide and Documentation Manual For Boastvhs for the PC", U.S. Department of Energy, (January 1992).
6. Craft, B.C., Hawkins, M., Terry, R.E.: *Applied Petroleum Reservoir Engineering*, 2<sup>nd</sup> Edition, Prentice Hall, Englewood Cliffs, NJ (1991).
7. Evinger, H.H., Muskat, M.: "Calculation of Theoretical Productivity Factor" *JPT* (September 1941). SPE TP 1352.
8. Vogel, J.V.: "Inflow Performance Relationships for Solution Gas Drive Wells". *JPT*. (June 1968) 83-92.
9. Tracy, G.W.: "Simplified Form of the Material Balance Equation," *Trans. AIME* (1955), 204.243
10. Turner, J.: "How Different Size Gas Caps and Pressure Maintenance Affect Amount of Recoverable Oil," *Oil Weekly* (June 12, 1944), 32.
11. Tsarevich, K.A.: "Calculation of the Flow Rates for the Center Well in a Circular Reservoir under Elastic Conditions," *Problems in Reservoir Hydrodynamics*, Part 1, Leningrad (1966) 9-34.
12. Cline, S.B.: "Reservoir Simulation as a Tool For Modifying Geological and Well Log Interpretations – A Fractured Pennsylvanian Sandstone Field Study", MS Thesis, University of Oklahoma, (1993).
13. Willhite, G. P: *Waterflooding*, SPE, Richardson, TX (1986)
14. Calhoun, J.C.: *Fundamentals of Reservoir Engineering*, University of Oklahoma Press, (1953)

15. Mattax, C.C., Dalton, D.L.: *Reservoir Simulation*, Monograph Series, SPE, Richardson, TX (1990) 13, 81.
16. Bass, D.M.: "Properties of Reservoir Rocks" *Petroleum Engineering Handbook*, SPE Richardson, TX (1992), 26-33.
17. Van Everdingen, A.F., Hurst, W.: "The Application of the Laplace Transformation to Flow Problems In Reservoirs", *Petroleum Transactions, AIIME*, (December, 1949), TP 2732.
18. Van Everdingen, A.F.: "The Skin Effect and Its Influence on the Productive Capacity of a Well", *Petroleum Transactions, AIIME*, Vol 198, (1953 ) TP 3581.
19. Stehfest, H.: "Algorithm 386: Numerical Inversion of Laplace Transforms," *Communications of the ACM*, 1970, 13, No. 1, 47-49.
20. Lee, J.: *Well Testing*, SPE Textbook Series, Dallas, TX (1982).
21. Matthews, C.S., Russell, D.G.: *Pressure Buildup and Flow Tests in Wells*, Monograph Series, SPE Dallas TX (1967). 1.
22. Earlougher, R.C.: *Advances in Well Test Analysis*, SPE Mongraph Series, SPE, Dallas TX (1977).
23. Joshi, S.D.: *Horizontal Well Technology*, PennWell Publishing Co., Tulsa (1991) 34, 62-65. 292.
24. Tiab, D.: "Direct Type Curve Synthesis of Pressure Transient Tests", SPE 18992, SPE Rocky Mountain Symposium, Denver, CO (March 6-8, 1989).
25. Tiab, D., Puthigai, S.K.: "Pressure Derivative Type Curves for Vertically Fractured Wells", *SPE Formation Evaluation*, (March 1988), 156-158.
26. Tiab, D.: "Analysis of Pressure and Pressure Derivative without Type Curve Matching-Vertically Fractured Wells in Closed Systems, SPE 26138, SPE meeting Anchorage Alaska, (May 1993).
27. Matalik, P.N., Godbole, S.P. and Joshi, S.D.: "Effect of Drainage Area Shapes on Horizontal Well Productivity", SPE paper, 18301, SPE Annual Conference Houston TX, (October 1988).
28. Kuchuk, F.J., Goode, P.A., et al: "Pressure Transient Analysis and Inflow Performance for Horizontal Wells", SPE paper 18300 Houston, TX (October 1988).
29. Babu, D.K., Odeh, A.S.: "Productivity of a Horizontal Well", SPE paper 18298, Houston, (October 1988) 373-382.

30. Joshi, S.D.: "Augmentation of Well Productivity With Slant and Horizontal Wells". *JPT*, (June 1988).
31. Slichter, C.S.: "Theoretical Investigation of the Motion of Ground Water," 19<sup>th</sup> annual report, U.S. Geological Survey (1897-1898) 301-84.
32. Joshi, S.D. "A Review of Horizontal Well and Drainhole Technology", Paper SPE 16868 SPE Annual Conference, Dallas 1987.
33. Joshi, S.D., Mutualik, P.N.: "Decline Curve Analysis Predicts Oil Recovery from Horizontal Wells". *Oil and Gas Journal*. (Sept. 7<sup>th</sup>, 1992).
34. Lock, C.D. and Sawyer, W.K. "Constant Pressure Injection in a Fractured Reservoir. Paper SPE 5594, SPE Annual Meeting Dallas, (Sept 28 1975).
35. Gringarten, A.: "Interpretation of Tests in Fissured and Multilayered Reservoirs With Double Porosity Behavior: Theory and Practice", SPE 10044, *JPT* April, 1984 549-564.
36. Camacho, R.G., Raghavan, R.: "Some Theoretical Results Useful in Analyzing Well Performance Under Solution Gas Drive". *SPE Formation Evaluation*, (June 1991), 190-191.
37. Camacho, R.: "Constant Pressure Production in Solution Gas Drive Reservoirs: Transient Flow". *SPE Formation Evaluation*, (June 1991), 199-208.
38. Fetkovich, M.J.: "The Isochronal Testing of Oil Wells". SPE 4529. SPE Preprint, 1973.
39. Ozkan, E., Raghavan, R.: "Horizontal Well Pressure Analysis", *SPE Formation Evaluation*, (December 1989), 567-575.
40. Russell, D.G.: "Transient Pressure Behavior in Vertically Fractured Reservoirs", *JPT*, Petroleum Transactions, October 1964, 1159-1170.
41. Mukherjee, H, Economides, M.: "A Parametric Comparison of Horizontal and Vertical Well Performance", *SPE Formation Evaluation*, (June 1991), 209-215.
42. Wiggins, M.: "Generalized Inflow Performance Relationships for Three Phase Flow", *SPE Reservoir Engineering*, (August 1994), 181-182.
43. Poston, S.W., Chen, H.Y.: "Fitting Type Curves to Austin Chalk Wells", SPE paper 21653, presented SPE meeting, Oklahoma City (April 7-9, 1991) 227-235.
44. Chen, H.Y., Raghavan, R.: "An Application of the Product Solution Principle for Instantaneous Source and Green's Functions", *SPE Formation Evaluation*, (June 1991).

45. Poston, S.W., Chen, H.Y, Raghavan, R: " Mathematical Development of Austin Chalk Type Curves" SPE 23527, SPE preprint 1991.
46. Cline, S.B., Tiab, D.: "Quantification of the Relative Importance of Fracture and Matrix Flow Units to Reservoir Storage Capacity and Transmissibility", SPE 27716. Permian Basin Oil and Gas Recovery Conference, (March 1994) 775-790.
47. Da Prat, G., Cinco,, L, Ramey, H.J.: :Decline Curve Analysis Using Type Curves for Two-Porosity Systems", SPE 9292, SPE Annual Meeting, Dallas TX (September 1980).
48. Agarwal, R.G., Gardner, D.C., et al: "Analyzing Well Production Data Using Combined-Type-Curve and Decline Curve Analysis Concepts", *SPE Reservoir Evaluation and Engineering*, (October 1999), 478-486.
49. Engler, T.W.: "Interpretation of Pressure Tests in Naturally Fractured Reservoirs by the Direct Synthesis Technique", PhD Dissertation, University of Oklahoma, (1995)

## Appendix A

### Derivation of the Saturated Analytic Approximation Equations and Relationship to IPR Relationships

As summarized in Chapter 3, for undersaturated conditions, the combined variation of viscosity and formation volume factor decreases approximately linearly with pressure as:

$$q = \frac{0.007078 k_h h}{\left( \ln \frac{r_e}{r_w} - 0.738 \right)} \int \frac{dp}{\mu_o B_o} \quad \dots \text{A1}$$

The integral is evaluated from  $P_{wf}$  to  $P_e$  (the pressure at the external boundary). Since  $1/\mu_o B_o$  is a straight line, the area is a trapezoid, so the integral can be represented by:

$$\int \frac{dp}{\mu_o B_o} = \frac{P_e - P_{wf}}{\left( \mu_o B_o \right)_{\bar{P}_R}} \quad \text{A2}$$

Where,

$$\frac{1}{\left( \mu_o B_o \right)_{\bar{P}_R}}$$

is the value at an average pressure  $\bar{P}_R = (P_e + P_{wf})/2$ . The resulting inflow equation, at average reservoir pressure for pseudosteady state conditions becomes:

$$q = \frac{0.007078 k_h h (\bar{P}_R - P_{wf})}{(\mu_o B_o)_{\bar{P}_R} \left( \ln \frac{r_e}{r_w} - 0.738 \right)} \quad \dots A3$$

Golan<sup>4</sup>(166) and Muskat et al<sup>7</sup> note that below the bubble point, (i.e. saturated reservoir conditions) equation 3 would become (neglecting skin and turbulence effects):

$$q = \frac{0.007078 h k_h}{\left( \ln \frac{r_e}{r_w} - 0.738 \right)} \int \frac{k_{ro}}{\mu_o B_o} dp \quad \dots A4$$

The integral is evaluated from  $P_{wf}$  to  $P_{Rave}$ .

Evinger and Muskat<sup>7</sup>(1942) and later Vogel<sup>8</sup> et al (1976) noted that the pressure function could be accurately represented versus pressure by a straight line ranging from  $k_{ro}/\mu_o B_o$  at reservoir pressure (up to the bubble point) to the origin. (Fig A-1) However, if this is the case, there is no need to evaluate the integral this way. If the straight-line assumption is valid, the problem reduces to expressing the area under the trapezoid situation as shown below.

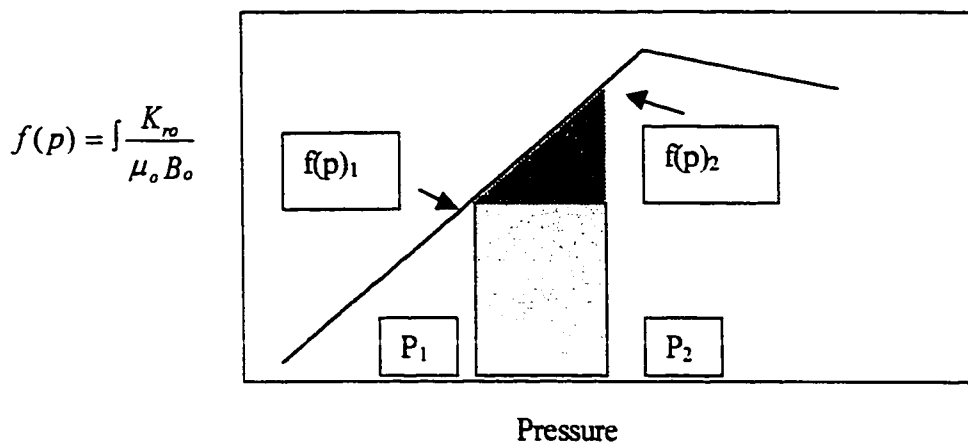


**Figure A-1 Mobility Function versus Pressure**

The area can be expressed as the sum of a triangle and rectangle:

$$A = (\Delta P)f(p_1) + 0.5(\Delta P)(f(p_2) - f(p_1))$$

$$A = (\Delta P)f(p_1) + 0.5(\Delta P)f(p_2) - 0.5(\Delta P)f(p_1)$$

$$A = 0.5(\Delta P)(f(p_1) + f(p_2))$$

$$A = \Delta P (f(p_1) + f(p_2))/2$$

Or substituting for the pressure functions:

$$Area = \Delta P \left( \frac{k_{ro}}{\mu_o B_o} \right)_{ave}$$

The value of  $(k_{ro}/\mu_o B_o)$  at any pressure can be obtained by calculating the slope of the line below the bubble point and multiplying by the pressure at the desired point.

Oil flow under saturated conditions can then be described above and below the bubble point if we substitute  $(k_{ro}/\mu_o B_o)_{ave}$  evaluated at average reservoir pressure  $P_R - P_{wf}$  or simply  $P_R$  if flowing bottom hole pressure is low.

$$q = \frac{0.007078 h k_h}{\left( \ln \frac{r_e}{r_w} - 0.738 \right)} \left[ \left( \overline{P}_R - P_{wf} \right) \left[ \frac{k_{ro}}{(\mu_o B_o)_{ave}} \right] \right]_{P_{ave} S_o} \quad ...A5$$

or more generally:

$$q_o = J(P_R - P_{wf})$$

Where  $J$  incorporates all of the terms in the above equation except the pressure differential so that:

$$J = \frac{0.007078 h k_h}{\left( \ln \frac{r_e}{r_w} - 0.738 \right)} \left[ \frac{k_{ro}}{(\mu_o B_o)_{ave}} \right] \quad A6$$

Therefore since we know the mobility as a function of pressure and saturation that is input to simulators we can use the same function to analytically check against simulation output. Actually it seems to me that  $K_{ro}$  should be computed at the average oil saturation at any given average pressure situation rather than at the average pressure as noted in Muskat'. Muskat never mentions this in his paper but perhaps the integral of  $K_{ro}$  should not be from  $P_{wf}$  to  $P_c$  but from  $S_{oi}$  to  $S_{oe}$  since  $K_{ro}$  is only indirectly related to pressure through the saturation function.

Now the above expression can be represented by the equivalent IPR depletion expression in terms of a backpressure constant C as follows:

Equation 4 can be written as:

$$q_o = C \int_{P_w}^{P_R} \frac{k_{ro}}{\mu_o B_o} dp \quad A7$$

Or as previously shown:

$$q_o = C' \text{ Area Under Curve}$$

Where C' is given as:

$$C' = \frac{0.007078 h k_h}{\left( \ln \frac{r_e}{r_w} - 0.738 \right)} \quad A8$$

Letting  $(k_{ro}/\mu_o B_o)$  be denoted by  $M_{PR}$  and  $M_{Pwf}$  for the respective pressures, the area under the curve is represented by the relationship:

$$\text{Area} = \frac{1}{2} \left[ \left( M_{PR} + \frac{M_{PR}}{P_R} P_{wf} \right) (P_R - P_{wf}) \right] \quad A8$$

$$\text{Area} = \frac{1}{2} \left[ \left( \frac{M_{PR}}{P_R} P_R + \frac{M_{PR} P_{wf} P_R}{P_R^2} \right) (P_R - P_{wf}) \right] \quad A9$$

$$\text{Area} = \frac{M_{PR}}{2P_R} (P_R + P_{wf}) (P_R - P_{wf}) \quad A10$$

Substituting this expression into the rate equation yields:

$$q_o = \frac{C M_{PR}}{2P_R} (P_R^2 - P_{wf}^2) \quad A11$$

Where C was previously defined. Combining the first terms and calling them C results in the equivalent to the pressure squared IPR relation:

$$q_o = C (P_R^2 - P_{wf}^2) \quad A12$$

Where C is defined below the bubble point as:

$$C = \frac{kh}{141.2\mu_o B_o} \frac{1}{2P_R} M_{PR} = \frac{kh}{141.2\mu_o B_o} \frac{1}{2P_R} \int_{P_w}^{P_R} \frac{k_{ro}}{\mu_o B_o} dp \quad A12$$

The addition of a turbulence term Dq<sub>o</sub> to the denominator of C and substitution into equation X, solving for q yields a back pressure equation with exponent n.

$$q_o = C (P_R^2 - P_{wf}^2)^n \quad A13$$

Where C is the backpressure constant approximated by:

$$C = \left[ \frac{kh}{141.2} \frac{1}{2P_R} \left( \frac{k_{ro}}{\mu_o B_o} \right) \right]^n \quad A14$$

For pseudosteady state, excluding damage and turbulence factors, the backpressure constant C varies only because of depletion and the resulting change in average  $(k_{ro}/\mu_o B_o)_{ave}$ . And as shown previously, these properties are evaluated at the average reservoir pressure. Plotting the well test data as  $q_o$  vs.  $\Delta P^2$  on log-log graphs determines the coefficient and the exponent of the backpressure equation.

This relationship can be useful in understanding the decline curves and relating Arps empirical decline curves with the exponential decline shown by Fetkovich. For instance the variation in the decline from the Fetkovich exponential decline is expressed by a "b" factor. The primary deviation is a result of the variation of  $k_{ro}/\mu_o B_o$  with declining reservoir pressure under pseudosteady state conditions.

It is shown in chapter 4 that the rate is expressed by Arps<sup>1</sup> as:

$$q = \frac{q_i}{(1 + bDt)^{\frac{1}{b}}} \quad A15$$

or defined in dimensionless decline parameters:

$$q_{dD} = \frac{q_i}{q_i} = [1 + bDt_{dD}]^{\frac{1}{b}} \quad A16$$

The decline D is assumed as unity in the literature. Exponential decline where b=0 is the equivalent of the Fetkovich<sup>38,42</sup> derivation is expressed in Arp's symbology as:

$$q_{dD} = e^{-r_{dD}}$$

A17

Now applying the definition of  $t_{dD}$ :

$$q_{dD} = \left[ 1 + b \frac{\frac{0.0063kt}{\frac{1}{2} \phi \mu c r_w^2 \left( \left( \frac{r_e}{r_w} \right)^2 - 1 \right) \left( \ln \frac{r_e}{r_w} - \frac{1}{2} \right)}} \right]^{\frac{1}{b}} \quad A18$$

Appendix C will illustrate methods of using these IPR relationships in conjunction with the type curve matching to extract relative permeability data from the rate-time production data.

## APPENDIX B

### **Program For Estimating Reservoir PVT Data**

The following program, OILPROP, was written in Pascal 3.0. All the user must know is the following information: Reservoir temperature in degrees F, oil gravity [deg API], gas gravity [air=1.0], initial reservoir pressure [psia], and either the bubble point pressure [psia] or the initial solution gas-oil ratio (RSOI[scf/stb]). The program will then determine the complete suite of PVT oil and gas properties: solution gas to oil ratio (RSO[scf/stb]), oil formation volume factor ( $B_o$ [bbl/stb]), and oil phase viscosity for oil ( $m_o$ [cp]). If the pressure is below the bubble point then the program will also compute the following gas properties: the gas deviation factor Z, the gas formation volume factor ( $B_g$ [bbl/scf]) and the gas phase viscosity ( $m_g$ [cp]). The user may specify the beginning and ending pressures to evaluate at any number of equally spaced pressures in between.

This program utilizes equations for oil and gas properties that can be found in Craft, Hawkins and Terry<sup>6</sup>.

The program first prompts the user for the input data. The program then proceeds according to the following pseudo-code flow chart:

```
WHILE PRESSURE >= MINIMUM PRESSURE SPECIFIED DO
    BEGIN
        IF BUBBLE POINT PRESSURE IS GIVEN THEN
            CALCULATE RSO
        ELSE
            USE RSOI TO CALCULATE BUBBLE POINT PRESSURE
            CALCULATE RSO
            IF PRESSURE > BUBBLE POINT PRESSURE THEN
                BEGIN
                    RSO=RSOB
                    CALC. OIL VIS. ABOVE BUBBLE
                END
            IF PRESSURE<=BUBBLE POINT THEN
                BEGIN
                    CALC. PSEUDO CRITICAL PROPS
                    CALC. THE Z FACTOR
                    CALC. GAS FORM. VOLUME FACTOR
                    CALC. THE GAS VISCOSITY
                    CALC. THE OIL VISCOSITY
                END
            CALCULATE THE OIL FORMATION VOLUME
            FACTOR
            PRINT RESULTS
        REPEAT PROCESS UNTIL ALL PRESSURE POINTS ARE
        EVALUATED
    END
```

RSO is calculated by the following equation, 1.26, from Craft Hawkins and Terry<sup>6</sup>.

$$R_{so} = \gamma_g \left( \frac{P}{18(10)^{YG}} \right)^{1.204} \text{ (scf / stb)} \quad \text{B1}$$

$\gamma_g$  = gas gravity

YG = 0.0091 T - 0.0125  $\rho_{0\text{API}}$

$\rho_0$  = API oil gravity

T = degrees Fahrenheit

P = Pressure psia

### Applicable Range

130 < P<sub>bubble</sub> (psia) < 7000

100 < T° F < 258

20 < GOR (scf/stb) < 1425

16.5 <  $\rho_0$  °API < 63.8

0.59 <  $\gamma_g$  < 0.95

1.024 < Bo (bbl/stb) < 2.05

When RSOI is known but the bubble point pressure is unknown then the above equation is solved for the bubble point pressure.

The following equations are used to determine the oil viscosity below and above the bubble point pressure respectively.

1)  $P \leq P_b$

$$A \mu_{od}^B (cp) \quad \text{B2}$$

$$A = 10.75 (R_{so} + 100)^{-0.515} \quad \text{B3}$$

$$B = 5.44 (R_{so} + 150)^{-0.338} \quad \text{B4}$$

$$\log(\log(\mu_{od} + 1)) = 1.8653 - 0.02508 \rho_{oAPI} - 0.5644 \log(T) \quad \text{B5}$$

### Applicable Range

$$\begin{aligned} 59 < T^{\circ F} &< 176 \\ -58 < T_{pour}^{\circ F} &< 59 \\ 5.0 < \rho_0 \text{ API} &< 58 \end{aligned}$$

2)  $P > P_b$

$$\mu_o = \mu_{ob} \left( \frac{P}{P_b} \right)^m (cp) \quad \text{B6}$$

$$m = 2.6P^{(1.187)} \exp(-11.513 - 8.98(10^{-6})P)$$

B7

$$\mu_{ob} = \mu_o \text{ at } P_{bubble}$$

### Applicable Range

$$\begin{aligned} 126 < P \text{ psig} &< 9500 \\ 0.117 < \mu_o &< 148 \\ 9.3 < \text{GOR scf/stb} &< 2199 \\ 15.3 < \rho_0 \text{ API} &< 59.5 \\ 0.511 < \gamma_g &< 1.351 \end{aligned}$$

The Z factor is calculated using the Abou Kassem equation, (equation 1.10 Craft and Hawkins<sup>6</sup>). My program uses the Newton-Raphson method to find the root of that equation which provides the Z value. This is an iterative process that also requires the derivative of the equation. The user can specify the iteration stopping criteria and the maximum number of iterations. The explanation of the terms in the below listed Abou Kassem equation can be found in the program listing.

$$Z = 1 + C_1(T_{pr}) \rho_r + C_2(T_{pr}) \rho_r^2 - C_3(T_{pr}) \rho_r^3 + C_4(\rho_r, T_{pr}) \quad B8$$

### Applicable range

$$\begin{aligned} 0.2 < P_{pr} &< 30 \\ 1.0 < T_{pr} &< 3.0 \text{ and } P_{pr} < 1.0 \text{ with } 0.7 < T_{pr} < 1.0 \end{aligned}$$

poor results if  $T_{pr} = 1.0$  and  $P_{pr} > 1.0$

Once Z is calculated, the gas formation volume factor is found from the following equation:

$$B_g = 0.00504 \left( \frac{ZT}{P} \right) \text{ (bbls / scf)} \quad \text{B9}$$

Z=gas deviation factor

T=°Rankine

P=pressure psia

The gas viscosity is determined from the following relation:

$$\mu_g = (10^4) K \exp(X \rho^Y) \quad \text{B10}$$

$$\rho = 1.4935(10)^{-3} \frac{PMW}{ZT} \quad \text{B11}$$

$$K = \frac{9.4 + 0.02MW(T)^{1.5}}{209 + 19MW + T} \quad \text{B12}$$

$$X = 3.5 + \frac{986}{T} + 0.01MW$$

B13

$$Y=2.4-0.2X$$

P=Pressure

T=Temperature °R

MW=molecular weight

### Applicable Range

$$\begin{aligned} 100 < P \text{ psia} &< 5000 \\ 100 < T^{\circ} \text{ F} &< 340 \\ 0.9 < \text{CO}_2 \% \text{ by mole} &< 3.2 \end{aligned}$$

\*Z must already be corrected for contaminants\*

The oil formation volume factor is determined from the following equations:

1)  $P < P_b$

$$B_o = 0.972 + 0.000147(F)^{1.175}$$

B14

$$F = R_{so} \left( \frac{\mu_g}{\mu_o} \right)^{0.5} + 1.25T$$

B15

$$\gamma_o = \frac{141.5}{131.5 + \rho_{oAPI}}$$

**B16**

2)  $P > P_b$

$$B_o = B_{ob} \exp(C_o(P_b - P))$$

**B17**

$$B_{ob} = B_o \text{ at } P_{bubble}$$

$$C_o = \frac{5 R_{sob} + 17.2 T - 1180 \gamma_g + 12.61 \rho_{oAPI} - 1433}{P(10^5)}$$

**B18**

### Applicable Range

$$\begin{aligned} 126 < P \text{ psig} &< 9500 \\ 1.006 < B_o \text{ bbl/stb} &< 2.226 \\ 9.3 < GOR \text{ scf/stb} &< 2199 \\ 15.3 < \rho_{oAPI} &< 59.5 \\ 0.511 < \gamma_g &< 1.351 \end{aligned}$$

The program was tested using the data provided in problem 1.20 in Craft, Hawkins and Terry<sup>6</sup>.

That input data was as follows:

Bubble Point Pressure = 2800

Gas Gravity = 0.8

Oil Gravity = 30 API

Temperature = 165° F

The test was run assuming an initial reservoir pressure of 3200 psia and the minimum pressure of interest was 800 psia. The results are included in this report. The program was also tested by substituting the initial solution gas to oil ratio for the bubble point pressure. Excellent agreement was obtained.

The program is simple to use and offers a quick method to accurately calculate reservoir oil and gas properties at a wide variety of application ranges of pressure and temperature. These results may aid the user in understanding and evaluating various reservoir characteristics.

THE INPUT DATA IS LISTED BELOW

THE FIRST Z ESTIMATE IS: 1.0000  
 THE % STOPPING CRITERIA IS: 0.0100  
 THE MAX. # ITERATIONS FOR Z IS: 50  
 THE RESERVOIR PRESSURE (psia) IS 3200.00  
 THE RESERVOIR TEMPERATURE IS (DEG F) 165.00  
 THE GAS GRAVITY IS 0.8000  
 THE API OIL GRAVITY IS 30.0000  
 THE BUBBLE POINT PRESSURE(psia) IS 2800.00

\*\*\*IF ZEROS APPEAR IN THE FOLLOWING TABLE IT MEANS\*\*\*  
 \*\*\*THAT THE PARAMETERS DO NOT APPLY AT THOSE \*\*\*  
 \*\*\*PRESSURES AND TEMPERATURES \*\*\*

| PRESSURE<br>psia | Z      | GAS VISCOCITY<br>cp | BG<br>bbl/scf | BO<br>bbl/stb | RSO<br>scf/stb | OIL VIS<br>cp |
|------------------|--------|---------------------|---------------|---------------|----------------|---------------|
| 3200.00          | 0.0000 | 0.0000              | 0.0000        | 1.3597        | 649.8896       | 0.8413        |
| 3080.00          | 0.0000 | 0.0000              | 0.0000        | 1.3614        | 649.8896       | 0.8315        |
| 2960.00          | 0.0000 | 0.0000              | 0.0000        | 1.3633        | 649.8896       | 0.8221        |
| 2840.00          | 0.0000 | 0.0000              | 0.0000        | 1.3653        | 649.8896       | 0.8131        |
| 2720.00          | 0.8083 | 0.0212              | 0.0009        | 1.3541        | 627.5990       | 0.8294        |
| 2600.00          | 0.8050 | 0.0206              | 0.0010        | 1.3365        | 594.4142       | 0.8602        |
| 2480.00          | 0.8028 | 0.0199              | 0.0010        | 1.3192        | 561.5405       | 0.8935        |
| 2360.00          | 0.8016 | 0.0193              | 0.0011        | 1.3022        | 528.9899       | 0.9297        |
| 2240.00          | 0.8016 | 0.0187              | 0.0011        | 1.2855        | 496.7752       | 0.9692        |
| 2120.00          | 0.8027 | 0.0181              | 0.0012        | 1.2691        | 464.9108       | 1.0123        |
| 2000.00          | 0.8052 | 0.0176              | 0.0013        | 1.2530        | 433.4125       | 1.0597        |
| 1880.00          | 0.8090 | 0.0170              | 0.0014        | 1.2372        | 402.2975       | 1.1120        |
| 1760.00          | 0.8141 | 0.0165              | 0.0015        | 1.2218        | 371.5853       | 1.1700        |
| 1640.00          | 0.8206 | 0.0160              | 0.0016        | 1.2068        | 341.2976       | 1.2345        |
| 1520.00          | 0.8284 | 0.0155              | 0.0017        | 1.1921        | 311.4591       | 1.3068        |
| 1400.00          | 0.8374 | 0.0151              | 0.0019        | 1.1777        | 282.0976       | 1.3884        |
| 1280.00          | 0.8475 | 0.0147              | 0.0021        | 1.1638        | 253.2457       | 1.4809        |
| 1160.00          | 0.8587 | 0.0143              | 0.0023        | 1.1503        | 224.9410       | 1.5866        |
| 1040.00          | 0.8709 | 0.0139              | 0.0026        | 1.1372        | 197.2284       | 1.7065        |
| 920.00           | 0.8839 | 0.0136              | 0.0030        | 1.1245        | 170.1617       | 1.8502        |
| 800.00           | 0.8976 | 0.0133              | 0.0035        | 1.1124        | 143.8075       | 2.0165        |

Table B-1 Sample PVT Program Output

```

PROGRAM OILPROP(INPUT,OUTPUT);

{$I c:\pas\scott\INFO.TXT}

VAR
CH,CHO:CHAR;
DEVICE:TEXT;
TRES,GASGRAV,PRESS,PBUB,PMIN,PMAX,ROOT,
PPR,TPR,PPC,TPC,STOPER,C1,C2,C3,C4,
BGI,RHO,MG,OILGRAV,BOB,BO,RSO,RSOI,RSOB,APIGRAV,
Z,N,OIL VISC,MEWLIVE,MEWABOVE,MEWOBUB:REAL;
ITERMAX:INTEGER;
(*ROOT is the first root estimate, STOPER is the iteration stopping
criteria expressed as % error, ITERMAX is the max # of iterations*)
(*-----*)
{$I c:\pas\scott\WHICHONE.PAS}

(*-----*)

PROCEDURE READATA;
(*This procedure prompts the user for the input data*)
BEGIN
WRITELN('INPUT RESERVOIR TEMP IN DEGREES F:');
READLN(TRES);
WRITELN('INPUT GAS GRAVITY:');
READLN(GASGRAV);
WRITELN('RESERVOIR PRESSURE:');
READLN(PRESS);
WRITELN('You may enter either Bubble Point pressure or solution gas ratio');
WRITELN('If you wish to enter bubble point pressure then type Y');
WRITELN('If not type N but you will then have to enter RSOI in the next step');
READLN(CHO);
IF (CHO= 'y') OR (CHO= 'Y') THEN
BEGIN
WRITELN('BUBBLE POINT PRESSURE=');
READLN(PBUB);
END
ELSE
BEGIN
WRITELN('RSOI=');
READLN(RSOI);
END;

WRITELN('INPUT OILGRAVITY IN API UNITS');

```

```

READLN(APIGRAV);
WRITELN('MAX PRESSURE TO EVALUATE');
READLN(PMAX);
WRITELN('MIN PRESSURE TO EVALUATE');
READLN(PMIN);
WRITELN('NUMBER OF POINTS TO EVALUATE ');
READLN(N);
END;
(*-----*)
PROCEDURE READATAZ;
(*this procedure reads in the Z factor estimate.stopper and max iterations*)
BEGIN
    WRITELN('SPECIFY THE INITIAL Z VALUE GUESS:');
    READLN(ROOT);
    WRITELN('SPECIFY THE % STOPPING CRITERIA FOR NEWTON
RAPHSON:');
    READLN(STOPER);
    WRITELN('SPECIFY THE MAXIMUM NUMBER OF ITERATIONS:');
    READLN(ITERMAX);
END;(*of readata*)

(*-----*)

PROCEDURE WRITEDATA;
(*this procedure writes the input data to the printer or screen*)
BEGIN
    WRITELN(DEVICE,'THE INPUT DATA IS LISTED BELOW');
    WRITELN(DEVICE);
    WRITELN(DEVICE,'THE FIRST Z ESTIMATE IS: ',ROOT:10:4);
    WRITELN(DEVICE,'THE % STOPPING CRITERIA IS: ',STOPER:10:4);
    WRITELN(DEVICE,'THE MAX. # ITERATIONS FOR Z IS: ',ITERMAX:10);
    WRITELN(DEVICE,'THE RESERVOIR PRESSURE (psia)IS ',PRESS:10:2);
    WRITELN(DEVICE,'THE RESERVOIR TEMPERATURE IS (DEG F)',TRES:10:2);
    WRITELN(DEVICE,'THE GAS GRAVITY IS ',GASGRAV:10:4);
    WRITELN(DEVICE,'THE API OIL GRAVITY IS ',APIGRAV:10:4);
    IF (CHO='Y') OR (CHO='y') THEN
        WRITELN(DEVICE,'THE BUBBLE POINT PRESSURE(psia) IS ',PBUB:10:2)
    ELSE
        WRITELN(DEVICE,'SOLUTION GAS RATIO (SCF/STB)RSOI IS ',RSOI:10:4);
    WRITELN(DEVICE);
    WRITELN(DEVICE,'***IF ZEROS APPEAR IN THE FOLLOWING TABLE IT
MEANS***');

    WRITELN(DEVICE,'***THAT THE PARAMETERS DO NOT APPLY AT THOSE
***');

```

```

      WRITELN(DEVICE,'***PRESSURES AND TEMPERATURES
      WRITELN(DEVICE);
END;(*of writedata*)

(*-----*)
FUNCTION DR(TRY:REAL):REAL;
(*This function evaluates Rho sub r in the Abou- Kassem equation*)
BEGIN
  DR:=0.27*PPR/(TRY*TPR);
END;
(*-----*)

PROCEDURE PSEUDOCRITICAL:
(*This procedure calculates the pseudocritical values for use in
 the calculation of the Z factor*)
BEGIN
  PPC:=756.8-131.0*GASGRAV-3.6*GASGRAV*GASGRAV;
  TPC:=169.2+349.5*GASGRAV-74*GASGRAV*GASGRAV;
  PPR:=PRESS/PPC;
  TPR:=(460+TRES)/TPC;
END;
(*-----*)

PROCEDURE CONSTANTS:
(* The procedure calculates some of the terms that are used in the
 Abou-Kassem equation evaluated in function funcvalue*)
BEGIN
  C1:=0.3265-1.07/TPR-(0.5339/(EXP(3*LN(TPR))))+
  (0.01569/(EXP(4*LN(TPR))))-
  (0.05165/(EXP(5*LN(TPR)))); 
  C2:=0.5475-0.7361/TPR+(0.1844/(TPR*TPR));
  C3:=0.1056*(-0.7361/TPR+0.1844/(TPR*TPR));
END;
(*-----*)

FUNCTION FUNCVALUE(TRY:REAL):REAL;
(*this function is specified by the user. We will find the root
 of this function later in the newtrap procedure. TRY is the root
 estimate input from the newtrap procedure*)
BEGIN

FUNCVALUE:=TRY-(1+C1*DR(TRY)+C2*DR(TRY)*DR(TRY)-
C3*EXP(5*LN(DR(TRY)))+
(0.6134*(1+0.721*DR(TRY)*DR(TRY))*((DR(TRY)*DR(TRY))/(
(EXP(3*LN(TPR))))*EXP(-0.721*DR(TRY)*DR(TRY))));

END;(*of function*)

```

```

(*-----*)
FUNCTION DERIV(TD:REAL):REAL;
(*this is the derivative of the above function. The derivative is
used in the calculation of the root. td is the root estimate
input from procedure newtrap*)
BEGIN
  DERIV:=1+(C1*DR(TD))/TD+(2*C2*DR(TD)*DR(TD))/TD-
  (5*C3*EXP(5*LN(DR(TD))))/TD+
  ((2*0.6234*DR(TD)*DR(TD))/(
  (TD*EXP(3*LN(TPR)))))*
  (1+0.721*DR(TD)*DR(TD)-EXP(2*LN((0.721*DR(TD)*DR(TD)))))*
  EXP(-0.721*DR(TD)*DR(TD));
END;(*of function*)

```

```

(*-----*)
PROCEDURE GASFVF;
(*This procedure calculates the gas formation volume factor in BBL/SCF*)
BEGIN
  BGI:=(0.00504*Z*(TRES+460))/PRESS;
END;
(*-----*)

```

```

PROCEDURE MEGAS:
(*This procedure calculates the gas viscosity in centipoise*)
var
MW,RHO,K,X,Y:REAL;
BEGIN
  MW:=28.97*GASGRAV;
  RHO:=1.4935*0.001*((PRESS*28.97*GASGRAV)/(Z*(460+TRES)));
  K:=(EXP(1.5*(LN((460+TRES))))*(9.4+0.02*MW))/(209+19*MW+(460+TRES));
  X:=3.5+(986/(460+TRES))+0.01*MW;
  Y:=2.4-0.2*X;
  MG:=0.0001*K*EXP(X*EXP(Y*LN(RHO)));
END;
(*-----*)

```

```

PROCEDURE OILFVF:
(*This procedure calculates the oil formation volume factor Bo in BBL/STB*)
VAR
CO,F:REAL;
BEGIN
  OILGRAV:=141.5/(131.5+APIGRAV);
  F:=RSO*EXP(0.5*LN(GASGRAV/OILGRAV))+1.25*TRES;
  BO:=0.972+0.000147*EXP(1.175*LN(F));

```

```

IF PRESS > PBUB THEN
BEGIN
  CO:=(5*RSOB+17.2*TRES-1180*GASGRAV+12.61*OILGRAV-1433)/(PRESS*
    EXP(5*LN(10)));
  BO:=BO*EXP(CO*(PBUB-PRESS));
END;
END;
(*-----*)
PROCEDURE RSOBELOWBUB;
(*This procedure calculates the residual gas saturation at the
bubble point and below the bubble point*)
VAR
  YG:REAL;
BEGIN
  YG:=0.00091*TRES-0.0125*APIGRAV;
  RSO:=GASGRAV*EXP(1.204*LN((PRESS/(18*EXP(YG*LN(10))))));
  RSOB:=GASGRAV*EXP(1.204*LN((PBUB/(18*EXP(YG*LN(10))))));
END;
(*-----*)

PROCEDURE PRESSBUB;
(*This procedure calculates the bubble point pressure if only the
initial residual gas saturation is known*)
VAR
  YG:REAL;
BEGIN
  YG:=0.00091*TRES-0.0125*APIGRAV;
  PBUB:=18*EXP(YG*LN(10))*EXP((1/1.204)*LN(RSOI/GASGRAV));
END;

(*-----*)
PROCEDURE NEWTRAP(VAR Xorig,Stopit:REAL;Maxit:INTEGER);
(*this procedure calculates the root of a given function using
the Newton-Rhapson method. The procedure requires the input of
Xorig=original root estimate, Stopit=stopping criteria, and
Maxit= the max # of iterations.*)
VAR
  Eraprox,Rootesta:REAL;
  Iter:INTEGER;
BEGIN
  Iter:=0;
  Eraprox:=1.1*Stoper;
  WHILE (Eraprox>Stoper) AND (Iter<Maxit) DO
    BEGIN
      Rootesta:=Xorig-(Funcvalue(Xorig)/Deriv(Xorig));

```

```

(*newtrapson equation where funcvalue is the function
and deriv is the derivative of the function*)
ITER:=ITER+1;
IF ROOTESTA <> 0.0 THEN (*tests to avoid zero division*)
    ERAPROX:= ABS((ROOTESTA-XORIG)/ROOTESTA)*100;
    (*calculates the approx error from preceding estimate*)
    XORIG:=ROOTESTA;
END;
Z:=ROOTESTA;
END;(*end of newtrap procedure*)

```

(\*-----\*)

```

PROCEDURE COMPARE(VAR ROOTESTA:REAL);
(*this procedure compares the function value with the calculated root
to zero. If it is close to zero the method has probably worked*)
BEGIN
    WRITELN(DEVICE);
    WRITELN(DEVICE,'IF THE FUNCTION VALUE IS CLOSE TO ZERO THE
METHOD WORKS');
    WRITELN(DEVICE,'THE FUNCTION VALUE WITH CALC. ROOT IS
',FUNCVALUE(ROOTESTA));
END;(*of compare*)

```

(\*-----\*)

```

PROCEDURE OILVIS:
(*This procedure calculates the oil viscosity both below the bubble
point (mewlive) and above the bubble point(mewabove)*)
VAR
    CONST1,CONST2,CONST3,MEWOD,A,B,ABUB,BBUB,MFACT:REAL;
BEGIN
    CONST1:=1.8635-0.025086*APIGRAV-0.5644*(LN(TRES)/LN(10));
    CONST2:=EXP(CONST1*LN(10));
    CONST3:=EXP(CONST2*LN(10));
    MEWOD:=CONST3-1.0;
    A:=10.715*EXP(-0.515*LN(RSO+100));
    B:=5.44*EXP(-0.338*LN(RSO+150));
    MEWLIVE:=A*EXP(B*LN(MEWOD));
    ABUB:=10.715*EXP(-0.515*LN(RSOB+100));
    BBUB:=5.44*EXP(-0.338*LN(RSOB+150));
    MEWOBUB:=ABUB*EXP(BBUB*LN(MEWOD));
    MFACT:=2.6*EXP(1.187*LN(PRESS))*EXP(-11.513-(8.98*0.00001*PRESS));
    MEWABOVE:=MEWOBUB*EXP(MFACT*LN(PRESS/PBUB));
END;

```

(\*-----\*)

PROCEDURE TITLES;

(\*This procedure prints the output titles\*)

BEGIN

WRITELN(DEVICE,'PRESSURE',' Z ','GAS VISCOCITY,' BG ',  
' BO '' RSO',' OIL VIS ');  
WRITELN(DEVICE,' psia',' ',' cp ',' bbl/scf,  
' bbl/stb',' scf/stb',' cp ');  
END:

(\*-----\*)

PROCEDURE PRINTRESULTS;

(\*This procedure prints the results to a printer or screen\*)

BEGIN

WRITELN(DEVICE,PRESS:9:2,Z:9:4, MG:12:4,BGI:9:4,BO:9:4,RSO:9:4,OILVISC:9:4  
);  
END:

(\*-----\*)

BEGIN(\*of main control program\*)

CHO:=':';

WHICHONE(DEVICE);

READATA;

READATAZ;

WRITEDATA;

TITLES;

WHILE PRESS >= PMIN DO

BEGIN

IF (CHO= 'y') OR (CHO= 'Y') THEN

RSOBELOWBUB

ELSE

PRESSBUB;

RSOBELOWBUB:

IF PRESS > PBUB THEN

BEGIN

RSO:=RSOB;

OILVIS;

OILVISC:=MEWABOVE;

Z:=0;MG:=0;BGI:=0;

END;

IF PRESS <= PBUB THEN

BEGIN

PSEUDOCRITICAL;

```

CONSTANTS;
NEWTRAP(ROOT,STOPER,ITERMAX);
GASFVF;
MEWGAS;
OILVIS;
OILVISC:=MEWLIVE;
END;
OILFVF;
PRINTRESULTS:
PRESS := PRESS-(PMAX-PMIN)/N;
END;
END. (*of main*)
 

PROCEDURE Whichone (VAR device: TEXT);
(*This "INCLUDED" procedure enables the user to assign the output to
either the console or printer. *)
 

VAR ch: CHAR;
i: INTEGER;

BEGIN (* of whichone procedure *)
CH:=' ';
CLRSCR;
WHILE (ch <> 'p') and (ch <> 'P') AND
(ch <> 'c') and (ch <> 'C') DO
BEGIN (* while *)
FOR i := 1 to 10 DO
WRITELN;
WRITE ('SELECT PRINTER OR CONSOLE (P/C) ==>');
READLN (ch);
IF (ch = 'p') or (ch = 'P')
THEN ASSIGN (device, 'LST:');
ELSE
BEGIN (* if *)
WRITELN;
WRITELN ('INVALID RESPONSE. PLEASE RETRY.');
WRITELN;
END; (* if *)
END; (* while *)
CLRSCR;
REWRITE (device)
END; (* of whichone procedure *)

```

## **Appendix C**

### **Guide To Estimating and Deriving the Reservoir Properties Needed In Reservoir Simulation and Two-Phase Analytical Calculations from Field Production Data**

Numerical simulations and two-phase analytical calculations such as presented in this dissertation require knowledge of certain fluid and rock properties. Normally these properties are not easily obtained or not available to the non-operating interests and thus must be estimated from production data. This section presents several original and some widely used methods to estimate all the properties required for input to simulation experiments. Methods for estimating absolute permeability methods are not included but a comprehensive discussion is given in my MS thesis, 1993.<sup>12</sup> A flow diagram of the process of estimating parameters is also given in that thesis.

#### **Estimating PVT Data**

PVT data can be generated from a simply a knowledge of the dead oil viscosity from a produced oil sample and produced gas-oil ratio (GOR) information obtained from production data. The details are described in the PVT section of this and my computer algorithms for calculation are shown in appendix B.

### Relative Permeability Data

Two methods, depending on the type of data available to the engineer are presented for calculating relative permeability data are. One method can be used when there is a core analysis available. Core analysis is used but then modified to fit field production information. The other method assumes no knowledge of core information but only field evidence of produced fluids ratios. An example is provided in which the matrix relative permeability to oil and gas is determined based on observed residual oil saturations as noted on core analysis and connate water saturations calculated from logs. The relative permeability to oil endpoint can be taken as the lowest residual oil saturation from the core or analogy to other field data. The water endpoint can be used as the lowest water saturation calculated from log analysis in a field or analogous formation.

### Capillary Pressure

Based on log calculated water saturation at various well locations and structure maps from a field, a capillary pressure relation can be developed to correspond to the transition zone found in the field or an analogous field. A discussion of the method and an example of capillary pressure curve estimation are shown in the capillary pressure section of this report. This capillary pressure curve was slightly modified to obtain a water saturation distribution that more closely resembled that calculated from well logs.

## C.2 RESERVOIR PROPERTIES

### C.2.1 Discussion of the PVT Data

Pressure, volume and temperature data can be generated from dead oil viscosity, gas gravity, initial produced GOR's, and initial reservoir pressure and temperature. No other data are often available or necessary to generate the PVT relations.

In this example, a service company laboratory measured a dead oil viscosity of 2.53 cp at the formation temperature of 116 degrees F. This oil viscosity corresponds to an API gravity of 38.1-degree oil. Gas gravity of 0.775 was estimated in this example based on the composition of the gas, which was primarily methane. Gas gravity can easily be estimated based on the composition, which will normally consist of predominantly methane, ethane and propane. The reader is referred to the Petroleum Engineering handbook for calculations using mole fractions.

Relative gas and oil production statistics can be obtained from operators or from the various state and private databases. This information should then be tabulated on a spreadsheet to identify producing gas to oil ratio (GOR) trends among wells within a field. GORs are then projected back to first production using linear or non-linear regression or trend analysis. This example (Table A-1) illustrates that the initial GOR was quite variable for the first reported

production from different wells. As the data indicate, no gas production was recorded for the field during the first six months of production. No pipeline was available during this time and gas was just vented to the atmosphere. Therefore the first GORs recorded in the field are likely higher than the initial solution GOR value. Therefore backward GOR projections were used to estimate an initial field GOR of 450 SCF/STB. This corresponds to a bubble point pressure of 1600 psia. Initial reservoir pressure was estimated as 1900 psia based on a normal pressure versus depth profile and comparison to initial pressures in fields of similar depth.

This example illustrates a logical and practical approach to estimating the information needed to input to the PVT program considering the typical set of data available to the engineer. Normally the initial GOR must be estimated from produced GORs some time after initial production, the initial reservoir pressure must be estimated from knowledge of the pressure versus depth profile for an area, and the gas gravity must be approximated from knowledge of the gas composition. Once these estimates are computed the engineer can use the algorithm of Appendix B to compute the PVT properties needed for simulation experiments.

### GOR ANALYSIS FOR PVT PROPERTIES

**CUMMULATIVE OIL PRODUCTION AND GOR DATA**  
**Shaded region indicates backward projection of data  
 using regression techniques**

Production tabulation of the first wells in the field  
 Pipeline installed in December 1983 gas flared until that time

| PROD<br>DATE | Aigner     |       | Warren Wells |       | Warren     |      | Warren     |      | Chenoweth  |       |
|--------------|------------|-------|--------------|-------|------------|------|------------|------|------------|-------|
|              | CUM<br>OIL | GOR   | CUM<br>OIL   | GOR   | CUM<br>OIL | GOR  | CUM<br>OIL | GOR  | CUM<br>OIL | GOR   |
| Jun-83       |            |       | 358          | 457.5 |            |      |            |      |            |       |
| Jul-83       |            |       | 716          | 468.2 |            |      |            |      |            |       |
| Aug-83       |            |       | 1413         | 489   |            |      |            |      |            |       |
| Sep-83       |            |       | 2489         | 521.1 |            |      |            |      |            |       |
| Oct-83       |            |       | 3389         | 547.9 |            |      |            |      |            |       |
| Nov-83       |            |       | 4642         | 585.3 |            |      |            |      |            |       |
| Dec-83       | 6263       | 341.4 | 6995         | 655.5 | 2973       |      | 874        |      |            |       |
| Jan-84       | 15585      | 445.8 | 9159         | 720   | 5224       |      | 6678       |      |            |       |
| Feb-84       | 17854      | 471.2 | 9981         | 744.6 | 5896       |      | 8760       |      | 2004       | 160.5 |
| Mar-84       | 21403      | 492   | 16298        | 933   | 7681       | 2521 | 13174      | 3690 | 4194       | 349.3 |
| Apr-84       | 25536      | 590   | 20796        | 852   | 8678       | 1805 | 20027      | 2817 | 5814       | 489   |
| May-84       | 30131      | 615   | 27662        | 1272  | 10843      | 2065 | 29690      | 2634 | 8157       | 691   |
| Jun-84       | 34393      | 637   | 31806        | 1835  | 12591      | 3694 | 37380      | 2711 | 10540      | 817   |
| Jul-84       | 39085      | 690   | 36020        | 2026  | 14335      | 3645 | 46610      | 2163 | 12788      | 760   |
| Aug-84       | 43280      | 774   | 39087        | 2863  | 15601      | 4669 | 60177      | 2674 | 14863      | 1182  |
| Sep-84       | 48148      | 754   | 41434        | 2851  | 16858      | 4423 | 70147      | 3342 | 16571      | 1105  |
| Oct-84       | 53199      | 989   | 43621        | 3236  | 17920      | 5186 | 78598      | 3629 | 18218      | 1630  |
| Nov-84       | 59625      | 1219  | 45264        | 4013  | 18797      | 5827 | 85118      | 4025 | 19738      | 1543  |
| Dec-84       | 64048      | 1301  | 46516        | 4513  | 18797      |      | 91235      | 3899 | 20862      | 2395  |
| Jan-85       |            |       |              |       |            |      |            |      |            |       |

**Table C-1 GOR Analysis for PVT Estimation**

Based on the estimated initial solution GOR, oil gravity, gas gravity and formation temperature, PVT properties were calculated using computer program OILPROP that uses the relations from Craft and Hawkins.<sup>6</sup> (see attached OILPROP program listing in Appendix

B) Table 2 shows the output from this program for the example. These relations are graphed on Figure 1. Data computed by this method serve as reasonable estimates of the formation PVT properties to use in reservoir simulation.

| PVT DATA         |        |                  |         |         |         |                  |
|------------------|--------|------------------|---------|---------|---------|------------------|
| PRESSURE<br>psia | Z      | GAS<br>VISCOSITY | Bg      | Bo      | RSO     | OIL<br>VISCOSITY |
|                  |        | cp               | bbl/scf | bbl/stb | mcf/stb | cp               |
| 2000             | 0.0000 | 0.0000           | 0.0000  | 1.2216  | 0.4430  | 0.8005           |
| 1868             | 0.0000 | 0.0000           | 0.0000  | 1.2228  | 0.4430  | 0.7886           |
| 1735             | 0.0000 | 0.0000           | 0.0000  | 1.2242  | 0.4430  | 0.7775           |
| 1602             | 0.0000 | 0.0000           | 0.0000  | 1.2258  | 0.4430  | 0.7673           |
| 1470             | 0.7814 | 0.0151           | 0.0015  | 1.2227  | 0.4337  | 0.7691           |
| 1338             | 0.7955 | 0.0145           | 0.0017  | 1.1994  | 0.3871  | 0.8200           |
| 1205             | 0.8115 | 0.0140           | 0.0020  | 1.1769  | 0.3415  | 0.8789           |
| 1073             | 0.8291 | 0.0135           | 0.0022  | 1.1552  | 0.2969  | 0.9480           |
| 941              | 0.8480 | 0.0130           | 0.0026  | 1.1345  | 0.2534  | 1.0299           |
| 809              | 0.8680 | 0.0127           | 0.0031  | 1.1147  | 0.2111  | 1.1286           |
| 676              | 0.8887 | 0.0123           | 0.0038  | 1.0959  | 0.1703  | 1.2495           |
| 544              | 0.9100 | 0.0120           | 0.0049  | 1.0783  | 0.1310  | 1.4004           |
| 412              | 0.9316 | 0.0117           | 0.0066  | 1.0619  | 0.0937  | 1.5928           |
| 279              | 0.9535 | 0.0115           | 0.0099  | 1.047   | 0.0587  | 1.8428           |
| 147              | 0.9755 | 0.0114           | 0.0193  | 1.0339  | 0.0271  | 2.1686           |
| 14.7             | 0.9976 | 0.0112           | 0.1970  | 1.0236  | 0.0017  | 2.5529           |

Table C-2 Program OILPROP Output

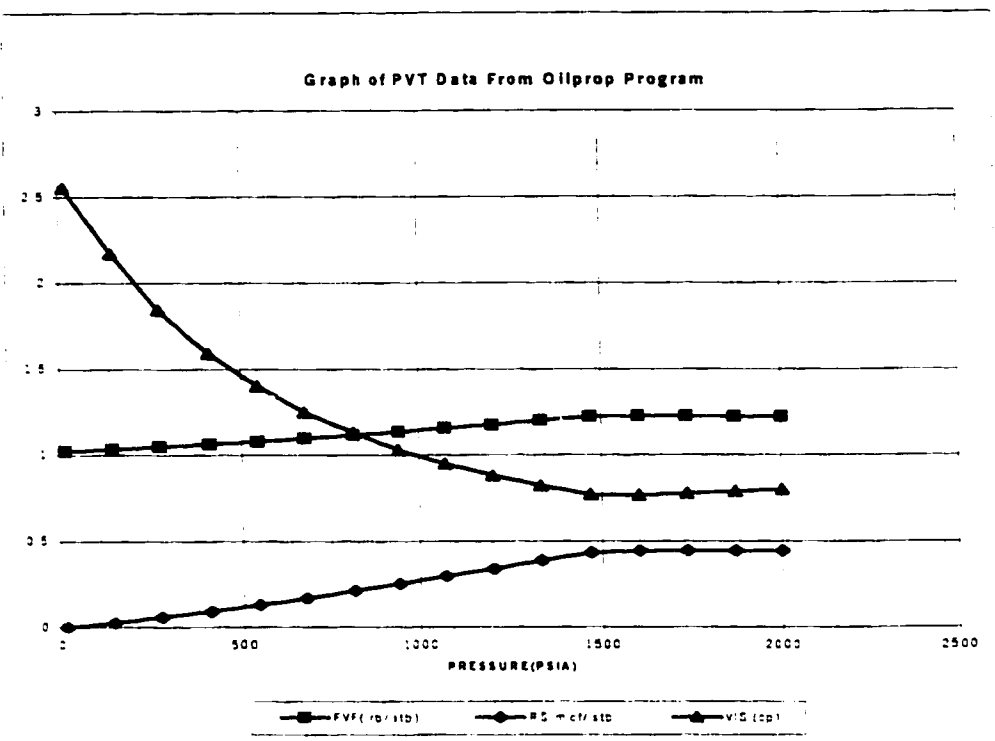


Figure C-1 Graph of PVT Data From Oilprop Program

### C.2.2 Oil-Water Relative Permeability Data

Relative permeability data can be generated empirically by using relationships that follow the general form as follows: A first estimate utilizes the following equations for water wet reservoirs from Willhite<sup>1</sup>

$$K_{rw} = (1-SwD)^x \quad C1$$

$$K_{ro} = C SwD^y \quad C2$$

$$SwD = \frac{S_w - S_{rw}}{1 - S_{or} - S_{rw}} \quad C3$$

$S_{iw}$  = irreducible water saturation

$S_{or}$  = residual oil saturation

$K_{ro}$  = oil relative permeability

$K_{rw}$  = water relative permeability

where C is generally in the range of 0.78, x between 2 and 3 and y between 3 and 4.

The first task is then to derive estimates for the residual oil saturation  $S_{or}$  and irreducible water saturation in the particular geologic formation in question. In the example shown here,  $S_{or}$  was based on the core analysis (Table 3A).  $S_{or}$  was assumed to be the geometric mean of  $1-S_w$  in the core. This is reasonable since presumably the core has been flushed by filtrate water during drilling thus reducing the zone to  $S_{or}$ .  $S_{iw}$  was taken as the lowest water saturation found in the field from log analysis.

The next step is to modify the exponents in the equation by trial and error until the curves that are generated explain the field phenomenon that is observed. The first try using the exponents of  $x=2.56$  and  $y=3.72$  with  $C=0.78$  did not explain the example field production (see Table 5C and Figure 2C). Field experience suggested that water was not produced until reaching 48-50% water saturation levels. The Willhite<sup>13</sup> relationships indicated that water flow would equal oil flow at 41% water saturation. This was not reasonable based on field experience. This points out the danger of using relations without verifying them with actual field experience and

shows the way to use field production data and well log calculations to calibrate generalized relationships.

#### EXAMPLE CORE ANALYSIS

| SAMPLE | DEPTH | POROSITY | PERM TO AIR(md) |       | WATER | GRAIN   | predict  |
|--------|-------|----------|-----------------|-------|-------|---------|----------|
|        |       | %        | HORIZ.          | VERT  | SAT   | DENSITY |          |
| 1      | 4655  | 2.40     | 0.11            | 0.01  | 81.50 | 2.76    | 0.224558 |
| 2      | 4656  | 7.10     | 0.16            | 0.11  | 72.80 | 2.65    | 3.480689 |
| 3      | 4657  | 10.10    | 0.16            | 0.57  | 67.00 | 2.65    | 8.481165 |
| 4      | 4658  | 10.80    | 8.30            | 14.00 | 52.80 | 2.65    | 10.04609 |
| 5      | 4659  | 9.30     | 10.00           | 10.00 | 41.80 | 2.66    | 6.884807 |
| 6      | 4660  | 10.30    | 14.00           | 14.00 | 48.10 | 2.67    | 8.911997 |
| 7      | 4661  | 12.20    | 9.90            | 4.70  | 57.80 | 2.66    | 13.66994 |
| 8      | 4662  | 11.70    | 13.00           | 4.10  | 46.60 | 2.66    | 12.29819 |
| 9      | 4663  | 13.30    | 51.00           | 39.00 | 45.90 | 2.66    | 17.00233 |
| 10     | 4664  | 7.30     | 9.20            | 6.20  | 44.90 | 2.70    | 3.73381  |
| 11     | 4665  | 4.00     | 0.27            | 0.34  | 57.10 | 2.73    | 0.816471 |
| 12     | 4666  | 5.60     | 7.20            | 0.02  | 62.50 | 2.65    | 1.910762 |
| 13     | 4667  | 5.60     | 0.10            | 1.78  | 76.60 | 3.06    | 1.910762 |

**Table C-3 Example Core Analysis**

#### RELATIVE PERMEABILITY ESTIMATES FROM WILLHITE GENERAL FORM

SWIRR= 0.2  
 SOR= 0.39

| SW    | SWD   | KO    | KW    |
|-------|-------|-------|-------|
| 0.200 | 0.000 | 0.910 | 0.000 |
| 0.210 | 0.024 | 0.875 | 0.000 |
| 0.260 | 0.146 | 0.706 | 0.000 |
| 0.300 | 0.244 | 0.582 | 0.000 |
| 0.350 | 0.366 | 0.439 | 0.001 |
| 0.400 | 0.488 | 0.312 | 0.006 |
| 0.450 | 0.610 | 0.202 | 0.026 |
| 0.500 | 0.732 | 0.111 | 0.085 |
| 0.550 | 0.854 | 0.042 | 0.232 |
| 0.583 | 0.934 | 0.012 | 0.417 |
| 0.584 | 0.937 | 0.011 | 0.425 |

**Table C-4 Relative Permeability Estimates from Willhite General Form**

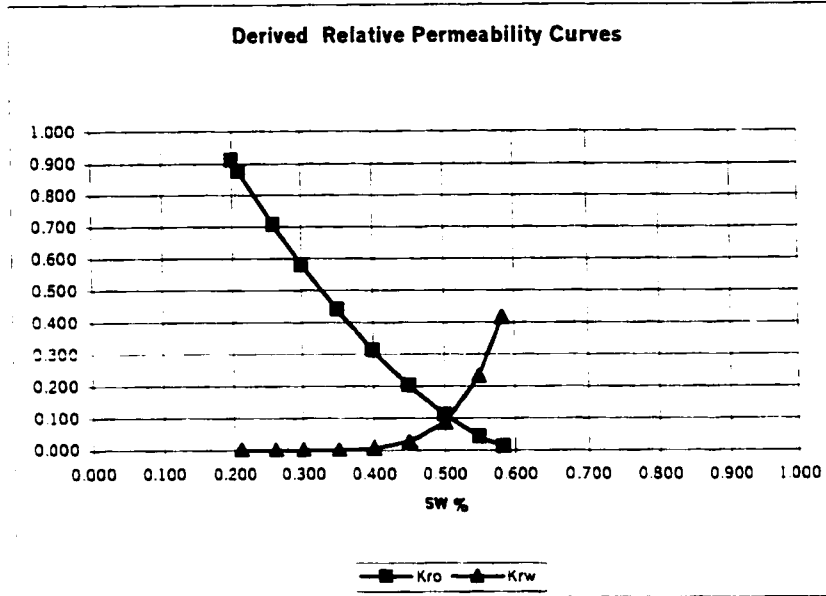


**Figure C-2 Derived Relative Permeability Curves**

Based on the water saturation calculations from log analysis and a comparison of those values with production data (Table C-5) it was apparent that the relative permeability data needed to be adjusted from that predicted by the initial equations. Based on the core analysis, the residual oil saturation of 39% (61% SW) was again chosen as one endpoint. The other endpoint was chosen as 80% oil saturation based on the highest log calculated oil saturation in the field. However, details of the curves were adjusted between endpoints by changing the constants and exponents in the equations to reflect the production actually found in the field. For instance, production and log analysis indicated that water was almost immobile up to 48% water saturation and then rose rapidly with increasing water saturation. Changing the constants and exponents on the generalized relative permeability relations resulted in the relative permeability curve shown in Figure 3A. This curve explained observed production in the field with the few exceptions and honored the petrophysical data.

**RATIO OF PRODUCED FLUID FLOWS**

| WELL NAME      | AVE.<br>PERM(md) | AVE.<br>Sw(%) | INITIAL     |               |             | RATIO OF FLUIDS |         |
|----------------|------------------|---------------|-------------|---------------|-------------|-----------------|---------|
|                |                  |               | OIL<br>BOPD | WATER<br>BWPD | GAS<br>MCFD | OIL/WTR         | OIL/GAS |
| Aigner 1-25    | 21.07            | 22.98         | 832         |               | 950         |                 | 0.88    |
| Warren 3C-24   | 18.71            | 25.14         | 210         |               | 300         |                 | 0.70    |
| Warren 3A-24   | 20.79            | 26.13         | 216         |               | 700         |                 | 0.31    |
| Aigner 4-25    | 11.99            | 26.78         | 144         |               | 210         |                 | 0.69    |
| Habben 1-30    | 11.02            | 31.00         | 330         |               |             |                 |         |
| Warren 6-30    | 10.99            | 33.70         | 181         | 0             | 500         |                 | 0.36    |
| Warren 1B-25   | 11.35            | 40.48         | 231         | 25            | 493         | 9.24            | 0.47    |
| Warren 4C-24   | 15.40            | 41.10         | 223         |               | 200         |                 | 1.12    |
| COP 1-23       | 9.80             | 42.00         | 19          | 8             |             | 2.38            |         |
| Habben 2-30    | 7.62             | 42.44         | 141         | 53            |             | 2.66            |         |
| Warren 4A-24   | 7.74             | 43.50         | 130         |               | 100         |                 | 1.30    |
| Bridal 1-26    | 9.90             | 43.90         | 20          | 20            | 35          | 1.00            | 0.57    |
| Warren 4-24    | 10.90            | 46.70         | 205         |               | 175         |                 | 1.17    |
| Spudds 2-24    | 3.56             | 46.70         |             |               |             |                 |         |
| Aigner 5-25    | 8.80             | 47.90         | 300         | 5             | 120         | 60.00           | 2.50    |
| Spudds 1-24    | 6.33             | 48.00         |             |               |             |                 |         |
| Luster 2-30    | 5.65             | 48.62         | 12          | 35            |             | 0.34            |         |
| Grace 1-A-25   | 9.10             | 49.21         | 241         |               | 100         |                 | 2.41    |
| Aigner 3-25    | 11.67            | 49.30         | 180         | 15            | 90          | 12.00           | 2.00    |
| Habben 4-30    | 4.28             | 49.50         | 94          | 40            | 98          | 2.35            | 0.96    |
| Chenoweth 1-23 | 13.24            | 49.88         | 130         | 30            | 100         | 4.33            | 1.30    |
| Heppler 1-23   | 7.99             | 50.11         | 36          | 2             |             | 18.00           |         |
| Habben 3-30    | 6.67             | 51.20         |             |               |             |                 |         |
| Warren 1-25    | 4.95             | 51.60         | 47          | 20            | 175         | 2.35            | 0.27    |
| Warren 1C-24   | 13.61            | 53.10         | 300         | 0             | 200         |                 | 1.50    |
| Forney 1-23    | 5.41             | 54.52         | 20          | 20            | 30          | 1.00            | 0.67    |
| Warren 6A-30   | 4.06             | 58.14         | 130         |               | 100         |                 | 1.30    |
| Ruth 1-23      | 10.38            | 58.17         |             |               |             |                 |         |
| Ruth 2-23      | 20.79            | 59.00         | 0           |               |             |                 |         |
| Spudds 3-24    | 7.90             | 62.91         |             |               |             |                 |         |
| Warren 5A-25   | 0.00             | 66.30         |             |               |             |                 |         |
| Reba 1-26      | 10.46            | 66.87         | 40          |               | 50          |                 | 0.80    |
| Luster 1-30    | 4.66             | 71.00         | 6           | 20            | 20          | 0.30            | 0.30    |
| Warren 1A-25   | 5.32             | 71.70         | 150         | 0             | 200         |                 | 0.75    |
| Warren 2-26    | 5.50             | 71.80         | 42          | 30            | 190         | 1.40            | 0.22    |
| Chenoweth 2-23 | 5.92             | 75.70         | 135         | 20            | 110         | 6.75            | 1.23    |
| Endres 1-26    | 6.92             | 77.00         | 42          | 2             |             | 21.00           |         |
| Chenoweth 3-23 | 3.90             | 85.41         | 33          | 10            | 80          | 3.30            | 0.41    |
| Warren 2A-26   | 5.25             | 87.13         | 60          | 10            | 42          | 6.00            | 1.43    |

**Table C-5 Ratio Of Produced Fluid Flows**

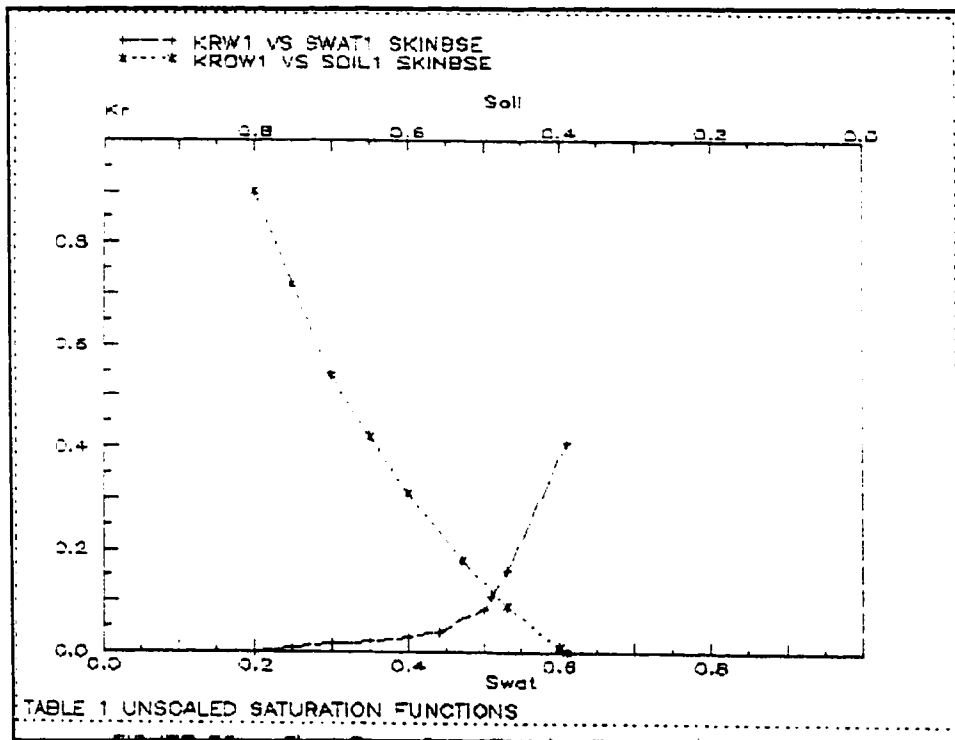


**Figure C-3 Final Relative Permeability Curve**

Often a fracture system is also present which requires a separate relative permeability curve. In this example because oil was produced from some wells at up to 75% water saturation even though the core data indicated that oil flow should cease at 61% water saturation. This results from the fracture system. In the fractures, both oil and water flow at higher relative saturation than in the matrix. To account for this, a separate linear relative permeability curve was used for the fractures that allowed oil to flow at higher water saturation than in the matrix. Conversely, water flowed at higher oil saturation. This is a reasonable explanation for the oil flow in wells with high water saturation.

### C 2.2.3 Using Producing Gas Oil Ratio to Determine Relative Permeability to Oil-Gas Curves

The producing gas-oil ratio is known to be a function of reservoir pressure and reservoir saturation. If one assumes that the pressure gradient is the same through both the gas and the oil phase, a radial flow system with incremental thickness dr, reservoir pressure P and pressure gradient dp/dr in psi/ft, a total of  $q_o$  reservoir barrels per day flowing past the radius r and  $q_g$  barrels of reservoir gas per day flowing past the radius r then applying Darcy's law the following expressions can be written for the velocity of oil and gas (v) respectively<sup>14</sup>:

$$v_o = \frac{q_o}{2\pi h} = \frac{-7.07 k_o dp}{2\pi \mu_o dr} \quad C4$$

$$v_g = \frac{q_g}{2\pi h} = \frac{-7.07 k_g dp}{2\pi \mu_g dr} \quad C5$$

The stock tank oil produced per day  $Q_o$  is of course  $q_o/B$  where B is the formation volume factor. The standard cubic feet of gas produced per day  $Q_g$  will be equal to the rate of movement of the reservoir gas converted to surface conditions plus the gas which is evolved from the oil produced, or:

$$Q_g = \frac{q_g}{v} + r Q_o \quad C6$$

where  $r$  is the gas in solution at the current pressure expressed as SCF/STB.

The producing gas-oil ratio is by definition however, the quotient  $Q_g/Q_o$  so by dividing the above equation through by  $Q_o = q_o/B$  and substituting into the oil and gas velocity relationships yields the following useful relationship:

$$R = \frac{q_g B}{q_o v} + r = \frac{k_g \mu_o B}{k_o \mu_g v} + r \quad C7$$

The quantities in this equation are only valid at the pressure and temperature existing at radius  $r$ .<sup>14</sup> Since these quantities are really not measurable and only an average pressure is measurable by shutting in the well other assumptions are necessary. If the value of  $\Delta P$  across the system approaches zero as a limit then one value of  $P$ , the average pressure would suffice to define the system. Therefore the assumption means that the production is occurring at zero pressure differential. This is often a reasonable approximation in practice.

In summary the assumptions are that 1) the pressure draw-down is zero, 2) the gas and oil are uniformly distributed 3) the gas and oil are flowing according to equilibrium relative permeability, and 4) the pressure gradients in the gas are the same as those in the oil phase.

The above-derived equation can be re-written as:

$$\frac{k_g}{k_o} = (R - r) \frac{\mu_g v}{\mu_o B}$$

C8

From material balance considerations the average oil saturation  $S_o$  can be expressed as:

$$S_o = \frac{(N - \Delta N)B}{Pore Volume} = \frac{(N - \Delta N)B}{NB_o / (1 - S_w)} = \left(1 - \frac{\Delta N}{N}\right) \frac{B}{B_o} (1 - S_w) \quad C9$$

These last two expressions involve only the average pressure at any given time, the cumulative production, and the producing gas-oil ratio at a given time. The water saturation is assumed constant. Calculations of  $k_g/k_o$  and  $S_o$  made at a number of times in the reservoir's history can be plotted to give the expected relationship. This is normally done on semi-log scale<sup>14</sup>. The following example provides an illustration of how the method works. The field data are tabulated in Table C-6. Using the average pressure, produced gas, production and formation volume factor a gas to oil relative permeability curve can be constructed as shown in figure C-4.

**Table C-6 Gas-Oil Relative Permeability Data and Construction**

N= 1.17E+08

| Average Pressure | R    | delta N  | data/N     | B     | V        | r   | m <u>o</u> /m <u>g</u> | S <sub>o</sub> | kg/ko   |
|------------------|------|----------|------------|-------|----------|-----|------------------------|----------------|---------|
| 3448             | 850  | 4.76E+05 | 0.00408584 | 1.443 | 0.00084  | 752 | 30.4                   | 0.71           | 0.00187 |
| 3303             | 920  | 1.74E+06 | 0.01498137 | 1.432 | 0.000875 | 725 | 32.1                   | 0.696          | 0.00321 |
| 3153             | 990  | 2.82E+06 | 0.02418884 | 1.42  | 0.00091  | 695 | 34                     | 0.684          | 0.00556 |
| 2938             | 1020 | 4.65E+06 | 0.03993133 | 1.403 | 0.00097  | 657 | 36.8                   | 0.664          | 0.00682 |
| 2813             | 1000 | 6.03E+06 | 0.05175966 | 1.393 | 0.00101  | 632 | 38.4                   | 0.652          | 0.00894 |
| 2678             | 1180 | 7.36E+06 | 0.06317597 | 1.382 | 0.001062 | 608 | 40.5                   | 0.638          | 0.01085 |
| 2533             | 1420 | 8.75E+06 | 0.07511588 | 1.371 | 0.00122  | 580 | 42.4                   | 0.625          | 0.0162  |
| 2453             | 1510 | 9.87E+06 | 0.08474678 | 1.364 | 0.001162 | 565 | 43.6                   | 0.615          | 0.01848 |
| 2318             | 1660 | 1.13E+07 | 0.09664378 | 1.354 | 0.00123  | 540 | 45.5                   | 0.609          | 0.0224  |
| 2153             | 1920 | 1.26E+07 | 0.1083176  | 1.34  | 0.00133  | 509 | 48                     | 0.589          | 0.0292  |
| 1978             | 2220 | 1.40E+07 | 0.12015451 | 1.326 | 0.001453 | 476 | 50.8                   | 0.575          | 0.0377  |
| 1818             | 2480 | 1.53E+07 | 0.13151073 | 1.313 | 0.00159  | 446 | 53.8                   | 0.563          | 0.0456  |
| 1658             | 2710 | 1.66E+07 | 0.14207725 | 1.301 | 0.001758 | 416 | 57.4                   | 0.55           | 0.054   |
| 1625             | 2800 | 1.69E+07 | 0.1453133  | 1.298 | 0.001795 | 410 | 58.2                   | 0.546          | 0.0567  |

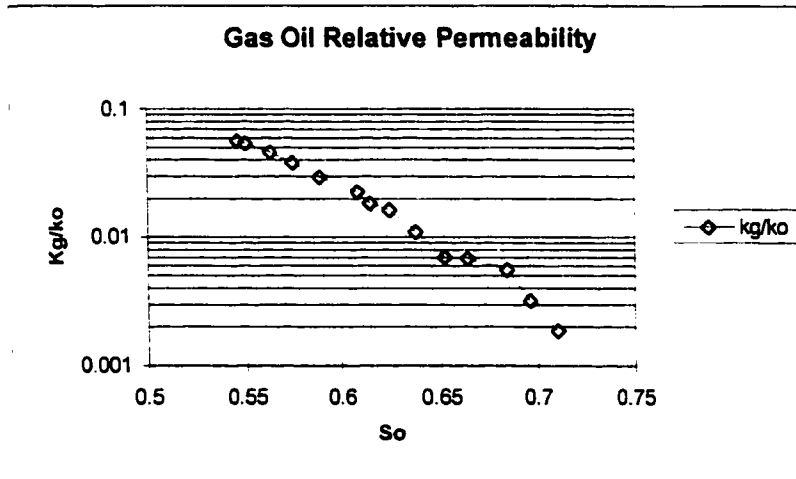


**Figure C-4 Gas Oil Relative Permeability**

#### C 2.2.4 Use of Decline Curves in Determining Contributions of Solution

##### Gas Energy and Estimating Mobility Functions

The rate decline path will be exponential where  $b=0$  and the Fetkovich radial solutions and Arps empirical solutions converge when the only reservoir energy is the compressibility of the rock and fluid. (See chapter 5 for my more general solutions) In a solution gas reservoir where water drive is absent the decline path will be more hyperbolic where  $b$  values of 0 to 0.5 exist. This deviation from  $b=0$  should give information that can be used in determining

**Figure 5.10 Composite Fetkovich Type Curve Transient and Exponential Depletion**

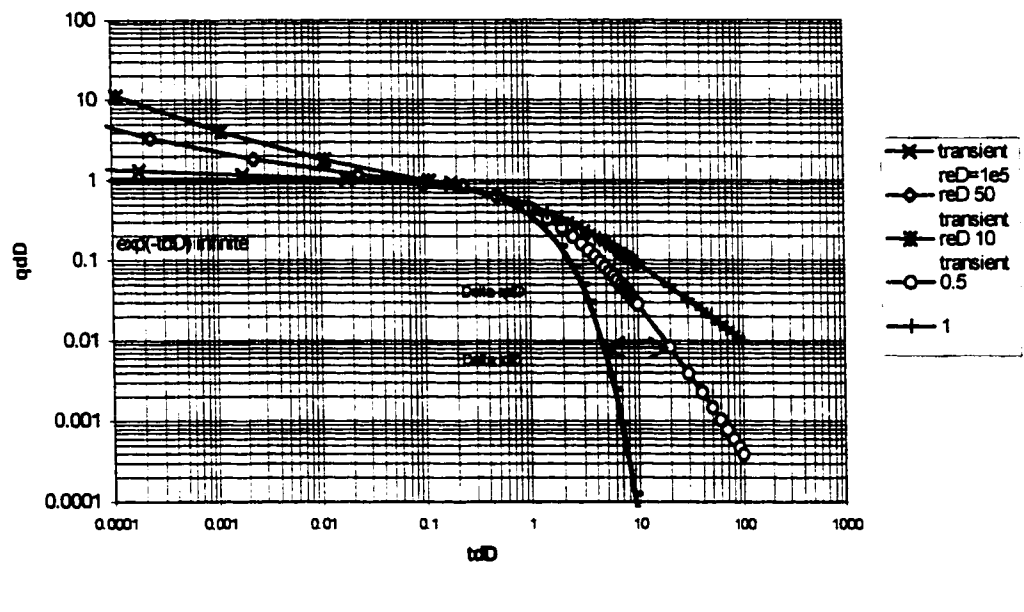


**Figure 5.10 Composite Fetkovich Type Curve Transient and Exponential Depletion**

the mobility-pressure function that was described in chapter 3 and the appendix A. This concept can be shown in reproduced figure 5.10 where  $\Delta q_{Dd}$  and  $\Delta t_{Dd}$  represent the deviation from the actual path and that predicted exponential path with no energy in the system other than the fluid and rock compressibility. The solution gas provides additional pressure support that more than offsets the increased resistance from the reduction in  $k_{ro}/(\mu_o B_o)$  with a reduction in pressure and oil saturation. Also with a purely exponential decline with no additional drive energy, the IPR will be constant with declining pressure. Field experience indicates that the IPR does change with depletion since exponential depletion is rare. Once the decline path is known from the above chart the difference between the decline path and the predicted exponential path should give information about the pressure mobility function and adjustments to IPR over time without the need for well testing techniques.

$$\int \frac{k_{ro}}{\mu_o B_o} dp \cong \frac{(P_R - P_{wf}) k_{ro}}{(\mu_o B_o)_{P_{wf}}} \quad C10$$

### Determination of Relative Permeability from Rate-Time Decline Data

In order to determine the ratio of  $k_g/k_o$ ,  $k_{ro}$ ,  $k_{rg}$  from rate-time data one needs to know the original oil in place, the current oil saturation and the productivity factor. The analysis (after Fetkovich work) uses the concept that once a well and its offsets have reached pseudo-steady state flow, a no-flow boundary will result at a distance between all wells. The distance to the

boundary of no-flow will depend on the flow rate of each offset well. Thus drainage volume of each well should remain constant if all wells are on decline and continue producing wide open against a common backpressure. If one assumes decline below the bubble point is proportional to:

$$\frac{(\bar{P}_R - P_{wf})}{\mu_o B_o} \quad C11$$

then the Pore Volume  $V_p$  can be determined from the expression:

$$V_p = \frac{5.615 \mu_o B_o}{(\mu c_t)_{\bar{P}_R} (\bar{P}_R - P_{wf}) t_{dD}} \frac{q(t)}{q_{Dd}} \quad C12$$

and the reserves in place are computed from:

$$N = \frac{V_p (1 - S_{wi})}{B_{oi}} \quad C13$$

The productivity factor is obtained from:<sup>38</sup>

$$PF = \frac{7.08 kh}{\ln \frac{r_e}{r_w} - \frac{1}{2}} = \frac{\mu_o B_o}{\bar{P} - P_{wf}} \frac{q(t)}{q_{Dd}} \quad C14$$

The relative permeability is then estimated from:

$$k_{ro} = \frac{q_o(\mu_o B_o)}{PF(\bar{P} - P_{wf})}$$

C15

A more rigorous approach uses the m(p) relationship from Fetkovich's isochronal testing of wells paper.<sup>38</sup> Pore volume is thus expressed as:

$$V_p = \frac{5.615 \left[ \frac{q(t)}{q_{Dd}} \frac{t}{t_{Dd}} \right]}{(\mu_o c_t)_{\bar{P}_R} \left[ \frac{\bar{P}_R - P_B}{(\mu_o B_o)_{\bar{P}_R P_b}} + \frac{P_b^2 - P_{wf}^2}{2P_b(\mu_o B_o)_{P_b}} \right]}$$

C16

And N is calculated in the same way using the above equation.

The productivity factor PF is then estimated by:

$$PF = \frac{7.08kh}{\ln \frac{r_e}{r_w}} = \frac{\frac{q(t)}{q_{Dd}}}{\left[ \frac{\bar{P}_R - P_B}{(\mu_o B_o)_{\bar{P}_R P_b}} + \frac{P_b^2 - P_{wf}^2}{2P_b(\mu_o B_o)_{P_b}} \right]}$$

C17

The relative permeability to oil is then computed below the bubble point by:

$$k_{ro} = \frac{2\bar{P}_R(\mu_o B_o)_{\bar{P}_R} q_o}{PF(P_R^2 - P_{wf}^2)}$$

C18

For each production period examined the new value of  $k_{ro}$  is calculated and the relative permeability relation is computed and plotted as a function of saturation.

### C 2.2.5 Use in Adjusting the IPR Curve with Depletion

It is well established that the inflow performance curve changes with decreasing reservoir pressure.

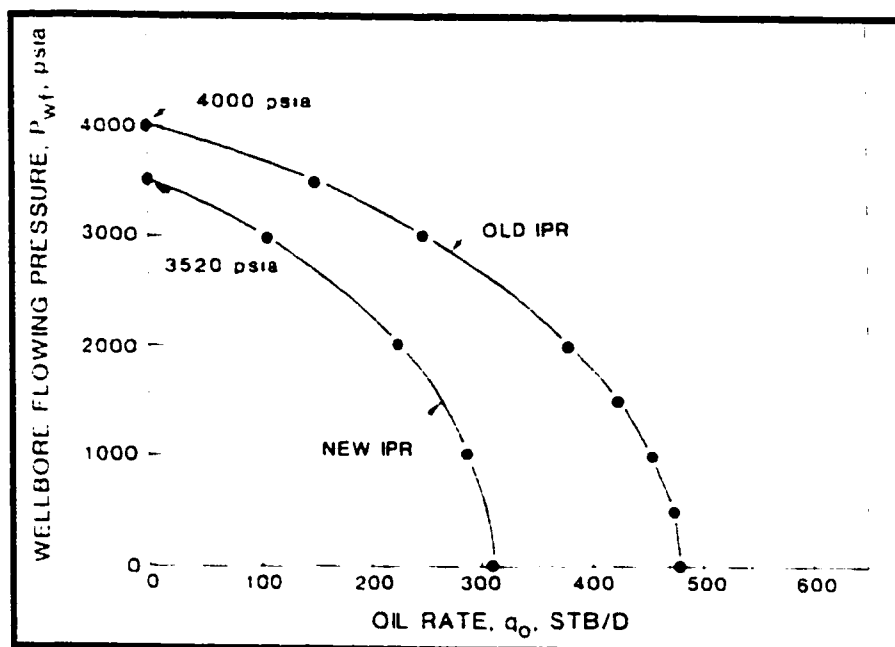


Figure C-5<sup>4</sup> Change in IPR with Depletion

In Appendix A it was shown that the IPR relations can be expressed as:

$$q_o = \frac{kh}{141.2\mu_o B_o} \frac{1}{2P_R} (P_R^2 - P_{wf}^2) k_{PR} \frac{1}{\ln \frac{r_e}{r_w} - \frac{3}{4}} \quad \text{C18}$$

OR:

$$q_o = C(P_R^2 - P_{wf}^2) \quad \text{C19}$$

$$q_o = C(P_R^2 - P_{wf}^2)$$

C19

Where:

$$C = \frac{kh}{141.2\mu_o B_o} \frac{1}{2P_R} k_{PR} \frac{1}{\ln \frac{r_e}{r_w} - \frac{3}{4}} \quad \text{C20}$$

As the reservoir pressure drops the resistance to oil flow increases since the ratio of  $\frac{k_{ro}}{\mu_o B_o}$

decreases as the average pressure decreases. Therefore the change in IPR with declining pressure should be related to the change in  $\frac{k_{ro}}{\mu_o B_o}$  that can be predicted from either the decline path method or the empirical method from field data presented earlier. Thus the IPR relation at any particular reservoir pressure should be expressed as:

$$q_o = C'(P_R^2 - P_{wf}^2) \quad \text{C21}$$

where:

$$q_o = q_{o \max} \left( \frac{\frac{k_{ro}}{\mu_o B_o} new}{\frac{k_{ro}}{\mu_o B_o} old} \right) \left( \frac{P_R new}{P_R old} \right) \left( 1 - \frac{P_{wf}}{P_R} \right)^n \quad \text{C22}$$

And if the IPRs are known then the inverse can be applied to determine the change in mobility function over time using the above relationship. Mattax and Dalton <sup>15</sup> presented a similar form previously developed by Whitson and Golan for above the bubble point conditions in which:

$$J_F = \frac{\left( \frac{k_{ro}}{\mu_o B_o} \right)_F}{\left( \frac{k_{ro}}{\mu_o B_o} \right)_P} J_P \quad C23$$

Thus the relationship can be used to determine the productivity at any future date ( $J_F$ ) if the mobility functions are known. Conversely it should be possible to infer the mobility functions if the performance functions are known. Mattax and Dalton indicate that the relationship can be used with small error below the bubble point also.

### C 2.2.5 Capillary Pressure Estimation

Capillary pressure can be thought of as a force per unit area resulting from the interaction of surface forces and the geometry of the medium in which they exist<sup>16</sup>. The effect of the capillary pressure relationship is to distribute the saturation properly over the depth of the reservoir. Although capillary pressure is not used in the analytical equations presented in this research, it is often needed in the numerical simulations. The following presents my method of determining capillary pressure without core experiments. The capillary pressure can be estimated from reservoir data alone by calculating the length of the oil to water transition zone and knowing the oil-water density contrast. The density is determined from an oil and water sample while the height of the oil column and transition zone is determined from production data and well log water saturation calculations. A transition zone of approximately 80 feet occurs in this example reservoir. The structurally highest well in the field occurs at a subsea depth of about

3510 feet. Based on log analysis, the water saturation gradually increases from a low of about 20% at the structurally highest part of the field to nearly 100% over about an 80-foot transition zone. The exact oil-water contact is unknown but is estimated to be 3590 feet subsea.

Capillary pressure is determined from the relationship  $P_c = (\rho_w - \rho_o)gh = \frac{2\sigma \cos\theta}{R}$ .

Based on oil and water density differences, the 80 foot transition zone of the example and the equations for capillary pressure, a preliminary curve can be developed to distribute the saturations across the transition zone as calculated from log analysis. It is a good idea to draw a map projection of the average water saturations within the field and to overlay this map on the structure map to make sure the two functions roughly agree. Table C-7 shows the results of the calculation. Figure C-6 shows the field average water saturation change with depth. Figure C-7 shows the capillary pressure curve calculated from the length of the transition zone and the oil and water density differences. Slight modifications to this capillary pressure data may be necessary to obtain an initial water saturation distribution that match the water saturation map generated from log analysis.

### **CAPILLARY PRESSURE DATA**

Pc=DELTA DENSITY\*g\*h= 2\*sigma\*cos/R  
OIL DENSITY = 50.33 #/cubic ft.  
WATER DENSITY= 71.76 #/cubic ft.  
TRANSITION ZONE= 80 FT.

| WATER<br>SAT. % | SUBSEA<br>DEPTH | Pc<br>psi |
|-----------------|-----------------|-----------|
| 20              | 3510            | 11.91     |
| 25              | 3520            | 10.42     |
| 30              | 3530            | 8.93      |
| 35              | 3540            | 7.44      |
| 40              | 3550            | 5.95      |
| 47              | 3560            | 4.46      |
| 53              | 3565            | 3.72      |
| 60              | 3570            | 2.98      |
| 75              | 3580            | 1.49      |
| 100             | 3590            | 0.00      |

**Table C-7 Capillary Pressure Calculation Data**

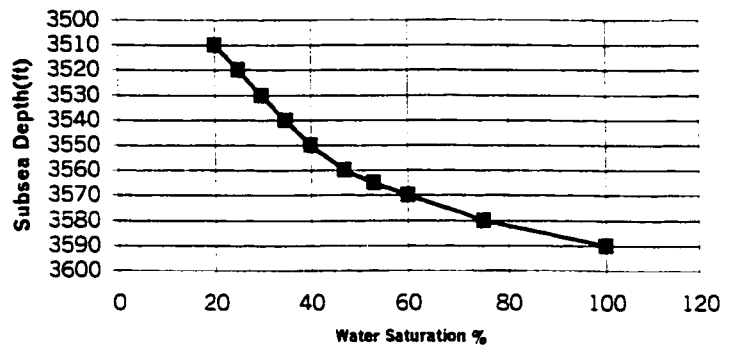


**Figure C-6 Saturation v. Depth Profile**

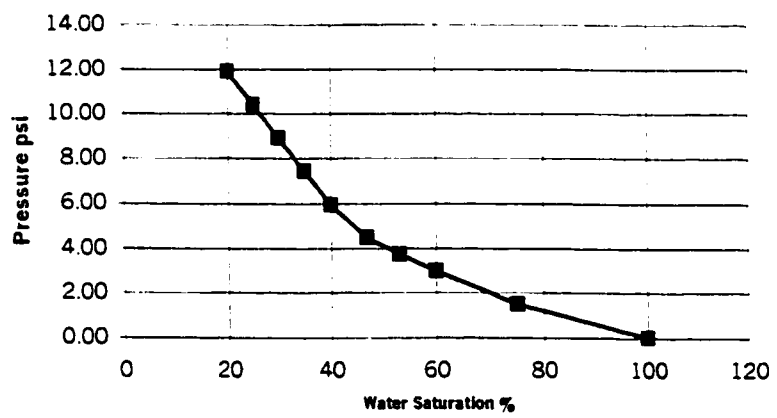


**Figure C-7 Capillary Pressure Profile**

**APPENDIX D**

**Tabular Generalized Type Curve Solutions**

**Table D-1 Tabular Data for Fetkovich Decline Type Curves Figures 5.1 – 5.4**

Infinite values from program, finite depletion values closed system from table c-5 Lee welltesting book ref 20

Radial Cases

| fetkovich constants |         |         |         | Depletion Portion |         |       |         |         |         |        |         |        |         |
|---------------------|---------|---------|---------|-------------------|---------|-------|---------|---------|---------|--------|---------|--------|---------|
|                     | c1      | 2.49573 |         | c1                | 3.41202 |       | c1      | 4.10517 |         |        |         |        |         |
|                     | c2      | 199.5   |         | c2                | 1249.5  |       | c2      | 4999.5  |         |        |         |        |         |
| infinite            | reD=20  | 20      |         | reD =50           | 50      |       | reD=100 | 100     |         |        |         |        |         |
| ID                  | qD      | ID      | tdID    | qD                | qdD     | ID    | tdID    | qD      | qdD     | ID     | tdID    | qD     | qdD     |
| 0.01                | 6.1289  | 100     | 0.20084 | 0.3394            | 0.84705 | 800   | 0.14074 | 0.2652  | 0.90487 | 2000   | 0.09745 | 0.2304 | 0.94583 |
| 0.1                 | 2.2488  | 130     | 0.2611  | 0.3174            | 0.79215 | 800   | 0.18765 | 0.2915  | 0.9946  | 3000   | 0.14617 | 0.2179 | 0.89452 |
| 1                   | 0.98443 | 160     | 0.32135 | 0.2975            | 0.74248 | 1000  | 0.23456 | 0.2393  | 0.8165  | 4000   | 0.1849  | 0.207  | 0.84977 |
| 10                  | 0.53392 | 200     | 0.40169 | 0.2728            | 0.68084 | 1300  | 0.30493 | 0.222   | 0.75747 | 5000   | 0.24362 | 0.1957 | 0.80749 |
| 100                 | 0.34556 | 240     | 0.48203 | 0.2502            | 0.62443 | 1600  | 0.37529 | 0.206   | 0.70288 | 6000   | 0.29234 | 0.1869 | 0.76726 |
| 1000                | 0.25098 | 300     | 0.60253 | 0.2197            | 0.54831 | 2000  | 0.46912 | 0.1885  | 0.63634 | 8000   | 0.38979 | 0.1686 | 0.66213 |
| 10000               | 0.19563 | 400     | 0.80338 | 0.177             | 0.44174 | 2400  | 0.56294 | 0.1682  | 0.5738  | 10000  | 0.48724 | 0.1536 | 0.63055 |
| 100000              | 0.16037 | 500     | 1.00422 | 0.1426            | 0.35589 | 3000  | 0.70368 | 0.1543  | 0.52648 | 13000  | 0.63341 | 0.1304 | 0.53531 |
| 1000000             | 0.13561 | 600     | 1.20566 | 0.1148            | 0.29851 | 4000  | 0.93824 | 0.1133  | 0.38658 | 16000  | 0.77958 | 0.1118 | 0.45898 |
| 1E+07               | 0.11742 | 700     | 1.40691 | 0.0925            | 0.23086 | 5000  | 1.17279 | 0.0833  | 0.28422 | 20000  | 0.97448 | 0.091  | 0.37357 |
| 1E+08               | 0.10351 | 800     | 1.60875 | 0.0745            | 0.18593 | 6000  | 1.40735 | 0.0682  | 0.2327  | 24000  | 1.16937 | 0.0741 | 0.30419 |
| 1E+09               | 0.09253 | 1000    | 2.00844 | 0.0483            | 0.12054 | 8000  | 1.87847 | 0.0418  | 0.14262 | 30000  | 1.46172 | 0.0645 | 0.26478 |
| 1E+10               | 0.08365 | 1300    | 2.81097 | 0.0283            | 0.07063 | 10000 | 2.34559 | 0.0254  | 0.08657 | 40000  | 1.94896 | 0.0326 | 0.13383 |
| 1E+11               | 0.07632 | 1600    | 3.21351 | 0.0132            | 0.03294 | 13000 | 3.04926 | 0.012   | 0.04094 | 50000  | 2.4362  | 0.0196 | 0.08005 |
| 1E+12               | 0.07017 | 2000    | 4.01688 | 0.0056            | 0.01398 | 16000 | 3.75294 | 0.0056  | 0.01911 | 60000  | 2.92344 | 0.0117 | 0.04803 |
|                     |         | 3000    | 6.02532 | 0.0006            | 0.0015  | 20000 | 4.69118 | 0.0021  | 0.00717 | 80000  | 3.86781 | 0.0042 | 0.01724 |
|                     |         |         |         |                   |         | 24000 | 5.62941 | 0.0006  | 0.00205 | 100000 | 4.87239 | 0.0015 | 0.00816 |
|                     |         |         |         |                   |         | 30000 | 7.03676 | 0.0002  | 0.00068 | 110000 | 5.35963 | 0.0009 | 0.00369 |

| c1      | 4.79832 | c1      | 5.71461 | c1       | 6.40776 |        |         |         |         |        |         |
|---------|---------|---------|---------|----------|---------|--------|---------|---------|---------|--------|---------|
| c2      | 19999.5 | c2      | 125000  | c2       | 500000  |        |         |         |         |        |         |
| reD=200 | 200     | reD=500 | 500     | reD=1000 | 1000    |        |         |         |         |        |         |
| ID      | tdID    | qD      | qdD     | ID       | tdID    | qD     | qdD     | ID      | tdID    | qD     | qdD     |
| 10000   | 0.10421 | 0.1943  | 0.93231 | 100000   | 0.13999 | 0.1568 | 0.89491 | 30000   | 0.00936 | 0.1773 | 1.1361  |
| 13000   | 0.13547 | 0.186   | 0.88249 | 130000   | 0.18199 | 0.1498 | 0.85605 | 40000   | 0.01248 | 0.1729 | 1.1079  |
| 18000   | 0.16673 | 0.182   | 0.87329 | 160000   | 0.22399 | 0.1435 | 0.82005 | 50000   | 0.01561 | 0.1667 | 1.0674  |
| 20000   | 0.20841 | 0.1742  | 0.83687 | 200000   | 0.27999 | 0.1354 | 0.77378 | 100000  | 0.03121 | 0.1604 | 1.0276  |
| 24000   | 0.25009 | 0.1688  | 0.80036 | 240000   | 0.33598 | 0.1277 | 0.72978 | 200000  | 0.08242 | 0.1518 | 0.9727  |
| 30000   | 0.31262 | 0.1562  | 0.7495  | 300000   | 0.41998 | 0.117  | 0.68861 | 300000  | 0.00364 | 0.1464 | 0.9381  |
| 40000   | 0.41682 | 0.1401  | 0.67224 | 400000   | 0.55997 | 0.1012 | 0.57832 | 400000  | 0.12485 | 0.1416 | 0.90734 |
| 50000   | 0.52103 | 0.1236  | 0.58307 | 500000   | 0.69996 | 0.0875 | 0.50003 | 500000  | 0.15808 | 0.1371 | 0.8785  |
| 60000   | 0.62523 | 0.1126  | 0.54029 | 600000   | 0.83998 | 0.0758 | 0.43202 | 600000  | 0.18727 | 0.1327 | 0.85031 |
| 80000   | 0.83365 | 0.0905  | 0.43425 | 800000   | 1.11994 | 0.0565 | 0.32288 | 700000  | 0.21848 | 0.1285 | 0.8234  |
| 100000  | 1.04208 | 0.0728  | 0.34932 | 1000000  | 1.39993 | 0.0422 | 0.24116 | 800000  | 0.2497  | 0.1244 | 0.79712 |
| 130000  | 1.35468 | 0.0524  | 0.25143 | 1300000  | 1.8199  | 0.0273 | 0.15801 | 900000  | 0.28091 | 0.1204 | 0.77149 |
| 160000  | 1.86729 | 0.0378  | 0.18138 | 1600000  | 2.23988 | 0.0176 | 0.10058 | 1000000 | 0.31212 | 0.1168 | 0.74714 |
| 200000  | 2.08412 | 0.0244  | 0.11708 | 2000000  | 2.79985 | 0.0098 | 0.056   | 1400000 | 0.43897 | 0.1024 | 0.65815 |
| 240000  | 2.50094 | 0.0138  | 0.06622 | 2400000  | 3.35982 | 0.0055 | 0.03143 | 2000000 | 0.62424 | 0.0844 | 0.54081 |
| 300000  | 3.12617 | 0.0082  | 0.03935 | 3000000  | 4.19978 | 0.0023 | 0.01314 | 2400000 | 0.74909 | 0.0741 | 0.47481 |
| 400000  | 4.16823 | 0.0028  | 0.01344 | 4000000  | 5.59971 | 0.0006 | 0.00285 | 3000000 | 0.93537 | 0.061  | 0.39087 |
| 500000  | 5.21029 | 0.0009  | 0.00432 | 5000000  | 6.99963 | 0.0001 | 0.00067 | 4000000 | 1.24849 | 0.0442 | 0.28322 |
|         |         |         |         |          |         |        |         | 5000000 | 1.56061 | 0.032  | 0.20505 |
|         |         |         |         |          |         |        |         | 7000000 | 2.18486 | 0.0167 | 0.10701 |
|         |         |         |         |          |         |        |         | 8400000 | 2.62183 | 0.0106 | 0.05792 |
|         |         |         |         |          |         |        |         | 1E+07   | 3.12122 | 0.0063 | 0.04037 |
|         |         |         |         |          |         |        |         | 1.4E+07 | 4.38671 | 0.0017 | 0.01089 |
|         |         |         |         |          |         |        |         | 2E+07   | 6.24244 | 0.0004 | 0.00256 |
|         |         |         |         |          |         |        |         | 3E+07   | 9.38368 | 0.0001 | 0.00084 |

**Table D-1 Tabular Data for Fetkovich Decline Type Curves Figures 5.1 – 5.4 Continued**

Infinite values from program, finite depletion values closed system from table c-5 Lee welltesting book ref 20

Radial Cases

| fetkovich constants |         |          |         | Depletion Portion |         |        |         |
|---------------------|---------|----------|---------|-------------------|---------|--------|---------|
| c1                  | 8.71034 | c1       | 11.0129 |                   |         |        |         |
| c2                  | 5E+07   | c2       | 5E+08   |                   |         |        |         |
| reD=10000           | 10000   | reD= 1e5 | 100000  |                   |         |        |         |
| depletion           |         |          |         |                   |         |        |         |
| ID                  | td0     | qd       | qd0     | ID                | td0     | qd     | qd0     |
| 3E+05               | 0.00889 | 0.1283   | 1.10012 | 1.4E+08           | 0.00254 | 0.1017 | 1.12001 |
| 4E+05               | 0.00918 | 0.124    | 1.08008 | 2E+08             | 0.00363 | 0.1    | 1.10129 |
| 5E+05               | 0.01148 | 0.1222   | 1.0844  | 2.4E+08           | 0.00436 | 0.099  | 1.09028 |
| 6E+05               | 0.01378 | 0.121    | 1.05395 | 3E+08             | 0.00545 | 0.098  | 1.07927 |
| 8E+05               | 0.01837 | 0.1188   | 1.03479 | 3.5E+08           | 0.00638 | 0.0971 | 1.06936 |
| 1E+07               | 0.02298 | 0.1174   | 1.02258 | 4E+08             | 0.00726 | 0.0966 | 1.06385 |
| 1E+07               | 0.02755 | 0.1162   | 1.01214 | 5E+08             | 0.00808 | 0.0956 | 1.05284 |
| 1E+07               | 0.03215 | 0.1152   | 1.00343 | 6E+08             | 0.0109  | 0.0948 | 1.04403 |
| 2E+07               | 0.03674 | 0.1143   | 0.99559 | 7E+08             | 0.01271 | 0.0941 | 1.03632 |
| 2E+07               | 0.04133 | 0.1135   | 0.98862 | 8E+08             | 0.01453 | 0.0935 | 1.02971 |
| 2E+07               | 0.04592 | 0.1128   | 0.98253 | 8.4E+08           | 0.01525 | 0.0933 | 1.02751 |
| 2E+07               | 0.05511 | 0.1115   | 0.9712  | 9E+08             | 0.01634 | 0.093  | 1.0242  |
| 3E+07               | 0.06888 | 0.1098   | 0.9564  | 1E+09             | 0.01816 | 0.0925 | 1.0187  |
| 4E+07               | 0.09184 | 0.1071   | 0.93288 | 1.4E+09           | 0.02542 | 0.0911 | 1.00328 |
| 5E+07               | 0.11481 | 0.105    | 0.91459 | 2E+09             | 0.03632 | 0.0896 | 0.98676 |
| 7E+07               | 0.16073 | 0.0998   | 0.88929 | 3E+09             | 0.05448 | 0.0877 | 0.95583 |
| 8E+07               | 0.18369 | 0.0975   | 0.84925 | 4E+09             | 0.07264 | 0.0861 | 0.94821 |
| 9E+07               | 0.20565 | 0.0952   | 0.82922 | 5E+09             | 0.0908  | 0.0845 | 0.93059 |
| 1E+08               | 0.22961 | 0.093    | 0.81006 | 6E+09             | 0.10886 | 0.0829 | 0.91297 |
| 1E+08               | 0.27553 | 0.0887   | 0.77261 | 7E+09             | 0.12712 | 0.0814 | 0.89645 |
| 1E+08               | 0.32146 | 0.0848   | 0.73689 | 8E+09             | 0.14528 | 0.0799 | 0.87993 |
| 2E+08               | 0.39034 | 0.0788   | 0.68837 | 9E+09             | 0.16344 | 0.0784 | 0.86341 |
| 2E+08               | 0.45922 | 0.0734   | 0.63934 | 1E+10             | 0.1816  | 0.077  | 0.848   |
| 2E+08               | 0.55107 | 0.0688   | 0.58185 | 1.3E+10           | 0.23609 | 0.0728 | 0.80174 |
| 3E+08               | 0.68884 | 0.068    | 0.5052  | 1.6E+10           | 0.29057 | 0.0689 | 0.75879 |
| 4E+08               | 0.91845 | 0.0458   | 0.39893 | 2E+10             | 0.38321 | 0.0639 | 0.70373 |
| 5E+08               | 1.14806 | 0.0362   | 0.31531 | 2.4E+10           | 0.43585 | 0.0594 | 0.65417 |
| 6E+08               | 1.37767 | 0.0286   | 0.24912 | 3E+10             | 0.54481 | 0.0531 | 0.58479 |
| 7E+08               | 1.60729 | 0.0226   | 0.19885 | 4E+10             | 0.72842 | 0.0441 | 0.48567 |
| 8E+08               | 1.8369  | 0.0178   | 0.15504 | 5E+10             | 0.90802 | 0.0366 | 0.40307 |
| 1E+09               | 2.29612 | 0.0111   | 0.09668 | 6E+10             | 1.09983 | 0.0304 | 0.33479 |
| 1E+09               | 3.21457 | 0.0043   | 0.03745 | 7E+10             | 1.27123 | 0.0253 | 0.27863 |
| 2E+09               | 4.56224 | 0.0011   | 0.00858 | 8E+10             | 1.45284 | 0.021  | 0.23127 |
| 3E+09               | 6.88836 | 0.0001   | 0.00087 | 9E+10             | 1.63444 | 0.0174 | 0.19162 |
|                     |         |          |         | 1E+11             | 1.81605 | 0.0145 | 0.15969 |
|                     |         |          |         | 1.3E+11           | 2.36086 | 0.0083 | 0.09141 |
|                     |         |          |         | 1.6E+11           | 2.90568 | 0.0048 | 0.05286 |
|                     |         |          |         | 2E+11             | 3.6321  | 0.0023 | 0.02533 |
|                     |         |          |         | 2.4E+11           | 4.35851 | 0.0011 | 0.01211 |
|                     |         |          |         | 3E+11             | 5.44814 | 0.0004 | 0.00441 |
|                     |         |          |         | 3.4E+11           | 6.17456 | 0.0002 | 0.0022  |

**Table D-2 Tabular Data for Fetkovich Decline Type Curves Figures 5.1 – 5.4 Transient Portion**

Infinite reservoir solutions-transient portion from program

| c1      | 1.8026  | 2.49573             | 3.41202 | 4.10517  | 4.79832             | 6.40776 |         |         |
|---------|---------|---------------------|---------|----------|---------------------|---------|---------|---------|
| c2      | 49.5    | 199.5               | 1249.5  | 4999.5   | 19999.5             | 500000  |         |         |
| reD     | 10      | reD 10<br>transient | 20      | 50       | reD 50<br>transient | 100     | 200     | 1000    |
| ID      | qd      | tdD                 | qdD     | tdD      | qdD                 | tdD     | qdD     | tdD     |
| 0.01    | 6.1269  | 0.0001              | 11.0479 | 2E-05    | 15.2981             | 2.3E-06 | 20.9119 | 4.9E-07 |
| 0.1     | 2.2488  | 0.0011              | 4.05365 | 0.0002   | 5.8124              | 2.3E-05 | 7.57295 | 4.9E-06 |
| 1       | 0.98443 | 0.0112              | 1.77452 | 0.00201  | 2.45687             | 0.00023 | 3.3589  | 4.9E-05 |
| 10      | 0.53392 | 0.1121              | 0.96244 | 0.02008  | 1.33252             | 0.00235 | 1.82175 | 0.00049 |
| 100     | 0.34558 | 1.1207              | 0.62229 | 0.02084  | 0.86243             | 0.02346 | 1.17905 | 0.00487 |
| 1000    | 0.25098 | 11.207              | 0.45238 | 0.00844  | 0.62633             | 0.23456 | 0.85628 | 0.04872 |
| 10000   | 0.19593 | 112.07              | 0.35318 | 0.00844  | 0.48859             | 2.34559 | 0.66852 | 0.48724 |
| 100000  | 0.16037 | 1120.7              | 0.28908 | 0.00844  | 0.40024             | 23.4559 | 0.54719 | 4.87239 |
| 1000000 | 0.13561 | 11207               | 0.24445 | 0.00844  | 0.33845             | 234.559 | 0.4627  | 48.7239 |
| 1E+07   | 0.11742 | 112072              | 0.21168 | 0.00844  | 0.29305             | 2345.59 | 0.40064 | 487.239 |
| 1E+08   | 0.10351 | 1E+08               | 0.18659 | 0.00844  | 0.25833             | 23455.9 | 0.35318 | 4872.39 |
| 1E+09   | 0.09253 | 1E+07               | 0.1668  | 0.008441 | 0.23094             | 234559  | 0.31572 | 48723.9 |
| 1E+10   | 0.08365 | 1E+08               | 0.15079 | 2E+07    | 0.20878             | 2345588 | 0.28543 | 487239  |
| 1E+11   | 0.07832 | 1E+09               | 0.13758 | 2E+08    | 0.19048             | 2.3E+07 | 0.26042 | 4872392 |
| 1E+12   | 0.07017 | 1E+10               | 0.12649 | 2E+09    | 0.17513             | 2.3E+08 | 0.23943 | 4.9E+07 |
|         |         |                     |         |          |                     |         | 0.28807 | 1E+07   |
|         |         |                     |         |          |                     |         | 0.33671 | 312122  |
|         |         |                     |         |          |                     |         |         | 0.44965 |

Infinite reservoir solutions-transient portion from program

| c1      | 8.71034                    | 11.0129 |                        |
|---------|----------------------------|---------|------------------------|
| c2      | 5E+07                      | 5E+09   |                        |
| reD     | 10000 transient<br>reD=1e5 | 100000  | INFINITE-<br>TRANSIENT |
| ID      | tdD                        | qdD     | tdD                    |
| 0.01    | 2.3E-11                    | 53.385  | 1.8E-13                |
| 0.1     | 2.3E-10                    | 19.588  | 1.8E-12                |
| 1       | 2.3E-09                    | 8.5747  | 1.8E-11                |
| 10      | 2.3E-08                    | 4.6506  | 1.8E-10                |
| 100     | 2.3E-07                    | 3.0099  | 1.8E-09                |
| 1000    | 2.3E-06                    | 2.1859  | 1.8E-08                |
| 10000   | 2.3E-05                    | 1.7086  | 1.8E-07                |
| 100000  | 0.00023                    | 1.3669  | 1.8E-06                |
| 1000000 | 0.0023                     | 1.1812  | 1.8E-05                |
| 1E+07   | 0.02298                    | 1.0228  | 0.00018                |
| 1E+08   | 0.22981                    | 0.9016  | 0.00182                |
| 1E+09   | 2.29812                    | 0.808   | 0.01816                |
| 1E+10   | 22.9812                    | 0.7286  | 0.1816                 |
| 1E+11   | 229.812                    | 0.6648  | 1.81605                |
| 1E+12   | 2298.12                    | 0.6112  | 18.1605                |
|         |                            |         | 0.77281                |
|         |                            |         | 0.00091                |
|         |                            |         | 0.00012                |
|         |                            |         | 10 4.5E-05             |

**Table D-3 Arps Depletion Solutions for Fetkovich Type Curves Figures 5.1 – 5.4**

Arps depletion solutions from program

| b values | 0       | 0.1    | 0.2     | 0.3     | 0.4     | 0.5     | 0.6     | 0.7     | 0.8     | 0.9     | 1       |
|----------|---------|--------|---------|---------|---------|---------|---------|---------|---------|---------|---------|
| t/D      | qdD     | qdD    | qdD     | qdD     | qdD     | qdD     | qdD     | qdD     | qdD     | qdD     | qdD     |
| 0.1      | 0.90484 | 0.9053 | 0.90573 | 0.90617 | 0.9066  | 0.90703 | 0.90745 | 0.90787 | 0.90828 | 0.90869 | 0.90909 |
| 0.5      | 0.60653 | 0.6139 | 0.62092 | 0.62759 | 0.63394 | 0.64    | 0.64579 | 0.65134 | 0.65666 | 0.66176 | 0.66667 |
| 1        | 0.36788 | 0.3855 | 0.40188 | 0.41705 | 0.4312  | 0.44444 | 0.45888 | 0.46858 | 0.47983 | 0.49009 | 0.5     |
| 1.5      | 0.22313 | 0.2472 | 0.26933 | 0.28981 | 0.30882 | 0.32653 | 0.34309 | 0.35862 | 0.37323 | 0.38699 | 0.4     |
| 2        | 0.13534 | 0.1615 | 0.18593 | 0.20874 | 0.23006 | 0.25    | 0.26372 | 0.28631 | 0.30289 | 0.31854 | 0.33333 |
| 2.5      | 0.08208 | 0.1074 | 0.13169 | 0.15484 | 0.17678 | 0.19753 | 0.21715 | 0.23571 | 0.25328 | 0.26992 | 0.28571 |
| 3        | 0.04979 | 0.0725 | 0.09537 | 0.11771 | 0.1393  | 0.16    | 0.17978 | 0.19853 | 0.2166  | 0.2337  | 0.25    |
| 3.5      | 0.0302  | 0.0497 | 0.07043 | 0.09137 | 0.11207 | 0.13223 | 0.15173 | 0.17049 | 0.18848 | 0.20572 | 0.22222 |
| 4        | 0.01832 | 0.0348 | 0.05292 | 0.07221 | 0.09174 | 0.11111 | 0.13008 | 0.1485  | 0.16632 | 0.18349 | 0.2     |
| 4.5      | 0.01111 | 0.0243 | 0.04039 | 0.05798 | 0.07623 | 0.09467 | 0.11298 | 0.13094 | 0.14844 | 0.16541 | 0.18182 |
| 5        | 0.00674 | 0.0173 | 0.03125 | 0.04716 | 0.06415 | 0.08163 | 0.09921 | 0.11654 | 0.13375 | 0.15044 | 0.16667 |
| 5.5      | 0.00409 | 0.0125 | 0.02449 | 0.03683 | 0.05459 | 0.07111 | 0.08795 | 0.1048  | 0.12148 | 0.13786 | 0.15385 |
| 6        | 0.00248 | 0.0081 | 0.0194  | 0.03232 | 0.04691 | 0.0625  | 0.0786  | 0.09487 | 0.1111  | 0.12713 | 0.14286 |
| 6.5      | 0.0015  | 0.0067 | 0.01554 | 0.02716 | 0.04067 | 0.05536 | 0.07074 | 0.08644 | 0.10221 | 0.11788 | 0.13333 |
| 7        | 0.00091 | 0.005  | 0.01256 | 0.02302 | 0.03553 | 0.04938 | 0.06407 | 0.07921 | 0.09453 | 0.10984 | 0.125   |
| 7.5      | 0.00055 | 0.0037 | 0.01024 | 0.01987 | 0.03125 | 0.04432 | 0.05835 | 0.07295 | 0.08783 | 0.10277 | 0.11765 |
| 8        | 0.00034 | 0.0028 | 0.00842 | 0.01692 | 0.02766 | 0.04    | 0.05341 | 0.06749 | 0.08193 | 0.09653 | 0.11111 |
| 8.5      | 0.0002  | 0.0021 | 0.00697 | 0.01465 | 0.02462 | 0.03628 | 0.0491  | 0.06269 | 0.07672 | 0.09096 | 0.10526 |
| 9        | 0.00012 | 0.0016 | 0.00581 | 0.01276 | 0.02203 | 0.03306 | 0.04533 | 0.05844 | 0.07207 | 0.08598 | 0.1     |
| 9.5      | 7.5E-05 | 0.0013 | 0.00488 | 0.01118 | 0.01981 | 0.03025 | 0.042   | 0.05465 | 0.0679  | 0.08149 | 0.09524 |
| 10       | 4.5E-05 | 0.001  | 0.00412 | 0.00984 | 0.01789 | 0.02778 | 0.03904 | 0.05127 | 0.06415 | 0.07743 | 0.09091 |
| 20       | 2.1E-09 | 2E-05  | 0.00032 | 0.00152 | 0.00412 | 0.00826 | 0.01391 | 0.02089 | 0.02897 | 0.03795 | 0.04762 |
| 30       | 9.4E-14 | 1E-06  | 5.9E-05 | 0.00046 | 0.00164 | 0.00391 | 0.00739 | 0.01209 | 0.01789 | 0.02468 | 0.03226 |
| 40       | 4.2E-18 | 1E-07  | 1.7E-05 | 0.00019 | 0.00084 | 0.00227 | 0.00468 | 0.00814 | 0.01264 | 0.01809 | 0.02436 |
| 50       | 1.9E-22 | 2E-08  | 6.2E-06 | 9.7E-06 | 0.00049 | 0.00148 | 0.00327 | 0.00598 | 0.00964 | 0.01421 | 0.01961 |
| 60       | 8.8E-27 | 4E-09  | 2.7E-06 | 5.5E-06 | 0.00032 | 0.00104 | 0.00243 | 0.00464 | 0.00771 | 0.01165 | 0.01639 |
| 70       | 4E-31   | 9E-10  | 1.3E-06 | 3.4E-06 | 0.00022 | 0.00077 | 0.00189 | 0.00374 | 0.00638 | 0.00984 | 0.01408 |
| 80       | 1.8E-35 | 3E-10  | 7E-07   | 2.2E-06 | 0.00016 | 0.00059 | 0.00152 | 0.0031  | 0.00542 | 0.00865 | 0.01235 |
| 90       | 8.2E-40 | 1E-10  | 4E-07   | 1.5E-06 | 0.00012 | 0.00047 | 0.00126 | 0.00263 | 0.00469 | 0.00747 | 0.01099 |
| 100      | 3.7E-44 | 4E-11  | 2.4E-07 | 1.1E-06 | 9.3E-06 | 0.00038 | 0.00106 | 0.00227 | 0.00412 | 0.00666 | 0.0099  |

**Table D-4 Equivalent Radial Transient Generalized Solutions Shape Factor 31.62**

| CA                           | 31.62               | Equivalent Radial in Transient Region |              |           |           |            |              |            |            |
|------------------------------|---------------------|---------------------------------------|--------------|-----------|-----------|------------|--------------|------------|------------|
|                              |                     |                                       |              |           |           |            |              |            |            |
|                              | log-term            | 1.34421927                            |              | 1.949557  |           | 2.74635034 |              | 3.34854055 |            |
|                              | c1c2                | 78.7565332                            | 78.852962    | 448.66156 | 448.02358 | 3958.51442 | 3950.9477    | 19311.7745 | 19273.9233 |
|                              | c1                  | 1.54733081                            |              | 2.244135  |           | 3.16132367 |              | 3.85450514 |            |
|                              | fokkovich constants |                                       |              |           |           |            |              |            |            |
| infinite reservoir solutions | A/w^2               | 311.017873                            |              | 1253.4955 |           | 7850.84004 |              | 31412.7849 |            |
|                              | c1                  | 1.55258509                            |              | 2.2457323 |           | 3.16202301 |              | 3.85517019 |            |
|                              | c2                  | 49.5                                  |              | 199.5     |           | 1249.5     |              | 4999.5     |            |
|                              | rD                  | 10 rD                                 | 10 transient | 20        |           | 50 rD      | 50 transient | 100        |            |
| ID                           | qD                  | tdD                                   | qdD          | tdD       | qdD       | tdD        | qdD          | tdD        | qdD        |
| 0.01                         | 6.1289              | 0.00013028                            | 9.4834358    | 2.229E-05 | 13.754079 | 2.5262E-05 | 19.375438    | 5.1782E-07 | 23.6238765 |
| 0.1                          | 2.2468              | 0.00130282                            | 3.4796375    | 0.0002229 | 5.0466109 | 2.5262E-05 | 7.1091851    | 5.1782E-08 | 8.66801116 |
| 1                            | 0.98443             | 0.01302821                            | 1.5232389    | 0.0022289 | 2.2091939 | 0.00025262 | 3.1121021    | 5.1782E-05 | 3.79449049 |
| 10                           | 0.53382             | 0.13028207                            | 0.8261509    | 0.0222885 | 1.1981886 | 0.0025262  | 1.687894     | 0.00051782 | 2.05799738 |
| 100                          | 0.34556             | 1.3028207                             | 0.5346856    | 0.2228851 | 0.7754833 | 0.025262   | 1.0624271    | 0.00517819 | 1.3319828  |
| 1000                         | 0.25098             | 13.028207                             | 0.3883181    | 2.2288515 | 0.5631881 | 0.25262002 | 0.7933658    | 0.05178188 | 0.96732661 |
| 10000                        | 0.19593             | 130.28207                             | 0.3031685    | 22.288515 | 0.4396634 | 2.52620022 | 0.6193982    | 0.5178188  | 0.75521319 |
| 100000                       | 0.16037             | 1302.8207                             | 0.2481454    | 222.88515 | 0.3506919 | 25.2620022 | 0.5069815    | 5.17818805 | 0.61814699 |
| 1000000                      | 0.13561             | 13028.207                             | 0.2098335    | 2228.8515 | 0.3043272 | 252.620022 | 0.4287071    | 51.7818805 | 0.52270644 |
| 10000000                     | 0.11742             | 130282.07                             | 0.1816876    | 22288.515 | 0.2635063 | 2526.20022 | 0.3712026    | 517.818805 | 0.45259599 |
| 100000000                    | 0.10351             | 1302820.7                             | 0.1601642    | 222885.15 | 0.2322904 | 25262.0022 | 0.3272286    | 5178.18805 | 0.39697983 |
| 1E+09                        | 0.092533            | 13028207                              | 0.1431792    | 2228851.5 | 0.2076565 | 252620.022 | 0.2925268    | 51781.8805 | 0.35666892 |
| 1E+10                        | 0.083663            | 130282070                             | 0.1294389    | 22288515  | 0.1877286 | 2526200.22 | 0.2644542    | 517818.805 | 0.32244092 |
| 1E+11                        | 0.076324            | 1302820895                            | 0.1180985    | 222885150 | 0.1712814 | 25262002.2 | 0.2412849    | 5178188.05 | 0.29419125 |
| 1E+12                        | 0.070173            | 13028E+10                             | 0.1085808    | 2.229E+09 | 0.1574777 | 252620022  | 0.2218396    | 51781880.5 | 0.27048219 |

**Table D-4 Equivalent Radial Transient Generalized Solutions Shape Factor 31.62 Continued**

| CA 31.62 Equivalent Radial in Transient Region |           |            |            |           |                            |            |            |           |                    |
|--|-----------|------------|------------|-----------|----------------------------|------------|------------|-----------|--------------------|
| logem  | 3.9506332 |            | 5.34858364 |           | 7.3485841                  |            | 9.34858408 |           |                    |
| c1c2   | 91143.538 | 90964.073  | 3084951.89 | 3078874.6 | 423851478                  | 423017014  | 5.3821E+10 | 5.381E+10 |                    |
| c1   | 4.5475739 |            | 6.15875463 |           | 8.4589551                  |            | 10.7811551 |           |                    |
| <i>feklovich constants</i>                     |           |            |            |           |                            |            |            |           |                    |
| A/w^2  | 125860.56 |            | 3141589.51 |           | 314159262                  |            | 3.1416E+10 |           |                    |
| c1   | 4.5483174 |            | 6.15775528 |           | 8.4603404                  |            | 10.7629255 |           |                    |
| c2   | 19999.5   |            | 499999.5   |           | 50000000                   |            | 5000000000 |           |                    |
| reD  | 200       |            | 1000       |           | 10000 transient<br>reD=1e5 |            | 100000     |           | INFINITE-TRANSIENT |
| tdD  | qdD       | tdD        | qdD        | tdD       | qdD                        | tdD        | qdD        | tdD       | qdD                |
| 1.097E-07                                      | 27.871626 | 3.2415E-08 | 37.734133  | 2.359E-11 | 51.84408                   | 1.8546E-13 | 65.954044  | 0.0001    | 0.9999             |
| 1.097E-06                                      | 10.226584 | 3.2415E-08 | 13.84531   | 2.359E-10 | 19.022498                  | 1.8546E-12 | 24.199688  | 0.001     | 0.9990005          |
| 1.097E-05                                      | 4.4767882 | 3.2415E-07 | 6.080894   | 2.359E-09 | 8.3272492                  | 1.8546E-11 | 10.593804  | 0.01      | 0.99004983         |
| 0.0001097                                      | 2.4280407 | 3.2415E-08 | 3.2872144  | 2.359E-08 | 4.5164053                  | 1.8546E-10 | 5.7455859  | 0.1       | 0.90483742         |
| 0.0010972                                      | 1.5714596 | 3.2415E-05 | 2.1275281  | 2.359E-07 | 2.9230765                  | 1.8546E-09 | 3.7186248  | 0.2       | 0.81873075         |
| 0.0109717                                      | 1.1412591 | 0.00032415 | 1.5450991  | 2.359E-06 | 2.1228594                  | 1.8546E-08 | 2.7006195  | 0.4       | 0.67032005         |
| 0.109717                                       | 0.8910082 | 0.00324154 | 1.2082929  | 2.359E-05 | 1.6573831                  | 1.8546E-07 | 2.1084331  | 0.6       | 0.54681164         |
| 1.0971705                                      | 0.7292944 | 0.03241542 | 0.9873587  | 0.0002359 | 1.3585826                  | 1.8546E-06 | 1.7257864  | 0.8       | 0.44932895         |
| 10.971705                                      | 0.6166695 | 0.32415416 | 0.8349175  | 0.0023593 | 1.1471189                  | 1.8546E-05 | 1.4593202  | 1         | 0.36787944         |
| 109.71705                                      | 0.5339781 | 3.24154163 | 0.7229281  | 0.0235932 | 0.9932505                  | 0.00018546 | 1.2635748  | 1.3       | 0.27253179         |
| 1097.1705                                      | 0.4707194 | 32.4154163 | 0.6372657  | 0.2359317 | 0.8755884                  | 0.00185457 | 1.1138872  | 1.9       | 0.14958852         |
| 10971.705                                      | 0.4208007 | 324.154163 | 0.589703   | 2.359317  | 0.7827325                  | 0.01854574 | 0.985762   | 2.5       | 0.082085           |
| 109717.05                                      | 0.3804182 | 3241.54163 | 0.515031   | 23.59317  | 0.707617                   | 0.18545738 | 0.9002029  | 3         | 0.04978707         |
| 1097170.5                                      | 0.347088  | 32415.4163 | 0.4699081  | 235.9317  | 0.6456213                  | 1.85457381 | 0.8213344  | 3.5       | 0.03019738         |
| 10971705                                       | 0.3191169 | 324154.163 | 0.4320379  | 2359.317  | 0.5935903                  | 18.5457381 | 0.7551425  | 5         | 0.00873795         |
|  |           |            |            |           |                            |            |            | 6         | 0.00247875         |
|  |           |            |            |           |                            |            |            | 7         | 0.00091188         |
|  |           |            |            |           |                            |            |            | 9         | 0.00012341         |
|  |           |            |            |           |                            |            |            | 10        | 4.54E-05           |

**Table D-5 Depletion Solutions Generalized for Figure 5.9**

New adaptation of Fetkovich for Other Shapes-Rectangular  $xy=2:1$  Well Near Boundary-Figure 5.9

Infinite values from infq.out, finite values from table c-5 Lee book

Depletion Region Stems Various Reservoir Sizes

|    |                     |           |           |                     |                      |           |            |           |        |            |  |
|----|---------------------|-----------|-----------|---------------------|----------------------|-----------|------------|-----------|--------|------------|--|
| CA | 10.8374             | logterm   | 2.4145937 |                     | logterm              | 3.2113871 |            |           |        |            |  |
|    | c1c2                | 555.68286 | 448.02359 |                     | c1c2                 | 4628.8057 | 3950.94775 |           |        |            |  |
|    | c1                  | 2.7794388 |           |                     | c1                   | 3.6966277 |            |           |        |            |  |
|    | fetkovich constants |           |           | fetkovich constants |                      |           |            |           |        |            |  |
|    | Equivalent          | A/hw^2    | 1253.4955 |                     | A/hw^2               | 7850.84   |            |           |        |            |  |
|    |                     | c1        | 2.2457323 |                     | c1                   | 3.162023  |            |           |        |            |  |
|    |                     | c2        | 199.5     |                     | c2                   | 1249.5    |            |           |        |            |  |
|    | infinite            | rdD       | 20        |                     | rdD =50<br>depletion |           | 50         |           |        |            |  |
|    | ID                  | qd        | ID        | tdID                | qd                   | qdD       | ID         | tdID      | qd     | qdD        |  |
|    | 0.01                | 6.1289    | 100       | 0.1799588           | 0.3394               | 0.9433415 | 600        | 0.1296231 | 0.2652 | 0.98034586 |  |
|    | 0.1                 | 2.2486    | 130       | 0.2339464           | 0.3174               | 0.8821939 | 800        | 0.1728308 | 0.2915 | 1.07756697 |  |
|    | 1                   | 0.98443   | 160       | 0.287934            | 0.2975               | 0.8268831 | 1000       | 0.2160384 | 0.2393 | 0.88480301 |  |
|    | 10                  | 0.53392   | 200       | 0.3599175           | 0.2728               | 0.7582309 | 1300       | 0.28085   | 0.222  | 0.82065135 |  |
|    | 100                 | 0.34558   | 240       | 0.431901            | 0.2502               | 0.6954156 | 1600       | 0.3458815 | 0.208  | 0.7615053  |  |
|    | 1000                | 0.25098   | 300       | 0.5398763           | 0.2197               | 0.6108427 | 2000       | 0.4320769 | 0.1885 | 0.68842108 |  |
|    | 10000               | 0.19583   | 400       | 0.719835            | 0.177                | 0.4919807 | 2400       | 0.5164823 | 0.1682 | 0.62177278 |  |
|    | 100000              | 0.16037   | 500       | 0.8997938           | 0.1426               | 0.396348  | 3000       | 0.6481153 | 0.1543 | 0.57038985 |  |
|    | 1000000             | 0.13561   | 600       | 1.0797526           | 0.1148               | 0.3190796 | 4000       | 0.8641538 | 0.1133 | 0.41882792 |  |
|    | 10000000            | 0.11742   | 700       | 1.2597113           | 0.0925               | 0.2570881 | 5000       | 1.0801922 | 0.0833 | 0.30792908 |  |
|    | 100000000           | 0.10351   | 800       | 1.4396701           | 0.0745               | 0.2070882 | 6000       | 1.2962307 | 0.0682 | 0.25211001 |  |
|    | 1E+09               | 0.092533  | 1000      | 1.7995878           | 0.0483               | 0.1342469 | 8000       | 1.7263076 | 0.0418 | 0.15451904 |  |
|    | 1E+10               | 0.083653  | 1300      | 2.3394639           | 0.0283               | 0.0786581 | 10000      | 2.1603845 | 0.0254 | 0.08389434 |  |
|    | 1E+11               | 0.076324  | 1600      | 2.8793402           | 0.0132               | 0.0366888 | 13000      | 2.8064998 | 0.012  | 0.04436653 |  |
|    | 1E+12               | 0.070173  | 2000      | 3.5991752           | 0.0066               | 0.0155649 | 16000      | 3.4566152 | 0.0056 | 0.02070112 |  |
|    |                     |           | 3000      | 5.3987628           | 0.0008               | 0.0016677 | 20000      | 4.3207689 | 0.0021 | 0.00776292 |  |
|    |                     |           |           |                     |                      |           | 24000      | 5.1849227 | 0.0006 | 0.00221798 |  |
|    |                     |           |           |                     |                      |           | 30000      | 6.4811534 | 0.0002 | 0.00073833 |  |

**Table D-5 Depletion Solutions Generalized for Figure 5.9 Continued**

| logterm             | 3.81357741  |             | logterm             | 4.415689975 |             |        |              |
|---------------------|-------------|-------------|---------------------|-------------|-------------|--------|--------------|
| c1c2                | 21963.74438 | 19273.92334 | c1c2                | 101872.2221 | 90864.07317 |        |              |
| c1                  | 4.389808956 |             | c1                  | 5.082877709 |             |        |              |
| felkovich constants |             |             | felkovich constants |             |             |        |              |
| A/hw^2              | 31412.78494 |             | A/hw^2              | 125860.5646 |             |        |              |
| c1                  | 3.855170186 |             | c1                  | 4.548317367 |             |        |              |
| c2                  | 4999.5      |             | c2                  | 19999.5     |             |        |              |
| reD=100             | 100         |             | reD=200             | 200         |             |        |              |
| tD                  | tdD         | qd          | qdD                 | tD          | tdD         | qd     | qdD          |
| 2000                | 0.080934948 | 0.2304      | 1.011411984         | 10000       | 0.098162186 | 0.1943 | 0.987603139  |
| 3000                | 0.136402422 | 0.2179      | 0.968539372         | 13000       | 0.127610842 | 0.186  | 0.945415254  |
| 4000                | 0.181869896 | 0.207       | 0.908690454         | 16000       | 0.157059497 | 0.182  | 0.825083743  |
| 5000                | 0.22733737  | 0.1967      | 0.863475422         | 20000       | 0.198324372 | 0.1742 | 0.885437297  |
| 6000                | 0.272804844 | 0.1869      | 0.820455294         | 24000       | 0.235588246 | 0.1668 | 0.847824002  |
| 8000                | 0.363739792 | 0.1686      | 0.74012179          | 30000       | 0.294486558 | 0.1582 | 0.793945498  |
| 10000               | 0.45467474  | 0.1536      | 0.674274656         | 40000       | 0.392648743 | 0.1401 | 0.712111167  |
| 13000               | 0.581077161 | 0.1304      | 0.572431088         | 50000       | 0.490810929 | 0.1236 | 0.626243685  |
| 16000               | 0.727479583 | 0.1118      | 0.490780641         | 60000       | 0.588973115 | 0.1126 | 0.57233203   |
| 20000               | 0.909349479 | 0.091       | 0.399472615         | 80000       | 0.785297487 | 0.0905 | 0.460000433  |
| 24000               | 1.091219375 | 0.0741      | 0.325284844         | 100000      | 0.981621858 | 0.0728 | 0.3700333497 |
| 30000               | 1.364024219 | 0.0645      | 0.283142678         | 130000      | 1.276108416 | 0.0524 | 0.268342792  |
| 40000               | 1.818698958 | 0.0326      | 0.143107772         | 160000      | 1.570594974 | 0.0378 | 0.192132777  |
| 50000               | 2.273373668 | 0.0195      | 0.085601275         | 200000      | 1.983243717 | 0.0244 | 0.124022216  |
| 60000               | 2.728048437 | 0.0117      | 0.051380765         | 240000      | 2.35588246  | 0.0138 | 0.070143712  |
| 90000               | 3.837387916 | 0.0042      | 0.018437198         | 300000      | 2.944865575 | 0.0082 | 0.041879587  |
| 100000              | 4.546747396 | 0.0015      | 0.006584713         | 400000      | 3.926487434 | 0.0026 | 0.014232058  |
| 110000              | 5.001422135 | 0.0009      | 0.003950828         | 500000      | 4.908109292 | 0.0009 | 0.00457459   |

**Table D-5 Depletion Solutions Generalized for Figure 5.9 Continued**

| logterm             | 5.211558113 |           | logterm             | 5.813620407 |             |        |             |
|---------------------|-------------|-----------|---------------------|-------------|-------------|--------|-------------|
| c1c2                | 751477.4937 | 683073.28 | c1c2                | 3353175.435 | 3078874.561 |        |             |
| c1                  | 5.999025695 |           | c1                  | 6.692058451 |             |        |             |
| fetkovich constants |             |           | fetkovich constants |             |             |        |             |
| A/hw^2              | 785395.0218 |           | A/hw^2              | 3141589.512 |             |        |             |
| c1                  | 5.464608096 |           | c1                  | 6.157755279 |             |        |             |
| c2                  | 124999.5    |           | c2                  | 499999.5    |             |        |             |
| reD=500             | 500         |           | reD=1000            | 1000        |             |        |             |
| ID                  | IdD         | qD        | qdD                 | ID          | IdD         | qD     | qdD         |
| 100000              | 0.133071184 | 0.1586    | 0.936447424         | 30000       | 0.008946743 | 0.1773 | 1.186501963 |
| 130000              | 0.172992539 | 0.1498    | 0.898654049         | 40000       | 0.011928981 | 0.1729 | 1.157056908 |
| 160000              | 0.212913865 | 0.1435    | 0.860880187         | 50000       | 0.014911239 | 0.1697 | 1.135642319 |
| 200000              | 0.266142368 | 0.1354    | 0.812268079         | 100000      | 0.029822478 | 0.1604 | 1.073406175 |
| 240000              | 0.319370842 | 0.1277    | 0.766075581         | 200000      | 0.050644956 | 0.1518 | 1.015854473 |
| 300000              | 0.399213553 | 0.117     | 0.701886006         | 300000      | 0.089467433 | 0.1484 | 0.979717357 |
| 400000              | 0.532264737 | 0.1012    | 0.6071014           | 400000      | 0.119289911 | 0.1416 | 0.947595477 |
| 500000              | 0.685355921 | 0.0875    | 0.524914748         | 500000      | 0.149112389 | 0.1371 | 0.917481214 |
| 600000              | 0.798427105 | 0.0758    | 0.453526343         | 600000      | 0.178934867 | 0.1327 | 0.888036156 |
| 800000              | 1.084589474 | 0.0665    | 0.338944962         | 700000      | 0.208757345 | 0.1285 | 0.858929511 |
| 1000000             | 1.330711842 | 0.0422    | 0.253158884         | 800000      | 0.238579822 | 0.1244 | 0.832492071 |
| 1300000             | 1.729925395 | 0.0273    | 0.163773401         | 900000      | 0.2684023   | 0.1204 | 0.805723837 |
| 1600000             | 2.129138947 | 0.0176    | 0.105582852         | 1000000     | 0.298224778 | 0.1166 | 0.780294015 |
| 2000000             | 2.661423684 | 0.0098    | 0.058790452         | 1400000     | 0.417514689 | 0.1024 | 0.685266785 |
| 2400000             | 3.193708421 | 0.0055    | 0.032994641         | 2000000     | 0.598449556 | 0.0844 | 0.564809733 |
| 3000000             | 3.992135527 | 0.0023    | 0.013797759         | 2400000     | 0.715739467 | 0.0741 | 0.495881531 |
| 4000000             | 5.322647369 | 0.0005    | 0.002999613         | 3000000     | 0.894674334 | 0.061  | 0.408215585 |
| 5000000             | 6.653559211 | 0.0001    | 0.000599903         | 4000000     | 1.192899112 | 0.0442 | 0.295788984 |
|                     |             |           |                     | 5000000     | 1.49112389  | 0.032  | 0.21414587  |
|                     |             |           |                     | 7000000     | 2.067573446 | 0.0167 | 0.111757376 |
|                     |             |           |                     | 8400000     | 2.505088136 | 0.0106 | 0.07093582  |
|                     |             |           |                     | 10000000    | 2.982247781 | 0.0063 | 0.042159968 |
|                     |             |           |                     | 14000000    | 4.175146893 | 0.0017 | 0.011376499 |
|                     |             |           |                     | 20000000    | 5.984495581 | 0.0004 | 0.002676823 |
|                     |             |           |                     | 30000000    | 8.946743342 | 0.0001 | 0.000669206 |

**Table D-5 Depletion Solutions Generalized for Figure 5.9 Continued**

| logterm             | 7.813620837  | logterm               | 9.813620841 |             |             |             |             |
|---------------------|--------------|-----------------------|-------------|-------------|-------------|-------------|-------------|
| c1c2                | 450873858.2  | c1c2                  | 58802982197 |             |             |             |             |
| c1                  | 8.994258946  | c1                    | 53814627319 |             |             |             |             |
| fetkovich constants |              | fetkovich constants   |             |             |             |             |             |
| A/w^2               | 314159262.2  | A/w^2                 | 31415926533 |             |             |             |             |
| c1                  | 8.460340372  | c1                    | 10.76292546 |             |             |             |             |
| c2                  | 49999999.5   | c2                    | 5000000000  |             |             |             |             |
| reD=10000           | 10000        | reD= 1e5<br>depletion | 100000      |             |             |             |             |
| ID                  | tdD          | qD                    | qdD         | ID          | tdD         | qD          | qdD         |
| 3000000             | 0.008656699  | 0.1263                | 1.135974905 | 140000000   | 0.002473368 | 0.1017      | 1.148849875 |
| 4000000             | 0.0086875598 | 0.124                 | 1.115288109 | 200000000   | 0.003533383 | 0.1         | 1.129645895 |
| 5000000             | 0.011094498  | 0.1222                | 1.099098443 | 240000000   | 0.004240059 | 0.099       | 1.118349438 |
| 6000000             | 0.013313397  | 0.121                 | 1.088305332 | 300000000   | 0.005300074 | 0.098       | 1.107052977 |
| 8000000             | 0.017751196  | 0.1188                | 1.068517983 | 350000000   | 0.00818342  | 0.0971      | 1.096888164 |
| 10000000            | 0.022188995  | 0.1174                | 1.055928    | 400000000   | 0.007068785 | 0.0966      | 1.091237935 |
| 12000000            | 0.026826794  | 0.1162                | 1.045132886 | 500000000   | 0.006833457 | 0.0956      | 1.079941476 |
| 14000000            | 0.031084583  | 0.1152                | 1.038138631 | 600000000   | 0.010600148 | 0.0948      | 1.070904309 |
| 16000000            | 0.035502382  | 0.1143                | 1.028043787 | 700000000   | 0.01236884  | 0.0941      | 1.062966787 |
| 18000000            | 0.039940191  | 0.1135                | 1.02084839  | 800000000   | 0.014133531 | 0.0935      | 1.056218912 |
| 20000000            | 0.04437799   | 0.1128                | 1.014552409 | 840000000   | 0.014840207 | 0.0933      | 1.05395962  |
| 24000000            | 0.053253588  | 0.1115                | 1.002859872 | 900000000   | 0.015900222 | 0.093       | 1.050570682 |
| 30000000            | 0.066566985  | 0.1098                | 9.987569632 | 1000000000  | 0.017666914 | 0.0925      | 1.044922453 |
| 40000000            | 0.06875598   | 0.1071                | 9.963285133 | 1400000000  | 0.024733679 | 0.0911      | 1.02910741  |
| 50000000            | 0.110944975  | 0.105                 | 9.944397189 | 2000000000  | 0.035333827 | 0.0896      | 1.012162722 |
| 70000000            | 0.155322985  | 0.0998                | 9.897627043 | 3000000000  | 0.053000741 | 0.0877      | 0.99069945  |
| 80000000            | 0.17751198   | 0.0975                | 9.876940247 | 4000000000  | 0.070687655 | 0.0861      | 0.972625116 |
| 90000000            | 0.199700955  | 0.0952                | 9.856253452 | 5000000000  | 0.088334568 | 0.0845      | 0.954550781 |
| 100000000           | 0.22188995   | 0.093                 | 9.836466082 | 6000000000  | 0.108001482 | 0.0829      | 0.936476447 |
| 120000000           | 0.26826794   | 0.0887                | 9.797790788 | 7000000000  | 0.123668395 | 0.0814      | 0.919531759 |
| 140000000           | 0.31084583   | 0.0848                | 9.760914307 | 8000000000  | 0.141335309 | 0.0799      | 0.90258707  |
| 170000000           | 0.377212916  | 0.0788                | 9.708747606 | 9000000000  | 0.159002223 | 0.0784      | 0.885642382 |
| 200000000           | 0.443779901  | 0.0734                | 9.660178607 | 10000000000 | 0.176669137 | 0.077       | 0.868627339 |
| 240000000           | 0.532535881  | 0.0688                | 9.600816498 | 13000000000 | 0.229669678 | 0.0728      | 0.822382212 |
| 300000000           | 0.656669851  | 0.068                 | 9.521657019 | 16000000000 | 0.282670619 | 0.0689      | 0.778326022 |
| 400000000           | 0.887556801  | 0.0458                | 9.41193706  | 20000000000 | 0.353338273 | 0.0539      | 0.721643727 |
| 500000000           | 1.109449752  | 0.0362                | 9.325592174 | 24000000000 | 0.424005928 | 0.0594      | 0.671009682 |
| 600000000           | 1.331339702  | 0.0286                | 9.257235806 | 30000000000 | 0.53000741  | 0.0531      | 0.599841197 |
| 700000000           | 1.553229652  | 0.0226                | 9.203270252 | 40000000000 | 0.708676547 | 0.0441      | 0.49817384  |
| 800000000           | 1.775119602  | 0.0178                | 9.160097809 | 50000000000 | 0.883345684 | 0.0386      | 0.413450398 |
| 1000000000          | 2.218899503  | 0.0111                | 9.099836274 | 60000000000 | 1.08001482  | 0.0304      | 0.343412352 |
| 1400000000          | 3.108458304  | 0.0043                | 9.038675313 | 70000000000 | 1.236683957 | 0.0253      | 0.285800411 |
| 2000000000          | 4.437799006  | 0.0011                | 9.009893685 | 80000000000 | 1.413353094 | 0.021       | 0.237225638 |
| 3000000000          | 6.6566698509 | 0.0001                | 9.000899426 | 90000000000 | 1.58002223  | 0.0174      | 0.196558386 |
|                     |              |                       | 1E+11       | 1.766691367 | 0.0145      | 0.163798655 |             |
|                     |              |                       | 1.3E+11     | 2.296696777 | 0.0083      | 0.083760606 |             |

**Table D-6 Depletion Solutions Generalized for Figure 5.7 Continued**

New adaptation of Fetkovich for rectangular shape  $xy=2:1$  Well at Center Figure 5.7

Infinite values from infq.out, finite values from table c-5 Lee book

Depletion Region Stems Various Reservoir Sizes

| CA         | 21.8369 logterm     | 2.1103279 |           |                       | logterm   | 2.9071212  |            |           |
|------------|---------------------|-----------|-----------|-----------------------|-----------|------------|------------|-----------|
|            | c1c2                | 485.66059 | 448.02359 | c1c2                  | 4190.2452 | 3860.94775 | c1         | 3.3463872 |
|            | fetkovich constants |           |           |                       |           |            |            |           |
| Equivalent | A/w^2               | 1253.4955 |           | A/w^2                 | 7850.84   |            |            |           |
|            | c1                  | 2.2457323 |           | c1                    | 3.162023  |            |            |           |
|            | c2                  | 199.5     |           | c2                    | 1249.5    |            |            |           |
| infinite   | rd0                 | 20        |           | rd0 = 50<br>depletion | 50        |            |            |           |
| ID         | qd                  | td        | td        | qd                    | qd0       | ID         | td         | qd        |
| 0.01       | 6.1289              | 100       | 0.2056051 | 0.3394                | 0.8244699 | 600        | 0.1431897  | 0.2652    |
| 0.1        | 2.2458              | 130       | 0.2676766 | 0.3174                | 0.7710276 | 800        | 0.1909196  | 0.2915    |
| 1          | 0.98443             | 160       | 0.3294482 | 0.2975                | 0.7226865 | 1000       | 0.2386495  | 0.2393    |
| 10         | 0.53392             | 200       | 0.4118102 | 0.2728                | 0.6626853 | 1300       | 0.3102444  | 0.222     |
| 100        | 0.34556             | 240       | 0.4941723 | 0.2502                | 0.6077854 | 1600       | 0.3818392  | 0.208     |
| 1000       | 0.25098             | 300       | 0.6177153 | 0.2197                | 0.5336949 | 2000       | 0.477299   | 0.1865    |
| 10000      | 0.19593             | 400       | 0.8236205 | 0.177                 | 0.4299681 | 2400       | 0.5727588  | 0.1682    |
| 100000     | 0.16037             | 500       | 1.0295256 | 0.1426                | 0.3464037 | 3000       | 0.7159486  | 0.1543    |
| 1000000    | 0.13561             | 600       | 1.2354307 | 0.1148                | 0.278872  | 4000       | 0.9545981  | 0.1133    |
| 10000000   | 0.11742             | 700       | 1.4413358 | 0.0925                | 0.2247009 | 5000       | 1.1932476  | 0.0833    |
| 100000000  | 0.10351             | 800       | 1.6472409 | 0.0745                | 0.1809753 | 6000       | 1.4318971  | 0.0682    |
| 1E+08      | 0.092533            | 1000      | 2.0590511 | 0.0483                | 0.1173303 | 8000       | 1.9091962  | 0.0418    |
| 1E+10      | 0.083653            | 1300      | 2.6767665 | 0.0283                | 0.0887463 | 10000      | 2.3864952  | 0.0254    |
| 1E+11      | 0.076324            | 1600      | 3.2944818 | 0.0132                | 0.0320654 | 13000      | 3.1024438  | 0.012     |
| 1E+12      | 0.070173            | 2000      | 4.1181023 | 0.0058                | 0.0136035 | 16000      | 3.8183923  | 0.0056    |
|            |                     | 3000      | 6.1771534 | 0.0008                | 0.0014575 | 20000      | 4.7729904  | 0.0021    |
|            |                     |           |           |                       |           | 24000      | 5.7275885  | 0.0006    |
|            |                     |           |           |                       |           | 30000      | 7.1594856  | 0.0002    |
|            |                     |           |           |                       |           |            | 0.00066929 |           |

**Table D-6 Depletion Solutions Generalized for Figure 5.7 Continued**

| logerm              | 3.508311526 |             | logerm              | 4.111404063 |             |        |             |
|---------------------|-------------|-------------|---------------------|-------------|-------------|--------|-------------|
| c1c2                | 20238.97575 | 19273.92334 | c1c2                | 94852.62108 | 90984.07317 |        |             |
| c1                  | 4.039568499 |             | c1                  | 4.732637252 |             |        |             |
| fetkovich constants |             |             | fetkovich constants |             |             |        |             |
| A/hw^2              | 31412.78494 |             | A/hw^2              | 125860.5646 |             |        |             |
| c1                  | 3.855170186 |             | c1                  | 4.548317387 |             |        |             |
| c2                  | 4899.5      |             | c2                  | 19989.5     |             |        |             |
| rd=100              | 100         |             | rd=200              | 200         |             |        |             |
| ID                  | tdD         | qD          | qdD                 | ID          | tdD         | qD     | qdD         |
| 2000                | 0.09881923  | 0.2304      | 0.930716582         | 10000       | 0.105426712 | 0.1943 | 0.919551418 |
| 3000                | 0.148228845 | 0.2179      | 0.880221976         | 13000       | 0.137054726 | 0.186  | 0.880270529 |
| 4000                | 0.19763846  | 0.207       | 0.836190679         | 16000       | 0.16868274  | 0.182  | 0.86133998  |
| 5000                | 0.247048075 | 0.1987      | 0.794583124         | 20000       | 0.210633425 | 0.1742 | 0.824425409 |
| 6000                | 0.29845769  | 0.1869      | 0.754996353         | 24000       | 0.25302411  | 0.1688 | 0.789403894 |
| 8000                | 0.39527692  | 0.1686      | 0.681071248         | 30000       | 0.316280137 | 0.1582 | 0.739237939 |
| 10000               | 0.49409615  | 0.1536      | 0.620477722         | 40000       | 0.421705849 | 0.1401 | 0.663042479 |
| 13000               | 0.642324995 | 0.1304      | 0.526759732         | 50000       | 0.527133562 | 0.1236 | 0.584983984 |
| 16000               | 0.79055384  | 0.1118      | 0.451623758         | 60000       | 0.632580274 | 0.1126 | 0.532894955 |
| 20000               | 0.9881923   | 0.091       | 0.387600733         | 80000       | 0.843413689 | 0.0905 | 0.428303671 |
| 24000               | 1.18583076  | 0.0741      | 0.299332026         | 100000      | 1.054267124 | 0.0728 | 0.344535982 |
| 30000               | 1.482288451 | 0.0645      | 0.260552168         | 130000      | 1.370547261 | 0.0524 | 0.247990182 |
| 40000               | 1.976384601 | 0.0326      | 0.131689933         | 160000      | 1.686827308 | 0.0378 | 0.178893688 |
| 50000               | 2.470480751 | 0.0195      | 0.078771586         | 200000      | 2.108534247 | 0.0244 | 0.115476349 |
| 60000               | 2.984576901 | 0.0117      | 0.047282951         | 240000      | 2.530241067 | 0.0138 | 0.065310394 |
| 80000               | 3.952769201 | 0.0042      | 0.016986188         | 300000      | 3.162801371 | 0.0082 | 0.038807825 |
| 100000              | 4.940961502 | 0.0015      | 0.008059353         | 400000      | 4.217058495 | 0.0028 | 0.013251384 |
| 110000              | 5.435057652 | 0.0009      | 0.003635612         | 500000      | 5.271335619 | 0.0009 | 0.004259374 |

**Table D-6 Depletion Solutions Generalized for Figure 5.7 Continued**

| logterm             | 4.807263231 |           | logterm             | 5.509354525 |             |
|---------------------|-------------|-----------|---------------------|-------------|-------------|
| c1c2                | 707604.0658 | 683073.28 | c1c2                | 3177681.198 | 3078874.581 |
| c1                  | 5.648785238 |           | c1                  | 6.341817994 |             |
| fetkovich constants |             |           | fetkovich constants |             |             |
| A/hw*2              | 785395.0218 |           | A/hw*2              | 3141589.512 |             |
| c1                  | 5.464608098 |           | c1                  | 6.157755279 |             |
| c2                  | 124999.5    |           | c2                  | 499999.5    |             |
| reD=500             | 500         |           | reD=1000            | 1000        |             |
| iD                  | tdD         | qD        | qdD                 | iD          | tdD         |
| 100000              | 0.141321969 | 0.1588    | 0.884589788         | 300000      | 0.009440848 |
| 130000              | 0.18371856  | 0.1498    | 0.846188029         | 400000      | 0.012587795 |
| 160000              | 0.226115151 | 0.1435    | 0.810600682         | 500000      | 0.015734744 |
| 200000              | 0.282643938 | 0.1354    | 0.784845521         | 1000000     | 0.031469488 |
| 240000              | 0.339172726 | 0.1277    | 0.721349875         | 2000000     | 0.062938978 |
| 300000              | 0.423965908 | 0.117     | 0.680907873         | 3000000     | 0.094408484 |
| 400000              | 0.585287877 | 0.1012    | 0.571857086         | 4000000     | 0.125877952 |
| 500000              | 0.705609848 | 0.0875    | 0.494268708         | 5000000     | 0.15734744  |
| 600000              | 0.847931815 | 0.0758    | 0.427048184         | 6000000     | 0.188816927 |
| 800000              | 1.130575754 | 0.0565    | 0.319156368         | 7000000     | 0.220286415 |
| 1000000             | 1.413219692 | 0.0422    | 0.238378737         | 8000000     | 0.251755903 |
| 1300000             | 1.8371856   | 0.0273    | 0.154211837         | 9000000     | 0.283225381 |
| 1600000             | 2.261151507 | 0.0176    | 0.09941862          | 10000000    | 0.314694879 |
| 2000000             | 2.826439384 | 0.0098    | 0.055358095         | 14000000    | 0.440572831 |
| 2400000             | 3.391727261 | 0.0055    | 0.031068319         | 20000000    | 0.629389758 |
| 3000000             | 4.239659076 | 0.0023    | 0.012982206         | 24000000    | 0.75626771  |
| 4000000             | 5.852878768 | 0.0005    | 0.002824393         | 30000000    | 0.944084837 |
| 5000000             | 7.06609848  | 0.0001    | 0.000584879         | 40000000    | 1.258779516 |
|                     |             |           |                     | 50000000    | 1.573474385 |
|                     |             |           |                     | 70000000    | 2.202864153 |
|                     |             |           |                     | 84000000    | 2.643436984 |
|                     |             |           |                     | 100000000   | 3.14694879  |
|                     |             |           |                     | 140000000   | 4.405728306 |
|                     |             |           |                     | 200000000   | 6.29389758  |
|                     |             |           |                     | 300000000   | 9.44084837  |
|                     |             |           |                     |             | 0.0001      |
|                     |             |           |                     |             | 0.000634182 |

**Table D-6 Depletion Solutions Generalized for Figure 5.7 Continued**

| logterm             | 7.509354955 | logterm               | 9.509354959 |
|---------------------|-------------|-----------------------|-------------|
| c1c2                | 433124417.1 | c1c2                  | 54848038065 |
| c1                  | 8.844018489 | c1                    | 53814627319 |
| felkovich constants |             | felkovich constants   |             |
| A/hw^2              | 314159262.2 | A/hw^2                | 31415926533 |
| c1                  | 8.460340372 | c1                    | 10.78292546 |
| c2                  | 49999999.5  | c2                    | 5000000000  |
| reD=10000           | 10000       | reD= 1e5<br>depletion | 100000      |
| tD                  | tdD         | qD                    | qdD         |
| 3000000             | 0.006926416 | 0.1263                | 1.091739535 |
| 4000000             | 0.009235222 | 0.124                 | 1.071858293 |
| 5000000             | 0.011544027 | 0.1222                | 1.058299059 |
| 6000000             | 0.013852832 | 0.121                 | 1.045926237 |
| 8000000             | 0.018470443 | 0.1188                | 1.026909366 |
| 10000000            | 0.023088054 | 0.1174                | 1.014807771 |
| 12000000            | 0.027705665 | 0.1162                | 1.004434948 |
| 14000000            | 0.032323278 | 0.1152                | 0.995790983 |
| 16000000            | 0.036940887 | 0.1143                | 0.988011313 |
| 18000000            | 0.041558497 | 0.1135                | 0.981086086 |
| 20000000            | 0.046176106 | 0.1128                | 0.975045286 |
| 24000000            | 0.055411133 | 0.1115                | 0.963808061 |
| 30000000            | 0.069264162 | 0.1098                | 0.94911323  |
| 40000000            | 0.092352217 | 0.1071                | 0.92577438  |
| 50000000            | 0.115440271 | 0.105                 | 0.907621941 |
| 70000000            | 0.161616379 | 0.0998                | 0.862673045 |
| 80000000            | 0.184704433 | 0.0975                | 0.842791803 |
| 90000000            | 0.207792487 | 0.0952                | 0.82291056  |
| 100000000           | 0.230880542 | 0.093                 | 0.803883719 |
| 120000000           | 0.27705665  | 0.0887                | 0.78872444  |
| 140000000           | 0.323232758 | 0.0846                | 0.731283984 |
| 170000000           | 0.392496921 | 0.0788                | 0.681148657 |
| 200000000           | 0.481761083 | 0.0734                | 0.634470957 |
| 240000000           | 0.55411133  | 0.0688                | 0.577420435 |
| 300000000           | 0.692641625 | 0.058                 | 0.501353072 |
| 400000000           | 0.923522165 | 0.0458                | 0.395696047 |
| 500000000           | 1.154402708 | 0.0362                | 0.312913469 |
| 600000000           | 1.38528325  | 0.0286                | 0.247218928 |
| 700000000           | 1.616163791 | 0.0226                | 0.195354818 |
| 800000000           | 1.847044333 | 0.0178                | 0.153863529 |
| 1000000000          | 2.308805416 | 0.0111                | 0.086948605 |
| 1400000000          | 3.22327583  | 0.0043                | 0.03718628  |
| 2000000000          | 4.817610832 | 0.0011                | 0.00850842  |
| 3000000000          | 6.926416249 | 0.0001                | 0.000854402 |
|                     |             | 1E+11                 | 1.623219271 |
|                     |             | 1.3E+11               | 2.370185053 |
|                     |             | 1.6E+11               | 2.917150834 |

**Table D-7 Depletion Solutions Generalized for Figure 5.8**

New adaptation of Fetkovich for rectangular shape x:y=4:1 Figure 5.8

Infinite values from infq.out, finite values from table c-5 Lee book

Depletion Region Stems Various Reservoir Sizes

|    |            |                     |           |           |                       |           |            |           |            |
|----|------------|---------------------|-----------|-----------|-----------------------|-----------|------------|-----------|------------|
| CA | 5.379      | logterm             | 2.7188173 |           | logterm               | 3.5158107 |            |           |            |
|    |            | c1c2                | 625.69539 | 448.02359 | c1c2                  | 5087.3053 | 3950.94775 |           |            |
|    |            | c1                  | 3.1298306 |           | c1                    | 4.0468184 |            |           |            |
|    |            | fetkovich constants |           |           | fetkovich constants   |           |            |           |            |
|    | Equivalent | A/tw^2              | 1253.4955 |           | A/tw^2                | 7850.84   |            |           |            |
|    |            | c1                  | 2.2457323 |           | c1                    | 3.162023  |            |           |            |
|    |            | c2                  | 199.5     |           | c2                    | 1249.5    |            |           |            |
|    | infinite   | reD                 | 20        |           | reD = 50<br>depletion | 50        |            |           |            |
|    | iD         | qD                  | iD        | tdiD      | qD                    | qdD       | iD         | tdiD      | qD         |
|    | 0.01       | 6.1289              | 100       | 0.1598222 | 0.3364                | 1.0621966 | 600        | 0.1184081 | 0.2652     |
|    | 0.1        | 2.2488              | 130       | 0.2077688 | 0.3174                | 0.9833447 | 800        | 0.1578748 | 0.2915     |
|    | 1          | 0.98443             | 160       | 0.2557155 | 0.2975                | 0.9310851 | 1000       | 0.1973435 | 0.2393     |
|    | 10         | 0.53392             | 200       | 0.3196444 | 0.2728                | 0.8537632 | 1300       | 0.2585466 | 0.222      |
|    | 100        | 0.34556             | 240       | 0.3835732 | 0.2502                | 0.7830336 | 1600       | 0.3157497 | 0.206      |
|    | 1000       | 0.25096             | 300       | 0.4794865 | 0.2197                | 0.6875798 | 2000       | 0.3948871 | 0.1855     |
|    | 10000      | 0.19593             | 400       | 0.6392887 | 0.177                 | 0.5539446 | 2400       | 0.4736245 | 0.1682     |
|    | 100000     | 0.16037             | 500       | 0.7991109 | 0.1426                | 0.4462853 | 3000       | 0.5920306 | 0.1543     |
|    | 1000000    | 0.13561             | 600       | 0.9589331 | 0.1148                | 0.3592816 | 4000       | 0.7893742 | 0.1133     |
|    | 10000000   | 0.11742             | 700       | 1.1187552 | 0.0925                | 0.2894908 | 5000       | 0.9867177 | 0.0833     |
|    | 100000000  | 0.10351             | 800       | 1.2785774 | 0.0745                | 0.2331575 | 6000       | 1.1840613 | 0.0682     |
|    | 1E+09      | 0.092533            | 1000      | 1.5982218 | 0.0483                | 0.1511612 | 8000       | 1.5787484 | 0.0418     |
|    | 1E+10      | 0.083653            | 1300      | 2.0776863 | 0.0283                | 0.0885885 | 10000      | 1.9734355 | 0.0254     |
|    | 1E+11      | 0.076324            | 1600      | 2.5571548 | 0.0132                | 0.0413111 | 13000      | 2.5854661 | 0.012      |
|    | 1E+12      | 0.070173            | 2000      | 3.1964435 | 0.0056                | 0.0175259 | 16000      | 3.1574968 | 0.0056     |
|    |            |                     | 3000      | 4.7948653 | 0.0006                | 0.0018778 | 20000      | 3.946871  | 0.0021     |
|    |            |                     |           |           |                       |           | 24000      | 4.7362452 | 0.0006     |
|    |            |                     |           |           |                       |           | 30000      | 5.9203065 | 0.0002     |
|    |            |                     |           |           |                       |           |            |           | 0.00080936 |

**Table D-7 Depletion Solutions Generalized for Figure 5.8 Continued**

| logterm             | 4.117800969  |             | logterm             | 4.719883534 |             |        |             |
|---------------------|--------------|-------------|---------------------|-------------|-------------|--------|-------------|
| c1c2                | 23748.28893  | 19273.92334 | c1c2                | 108890.8467 | 90984.07317 |        |             |
| c1                  | 4.740000695  |             | c1                  | 5.433089447 |             |        |             |
| fetkovich constants |              |             | fetkovich constants |             |             |        |             |
| A/tw^2              | 31412.78494  |             | A/tw^2              | 125660.5646 |             |        |             |
| c1                  | 3.855170186  |             | c1                  | 4.548317367 |             |        |             |
| c2                  | 4999.5       |             | c2                  | 19999.5     |             |        |             |
| reD=100             | 100          |             | reD=200             | 200         |             |        |             |
| tD                  | tdD          | qd          | qdD                 | tD          | tdD         | qd     | qdD         |
| 2000                | 0.084216685  | 0.2304      | 1.06209616          | 10000       | 0.091835083 | 0.1943 | 1.055645364 |
| 3000                | 0.126324997  | 0.2179      | 1.032846151         | 13000       | 0.119385609 | 0.186  | 1.010550917 |
| 4000                | 0.168433329  | 0.207       | 0.981180144         | 16000       | 0.146938134 | 0.182  | 0.968818639 |
| 5000                | 0.210541662  | 0.1967      | 0.932358137         | 20000       | 0.183670167 | 0.1742 | 0.946440666 |
| 6000                | 0.252649994  | 0.1869      | 0.88590813          | 24000       | 0.2204042   | 0.1668 | 0.908235984 |
| 8000                | 0.336886658  | 0.1686      | 0.799164117         | 30000       | 0.27550525  | 0.1562 | 0.848645448 |
| 10000               | 0.421083323  | 0.1536      | 0.728064107         | 40000       | 0.367340334 | 0.1401 | 0.78117303  |
| 13000               | 0.54740832   | 0.1304      | 0.618096091         | 50000       | 0.459175417 | 0.1236 | 0.671527384 |
| 16000               | 0.673733317  | 0.1118      | 0.529932078         | 60000       | 0.551010501 | 0.1126 | 0.61176362  |
| 20000               | 0.842166848  | 0.091       | 0.431340063         | 80000       | 0.734680688 | 0.0905 | 0.491692785 |
| 24000               | 1.010599975  | 0.0741      | 0.351234052         | 100000      | 0.918350835 | 0.0728 | 0.396527456 |
| 30000               | 1.263249989  | 0.0645      | 0.305730045         | 130000      | 1.193856065 | 0.0524 | 0.284692839 |
| 40000               | 1.684333282  | 0.0326      | 0.154524023         | 160000      | 1.469381336 | 0.0378 | 0.205370025 |
| 50000               | 2.105416615  | 0.0195      | 0.092430014         | 200000      | 1.83670167  | 0.0244 | 0.132566895 |
| 60000               | 2.526499938  | 0.0117      | 0.055458008         | 240000      | 2.204042004 | 0.0138 | 0.074976358 |
| 80000               | 3.3688666585 | 0.0042      | 0.019608003         | 300000      | 2.755052505 | 0.0082 | 0.044551169 |
| 100000              | 4.210833231  | 0.0015      | 0.007110001         | 400000      | 3.67340334  | 0.0028 | 0.015212594 |
| 110000              | 4.631916554  | 0.0009      | 0.004286001         | 500000      | 4.591754174 | 0.0009 | 0.004889763 |

**Table D-7 Depletion Solutions Generalized for Figure 5.8 Continued**

| logterm             | 5.515782672 |           | logterm             | 6.117843986 |             |
|---------------------|-------------|-----------|---------------------|-------------|-------------|
| c1c2                | 796344.8187 | 683073.28 | c1c2                | 3528645.262 | 3078874.581 |
| c1                  | 6.349217433 |           | c1                  | 7.042250189 |             |
| fetkovich constants |             |           | fetkovich constants |             |             |
| A/hw^2              | 785395.0218 |           | A/hw^2              | 3141589.512 |             |
| c1                  | 5.464608098 |           | c1                  | 6.157755279 |             |
| c2                  | 124899.5    |           | c2                  | 499999.5    |             |
| reD=500             | 500         |           | reD=1000            | 1000        |             |
| ID                  | tdID        | qD        | qdD                 | ID          | tdID        |
| 100000              | 0.125731629 | 0.1586    | 0.69428745          | 30000       | 0.008501848 |
| 130000              | 0.163451118 | 0.1498    | 0.951112772         | 40000       | 0.011335795 |
| 160000              | 0.201170607 | 0.1435    | 0.911112702         | 50000       | 0.014169744 |
| 200000              | 0.251463259 | 0.1354    | 0.85968404          | 100000      | 0.028339488 |
| 240000              | 0.301755911 | 0.1277    | 0.810795086         | 200000      | 0.058678976 |
| 300000              | 0.377194888 | 0.117     | 0.74285844          | 300000      | 0.085018484 |
| 400000              | 0.502926518 | 0.1012    | 0.642540804         | 400000      | 0.113357952 |
| 500000              | 0.628658147 | 0.0875    | 0.555558525         | 500000      | 0.14169744  |
| 600000              | 0.754389776 | 0.0756    | 0.480000838         | 600000      | 0.170036928 |
| 800000              | 1.005853035 | 0.0685    | 0.358730785         | 700000      | 0.198376416 |
| 1000000             | 1.257316294 | 0.0422    | 0.287936976         | 800000      | 0.226715904 |
| 1300000             | 1.634511182 | 0.0273    | 0.173333636         | 900000      | 0.255055382 |
| 1600000             | 2.011706071 | 0.0176    | 0.111746227         | 1000000     | 0.28339488  |
| 2000000             | 2.514632588 | 0.0098    | 0.062222331         | 1400000     | 0.396752832 |
| 2400000             | 3.017559108 | 0.0055    | 0.034920698         | 2000000     | 0.58678976  |
| 3000000             | 3.771948882 | 0.0023    | 0.0146032           | 2400000     | 0.680147712 |
| 4000000             | 5.029265176 | 0.0005    | 0.003174609         | 3000000     | 0.85018464  |
| 5000000             | 6.28658147  | 0.0001    | 0.000634922         | 4000000     | 1.133579518 |
|                     |             |           |                     | 5000000     | 1.416974398 |
|                     |             |           |                     | 7000000     | 1.983764158 |
|                     |             |           |                     | 8400000     | 2.380516991 |
|                     |             |           |                     | 10000000    | 2.833948798 |
|                     |             |           |                     | 14000000    | 3.987528318 |
|                     |             |           |                     | 20000000    | 5.687897597 |
|                     |             |           |                     | 30000000    | 8.501846395 |
|                     |             |           |                     |             | 0.0001      |
|                     |             |           |                     |             | 0.000704225 |

**Table D-7 Depletion Solutions Generalized for Figure 5.8 Continued**

| logarm              | 8.117844396 | logarm                | 10.1178444  |
|---------------------|-------------|-----------------------|-------------|
| c1c2                | 468220858.2 | c1c2                  | 58357682217 |
| c1                  | 9.344450684 | c1                    | 53814627319 |
| fetkovich constants |             | fetkovich constants   |             |
| A/hw^2              | 314159262.2 | A/hw^2                | 31415926533 |
| c1                  | 8.460340372 | c1                    | 10.76292546 |
| c2                  | 49999999.5  | c2                    | 5000000000  |
| reD=10000           | 10000       | reD= 1e5<br>depletion | 100000      |
| ID                  | tdID        | qD                    | qdD         |
| ID                  | tdID        | qD                    | qdD         |
| 3000000             | 0.005407233 | 0.1263                | 1.180204121 |
| 4000000             | 0.008542977 | 0.124                 | 1.158711885 |
| 5000000             | 0.010678721 | 0.1222                | 1.141891874 |
| 6000000             | 0.012814465 | 0.121                 | 1.130678533 |
| 8000000             | 0.017085954 | 0.1188                | 1.110120741 |
| 10000000            | 0.021357442 | 0.1174                | 1.09703851  |
| 12000000            | 0.025628931 | 0.1162                | 1.085825169 |
| 14000000            | 0.029900419 | 0.1152                | 1.076480719 |
| 16000000            | 0.034171908 | 0.1143                | 1.068070713 |
| 18000000            | 0.038443398 | 0.1135                | 1.060565153 |
| 20000000            | 0.042714885 | 0.1128                | 1.054054037 |
| 24000000            | 0.051257862 | 0.1115                | 1.041908251 |
| 30000000            | 0.084072327 | 0.1098                | 1.026020685 |
| 40000000            | 0.08542977  | 0.1071                | 1.000790668 |
| 50000000            | 0.106787212 | 0.105                 | 9.981167322 |
| 70000000            | 0.149502097 | 0.0998                | 9.932578178 |
| 80000000            | 0.170859539 | 0.0975                | 9.911083942 |
| 90000000            | 0.192216981 | 0.0952                | 9.889591705 |
| 100000000           | 0.213574424 | 0.093                 | 9.869033914 |
| 120000000           | 0.256289309 | 0.0887                | 9.828852778 |
| 140000000           | 0.299004193 | 0.0846                | 9.790540528 |
| 170000000           | 0.36307652  | 0.0788                | 9.736342714 |
| 200000000           | 0.427148848 | 0.0734                | 9.68588268  |
| 240000000           | 0.512578617 | 0.0688                | 9.624208308 |
| 300000000           | 0.640723271 | 0.058                 | 9.54197814  |
| 400000000           | 0.854297695 | 0.0458                | 9.427975841 |
| 500000000           | 1.067872119 | 0.0362                | 9.338269115 |
| 600000000           | 1.261446543 | 0.0286                | 9.25725129  |
| 700000000           | 1.495020966 | 0.0226                | 9.211184585 |
| 800000000           | 1.70859539  | 0.0178                | 9.168331222 |
| 1000000000          | 2.135744238 | 0.0111                | 9.103723403 |
| 1400000000          | 2.980041933 | 0.0043                | 9.040181138 |
| 2000000000          | 4.271488476 | 0.0011                | 9.010278866 |
| 3000000000          | 6.407232713 | 0.0001                | 9.000934445 |
|                     |             | 1E+11                 | 1.713570454 |
|                     |             | 1.3E+11               | 2.22764159  |
|                     |             | 1.6E+11               | 2.741712726 |

**Table D-8 Derivative Solutions for Type Curve**

| red<br>c1<br>1.8025851 |           |           |          | red<br>c1<br>2.49573227 |            |            |          | red<br>c1<br>3.412023 |            |          |          |
|------------------------|-----------|-----------|----------|-------------------------|------------|------------|----------|-----------------------|------------|----------|----------|
| ID                     | qD'       | qDd'      | qDd^2ID  | ID                      | qD'        | qDd'       | qDd^2ID  | ID                    | qD'        | qDd'     | qDd^2ID  |
| 8.97E-05               |           |           |          | 8.03E-05                |            |            |          | 7.04E-05              |            |          |          |
| 1.01E-04               | 29775.045 | 53672.053 | 5.41E+00 | 1.00E-04                | 13000.0852 | 32444.7321 | 3.26E+00 | 9.38E-05              | 5179.77644 | 17673.52 | 1.88E+00 |
| 1.12E-04               | 28155.888 | 47148.211 | 5.28E+00 | 1.21E-04                | 9828.41694 | 24524.1059 | 2.98E+00 | 1.17E-04              | 3675.76078 | 12541.78 | 1.47E+00 |
| 2.24E-04               | 10675.902 | 19244.222 | 4.31E+00 | 1.41E-04                | 7772.56857 | 19398.2502 | 2.73E+00 | 1.41E-04              | 2716.94699 | 9270.285 | 1.30E+00 |
| 3.38E-04               | 5241.0206 | 9447.3856 | 3.18E+00 | 1.61E-04                | 8350.64695 | 15849.5148 | 2.55E+00 | 1.64E-04              | 2222.341   | 7582.679 | 1.25E+00 |
| 4.48E-04               | 3299.2985 | 5947.2653 | 2.67E+00 | 1.81E-04                | 5319.78653 | 13276.7208 | 2.40E+00 | 1.88E-04              | 1928.57308 | 6580.338 | 1.23E+00 |
| 5.60E-04               | 2329.7772 | 4199.8217 | 2.35E+00 | 2.01E-04                | 4676.77478 | 11671.9777 | 2.34E+00 | 2.35E-04              | 1397.80868 | 4769.355 | 1.12E+00 |
| 6.72E-04               | 1760.9755 | 3174.3081 | 2.13E+00 | 4.02E-04                | 1923.1715  | 4799.72118 | 1.93E+00 | 4.89E-04              | 571.768351 | 1950.887 | 0.9152   |
| 7.85E-04               | 1302.8547 | 2510.7392 | 1.97E+00 | 6.03E-04                | 952.948998 | 2378.30481 | 1.43E+00 | 7.04E-04              | 280.444828 | 991.0044 | 0.86735  |
| 8.97E-04               | 1138.0568 | 2051.4622 | 1.84E+00 | 8.03E-04                | 604.881326 | 1509.62185 | 1.21E+00 | 9.38E-04              | 187.61149  | 640.1347 | 0.8006   |
| 1.01E-03               | 953.16004 | 1718.1521 | 1.73E+00 | 1.00E-03                | 429.33279  | 1071.4997  | 1.08E+00 | 1.17E-03              | 135.375153 | 461.9031 | 0.54172  |
| 1.12E-03               | 838.49914 | 1511.406  | 1.69E+00 | 1.21E-03                | 317.272174 | 791.826404 | 0.95423  | 1.41E-03              | 104.269374 | 355.7695 | 0.50071  |
| 2.24E-03               | 344.65141 | 621.2635  | 1.39E+00 | 1.41E-03                | 259.548272 | 647.782999 | 0.91089  | 1.84E-03              | 83.7849331 | 285.8781 | 0.46938  |
| 3.38E-03               | 170.74072 | 307.77467 | 1.03E+00 | 1.61E-03                | 225.261315 | 582.191934 | 0.90333  | 1.88E-03              | 69.4726752 | 237.0424 | 0.44481  |
| 4.48E-03               | 108.40747 | 195.41358 | 0.87602  | 2.01E-03                | 163.252198 | 407.433778 | 0.81829  | 2.11E-03              | 58.9800003 | 201.2411 | 0.42482  |
| 5.60E-03               | 76.949077 | 138.70726 | 0.77726  | 4.02E-03                | 66.7813323 | 166.688326 | 0.68949  | 2.35E-03              | 52.3375457 | 178.5789 | 0.41887  |
| 6.72E-03               | 58.875093 | 102.5222  | 0.68939  | 6.03E-03                | 33.9061565 | 84.6181933 | 0.50985  | 4.89E-03              | 22.9781905 | 78.40211 | 0.3678   |
| 7.85E-03               | 48.504391 | 83.828122 | 0.65764  | 8.03E-03                | 21.9055019 | 54.6702681 | 0.43921  | 7.04E-03              | 12.1825843 | 41.58719 | 0.2925   |
| 8.97E-03               | 40.377147 | 72.783243 | 0.65256  | 1.00E-02                | 15.8198759 | 39.4821749 | 0.39648  | 9.38E-03              | 8.08422472 | 27.58358 | 0.2588   |
| 1.12E-02               | 29.2601   | 52.743821 | 0.5911   | 1.21E-02                | 12.178453  | 30.3941582 | 0.36828  | 1.17E-02              | 5.94734046 | 20.29246 | 0.23799  |
| 2.24E-02               | 11.986644 | 21.570893 | 0.48349  | 1.41E-02                | 9.78553815 | 24.4220784 | 0.34335  | 1.41E-02              | 4.84819298 | 15.85974 | 0.22321  |
| 3.38E-02               | 6.0783893 | 10.956814 | 0.36839  | 1.61E-02                | 8.1091879  | 20.238362  | 0.32519  | 1.84E-02              | 3.78819075 | 12.91857 | 0.21211  |
| 4.48E-02               | 3.9279484 | 7.0804613 | 0.31741  | 1.81E-02                | 6.88429028 | 17.1813454 | 0.31057  | 1.88E-02              | 3.17368036 | 10.82667 | 0.2032   |
| 5.60E-02               | 2.8339864 | 5.1085017 | 0.28626  | 2.01E-02                | 6.11619873 | 15.2643896 | 0.30657  | 2.11E-02              | 2.71783929 | 9.27333  | 0.19578  |
| 6.72E-02               | 2.1828836 | 3.9348334 | 0.26459  | 4.02E-02                | 2.68426063 | 6.6891959  | 0.2691   | 2.35E-02              | 2.42889095 | 8.287432 | 0.19439  |
| 7.85E-02               | 1.7546986 | 3.1829935 | 0.24814  | 6.03E-02                | 1.42343802 | 3.55252021 | 0.21405  | 4.89E-02              | 1.1139237  | 3.800733 | 0.1783   |
| 8.97E-02               | 1.4533199 | 2.6197328 | 0.23488  | 8.03E-02                | 0.94712206 | 2.3837631  | 0.1899   | 7.04E-02              | 0.61879097 | 2.111329 | 0.14857  |
| 0.10087                | 1.2360667 | 2.2281154 | 0.22475  | 1.00E-01                | 0.70752129 | 1.76578371 | 0.17732  | 9.38E-02              | 0.43684797 | 1.490877 | 0.13988  |
| 0.11207                | 1.1052608 | 1.9823262 | 0.22328  | 0.12051                 | 0.57221573 | 1.42809725 | 0.1721   | 1.17E-01              | 0.3537087  | 1.206865 | 0.14154  |
| 0.22414                | 0.5845577 | 1.0717409 | 0.24022  | 0.14059                 | 0.49197007 | 1.22782559 | 0.17262  | 0.14074               | 0.31194808 | 1.054374 | 0.1498   |
| 0.33622                | 0.4441272 | 0.800577  | 0.26917  | 0.16068                 | 0.44168006 | 1.10231518 | 0.17712  | 0.16419               | 0.28856303 | 0.984662 | 0.16167  |
|                        |           |           |          | 0.18076                 | 0.40886349 | 1.02041381 | 0.18445  | 0.18765               | 0.27398421 | 0.934772 | 0.17541  |
|                        |           |           |          | 0.20084                 | 0.38985093 | 0.97298355 | 0.19541  | 0.21111               | 0.26364958 | 0.899578 | 0.18991  |
|                        |           |           |          | 0.40169                 | 0.29780231 | 0.74323483 | 0.29655  | 0.23456               | 0.25600878 | 0.873508 | 0.20489  |

**Table D-8 Derivative Solutions For Type Curve Continued**

| ID       | qD'      | 100      |          |                     | ID         | 200         |            |                     | ID       | 1000     |          |                     |
|----------|----------|----------|----------|---------------------|------------|-------------|------------|---------------------|----------|----------|----------|---------------------|
|          |          | c1       | 4.10517  | qDd <sup>m</sup> ID |            | c1          | 4.79831737 | qDd <sup>m</sup> ID |          | c1       | 6.407755 | qDd <sup>m</sup> ID |
| 3.41E-06 |          |          |          | 7.29E-06            |            |             |            |                     | 6.24E-05 |          |          |                     |
| 3.90E-05 | 9286.604 | 38123.09 | 1.49E+00 | 8.34E-06            | 43418.727  | 208336.832  | 1.74E+00   | 9.38E-05            | 480.731  | 2952.252 | 0.27644  |                     |
| 4.87E-05 | 6727.817 | 27618.83 | 1.35E+00 | 1.04E-05            | 31457.9456 | 150945.207  | 1.573      | 1.25E-04            | 312.7468 | 2004.005 | 0.2502   |                     |
| 9.74E-05 | 2752.72  | 11300.39 | 1.10E+00 | 2.08E-05            | 8580.3808  | 41171.3902  | 1.2871     | 1.58E-04            | 234.0113 | 1499.487 | 0.23401  |                     |
| 1.48E-04 | 1397.86  | 5738.455 | 0.83879  | 3.13E-05            | 4902.61508 | 23624.3031  | 0.98054    | 1.87E-04            | 185.2384 | 1188.949 | 0.22228  |                     |
| 1.95E-04 | 903.1022 | 3707.388 | 0.72257  | 4.17E-05            | 3378.34906 | 16210.381   | 0.84461    | 2.18E-04            | 152.4824 | 977.0699 | 0.21348  |                     |
| 2.44E-04 | 651.9838 | 2678.504 | 0.65205  | 5.21E-05            | 2539.956   | 12187.515   | 0.782      | 2.50E-04            | 128.7812 | 825.0701 | 0.20802  |                     |
| 2.92E-04 | 501.9476 | 2080.58  | 0.60239  | 6.25E-05            | 2010.8371  | 9848.63457  | 0.70381    | 2.81E-04            | 111.2554 | 712.8974 | 0.20026  |                     |
| 3.41E-04 | 403.1924 | 1655.173 | 0.56453  | 7.29E-05            | 1650.12682 | 7917.83122  | 0.68007    | 3.12E-04            | 100.2206 | 642.1889 | 0.20044  |                     |
| 3.90E-04 | 334.4877 | 1373.047 | 0.5362   | 8.34E-05            | 1300.19073 | 6670.57832  | 0.6256     | 6.24E-04            | 47.32527 | 303.2488 | 0.1893   |                     |
| 4.39E-04 | 283.963  | 1165.717 | 0.51119  | 9.38E-05            | 1194.04202 | 5729.39257  | 0.59708    | 9.38E-04            | 26.82487 | 171.8872 | 0.16096  |                     |
| 4.87E-04 | 251.7544 | 1033.495 | 0.50356  | 1.04E-04            | 588.798801 | 2825.20033  | 0.5888     | 1.25E-03            | 18.51982 | 118.6692 | 0.1482   |                     |
| 9.74E-04 | 103.1395 | 423.4053 | 0.4126   | 2.08E-04            | 344.88651  | 1854.78858  | 0.51732    | 1.58E-03            | 14.00108 | 897.1549 | 0.14001  |                     |
| 1.48E-03 | 58.66818 | 240.8429 | 0.36204  | 3.13E-04            | 205.721436 | 987.116741  | 0.41145    | 1.87E-03            | 11.20354 | 71.7893  | 0.13439  |                     |
| 1.95E-03 | 38.894   | 159.6665 | 0.31119  | 4.17E-04            | 145.600081 | 698.635395  | 0.38401    | 2.18E-03            | 9.299083 | 59.58625 | 0.13019  |                     |
| 2.44E-03 | 28.62409 | 117.5058 | 0.28627  | 5.21E-04            | 111.5814   | 535.402972  | 0.33475    | 2.50E-03            | 7.900544 | 50.62475 | 0.12841  |                     |
| 2.92E-03 | 22.39803 | 91.94773 | 0.2688   | 6.25E-04            | 89.7408875 | 430.604298  | 0.3141     | 2.81E-03            | 6.850546 | 43.89682 | 0.12331  |                     |
| 3.41E-03 | 18.24733 | 74.90838 | 0.25549  | 7.29E-04            | 74.570808  | 357.814403  | 0.29819    | 3.12E-03            | 6.175035 | 39.56811 | 0.1235   |                     |
| 3.90E-03 | 15.27353 | 62.70043 | 0.2444   | 8.33E-04            | 63.4652289 | 304.52831   | 0.2858     | 6.24E-03            | 2.997517 | 19.20736 | 0.1199   |                     |
| 4.39E-03 | 13.073   | 53.66688 | 0.23534  | 9.38E-04            | 56.0884037 | 284.235878  | 0.27536    | 9.38E-03            | 1.732491 | 11.10138 | 0.10395  |                     |
| 4.87E-03 | 11.69381 | 48.00509 | 0.2339   | 1.04E-03            | 27.3235287 | 131.108953  | 0.27324    | 1.25E-02            | 1.212513 | 7.769483 | 0.097    |                     |
| 9.74E-03 | 5.359458 | 22.00148 | 0.2144   | 2.08E-03            | 16.7067767 | 80.1644169  | 0.25061    | 0.01581             | 0.925086 | 5.927592 | 0.09251  |                     |
| 1.48E-02 | 2.952241 | 12.11945 | 0.17715  | 3.13E-03            | 10.3498207 | 49.8617245  | 0.207      | 0.01873             | 0.742454 | 4.757462 | 0.08909  |                     |
| 1.95E-02 | 2.002131 | 8.219087 | 0.16019  | 4.17E-03            | 7.48579822 | 35.9872188  | 0.1874     | 0.02185             | 0.619929 | 3.972356 | 0.08879  |                     |
| 2.44E-02 | 1.499848 | 6.15713  | 0.15     | 5.21E-03            | 5.84156548 | 28.0296851  | 0.17525    | 0.02497             | 0.530038 | 3.396356 | 0.08481  |                     |
| 2.92E-02 | 1.187398 | 4.874481 | 0.1425   | 6.25E-03            | 4.74845662 | 22.7848019  | 0.1662     | 0.02808             | 0.455888 | 2.92122  | 0.08206  |                     |
| 3.41E-02 | 0.977395 | 4.012373 | 0.13685  | 7.29E-03            | 3.99838277 | 19.1856085  | 0.15994    | 0.03121             | 0.415797 | 2.884328 | 0.08316  |                     |
| 3.90E-02 | 0.82742  | 3.396701 | 0.1324   | 8.34E-03            | 3.43992207 | 16.5058378  | 0.1548     | 0.06242             | 0.224324 | 1.437412 | 0.08673  |                     |
| 4.39E-02 | 0.712421 | 2.92461  | 0.12825  | 9.38E-03            | 2.99840432 | 14.3776889  | 0.14983    | 0.09364             | 0.164171 | 1.051987 | 0.09885  |                     |
| 4.87E-02 | 0.641935 | 2.635252 | 0.1284   | 1.04E-02            | 1.49337413 | 7.16588303  | 0.14934    | 0.12485             | 0.149073 | 0.955226 | 0.11926  |                     |
| 9.74E-02 | 0.336686 | 1.38207  | 0.13468  | 2.08E-02            | 0.94530184 | 4.53585823  | 0.1418     | 0.15808             | 0.142411 | 0.912534 | 0.14241  |                     |
| 1.48E-01 | 0.245045 | 1.005952 | 0.14704  | 3.13E-02            | 0.60223957 | 2.88973658  | 0.12045    | 0.16727             | 0.137536 | 0.881294 | 0.16504  |                     |
| 0.1949   | 0.220623 | 0.905695 | 0.17652  | 4.17E-02            | 0.44398805 | 2.130396556 | 0.111      | 0.21849             | 0.133111 | 0.852945 | 0.18636  |                     |
| 0.24362  | 0.207549 | 0.852024 | 0.20757  | 5.21E-02            | 0.34359405 | 1.64867329  | 0.10572    | 0.2497              | 0.128836 | 0.825551 | 0.20814  |                     |
| 0.29234  | 0.198924 | 0.808408 | 0.23833  | 6.25E-02            | 0.2940786  | 1.41106247  | 0.10308    | 0.28091             | 0.124811 | 0.799758 | 0.22468  |                     |
| 0.34107  | 0.187101 | 0.768083 | 0.28197  | 7.29E-02            | 0.26199232 | 1.25712229  | 0.10293    | 0.31212             | 0.121126 | 0.778144 | 0.24225  |                     |
| 0.38879  | 0.177627 | 0.729188 | 0.28423  | 8.34E-02            | 0.24086121 | 1.15476889  | 0.1048     |                     |          |          |          |                     |
|          |          |          |          | 9.38E-02            | 0.22896505 | 1.09864896  | 0.1083     |                     |          |          |          |                     |
|          |          |          |          | 0.10421             | 0.18522679 | 0.88877693  | 0.11449    |                     |          |          |          |                     |
|          |          |          |          | 0.20841             | 0.16387454 | 0.78832205  | 0.18523    |                     |          |          |          |                     |
|          |          |          |          | 0.31262             | 0.14684745 | 0.70510052  | 0.24582    |                     |          |          |          |                     |
|          |          |          |          | 0.41682             |            | 0.2939      |            |                     |          |          |          |                     |

**Table D-8 Derivative Solutions For Type Curve Continued**

| red<br>c1<br>10000<br>8.71034037 |          |            |         | red<br>c1<br>100000<br>11.0129255 |        |            |         |
|----------------------------------|----------|------------|---------|-----------------------------------|--------|------------|---------|
| ID                               | qD'      | qdD'       | qdD^2D  | ID                                | qD'    | qdD'       | qdD^2D  |
| 1.84E-06                         |          |            |         | 7.28E-06                          |        |            |         |
| 2.07E-05                         | 932.5598 | 8122.91314 | 0.16786 | 9.08E-08                          | 1120.1 | 12335.8314 | 0.11201 |
| 2.30E-05                         | 843.9079 | 7350.72514 | 0.16878 | 1.09E-05                          | 905.11 | 9867.87812 | 0.10861 |
| 4.50E-05                         | 407.5038 | 3549.49897 | 0.183   | 1.27E-05                          | 757.52 | 8342.51101 | 0.10605 |
| 6.89E-05                         | 235.4988 | 2051.27461 | 0.1413  | 1.45E-05                          | 650.02 | 7158.59031 | 0.104   |
| 9.18E-05                         | 164.4873 | 1432.73894 | 0.13158 | 1.63E-05                          | 570.02 | 6277.53304 | 0.1026  |
| 1.15E-04                         | 125.7357 | 1086.20077 | 0.12574 | 1.82E-05                          | 516.56 | 5688.87665 | 0.10331 |
| 1.38E-04                         | 101.0063 | 879.799868 | 0.12121 | 3.63E-05                          | 256.75 | 2827.58532 | 0.1027  |
| 1.61E-04                         | 84.25636 | 733.901574 | 0.11798 | 5.45E-05                          | 152.25 | 1678.73134 | 0.09135 |
| 1.84E-04                         | 72.00614 | 627.197997 | 0.11521 | 7.28E-05                          | 107.75 | 1188.62757 | 0.0862  |
| 2.07E-04                         | 62.75584 | 546.624728 | 0.11298 | 9.08E-05                          | 83.255 | 916.885091 | 0.08326 |
| 2.30E-04                         | 56.94053 | 485.97143  | 0.11388 | 1.09E-04                          | 67.502 | 743.39207  | 0.081   |
| 4.59E-04                         | 27.95026 | 243.458295 | 0.1118  | 1.27E-04                          | 58.501 | 622.246696 | 0.0791  |
| 6.89E-04                         | 16.39958 | 142.845944 | 0.0984  | 1.45E-04                          | 48.751 | 536.894273 | 0.078   |
| 9.18E-04                         | 11.54936 | 100.598835 | 0.0924  | 1.63E-04                          | 48.095 | 529.66685  | 0.07695 |
| 1.15E-03                         | 8.874297 | 77.2981448 | 0.08875 | 1.82E-04                          | 42.941 | 472.901371 | 0.07729 |
| 1.38E-03                         | 7.150359 | 62.2820843 | 0.08581 | 3.63E-04                          | 38.901 | 428.40859  | 0.0778  |
| 1.61E-03                         | 5.975302 | 52.046911  | 0.08368 | 5.45E-04                          | 17.437 | 192.037684 | 0.08975 |
| 1.84E-03                         | 5.150242 | 44.8803626 | 0.0824  | 7.28E-04                          | 11.087 | 121.875516 | 0.0884  |
| 2.07E-03                         | 4.500243 | 38.1986451 | 0.081   | 9.08E-04                          | 8.0312 | 88.4474546 | 0.08425 |
| 2.30E-03                         | 4.057488 | 35.3421018 | 0.08115 | 1.09E-03                          | 6.2404 | 68.7253585 | 0.0824  |
| 4.59E-03                         | 2.029994 | 17.6819389 | 0.0812  | 1.27E-03                          | 5.1043 | 56.2132893 | 0.08125 |
| 6.89E-03                         | 1.202477 | 10.4739853 | 0.07215 | 1.45E-03                          | 4.3144 | 47.5141598 | 0.0804  |
| 9.18E-03                         | 0.854949 | 7.44686422 | 0.0684  | 1.63E-03                          | 3.7407 | 41.1963105 | 0.05985 |
| 1.15E-02                         | 0.657448 | 5.72659176 | 0.08575 | 1.82E-03                          | 3.3799 | 37.2222222 | 0.05084 |
| 1.38E-02                         | 0.532531 | 4.83852798 | 0.08391 | 3.63E-03                          | 3.05   | 33.5887577 | 0.051   |
| 1.61E-02                         | 0.450024 | 3.91986561 | 0.083   | 5.45E-03                          | 1.3782 | 15.156521  | 0.05505 |
| 1.84E-02                         | 0.385018 | 3.35383928 | 0.0816  | 7.28E-03                          | 0.8733 | 9.61803197 | 0.0524  |
| 2.07E-02                         | 0.335018 | 2.91812243 | 0.0803  | 9.08E-03                          | 0.6375 | 7.02114479 | 0.051   |
| 0.022981                         | 0.304823 | 2.65511084 | 0.08098 | 1.09E-02                          | 0.115  | 4.57075991 | 0.0488  |
| 0.045922                         | 0.166898 | 1.45374788 | 0.08678 | 0.012712                          | 0.35   | 3.85462555 | 0.049   |
| 0.068884                         | 0.122848 | 1.07004529 | 0.07371 | 0.014528                          | 0.3025 | 3.3314978  | 0.0484  |
| 0.091845                         | 0.112057 | 0.97814459 | 0.08965 | 0.016344                          | 0.285  | 2.9185022  | 0.0477  |
| 0.11481                          | 0.107798 | 0.9389426  | 0.1078  | 0.01816                           | 0.2419 | 2.66365839 | 0.04837 |
| 0.13777                          | 0.105008 | 0.91464034 | 0.12601 | 0.036321                          | 0.1324 | 1.4580821  | 0.05298 |
| 0.16073                          | 0.102508 | 0.89288381 | 0.14351 | 0.0544481                         | 0.098  | 1.07955087 | 0.05882 |
| 0.18369                          | 0.100058 | 0.87152267 | 0.16009 | 0.072642                          | 0.0897 | 0.96758294 | 0.07174 |
| 0.20665                          | 0.097778 | 0.85168159 | 0.178   | 0.090802                          | 0.0866 | 0.95380058 | 0.08661 |
| 0.22961                          | 0.095651 | 0.83315187 | 0.1913  | 0.10988                           | 0.0848 | 0.93346182 | 0.10171 |
| 0.45922                          | 0.078168 | 0.66345107 | 0.30467 | 0.12712                           | 0.0832 | 0.9157489  | 0.11641 |
|                                  |          |            |         | 0.14528                           | 0.0816 | 0.89812775 | 0.13048 |
|                                  |          |            |         | 0.16344                           | 0.0801 | 0.88215859 | 0.14418 |
|                                  |          |            |         | 0.1816                            | 0.0788 | 0.86734581 | 0.15751 |
|                                  |          |            |         | 0.36321                           | 0.0657 | 0.72382368 | 0.2629  |
|                                  |          |            |         | 0.54481                           | 0.0546 | 0.60131056 | 0.3276  |
|                                  |          |            |         | 0.72642                           | 0.0454 | 0.49951819 | 0.38288 |
|                                  |          |            |         | 0.90802                           | 0.0377 | 0.4148587  | 0.3787  |
|                                  |          |            |         | 1.09E+00                          | 0.0313 | 0.34440162 | 0.37526 |

**Table D-9 Arps Derivative Solutions For Type Curve**

| b values | 0          | 0.1        | 0.2     | 0.3     | 0.4      | 0.5      | 0.6     | 0.7      | 0.8      | 0.9        | 1       |
|----------|------------|------------|---------|---------|----------|----------|---------|----------|----------|------------|---------|
| tDd      | qDdtDd     |            |         |         |          |          |         |          |          |            |         |
| 0.1      | 0.09048374 | 0.08963237 | 0.0888  | 0.08798 | 0.087173 | 0.086384 | 0.08561 | 0.084848 | 0.0841   | 0.08336591 | 0.08264 |
| 0.5      | 0.30326533 | 0.29233964 | 0.28224 | 0.27285 | 0.264141 | 0.256    | 0.24838 | 0.241238 | 0.234521 | 0.228194   | 0.22222 |
| 1        | 0.36787944 | 0.3504939  | 0.3349  | 0.32081 | 0.308001 | 0.296298 | 0.28555 | 0.275638 | 0.266463 | 0.25794068 | 0.25    |
| 1.5      | 0.33469524 | 0.32241483 | 0.31076 | 0.2998  | 0.289515 | 0.279883 | 0.27086 | 0.262407 | 0.254472 | 0.24701639 | 0.24    |
| 2        | 0.27067057 | 0.26917597 | 0.26582 | 0.26092 | 0.255809 | 0.25     | 0.24429 | 0.238594 | 0.232991 | 0.22752531 | 0.22222 |
| 2.5      | 0.2052125  | 0.21474836 | 0.21948 | 0.22119 | 0.220971 | 0.219479 | 0.21715 | 0.214284 | 0.211065 | 0.20763347 | 0.20408 |
| 3        | 0.14938121 | 0.16739573 | 0.17881 | 0.18588 | 0.189851 | 0.192    | 0.19262 | 0.192227 | 0.191115 | 0.18948912 | 0.1875  |
| 3.5      | 0.10569084 | 0.12894265 | 0.145   | 0.155   | 0.163429 | 0.168295 | 0.17131 | 0.172956 | 0.173602 | 0.17350014 | 0.17284 |
| 4        | 0.07326256 | 0.09877804 | 0.1176  | 0.13129 | 0.141141 | 0.148148 | 0.15303 | 0.15632  | 0.158398 | 0.15955285 | 0.18    |
| 4.5      | 0.04999048 | 0.07553783 | 0.09565 | 0.11098 | 0.122507 | 0.131088 | 0.13741 | 0.141984 | 0.145214 | 0.14739819 | 0.14878 |
| 5        | 0.03368973 | 0.0578061  | 0.07813 | 0.09431 | 0.106917 | 0.116818 | 0.12402 | 0.129598 | 0.133748 | 0.13676725 | 0.13889 |
| 5.5      | 0.02247724 | 0.04433166 | 0.06413 | 0.08059 | 0.083829 | 0.104295 | 0.11249 | 0.118847 | 0.12373  | 0.12742989 | 0.13018 |
| 6        | 0.01487251 | 0.03410605 | 0.05292 | 0.05925 | 0.062789 | 0.09375  | 0.10252 | 0.109468 | 0.114931 | 0.11916339 | 0.12245 |
| 6.5      | 0.00977235 | 0.02633844 | 0.04391 | 0.05084 | 0.073427 | 0.084673 | 0.09384 | 0.101238 | 0.10716  | 0.11186074 | 0.11556 |
| 7        | 0.00838317 | 0.0204249  | 0.03663 | 0.05198 | 0.065442 | 0.076818 | 0.08625 | 0.093979 | 0.100259 | 0.10532405 | 0.10938 |
| 7.5      | 0.00414813 | 0.01580899 | 0.03072 | 0.04538 | 0.058584 | 0.069981 | 0.07957 | 0.087541 | 0.0941   | 0.09945957 | 0.10381 |
| 8        | 0.0026837  | 0.0124478  | 0.0259  | 0.03981 | 0.052689 | 0.064    | 0.07367 | 0.081803 | 0.088577 | 0.09417322 | 0.09877 |
| 8.5      | 0.00172948 | 0.0097843  | 0.02194 | 0.03608 | 0.04757  | 0.058741 | 0.06842 | 0.078665 | 0.0836   | 0.08938889 | 0.09418 |
| 9        | 0.00111068 | 0.00772597 | 0.01868 | 0.03105 | 0.043111 | 0.054085 | 0.06374 | 0.072045 | 0.079097 | 0.08603536 | 0.09    |
| 9.50E+00 | 0.00071109 | 0.00612634 | 0.01597 | 0.02759 | 0.036208 | 0.049971 | 0.05955 | 0.068782 | 0.075007 | 0.08108392 | 0.08617 |
| 1.00E+01 | 0.000454   | 0.00488281 | 0.01372 | 0.02481 | 0.035777 | 0.046298 | 0.05577 | 0.064089 | 0.071278 | 0.07742637 | 0.08264 |
| 2.00E+01 | 4.1223E-08 | 0.0001129  | 0.00128 | 0.00435 | 0.009145 | 0.015026 | 0.0214  | 0.027849 | 0.034082 | 0.03994285 | 0.04535 |
| 3.00E+01 | 2.8073E-12 | 7.1526E-06 | 0.00025 | 0.00139 | 0.003787 | 0.007324 | 0.01167 | 0.01648  | 0.021468 | 0.02642469 | 0.03122 |
| 4.00E+01 | 1.6993E-16 | 8.192E-07  | 7.5E-05 | 0.0006  | 0.001975 | 0.004319 | 0.00749 | 0.011234 | 0.015325 | 0.01958194 | 0.0236  |
| 5.00E+01 | 9.6437E-21 | 1.3782E-07 | 2.8E-05 | 0.0003  | 0.001178 | 0.002845 | 0.00527 | 0.008308 | 0.011755 | 0.015442   | 0.01922 |
| 6.00E+01 | 5.2539E-25 | 3.0344E-08 | 1.2E-05 | 0.00017 | 0.000788 | 0.002014 | 0.00395 | 0.008474 | 0.009445 | 0.01270727 | 0.01612 |
| 7.00E+01 | 2.7828E-29 | 8.1481E-09 | 6.1E-06 | 0.00011 | 0.000533 | 0.0015   | 0.00308 | 0.005236 | 0.007841 | 0.01078593 | 0.01389 |
| 8.00E+01 | 1.4439E-33 | 2.5493E-09 | 3.3E-06 | 7E-05   | 0.000388 | 0.001161 | 0.00249 | 0.004353 | 0.006689 | 0.00931984 | 0.01219 |
| 9.00E+01 | 7.3748E-38 | 9E-10      | 1.9E-06 | 4.8E-06 | 0.000292 | 0.000925 | 0.00206 | 0.003697 | 0.005778 | 0.00820293 | 0.01087 |
| 1.00E+02 | 3.7201E-42 | 3.5049E-10 | 1.2E-06 | 3.4E-06 | 0.000227 | 0.000754 | 0.00173 | 0.003192 | 0.005081 | 0.00731553 | 0.0098  |
| 5.00E+02 |            |            |         |         |          |          | 0.00012 | 0.000329 | 0.000695 | 0.00124655 | 0.00199 |
| 1.00E+03 |            |            |         |         |          |          | 3.9E-05 | 0.000123 | 0.000293 | 0.00057843 | 0.001   |

## **APPENDIX E**

### **DERIVATION OF GENERALIZED DECLINE CURVE EQUATIONS**

## **Derivation of Generalized Decline Curve Equations**

Fetkovich<sup>3</sup> (1980) presented a useful form of the solution of Tsarevich and Kuranov<sup>11</sup> (1966) to prepare type curves of dimensionless rate versus dimensionless time. Observation of the type curves shows that transition from the infinite acting transient to the PSS is instantaneous at  $t_{pss}$ . Irregular outer geometry will however affect the infinite acting period and postpone true pseudo-steady state production and cause a transition zone. This research will show how to extend and construct type curves to illustrate this phenomenon for various reservoir shape factors and well positions within the reservoir.

Fetkovich prepared a type curve of dimensionless rate versus dimensionless time using the following relationship<sup>4</sup>.

$$q_D = \frac{141.5 q \mu B}{kh(P_i - P_{wf})} \quad \text{E1}$$

$$t_D = \frac{0.00634 k t}{\phi \mu c_i r_{wa}^2} \quad \text{E2}$$

$$r_{wa} = r_w e^{-S} \quad \text{E3}$$

$$r_{wa} = \frac{x_f}{2} \quad \text{E4}$$

An irregular outer geometry or off center well location can create a period of transition between transient and PSS production. This transition zone has not been the focus of much research but it may provide valuable information about the reservoir shape and permit more accurate curve fitting.

A general expression for PSS decline for constant pressure according to the analytical solution is:

$$q_D = A e^{-B t_D} \quad \text{E5}$$

Where A and B are constants defined by the ratio  $r_e/r_{wa}$ . Fetkovich developed expressions for A and B which reflect different ratios of  $r_e/r_{wa}$ . The higher the ratio the larger is the time to pseudosteady state  $t_{DPSS}$ .

$$A = \frac{1}{\ln(r_e / r_{wa}) - 0.5} \quad \text{E6}$$

$$B = \frac{2A}{(r_e / r_{wa})^2 - 1} \quad \text{E7}$$

The expressions for A and B reflect the observation that different ratios of  $r_e/r_{wa}$  give different depletion stems. The higher the ratio of  $r_e/r_{wa}$  the larger the time to pseudosteady state  $t_{DPSS}$  and the lower is  $q_D$  at the start of depletion.

Exponential decline, according to the analytical solution, is substantiated by many field observations. The primary observation in Arp's<sup>1</sup> work (1945) suggested that all conventional depletion declines can be expressed by three types of: hyperbolic, exponential and harmonic.

Perhaps not well known, the Fetkovich Type Curves are based on a strictly radial system operating above the bubble point with the well centrally located. It is obviously desirable to derive a more general case that would apply to any particular reservoir drainage shape such as rectangular, triangular, and reservoirs in which the well is displaced from the reservoir center. It would also be desirable to modify the curves for cases below the bubble point. This method utilizes shape factors derived for these various conditions such as shown in Earlouger's Table C-1 in *Advances in Well Testing*. Application of these factors to the Fetkovich system is not straightforward. I have derived a system that will incorporate all reservoir shapes, positions and later will be applied to vertically fractured and horizontal wells using an equivalent well bore radius concept.

Based on the productivity and decline theory of the previous section Fetkovich defined  $q_{Dd}$  as:

$$q_{Dd} = \frac{q(t)}{q_{\max}} = \frac{141.3 \mu B q(t)}{kh(P_i - P_{wf})} \left[ \ln \frac{r_e}{r_w} - \frac{1}{2} \right] = q_D \left[ \ln \frac{r_e}{r_w} - \frac{1}{2} \right] = q_D c_1 \quad E8$$

Now instead of using the radial form let us begin with a more general equation such as that found on page 243 in Craft and Hawkins in terms of the shape factors and drainage area A so that:

$$q(t) = \frac{kh(P_i - P_{wf})}{162.6\mu B} \left[ \log \frac{4A}{1.781C_A r_w^2} \right] = \frac{kh(P_i - P_{wf})}{141.3\mu B} \left[ 1.151 \log \frac{4A}{1.781C_A r_w^2} \right] \quad E9$$

Then applying the Fetkovich definition above and converting constants to Fetkovich's definitions of  $q_D$ :

$$q_{Dd} = \frac{q(t)}{q_i} = \frac{\frac{q(t)}{kh(P_i - P_{wf})}}{141.3\mu B \left[ 1.151 \log \frac{4A}{1.781C_A r_w^2} \right]} \quad E10$$

But since:

$$q_D = \frac{141.3\mu B q(t)}{kh(P_i - P_{wf})} \quad E11$$

$$q_{Dd} = \frac{q(t)}{q_{i,\max}} = q_D \left[ 1.151 \left[ \log \frac{4A}{1.781C_A r_w^2} \right] \right] \quad E12$$

Therefore we only need to adjust the dimensionless rate values of VanEverdingen and Hurst by the appropriate shape factors, well position and well radius. Since it is desirable

to present the more general forms in terms of  $A/r_w^2$  the equivalent radial solutions to  $q_D$  and  $t_D$  at the various  $r_{eD}=r_e/r_w$  values can be obtained by finding equivalent expressions in terms of  $A/r_w^2$  and the various shape factors using the following relationship:

$$\frac{A}{r_w^2} = \pi \left( \frac{r_e}{r_w} \right)^2 - \pi = \pi \left( \left( \frac{r_e}{r_w} \right)^2 - 1 \right) \quad E13$$

I have confirmed that when the circular shape factor is used, the above derivation is identical to the Fetkovich radial form. Compare Figures 5.6 with 5.2 in chapter 5.

In a similar manner the dimensionless time  $t_{Dd}$  was defined by Fetkovich as:

$$t_{Dd} = \left[ \frac{q_{i,\max}}{N_{pu}} \right] t = D_i t = \frac{0.00634kt}{\phi\mu c_i r_w^2} \left[ \frac{1}{\frac{1}{2} \left[ \left( \frac{r_e}{r_w} \right)^2 - 1 \right] \left[ \ln \left( \frac{r_e}{r_w} \right) - \frac{1}{2} \right]} \right] = t_D \left[ \frac{1}{\frac{1}{2} \left[ \left( \frac{r_e}{r_w} \right)^2 - 1 \right] \left[ \ln \left( \frac{r_e}{r_w} \right) - \frac{1}{2} \right]} \right] \quad E14$$

or:

$$t_{Dd} = t_D \frac{2}{c_1 c_2} \quad E15$$

Likewise the more general dimensionless time decline can be derived in a manner similar to that of Fetkovich but in terms of the reservoir shape and drainage size factors:

$$t_{Dd} = \left[ \frac{q_{i,\max}}{N_i} \right] t = D_i t \quad E16$$

where :

$$q_{i,\max} = \frac{k h P_i}{162.6 \mu B} \left[ \frac{1}{\log \frac{4A}{1.781 C_A r_w^2}} \right] \quad E17$$

and :

$$N_i = \frac{A \phi c_i h P_i}{5.615 B} \quad E18$$

$$t_{Dd} = \frac{q_{i,\max}}{N_i} t = \frac{\frac{k h P_i}{162.6 \mu B} \left[ \frac{1}{\log \frac{4A}{1.781 C_A r_w^2}} \right]}{\frac{A \phi c_i h P_i}{5.615 B}} t \quad E19$$

$$t_{Dd} = \frac{q_{\max}}{N_i} t = \frac{0.00634kt}{\phi\mu c_i A} \left[ \frac{\frac{5.44678}{4A}}{\log \frac{1.781C_A r_w^2}{r_w^2}} \right] \quad E20$$

$$t_{Dd} = \frac{0.00634kt}{\phi\mu c_i r_w^2} \frac{r_w^2}{A} \left[ \frac{\frac{5.44678}{4A}}{\log \frac{1.781C_A r_w^2}{r_w^2}} \right] = t_D \frac{r_w^2}{A} \left[ \frac{\frac{5.44678}{4A}}{\log \frac{1.781C_A r_w^2}{r_w^2}} \right] \quad E21$$

or putting in a similar arrangement to that of the Fetkovich radial form:

$$t_{Dd} = \frac{\frac{t_D}{4A}}{\frac{A}{r_w^2} \frac{\log \frac{4A}{1.781C_A r_w^2}}{5.44678}} = \frac{\frac{t_D}{0.183594A}}{\frac{r_w^2}{\log \frac{4A}{1.781C_A r_w^2}}} = \frac{t_D}{0.183594(c_1 c_2)} \quad E22$$

Where  $c_2$  is:

$$c_2 = \frac{A}{r_w^2} \quad E23$$

As compared to  $c_2$  in the Fetkovich radial case:

$$c_2 = \frac{r_e}{r_w^2} - 1 \quad E24$$

And:

$$c_l = \log \frac{4A}{1.781C_A r_w^2} \quad \text{E25}$$

Again comparing this to the Fetkovich equivalent forms one notes the similarities:

$$c_l = \ln \frac{r_e}{r_w} - \frac{1}{2} \quad \text{E25}$$

**APPENDIX F**

**BACKGROUND OF EFFECTIVE WELLBORE RADIUS OF A**

**HORIZONTAL WELL**

## Derivation of Effective Wellbore Radius Of A Horizontal Well

The effective wellbore radius is the theoretical well radius required matching the observed production rate. Thus stimulated wells will have effective wellbore radius greater than the drilled wellbore radius, and damaged wells will have an effective wellbore radius smaller than the drilled wellbore radius.

Due to the longer well length, for a given time period under similar operating conditions, a horizontal well would drain a larger reservoir area than a vertical well. Then each horizontal well would drain either a square or a circular drainage area with a rectangular drainage area at the center. This concept implies that the reservoir thickness is considerably less than the length of the sides of the drainage area. It is possible to calculate the drainage area of a horizontal well by assuming an elliptical drainage area in the horizontal plane with each end of the well as a foci of a drainage ellipse.

Slichter<sup>31,41</sup> showed that ellipses could represent constant pressure (constant porosity) curves (see Figures F-1, F-2) while the hyperbolas represent constant streamlines (constant potential) as:

$$w(z) = \phi + i\Psi = \cosh^{-1}(z/\Delta r) \quad F1$$

By definition  $z=x+iy$ . Substituting this into the equation and equation real and imaginary parts yields:

$$x = \Delta r \cosh \phi \cos \Psi \quad F2$$

$$y = \Delta r \sinh \phi \sin \Psi \quad F3$$

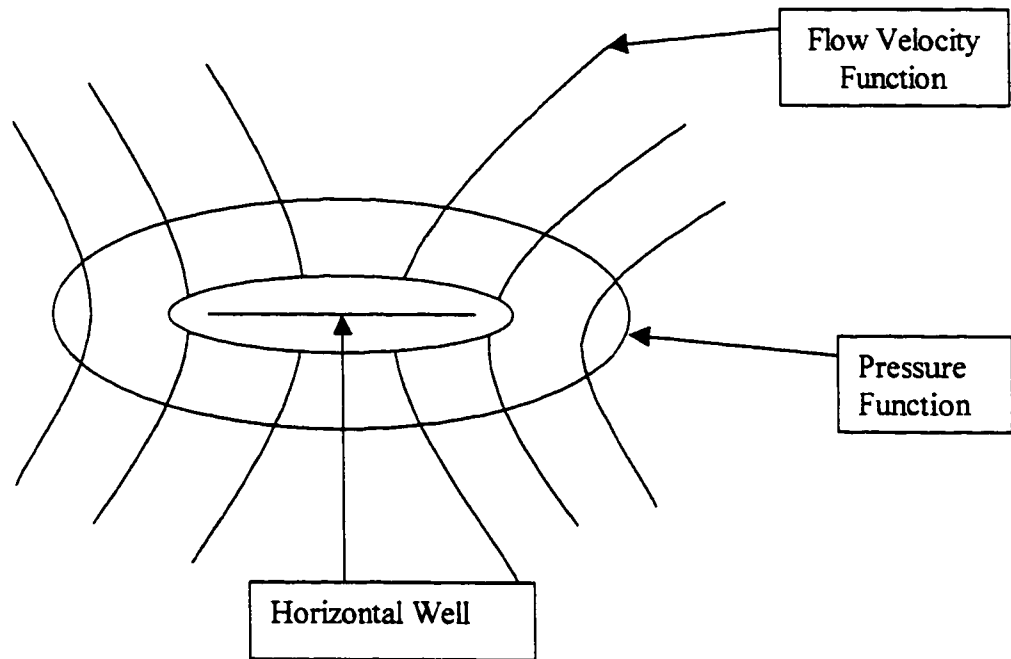


**Figure F1 Potential Flow to a Horizontal Well-Horizontal plane**

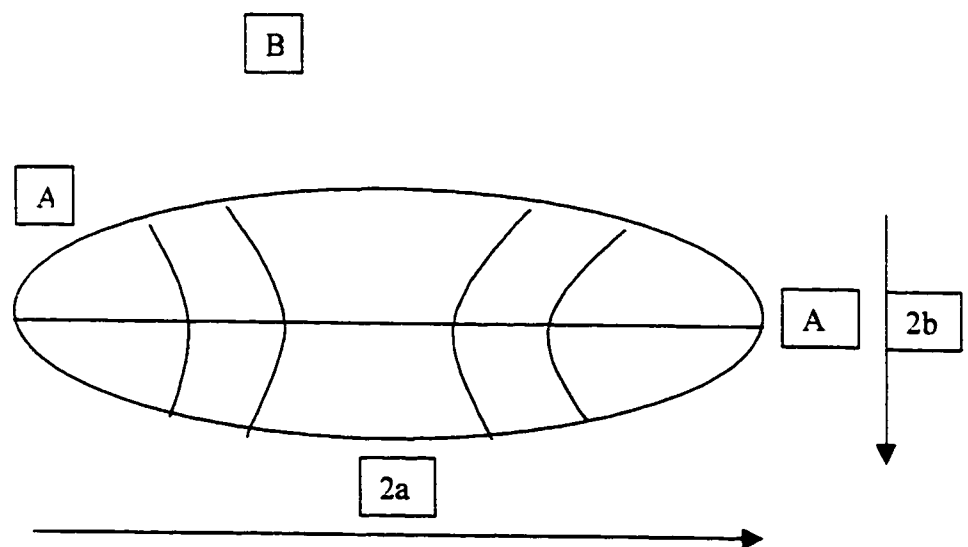
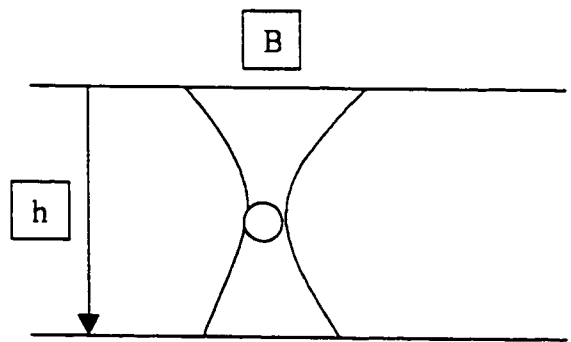
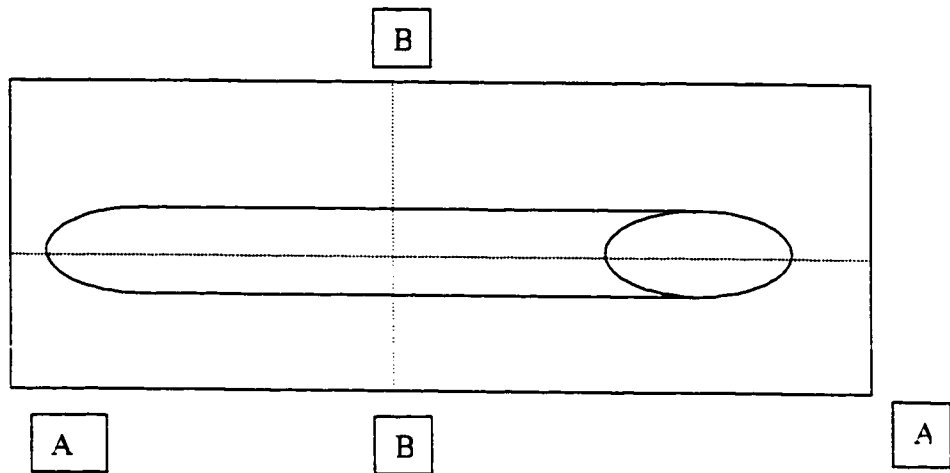


**Figure F-2 Division of 3D Horizontal Well Into Two 2-D Problems**

The equation with the hyperbolic function represents a classic equation of an ellipse, while the equation with the trigonometric functions represents the equation of the hyperbola. Therefore the above equations can be reformulated as

$$\phi = \cosh^{-1} H^*$$

$$\Psi = \cos^{-1} H^*$$

where:

$$H^* = \left[ \frac{x^2 + y^2 + \Delta r^2 \pm \sqrt{(x^2 + y^2 + \Delta r^2)^2 - 4\Delta r^2 x^2}}{2\Delta r^2} \right]^{1/2} \quad F4$$

The plus sign refers to  $\phi$  and the minus sign refers to  $\Psi$ . The pressure drop between drainage boundary and well,  $\Delta p$  is the same as  $p_e$  because wellbore pressure is assumed to be zero. The potential function  $\phi$  is the same as the pressure,  $p$ . At drainage radius  $r_{eH}$ , half the major and minor axes of the ellipse of constant pressure are  $a$  and  $b$ . Hence the pressure at the drainage boundary  $p_e$  is:

$$p_e = \cosh^{-1} \frac{a}{\Delta r} = \ln \frac{\left( a + \sqrt{a^2 - \Delta r^2} \right)}{\Delta r} \quad F5$$

Because wellbore pressure is assumed to be zero, the pressure drop between the drainage boundary and well,  $\Delta p$ , is the same as  $p_e$  defined above,. Substituting this into Darcy's porous medium equation yields:

$$q_1 = \frac{2\pi k_o \Delta p / \mu}{\ln \left( \frac{a + \sqrt{a^2 - \Delta r^2}}{\Delta r} \right)} \quad F6$$

where  $\Delta r$  is the half length =  $L/2$ . Therefore this equation represents the flow to a horizontal well from a horizontal plane.

Since drainage radius is normally used in the calculations, the horizontal well drainage radius  $r_{eH}$  can be represented by equating the areas of a circle and ellipse which reduces to:

$$r_{eH} = \sqrt{ab} \quad F7$$

where  $a$  and  $b$  are the major and minor axes of a drainage ellipse and  $\pm L/2$  represent the foci of the drainage ellipse. Thus using the properties of an ellipse,  $b$  can be defined as:

$$b = \sqrt{a^2 - (L/2)^2} \quad F8$$

which upon substituting into the radius equation above yields:

$$r_{eH} = a [1 - (L/2a)^2]^{1/4} \quad F9$$

If  $L/2a$  is less than 0.5, the effective horizontal radius is approximately equal to  $a$ . The flow in the vertical plan can be calculated in a similar manner and yields:

$$q_2 = \frac{2\pi k \Delta p / \mu}{\ln(h / 2r_s)} \quad \text{F10}$$

If we let  $k_H$  represent the horizontal permeability and  $K_v$  theoretical permeability in a reservoir of thickness  $h$ , then the influence of anisotropy in the horizontal versus vertical direction can be represented (Muscat) by the geometric mean of  $K_v$  and  $K_H$ . Therefore equation for  $q_1$  can be modified to:

$$q_1 = \frac{2\pi \sqrt{K_v K_H} h \Delta p / (\mu / B_o)}{\ln\left(\frac{a + \sqrt{a^2 - (L/2)^2}}{L/2}\right)} \quad \text{F11}$$

and for the vertical flow in a horizontal well of length  $L$  the vertical flow  $q_2$  can be represented as:

$$q_2 = \frac{2\pi \sqrt{k_v k_H} \Delta p / (\mu / B_o)}{\ln(h / 2r_s)} \quad \text{F12}$$

Now expressing  $q_1$  and  $q_2$  in terms of flow resistance and summing the results yields the flow of a horizontal well as:

$$q_H = \frac{2\pi k_h \Delta p / (\mu / B_o)}{\ln \left[ \frac{a + \sqrt{a^2 - (L/2)^2}}{L/2} \right] + \frac{\beta^2 h}{L} \ln \frac{h}{2r_w}}$$
F13

where :

$$\beta = \left( \frac{k_h}{k_v} \right)^{\frac{1}{2}}$$
F14

The effective radius of a horizontal well can then be calculated by converting the productivity of a horizontal well into that of an equivalent vertical well. As demonstrated earlier the effective wellbore radius can be defined as:

$$r_w = r_w e^{-s}$$
F15

or as shown from type curve matching, it can be obtained from the infinite acting portion of the type curve by:

$$r_{wa} = \frac{r_e}{\left( \frac{r_e}{r_{wa}} \right)_{match}}$$
F16

The following relationship equates the vertical well that is required to produce oil at the same rate as that of a horizontal well, assuming equal drainage volumes, equal actual well bore radii, and equal productivity indices,  $(q/\Delta P)_h = (q/\Delta P)_v$ .

$$\left[ \frac{2\pi k_h}{\mu B \ln\left(\frac{r_e}{r_w}\right)} \right]_v = \left[ \frac{2\pi k_h}{\ln\left[ \frac{a + \sqrt{a^2 - (L/2)^2}}{L/2} \right] + (h/L) \ln[h/(2r_w)]} \right]_h \quad F17$$

Solving for  $r_w$ , yields:

$$r_w = \frac{0.5 r_{eh} L}{a \left[ 1 + \sqrt{1 - \left[ \frac{L}{2a} \right]^2} \right] \frac{h}{2r_w}} \quad F18$$

where:

$$a = 0.5L \left[ 0.5 + \sqrt{0.25 + \left( \frac{2r_{eh}}{L} \right)^4} \right]^{\frac{1}{2}} \quad F19$$

If the reservoir were anisotropic then the effective wellbore radius would be:

$$r_w = \frac{0.5 r_{eh} L}{a \left[ 1 + \sqrt{1 - \left[ \frac{L}{2a} \right]^2} \right] \frac{\beta h}{2r_w}} \quad F20$$

where :

$$\beta = \left( \frac{k_h}{k_v} \right)^{\frac{1}{2}} \quad F21$$

## APPENDIX G

### Fracture Model Tabular Experimental Results

| Model Type 1 |                |          |          |          |         |          |     |        |          |          |          |          |                       |
|--------------|----------------|----------|----------|----------|---------|----------|-----|--------|----------|----------|----------|----------|-----------------------|
| 28 by<br>28  | phimatrix 0.01 | 2XeL 8.5 | ocep     | 3.373    |         |          |     |        |          |          |          |          |                       |
|              | w 0.036        |          | (mmbo)   |          |         |          |     |        |          |          |          |          |                       |
|              | kmatrice 0.1   |          | Sor 0.75 |          |         |          |     |        |          |          |          |          |                       |
|              | kfracture 1000 |          |          |          |         |          |     |        |          |          |          |          |                       |
| delta t      | average        | cum oil  | oil rate | gas rate | cum gas |          |     |        |          |          |          |          | t <sub>p</sub> (days) |
| days         | pressure       | mbo      | bopd     | mcfd     | mmcf    | dt hours | dq  | dp     | qdq      | dplq     | q cum/dp | q cum/lq | qcum/bq               |
| 6            | 1932           | 8.81     | 460      | 584      | 8.026   | 144      | 68  | 6.7847 | 0.147626 | 129.556  | 19.15217 |          |                       |
| 8            | 1925           | 9.672    | 415      | 470      | 8.974   | 192      | 45  | 75     | 5.5333   | 0.180723 | 128.96   | 23.30602 | 214.93                |
| 10           | 1920           | 10.42    | 380      | 410      | 9.904   | 240      | 80  | 80     | 4.75     | 0.210526 | 130.25   | 27.42105 | 130.25                |
| 12           | 1914           | 11.16    | 367      | 376      | 10.67   | 288      | 93  | 86     | 4.2674   | 0.234332 | 129.767  | 30.40872 | 120                   |
| 14           | 1910           | 11.89    | 363      | 340      | 11.37   | 336      | 97  | 90     | 4.0333   | 0.247934 | 132.111  | 32.75482 | 122.58                |
| 16           | 1898           | 12.61    | 360      | 318      | 12.01   | 384      | 100 | 94     | 3.8298   | 0.261111 | 134.149  | 36.02778 | 126.1                 |
| 18           | 1892           | 13.33    | 358      | 302      | 12.63   | 432      | 102 | 98     | 3.6531   | 0.273743 | 136.02   | 37.23464 | 130.69                |
| 20           | 1889           | 14.04    | 356      | 290      | 13.21   | 480      | 104 | 101    | 3.5248   | 0.283708 | 139.01   | 39.4382  | 135                   |
| 22           | 1895           | 14.75    | 353      | 281      | 13.78   | 528      | 107 | 105    | 3.3619   | 0.29745  | 140.476  | 41.7847  | 137.85                |
| 24           | 1892           | 15.45    | 349      | 274      | 14.33   | 576      | 111 | 108    | 3.2315   | 0.309458 | 143.056  | 44.28934 | 139.19                |
| 26           | 1889           | 16.14    | 344      | 268      | 14.87   | 624      | 116 | 111    | 3.0981   | 0.322674 | 145.405  | 46.9186  | 139.14                |
| 31           | 1880           | 17.65    | 332      | 249      | 16.7    | 744      | 126 | 120    | 2.7667   | 0.361446 | 147.083  | 53.16265 | 137.89                |
| 62           | 1841           | 27.31    | 309      | 167      | 23.22   | 1488     | 151 | 159    | 1.9434   | 0.514563 | 171.761  | 88.38188 | 180.86                |
| 123          | 1787           | 44.42    | 233      | 183      | 32.97   | 2952     | 227 | 213    | 1.0039   | 0.914163 | 208.545  | 190.6438 | 196.68                |
| 214          | 1728           | 64.6     | 203      | 116      | 44.52   | 5136     | 257 | 272    | 0.7463   | 1.339901 | 237.5    | 318.2266 | 251.36                |
| 395          | 1638           | 98.08    | 143      | 92       | 63.66   | 9480     | 317 | 361    | 0.3961   | 2.524476 | 266.15   | 671.8881 | 303.09                |
| 576          | 1572           | 120.9    | 125      | 85       | 79.8    | 13824    | 335 | 428    | 0.2921   | 3.424    | 282.477  | 987.2    | 360.9                 |
| 942          | 1480           | 158.4    | 86       | 77       | 111.2   | 22608    | 374 | 520    | 0.1654   | 6.046512 | 304.615  | 1841.86  | 423.53                |
| 1308         | 1434           | 187.3    | 74       | 61       | 134.3   | 31382    | 386 | 566    | 0.1307   | 7.648649 | 330.919  | 2531.081 | 485.23                |
| 2304         | 1383           | 250      | 56       | 41       | 181.9   | 55296    | 404 | 637    | 0.0879   | 11.375   | 382.465  | 4464.286 | 618.81                |
| 3400         | 1306           | 303.4    | 40       | 33       | 223.3   | 81600    | 420 | 694    | 0.0578   | 17.35    | 437.176  | 7585     | 722.38                |
| 5998         | 1217           | 401.8    | 31       | 28       | 294.6   | 143904   | 429 | 783    | 0.0396   | 26.25808 | 513.156  | 12981.29 | 936.6                 |
| 8562         | 1150           | 474.4    | 27       | 21       | 353.1   | 206208   | 433 | 850    | 0.0318   | 31.48148 | 558.118  | 17570.37 | 1096.6                |
| 11188        | 1083           | 536.1    | 21       | 19       | 406.6   | 268512   | 439 | 907    | 0.0232   | 43.19048 | 591.068  | 25528.57 | 1221.2                |
| 13784        | 1048           | 588.7    | 20       | 18       | 452.1   | 330816   | 440 | 962    | 0.021    | 47.6     | 618.382  | 29435    | 1338                  |
| 16380        | 1005           | 634.9    | 16       | 16       | 497.3   | 383120   | 444 | 995    | 0.0161   | 62.1875  | 638.09   | 39881.25 | 1430                  |
| 18976        | 968            | 675.7    | 15       | 15       | 537.6   | 455424   | 445 | 1032   | 0.0145   | 68.8     | 654.748  | 45046.67 | 1518.4                |
| 21572        | 933            | 712.9    | 13       | 15       | 577.3   | 517728   | 447 | 1067   | 0.0122   | 82.07692 | 668.136  | 54838.46 | 1594.9                |
| 24168        | 901            | 745.8    | 12       | 14       | 614.2   | 580032   | 448 | 1099   | 0.0109   | 91.58333 | 678.617  | 62150    | 1654.7                |

Table G-1 Model 1 Type 1 Fracture Simulation Output and Calculations

| Model Type1 |         |                |          |            |           |             |             |
|-------------|---------|----------------|----------|------------|-----------|-------------|-------------|
| 28 by 28    |         | phmatrix 0.01  |          |            | 2XeL 8.5  |             |             |
|             |         | w 0.036        |          |            |           |             |             |
|             |         | kmatrix 0.1    |          |            | Sol 0.75  |             |             |
|             |         | kfracture 1000 |          |            |           |             |             |
| delta t     | cum oil | days/days      |          |            | hours     |             |             |
| days        | mbo     | dq/q           | dp/p     | (tp+dt)/dt | sqrt dt   | sqrt dt     | d(dq/q)     |
| 6           | 8810    | 0              | 0.035197 | 4.192029   | 2.4494897 |             | 12          |
| 8           | 9872    | 0.10843        | 0.038861 | 3.913253   | 2.8284271 | 13.85840646 |             |
| 10          | 10420   | 0.21053        | 0.041667 | 3.742105   | 3.1622777 | 15.49193338 | 0.036243065 |
| 12          | 11160   | 0.25341        | 0.044632 | 3.53408    | 3.4841016 | 16.97058275 | 0.014172829 |
| 14          | 11890   | 0.26722        | 0.04712  | 3.33963    | 3.7416574 | 18.33030278 | 0.008092946 |
| 16          | 12610   | 0.27778        | 0.049318 | 3.189236   | 4         | 19.56581794 | 0.004424643 |
| 18          | 13330   | 0.28462        | 0.051525 | 3.068581   | 4.2426407 | 20.78460669 | 0.003589263 |
| 20          | 14040   | 0.29213        | 0.053186 | 2.97191    | 4.472136  | 21.9089023  | 0.004549987 |
| 22          | 14750   | 0.30312        | 0.056409 | 2.896305   | 4.6904158 | 22.97825059 | 0.008479186 |
| 24          | 15450   | 0.31805        | 0.057082 | 2.844556   | 4.8889795 | 24          | 0.008523289 |
| 26          | 16140   | 0.33721        | 0.058761 | 2.804582   | 5.0990185 | 24.87999199 | 0.009641513 |
| 31          | 17850   | 0.38554        | 0.06383  | 2.714924   | 5.5677844 | 27.27638339 | 0.004207329 |
| 62          | 27310   | 0.48867        | 0.086366 | 2.425514   | 7.8740079 | 38.57460304 | 0.006396987 |
| 123         | 44420   | 0.97425        | 0.119194 | 2.549949   | 11.090537 | 54.33231063 | 0.005114057 |
| 214         | 64800   | 1.26601        | 0.157407 | 2.48704    | 14.628739 | 71.66588147 | 0.004568141 |
| 395         | 96080   | 2.21678        | 0.220256 | 2.700983   | 19.874607 | 97.36529156 | 0.00390606  |
| 576         | 120900  | 2.68           | 0.272265 | 2.679167   | 24        | 117.5755077 | 0.003897722 |
| 942         | 158400  | 4.34884        | 0.351351 | 2.955286   | 30.692019 | 150.359669  | 0.003464776 |
| 1308        | 187300  | 5.21622        | 0.3947   | 2.935077   | 36.166283 | 177.1778787 | 0.002103854 |
| 2304        | 250000  | 7.21429        | 0.467351 | 2.937624   | 48        | 235.1510153 | 0.002525706 |
| 3400        | 303400  | 10.5           | 0.531394 | 3.230882   | 58.309519 | 285.6571371 | 0.001794264 |
| 5986        | 401800  | 13.6387        | 0.643385 | 3.161656   | 77.433843 | 379.346807  | 0.001066456 |
| 8562        | 474400  | 16.037         | 0.73913  | 3.044959   | 92.693042 | 454.1013103 | 0.00136095  |
| 11188       | 536100  | 20.9048        | 0.829826 | 3.281782   | 105.77334 | 518.1814354 | 0.001148491 |
| 13784       | 588700  | 22             | 0.908387 | 3.135447   | 117.40528 | 575.166063  | 0.00131842  |
| 16380       | 634900  | 27.75          | 0.99005  | 3.422543   | 127.98437 | 626.9928229 | 0.001476631 |
| 18976       | 675700  | 29.6667        | 1.086116 | 3.373876   | 137.7534  | 674.8510947 | 0.001277854 |
| 21572       | 712900  | 34.3846        | 1.143623 | 3.542113   | 146.8741  | 719.533182  | 0.001476631 |
| 24168       | 745800  | 37.3333        | 1.219756 | 3.571582   | 155.46061 | 761.5983193 |             |

Table G-1 Model 1 Type 1 Fracture Simulation Output and Calculations -Continued

| days  | mbo    | The pressure decline can be compared with actual pressures as a function of time |          |          |              |         |         |            |          |         |          |            |  |
|-------|--------|--|----------|----------|--------------|---------|---------|------------|----------|---------|----------|------------|--|
|       |        | $q''t$   | $1/q''t$ | $1/q'$   | $q'$ (deriv) | $q''at$ | $t''Q'$ | $t''Q''at$ | $p'$     | $p''at$ | $t''p'$  | $t''p''at$ |  |
| 6     | 8810   |  |          |          |              |         |         |            |          |         |          |            |  |
| 8     | 9572   | 2E+05  | 0.0004   | 0.00005  | 20000        | 20000   | 160000  | 160000     | 3        | 3       | 24       | 24         |  |
| 10    | 10420  | 1E+05  | 0.0008   | 8.33E-05 | 12000        | 12000   | 120000  | 120000     | 3        | 3       | 28       | 28         |  |
| 12    | 11160  | 51000  | 0.0028   | 0.000235 | 4250         | 4250    | 51000   | 51000      | 3        | 3       | 30       | 30         |  |
| 14    | 11890  | 24500  | 0.008    | 0.000571 | 1750         | 1750    | 24500   | 24500      | 2        | 2       | 28       | 28         |  |
| 16    | 12610  | 20000  | 0.0128   | 0.0008   | 1250         | 1250    | 20000   | 20000      | 2        | 2       | 32       | 32         |  |
| 18    | 13330  | 18000  | 0.018    | 0.001    | 1000         | 1000    | 18000   | 18000      | 2        | 2       | 32       | 32         |  |
| 20    | 14040  | 25000  | 0.016    | 0.0008   | 1250         | 1250    | 25000   | 25000      | 2        | 2       | 35       | 35         |  |
| 22    | 14750  | 38500  | 0.0126   | 0.000571 | 1750         | 1750    | 38500   | 38500      | 2        | 2       | 36       | 36         |  |
| 24    | 15450  | 54000  | 0.0107   | 0.000444 | 2250         | 2250    | 54000   | 54000      | 2        | 2       | 36       | 36         |  |
| 26    | 16140  | 64257  | 0.0105   | 0.000405 | 2428.6       | 2471    | 63143   | 64257      | 1.714286 | 1.58571 | 44.57143 | 41.229     |  |
| 31    | 17650  | 67281  | 0.0143   | 0.000481 | 972.22       | 2170    | 30139   | 67281      | 1.333333 | 1.72473 | 41.33333 | 53.467     |  |
| 62    | 27310  | 56529  | 0.068    | 0.001097 | 1076.1       | 911.8   | 66717   | 56529      | 1.01087  | 1.13244 | 62.67391 | 70.211     |  |
| 123   | 44420  | 1E+05  | 0.1401   | 0.001139 | 697.37       | 878.2   | 85776   | 108019     | 0.743421 | 0.79018 | 91.44079 | 97.192     |  |
| 214   | 64600  | 70680  | 0.6479   | 0.003028 | 330.88       | 330.3   | 70809   | 70680      | 0.544118 | 0.58695 | 116.4412 | 127.53     |  |
| 395   | 96080  | 85110  | 1.8332   | 0.004641 | 215.47       | 215.5   | 85110   | 85110      | 0.430939 | 0.43094 | 170.221  | 170.22     |  |
| 576   | 120800 | 58637  | 5.6581   | 0.009823 | 104.2        | 101.8   | 60022   | 58637      | 0.290676 | 0.33088 | 167.4298 | 190.57     |  |
| 942   | 158400 | 65631  | 13.52    | 0.014353 | 69.672       | 69.67   | 65631   | 65631      | 0.188525 | 0.18852 | 177.5902 | 177.59     |  |
| 1308  | 187300 | 37713  | 45.365   | 0.034683 | 22.026       | 28.83   | 28811   | 37713      | 0.085903 | 0.11107 | 112.3612 | 145.27     |  |
| 2304  | 250000 | 37828  | 140.33   | 0.080807 | 16.252       | 16.42   | 37446   | 37828      | 0.081185 | 0.08211 | 140.9713 | 143.09     |  |
| 3400  | 303400 | 38400  | 301.04   | 0.088542 | 6.7714       | 11.29   | 23023   | 38400      | 0.039545 | 0.04675 | 134.4529 | 158.94     |  |
| 5996  | 401800 | 15013  | 2394.7   | 0.399385 | 2.5039       | 2.504   | 15013   | 15013      | 0.030046 | 0.03005 | 180.1572 | 180.16     |  |
| 8592  | 474400 | 16549  | 4481     | 0.5192   | 1.926        | 1.926   | 16549   | 16549      | 0.023883 | 0.02388 | 205.2018 | 205.2      |  |
| 11188 | 536100 | 15084  | 6298.3   | 0.741714 | 1.3482       | 1.348   | 15084   | 15084      | 0.019846 | 0.01985 | 219.7951 | 219.8      |  |
| 13784 | 588700 | 13274  | 14313    | 1.0384   | 0.983        | 0.983   | 13274   | 13274      | 0.018949 | 0.01895 | 233.6271 | 233.63     |  |
| 16380 | 634900 | 15774  | 17009    | 1.0384   | 0.983        | 0.983   | 15774   | 15774      | 0.015408 | 0.01541 | 252.3883 | 252.39     |  |
| 18876 | 675700 | 10685  | 32841    | 1.730667 | 0.5778       | 0.578   | 10685   | 10685      | 0.013867 | 0.01387 | 263.1495 | 263.15     |  |
| 21572 | 712900 | 12465  | 37334    | 1.730667 | 0.5778       | 0.578   | 12465   | 12465      | 0.012904 | 0.0129  | 278.3752 | 278.38     |  |

Table G-1 Model 1 Type 1 Fracture Simulation Output and Calculations -Continued

| days  | Qsmooth | Q'smooth | Q'smooth      | Q" | Q"t       |
|-------|---------|----------|---------------|----|-----------|
| 6     |         |          |               |    |           |
| 8     | -403    | 403      |               |    |           |
| 10    | -372    | 372      | 8750 8750     |    | 87500     |
| 12    | -368    | 368      | 2375 2375     |    | 28500     |
| 14    | -363    | 363      | 1875 1875     |    | 28250     |
| 16    | -360    | 360      | 1250 1250     |    | 20000     |
| 18    | -358    | 358      | 1250 1250     |    | 22500     |
| 20    | -355    | 355      | 1250 1250     |    | 25000     |
| 22    | -353    | 353      | 1875 1875     |    | 41250     |
| 24    | -348    | 348      | 4946 4946.429 |    | 118714.29 |
| 26    | -333    | 333      | 6850 6309.268 |    | 164040.96 |
| 31    | -303    | 303      | 5070 877.44   |    | 27200.64  |
| 62    | -301    | 301      | 291 504.5003  |    | 31279.019 |
| 123   | -257    | 257      | 660 627.4475  |    | 77178.045 |
| 214   | -206    | 206      | 467 372.7803  |    | 78774.98  |
| 395   | -156    | 156      | 221 221.2676  |    | 87400.695 |
| 578   | -126    | 126      | 142 118.4908  |    | 68250.713 |
| 942   | -91     | 91       | 70 69.66672   |    | 65626.052 |
| 1308  | -75     | 75       | 37 25.35468   |    | 33163.927 |
| 2304  | -56     | 56       | 14 13.93324   |    | 32102.196 |
| 3400  | -46     | 46       | 8 6.295238    |    | 21403.809 |
| 5998  | -33     | 33       | 4 3.7836      |    | 22686.466 |
| 8592  | -26     | 26       | 2 2.10336     |    | 18072.072 |
| 11188 | -22     | 22       | 1 1.316919    |    | 14733.687 |
| 13784 | -19     | 19       | 1 1.012729    |    | 13959.458 |
| 16380 | -17     | 17       | 1 0.771603    |    | 12638.859 |
| 18976 | -15     | 15       | 3 3.227378    |    |           |
| 21572 |         |          |               |    |           |

Table G-1 Model 1 Type 1 Fracture Simulation Output and Calculations -Continued

| Model Type 1h |                 |           |            |          |         |          |     |      |        |          |          |          |          |
|---------------|-----------------|-----------|------------|----------|---------|----------|-----|------|--------|----------|----------|----------|----------|
| 28 by<br>28   | phi matrix 0.01 | 2Xe/L 8.5 | coip 3.373 |          |         |          |     |      |        |          |          |          |          |
|               | w 0.036         |           | (mmbo)     |          |         |          |     |      |        |          |          |          |          |
|               | kmatrix 0.1     |           | Sci 0.75   |          |         |          |     |      |        |          |          |          |          |
|               | kfracture 4000  |           |            |          |         |          |     |      |        |          |          |          |          |
| delta q       |                 |           |            |          |         |          |     |      |        |          |          |          |          |
| delta t       | average         | cum oil   | oil rate   | gas rate | cum gas |          |     |      |        |          |          |          | t(days)  |
| days          | pressure        | mbo       | bopd       | mcfd     | mmcf    | dt hours | dq  | dp   | q/dp   | q/dq     | q cum/dp | q cum/q  | q cum/dq |
| 6             | 1827            | 9.151     | 475        | 662      | 8.183   | 144      |     | 73   | 6.5058 | 0.153684 | 125.356  | 19.26526 |          |
| 8             | 1821            | 10.06     | 436        | 528      | 9.22    | 182      | 39  | 79   | 5.519  | 0.181183 | 127.342  | 23.07339 | 257.95   |
| 10            | 1916            | 10.9      | 426        | 435      | 10.18   | 240      | 49  | 84   | 5.0714 | 0.197183 | 128.782  | 25.58685 | 222.45   |
| 12            | 1911            | 11.73     | 419        | 391      | 11.04   | 288      | 58  | 89   | 4.7079 | 0.212411 | 131.798  | 27.98523 | 209.48   |
| 14            | 1907            | 12.54     | 416        | 362      | 11.84   | 336      | 59  | 93   | 4.4731 | 0.223558 | 134.839  | 30.14423 | 212.54   |
| 16            | 1902            | 13.35     | 414        | 343      | 12.58   | 384      | 61  | 98   | 4.2245 | 0.236715 | 136.224  | 32.24638 | 218.85   |
| 18            | 1899            | 14.16     | 412        | 330      | 13.3    | 432      | 63  | 101  | 4.0792 | 0.245146 | 140.198  | 34.36883 | 224.75   |
| 20            | 1895            | 14.96     | 408        | 322      | 14      | 480      | 67  | 105  | 3.8857 | 0.257353 | 142.478  | 36.85667 | 223.28   |
| 22            | 1891            | 15.76     | 403        | 317      | 14.67   | 528      | 72  | 109  | 3.6972 | 0.270471 | 144.587  | 39.1067  | 218.89   |
| 24            | 1888            | 16.54     | 396        | 313      | 15.34   | 576      | 79  | 112  | 3.5357 | 0.282828 | 147.679  | 41.76768 | 209.37   |
| 26            | 1885            | 17.31     | 389        | 308      | 15.98   | 624      | 86  | 115  | 3.3826 | 0.295563 | 150.522  | 44.49671 | 201.28   |
| 31            | 1878            | 19.1      | 394        | 237      | 17.82   | 744      | 81  | 124  | 3.1774 | 0.314721 | 154.032  | 48.47716 | 235.8    |
| 62            | 1837            | 30.54     | 353        | 230      | 25.31   | 1488     | 122 | 163  | 2.1656 | 0.481756 | 187.362  | 85.51558 | 250.33   |
| 123           | 1785            | 51.24     | 302        | 157      | 36.47   | 2952     | 173 | 215  | 1.4047 | 0.711921 | 238.326  | 189.6689 | 296.18   |
| 214           | 1728            | 78.34     | 243        | 140      | 49.81   | 5136     | 232 | 272  | 0.8834 | 1.119342 | 280.662  | 314.1564 | 329.05   |
| 395           | 1641            | 111.9     | 148        | 163      | 76.07   | 9480     | 327 | 359  | 0.4123 | 2.425678 | 311.699  | 756.0811 | 342.2    |
| 576           | 1576            | 135.1     | 113        | 101      | 98.98   | 13824    | 362 | 424  | 0.2665 | 3.752212 | 318.632  | 1186.575 | 373.2    |
| 942           | 1494            | 173.4     | 93         | 84       | 127.7   | 22608    | 382 | 508  | 0.1838 | 5.44086  | 342.688  | 1884.516 | 453.93   |
| 1308          | 1441            | 202.4     | 73         | 59       | 153.3   | 31392    | 402 | 569  | 0.1306 | 7.857534 | 362.075  | 2772.603 | 503.48   |
| 2304          | 1359            | 268.9     | 57         | 53       | 200     | 55296    | 418 | 641  | 0.0889 | 11.24581 | 419.501  | 4717.544 | 643.3    |
| 3400          | 1301            | 320.6     | 48         | 23       | 242.8   | 81600    | 427 | 699  | 0.0687 | 14.5625  | 458.655  | 6579.167 | 750.82   |
| 5996          | 1207            | 419.9     | 29         | 27       | 320.6   | 143804   | 446 | 793  | 0.0366 | 27.34483 | 529.508  | 14479.31 | 941.48   |
| 8592          | 1139            | 494.9     | 26         | 25       | 379.9   | 208208   | 449 | 851  | 0.0302 | 33.11538 | 574.797  | 19034.82 | 1102.2   |
| 11188         | 1083            | 553       | 22         | 18       | 433.3   | 268512   | 453 | 917  | 0.024  | 41.68182 | 603.053  | 25136.36 | 1220.8   |
| 13784         | 1035            | 607.2     | 18         | 19       | 482     | 330816   | 457 | 985  | 0.0187 | 53.61111 | 629.223  | 33733.33 | 1328.7   |
| 16380         | 994             | 651.3     | 17         | 16       | 528.7   | 393120   | 458 | 1008 | 0.0169 | 58.17647 | 647.416  | 38311.76 | 1422.1   |
| 18976         | 955             | 693.3     | 15         | 17       | 569.9   | 455424   | 460 | 1045 | 0.0144 | 68.66667 | 663.445  | 46220    | 1507.2   |
| 21572         | 919             | 728.6     | 13         | 15       | 610.4   | 517728   | 462 | 1081 | 0.012  | 83.15385 | 674.008  | 56046.15 | 1577.1   |
| 24168         | 886             | 761.8     | 12         | 15       | 648.9   | 580032   | 463 | 1114 | 0.0108 | 92.83333 | 683.842  | 63483.33 | 1645.4   |

Table G-2 Model 1 Type 1h Fracture Simulation Output and Calculations

| Model Type 1h |         |                           |          |   |           |             |               |             |       |
|---------------|---------|---------------------------|----------|---|-----------|-------------|---------------|-------------|-------|
| 28 by 28      |         | phimatrix 0.01<br>w 0.036 |          | 2xel 8.5<br>kmatrix 0.1<br>Sai 0.75<br>kfraction 4000 |           |             | cop<br>(mmbo) |             | 3.373 |
| delta t       | cum oil | days/days                 |          |   |           | hours       |               |             |       |
| days          | mbo     | dq/q                      | dq/p     | (t0+dt)/dt  | sqr dt    | sqr dt      | t/q           | d(dq/q)     |       |
| 5             | 9151    | 0                         | 0.037883 | 4.210877  | 2.4494897 | 12          | 0.002105263   |             |       |
| 8             | 10080   | 0.08945                   | 0.041124 | 3.884174  | 2.8284271 | 13.85640646 | 0.002293578   |             |       |
| 10            | 10900   | 0.11502                   | 0.043841 | 3.558885  | 3.1622777 | 15.49193338 | 0.002347418   | 0.011050503 |       |
| 12            | 11730   | 0.13385                   | 0.046572 | 3.332936  | 3.4841016 | 16.97058275 | 0.002388635   | 0.008700882 |       |
| 14            | 12540   | 0.14183                   | 0.048768 | 3.153158  | 3.7416574 | 18.33030278 | 0.002403846   | 0.003422881 |       |
| 16            | 13350   | 0.14734                   | 0.051525 | 3.015399  | 4         | 19.59581794 | 0.002415459   | 0.002771425 |       |
| 18            | 14160   | 0.15291                   | 0.053185 | 2.908385  | 4.2426407 | 20.78460969 | 0.002427184   | 0.004218173 |       |
| 20            | 14980   | 0.16422                   | 0.055409 | 2.833333  | 4.472136  | 21.9089023  | 0.00245098    | 0.006436857 |       |
| 22            | 15780   | 0.17866                   | 0.057641 | 2.777577  | 4.6904158 | 22.97825059 | 0.00248139    | 0.008819816 |       |
| 24            | 16540   | 0.18949                   | 0.059322 | 2.74032   | 4.8989795 | 24          | 0.002525253   | 0.01060491  |       |
| 26            | 17310   | 0.22108                   | 0.061008 | 2.711489  | 5.0990195 | 24.97996199 | 0.002570694   | 0.00868983  |       |
| 31            | 19100   | 0.20558                   | 0.066098 | 2.583779  | 5.5677844 | 27.27636339 | 0.002538071   | 0.003459149 |       |
| 62            | 30540   | 0.34561                   | 0.088732 | 2.395413  | 7.8740079 | 38.57460304 | 0.002832861   | 0.003991999 |       |
| 123           | 51240   | 0.57285                   | 0.120448 | 2.379422  | 11.090537 | 54.33231063 | 0.003311258   | 0.004007391 |       |
| 214           | 76340   | 0.95473                   | 0.157407 | 2.46802   | 14.628739 | 71.66589147 | 0.004115226   | 0.006016955 |       |
| 395           | 111900  | 2.20946                   | 0.218769 | 2.914129  | 19.874607 | 97.36529156 | 0.006758757   | 0.006212175 |       |
| 576           | 136100  | 3.20354                   | 0.269036 | 3.075851  | 24        | 117.5755077 | 0.008849558   | 0.003469959 |       |
| 942           | 173400  | 4.10753                   | 0.338688 | 2.979316  | 30.692019 | 150.359569  | 0.010752688   | 0.003146598 |       |
| 1308          | 202400  | 5.50885                   | 0.387925 | 3.119727  | 36.166283 | 177.1778767 | 0.01369863    | 0.002368434 |       |
| 2304          | 268900  | 7.33333                   | 0.47167  | 3.047545  | 48        | 235.1510153 | 0.01754386    | 0.001619873 |       |
| 3400          | 320800  | 8.89583                   | 0.537278 | 2.984461  | 58.308619 | 285.6571371 | 0.020633333   | 0.0021793   |       |
| 5986          | 419900  | 15.3793                   | 0.657001 | 3.414828  | 77.433843 | 379.346807  | 0.034482759   | 0.00161275  |       |
| 8562          | 494900  | 17.2692                   | 0.755926 | 3.215388  | 92.693042 | 454.1013103 | 0.038461538   | 0.001003775 |       |
| 11188         | 553000  | 20.5909                   | 0.846722 | 3.246725  | 105.77334 | 518.1814354 | 0.045454546   | 0.001563879 |       |
| 13784         | 607200  | 25.3889                   | 0.932387 | 3.447282  | 117.40528 | 575.188063  | 0.055555556   | 0.001223087 |       |
| 16380         | 661300  | 26.9412                   | 1.012072 | 3.338836  | 127.98437 | 626.9628229 | 0.058823529   | 0.001016521 |       |
| 18976         | 693300  | 30.6667                   | 1.094241 | 3.435708  | 137.7534  | 674.8510947 | 0.066666667   | 0.001655872 |       |
| 21572         | 728600  | 35.5385                   | 1.176279 | 3.598097  | 146.8741  | 719.533182  | 0.076923077   | 0.001524782 |       |
| 24168         | 761800  | 38.5833                   | 1.257336 | 3.626752  | 155.46061 | 761.5983193 | 0.083333333   |             |       |

Table G-2 Model 1 Type 1h Fracture Simulation Output and Calculations - Continued

| delta t: cum oil |        | the pressure decline can be compared with actual pressures as a function of time |          |            |        |        |         |          |         |                   |                       |
|------------------|--------|--|----------|------------|--------|--------|---------|----------|---------|-------------------|-----------------------|
| days             | mbo    | 1/q <sup>n</sup> t   | 1/q'     | q' (deriv) | q' alt | PQ     | PQ' alt | p'       | p' alt  | t <sup>n</sup> p' | t <sup>n</sup> p' alt |
| 6                | 9151   |  |          |            |        |        |         |          |         |                   |                       |
| 8                | 10060  | 0.0007   | 8.16E-05 | 12250      | 12250  | 98000  | 98000   | 3        | 3       | 22                | 22                    |
| 10               | 10900  | 0.0024   | 0.000235 | 4250       | 4250   | 42500  | 42500   | 3        | 3       | 25                | 25                    |
| 12               | 11730  | 0.0048   | 0.0004   | 2500       | 2500   | 30000  | 30000   | 2        | 2       | 27                | 27                    |
| 14               | 12540  | 0.0112   | 0.0008   | 1250       | 1250   | 17500  | 17500   | 2        | 2       | 32                | 32                    |
| 16               | 13350  | 0.016  | 0.001    | 1000       | 1000   | 16000  | 16000   | 2        | 2       | 32                | 32                    |
| 18               | 14160  | 0.012  | 0.000867 | 1500       | 1500   | 27000  | 27000   | 2        | 2       | 32                | 32                    |
| 20               | 14960  | 0.0089   | 0.000444 | 2250       | 2250   | 45000  | 45000   | 2        | 2       | 40                | 40                    |
| 22               | 15760  | 0.0073   | 0.000333 | 3000       | 3000   | 58000  | 58000   | 2        | 2       | 39                | 39                    |
| 24               | 16540  | 0.0069   | 0.000285 | 3500       | 3500   | 84000  | 84000   | 2        | 2       | 36                | 36                    |
| 26               | 17310  | 0.0117   | 0.000452 | 285.71     | 2214   | 7428.6 | 57571   | 1.714285 | 1.58571 | 44.57143          | 41.229                |
| 31               | 19100  | -0.046   | -0.00148 | 1000       | 677    | 31000  | -21000  | 1.333333 | 1.72473 | 41.33333          | 53.467                |
| 62               | 30540  | 0.0535   | 0.000863 | 1000       | 1159   | 62000  | 71836   | 0.98913  | 1.12139 | 61.32609          | 69.526                |
| 123              | 51240  | 0.1617   | 0.001315 | 723.68     | 780.7  | 89013  | 93570   | 0.717105 | 0.78173 | 88.20395          | 93.692                |
| 214              | 76340  | 0.3525   | 0.001647 | 586.18     | 607    | 121162 | 129906  | 0.528412 | 0.57762 | 113.2941          | 123.61                |
| 385              | 111900 | 1.0899   | 0.002785 | 359.12     | 359.1  | 141851 | 141851  | 0.41989  | 0.41989 | 165.8584          | 165.86                |
| 578              | 135100 | 3.806  | 0.006781 | 100.55     | 147.5  | 57916  | 84941   | 0.268739 | 0.31442 | 154.7834          | 181.11                |
| 942              | 173400 | 17.239   | 0.0183   | 54.645     | 54.64  | 51475  | 51475   | 0.184426 | 0.18443 | 173.7295          | 173.73                |
| 1308             | 202400 | 29.541   | 0.022585 | 26.432     | 44.28  | 34573  | 57915   | 0.098119 | 0.12802 | 129.6476          | 167.45                |
| 2304             | 268900 | 186.93   | 0.081132 | 11.95      | 12.33  | 27533  | 28398   | 0.066922 | 0.06833 | 154.1874          | 157.43                |
| 3400             | 320600 | 427.85   | 0.125839 | 7.584      | 7.947  | 25785  | 27019   | 0.04117  | 0.04796 | 139.9783          | 163.06                |
| 5998             | 419900 | 1415.1   | 0.236    | 4.2373     | 4.237  | 25407  | 25407   | 0.031202 | 0.0312  | 187.0863          | 187.09                |
| 8592             | 494900 | 6372.8   | 0.741714 | 1.3482     | 1.348  | 11584  | 11584   | 0.023883 | 0.02388 | 205.2018          | 205.2                 |
| 11188            | 553000 | 7261   | 0.649    | 1.5408     | 1.541  | 17239  | 17239   | 0.020031 | 0.02003 | 224.1048          | 224.1                 |
| 13784            | 607200 | 14313  | 1.0384   | 0.983      | 0.983  | 13274  | 13274   | 0.017142 | 0.01714 | 236.282           | 236.28                |
| 16380            | 651300 | 28348  | 1.730687 | 0.5778     | 0.578  | 9464.6 | 9464.6  | 0.015408 | 0.01541 | 252.3883          | 252.39                |
| 18976            | 683300 | 24631  | 1.298    | 0.7704     | 0.77   | 14619  | 14619   | 0.014445 | 0.01445 | 274.114           | 274.11                |
| 21572            | 728600 | 37334  | 1.730687 | 0.5778     | 0.578  | 12465  | 12465   | 0.01329  | 0.01329 | 286.6849          | 286.68                |

Table G-2 Model 1 Type 1h Fracture Simulation Output and Calculations - Continued

| days  | Q'smooth | Q' smooth | Q'smooth | Q'       |
|-------|----------|-----------|----------|----------|
| 6     |          |           |          |          |
| 8     | -437     | 437       |          |          |
| 10    | -418     | 418       | 6813     | 6812.5   |
| 12    | -410     | 410       | 3125     | 3125     |
| 14    | -405     | 405       | 1250     | 1250     |
| 16    | -405     | 405       | 625      | 625      |
| 18    | -403     | 403       | 1250     | 1250     |
| 20    | -400     | 400       | 1875     | 1875     |
| 22    | -395     | 395       | 3125     | 3125     |
| 24    | -388     | 388       | 4429     | 4428.571 |
| 26    | -377     | 377       | 4882     | 3995.392 |
| 31    | -360     | 360       | 3080     | 507.1394 |
| 62    | -359     | 359       | 280      | 498.5175 |
| 123   | -314     | 314       | 728      | 722.0733 |
| 214   | -249     | 249       | 833      | 557.1037 |
| 395   | -162     | 162       | 356      | 356.0315 |
| 576   | -120     | 120       | 181      | 128.6865 |
| 942   | -92      | 92        | 61       | 60.79999 |
| 1308  | -76      | 76        | 37       | 25.33205 |
| 2304  | -57      | 57        | 15       | 14.98098 |
| 3400  | -45      | 45        | 10       | 6.464455 |
| 5996  | -34      | 34        | 4        | 3.637876 |
| 8592  | -26      | 26        | 2        | 2.299971 |
| 11188 | -22      | 22        | 1        | 1.290951 |
| 13784 | -19      | 19        | 1        | 0.971923 |
| 16380 | -17      | 17        | 1        | 0.779022 |
| 18976 | -15      | 15        | 1        | 0.652895 |
| 21572 | -13      | 13        |          |          |

Table G-2 Model 1 Type 1h Fracture Simulation Output and Calculations - Continued

Table G-3 Model 1 Type 1a Fracture Simulation Output and Calculations

| model Type1n |          |                |          |          |          |          |           |        |          |          | kfracture   | 1000     |          |  |
|--------------|----------|----------------|----------|----------|----------|----------|-----------|--------|----------|----------|-------------|----------|----------|--|
| 28 by 28     |          | phmatrix 0.009 |          |          | 2XeL 8.5 |          | oap 3.373 |        |          | w 0.146  | kmatrix 0.1 |          | Sor 0.75 |  |
| delta t      | average  | cum oil        | oil rate | gas rate | cum gas  |          |           |        |          |          | tp(days)    |          |          |  |
| days         | pressure | mbo            | bopd     | mcfd     | mmcf     | dt hours | dq        | dp     | qd/p     | dp/q     | q cum/dp    | q cum/q  | qcum/dq  |  |
| 6            | 1921     | 10.6           | 814      |          |          | 144      | 79        | 10.304 | 0.097052 | 134.177  | 13.02211    |          |          |  |
| 8            | 1912     | 12.13          | 739      |          |          | 192      | 75        | 88     | 8.3977   | 0.11908  | 137.841     | 16.41407 | 161.73   |  |
| 10           | 1905     | 13.47          | 644      |          |          | 240      | 170       | 95     | 6.7789   | 0.147518 | 141.789     | 20.91615 | 79.235   |  |
| 12           | 1898     | 14.83          | 560      |          |          | 288      | 254       | 102    | 5.4902   | 0.182143 | 143.431     | 28.125   | 57.598   |  |
| 14           | 1893     | 15.82          | 476      |          |          | 336      | 338       | 107    | 4.4486   | 0.22479  | 145.981     | 32.81513 | 46.213   |  |
| 16           | 1887     | 16.49          | 422      |          |          | 384      | 392       | 113    | 3.7345   | 0.267773 | 145.929     | 39.07583 | 42.066   |  |
| 18           | 1881     | 17.3           | 402      |          |          | 432      | 412       | 119    | 3.3782   | 0.29802  | 145.378     | 43.03483 | 41.99    |  |
| 20           | 1876     | 18.08          | 389      |          |          | 480      | 425       | 124    | 3.1371   | 0.318768 | 145.806     | 46.47815 | 42.541   |  |
| 22           | 1871     | 18.85          | 383      |          |          | 528      | 431       | 129    | 2.966    | 0.336815 | 146.124     | 49.21671 | 43.735   |  |
| 24           | 1866     | 19.61          | 382      |          |          | 576      | 432       | 134    | 2.8507   | 0.350785 | 146.343     | 51.33508 | 45.384   |  |
| 26           | 1862     | 20.38          | 380      |          |          | 624      | 434       | 138    | 2.7538   | 0.363158 | 147.681     | 53.83158 | 46.959   |  |
| 37           | 1844     | 24.51          | 373      |          |          | 888      | 441       | 156    | 2.391    | 0.418231 | 157.115     | 65.71046 | 55.578   |  |
| 48           | 1828     | 28.56          | 366      |          |          | 1152     | 448       | 172    | 2.1279   | 0.468945 | 166.047     | 78.03279 | 63.75    |  |
| 59           | 1815     | 32.61          | 369      |          |          | 1416     | 445       | 185    | 1.9846   | 0.501356 | 178.27      | 88.37398 | 73.281   |  |
| 70           | 1803     | 36.67          | 368      |          |          | 1680     | 446       | 197    | 1.868    | 0.535328 | 186.142     | 99.64674 | 82.22    |  |
| 81           | 1792     | 40.65          | 357      |          |          | 1944     | 457       | 208    | 1.7163   | 0.582633 | 195.433     | 113.8655 | 88.95    |  |
| 92           | 1781     | 44.5           | 344      |          |          | 2208     | 470       | 219    | 1.5708   | 0.636628 | 203.196     | 129.3605 | 94.681   |  |
| 103          | 1771     | 48.22          | 335      |          |          | 2472     | 479       | 229    | 1.4629   | 0.683582 | 210.568     | 143.9403 | 100.67   |  |
| 114          | 1762     | 51.85          | 328      |          |          | 2736     | 486       | 238    | 1.3782   | 0.72561  | 217.899     | 158.1098 | 106.71   |  |
| 125          | 1753     | 55.43          | 323      |          |          | 3000     | 491       | 247    | 1.3077   | 0.764708 | 224.413     | 171.6099 | 112.89   |  |
| 136          | 1744     | 58.95          | 318      |          |          | 3264     | 498       | 258    | 1.2422   | 0.805031 | 230.273     | 185.3774 | 118.85   |  |
| 147          | 1735     | 62.42          | 313      |          |          | 3528     | 501       | 264    | 1.1856   | 0.84345  | 236.439     | 199.4249 | 124.59   |  |
| 158          | 1728     | 65.82          | 307      |          |          | 3792     | 507       | 272    | 1.1287   | 0.885993 | 241.985     | 214.3974 | 129.82   |  |
| 169          | 1720     | 69.17          | 302      |          |          | 4056     | 512       | 280    | 1.0786   | 0.927152 | 247.036     | 229.0397 | 135.1    |  |
| 180          | 1713     | 72.45          | 298      |          |          | 4320     | 518       | 287    | 1.0314   | 0.969565 | 252.439     | 244.7635 | 139.88   |  |
| 191          | 1705     | 75.67          | 290      |          |          | 4584     | 524       | 296    | 0.9831   | 1.017241 | 258.508     | 260.931  | 144.41   |  |
| 222          | 1686     | 84.45          | 277      |          |          | 5328     | 537       | 314    | 0.8822   | 1.133574 | 268.949     | 304.8736 | 157.26   |  |
| 253          | 1669     | 92.81          | 260      |          |          | 6072     | 554       | 331    | 0.7855   | 1.273077 | 280.393     | 366.9815 | 167.53   |  |
| 284          | 1662     | 100.5          | 243      |          |          | 6816     | 571       | 348    | 0.6983   | 1.432099 | 288.793     | 413.5802 | 176.01   |  |
| 345          | 1621     | 114.8          | 216.4    |          |          | 8280     | 597.8     | 379    | 0.571    | 1.751386 | 302.902     | 530.4991 | 192.1    |  |
| 405          | 1583     | 127.6          | 208.3    |          |          | 9744     | 607.7     | 407    | 0.5069   | 1.972855 | 313.514     | 618.5167 | 209.97   |  |
| 772          | 1472     | 189.2          | 141.6    |          |          | 18528    | 672.4     | 528    | 0.2682   | 3.728814 | 358.333     | 1338.158 | 281.38   |  |
| 1138         | 1407     | 234.5          | 111      |          |          | 27312    | 703       | 583    | 0.1872   | 5.342342 | 395.447     | 2112.613 | 333.57   |  |
| 1504         | 1365     | 270.4          | 85       |          |          | 36096    | 729       | 635    | 0.1339   | 7.470588 | 425.827     | 3181.176 | 370.92   |  |
| 1670         | 1326     | 297.9          | 64.7     |          |          | 44880    | 749.3     | 674    | 0.096    | 10.41731 | 441.988     | 4604.328 | 397.57   |  |
| 2236         | 1293     | 319.1          | 52       |          |          | 53664    | 762       | 707    | 0.0736   | 13.59815 | 451.344     | 6136.538 | 418.77   |  |
| 2602         | 1265     | 336.6          | 44.5     |          |          | 62448    | 789.5     | 735    | 0.0605   | 16.51686 | 457.959     | 7554.045 | 437.43   |  |
| 3698         | 1202     | 379.3          | 35.1     |          |          | 88752    | 778.9     | 798    | 0.044    | 22.73504 | 475.313     | 10808.27 | 488.97   |  |
| 4794         | 1157     | 414.9          | 31       |          |          | 115058   | 783       | 843    | 0.0368   | 27.19355 | 492.171     | 13383.87 | 529.89   |  |
| 5890         | 1122     | 448.3          | 30       |          |          | 141380   | 784       | 878    | 0.0342   | 29.26867 | 510.592     | 14943.33 | 571.81   |  |
| 6986         | 1091     | 479.3          | 27       |          |          | 167884   | 787       | 908    | 0.0297   | 33.68887 | 527.283     | 17751.85 | 609.02   |  |
| 8082         | 1084     | 507.1          | 24.6     |          |          | 193958   | 799.4     | 938    | 0.0263   | 38.04878 | 541.774     | 20813.82 | 842.39   |  |
| 9178         | 1039     | 533.7          | 23.9     |          |          | 220272   | 790.1     | 961    | 0.0249   | 40.20921 | 565.356     | 22330.54 | 875.48   |  |
| 10274        | 1015     | 558.9          | 22       |          |          | 246576   | 792       | 985    | 0.0223   | 44.77273 | 587.411     | 25404.55 | 705.68   |  |

| model Type1n |         | kfracture 1000  |          | kmatrix 0.1 |           | cop 3.373 |  |
|--------------|---------|-----------------|----------|-------------|-----------|-----------|--|
| 28 by 28     |         | primatix 0.0089 |          | 2XeL 8.5    |           |           |  |
| delta t      | cum oil |                 |          | days/days   | hours     |           |  |
| days         | mbo     | dq/q            | dp/p     | (p+dt)/dt   | sqr dt    | sqr dt    |  |
| 6            | 10800   | 0               | 0.041124 | 3.170352    | 2.4494897 | 12        |  |
| 8            | 12130   | 0.10149         | 0.046025 | 3.051759    | 2.8284271 | 13.858406 |  |
| 10           | 13470   | 0.26398         | 0.049899 | 3.091615    | 3.1622777 | 15.481933 |  |
| 12           | 14830   | 0.45357         | 0.053741 | 3.177083    | 3.4641016 | 16.970563 |  |
| 14           | 15620   | 0.71008         | 0.056524 | 3.343938    | 3.7416574 | 18.330303 |  |
| 16           | 16490   | 0.92891         | 0.059683 | 3.442239    | 4         | 19.595918 |  |
| 18           | 17300   | 1.02488         | 0.063264 | 3.390824    | 4.2426407 | 20.78461  |  |
| 20           | 18080   | 1.09254         | 0.066098 | 3.323907    | 4.472136  | 21.908802 |  |
| 22           | 18850   | 1.12533         | 0.068847 | 3.237123    | 4.6904158 | 22.978251 |  |
| 24           | 19610   | 1.13089         | 0.071811 | 3.138962    | 4.8989795 | 24        |  |
| 26           | 20380   | 1.14211         | 0.074114 | 3.082753    | 5.0990195 | 24.979962 |  |
| 37           | 24510   | 1.18231         | 0.084598 | 2.775958    | 6.0827825 | 29.799329 |  |
| 48           | 28560   | 1.22404         | 0.094062 | 2.625683    | 6.9282032 | 33.941125 |  |
| 58           | 32610   | 1.20598         | 0.101928 | 2.497864    | 7.6811457 | 37.629775 |  |
| 70           | 36670   | 1.21198         | 0.109262 | 2.423525    | 8.3666003 | 40.987803 |  |
| 91           | 40850   | 1.28011         | 0.116071 | 2.405747    | 9         | 44.090815 |  |
| 92           | 44500   | 1.36628         | 0.122985 | 2.408092    | 9.591683  | 46.98936  |  |
| 103          | 48220   | 1.42985         | 0.129305 | 2.397479    | 10.148892 | 49.718212 |  |
| 114          | 51880   | 1.48171         | 0.135074 | 2.386928    | 10.677078 | 52.306787 |  |
| 125          | 55430   | 1.52012         | 0.140901 | 2.372879    | 11.18034  | 54.772256 |  |
| 136          | 58850   | 1.55975         | 0.146788 | 2.363089    | 11.681904 | 57.131427 |  |
| 147          | 62420   | 1.60064         | 0.152074 | 2.358632    | 12.124356 | 59.39697  |  |
| 158          | 65820   | 1.65147         | 0.157407 | 2.358946    | 12.569805 | 61.579217 |  |
| 169          | 69170   | 1.69536         | 0.162791 | 2.355265    | 13        | 63.686733 |  |
| 180          | 72450   | 1.75            | 0.167542 | 2.359797    | 13.418408 | 65.726707 |  |
| 191          | 75870   | 1.8089          | 0.173021 | 2.366131    | 13.820275 | 67.705244 |  |
| 222          | 84450   | 1.93863         | 0.186524 | 2.373305    | 14.869884 | 72.99315  |  |
| 253          | 92810   | 2.13077         | 0.198322 | 2.410915    | 15.905874 | 77.923039 |  |
| 284          | 100500  | 2.34979         | 0.210654 | 2.458268    | 16.8523   | 82.55807  |  |
| 345          | 114800  | 2.76155         | 0.233805 | 2.537678    | 18.574176 | 90.994505 |  |
| 406          | 127600  | 2.94571         | 0.255483 | 2.52344     | 20.149442 | 98.711701 |  |
| 772          | 188200  | 4.74859         | 0.358698 | 2.730775    | 27.784888 | 136.1176  |  |
| 1138         | 234500  | 6.33333         | 0.421484 | 2.858426    | 33.734256 | 165.26343 |  |
| 1504         | 270400  | 8.57647         | 0.465201 | 3.115144    | 38.781439 | 189.98947 |  |
| 1870         | 297900  | 11.5811         | 0.508298 | 3.462207    | 43.243497 | 211.849   |  |
| 2236         | 319100  | 14.6538         | 0.54679  | 3.744427    | 47.286352 | 231.65492 |  |
| 2602         | 338800  | 17.2921         | 0.581028 | 3.907012    | 51.009803 | 249.89598 |  |
| 3698         | 379300  | 22.1909         | 0.653884 | 3.922192    | 60.811163 | 297.91274 |  |
| 4794         | 414900  | 25.2581         | 0.728608 | 3.791796    | 69.238717 | 339.19905 |  |
| 5880         | 448300  | 28.1333         | 0.782531 | 3.537068    | 76.746335 | 375.97872 |  |
| 6966         | 479300  | 29.1481         | 0.833181 | 3.541081    | 83.582295 | 409.46795 |  |
| 8082         | 507100  | 32.0894         | 0.878699 | 3.550584    | 89.899944 | 440.41798 |  |
| 9178         | 533700  | 33.0568         | 0.924828 | 3.433051    | 95.801879 | 469.33144 |  |
| 10274        | 558900  | 36              | 0.970443 | 3.472702    | 101.36074 | 496.5642  |  |

Table G-3 Model 1 Type 1n Fracture Simulation Output and Calculations - Continued

Table G-3 Model 1 Type Ia Fracture Simulation Output and Calculations - Continued

| delta t<br>days | cum oil<br>mbo | the pressure decline can be compared with actual pressures as a function of time |                    |                   |           |       |                               |                                   |          |         |                   |                       |
|-----------------|----------------|--|--------------------|-------------------|-----------|-------|-------------------------------|-----------------------------------|----------|---------|-------------------|-----------------------|
|                 |                | q <sup>n</sup> t   | 1/q <sup>n</sup> t | 1/tq <sup>n</sup> | q' (derv) | q'alt | t <sup>n</sup> q <sup>n</sup> | t <sup>n</sup> q <sup>n</sup> alt | p'       | p' alt  | t <sup>n</sup> p' | t <sup>n</sup> p' alt |
| 6               | 10800          |  |                    |                   |           |       |                               |                                   |          |         |                   |                       |
| 8               | 12130          | 3E+05  | 0.0002             | 2.35E-05          | 42500     | 42500 | 340000                        | 340000                            | 4        | 4       | 32                | 32                    |
| 10              | 13470          | 4E+05  | 0.0002             | 2.23E-05          | 44750     | 44750 | 447500                        | 447500                            | 4        | 4       | 35                | 35                    |
| 12              | 14830          | 5E+05  | 0.0003             | 2.38E-05          | 42000     | 42000 | 504000                        | 504000                            | 3        | 3       | 38                | 38                    |
| 14              | 15620          | 5E+05  | 0.0004             | 2.9E-05           | 34500     | 34500 | 483000                        | 483000                            | 3        | 3       | 39                | 39                    |
| 16              | 16490          | 3E+05  | 0.0009             | 5.41E-05          | 18500     | 18500 | 298000                        | 298000                            | 3        | 3       | 48                | 48                    |
| 18              | 17300          | 1E+05  | 0.0022             | 0.000121          | 8250      | 8250  | 148500                        | 148500                            | 3        | 3       | 50                | 50                    |
| 20              | 18080          | 95000  | 0.0042             | 0.000211          | 4750      | 4750  | 95000                         | 95000                             | 3        | 3       | 50                | 50                    |
| 22              | 18850          | 38600  | 0.0126             | 0.000571          | 1750      | 1750  | 38500                         | 38500                             | 3        | 3       | 55                | 55                    |
| 24              | 19610          | 18000  | 0.032              | 0.001333          | 750       | 750   | 18000                         | 18000                             | 2        | 2       | 54                | 54                    |
| 26              | 20380          | 24545  | 0.0275             | 0.001058          | 692.31    | 944.1 | 18000                         | 24545                             | 1.692308 | 1.94406 | 44                | 50.545                |
| 37              | 24510          | 23545  | 0.0581             | 0.001571          | 636.38    | 636.4 | 23545                         | 23545                             | 1.545455 | 1.54545 | 57.18182          | 57.182                |
| 48              | 28580          | 8727   | 0.264              | 0.0055            | 181.82    | 181.8 | 8727.3                        | 8727.3                            | 1.318182 | 1.31818 | 63.27273          | 63.273                |
| 59              | 32610          | -6364  | -0.649             | -0.011            | -90.91    | -90.9 | -6364                         | -6363.6                           | 1.136364 | 1.13636 | 67.04545          | 67.045                |
| 70              | 36670          | 38182  | 0.1283             | 0.001833          | 545.45    | 545.5 | 38182                         | 38182                             | 1.045455 | 1.04545 | 73.18182          | 73.182                |
| 81              | 40650          | 88364  | 0.0742             | 0.000917          | 1080.9    | 1091  | 88364                         | 88364                             | 1        | 1       | 81                | 81                    |
| 92              | 44500          | 92000  | 0.092              | 0.001             | 1000      | 1000  | 92000                         | 92000                             | 0.954545 | 0.95455 | 87.81818          | 87.818                |
| 103             | 48220          | 74908  | 0.1416             | 0.001375          | 727.27    | 727.3 | 74908                         | 74908                             | 0.883636 | 0.88364 | 88.95455          | 88.955                |
| 114             | 51860          | 62182  | 0.209              | 0.001833          | 545.45    | 545.5 | 62182                         | 62182                             | 0.818182 | 0.81818 | 93.27273          | 93.273                |
| 125             | 55430          | 58818  | 0.275              | 0.0022            | 454.55    | 454.5 | 58818                         | 58818                             | 0.818182 | 0.81818 | 102.2727          | 102.27                |
| 136             | 59950          | 61818  | 0.2982             | 0.0022            | 454.55    | 454.5 | 61818                         | 61818                             | 0.772727 | 0.77273 | 105.0909          | 105.09                |
| 147             | 62420          | 73500  | 0.294              | 0.002             | 500       | 500   | 73500                         | 73500                             | 0.727273 | 0.72727 | 106.9091          | 106.91                |
| 158             | 65820          | 79000  | 0.316              | 0.002             | 500       | 500   | 79000                         | 79000                             | 0.727273 | 0.72727 | 114.9091          | 114.91                |
| 169             | 69170          | 94500  | 0.338              | 0.002             | 500       | 500   | 84500                         | 84500                             | 0.681818 | 0.68182 | 115.2273          | 115.23                |
| 180             | 72450          | 98182  | 0.33               | 0.001833          | 545.45    | 545.5 | 98182                         | 98182                             | 0.681818 | 0.68182 | 122.7273          | 122.73                |
| 191             | 75870          | 97874  | 0.3727             | 0.001951          | 452.38    | 512.4 | 85405                         | 97874                             | 0.642857 | 0.69732 | 122.7857          | 133.19                |
| 222             | 84450          | 1E+05  | 0.4588             | 0.002067          | 483.87    | 483.9 | 107419                        | 107419                            | 0.580645 | 0.58065 | 128.9032          | 128.9                 |
| 253             | 92810          | 1E+05  | 0.4614             | 0.001824          | 548.39    | 548.4 | 138742                        | 138742                            | 0.548387 | 0.54839 | 138.7419          | 138.74                |
| 284             | 100500         | 1E+05  | 0.5563             | 0.001959          | 473.91    | 510.5 | 134591                        | 144993                            | 0.521739 | 0.53484 | 148.1739          | 151.9                 |
| 345             | 114800         | 1E+05  | 1.1469             | 0.003324          | 300.82    | 300.8 | 103783                        | 103783                            | 0.483807 | 0.48381 | 168.8443          | 168.84                |
| 406             | 127600         | 67873  | 2.4286             | 0.005982          | 175.18    | 187.2 | 71121                         | 67873                             | 0.348946 | 0.44067 | 141.6721          | 178.91                |
| 772             | 188200         | 1E+05  | 5.9297             | 0.007681          | 130.19    | 130.2 | 100508                        | 100508                            | 0.254098 | 0.2541  | 196.1639          | 196.16                |
| 1138            | 234500         | 87903  | 14.718             | 0.012933          | 77.322    | 77.32 | 87903                         | 87903                             | 0.146175 | 0.14617 | 166.347           | 166.35                |
| 1504            | 270400         | 95130  | 23.778             | 0.01581           | 63.251    | 63.25 | 95130                         | 95130                             | 0.110656 | 0.11066 | 166.4252          | 166.43                |
| 1870            | 297800         | 84303  | 41.48              | 0.022182          | 45.062    | 45.08 | 84303                         | 84303                             | 0.098361 | 0.09836 | 183.9344          | 183.93                |
| 2236            | 319100         | 81704  | 81.027             | 0.036238          | 27.598    | 27.8  | 81704                         | 81704                             | 0.083333 | 0.08333 | 186.3333          | 186.33                |
| 2602            | 336600         | 45558  | 148.81             | 0.057114          | 11.58     | 17.51 | 30078                         | 45558                             | 0.062244 | 0.07174 | 181.9576          | 186.67                |
| 3698            | 379300         | 22775  | 800.45             | 0.16237           | 6.1588    | 6.159 | 22775                         | 22775                             | 0.04927  | 0.04927 | 182.2007          | 182.2                 |
| 4794            | 414900         | 11154  | 2080.5             | 0.429804          | 2.3266    | 2.327 | 11154                         | 11154                             | 0.036496 | 0.0365  | 174.9635          | 174.96                |
| 5890            | 448300         | 10748  | 3227.7             | 0.548             | 1.8248    | 1.825 | 10748                         | 10748                             | 0.030108 | 0.03011 | 177.3449          | 177.34                |
| 6986            | 479300         | 17210  | 2835.8             | 0.405926          | 2.4635    | 2.464 | 17210                         | 17210                             | 0.02846  | 0.02846 | 184.8485          | 184.85                |
| 8082            | 507100         | 11430  | 5714.8             | 0.707097          | 1.4142    | 1.414 | 11430                         | 11430                             | 0.023723 | 0.02372 | 191.7283          | 191.73                |
| 9178            | 533700         | 10886  | 7737.8             | 0.843077          | 1.1881    | 1.188 | 10886                         | 10886                             | 0.022354 | 0.02235 | 205.1651          | 205.17                |

| delta t | cum  |           |            |           | 2 smooths |           |            |
|---------|------|-----------|------------|-----------|-----------|-----------|------------|
|         | days | Q' smooth | -Q' smooth | Q"        | Q"        | Q" smooth | Q"t        |
| 6       |      |           |            |           |           |           |            |
| 8       | -718 | 718       |            |           |           |           |            |
| 10      | -625 | 625       | -45000     | 45000     |           | 45000     | 450000     |
| 12      | -538 | 538       | -40000     | 40000     |           | 40000     | 480000     |
| 14      | -465 | 465       | -28375     | 28375     |           | 28375     | 411250     |
| 16      | -420 | 420       | -16875     | 16875     |           | 16875     | 270000     |
| 18      | -388 | 388       | -8125      | 8125      |           | 8125      | 146250     |
| 20      | -388 | 388       | -3750      | 3750      |           | 3750      | 75000      |
| 22      | -383 | 383       | -1250      | 1250      |           | 1250      | 27500      |
| 24      | -383 | 383       | 257.8871   | -257.8871 |           | -258      | -6188.8112 |
| 26      | -384 | 384       | -821.678   | 821.6783  |           | -273      | 21363.636  |
| 37      | -372 | 372       | -697.711   | 697.7114  |           | 698       | 25815.321  |
| 48      | -368 | 368       | -144.628   | 144.6281  |           | 145       | 6642.1488  |
| 59      | -369 | 369       | -123.987   | 123.9889  |           | 124       | 7314.0496  |
| 70      | -365 | 365       | -578.512   | 578.5124  |           | 579       | 40495.858  |
| 81      | -356 | 356       | -971.074   | 971.0744  |           | 971       | 78657.025  |
| 92      | -344 | 344       | -971.074   | 971.0744  |           | 971       | 88338.843  |
| 103     | -335 | 335       | -743.802   | 743.8017  |           | 744       | 78811.57   |
| 114     | -328 | 328       | -557.851   | 557.8512  |           | 558       | 63565.041  |
| 125     | -322 | 322       | -454.545   | 454.5455  |           | 455       | 56818.182  |
| 136     | -318 | 318       | -454.545   | 454.5455  |           | 455       | 61818.182  |
| 147     | -312 | 312       | -495.868   | 495.8678  |           | 496       | 72892.562  |
| 158     | -307 | 307       | -495.868   | 495.8678  |           | 496       | 78347.107  |
| 169     | -301 | 301       | -516.529   | 516.5289  |           | 517       | 87293.388  |
| 180     | -295 | 295       | -505.675   | 505.6747  |           | 506       | 91021.442  |
| 191     | -290 | 290       | -452.451   | 452.4508  |           | 466       | 86418.098  |
| 222     | -278 | 278       | -505.933   | 505.9327  |           | 506       | 112317.05  |
| 253     | -259 | 259       | -531.978   | 531.9775  |           | 532       | 134590.31  |
| 284     | -243 | 243       | -399.346   | 399.3459  |           | 447       | 113414.23  |
| 345     | -222 | 222       | -324.31    | 324.3099  |           | 324       | 111886.91  |
| 406     | -204 | 204       | -178.204   | 178.2035  |           | 279       | 72350.623  |
| 772     | -146 | 146       | -127.014   | 127.014   |           | 127       | 98054.798  |
| 1138    | -111 | 111       | -81.1834   | 81.18337  |           | 81        | 92388.679  |
| 1504    | -87  | 87        | -60.6542   | 60.65424  |           | 61        | 91223.984  |
| 1870    | -67  | 67        | -46.0972   | 46.09723  |           | 46        | 86201.813  |
| 2236    | -53  | 53        | -28.5963   | 28.59626  |           | 28        | 63941.241  |
| 2602    | -46  | 46        | -11.7292   | 11.72917  |           | 17        | 30519.306  |
| 3668    | -36  | 36        | -6.44137   | 6.441373  |           | 6         | 23820.196  |
| 4794    | -31  | 31        | -2.8928    | 2.892902  |           | 3         | 13868.572  |
| 5800    | -29  | 29        | -2.12285   | 2.122849  |           | 2         | 12503.58   |
| 6986    | -27  | 27        | -2.08122   | 2.081224  |           | 2         | 14539.433  |
| 8082    | -25  | 25        | -1.45686   | 1.456857  |           | 1         | 11774.319  |
| 9178    | -24  | 24        | -1.33196   | 1.331964  |           | 1         | 12224.945  |

Table G-3 Model 1 Type Ia Fracture Simulation Output and Calculations - Continued

**Table G-4 Model 1 Type 1nh Fracture Simulation Output and Calculations**

| model Type1nh |          |                 |          |          |          |          |           |      |        | kfracture 4000 |             |          |          |  |
|---------------|----------|-----------------|----------|----------|----------|----------|-----------|------|--------|----------------|-------------|----------|----------|--|
| 28 by 28      |          | phimatrix 0.009 |          |          | 2XeL 6.5 |          | cop 3.373 |      |        | w 0.146        | kmatrix 0.1 |          | Sai 0.75 |  |
| delta t       | average  | cum oil         | oil rate | gas rate | cum gas  |          |           |      |        |                |             |          |          |  |
| days          | pressure | mbo             | bopd     | mcfd     | mmcf     | dt hours | dq        | dp   | qd/p   | dq/q           | q cum/dp    | q cum/q  | qcum/dq  |  |
| 6             | 1809     | 11.24           | 920      |          |          | 144      |           | 91   | 10.11  | 0.088913       | 123.516     | 12.21739 |          |  |
| 8             | 1800     | 12.98           | 833      |          |          | 192      | 87        | 100  | 8.33   | 0.120048       | 129.8       | 15.58223 | 149.2    |  |
| 10            | 1893     | 14.45           | 708      |          |          | 240      | 212       | 107  | 6.6168 | 0.15113        | 135.047     | 20.4096  | 68.16    |  |
| 12            | 1887     | 15.69           | 582      |          |          | 288      | 328       | 113  | 5.2389 | 0.190878       | 138.85      | 26.50338 | 47.835   |  |
| 14            | 1882     | 16.73           | 491      |          |          | 336      | 429       | 118  | 4.161  | 0.240326       | 141.78      | 34.07332 | 38.998   |  |
| 16            | 1876     | 17.62           | 440      |          |          | 384      | 480       | 124  | 3.5484 | 0.281818       | 142.097     | 40.04545 | 36.708   |  |
| 18            | 1871     | 18.48           | 428      |          |          | 432      | 492       | 129  | 3.3178 | 0.301402       | 143.256     | 43.17757 | 37.561   |  |
| 20            | 1866     | 19.33           | 425      |          |          | 480      | 495       | 134  | 3.1718 | 0.315294       | 144.254     | 45.48235 | 39.051   |  |
| 22            | 1862     | 20.18           | 424      |          |          | 528      | 496       | 138  | 3.0725 | 0.325472       | 146.232     | 47.58434 | 40.685   |  |
| 24            | 1858     | 21.03           | 423      |          |          | 576      | 497       | 142  | 2.9789 | 0.335697       | 148.099     | 49.71631 | 42.314   |  |
| 26            | 1855     | 21.87           | 422      |          |          | 624      | 498       | 145  | 2.9103 | 0.343802       | 150.828     | 51.82484 | 43.916   |  |
| 37            | 1836     | 26.47           | 414      |          |          | 888      | 506       | 164  | 2.5244 | 0.398135       | 161.402     | 63.9372  | 52.312   |  |
| 48            | 1821     | 30.99           | 410      |          |          | 1152     | 510       | 179  | 2.2905 | 0.436585       | 173.128     | 75.58537 | 60.765   |  |
| 59            | 1808     | 35.51           | 413      |          |          | 1416     | 507       | 192  | 2.151  | 0.464891       | 184.948     | 85.98063 | 70.039   |  |
| 70            | 1795     | 40.07           | 413      |          |          | 1680     | 507       | 205  | 2.0146 | 0.496388       | 195.463     | 97.02179 | 79.034   |  |
| 81            | 1784     | 44.54           | 402      |          |          | 1944     | 518       | 216  | 1.8611 | 0.537313       | 206.204     | 110.798  | 85.985   |  |
| 92            | 1773     | 48.86           | 389      |          |          | 2208     | 531       | 227  | 1.7137 | 0.583548       | 215.33      | 125.6555 | 92.053   |  |
| 103           | 1762     | 53.1            | 380      |          |          | 2472     | 540       | 238  | 1.5966 | 0.626316       | 223.109     | 139.7368 | 98.333   |  |
| 114           | 1753     | 57.24           | 373      |          |          | 2736     | 547       | 247  | 1.5101 | 0.662198       | 231.741     | 153.4584 | 104.64   |  |
| 125           | 1744     | 61.32           | 368      |          |          | 3000     | 552       | 256  | 1.4375 | 0.696652       | 239.531     | 165.6304 | 111.09   |  |
| 136           | 1734     | 65.34           | 363      |          |          | 3264     | 557       | 268  | 1.3847 | 0.732782       | 245.639     | 180      | 117.31   |  |
| 147           | 1726     | 69.31           | 358      |          |          | 3528     | 562       | 274  | 1.3066 | 0.765363       | 252.956     | 193.6034 | 123.33   |  |
| 158           | 1718     | 73.22           | 353      |          |          | 3792     | 567       | 282  | 1.2518 | 0.798867       | 259.645     | 207.4221 | 129.14   |  |
| 169           | 1710     | 77.08           | 347      |          |          | 4056     | 573       | 290  | 1.1986 | 0.835735       | 265.724     | 222.0749 | 134.49   |  |
| 180           | 1702     | 80.84           | 341      |          |          | 4320     | 579       | 298  | 1.1443 | 0.8739         | 271.275     | 237.0674 | 139.82   |  |
| 191           | 1694     | 84.55           | 335      |          |          | 4584     | 585       | 308  | 1.0948 | 0.913433       | 278.307     | 252.3881 | 144.53   |  |
| 222           | 1674     | 94.71           | 322      |          |          | 5328     | 598       | 326  | 0.9877 | 1.012422       | 290.521     | 294.1304 | 158.38   |  |
| 253           | 1656     | 104.5           | 308      |          |          | 6072     | 611       | 345  | 0.8857 | 1.116505       | 302.899     | 338.1877 | 171.03   |  |
| 284           | 1638     | 113.9           | 298.4    |          |          | 6816     | 621.6     | 362  | 0.8243 | 1.213137       | 314.841     | 381.7024 | 183.24   |  |
| 345           | 1606     | 131.5           | 281      |          |          | 8280     | 639       | 384  | 0.7132 | 1.402135       | 333.756     | 467.9715 | 205.79   |  |
| 406           | 1578     | 147.9           | 274      |          |          | 9744     | 646       | 422  | 0.6493 | 1.540148       | 350.474     | 539.781  | 228.95   |  |
| 772           | 1450     | 222.8           | 160      |          |          | 18528    | 760       | 550  | 0.2809 | 3.4375         | 405.091     | 1392.5   | 293.16   |  |
| 1138          | 1372     | 268.3           | 88       |          |          | 27312    | 832       | 628  | 0.1401 | 7.136384       | 424.045     | 3026.136 | 320.07   |  |
| 1504          | 1320     | 292.8           | 82       |          |          | 36098    | 858       | 680  | 0.0912 | 10.96774       | 430.588     | 4722.581 | 341.26   |  |
| 1870          | 1281     | 312.6           | 48       |          |          | 44880    | 872       | 719  | 0.0688 | 14.97917       | 434.771     | 6512.5   | 358.49   |  |
| 2238          | 1251     | 329.2           | 44       |          |          | 53884    | 878       | 749  | 0.0587 | 17.02273       | 439.519     | 7481.818 | 375.8    |  |
| 2602          | 1226     | 344.8           | 41       |          |          | 62448    | 879       | 774  | 0.053  | 18.87805       | 445.478     | 8408.756 | 382.26   |  |
| 3698          | 1172     | 384.8           | 33.8     |          |          | 88752    | 886.2     | 828  | 0.0408 | 24.49704       | 464.493     | 11378.7  | 433.99   |  |
| 4794          | 1133     | 423             | 35.4     |          |          | 115056   | 884.6     | 887  | 0.0408 | 24.49153       | 487.888     | 11949.15 | 478.18   |  |
| 5890          | 1096     | 458.4           | 29.3     |          |          | 141380   | 890.7     | 902  | 0.0325 | 30.78498       | 508.204     | 15845.05 | 514.65   |  |
| 6866          | 1068     | 488.5           | 26.7     |          |          | 167684   | 893.3     | 932  | 0.0286 | 34.90837       | 524.142     | 18295.88 | 546.85   |  |
| 8082          | 1041     | 517.9           | 26.4     |          |          | 193988   | 893.6     | 959  | 0.0275 | 36.32576       | 540.042     | 19817.42 | 579.57   |  |
| 9178          | 1016     | 545.3           | 23.4     |          |          | 220272   | 896.6     | 984  | 0.0238 | 42.05128       | 554.167     | 23303.42 | 608.19   |  |
| 10274         | 993      | 589.4           | 21       |          |          | 246576   | 899       | 1007 | 0.0209 | 47.95238       | 585.442     | 27114.29 | 633.37   |  |

| model Type1nh |         | w 0.146         |          | kfracture 4000 |           | kmatrx 0.1  |             |
|---------------|---------|-----------------|----------|----------------|-----------|-------------|-------------|
| 28 by 28      |         | phimatrx 0.0089 |          | 2X&L 8.5       |           | oop 3.373   |             |
| delta t       | cum oil | days/days       |          |                |           | hours       |             |
| days          | mbo     | dq/q            | dp/p     | (p+dt)/dt      | sqr dt    | sqr dt      | 1/q         |
| 6             | 11240   | 0               | 0.047659 | 3.036232       | 2.4494897 | 12          | 0.001086957 |
| 8             | 12980   | 0.10444         | 0.052632 | 2.947779       | 2.8284271 | 13.85640646 | 0.00120048  |
| 10            | 14450   | 0.29844         | 0.058524 | 3.04096        | 3.1622777 | 15.49183338 | 0.001412429 |
| 12            | 15690   | 0.55405         | 0.059683 | 3.206615       | 3.4641016 | 16.97056275 | 0.001689189 |
| 14            | 16730   | 0.87373         | 0.062699 | 3.433809       | 3.7416574 | 18.33030278 | 0.00203666  |
| 16            | 17820   | 1.09091         | 0.068098 | 3.502841       | 4         | 19.58591794 | 0.002272727 |
| 18            | 18480   | 1.14953         | 0.068947 | 3.396754       | 4.2426407 | 20.78460969 | 0.002336449 |
| 20            | 19330   | 1.16471         | 0.071811 | 3.274118       | 4.472136  | 21.90890223 | 0.002352941 |
| 22            | 20180   | 1.16681         | 0.074114 | 3.163379       | 4.6604158 | 22.97825056 | 0.002358491 |
| 24            | 21030   | 1.17494         | 0.078426 | 3.071513       | 4.8989795 | 24          | 0.002364065 |
| 26            | 21870   | 1.18009         | 0.078167 | 2.993256       | 5.0990195 | 24.97999199 | 0.002369668 |
| 37            | 26470   | 1.22222         | 0.089325 | 2.726032       | 6.0827825 | 29.79932685 | 0.002415459 |
| 48            | 30990   | 1.2439          | 0.096298 | 2.574695       | 6.9282032 | 33.9411255  | 0.002439024 |
| 59            | 35510   | 1.2276          | 0.106195 | 2.457299       | 7.6811457 | 37.82977544 | 0.002421308 |
| 70            | 40070   | 1.2276          | 0.114206 | 2.386026       | 8.3866003 | 40.96780306 | 0.002421308 |
| 81            | 44540   | 1.28858         | 0.121076 | 2.367852       | 9         | 44.09081537 | 0.002487562 |
| 92            | 48680   | 1.36504         | 0.128032 | 2.365821       | 9.591663  | 46.9883605  | 0.002570684 |
| 103           | 53100   | 1.42105         | 0.135074 | 2.356668       | 10.148892 | 49.71921158 | 0.002631579 |
| 114           | 57240   | 1.46849         | 0.140801 | 2.346127       | 10.677078 | 52.30678732 | 0.002680965 |
| 125           | 61320   | 1.5             | 0.146789 | 2.333043       | 11.18034  | 54.77225575 | 0.002717391 |
| 136           | 65340   | 1.53444         | 0.153403 | 2.323529       | 11.661904 | 57.13142743 | 0.002754821 |
| 147           | 68310   | 1.58983         | 0.158749 | 2.31703        | 12.124356 | 59.39696962 | 0.002793296 |
| 158           | 73220   | 1.60623         | 0.164144 | 2.312798       | 12.569805 | 61.57921727 | 0.002832881 |
| 169           | 77080   | 1.6513          | 0.169591 | 2.314053       | 13        | 63.68673331 | 0.002881844 |
| 180           | 80840   | 1.69795         | 0.175088 | 2.317041       | 13.416408 | 65.72670569 | 0.002832551 |
| 191           | 84550   | 1.74627         | 0.180636 | 2.321403       | 13.820275 | 67.70524352 | 0.002985075 |
| 222           | 94710   | 1.85714         | 0.194743 | 2.324912       | 14.899664 | 72.99315036 | 0.00310559  |
| 253           | 104500  | 1.97735         | 0.208459 | 2.33671        | 15.905974 | 77.92303866 | 0.003236246 |
| 284           | 113900  | 2.08311         | 0.221001 | 2.344023       | 16.8523   | 82.55905976 | 0.003351208 |
| 345           | 131500  | 2.27402         | 0.24533  | 2.356439       | 18.574176 | 90.99450533 | 0.003558719 |
| 406           | 147900  | 2.35766         | 0.267427 | 2.32951        | 20.149442 | 98.71170143 | 0.003649635 |
| 772           | 222800  | 4.75            | 0.37931  | 2.803756       | 27.784888 | 135.1175982 | 0.00625     |
| 1138          | 286300  | 9.45455         | 0.457726 | 3.659171       | 33.734256 | 165.2634261 | 0.011363636 |
| 1504          | 292800  | 13.8387         | 0.515152 | 4.140014       | 38.781439 | 189.9884734 | 0.016129032 |
| 1870          | 312800  | 18.1667         | 0.56128  | 4.48262        | 43.243497 | 211.8480028 | 0.020833333 |
| 2236          | 329200  | 19.9091         | 0.598721 | 4.346073       | 47.286362 | 231.6548158 | 0.022727273 |
| 2602          | 344800  | 21.439          | 0.631321 | 4.232035       | 51.009803 | 249.8969784 | 0.024390244 |
| 3698          | 384600  | 26.2189         | 0.706485 | 4.076987       | 60.811183 | 297.9127389 | 0.029585799 |
| 4794          | 423000  | 24.9887         | 0.765225 | 3.492522       | 69.238717 | 339.1990565 | 0.026248588 |
| 5890          | 458400  | 30.3993         | 0.821494 | 3.656206       | 76.746335 | 375.9787228 | 0.034129693 |
| 6986          | 488500  | 33.4569         | 0.872658 | 3.818935       | 83.582295 | 409.4679475 | 0.037453184 |
| 8082          | 517900  | 33.8485         | 0.92123  | 3.427298       | 89.899944 | 440.4179833 | 0.037878788 |
| 9178          | 545300  | 38.3162         | 0.988504 | 3.538052       | 96.801879 | 469.3314394 | 0.042736043 |
| 10274         | 586400  | 42.8095         | 1.014099 | 3.839117       | 101.38074 | 498.5841952 | 0.047819048 |

Table G-4 Model 1 Type 1nh Fracture Simulation Output and Calculations - Continued

Table G-4 Model 1 Type I Inh Fracture Simulation Output and Calculations - Continued

| days | cum oil | the pressure decline can be compared with actual pressures as a function of time |                  |            |       |                  |                    |          |         |                  |                      |
|------|---------|--|------------------|------------|-------|------------------|--------------------|----------|---------|------------------|----------------------|
|      |         | 1/q <sup>n</sup> t   | 1/q <sup>n</sup> | q' (derrv) | q'alt | p <sup>n</sup> t | p <sup>n</sup> alt | p'       | p' alt  | r <sup>n</sup> p | r <sup>n</sup> p'alt |
| 6    | 11240   |  |                  |            |       |                  |                    |          |         |                  |                      |
| 8    | 12980   | 0.0002   | 1.89E-05         | 53000      | 53000 | 424000           | 424000             | 4        | 4       | 32               | 32                   |
| 10   | 14450   | 0.0002   | 1.88E-05         | 60250      | 60250 | 602500           | 602500             | 3        | 3       | 33               | 33                   |
| 12   | 15890   | 0.0002   | 1.84E-05         | 54250      | 54250 | 651000           | 651000             | 3        | 3       | 33               | 33                   |
| 14   | 16730   | 0.0004   | 2.63E-05         | 38000      | 38000 | 532000           | 532000             | 3        | 3       | 39               | 39                   |
| 16   | 17620   | 0.001  | 6.35E-05         | 15750      | 15750 | 252000           | 252000             | 3        | 3       | 44               | 44                   |
| 18   | 18480   | 0.0048   | 0.000267         | 3750       | 3750  | 67500            | 67500              | 3        | 3       | 45               | 45                   |
| 20   | 19330   | 0.02   | 0.001            | 1000       | 1000  | 20000            | 20000              | 2        | 2       | 45               | 45                   |
| 22   | 20180   | 0.044  | 0.002            | 500        | 500   | 11000            | 11000              | 2        | 2       | 44               | 44                   |
| 24   | 21030   | 0.048  | 0.002            | 500        | 500   | 12000            | 12000              | 2        | 2       | 42               | 42                   |
| 26   | 21870   | 0.0376   | 0.001444         | 692.31     | 535   | 18000            | 13909              | 1.692308 | 1.53497 | 44               | 39.908               |
| 37   | 26470   | 0.0878   | 0.001833         | 545.45     | 545.5 | 20182            | 20182              | 1.545455 | 1.54545 | 57.18182         | 57.182               |
| 48   | 30990   | 1.066  | 0.022            | 45.455     | 45.45 | 2181.8           | 2181.8             | 1.272727 | 1.27273 | 61.09091         | 61.091               |
| 56   | 35510   | -0.433   | -0.00733         | -136.4     | -136  | 8045             | 8045.5             | 1.181818 | 1.18182 | 60.72727         | 60.727               |
| 70   | 40070   | 0.14   | 0.002            | 500        | 500   | 35000            | 35000              | 1.090909 | 1.09091 | 76.36364         | 76.364               |
| 81   | 44540   | 0.0743   | 0.000917         | 1080.9     | 1081  | 88364            | 88364              | 1        | 1       | 81               | 81                   |
| 92   | 48880   | 0.082  | 0.001            | 1000       | 1000  | 92000            | 92000              | 1        | 1       | 92               | 92                   |
| 103  | 53100   | 0.1416   | 0.001375         | 727.27     | 727.3 | 74909            | 74909              | 0.909091 | 0.90909 | 93.63636         | 93.636               |
| 114  | 57240   | 0.208  | 0.001833         | 545.45     | 545.5 | 62182            | 62182              | 0.818182 | 0.81818 | 93.27273         | 93.273               |
| 125  | 61320   | 0.275  | 0.0022           | 454.55     | 454.5 | 56818            | 56818              | 0.863636 | 0.86364 | 107.9545         | 107.95               |
| 136  | 65340   | 0.2962   | 0.0022           | 454.55     | 454.5 | 61818            | 61818              | 0.818182 | 0.81818 | 111.2727         | 111.27               |
| 147  | 69310   | 0.3234   | 0.0022           | 454.55     | 454.5 | 66818            | 66818              | 0.727273 | 0.72727 | 108.9091         | 108.91               |
| 158  | 73220   | 0.316  | 0.002            | 500        | 500   | 79000            | 79000              | 0.727273 | 0.72727 | 114.9091         | 114.91               |
| 169  | 77080   | 0.3068   | 0.001833         | 545.45     | 545.5 | 92182            | 92182              | 0.727273 | 0.72727 | 122.9091         | 122.91               |
| 180  | 80840   | 0.33   | 0.001833         | 545.45     | 545.5 | 98182            | 98182              | 0.727273 | 0.72727 | 130.9091         | 130.91               |
| 191  | 84550   | 0.4222   | 0.002211         | 452.38     | 512.4 | 86405            | 97874              | 0.666667 | 0.70577 | 127.3333         | 134.8                |
| 222  | 94710   | 0.5294   | 0.002385         | 419.35     | 419.4 | 93097            | 93097              | 0.629032 | 0.62903 | 138.6452         | 139.65               |
| 253  | 104500  | 0.6547   | 0.002527         | 380.65     | 380.6 | 96303            | 96303              | 0.580645 | 0.58065 | 146.9032         | 146.9                |
| 284  | 113800  | 0.9331   | 0.003286         | 304.35     | 322.8 | 88435            | 91685              | 0.532609 | 0.54037 | 151.2609         | 153.48               |
| 345  | 131500  | 1.725  | 0.005            | 200        | 200   | 69000            | 69000              | 0.491803 | 0.4918  | 168.6721         | 169.67               |
| 406  | 147900  | 1.4327   | 0.003529         | 283.37     | 142.9 | 115049           | 58000              | 0.36534  | 0.4434  | 148.3279         | 180.02               |
| 772  | 222800  | 3.0382   | 0.003935         | 254.1      | 254.1 | 198164           | 198164             | 0.281421 | 0.28142 | 217.2568         | 217.26               |
| 1138 | 266300  | 8.5002   | 0.007489         | 133.88     | 133.9 | 152355           | 152355             | 0.177598 | 0.1776  | 202.1038         | 202.1                |
| 1504 | 292800  | 27.523   | 0.0183           | 54.645     | 54.64 | 82188            | 82188              | 0.124317 | 0.12432 | 186.9727         | 186.97               |
| 1870 | 312800  | 78.047   | 0.040887         | 24.59      | 24.58 | 45984            | 45984              | 0.094262 | 0.09426 | 178.2705         | 178.27               |
| 2236 | 329200  | 233.82   | 0.104571         | 9.5628     | 9.563 | 21383            | 21383              | 0.075137 | 0.07514 | 168.0056         | 168.01               |
| 2602 | 344800  | 372.95   | 0.143333         | 6.9767     | 7.789 | 18153            | 20268              | 0.054036 | 0.06354 | 140.6005         | 165.33               |
| 3698 | 384600  | 1447.5   | 0.391429         | 2.5547     | 2.555 | 9447.4           | 9447.4             | 0.042427 | 0.04243 | 156.8951         | 156.9                |
| 4794 | 423000  | 2336.2   | 0.487111         | 2.0529     | 2.053 | 9841.7           | 9841.7             | 0.033759 | 0.03376 | 161.8412         | 161.84               |
| 5890 | 458400  | 1484   | 0.251954         | 3.989      | 3.989 | 23377            | 23377              | 0.029663 | 0.02966 | 174.6578         | 174.66               |
| 6988 | 488500  | 5280.5   | 0.755852         | 1.323      | 1.323 | 9242.4           | 9242.4             | 0.026004 | 0.026   | 181.8615         | 181.86               |
| 8082 | 517900  | 5388.4   | 0.684242         | 1.5055     | 1.505 | 12167            | 12167              | 0.023723 | 0.02372 | 191.7263         | 191.73               |
| 9178 | 545300  | 3725.6   | 0.405926         | 2.4635     | 2.464 | 22610            | 22610              | 0.021898 | 0.0219  | 200.9781         | 200.98               |

| data t | cum       |            |          | 2 smooths |           |
|--------|-----------|------------|----------|-----------|-----------|
| days   | Q' smooth | -Q' smooth | Q"       | Q"        | Q" smooth |
| 6      |           |            |          |           |           |
| 8      | -803      | 803        |          |           |           |
| 10     | -678      | 678        | -58125   | 58125     | 58125     |
| 12     | -570      | 570        | -48750   | 48750     | 48750     |
| 14     | -483      | 483        | -33125   | 33125     | 33125     |
| 16     | -438      | 438        | -13750   | 13750     | 13750     |
| 18     | -428      | 428        | -3125    | 3125      | 3125      |
| 20     | -425      | 425        | -625     | 625       | 625       |
| 22     | -425      | 425        | -625     | 625       | 625       |
| 24     | -423      | 423        | -1319.93 | 1319.93   | 1320      |
| 26     | -420      | 420        | -611.888 | 611.8881  | 1248      |
| 37     | -415      | 415        | -400.509 | 400.5088  | 401       |
| 48     | -411      | 411        | -82.6446 | 82.64463  | 83        |
| 59     | -413      | 413        | -20.6612 | 20.66116  | 21        |
| 70     | -410      | 410        | -557.851 | 557.8512  | 558       |
| 81     | -400      | 400        | -971.074 | 971.0744  | 971       |
| 92     | -389      | 389        | -929.752 | 929.7521  | 930       |
| 103    | -380      | 380        | -702.479 | 702.4793  | 702       |
| 114    | -374      | 374        | -537.19  | 537.1901  | 537       |
| 125    | -368      | 368        | -475.207 | 475.2086  | 475       |
| 136    | -363      | 363        | -454.545 | 454.5455  | 455       |
| 147    | -358      | 358        | -495.868 | 495.8678  | 496       |
| 158    | -352      | 352        | -537.19  | 537.1901  | 537       |
| 169    | -348      | 348        | -537.19  | 537.1901  | 537       |
| 180    | -340      | 340        | -526.685 | 526.6849  | 527       |
| 191    | -335      | 335        | -444.77  | 444.7703  | 491       |
| 222    | -322      | 322        | -407.426 | 407.4264  | 407       |
| 253    | -310      | 310        | -379.085 | 379.0854  | 379       |
| 284    | -298      | 298        | -335.083 | 335.0827  | 349       |
| 345    | -279      | 279        | -316.329 | 316.3295  | 316       |
| 406    | -260      | 260        | -273.884 | 273.8839  | 305       |
| 772    | -162      | 162        | -224.114 | 224.1141  | 224       |
| 1138   | -96       | 96         | -134.559 | 134.5591  | 135       |
| 1504   | -63       | 63         | -62.7072 | 62.70716  | 63        |
| 1870   | -50       | 50         | -26.3148 | 26.31481  | 26        |
| 2236   | -44       | 44         | -11.8624 | 11.86237  | 12        |
| 2602   | -41       | 41         | -5.68865 | 5.688654  | 7         |
| 3698   | -36       | 36         | -3.3648  | 3.364799  | 3         |
| 4794   | -34       | 34         | -2.64315 | 2.643155  | 3         |
| 5890   | -30       | 30         | -2.97615 | 2.976151  | 3         |
| 6986   | -27       | 27         | -1.81057 | 1.810555  | 2         |
| 8082   | -26       | 26         | -1.66498 | 1.664979  | 2         |
| 9178   | -23       | 23         | -2.16447 | 2.164473  | 2         |

Table G-4 Model I Type 1uh Fracture Simulation Output and Calculations - Continued

| model Type2 |          |           |          |          |         |                 |       |      |        |          |          |          |          |  |  |          |  |  |  |  |  |  |  |  |  |
|-------------|----------|-----------|----------|----------|---------|-----------------|-------|------|--------|----------|----------|----------|----------|--|--|----------|--|--|--|--|--|--|--|--|--|
| 28 by 28    |          | phimatrix | 0.11     | 2Xe/L    | 8.5     | coirp(mm<br>bo) | 3.373 |      |        |          |          |          |          |  |  |          |  |  |  |  |  |  |  |  |  |
|             |          | w         | 0.007    |          |         |                 |       |      |        |          |          |          |          |  |  |          |  |  |  |  |  |  |  |  |  |
|             |          | kmatrix   | 0.1      | Soi      | 0.75    |                 |       |      |        |          |          |          |          |  |  |          |  |  |  |  |  |  |  |  |  |
|             |          | kfracture | 1000     |          |         |                 |       |      |        |          |          |          |          |  |  |          |  |  |  |  |  |  |  |  |  |
| delta q     |          |           |          |          |         |                 |       |      |        |          |          |          |          |  |  |          |  |  |  |  |  |  |  |  |  |
| delta t     | average  | curr oil  | oil rate | gas rate | cum gas |                 |       |      |        |          |          |          |          |  |  | tx(days) |  |  |  |  |  |  |  |  |  |
| days        | pressure | mbo       | bopd     | mcf/d    | mmcf    | dt hours        | dq    | dp   | q/dp   | d/q      | q cum/dp | q cum/q  | q cum/dq |  |  |          |  |  |  |  |  |  |  |  |  |
| 5           | 1863     | 13.18     | 1548     | 808      | 9.345   | 144             |       | 137  | 11.299 | 0.088501 | 36.2044  | 8.514212 |          |  |  |          |  |  |  |  |  |  |  |  |  |
| 8           | 1838     | 16.19     | 1444     | 974      | 11.15   | 192             | 104   | 162  | 8.9136 | 0.112188 | 99.8383  | 11.21191 | 155.67   |  |  |          |  |  |  |  |  |  |  |  |  |
| 10          | 1814     | 18.95     | 1321     | 950      | 13.12   | 240             | 227   | 186  | 7.1022 | 0.140802 | 101.882  | 14.34519 | 83.48    |  |  |          |  |  |  |  |  |  |  |  |  |
| 12          | 1792     | 21.55     | 1289     | 804      | 14.72   | 288             | 259   | 208  | 6.1971 | 0.161365 | 103.606  | 16.71839 | 83.205   |  |  |          |  |  |  |  |  |  |  |  |  |
| 14          | 1771     | 24.1      | 1253     | 824      | 16.33   | 336             | 295   | 229  | 5.4716 | 0.182761 | 105.24   | 19.23384 | 81.685   |  |  |          |  |  |  |  |  |  |  |  |  |
| 16          | 1751     | 26.55     | 1220     | 727      | 17.89   | 384             | 328   | 249  | 4.8996 | 0.204098 | 106.627  | 21.7623  | 80.945   |  |  |          |  |  |  |  |  |  |  |  |  |
| 18          | 1732     | 28.93     | 1183     | 744      | 19.41   | 432             | 385   | 268  | 4.3398 | 0.230438 | 107.948  | 24.87532 | 75.143   |  |  |          |  |  |  |  |  |  |  |  |  |
| 20          | 1714     | 31.23     | 1183     | 499      | 20.7    | 480             | 365   | 286  | 4.1384 | 0.241758 | 109.196  | 26.39899 | 85.582   |  |  |          |  |  |  |  |  |  |  |  |  |
| 22          | 1698     | 33.55     | 1152     | 631      | 21.9    | 528             | 395   | 302  | 3.8146 | 0.262153 | 111.093  | 29.12326 | 84.722   |  |  |          |  |  |  |  |  |  |  |  |  |
| 24          | 1682     | 35.82     | 1163     | 556      | 22.98   | 576             | 385   | 318  | 3.6572 | 0.273431 | 112.642  | 30.79966 | 83.039   |  |  |          |  |  |  |  |  |  |  |  |  |
| 26          | 1667     | 37.95     | 1084     | 630      | 24.32   | 624             | 484   | 333  | 3.1952 | 0.31297  | 113.964  | 35.66729 | 78.409   |  |  |          |  |  |  |  |  |  |  |  |  |
| 31          | 1634     | 43.14     | 1055     | 545      | 27.7    | 744             | 483   | 368  | 2.8825 | 0.346919 | 117.869  | 40.891   | 87.505   |  |  |          |  |  |  |  |  |  |  |  |  |
| 62          | 1541     | 70.68     | 793      | 458      | 43.55   | 1488            | 755   | 459  | 1.7277 | 0.578815 | 153.987  | 89.12969 | 93.616   |  |  |          |  |  |  |  |  |  |  |  |  |
| 123         | 1483     | 114.6     | 697      | 331      | 67.49   | 2952            | 851   | 517  | 1.3482 | 0.74175  | 221.663  | 164.4169 | 134.67   |  |  |          |  |  |  |  |  |  |  |  |  |
| 214         | 1430     | 171.8     | 591      | 300      | 96.56   | 5136            | 957   | 570  | 1.0368 | 0.964467 | 301.404  | 290.6937 | 179.52   |  |  |          |  |  |  |  |  |  |  |  |  |
| 395         | 1355     | 268.4     | 481      | 212      | 143.9   | 9480            | 1067  | 645  | 0.7457 | 1.340956 | 416.124  | 558.0042 | 251.55   |  |  |          |  |  |  |  |  |  |  |  |  |
| 576         | 1297     | 351.8     | 439      | 214      | 184.8   | 13824           | 1106  | 703  | 0.8245 | 1.601367 | 500.427  | 801.3867 | 317.22   |  |  |          |  |  |  |  |  |  |  |  |  |
| 942         | 1203     | 494.2     | 349      | 168      | 256.5   | 22608           | 1199  | 797  | 0.4378 | 2.283668 | 620.075  | 1416.046 | 412.18   |  |  |          |  |  |  |  |  |  |  |  |  |
| 1308        | 1129     | 611.8     | 290      | 153      | 319.5   | 31382           | 1258  | 871  | 0.333  | 3.003448 | 702.411  | 2109.655 | 486.33   |  |  |          |  |  |  |  |  |  |  |  |  |
| 2304        | 969      | 845.8     | 179      | 216      | 498.3   | 55296           | 1389  | 1031 | 0.1736 | 5.759777 | 820.369  | 4725.14  | 617.82   |  |  |          |  |  |  |  |  |  |  |  |  |
| 3400        | 812      | 1007      | 111      | 224      | 719.7   | 81600           | 1437  | 1168 | 0.0934 | 10.7027  | 847.643  | 9072.072 | 700.77   |  |  |          |  |  |  |  |  |  |  |  |  |
| 5696        | 511      | 1179      | 38       | 128      | 1161    | 143904          | 1510  | 1489 | 0.0255 | 39.18421 | 791.807  | 31026.32 | 780.79   |  |  |          |  |  |  |  |  |  |  |  |  |
| 8592        | 382      | 1244      | 17       | 54       | 1371    | 205208          | 1531  | 1638 | 0.0104 | 96.35294 | 759.463  | 73176.47 | 812.54   |  |  |          |  |  |  |  |  |  |  |  |  |
| 11188       | 298      | 1276      | 9.2      | 34       | 1488    | 268512          | 1539  | 1702 | 0.0054 | 185      | 749.708  | 138865.7 | 829.22   |  |  |          |  |  |  |  |  |  |  |  |  |
| 13784       | 298      | 1295      | 6        | 22       | 1558    | 330816          | 1542  | 1734 | 0.0035 | 289      | 746.828  | 215833.3 | 839.82   |  |  |          |  |  |  |  |  |  |  |  |  |
| 16380       | 254      | 1309      | 4.8      | 17.2     | 1608    | 393120          | 1543  | 1746 | 0.0027 | 363.75   | 749.714  | 272708.3 | 848.24   |  |  |          |  |  |  |  |  |  |  |  |  |
| 18976       | 246      | 1320      | 4        | 14.3     | 1647    | 455424          | 1544  | 1754 | 0.0023 | 438.5    | 752.586  | 330000   | 864.92   |  |  |          |  |  |  |  |  |  |  |  |  |
| 21572       | 239      | 1330      | 3.3      | 11.9     | 1681    | 517728          | 1545  | 1761 | 0.0019 | 533.6364 | 755.253  | 403030.3 | 881.01   |  |  |          |  |  |  |  |  |  |  |  |  |
| 24168       | 233      | 1337      | 2.8      | 10.2     | 1708    | 580032          | 1546  | 1767 | 0.0016 | 631.0714 | 756.65   | 477500   | 865.26   |  |  |          |  |  |  |  |  |  |  |  |  |

Table G-5 Model 2 Type 2 Fracture Simulation Output and Calculations

| model Type2 |         |                          |          |            |           |                  |             |  |
|-------------|---------|--------------------------|----------|------------|-----------|------------------|-------------|--|
| 28 by 28    |         | phimatrx 0.11<br>w 0.007 |          | 2xarL 8.5  |           | ocip(mmbo) 3.373 |             |  |
|             |         | kmatrix 0.1              |          | Sci 0.75   |           |                  |             |  |
|             |         | kfracture 1000           |          |            |           |                  |             |  |
| delta t     | cum oil |                          |          |            | days/days |                  |             |  |
| days        | mbo     | dq/q                     | dp/p     | (tp+dt)/dt | sqrt dt   | sqrt dt          | hours       |  |
| 6           | 13180   | 0                        | 0.073537 | 2.419035   | 2.4484897 |                  | 12          |  |
| 8           | 16190   | 0.07202                  | 0.068136 | 2.401489   | 2.8284271 | 13.85640546      |             |  |
| 10          | 18950   | 0.17184                  | 0.102536 | 2.434519   | 3.1622777 | 15.49193338      | 0.032227198 |  |
| 12          | 21550   | 0.20063                  | 0.116071 | 2.393199   | 3.4641016 | 16.97056275      | 0.01589686  |  |
| 14          | 24100   | 0.23543                  | 0.129305 | 2.373846   | 3.7416574 | 18.33030278      | 0.016980376 |  |
| 16          | 26550   | 0.26885                  | 0.142204 | 2.380143   | 4         | 19.59591794      | 0.023901384 |  |
| 18          | 28930   | 0.33104                  | 0.154734 | 2.381952   | 4.2426407 | 20.78460969      | 0.009921289 |  |
| 20          | 31230   | 0.30854                  | 0.165851 | 2.318949   | 4.472136  | 21.9089023       | 0.003177397 |  |
| 22          | 33550   | 0.34375                  | 0.177856 | 2.323785   | 4.6904158 | 22.97825059      | 0.005625699 |  |
| 24          | 35820   | 0.33104                  | 0.189051 | 2.283319   | 4.8989795 |                  | 24          |  |
| 26          | 37950   | 0.45489                  | 0.19976  | 2.371818   | 5.0690195 | 24.97999199      | 0.019465452 |  |
| 31          | 43140   | 0.4673                   | 0.22399  | 2.319054   | 5.5577644 | 27.27636339      | 0.01381093  |  |
| 62          | 70680   | 0.95208                  | 0.297859 | 2.437579   | 7.8740079 | 38.57460304      | 0.00819183  |  |
| 123         | 114600  | 1.22095                  | 0.348618 | 2.336739   | 11.090537 | 54.33231083      | 0.00438653  |  |
| 214         | 171800  | 1.61929                  | 0.398601 | 2.358382   | 14.828739 | 71.66586147      | 0.003666722 |  |
| 395         | 268400  | 2.2183                   | 0.476015 | 2.412666   | 19.874607 | 97.36529156      | 0.002505267 |  |
| 576         | 351800  | 2.5282                   | 0.54202  | 2.391262   | 24        | 117.5755077      | 0.002225292 |  |
| 942         | 494200  | 3.43553                  | 0.66251  | 2.503233   | 30.692019 | 150.359569       | 0.002475048 |  |
| 1308        | 611800  | 4.33793                  | 0.771479 | 2.612886   | 36.166283 | 177.1778787      | 0.003082889 |  |
| 2304        | 845800  | 7.64804                  | 1.063963 | 3.050842   | 48        | 235.1510153      | 0.00411473  |  |
| 3400        | 1007000 | 12.9459                  | 1.483054 | 3.668256   | 58.309519 | 285.6571371      | 0.00869144  |  |
| 5996        | 1179000 | 39.7368                  | 2.913894 | 6.174502   | 77.433843 | 379.346807       | 0.014852249 |  |
| 8582        | 1244000 | 90.0588                  | 4.524862 | 9.516815   | 92.683042 | 454.1013103      | 0.024561639 |  |
| 11188       | 1276000 | 167.261                  | 5.711409 | 13.39682   | 105.77334 | 518.1814354      | 0.032153539 |  |
| 13784       | 1286000 | 257                      | 6.518797 | 16.65825   | 117.40828 | 575.168083       | 0.029707074 |  |
| 16380       | 1309000 | 321.5                    | 6.874016 | 17.64886   | 127.98437 | 626.9928229      | 0.024845917 |  |
| 18978       | 1320000 | 386                      | 7.130081 | 18.39039   | 137.7534  | 674.8510947      | 0.028233996 |  |
| 21572       | 1330000 | 468.091                  | 7.368201 | 19.68303   | 146.8741  | 719.533182       | 0.03194475  |  |
| 24168       | 1337000 | 551.857                  | 7.583691 | 20.75753   | 155.46061 | 761.5983193      |             |  |

Table G-5 Model 2 Type 2 Fracture Simulation Output and Calculations - Continued

| delta t<br>days | cum oil<br>mbo | the pressure decline can be compared with actual pressures as a function of time |          |           |       |        |         |          |         |          |         |
|-----------------|----------------|--|----------|-----------|-------|--------|---------|----------|---------|----------|---------|
|                 |                | 1/q''t   | 1/k'     | q' (derv) | q'att | r'Q'   | r'Q'att | p'       | p'att   | r'p'     | r'p'att |
| 6               | 13180          |  |          |           |       |        |         |          |         |          |         |
| 8               | 16190          | 0.0001   | 1.78E-05 | 58750     | 58750 | 454000 | 454000  | 12       | 12      | 98       | 98      |
| 10              | 18850          | 0.0003   | 2.58E-05 | 38750     | 38750 | 387500 | 387500  | 12       | 12      | 115      | 115     |
| 12              | 21550          | 0.0007   | 5.88E-05 | 17000     | 17000 | 204000 | 204000  | 11       | 11      | 129      | 129     |
| 14              | 24100          | 0.0008   | 5.8E-05  | 17250     | 17250 | 241500 | 241500  | 10       | 10      | 144      | 144     |
| 16              | 26550          | 0.0007   | 4.44E-05 | 22500     | 22500 | 380000 | 380000  | 10       | 10      | 156      | 156     |
| 18              | 28930          | 0.0019   | 0.000108 | 9250      | 9250  | 188500 | 188600  | 9        | 9       | 167      | 167     |
| 20              | 31230          | 0.0073   | 0.000364 | 2750      | 2750  | 55000  | 55000   | 9        | 9       | 170      | 170     |
| 22              | 33550          | 0.0044   | 0.0002   | 5000      | 5000  | 110000 | 110000  | 8        | 8       | 176      | 176     |
| 24              | 35820          | 0.0011   | 4.55E-05 | 22000     | 22000 | 528000 | 528000  | 8        | 8       | 186      | 186     |
| 26              | 37950          | 0.0017   | 6.48E-05 | 15429     | 35871 | 401143 | 932657  | 6.857143 | 7.24286 | 178.2857 | 188.31  |
| 31              | 43140          | 0.0041   | 0.000133 | 7527.8    | 2724  | 233381 | 84439   | 3.5      | 6.1     | 108.5    | 189.1   |
| 62              | 70680          | 0.0158   | 0.000257 | 3891.3    | 6134  | 241281 | 380313  | 1.641304 | 2.30952 | 101.7609 | 143.19  |
| 123             | 114600         | 0.0626   | 0.000752 | 1328.9    | 1410  | 163461 | 173388  | 0.730263 | 0.80287 | 88.82237 | 98.766  |
| 214             | 171800         | 0.2695   | 0.001259 | 794.12    | 978.5 | 169941 | 208389  | 0.470588 | 0.52619 | 100.7059 | 112.61  |
| 395             | 268400         | 0.9407   | 0.002382 | 419.89    | 419.9 | 165856 | 165856  | 0.367403 | 0.3674  | 145.1243 | 145.12  |
| 576             | 351800         | 2.3869   | 0.004144 | 241.32    | 238.6 | 138998 | 136299  | 0.277879 | 0.29939 | 160.0586 | 172.45  |
| 942             | 494200         | 4.6278   | 0.004913 | 203.55    | 203.6 | 191746 | 191746  | 0.229508 | 0.22951 | 216.1967 | 216.2   |
| 1308            | 611800         | 10.479   | 0.008012 | 124.82    | 147.8 | 163260 | 193384  | 0.171806 | 0.19102 | 224.7225 | 249.86  |
| 2304            | 845800         | 26.927   | 0.011887 | 85.584    | 87.93 | 197140 | 202580  | 0.15153  | 0.15236 | 349.1243 | 351.04  |
| 3400            | 1E+06          | 89.027   | 0.026184 | 38.191    | 51.97 | 129848 | 176709  | 0.124052 | 0.13514 | 421.7768 | 459.49  |
| 5998            | 1E+06          | 331.18   | 0.055234 | 18.105    | 18.1  | 108556 | 108556  | 0.086672 | 0.08667 | 519.6841 | 519.68  |
| 8592            | 1E+06          | 1548.9   | 0.180278 | 5.547     | 5.547 | 47880  | 47880   | 0.041025 | 0.04102 | 352.4838 | 352.48  |
| 11188           | 1E+06          | 5280.7   | 0.472    | 2.1186    | 2.119 | 23703  | 23703   | 0.01849  | 0.01849 | 208.8659 | 208.87  |
| 13784           | 1E+06          | 18265  | 1.18     | 0.8475    | 0.847 | 11681  | 11681   | 0.008475 | 0.00847 | 116.8136 | 116.81  |
| 16380           | 1E+06          | 42522  | 2.586    | 0.3852    | 0.386 | 6309.7 | 6309.7  | 0.003852 | 0.00385 | 63.09707 | 63.097  |
| 18978           | 1E+06          | 65682  | 3.461333 | 0.2889    | 0.289 | 5482.3 | 5482.3  | 0.002889 | 0.00289 | 54.8228  | 54.823  |
| 21572           | 1E+06          | 93335  | 4.326867 | 0.2311    | 0.231 | 4985.8 | 4985.8  | 0.002504 | 0.0025  | 54.0131  | 54.013  |

Table G-5 Model 2 Type 2 Fracture Simulation Output and Calculations - Continued

| delta t<br>days | 2 smooths |            |       |           |           |  |
|-----------------|-----------|------------|-------|-----------|-----------|--|
|                 | Q' smooth | Q'' smooth | Q"    | Q' smooth | Q''t      |  |
| 6               |           |            |       |           |           |  |
| 8               | -1443     | 1443       |       |           |           |  |
| 10              | -1340     | 1340       | 38750 | 38750     | 387500    |  |
| 12              | -1288     | 1288       | 22500 | 22500     | 270000    |  |
| 14              | -1250     | 1250       | 20000 | 20000     | 280000    |  |
| 16              | -1208     | 1208       | 20000 | 20000     | 320000    |  |
| 18              | -1170     | 1170       | 13125 | 13125     | 236250    |  |
| 20              | -1155     | 1155       | 5625  | 5625      | 112500    |  |
| 22              | -1148     | 1148       | 13750 | 13750     | 302500    |  |
| 24              | -1100     | 1100       | 22554 | 22554     | 541285.71 |  |
| 26              | -1057     | 1057       | 11826 | 17545     | 307486.97 |  |
| 31              | -1017     | 1017       | 6268  | 7732      | 194299.17 |  |
| 52              | -832      | 832        | 3629  | 4789      | 225027.76 |  |
| 123             | -683      | 683        | 1545  | 1837      | 190015.62 |  |
| 214             | -587      | 587        | 684   | 816       | 146363.86 |  |
| 395             | -497      | 497        | 441   | 441       | 174350.45 |  |
| 576             | -437      | 437        | 260   | 297       | 149577.1  |  |
| 942             | -355      | 355        | 190   | 190       | 178807.54 |  |
| 1308            | -298      | 298        | 119   | 142       | 155855.21 |  |
| 2304            | -193      | 193        | 84    | 88        | 192750.27 |  |
| 3400            | -123      | 123        | 40    | 54        | 135799.95 |  |
| 5996            | -46       | 46         | 20    | 20        | 120571.68 |  |
| 8592            | -19       | 19         | 7     | 7         | 59284.047 |  |
| 11188           | -10       | 10         | 2     | 2         | 26562.14  |  |
| 13784           | -6        | 6          | 1     | 1         | 13294.722 |  |
| 16380           | -5        | 5          | 0     | 0         |           |  |
| 18976           | -4        | 4          | 1     | 1         |           |  |
| 21572           |           |            |       |           |           |  |

Table G-5 Model 2 Type 2 Fracture Simulation Output and Calculations - Continued

| model Type2h   |          |                |          |           |         |           |      |      |        |          |          |          |         |
|----------------|----------|----------------|----------|-----------|---------|-----------|------|------|--------|----------|----------|----------|---------|
| 28 by 28       |          | phimatrix 0.11 |          | 2Xe/L 8.5 |         | cop 3.373 |      |      |        |          |          |          |         |
|                |          | w 0.007        |          |           |         | (mmbo)    |      |      |        |          |          |          |         |
|                |          | kmatrix 10.1   |          | Sci 0.75  |         |           |      |      |        |          |          |          |         |
|                |          | kfraction 4000 |          |           |         |           |      |      |        |          |          |          |         |
| <b>delta q</b> |          |                |          |           |         |           |      |      |        |          |          |          |         |
| delta t        | average  | cum oil        | oil rate | gas rate  | cum gas |           |      |      |        |          |          | tp(days) |         |
| days           | pressure | mbo            | bopd     | mcfd      | mmcf    | dt hours  | dq   | dp   | q/dp   | dp/q     | q cum/dp | q cum/q  | qcum/dq |
| 6              | 1840     | 14.84          | 1780     | 1165      | 10.23   | 144       |      | 160  | 11.125 | 0.069888 | 92.75    | 9.337079 |         |
| 8              | 1810     | 18.27          | 1676     | 1226      | 12.73   | 192       | 104  | 190  | 8.8211 | 0.113365 | 98.1579  | 10.90085 | 175.87  |
| 10             | 1782     | 21.52          | 1611     | 1152      | 15.1    | 240       | 169  | 218  | 7.3899 | 0.13532  | 98.7156  | 13.35816 | 127.34  |
| 12             | 1756     | 24.77          | 1605     | 1077      | 17.16   | 288       | 175  | 244  | 6.5779 | 0.152025 | 101.516  | 15.43302 | 141.54  |
| 14             | 1733     | 27.91          | 1548     | 982       | 19.17   | 336       | 232  | 287  | 5.7978 | 0.172481 | 104.532  | 18.02972 | 120.3   |
| 16             | 1711     | 30.97          | 1511     | 898       | 21.2    | 384       | 269  | 289  | 5.2284 | 0.191284 | 107.163  | 20.49636 | 115.13  |
| 18             | 1691     | 33.94          | 1494     | 856       | 22.95   | 432       | 286  | 309  | 4.835  | 0.206827 | 109.838  | 22.71754 | 118.67  |
| 20             | 1673     | 36.88          | 1453     | 883       | 24.81   | 480       | 327  | 327  | 4.4434 | 0.225052 | 112.783  | 25.38197 | 112.78  |
| 22             | 1656     | 39.67          | 1373     | 958       | 26.73   | 528       | 407  | 344  | 3.9913 | 0.250546 | 115.32   | 28.89294 | 97.469  |
| 24             | 1640     | 42.44          | 1375     | 851       | 28.38   | 576       | 405  | 360  | 3.8194 | 0.261818 | 117.889  | 30.86545 | 104.79  |
| 26             | 1626     | 45.16          | 1344     | 798       | 29.95   | 624       | 436  | 374  | 3.5936 | 0.278274 | 120.749  | 33.60119 | 103.58  |
| 31             | 1594     | 51.2           | 1246     | 798       | 34.41   | 744       | 534  | 406  | 3.089  | 0.325843 | 128.108  | 41.09149 | 95.88   |
| 32             | 1520     | 65.03          | 1006     | 621       | 54.54   | 1488      | 774  | 480  | 2.0958 | 0.477137 | 179.229  | 85.5169  | 111.15  |
| 123            | 1457     | 142.4          | 882      | 475       | 86.74   | 2952      | 888  | 543  | 1.8243 | 0.615846 | 262.247  | 161.4512 | 158.57  |
| 214            | 1397     | 216            | 751      | 432       | 124.6   | 5136      | 1029 | 603  | 1.2454 | 0.802929 | 358.209  | 287.6165 | 209.91  |
| 396            | 1310     | 339.8          | 642      | 299       | 186.1   | 9480      | 1138 | 690  | 0.9304 | 1.074786 | 492.484  | 529.2835 | 298.59  |
| 578            | 1242     | 444.2          | 540      | 285       | 238.2   | 13824     | 1240 | 758  | 0.7124 | 1.403704 | 588.016  | 822.5826 | 358.23  |
| 942            | 1132     | 612.1          | 386      | 284       | 334.5   | 22608     | 1394 | 968  | 0.4447 | 2.248705 | 705.184  | 1585.751 | 439.1   |
| 1308           | 1040     | 736.9          | 301      | 278       | 433.6   | 31392     | 1479 | 960  | 0.3135 | 3.189369 | 787.604  | 2448.173 | 498.24  |
| 2304           | 841      | 959.8          | 170      | 258       | 696.9   | 55298     | 1610 | 1159 | 0.1467 | 6.817647 | 827.955  | 5844.706 | 595.02  |
| 3400           | 681      | 1099           | 90       | 235       | 983.8   | 81600     | 1690 | 1339 | 0.0872 | 14.87778 | 820.762  | 12211.11 | 650.3   |
| 5996           | 391      | 1230           | 28       | 82        | 1343    | 143904    | 1752 | 1609 | 0.0174 | 57.48429 | 784.45   | 43928.57 | 702.05  |
| 8592           | 297      | 1277           | 12.3     | 43        | 1499    | 208208    | 1768 | 1703 | 0.0072 | 138.4553 | 749.853  | 103821.1 | 722.41  |
| 11186          | 262      | 1302           | 7.6      | 26.3      | 1584    | 268512    | 1772 | 1738 | 0.0044 | 228.6842 | 748.137  | 171315.8 | 734.6   |
| 13784          | 248      | 1319           | 5.7      | 20        | 1643    | 330816    | 1774 | 1752 | 0.0033 | 307.3684 | 752.854  | 231403.5 | 743.39  |
| 16380          | 240      | 1332           | 4.6      | 16.1      | 1699    | 393120    | 1775 | 1760 | 0.0026 | 382.6087 | 755.818  | 289565.2 | 750.25  |
| 18976          | 233      | 1343           | 3.7      | 13.2      | 1727    | 455424    | 1776 | 1767 | 0.0021 | 477.5676 | 780.045  | 362973   | 758.07  |
| 21572          | 226      | 1352           | 3        | 10.8      | 1758    | 517728    | 1777 | 1772 | 0.0017 | 590.6887 | 782.98   | 450886.7 | 780.83  |
| 24168          | 224      | 1359           | 2.6      | 9.4       | 1784    | 580032    | 1777 | 1776 | 0.0015 | 683.0769 | 785.203  | 522882.3 | 784.6   |

Table G-6 Model 2 Type 2h Fracture Simulation Output and Calculations

| model Type2h |         |         |                |            |           |             |                     |             |  |
|--------------|---------|---------|----------------|------------|-----------|-------------|---------------------|-------------|--|
| 28 by 28     |         |         | phimatrix 0.11 |            | 2XeL 8.5  |             | oip 3.373<br>(mmbo) |             |  |
|              |         |         | w 0.007        |            |           |             |                     |             |  |
|              |         |         | kmatrix 10.1   |            | Sol 0.75  |             |                     |             |  |
|              |         |         | kfracture 4000 |            |           |             |                     |             |  |
| delta t      | cum oil |         |                | days/days  |           |             | hours               |             |  |
| days         | mbo     | dg/q    | dq/p           | (tp+dt)/dt | sort dt   | sort dt     | sort dt             | 1/q'        |  |
| 5            | 14840   | 0       | 0.086957       | 2.389513   | 2.4494897 |             | 12                  | 0.000581798 |  |
| 8            | 18270   | 0.06205 | 0.104972       | 2.362619   | 2.8284271 | 13.85640646 |                     | 0.000596659 |  |
| 10           | 21520   | 0.1049  | 0.122334       | 2.335816   | 3.1622777 | 15.49193338 |                     | 0.000620732 |  |
| 12           | 24770   | 0.10903 | 0.138952       | 2.286085   | 3.4641016 | 16.97056275 |                     | 0.000623053 |  |
| 14           | 27910   | 0.14887 | 0.154088       | 2.287837   | 3.7416574 | 18.33030278 |                     | 0.000645995 |  |
| 16           | 30970   | 0.17803 | 0.168907       | 2.281023   |           | 4           | 19.59591794         | 0.000681813 |  |
| 18           | 33940   | 0.19143 | 0.182732       | 2.262085   | 4.2426407 | 20.78460989 |                     | 0.000689344 |  |
| 20           | 36880   | 0.22505 | 0.195457       | 2.269088   | 4.472136  | 21.9086023  |                     | 0.000688231 |  |
| 22           | 39670   | 0.29643 | 0.207729       | 2.313315   | 4.6904158 | 22.97825058 |                     | 0.000728332 |  |
| 24           | 42440   | 0.29455 | 0.219512       | 2.286081   | 4.8989795 |             | 24                  | 0.000727273 |  |
| 26           | 45160   | 0.3244  | 0.230012       | 2.292353   | 5.0990195 | 24.97999199 |                     | 0.000744048 |  |
| 31           | 51200   | 0.42857 | 0.254705       | 2.325532   | 5.5677644 | 27.27636339 |                     | 0.000802568 |  |
| 62           | 86030   | 0.76938 | 0.315789       | 2.379305   | 7.8740079 | 38.57460304 |                     | 0.000994036 |  |
| 123          | 142400  | 1.01814 | 0.372684       | 2.312812   | 11.090537 | 54.33231083 |                     | 0.001133787 |  |
| 214          | 216000  | 1.37017 | 0.431639       | 2.344002   | 14.626739 | 71.66589147 |                     | 0.001331558 |  |
| 395          | 339800  | 1.77259 | 0.526718       | 2.336958   | 19.874607 | 97.36529156 |                     | 0.001557632 |  |
| 576          | 444200  | 2.2963  | 0.610308       | 2.428112   |           | 24          | 117.5755077         | 0.001851852 |  |
| 942          | 612100  | 3.6114  | 0.768784       | 2.683388   | 30.692019 | 150.359569  |                     | 0.002590674 |  |
| 1308         | 738600  | 4.91362 | 0.923077       | 2.871692   | 36.166283 | 177.1778767 |                     | 0.003222259 |  |
| 2304         | 959600  | 9.47058 | 1.378121       | 3.446959   |           | 48          | 235.1510153         | 0.005882353 |  |
| 3400         | 1098000 | 18.7778 | 2.025719       | 4.581503   | 58.309519 | 285.6571371 |                     | 0.011111111 |  |
| 5998         | 1230000 | 62.5714 | 4.11509        | 8.326313   | 77.433843 | 379.346807  |                     | 0.035714286 |  |
| 8592         | 1277000 | 143.715 | 5.734007       | 13.08347   | 92.683042 | 454.1013103 |                     | 0.081300813 |  |
| 11188        | 1302000 | 233.211 | 6.833568       | 16.31246   | 105.77334 | 518.1814354 |                     | 0.131576947 |  |
| 13784        | 1319000 | 311.281 | 7.054516       | 17.78783   | 117.40528 | 575.166063  |                     | 0.175438595 |  |
| 16380        | 1332000 | 385.957 | 7.333333       | 18.67797   | 127.98437 | 626.9928229 |                     | 0.217391304 |  |
| 18978        | 1343000 | 480.081 | 7.583681       | 20.128     | 137.7534  | 674.8510947 |                     | 0.27027027  |  |
| 21572        | 1352000 | 592.333 | 7.77193        | 21.89128   | 146.8741  | 719.533182  |                     | 0.333333333 |  |
| 24168        | 1359000 | 683.615 | 7.928571       | 22.62745   | 155.46051 | 761.5983193 |                     | 0.384615385 |  |

Table G-6 Model 2 Type 2h Fracture Simulation Output and Calculations - Continued

| delta t | cum oil | the pressure decline can be compared with actual pressures as a function of time |     |                    |                    |           |                   |                     |                                    |          |                   |                     |                                    |
|---------|---------|--|-----|--------------------|--------------------|-----------|-------------------|---------------------|------------------------------------|----------|-------------------|---------------------|------------------------------------|
|         |         | days   | mbo | 1/q <sup>n</sup> t | 1/t <sup>1/2</sup> | q' (derv) | q' <sup>alt</sup> | t <sup>1/2</sup> Q' | t <sup>1/2</sup> Q' <sup>alt</sup> | p'       | p' <sup>alt</sup> | t <sup>1/2</sup> p' | t <sup>1/2</sup> p' <sup>alt</sup> |
| 6       | 14840   |  |     |                    |                    |           |                   |                     |                                    |          |                   |                     |                                    |
| 8       | 18270   |  |     | 0.0002             | 2.37E-05           | 42250     | 42250             | 338000              | 338000                             | 15       | 15                | 116                 | 116                                |
| 10      | 21520   |  |     | 0.0006             | 5.63E-05           | 17750     | 17750             | 177500              | 177500                             | 14       | 14                | 135                 | 135                                |
| 12      | 24770   |  |     | 0.0008             | 6.35E-05           | 15750     | 15750             | 189000              | 189000                             | 12       | 12                | 147                 | 147                                |
| 14      | 27910   |  |     | 0.0008             | 4.26E-05           | 23500     | 23500             | 329000              | 329000                             | 11       | 11                | 158                 | 158                                |
| 16      | 30970   |  |     | 0.0012             | 7.41E-05           | 13500     | 13500             | 216000              | 216000                             | 11       | 11                | 168                 | 168                                |
| 18      | 33840   |  |     | 0.0012             | 6.9E-05            | 14500     | 14500             | 261000              | 261000                             | 10       | 10                | 171                 | 171                                |
| 20      | 36880   |  |     | 0.0007             | 3.31E-05           | 30250     | 30250             | 605000              | 605000                             | 9        | 9                 | 175                 | 175                                |
| 22      | 39670   |  |     | 0.0011             | 5.13E-05           | 19500     | 19500             | 429000              | 429000                             | 8        | 8                 | 182                 | 182                                |
| 24      | 42440   |  |     | 0.0033             | 0.000138           | 7250      | 7250              | 174000              | 174000                             | 8        | 8                 | 180                 | 180                                |
| 26      | 45160   |  |     | 0.0016             | 6E-05              | 18429     | 16671             | 479143              | 433457                             | 6.571429 | 6.82857           | 170.8571            | 177.54                             |
| 31      | 51200   |  |     | 0.0017             | 5.57E-05           | 9388.9    | 17953             | 291056              | 556544                             | 2.944444 | 5.84265           | 91.27778            | 181.12                             |
| 62      | 86030   |  |     | 0.0107             | 0.000172           | 3968.5    | 5818              | 245304              | 360728                             | 1.48913  | 1.93075           | 92.32609            | 119.71                             |
| 123     | 142400  |  |     | 0.0685             | 0.000557           | 1877.6    | 1795              | 206349              | 220750                             | 0.808211 | 0.88282           | 99.53289            | 108.6                              |
| 214     | 216000  |  |     | 0.1848             | 0.000863           | 882.35    | 1159              | 188824              | 248115                             | 0.540441 | 0.59956           | 115.6544            | 128.31                             |
| 365     | 339800  |  |     | 0.6777             | 0.001716           | 582.87    | 582.9             | 230235              | 230235                             | 0.428177 | 0.42818           | 169.1298            | 169.13                             |
| 576     | 444200  |  |     | 1.1158             | 0.001937           | 468.01    | 516.3             | 269572              | 297385                             | 0.325411 | 0.35083           | 187.4369            | 202.08                             |
| 942     | 612100  |  |     | 2.8851             | 0.003063           | 326.5     | 326.5             | 307586              | 307586                             | 0.275956 | 0.27596           | 259.9508            | 259.95                             |
| 1308    | 738900  |  |     | 6.375              | 0.004874           | 158.59    | 205.2             | 207436              | 268371                             | 0.213656 | 0.23751           | 279.4628            | 310.66                             |
| 2304    | 958800  |  |     | 22.227             | 0.009847           | 100.86    | 103.7             | 232382              | 238829                             | 0.161166 | 0.18287           | 417.4073            | 421.32                             |
| 3400    | 1E+06   |  |     | 58.205             | 0.017119           | 38.462    | 58.41             | 130769              | 198808                             | 0.121885 | 0.14635           | 414.4095            | 497.61                             |
| 5996    | 1E+06   |  |     | 400.66             | 0.086821           | 14.985    | 14.97             | 89732               | 89732                              | 0.070108 | 0.07011           | 420.3657            | 420.37                             |
| 8582    | 1E+06   |  |     | 2188.7             | 0.25451            | 3.9291    | 3.929             | 33759               | 33759                              | 0.024846 | 0.02485           | 213.4781            | 213.48                             |
| 11188   | 1E+06   |  |     | 8801.2             | 0.788857           | 1.2712    | 1.271             | 14222               | 14222                              | 0.009438 | 0.00944           | 105.5878            | 105.59                             |
| 13784   | 1E+06   |  |     | 23856              | 1.730887           | 0.5778    | 0.578             | 7984.6              | 7984.6                             | 0.004237 | 0.00424           | 58.40678            | 58.407                             |
| 16380   | 1E+06   |  |     | 42522              | 2.588              | 0.3852    | 0.385             | 6308.7              | 6308.7                             | 0.002889 | 0.00289           | 47.3228             | 47.323                             |
| 18976   | 1E+06   |  |     | 61577              | 3.245              | 0.3082    | 0.308             | 5847.8              | 5847.8                             | 0.002311 | 0.00231           | 43.85824            | 43.858                             |
| 21572   | 1E+06   |  |     | 101820             | 4.72               | 0.2119    | 0.212             | 4570.3              | 4570.3                             | 0.001733 | 0.00173           | 37.39368            | 37.394                             |

Table G-6 Model 2 Type 2h Fracture Simulation Output and Calculations - Continued

| days  | 2 smooths |           |       |             |           |  |
|-------|-----------|-----------|-------|-------------|-----------|--|
|       | Q' smooth | Q''smooth | Q"    | Q''' smooth | Q'''t     |  |
| 6     |           |           |       |             |           |  |
| 8     | -1670     | 1670      |       |             |           |  |
| 10    | -1625     | 1625      | 18125 | 18125       | 181250    |  |
| 12    | -1598     | 1598      | 18750 | 18750       | 225000    |  |
| 14    | -1550     | 1550      | 22500 | 22500       | 315000    |  |
| 16    | -1508     | 1508      | 18125 | 18125       | 280000    |  |
| 18    | -1478     | 1478      | 18750 | 18750       | 337500    |  |
| 20    | -1433     | 1433      | 21875 | 21875       | 437500    |  |
| 22    | -1390     | 1390      | 15000 | 15000       | 330000    |  |
| 24    | -1373     | 1373      | 18357 | 18357       | 440571.43 |  |
| 26    | -1317     | 1317      | 25176 | 26849       | 654566.31 |  |
| 31    | -1196     | 1196      | 7229  | 21345       | 224088.11 |  |
| 62    | -1056     | 1056      | 3461  | 3979        | 214605.47 |  |
| 123   | -878      | 878       | 1903  | 2241        | 234111.55 |  |
| 214   | -767      | 767       | 910   | 1063        | 194674.73 |  |
| 395   | -630      | 630       | 633   | 633         | 250204.44 |  |
| 578   | -638      | 538       | 421   | 467         | 242744.88 |  |
| 942   | -400      | 400       | 312   | 312         | 293788.25 |  |
| 1308  | -309      | 309       | 163   | 216         | 213358.79 |  |
| 2304  | -178      | 178       | 98    | 101         | 225802.89 |  |
| 3400  | -104      | 104       | 39    | 55          | 132070.19 |  |
| 5988  | -34       | 34        | 17    | 17          | 104566.34 |  |
| 8592  | -14       | 14        | 5     | 5           | 43347.475 |  |
| 11188 | -8        | 8         | 2     | 2           | 17431.404 |  |
| 13784 | -6        | 6         | 1     | 1           | 9204.038  |  |
| 16380 | -5        | 5         | 0     | 0           |           |  |
| 18976 | -4        | 4         | 1     | 1           |           |  |
| 21572 |           |           |       |             |           |  |

Table G-6 Model 2 Type 2b Fracture Simulation Output and Calculations - Continued

| model Type3 |          |                |          |          |           |          |       |     |        |          |          |          |         |          |
|-------------|----------|----------------|----------|----------|-----------|----------|-------|-----|--------|----------|----------|----------|---------|----------|
| 28 by<br>28 |          | phmatrix 0.11  | 2XeL 8.5 |          | oap 3.373 |          |       |     |        |          |          |          |         |          |
|             |          | w 0.007        |          |          | (mmbo)    |          |       |     |        |          |          |          |         |          |
|             |          | kmatrix 0.1    |          |          | Sor 0.75  |          |       |     |        |          |          |          |         |          |
|             |          | kfracture 1000 |          |          |           |          |       |     |        |          |          |          |         |          |
| delta q     |          |                |          |          |           |          |       |     |        |          |          |          |         |          |
| delta t     | average  | cum oil        | oil rate | gas rate | cum gas   |          |       |     |        |          |          |          |         | tp(days) |
| days        | pressure | mbo            | bopd     | mcfd/d   | mmcfd     | dt hours | dq    | dp  | qdq    | dp/dq    | q cum/dp | q cum/q  | qcum/dq |          |
| 6           | 1935     | 7.57           | 365      | 592      | 7.922     | 144      |       | 66  | 5.6154 | 0.178082 | 116.462  | 20.73973 |         |          |
| 8           | 1931     | 8.242          | 322      | 420      | 8.843     | 192      | 43    | 68  | 4.6657 | 0.214286 | 119.449  | 25.59627 | 191.67  |          |
| 10          | 1928     | 8.886          | 278      | 351      | 9.5       | 240      | 87    | 72  | 3.8811 | 0.258993 | 123.139  | 31.88208 | 101.91  |          |
| 14          | 1923     | 10.01          | 264      | 239      | 10.53     | 336      | 101   | 77  | 3.4286 | 0.291887 | 130      | 37.91657 | 99.109  |          |
| 16          | 1921     | 10.53          | 254      | 219      | 10.96     | 384      | 111   | 79  | 3.2152 | 0.311024 | 133.291  | 41.45669 | 94.885  |          |
| 18          | 1919     | 11.05          | 232      | 254      | 11.34     | 432      | 133   | 81  | 2.8842 | 0.349138 | 136.42   | 47.62931 | 83.083  |          |
| 20          | 1916     | 11.53          | 238      | 194      | 11.72     | 480      | 127   | 84  | 2.8333 | 0.352941 | 137.262  | 48.44538 | 90.787  |          |
| 22          | 1915     | 12             | 218      | 202      | 12.07     | 528      | 147   | 85  | 2.5847 | 0.388908 | 141.178  | 55.04587 | 81.833  |          |
| 24          | 1913     | 12.48          | 225      | 168      | 12.35     | 576      | 140   | 87  | 2.5862 | 0.388667 | 143.448  | 55.46867 | 88.143  |          |
| 26          | 1911     | 12.94          | 213      | 183      | 12.64     | 624      | 152   | 89  | 2.3933 | 0.41784  | 145.393  | 60.75117 | 85.132  |          |
| 31          | 1906     | 13.83          | 209      | 145      | 12.78     | 744      | 158   | 94  | 2.2234 | 0.449781 | 147.128  | 66.17225 | 88.654  |          |
| 62          | 1885     | 19.45          | 168      | 96       | 17.4      | 1488     | 197   | 115 | 1.4609 | 0.684524 | 169.13   | 115.7738 | 98.731  |          |
| 123         | 1854     | 28.68          | 146      | 71       | 22.54     | 2952     | 219   | 146 | 1      | 1        | 198.438  | 198.4384 | 130.96  |          |
| 214         | 1820     | 40.41          | 121      | 66       | 28.75     | 5136     | 244   | 180 | 0.6722 | 1.487603 | 224.5    | 333.9669 | 165.61  |          |
| 385         | 1769     | 59.03          | 68       | 56       | 39.41     | 9480     | 277   | 231 | 0.381  | 2.625    | 255.541  | 670.7955 | 213.1   |          |
| 576         | 1729     | 73.47          | 70       | 49       | 48.98     | 13824    | 295   | 271 | 0.2583 | 3.871429 | 271.107  | 1049.571 | 249.05  |          |
| 842         | 1666     | 98.83          | 54       | 41       | 63.07     | 22608    | 311   | 334 | 0.1617 | 6.185185 | 289.91   | 1793.148 | 311.35  |          |
| 1308        | 1617     | 116.3          | 51       | 31       | 74.13     | 31382    | 314   | 383 | 0.1332 | 7.509804 | 303.655  | 2280.362 | 370.38  |          |
| 2304        | 1527     | 155.3          | 38       | 25       | 103.6     | 55298    | 327   | 473 | 0.0803 | 12.44737 | 328.33   | 4088.842 | 474.92  |          |
| 3400        | 1469     | 190            | 30       | 17       | 124.1     | 81600    | 335   | 531 | 0.0585 | 17.7     | 357.815  | 6333.333 | 587.16  |          |
| 5986        | 1381     | 254.3          | 20       | 16       | 170.6     | 143904   | 345   | 619 | 0.0323 | 30.95    | 410.824  | 12715    | 737.1   |          |
| 8592        | 1329     | 302.8          | 18.6     | 9.8      | 202.8     | 208208   | 348.4 | 671 | 0.0277 | 36.07527 | 451.267  | 18279.57 | 874.13  |          |
| 11188       | 1289     | 347.8          | 15.3     | 13.3     | 232.4     | 268512   | 349.7 | 711 | 0.0215 | 46.47059 | 489.17   | 22732.03 | 994.57  |          |
| 13784       | 1252     | 382.7          | 12.6     | 8.6      | 262.3     | 330816   | 352.4 | 748 | 0.0168 | 59.36508 | 511.631  | 30373.02 | 1086    |          |
| 16380       | 1222     | 413.9          | 11.7     | 8.7      | 286.3     | 363120   | 353.3 | 778 | 0.015  | 68.49573 | 532.005  | 36378.07 | 1171.5  |          |
| 18976       | 1196     | 444.5          | 11.8     | 8.8      | 307.5     | 455424   | 353.2 | 804 | 0.0147 | 68.13559 | 552.881  | 37689.49 | 1258.5  |          |
| 21572       | 1169     | 473.1          | 10       | 9.1      | 330.5     | 517728   | 356   | 831 | 0.012  | 63.1     | 569.314  | 47310    | 1332.7  |          |
| 24168       | 1145     | 497.3          | 8.9      | 8.1      | 362.2     | 580032   | 358.1 | 855 | 0.0104 | 96.06742 | 581.637  | 58878.4  | 1308.5  |          |

Table G-7 Model 3 Type 3 Fracture Simulation Output and Calculations

| model Type3 |         |                           |          |            |           |                     |             |  |
|-------------|---------|---------------------------|----------|------------|-----------|---------------------|-------------|--|
| 28 by 28    |         | phimatrix 0.11<br>w 0.007 |          | 2XeL 8.5   |           | oop 3.373<br>(mmbo) |             |  |
|             |         | kmatrix 0.1               |          | Sci 0.75   |           |                     |             |  |
|             |         | kfracture 1000            |          |            |           |                     |             |  |
| delta t     | cum oil |                           |          | days/days  |           | hours               |             |  |
| days        | mbo     | dq/q                      | dp/p     | (dp+dt)/dt | sqr1 dt   | sqr1 dt             | d(dq/q)/dt  |  |
| 6           | 7570    | 0                         | 0.033592 | 4.456621   | 2.4494897 |                     | 12          |  |
| 8           | 8242    | 0.13354                   | 0.035733 | 4.198534   | 2.8284271 | 13.85640648         |             |  |
| 10          | 8866    | 0.31295                   | 0.037344 | 4.188209   | 3.1622777 | 15.49193338         | 0.041505897 |  |
| 14          | 10010   | 0.38258                   | 0.040042 | 3.708333   | 3.7416574 | 18.33030278         | 0.020676372 |  |
| 16          | 10530   | 0.43701                   | 0.041124 | 3.591043   | 4         | 19.59591794         | 0.047675026 |  |
| 18          | 11050   | 0.57328                   | 0.042209 | 3.646073   | 4.2426407 | 20.78460989         | 0.024151393 |  |
| 20          | 11530   | 0.53361                   | 0.043841 | 3.422288   | 4.472138  | 21.90660223         | 0.025256016 |  |
| 22          | 12000   | 0.67431                   | 0.044386 | 3.502085   | 4.6904158 | 22.97825056         | 0.022152194 |  |
| 24          | 12480   | 0.62222                   | 0.045478 | 3.311111   | 4.8989795 | 24                  | 0.009825774 |  |
| 26          | 12940   | 0.71362                   | 0.046572 | 3.336584   | 5.0990195 | 24.97969199         | 0.017741323 |  |
| 31          | 13830   | 0.74641                   | 0.048318 | 3.134589   | 5.5677544 | 27.27636339         | 0.012750112 |  |
| 62          | 19450   | 1.17262                   | 0.061008 | 2.86732    | 7.8740079 | 38.57460304         | 0.00819118  |  |
| 123         | 28680   | 1.5                       | 0.078749 | 2.59705    | 11.090537 | 54.33231083         | 0.005552039 |  |
| 214         | 40410   | 2.01653                   | 0.098901 | 2.560593   | 14.628739 | 71.65589147         | 0.008057821 |  |
| 395         | 59030   | 3.14773                   | 0.130582 | 2.698216   | 19.874607 | 97.36529158         | 0.008071151 |  |
| 576         | 73470   | 4.21429                   | 0.156738 | 2.822173   | 24        | 117.5755077         | 0.004774282 |  |
| 942         | 96830   | 5.75826                   | 0.20048  | 2.903554   | 30.692018 | 150.356669          | 0.002653794 |  |
| 1308        | 116300  | 6.15686                   | 0.236858 | 2.743419   | 36.168283 | 177.1778767         | 0.002089577 |  |
| 2304        | 155300  | 8.60526                   | 0.309758 | 2.773803   | 48        | 235.1510153         | 0.002394744 |  |
| 3400        | 190000  | 11.1657                   | 0.36147  | 2.862745   | 58.309519 | 285.6571371         | 0.002341478 |  |
| 5906        | 254300  | 17.25                     | 0.448226 | 3.12058    | 77.433843 | 379.346807          | 0.001436246 |  |
| 8502        | 302800  | 18.6237                   | 0.504891 | 2.894736   | 92.693042 | 454.1013103         | 0.001079778 |  |
| 11188       | 347800  | 22.8562                   | 0.55159  | 3.031822   | 105.77334 | 518.1614354         | 0.001799807 |  |
| 13784       | 382700  | 27.9683                   | 0.597444 | 3.203498   | 117.40528 | 575.168063          | 0.001413785 |  |
| 16380       | 413900  | 30.1966                   | 0.636661 | 3.159711   | 127.98437 | 626.9928229         | 0.000378265 |  |
| 18976       | 444500  | 29.9322                   | 0.672241 | 2.985112   | 137.7534  | 674.8510947         | 0.00102146  |  |
| 21572       | 473100  | 36.5                      | 0.710864 | 3.193121   | 146.8741  | 719.533182          | 0.001941262 |  |
| 24168       | 497300  | 40.0112                   | 0.746725 | 3.312      | 155.46081 | 761.5983193         |             |  |

Table G-7 Model 3 Type 3 Fracture Simulation Output and Calculations - Continued

| delta t: cum oil |        | the pressure decline can be compared with actual pressures as a function of time |          |           |       |                   |                      |          |         |                   |                      |
|------------------|--------|--|----------|-----------|-------|-------------------|----------------------|----------|---------|-------------------|----------------------|
| days             | mbo    | 1/q* <sup>n</sup> t  | 1/q'     | q' (dsmv) | q'alt | t <sup>n</sup> Q' | t <sup>n</sup> Q'alt | p'       | p'alt   | t <sup>n</sup> p' | t <sup>n</sup> p'alt |
| 6                | 7570   |  |          |           |       |                   |                      |          |         |                   |                      |
| 8                | 8242   | 0.0004   | 4.6E-05  | 21750     | 21750 | 174000            | 174000               | 2        | 2       | 14                | 14                   |
| 10               | 8868   | 0.001  | 0.000103 | 9887      | 15833 | 98887             | 158333               | 1        | 1       | 13                | 14                   |
| 14               | 10010  | 0.0035   | 0.00025  | 4000      | 4500  | 56000             | 63000                | 1        | 1       | 16                | 15                   |
| 16               | 10530  | 0.002  | 0.000125 | 8000      | 8000  | 128000            | 128000               | 1        | 1       | 16                | 16                   |
| 18               | 11050  | 0.0045   | 0.00025  | 4000      | 4000  | 72000             | 72000                | 1        | 1       | 23                | 23                   |
| 20               | 11530  | 0.0057   | 0.000286 | 3500      | 3500  | 70000             | 70000                | 1        | 1       | 20                | 20                   |
| 22               | 12000  | 0.0068   | 0.000306 | 3250      | 3250  | 71500             | 71500                | 1        | 1       | 17                | 17                   |
| 24               | 12480  | 0.0192   | 0.0008   | 1250      | 1250  | 30000             | 30000                | 1        | 1       | 24                | 24                   |
| 26               | 12940  | 0.0114   | 0.000438 | 2285.7    | 4514  | 58429             | 117371               | 1        | 1       | 26                | 26                   |
| 31               | 13830  | 0.0248   | 0.0008   | 1250      | 872.6 | 38753             | 27050                | 0.722222 | 0.9552  | 22.38889          | 29.611               |
| 62               | 19450  | 0.0805   | 0.00146  | 684.78    | 998.5 | 42457             | 61904                | 0.565217 | 0.8204  | 35.04348          | 38.465               |
| 123              | 26680  | 0.3878   | 0.003234 | 309.21    | 326.2 | 38033             | 40119                | 0.427632 | 0.45419 | 52.59868          | 55.866               |
| 214              | 40410  | 1.0036   | 0.00469  | 213.24    | 243.8 | 45632             | 52175                | 0.3125   | 0.34289 | 66.875            | 73.379               |
| 395              | 59030  | 2.8037   | 0.007098 | 140.88    | 140.9 | 55649             | 55649                | 0.251381 | 0.25138 | 99.29558          | 99.298               |
| 576              | 73470  | 9.2688   | 0.016088 | 62.157    | 81.01 | 35803             | 46880                | 0.1883   | 0.20483 | 108.4807          | 117.98               |
| 942              | 98830  | 36.292   | 0.038526 | 25.956    | 25.96 | 24451             | 24451                | 0.153005 | 0.15301 | 144.1311          | 144.13               |
| 1308             | 116300 | 111.34   | 0.085125 | 11.747    | 9.501 | 15366             | 12428                | 0.102056 | 0.12219 | 133.489           | 159.82               |
| 2304             | 155300 | 229.52   | 0.099619 | 10.038    | 10.31 | 23128             | 23762                | 0.070746 | 0.07254 | 162.9981          | 167.12               |
| 3400             | 190000 | 687.38   | 0.205111 | 4.8754    | 6.276 | 16576             | 21338                | 0.039545 | 0.04727 | 134.4529          | 160.73               |
| 5998             | 254300 | 2730.8   | 0.455439 | 2.1957    | 2.198 | 13185             | 13185                | 0.026986 | 0.02698 | 161.8795          | 161.68               |
| 8582             | 302800 | 9481.4   | 1.104681 | 0.9052    | 0.905 | 7777.8            | 7777.8               | 0.01772  | 0.01772 | 152.2465          | 152.25               |
| 11188            | 347800 | 9681.3   | 0.865333 | 1.1556    | 1.156 | 12829             | 12829                | 0.014831 | 0.01483 | 165.9237          | 165.92               |
| 13784            | 382700 | 19880  | 1.442222 | 0.6934    | 0.693 | 9557.5            | 9557.5               | 0.012904 | 0.0129  | 177.8752          | 177.88               |
| 16380            | 413900 | 105306   | 6.49     | 0.1541    | 0.154 | 2523.9            | 2523.9               | 0.010786 | 0.01079 | 178.6718          | 178.67               |
| 18976            | 444500 | 57965  | 3.054118 | 0.3274    | 0.327 | 6213.3            | 6213.3               | 0.010208 | 0.01021 | 193.7072          | 193.71               |
| 21572            | 473100 | 38621  | 1.790345 | 0.5586    | 0.558 | 12049             | 12049                | 0.009823 | 0.00982 | 211.8975          | 211.9                |

Table G-7 Model 3 Type 3 Fracture Simulation Output and Calculations - Continued

| days  | 2 smooths |            |      |           |           |
|-------|-----------|------------|------|-----------|-----------|
|       | Q' smooth | Q'' smooth | Q"   | Q' smooth | Q'''1     |
| 6     |           |            |      |           |           |
| 8     | -324      | 324        |      |           |           |
| 10    | -303      | 303        | 9222 | 9778      | 92222.222 |
| 14    | -269      | 269        | 7222 | 5778      | 101111.11 |
| 16    | -260      | 260        | 4667 | 4667      | 74666.667 |
| 18    | -250      | 250        | 5625 | 5625      | 101250    |
| 20    | -238      | 238        | 3125 | 3125      | 62500     |
| 22    | -238      | 238        | 625  | 625       | 13750     |
| 24    | -235      | 235        | 5589 | 5589      | 134142.86 |
| 26    | -215      | 215        | 8078 | 9188      | 210018.9  |
| 31    | -178      | 178        | 1221 | 6351      | 37849.386 |
| 62    | -171      | 171        | 383  | 315       | 24354.646 |
| 123   | -142      | 142        | 335  | 381       | 41266.184 |
| 214   | -120      | 120        | 187  | 215       | 40118.604 |
| 365   | -91       | 91         | 126  | 126       | 49858.61  |
| 576   | -74       | 74         | 60   | 77        | 34554.775 |
| 942   | -59       | 59         | 34   | 34        | 32270.07  |
| 1308  | -49       | 49         | 17   | 22        | 22014.316 |
| 2304  | -36       | 36         | 9    | 10        | 21816.532 |
| 3400  | -30       | 30         | 4    | 5         | 12785.686 |
| 5986  | -22       | 22         | 2    | 2         | 13403.52  |
| 8592  | -18       | 18         | 1    | 1         | 10486.264 |
| 11188 | -15       | 15         | 1    | 1         | 11371.916 |
| 13784 | -13       | 13         | 1    | 1         | 9255.1715 |
| 16380 | -12       | 12         | 0    | 0         | 4192.6884 |
| 18976 | -11       | 11         | 0    | 0         | 6335.455  |
| 21572 | -10       | 10         | 2    | 2         | 47374.294 |

Table G-7 Model 3 Type 3 Fracture Simulation Output and Calculations - Continued

| model Type 3h |                  |             |               |                |              |          |       |     |        |          |          |          |           |
|---------------|------------------|-------------|---------------|----------------|--------------|----------|-------|-----|--------|----------|----------|----------|-----------|
| 28 by<br>28   | phimatnx         | 0.11        | 2XeL          | 8.5            | oap 3.373    |          |       |     |        |          |          |          |           |
|               | w                | 0.007       |               |                | (mmbo)       |          |       |     |        |          |          |          |           |
|               | kmatrix          | 0.1         | Sor           | 0.75           |              |          |       |     |        |          |          |          |           |
|               | kfracture        | 4000        |               |                |              |          |       |     |        |          |          |          |           |
| delta t       | delta q          |             |               |                |              |          |       |     |        |          |          |          |           |
| days          | average pressure | cum oil mbo | oil rate bopd | gas rate mcf/d | cum gas mmcf | dt hours | dq    | dp  | q/dp   | dq/q     | q cum/dp | q cum/q  | qcum/dq   |
| 5             | 1934             | 7.897       | 378           | 734            | 8.043        | 144      |       | 56  | 5.7273 | 0.174603 | 119.652  | 20.89153 |           |
| 8             | 1930             | 8.659       | 365           | 470            | 9.059        | 192      | 13    | 70  | 5.2143 | 0.191781 | 123.7    | 23.72329 | 666.08    |
| 10            | 1927             | 9.393       | 303           | 453            | 9.8          | 240      | 75    | 73  | 4.1507 | 0.240924 | 128.671  |          | 31 125.24 |
| 14            | 1921             | 10.81       | 303           | 273            | 10.9         | 336      | 75    | 79  | 3.8354 | 0.260726 | 136.835  | 35.87657 | 144.13    |
| 16            | 1918             | 11.41       | 297           | 258            | 11.42        | 384      | 81    | 82  | 3.622  | 0.278094 | 139.146  | 38.41751 | 140.88    |
| 18            | 1916             | 11.98       | 288           | 251            | 11.92        | 432      | 90    | 84  | 3.4288 | 0.291667 | 142.738  | 41.63194 | 133.22    |
| 20            | 1914             | 12.6        | 284           | 232            | 12.36        | 480      | 94    | 86  | 3.3023 | 0.302817 | 146.512  | 44.36862 | 134.04    |
| 22            | 1912             | 13.17       | 279           | 221            | 12.79        | 528      | 99    | 88  | 3.1705 | 0.315412 | 149.659  | 47.2043  | 133.03    |
| 24            | 1910             | 13.72       | 278           | 209            | 13.22        | 576      | 100   | 90  | 3.0889 | 0.323741 | 152.444  | 49.35252 | 137.2     |
| 26            | 1908             | 14.29       | 282           | 182            | 13.6         | 624      | 96    | 92  | 3.0852 | 0.328241 | 155.326  | 50.67376 | 148.85    |
| 31            | 1903             | 15.5        | 256           | 188            | 14.68        | 744      | 122   | 97  | 2.6392 | 0.378906 | 159.794  | 60.54688 | 127.05    |
| 62            | 1881             | 22.64       | 205           | 141            | 19.39        | 1488     | 173   | 119 | 1.7227 | 0.580488 | 190.252  | 110.439  | 130.87    |
| 123           | 1850             | 33.56       | 148           | 114            | 26.36        | 2952     | 230   | 150 | 0.9887 | 1.013514 | 223.733  | 226.7588 | 145.91    |
| 214           | 1815             | 46.5        | 128           | 78             | 33.38        | 5136     | 250   | 185 | 0.6919 | 1.445313 | 251.351  | 363.2813 | 186       |
| 395           | 1761             | 64.74       | 81            | 65             | 47.82        | 9480     | 297   | 239 | 0.3389 | 2.960617 | 270.879  | 799.2593 | 217.98    |
| 576           | 1721             | 79.04       | 77            | 43             | 56.48        | 13824    | 301   | 279 | 0.278  | 3.623377 | 283.297  | 1026.494 | 262.59    |
| 942           | 1658             | 103.7       | 59            | 34             | 69.62        | 22608    | 319   | 342 | 0.1725 | 5.798661 | 303.216  | 1757.627 | 325.08    |
| 1308          | 1608             | 123.4       | 44            | 45             | 84.12        | 31362    | 334   | 392 | 0.1122 | 8.908091 | 314.795  | 2804.545 | 369.46    |
| 2304          | 1519             | 160.8       | 34            | 21             | 113.6        | 55296    | 344   | 481 | 0.0707 | 14.14706 | 334.304  | 4729.412 | 467.44    |
| 3400          | 1462             | 196.8       | 26            | 28             | 133.9        | 81600    | 352   | 538 | 0.0483 | 20.69231 | 365.799  | 7569.231 | 559.09    |
| 5996          | 1372             | 259         | 20            | 15             | 183.1        | 143804   | 358   | 628 | 0.0318 | 31.4     | 412.42   | 12950    | 723.46    |
| 8592          | 1322             | 308         | 18.4          | 11.9           | 214.3        | 206208   | 359.6 | 678 | 0.0271 | 36.84783 | 455.752  | 16783.48 | 859.29    |
| 11188         | 1279             | 353.2       | 14.5          | 13             | 248.1        | 268512   | 363.5 | 721 | 0.0201 | 49.72414 | 489.875  | 24358.62 | 971.66    |
| 13784         | 1243             | 387         | 12.4          | 10.2           | 277.5        | 330616   | 365.6 | 757 | 0.0164 | 61.04839 | 511.229  | 31209.68 | 1058.5    |
| 16380         | 1213             | 418.3       | 12.1          | 8.3            | 299.9        | 363120   | 365.9 | 787 | 0.0154 | 65.04132 | 531.512  | 34570.25 | 1143.2    |
| 18976         | 1186             | 449.9       | 10.8          | 11.1           | 322          | 455424   | 367.2 | 814 | 0.0133 | 75.37037 | 552.703  | 41657.41 | 1225.2    |
| 21572         | 1160             | 477.1       | 10.3          | 7.6            | 345.4        | 517728   | 367.7 | 840 | 0.0123 | 81.5534  | 567.976  | 46320.39 | 1297.5    |
| 24168         | 1137             | 500.9       | 8.6           | 7.4            | 386.2        | 580032   | 369.4 | 863 | 0.01   | 100.3488 | 580.417  | 58244.19 | 1356      |

Table G-8 Model 3 Type 3b Fracture Simulation Output and Calculations

| model Type 3h |         |                |          |             |           |                     |    |             |  |
|---------------|---------|----------------|----------|-------------|-----------|---------------------|----|-------------|--|
| 28 by 28      |         | phimatrix 0.11 |          | 2x6L 8.5    |           | cap 3.373<br>(mmbo) |    |             |  |
|               |         | w 0.007        |          | kmatrix 0.1 |           | Sci 0.75            |    |             |  |
|               |         | kfraction 4000 |          |             |           |                     |    |             |  |
| delta t       | cum oil |                |          | days/days   |           | hours               |    |             |  |
| days          | mbo     | dq/q           | dp/p     | (p+dl)/dt   | sqrt dt   | sqrt dt             |    | 1/q         |  |
| 8             | 7897    | 0              | 0.034126 | 4.481922    | 2.4484867 |                     | 12 | 0.002645503 |  |
| 8             | 8859    | 0.03562        | 0.036269 | 3.965411    | 2.8284271 | 13.85640646         |    | 0.002738726 |  |
| 10            | 9393    | 0.24752        | 0.037883 | 4.1         | 3.1622777 | 15.49193338         |    | 0.00330033  |  |
| 14            | 10810   | 0.24752        | 0.041124 | 3.548326    | 3.7416574 | 18.33030278         |    | 0.00330033  |  |
| 16            | 11410   | 0.27273        | 0.042753 | 3.401094    | 4         | 19.59591794         |    | 0.003367003 |  |
| 18            | 11990   | 0.3125         | 0.043841 | 3.312885    | 4.2426407 | 20.78460989         |    | 0.003472222 |  |
| 20            | 12600   | 0.33099        | 0.044932 | 3.21831     | 4.472136  | 21.9086023          |    | 0.003521127 |  |
| 22            | 13170   | 0.35484        | 0.046025 | 3.14585     | 4.6904158 | 22.97825059         |    | 0.003584229 |  |
| 24            | 13720   | 0.35971        | 0.04712  | 3.056356    | 4.8989795 |                     | 24 | 0.003597122 |  |
| 26            | 14290   | 0.34043        | 0.048218 | 2.948991    | 5.0990195 | 24.97999199         |    | 0.003548099 |  |
| 31            | 15500   | 0.47658        | 0.050972 | 2.953125    | 5.5677644 | 27.27636339         |    | 0.00390625  |  |
| 62            | 22840   | 0.8439         | 0.063264 | 2.781275    | 7.8740079 | 38.57460304         |    | 0.004878049 |  |
| 123           | 33560   | 1.55405        | 0.081081 | 2.843551    | 11.090537 | 54.33231083         |    | 0.006756757 |  |
| 214           | 46500   | 1.95313        | 0.101928 | 2.697576    | 14.528739 | 71.68589147         |    | 0.0078125   |  |
| 385           | 64740   | 3.68867        | 0.135718 | 3.023441    | 19.874607 | 97.36529158         |    | 0.012345679 |  |
| 576           | 79040   | 3.90809        | 0.162115 | 2.782107    | 24        | 117.5755077         |    | 0.012987013 |  |
| 942           | 103700  | 5.40678        | 0.206273 | 2.855846    | 30.692019 | 150.359589          |    | 0.016949153 |  |
| 1308          | 123400  | 7.59091        | 0.243781 | 3.144148    | 36.186283 | 177.1778767         |    | 0.022727273 |  |
| 2304          | 160800  | 10.1176        | 0.316656 | 3.052696    | 48        | 235.1510153         |    | 0.029411765 |  |
| 3400          | 198800  | 13.5385        | 0.367989 | 3.226244    | 58.309519 | 285.6571371         |    | 0.038461538 |  |
| 5998          | 256000  | 17.9           | 0.457726 | 3.159773    | 77.433843 | 379.346807          |    | 0.05        |  |
| 8592          | 308000  | 19.5435        | 0.512859 | 2.954548    | 92.693042 | 454.1013103         |    | 0.064347826 |  |
| 11188         | 353200  | 25.089         | 0.563722 | 3.17721     | 105.77334 | 518.1814354         |    | 0.088965517 |  |
| 13784         | 387000  | 29.4839        | 0.60901  | 3.264196    | 117.40526 | 575.166063          |    | 0.080645161 |  |
| 16380         | 418300  | 30.2397        | 0.648805 | 3.110516    | 127.98437 | 626.9928229         |    | 0.082644628 |  |
| 18976         | 449900  | 34             | 0.688341 | 3.195268    | 137.7534  | 674.8510947         |    | 0.082592593 |  |
| 21572         | 477100  | 35.999         | 0.724138 | 3.147246    | 146.8741  | 719.533182          |    | 0.087087379 |  |
| 24168         | 500900  | 42.9535        | 0.759015 | 3.409971    | 155.48081 | 761.5983193         |    | 0.11627907  |  |

Table G-8 Model 3 Type 3h Fracture Simulation Output and Calculations - Continued

| delta t | cum oil | the pressure decline can be compared with actual pressures as a function of time |     |                    |          |            |        |        |         |          |         |          |         |
|---------|---------|--|-----|--------------------|----------|------------|--------|--------|---------|----------|---------|----------|---------|
|         |         | days   | mbo | 1/q <sup>n-1</sup> | 1/q'     | q' (deriv) | q' att | r'Q'   | r'Q'att | p'       | p' att  | r'p'     | r'p'att |
| 6       | 7897    |  |     |                    |          |            |        |        |         |          |         |          |         |
| 8       | 8550    |  |     | 0.0004             | 5.33E-05 | 18750      | 18750  | 150000 | 150000  | 2        | 2       | 14       | 14      |
| 10      | 9303    |  |     | 0.0005             | 4.84E-05 | 10333      | 20887  | 103333 | 208887  | 2        | 2       | 15       | 15      |
| 14      | 10810   |  |     | 0.007              | 0.0005   | 1000       | 2000   | 14000  | 28000   | 2        | 2       | 21       | 21      |
| 16      | 11410   |  |     | 0.0043             | 0.000287 | 3750       | 3750   | 60000  | 60000   | 1        | 1       | 20       | 20      |
| 18      | 11990   |  |     | 0.0055             | 0.000308 | 3250       | 3250   | 58500  | 58500   | 1        | 1       | 18       | 18      |
| 20      | 12600   |  |     | 0.0089             | 0.000444 | 2250       | 2250   | 45000  | 45000   | 1        | 1       | 20       | 20      |
| 22      | 13170   |  |     | 0.0147             | 0.000857 | 1500       | 1500   | 33000  | 33000   | 1        | 1       | 22       | 22      |
| 24      | 13720   |  |     | -0.032             | -0.00133 | -750       | -750   | -18000 | -18000  | 1        | 1       | 24       | 24      |
| 26      | 14290   |  |     | 0.455              | 0.0175   | 3142.9     | 57.14  | 81714  | 1485.7  | 1        | 1       | 26       | 26      |
| 31      | 15500   |  |     | 0.0086             | 0.000212 | 2138.9     | 4705   | 66308  | 145894  | 0.75     | 0.95988 | 23.25    | 29.75   |
| 62      | 22640   |  |     | 0.0441             | 0.00711  | 1173.9     | 1405   | 72783  | 87152   | 0.576087 | 0.64179 | 35.71739 | 39.791  |
| 123     | 33580   |  |     | 0.1899             | 0.001544 | 508.58     | 647.6  | 62308  | 79658   | 0.434211 | 0.4586  | 53.40789 | 56.408  |
| 214     | 46500   |  |     | 0.918              | 0.00429  | 246.32     | 233.1  | 52713  | 49899   | 0.327208 | 0.35575 | 70.02205 | 76.131  |
| 395     | 64740   |  |     | 2.8037             | 0.007098 | 140.88     | 140.9  | 55649  | 55649   | 0.259689 | 0.25967 | 102.5681 | 102.57  |
| 576     | 79040   |  |     | 18.545             | 0.032195 | 40.219     | 31.05  | 23165  | 17891   | 0.1883   | 0.20483 | 106.4607 | 117.98  |
| 942     | 103700  |  |     | 20.885             | 0.022182 | 45.082     | 45.08  | 42467  | 42467   | 0.154372 | 0.15437 | 145.418  | 145.42  |
| 1308    | 123400  |  |     | 40.039             | 0.030611 | 18.355     | 32.67  | 24009  | 42730   | 0.102058 | 0.12391 | 133.486  | 162.08  |
| 2304    | 160800  |  |     | 263.76             | 0.114479 | 8.6042     | 8.735  | 19824  | 20126   | 0.06979  | 0.07158 | 160.7954 | 164.91  |
| 3400    | 198800  |  |     | 584.34             | 0.171855 | 3.792      | 5.819  | 12893  | 19783   | 0.036816 | 0.04686 | 135.3738 | 159.32  |
| 5996    | 259000  |  |     | 4096.2             | 0.683158 | 1.4638     | 1.484  | 8776.9 | 8776.9  | 0.026965 | 0.02698 | 161.6795 | 161.68  |
| 8592    | 308000  |  |     | 8110.8             | 0.944    | 1.0593     | 1.059  | 9101.7 | 9101.7  | 0.017912 | 0.01791 | 153.9014 | 153.9   |
| 11188   | 353200  |  |     | 9681.3             | 0.865333 | 1.1556     | 1.156  | 12929  | 12929   | 0.015216 | 0.01522 | 170.2334 | 170.23  |
| 13784   | 387000  |  |     | 29819              | 2.163333 | 0.4622     | 0.462  | 6371.6 | 6371.6  | 0.012712 | 0.01271 | 175.2203 | 175.22  |
| 16380   | 418300  |  |     | 53153              | 3.245    | 0.3082     | 0.308  | 5047.8 | 5047.8  | 0.010978 | 0.01098 | 179.8267 | 179.83  |
| 18976   | 449900  |  |     | 54735              | 2.884444 | 0.3467     | 0.347  | 6578.7 | 6578.7  | 0.010208 | 0.01021 | 193.7072 | 193.71  |
| 21572   | 477100  |  |     | 50910              | 2.36     | 0.4237     | 0.424  | 9140.7 | 9140.7  | 0.009438 | 0.00944 | 203.5878 | 203.59  |

Table G-8 Model 3 Type 3b Fracture Simulation Output and Calculations - Continued

| delta t<br>days | 2 smooths |            |       |           |
|-----------------|-----------|------------|-------|-----------|
|                 | Q' smooth | Q'' smooth | Q"    | Q" smooth |
| 6               |           |            |       |           |
| 8               | -374      | 374        |       |           |
| 10              | -363      | 363        | 9319  | 7472      |
| 14              | -318      | 318        | 11292 | 11417     |
| 16              | -295      | 295        | 5146  | 5146      |
| 18              | -298      | 298        | 0     | 0         |
| 20              | -295      | 295        | 4375  | 4375      |
| 22              | -280      | 280        | 3750  | 3750      |
| 24              | -280      | 280        | 1821  | 1821      |
| 26              | -273      | 273        | 5860  | 4450      |
| 31              | -240      | 240        | 1658  | 5862      |
| 62              | -213      | 213        | 828   | 854       |
| 123             | -164      | 164        | 557   | 637       |
| 214             | -128      | 128        | 273   | 334       |
| 395             | -90       | 90         | 147   | 147       |
| 578             | -75       | 75         | 54    | 68        |
| 942             | -61       | 61         | 35    | 35        |
| 1308            | -49       | 49         | 19    | 26        |
| 2304            | -35       | 35         | 9     | 10        |
| 3400            | -30       | 30         | 4     | 4         |
| 5996            | -22       | 22         | 2     | 2         |
| 8592            | -18       | 18         | 1     | 1         |
| 11188           | -15       | 15         | 1     | 1         |
| 13784           | -13       | 13         | 1     | 1         |
| 16380           | -12       | 12         | 0     | 0         |
| 18976           | -11       | 11         | 0     | 0         |
| 21572           | -10       | 10         | 2     | 2         |

Table G-8 Model 3 Type 3b Fracture Simulation Output and Calculations - Continued

| model Type4h |          |                |          |           |         |          |      |      |        |          |          |          |          |  |  |  |  |  |  |  |  |  |
|--------------|----------|----------------|----------|-----------|---------|----------|------|------|--------|----------|----------|----------|----------|--|--|--|--|--|--|--|--|--|
| 28 by<br>28  |          | phimatrix 0.11 | 2XeL 8.5 | cap 3.373 |         |          |      |      |        |          |          |          |          |  |  |  |  |  |  |  |  |  |
|              |          | w 0.007        |          | (mmbo)    |         |          |      |      |        |          |          |          |          |  |  |  |  |  |  |  |  |  |
|              |          | kmatrix 10.1   |          | Sci 0.75  |         |          |      |      |        |          |          |          |          |  |  |  |  |  |  |  |  |  |
|              |          | kfracture 4000 |          |           |         |          |      |      |        |          |          |          |          |  |  |  |  |  |  |  |  |  |
|              |          | k partitions   |          |           |         |          |      |      |        |          |          |          |          |  |  |  |  |  |  |  |  |  |
|              |          |                |          |           |         |          |      |      |        |          |          |          |          |  |  |  |  |  |  |  |  |  |
|              |          | delta q        |          |           |         |          |      |      |        |          |          |          |          |  |  |  |  |  |  |  |  |  |
| delta t      | average  | cum oil        | oil rate | gas rate  | cum gas |          |      |      |        |          |          |          | t(days)  |  |  |  |  |  |  |  |  |  |
| days         | pressure | mbo            | bopd     | mcf/d     | mmcf    | dt hours | dq   | dp   | q/dp   | dp/q     | q cum/dp | q cum/q  | q cum/dq |  |  |  |  |  |  |  |  |  |
| 5            | 1842     | 14.78          | 1773     | 1141      | 10.2    | 144      |      | 158  | 11.222 | 0.089114 | 93.5443  | 8336153  |          |  |  |  |  |  |  |  |  |  |
| 8            | 1812     | 18.19          | 1666     | 1223      | 12.68   | 192      | 107  | 188  | 8.8817 | 0.112845 | 98.7553  | 10.91837 | 170      |  |  |  |  |  |  |  |  |  |
| 10           | 1784     | 21.41          | 1586     | 1185      | 15.08   | 240      | 187  | 216  | 7.3426 | 0.136192 | 99.1204  | 13.49937 | 114.49   |  |  |  |  |  |  |  |  |  |
| 12           | 1759     | 24.68          | 1607     | 1036      | 17.08   | 288      | 166  | 241  | 6.888  | 0.148988 | 102.324  | 15.34536 | 148.55   |  |  |  |  |  |  |  |  |  |
| 14           | 1735     | 27.76          | 1513     | 1091      | 19.2    | 336      | 260  | 285  | 5.7084 | 0.175149 | 104.755  | 18.34785 | 106.77   |  |  |  |  |  |  |  |  |  |
| 16           | 1713     | 30.77          | 1513     | 868       | 21.18   | 384      | 280  | 287  | 5.2718 | 0.189889 | 107.213  | 20.33708 | 118.35   |  |  |  |  |  |  |  |  |  |
| 18           | 1693     | 33.79          | 1498     | 908       | 22.92   | 432      | 277  | 307  | 4.873  | 0.205214 | 110.065  | 22.5869  | 121.99   |  |  |  |  |  |  |  |  |  |
| 20           | 1675     | 36.73          | 1453     | 921       | 24.69   | 480      | 320  | 325  | 4.4708 | 0.223675 | 113.015  | 25.27873 | 114.78   |  |  |  |  |  |  |  |  |  |
| 22           | 1658     | 39.53          | 1410     | 877       | 26.49   | 528      | 363  | 342  | 4.1228 | 0.242553 | 115.585  | 28.03546 | 108.9    |  |  |  |  |  |  |  |  |  |
| 24           | 1642     | 42.28          | 1411     | 581       | 28.08   | 576      | 362  | 358  | 3.9413 | 0.253721 | 118.101  | 29.98456 | 116.8    |  |  |  |  |  |  |  |  |  |
| 26           | 1629     | 45.07          | 1392     | 686       | 29.24   | 624      | 381  | 371  | 3.752  | 0.268523 | 121.482  | 32.37787 | 118.29   |  |  |  |  |  |  |  |  |  |
| 31           | 1597     | 51.35          | 1245     | 803       | 34.01   | 744      | 528  | 403  | 3.0893 | 0.323695 | 127.419  | 41.24498 | 97.254   |  |  |  |  |  |  |  |  |  |
| 62           | 1521     | 86.02          | 1007     | 604       | 54.07   | 1488     | 788  | 479  | 2.1023 | 0.47567  | 179.582  | 85.42205 | 112.3    |  |  |  |  |  |  |  |  |  |
| 123          | 1458     | 142            | 857      | 458       | 85.98   | 2952     | 906  | 542  | 1.5996 | 0.625144 | 261.993  | 163.7832 | 156.73   |  |  |  |  |  |  |  |  |  |
| 214          | 1398     | 215.1          | 758      | 380       | 123.5   | 5138     | 1015 | 602  | 1.2591 | 0.794195 | 357.309  | 283.7731 | 211.92   |  |  |  |  |  |  |  |  |  |
| 395          | 1312     | 337.9          | 610      | 330       | 185     | 9480     | 1163 | 688  | 0.8886 | 1.127889 | 491.134  | 553.9344 | 290.54   |  |  |  |  |  |  |  |  |  |
| 576          | 1244     | 440.8          | 535      | 283       | 236.9   | 13824    | 1237 | 756  | 0.708  | 1.410448 | 583.201  | 822.5746 | 366.43   |  |  |  |  |  |  |  |  |  |
| 942          | 1135     | 606.2          | 388      | 280       | 333     | 22808    | 1385 | 865  | 0.4486 | 2.229381 | 700.809  | 1562.371 | 437.69   |  |  |  |  |  |  |  |  |  |
| 1308         | 1045     | 730.9          | 300      | 271       | 427.5   | 31382    | 1473 | 956  | 0.3141 | 3.183333 | 786.34   | 2438.333 | 496.2    |  |  |  |  |  |  |  |  |  |
| 2304         | 848      | 955.1          | 173      | 260       | 685.2   | 55296    | 1600 | 1152 | 0.1502 | 6.65896  | 829.08   | 5520.809 | 596.94   |  |  |  |  |  |  |  |  |  |
| 3400         | 689      | 1065           | 92       | 234       | 950.5   | 81600    | 1681 | 1331 | 0.0891 | 14.48739 | 822.69   | 11802.17 | 651.4    |  |  |  |  |  |  |  |  |  |
| 5996         | 398      | 1228           | 29       | 95        | 1346    | 14304    | 1744 | 1604 | 0.0181 | 55.31034 | 785.586  | 42344.83 | 704.13   |  |  |  |  |  |  |  |  |  |
| 8592         | 299      | 1277           | 12.6     | 43.6      | 1508    | 208208   | 1780 | 1701 | 0.0074 | 135      | 750.735  | 101349.2 | 725.4    |  |  |  |  |  |  |  |  |  |
| 11188        | 263      | 1302           | 7.6      | 26.6      | 1584    | 268512   | 1785 | 1737 | 0.0044 | 228.5526 | 749.568  | 171315.8 | 737.51   |  |  |  |  |  |  |  |  |  |
| 13784        | 249      | 1319           | 5.7      | 20.1      | 1653    | 330816   | 1787 | 1751 | 0.0033 | 307.193  | 753.284  | 231403.5 | 746.34   |  |  |  |  |  |  |  |  |  |
| 16380        | 241      | 1332           | 4.6      | 16.2      | 1700    | 363120   | 1788 | 1759 | 0.0026 | 382.3913 | 757.248  | 286855.2 | 753.22   |  |  |  |  |  |  |  |  |  |
| 18976        | 234      | 1343           | 3.7      | 13.4      | 1738    | 455424   | 1789 | 1765 | 0.0021 | 477.2973 | 760.478  | 362973   | 759.06   |  |  |  |  |  |  |  |  |  |
| 21572        | 228      | 1351           | 3        | 10.9      | 1770    | 517728   | 1770 | 1772 | 0.0017 | 590.6667 | 762.415  | 450333.3 | 763.28   |  |  |  |  |  |  |  |  |  |
| 24168        | 224      | 1368           | 2.6      | 9.4       | 1798    | 58032    | 1770 | 1776 | 0.0015 | 683.0789 | 764.64   | 522307.7 | 767.06   |  |  |  |  |  |  |  |  |  |

Table G-9 Model 4 Type 4h Fracture Simulation Output and Calculations

| model Type4h |         |                          |          |   |           |                      |  |
|--------------|---------|--------------------------|----------|---|-----------|----------------------|--|
| 28 by 28     |         | phimatrx 0.11<br>w 0.007 |          | 2XeL 8.5<br>kmatrx 10.1<br>kfracture 4000<br>k partitions |           | odip 3.373<br>(mmbo) |  |
| <hr/>        |         |                          |          |   |           |                      |  |
| delta t      | cum oil |                          |          | days/days   |           | hours                |  |
| days         | mbo     | dp/dq                    | dpp      | (tp+dt)/dt  | sqrt dt   | sqrt dt              |  |
| 6            | 14780   | 0                        | 0.085776 | 2.389356  | 2.4494897 | 12                   |  |
| 8            | 18190   | 0.06423                  | 0.103753 | 2.384798  | 2.8284271 | 13.85640646          |  |
| 10           | 21410   | 0.11791                  | 0.121076 | 2.349937  | 3.1622777 | 15.49193338          |  |
| 12           | 24660   | 0.1033                   | 0.13701  | 2.27878   | 3.4841016 | 16.87056275          |  |
| 14           | 27760   | 0.17184                  | 0.152738 | 2.310547  | 3.7416574 | 18.33030278          |  |
| 16           | 30770   | 0.17184                  | 0.167542 | 2.271087  | 4         | 19.59591794          |  |
| 18           | 33790   | 0.18516                  | 0.181335 | 2.254828  | 4.2426407 | 20.78460989          |  |
| 20           | 36730   | 0.22023                  | 0.19403  | 2.263637  | 4.472136  | 21.9089023           |  |
| 22           | 39630   | 0.25745                  | 0.206273 | 2.274339  | 4.6904158 | 22.97825059          |  |
| 24           | 42280   | 0.25856                  | 0.218027 | 2.248524  | 4.8989795 | 24                   |  |
| 26           | 45070   | 0.27371                  | 0.227747 | 2.245303  | 5.0990195 | 24.97999199          |  |
| 31           | 51350   | 0.4241                   | 0.252348 | 2.330483  | 5.5677644 | 27.27636339          |  |
| 62           | 86020   | 0.76068                  | 0.314924 | 2.377775  | 7.8740079 | 38.57460304          |  |
| 123          | 142000  | 1.04498                  | 0.371742 | 2.33157   | 11.080537 | 54.33231063          |  |
| 214          | 215100  | 1.33905                  | 0.430615 | 2.326042  | 14.828739 | 71.66589147          |  |
| 395          | 337900  | 1.90658                  | 0.52439  | 2.402366  | 19.874607 | 97.36529156          |  |
| 576          | 440800  | 2.30784                  | 0.607717 | 2.428081  | 24        | 117.5755077          |  |
| 942          | 608200  | 3.56959                  | 0.762115 | 2.658568  | 30.892019 | 150.356569           |  |
| 1308         | 730900  | 4.91                     | 0.913878 | 2.86264   | 36.166283 | 177.1778767          |  |
| 2304         | 955100  | 9.24855                  | 1.358491 | 3.396185  | 48        | 235.1510153          |  |
| 3400         | 1096000 | 18.2717                  | 1.989537 | 4.500638  | 58.309519 | 265.6571371          |  |
| 5996         | 1228000 | 60.1379                  | 4.050505 | 8.062179  | 77.433843 | 379.346807           |  |
| 8592         | 1277000 | 139.714                  | 5.688963 | 12.79578  | 92.663042 | 454.1013103          |  |
| 11188        | 1302000 | 232.289                  | 8.604563 | 16.31246  | 105.77334 | 518.1814354          |  |
| 13784        | 1319000 | 310.053                  | 7.032129 | 17.78783  | 117.40528 | 575.166063           |  |
| 16380        | 1332000 | 384.435                  | 7.298755 | 18.67797  | 127.98437 | 626.9928229          |  |
| 18976        | 1343000 | 478.189                  | 7.547009 | 20.128  | 137.7534  | 674.8510947          |  |
| 21572        | 1351000 | 590                      | 7.77193  | 21.87583  | 146.8741  | 719.533182           |  |
| 24168        | 1358000 | 680.923                  | 7.926571 | 22.61154  | 155.46061 | 761.5963193          |  |

Table G-9 Model 4 Type 4h Fracture Simulation Output and Calculations - Continued

| delta t | cum oil | the pressure decline can be compared with actual pressures as a function of time |     |                    |          |           |       |                  |                      |          |         |                   |                      |
|---------|---------|--|-----|--------------------|----------|-----------|-------|------------------|----------------------|----------|---------|-------------------|----------------------|
|         |         | days   | mbo | 1/q <sup>n</sup> t | 1/q'     | q' (dinv) | q'att | t <sup>n</sup> Q | t <sup>n</sup> Q'att | p'       | p' att  | t <sup>n</sup> p' | t <sup>n</sup> p'att |
| 6       | 14780   |  |     |                    |          |           |       |                  |                      |          |         |                   |                      |
| 8       | 18190   |  |     | 0.0002             | 2.14E-05 | 46750     | 46750 | 374000           | 374000               | 15       | 15      | 116               | 116                  |
| 10      | 21410   |  |     | 0.0007             | 6.78E-05 | 14750     | 14750 | 147500           | 147500               | 13       | 13      | 133               | 133                  |
| 12      | 24660   |  |     | 0.0007             | 5.48E-05 | 18250     | 18250 | 219000           | 219000               | 12       | 12      | 147               | 147                  |
| 14      | 27760   |  |     | 0.0006             | 4.26E-05 | 23500     | 23500 | 328000           | 328000               | 12       | 12      | 161               | 161                  |
| 16      | 30770   |  |     | 0.0038             | 0.000235 | 4250      | 4250  | 68000            | 68000                | 11       | 11      | 168               | 168                  |
| 18      | 33790   |  |     | 0.0012             | 6.87E-05 | 15000     | 15000 | 270000           | 270000               | 10       | 10      | 171               | 171                  |
| 20      | 36730   |  |     | 0.0009             | 4.65E-05 | 21500     | 21500 | 430000           | 430000               | 9        | 9       | 175               | 175                  |
| 22      | 39630   |  |     | 0.0021             | 9.52E-05 | 10500     | 10500 | 231000           | 231000               | 8        | 8       | 182               | 182                  |
| 24      | 42280   |  |     | 0.0053             | 0.000222 | 4500      | 4500  | 108000           | 108000               | 7        | 7       | 174               | 174                  |
| 26      | 45070   |  |     | 0.0017             | 6.59E-05 | 23714     | 15185 | 616571           | 394829               | 6.428571 | 6.47143 | 167.1429          | 168.26               |
| 31      | 51350   |  |     | 0.0012             | 3.79E-05 | 10684     | 26383 | 331528           | 817872               | 3        | 5.85161 | 93                | 181.4                |
| 62      | 86020   |  |     | 0.0106             | 0.000171 | 4108.7    | 5864  | 254739           | 363556               | 1.51087  | 1.97353 | 93.67391          | 122.36               |
| 123     | 142000  |  |     | 0.0863             | 0.000539 | 1638.2    | 1855  | 201493           | 228131               | 0.809211 | 0.88292 | 99.53289          | 108.6                |
| 214     | 215100  |  |     | 0.1999             | 0.000934 | 944.85    | 1071  | 202199           | 229115               | 0.538765 | 0.58771 | 114.8676          | 127.91               |
| 385     | 337900  |  |     | 0.6441             | 0.001631 | 813.28    | 813.3 | 242238           | 242238               | 0.425414 | 0.42541 | 168.0387          | 168.04               |
| 576     | 440600  |  |     | 1.414              | 0.002455 | 405.85    | 407.4 | 233770           | 234640               | 0.323583 | 0.34992 | 186.3839          | 201.55               |
| 942     | 606200  |  |     | 2.9218             | 0.003102 | 322.4     | 322.4 | 303705           | 303705               | 0.271858 | 0.27186 | 258.0902          | 258.09               |
| 1308    | 730900  |  |     | 6.2259             | 0.00476  | 157.86    | 210.1 | 206476           | 274799               | 0.21072  | 0.23297 | 275.6211          | 304.73               |
| 2304    | 955100  |  |     | 22.591             | 0.008605 | 99.428    | 102   | 229078           | 234882               | 0.179732 | 0.18138 | 414.1033          | 417.9                |
| 3400    | 1E+06   |  |     | 57.462             | 0.0169   | 39.003    | 59.17 | 132611           | 201178               | 0.122427 | 0.14606 | 416.2514          | 496.59               |
| 5996    | 1E+06   |  |     | 392.08             | 0.08639  | 15.293    | 15.29 | 91686            | 91686                | 0.071263 | 0.07126 | 427.2958          | 427.3                |
| 8592    | 1E+06   |  |     | 2084.6             | 0.242617 | 4.1217    | 4.122 | 35414            | 35414                | 0.025616 | 0.02562 | 220.0955          | 220.1                |
| 11188   | 1E+06   |  |     | 8418.6             | 0.752464 | 1.329     | 1.329 | 148688           | 148688               | 0.00963  | 0.00963 | 107.7427          | 107.74               |
| 13784   | 1E+06   |  |     | 23856              | 1.730687 | 0.5778    | 0.578 | 7964.6           | 7964.6               | 0.004237 | 0.00424 | 58.40678          | 58.407               |
| 16380   | 1E+06   |  |     | 42522              | 2.596    | 0.3852    | 0.385 | 6309.7           | 6309.7               | 0.002889 | 0.00289 | 47.3226           | 47.323               |
| 18976   | 1E+06   |  |     | 81577              | 3.245    | 0.3082    | 0.308 | 5847.8           | 5847.8               | 0.002504 | 0.0025  | 47.5131           | 47.513               |
| 21572   | 1E+06   |  |     | 101820             | 4.72     | 0.2119    | 0.212 | 4570.3           | 4570.3               | 0.00193  | 0.00193 | 41.54854          | 41.549               |

Table G-9 Model 4 Type 4h Fracture Simulation Output and Calculations - Continued

| days  | 2 smooths |          |       |           |           |
|-------|-----------|----------|-------|-----------|-----------|
|       | Q' smooth | Q'smooth | Q"    | Q' smooth | Q"t       |
| 6     |           |          |       |           |           |
| 8     | -1658     | 1658     |       |           |           |
| 10    | -1618     | 1618     | 17500 | 17500     | 175000    |
| 12    | -1588     | 1588     | 22500 | 22500     | 270000    |
| 14    | -1528     | 1528     | 20000 | 20000     | 280000    |
| 16    | -1508     | 1508     | 9375  | 9375      | 150000    |
| 18    | -1490     | 1490     | 18125 | 18125     | 326250    |
| 20    | -1435     | 1435     | 25625 | 25625     | 512500    |
| 22    | -1388     | 1388     | 12500 | 12500     | 275000    |
| 24    | -1385     | 1385     | 8054  | 8064      | 183285.71 |
| 26    | -1355     | 1355     | 21159 | 17378     | 550133.64 |
| 31    | -1237     | 1237     | 8458  | 21225     | 262225.37 |
| 62    | -1051     | 1051     | 3968  | 4989      | 246042.96 |
| 123   | -872      | 872      | 1903  | 2243      | 234053.44 |
| 214   | -782      | 782      | 912   | 1081      | 195144.55 |
| 395   | -624      | 624      | 639   | 639       | 252410.06 |
| 576   | -530      | 530      | 416   | 487       | 239847.64 |
| 942   | -398      | 398      | 301   | 301       | 283839.44 |
| 1308  | -310      | 310      | 160   | 208       | 208850.2  |
| 2304  | -179      | 179      | 98    | 101       | 225423.39 |
| 3400  | -105      | 105      | 39    | 56        | 132287.33 |
| 5996  | -35       | 35       | 17    | 17        | 104756.05 |
| 8592  | -14       | 14       | 5     | 5         | 44622.401 |
| 11188 | -8        | 8        | 2     | 2         | 18261.471 |
| 13784 | -6        | 6        | 1     | 1         | 9204.038  |
| 16380 | -5        | 5        | 0     | 0         | 6684.0119 |
| 18976 | -4        | 4        | 1     | 1         |           |
| 21572 |           |          |       |           |           |

Table G-9 Model 4 Type 4h Fracture Simulation Output and Calculations - Continued